Fracture characteristics from two reactivated basement fault zones: examples from Norway and Shetland

Sleight, Janine Michelle

Fracture Characteristics from Two Reactivated Basement Fault Zones: Examples from Norway and Shetland

by

Janine Michelle Sleight

A thesis submitted in fulfilment of the requirements of the University of Durham for the degree of Doctor of Philosophy

Department of Geological Sciences
University of Durham
2001

Volume II of II

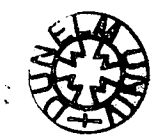

LIST OF FIGURES

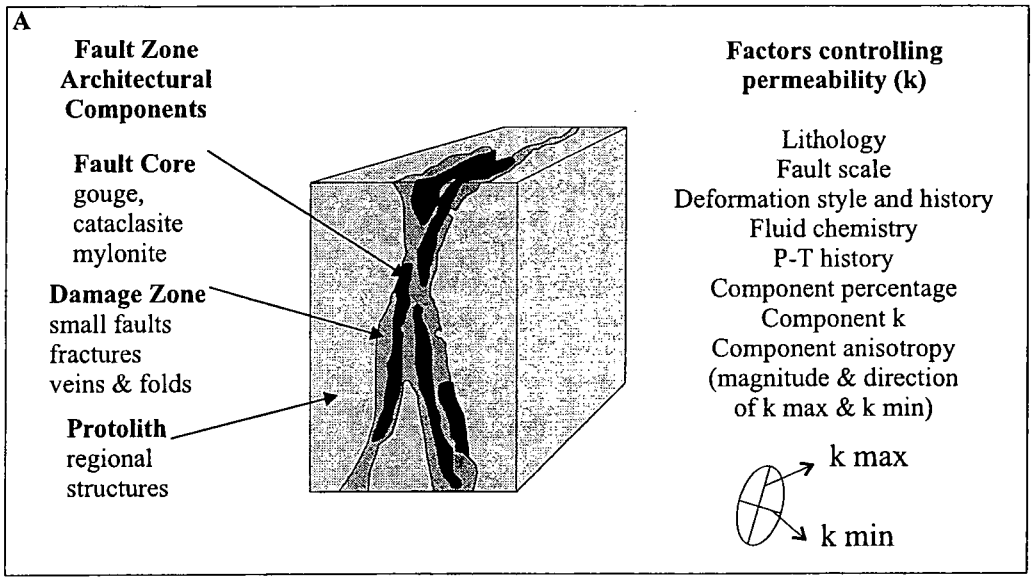

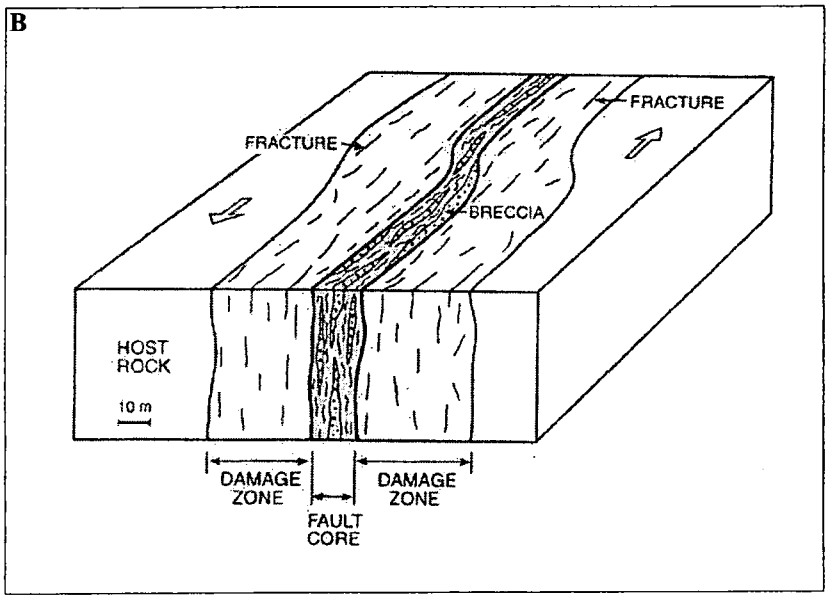

Figure 1.1 Principal components of an upper crustal fault zone
(**A** - after Caine et al., 1996, **B** - after Gudmundson et al., 2001)

A

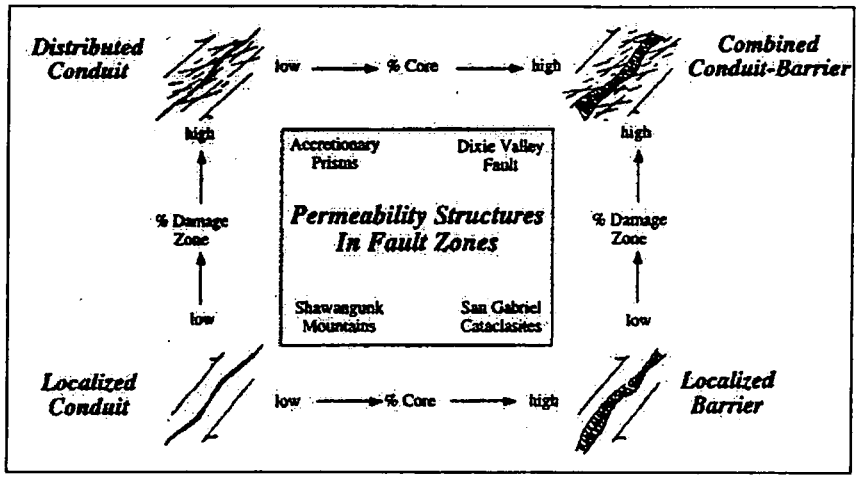

B

Permeability Structure	Architectural Style	Fault Core	Damage Zone
Localised conduit	Localised slip along single curviplanar surface, or along discretely segmented planes	Poorly developed or absent	Poorly developed or absent
Distributed conduit	Distributed slip accommodated along distributed surfaces and fractures	Poorly developed as narrow discrete, discontinuous bands, or absent	Well developed, discrete slip surfaces and fracture network
Localised barrier	Localised slip accommodated within cataclastic zone	Well developed fault core cataclasites	Poorly developed or absent
Combined conduit-barrier	Deformation accommodated within localised cataclastic zone and distributed zone of subsidiary structures	Well developed fault core cataclasites	Well developed, discrete slip surfaces and fracture network

Figure 1.2 A – Four end members of fault zone architecture and fluid-related flow, depending on relative permeabilities of the fault core and damage zone
B – Fault zone architectural styles and permeability structure (after Caine et al., 1996)

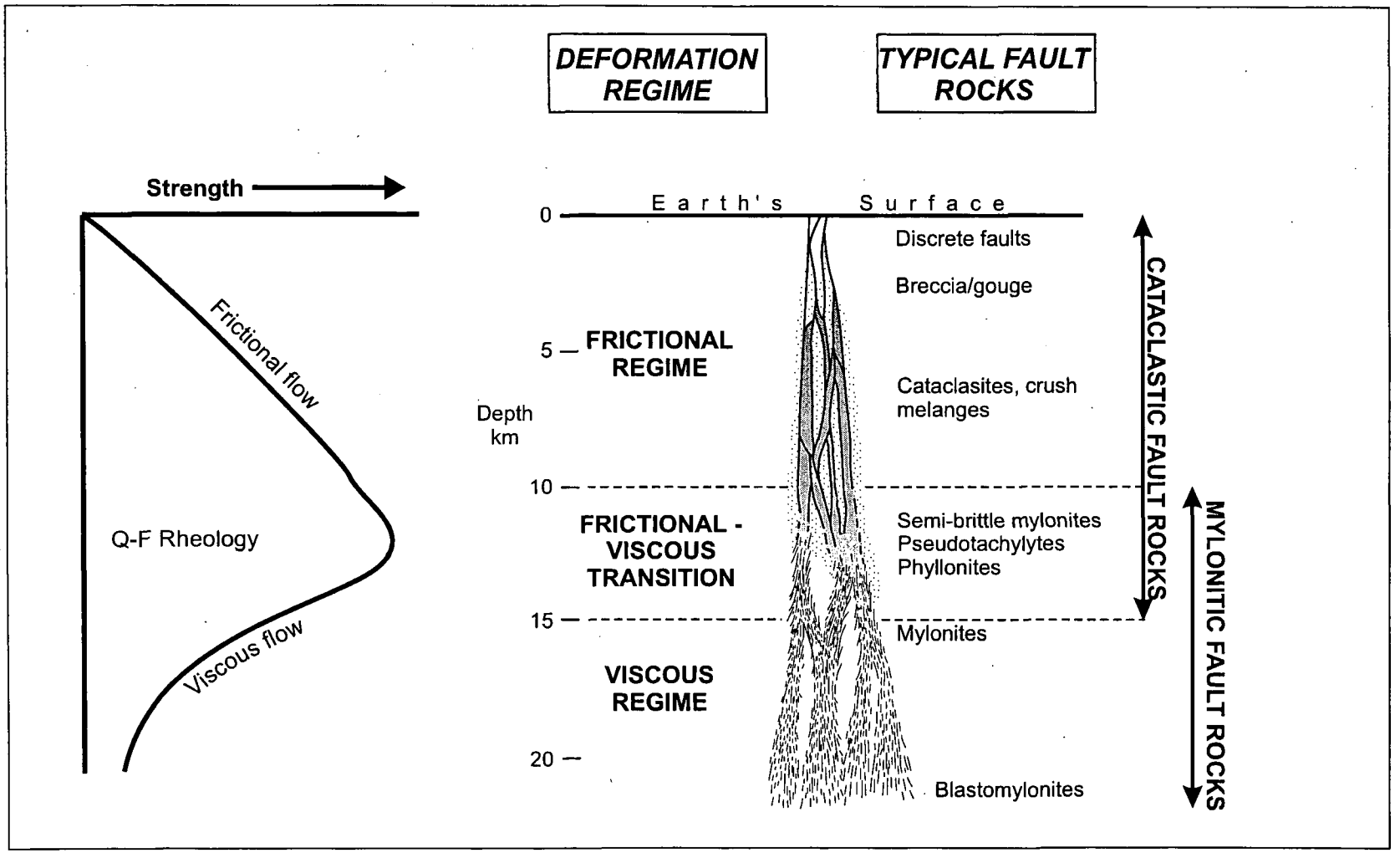

Figure 1.3 Notional vertical fault zone illustrating deformation processes and fault rock assemblages (after Holdsworth et al., 2001, and Sibson 1977)

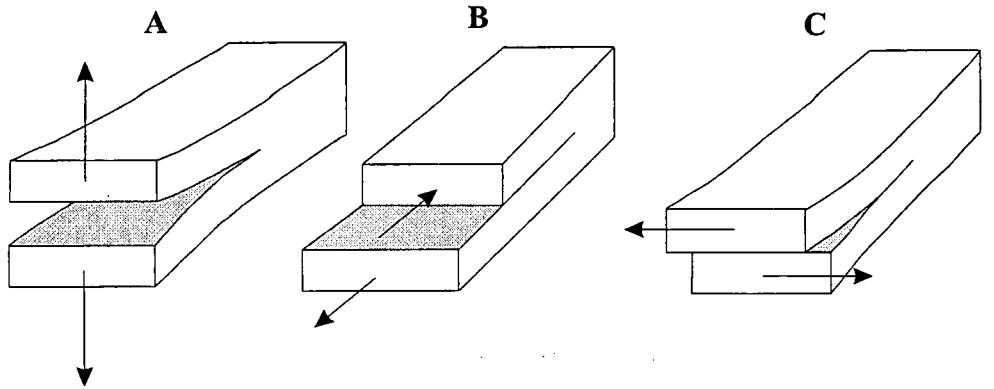

Figure 1.4 Schematic diagram of the three fundamental modes of fracture
A = mode I, tensile or opening mode
B = mode II, shear fracture
C = mode III, shear fracture
(after Atkinson 1987)

STRAIN REGIME

STRUCTURAL SEQUENCE	Tensile (tensile normal stress)	Shear (compressive normal stress)
Initial	JOINTS	DEFORMATION BANDS
Overprinted	JOINTED FAULTS	FAULTED JOINTS

Figure 1.6 Classification of fractures by opening displacement (after Schultz 2000)

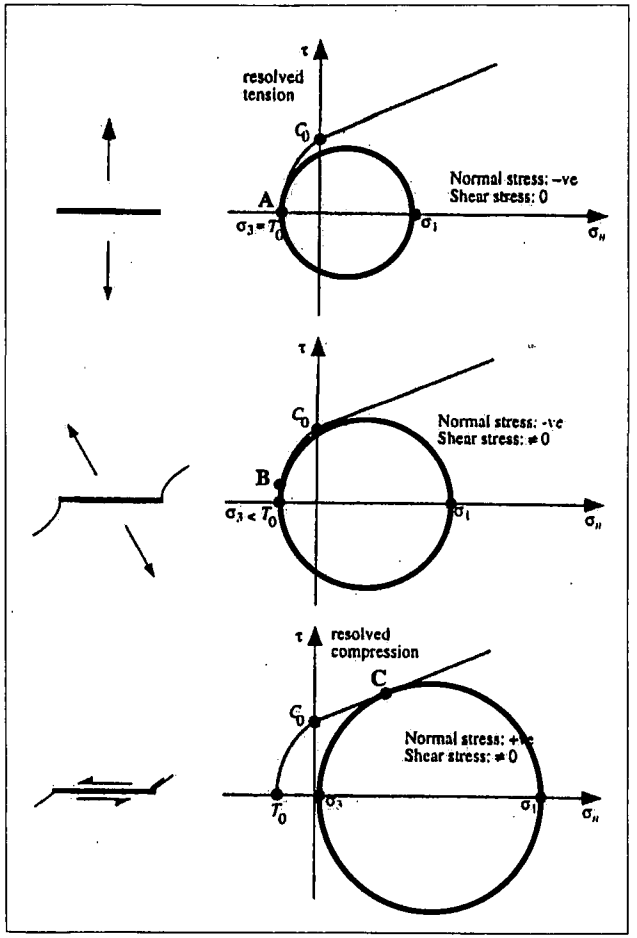

Figure 1.5 Mohr-Coulomb diagrams illustrating modes of fracture propagation
A = mode I fracture (e.g. extensional joint)
B = mixed-mode fractures
C = mode II and mode III, shear fractures
(after Schultz 2000)

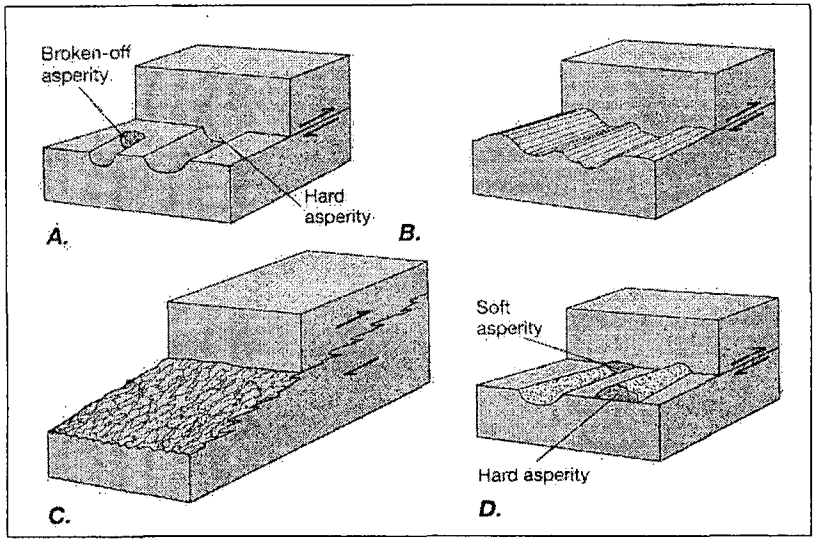

Figure 1.7 Slickenlines and lineations on fault surfaces
A - slickenlines formed by scratching and gouging by hard asperities in wall rocks
B - slickenlines formed by linear irregularities on the fault surface (ridge-in-groove)
C - Spikes on a stickolite (solution surface subparallel to movement direction)
D - Lineations formed by smeared mineral grains and soft asperities, or the collection of gouge behind a hard asperity
(after Twiss & Moores 1992)

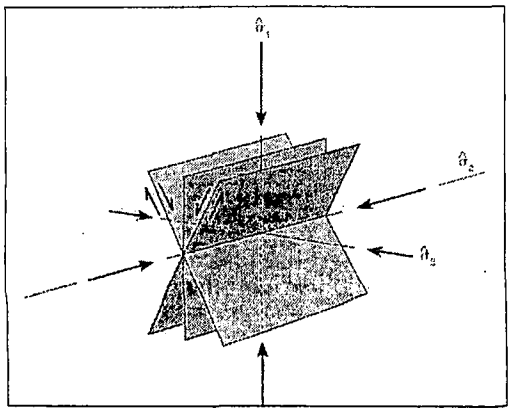

Figure 1.8 Conjugate fault pair bisected by an extension fracture (after Twiss & Moores 1992)

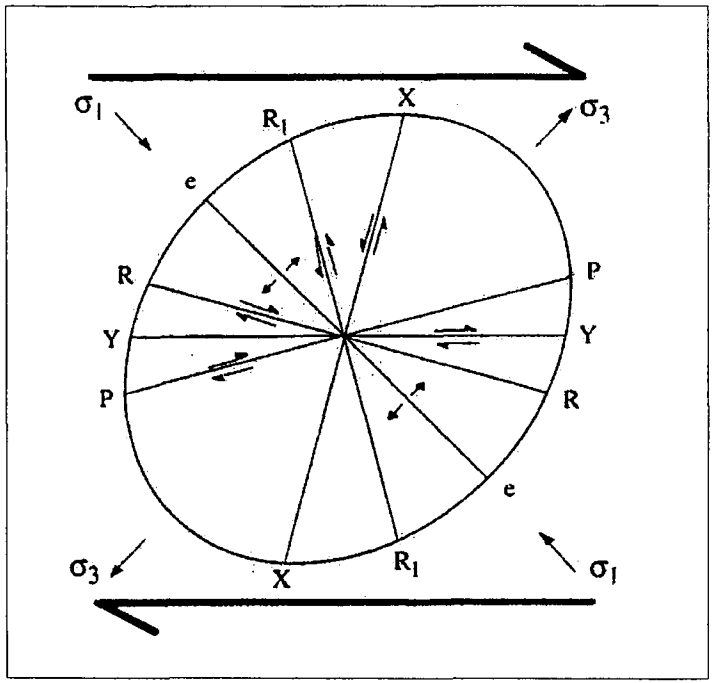

Figure 1.9 Subsidiary en-echelon structures that may occur within fault zones during simple shear (dextral shear in this diagram)
R and R_1 = Riedel and conjugate Riedel shears
P-shears, X-shears, Y-shears, extension joints (e)
(after Hancock 1985)

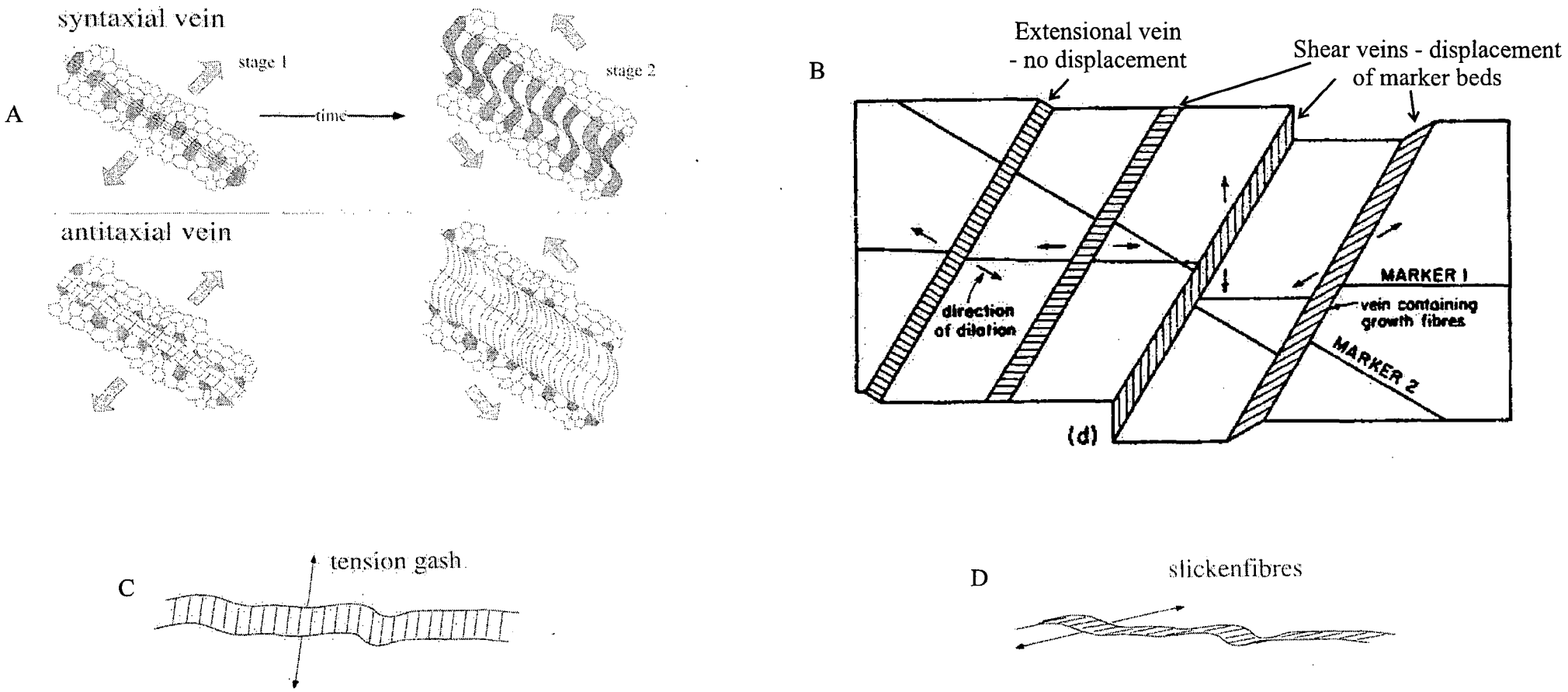

Figure 1.10 Fibrous vein infills
A - Syntaxial and antitaxial fibrous vein infills as illustrators of displacement (after Passchier & Trouw 1996)
B - The fibres in undeformed extensional veins are perpendicular to the vein margin, fibres in shear veins fractures are oblique (after Hancock 1985)
C - Veins that lie at a high angle to the extension direction are known as tension gashes (after Passchier & Trouw 1996)
D - Fibrous infills formed at a small angle to the opening direction are known as slickenfibres (after Passchier & Trouw 1996)

A

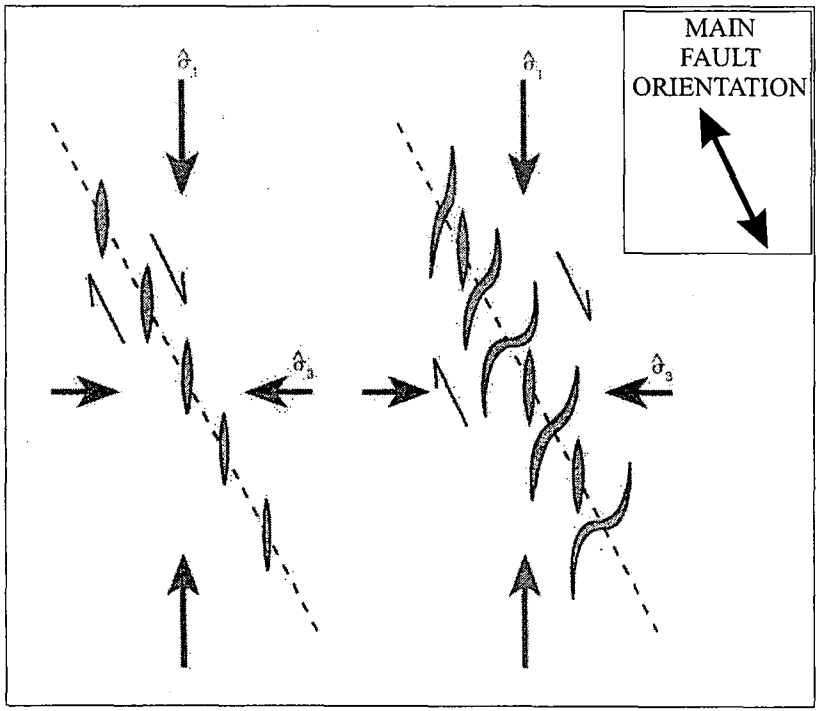

B

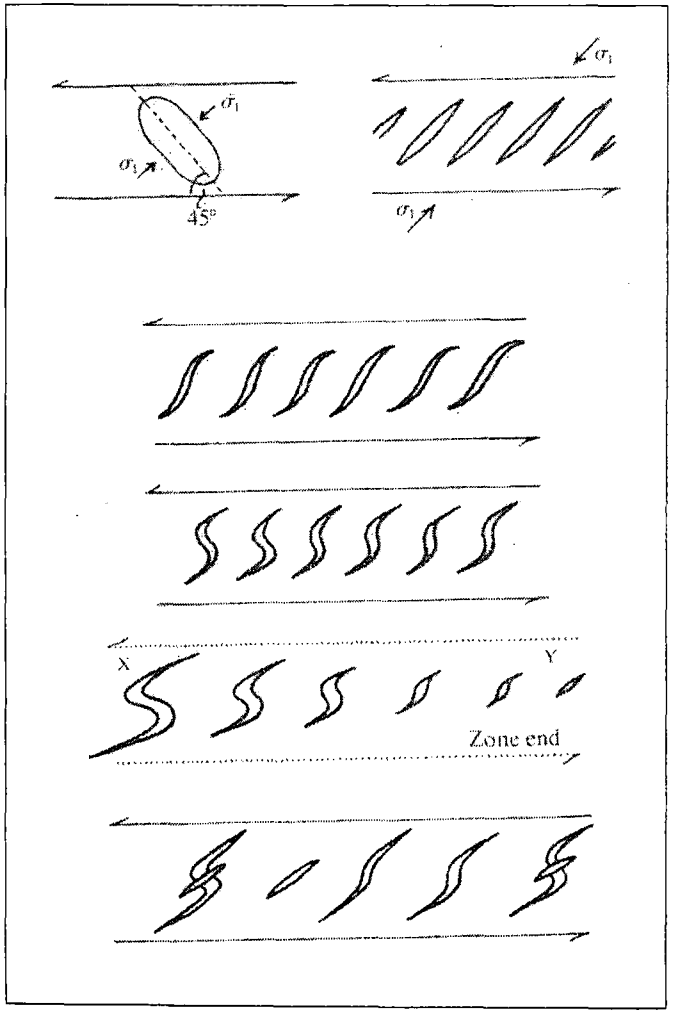

Figure 1.11 En-echelon tension gashes as kinematic indicators
A - (after Twiss & Moores 1992), acute angle between en-echelon tension gash and fault plane as a direct indicator of movement direction
B - (after Price & Cosgrove 1991), development of sigmoidal tension gashes with progressive deformation, cross-cut by a later set.

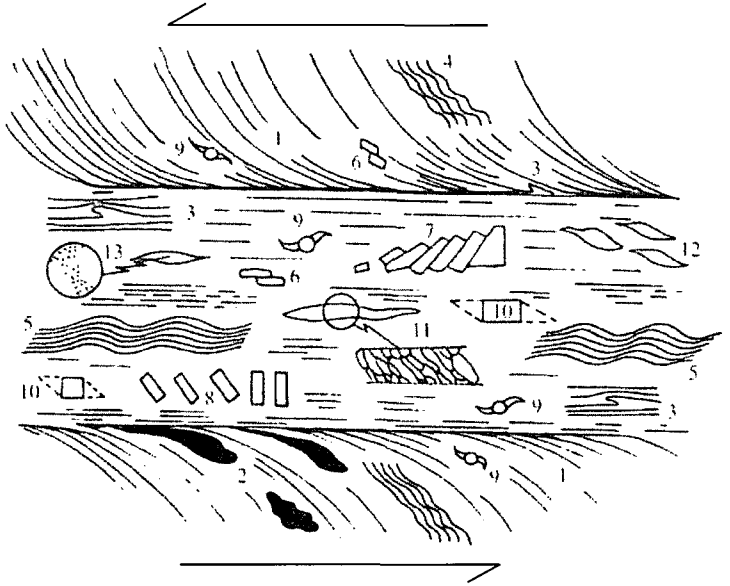

A Viscous kinematic indicators (after Price and Cosgrove 1991
1 - rotation of foliation
2 - rotation of deformed markers
3 - asymmetry of interfolial folds
4 - shear bands in the margin
5 - shear bands in the centre of the shear zone
6 - sheared porphyroclasts
7 - rotation of fragments due to shear fractures
8 - rotation of fragments due to tensile fractures
9 - asymmetry of trails around rotating clasts
10 - asymmetry of tails around non-rotation clasts
11 - asymmetry of elongate recrystallised quartz grains
12 - asymmetry of mica porphyroclasts
13 - asymmetry of quartz c-axia fabrics

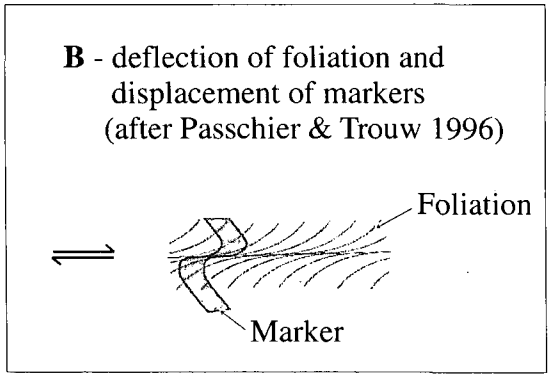

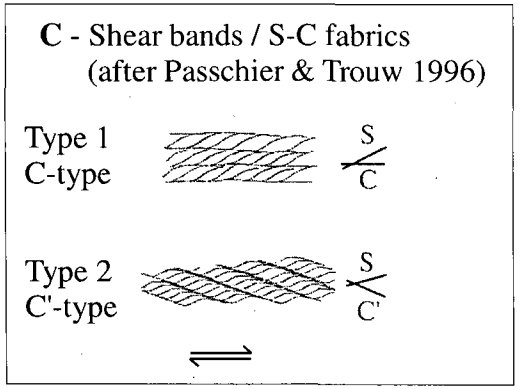

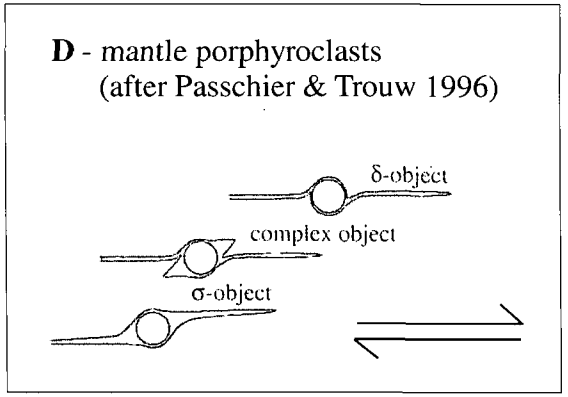

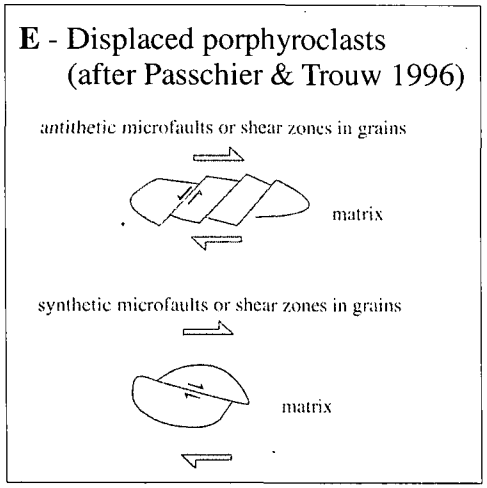

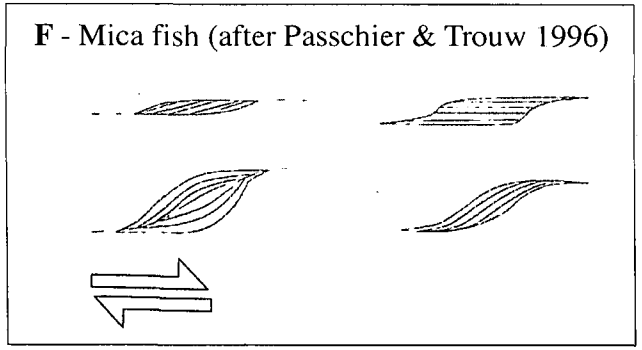

Figure 1.12 Viscous kinematic indicators

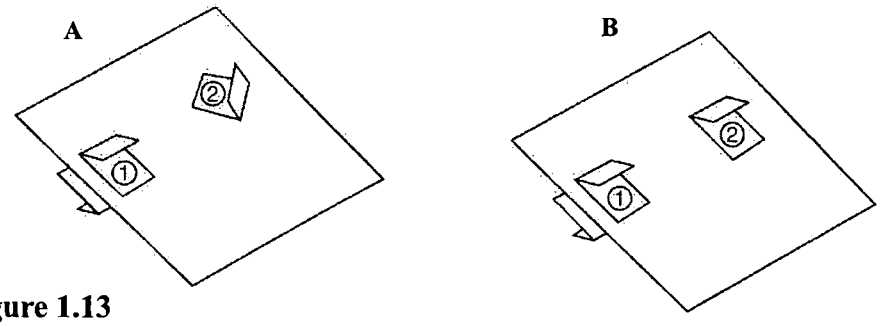

Figure 1.13
A - Geometric reactivation, reactivated structures display *different* senses of relative displacement for successive events
B - Kinematic reactivation, reactivated structures display *similar* senses of relative displacement for successive events
(after Holdsworth et al., 1997)

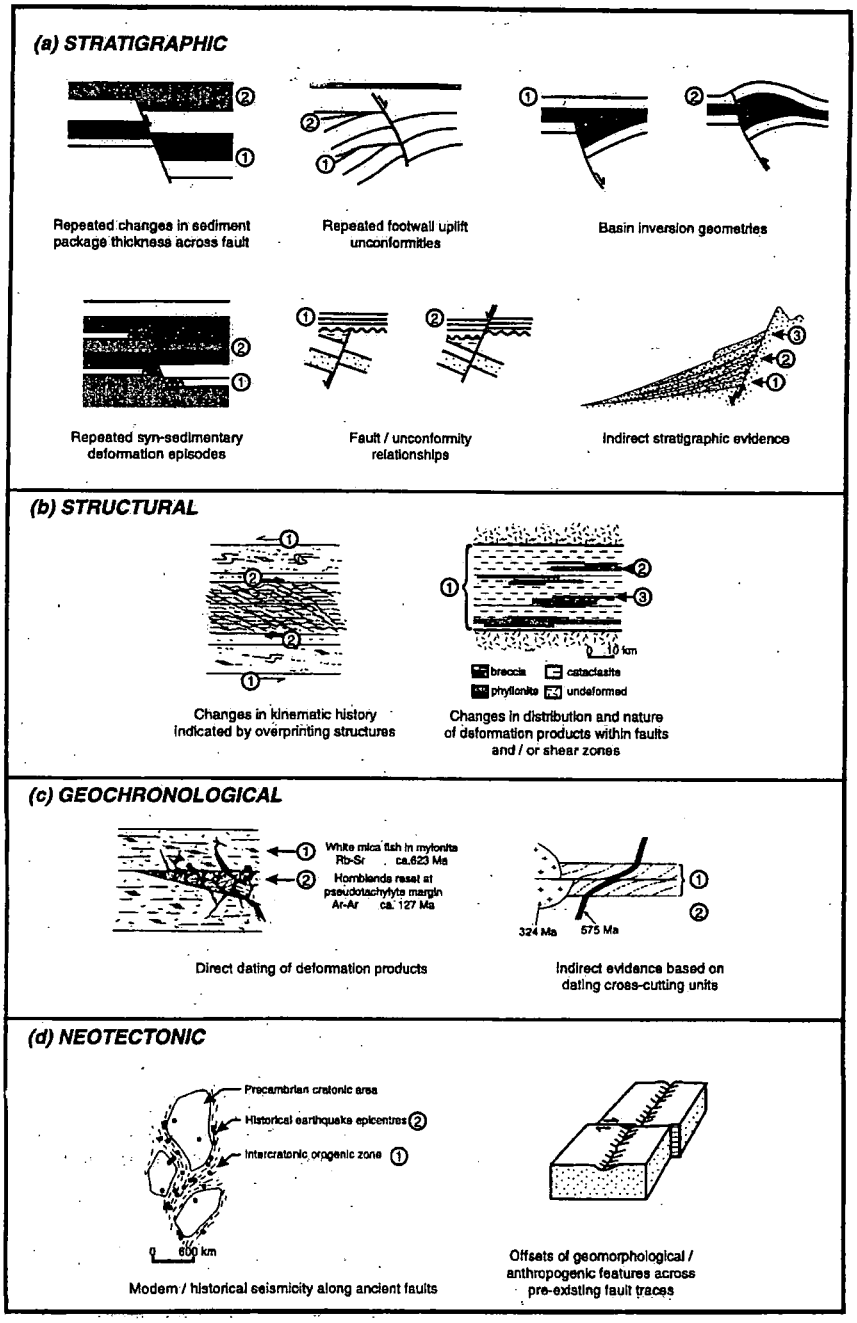

Figure 1.14 The criteria considered reliable for recognising reactivation: stratigraphic, structural, geochronological and neotectonic (after Holdsworth et al., 1997)

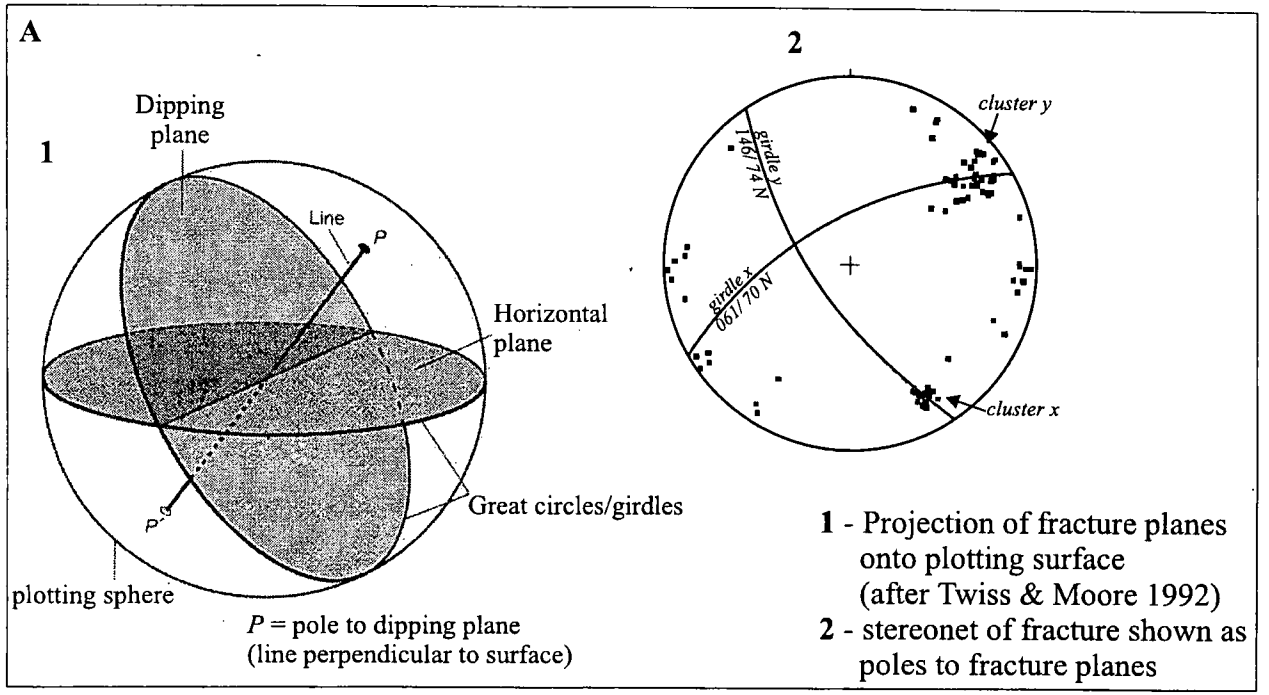

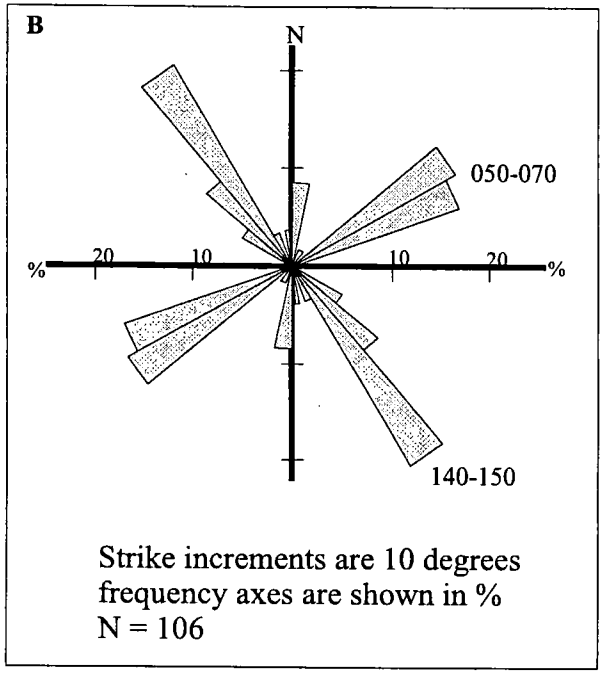

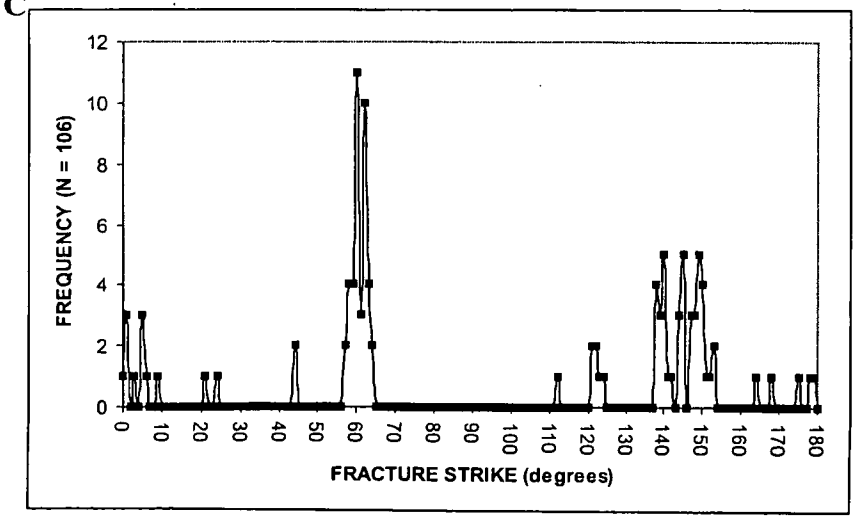

Figure 1.15 Three ways to illustrate the same data set of fracture orientation values
A - Stereographic projection plot, known as stereonets
B - Rose diagram
C - Von Mises diagram

NB each example (A2, B& C) is plotted for the same fracture dataset, locality 157, MTFC, Norway

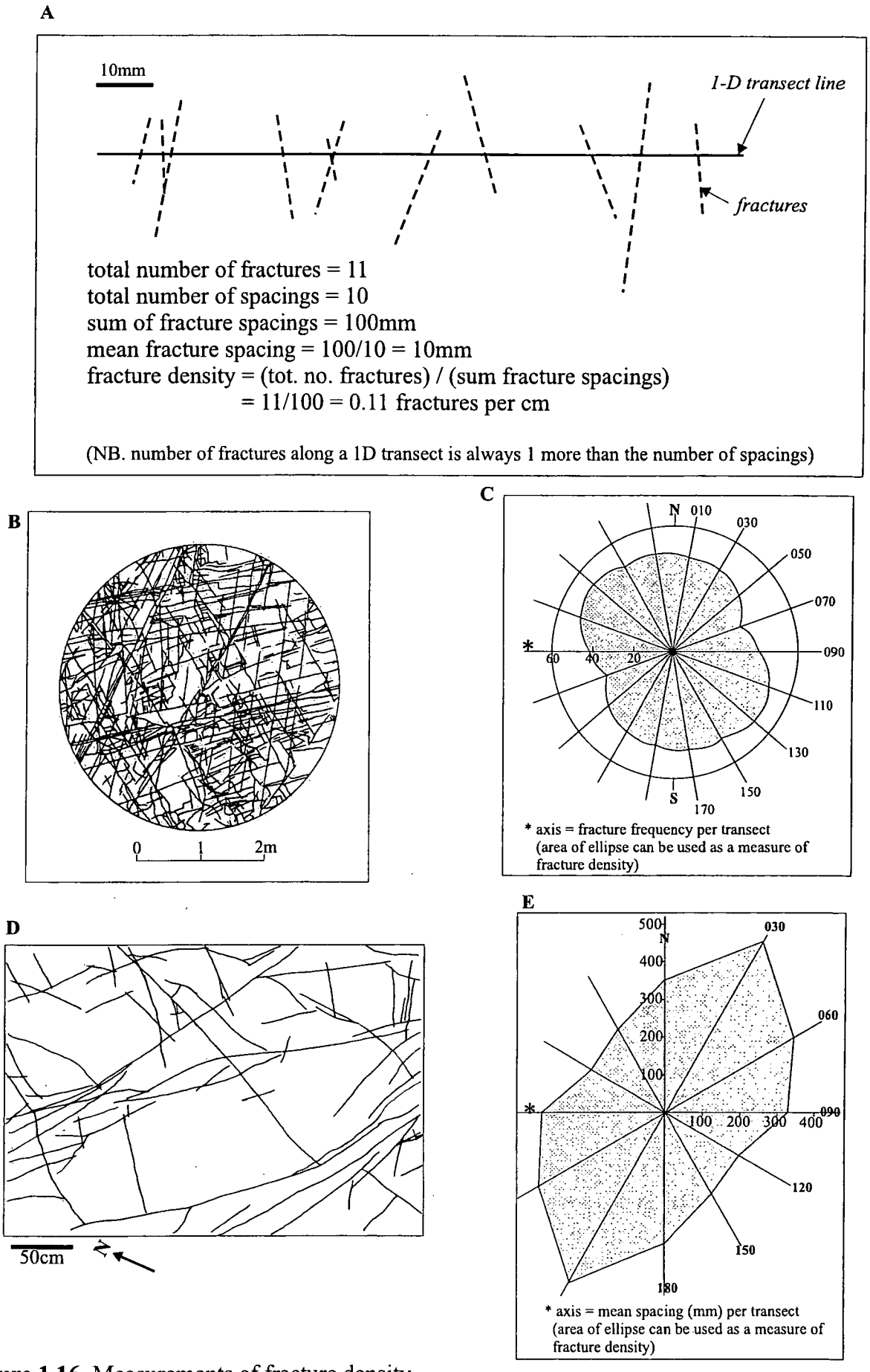

Figure 1.16 Measurements of fracture density

A - along a 1-dimensional line transect (schematic)

B & C - fracture frequency measured along equal-length transects (every 20°) within a circular sample area to produce a rose diagram (after Hudson & Priest, 1983)

D & E - mean spacing measured across a rectangular sample area along transects (every 30°). Mean spacing (instead of fracture frequency as in C) is used to to create rose diagram as not all transects are the same length. (Method proposed in this study, actual data set from locality 132a, MTFC.)

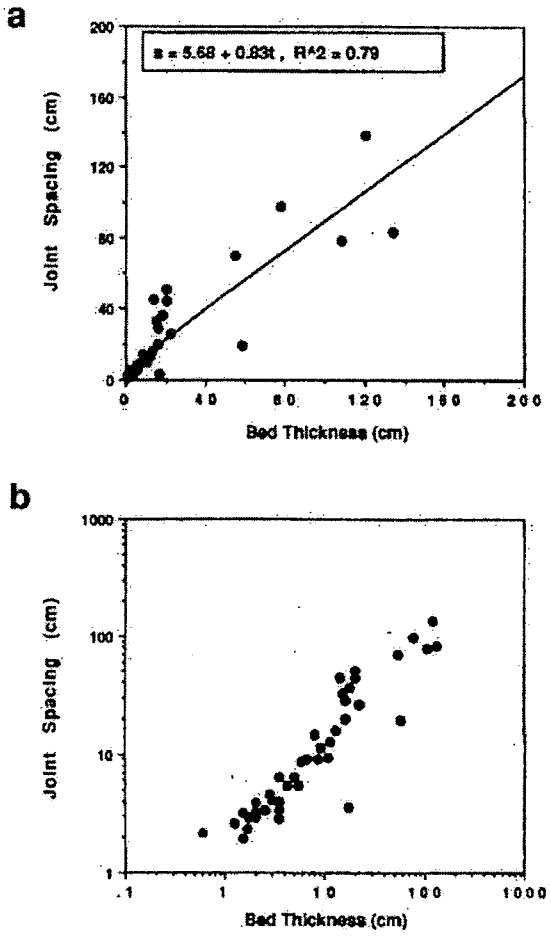

Figure 1.17a Linear relationship between fracture spacing and bed thickness for a sandstone lithology
a - linear axes, b - logarithmic axes (after Ji & Saruwatari 1998)

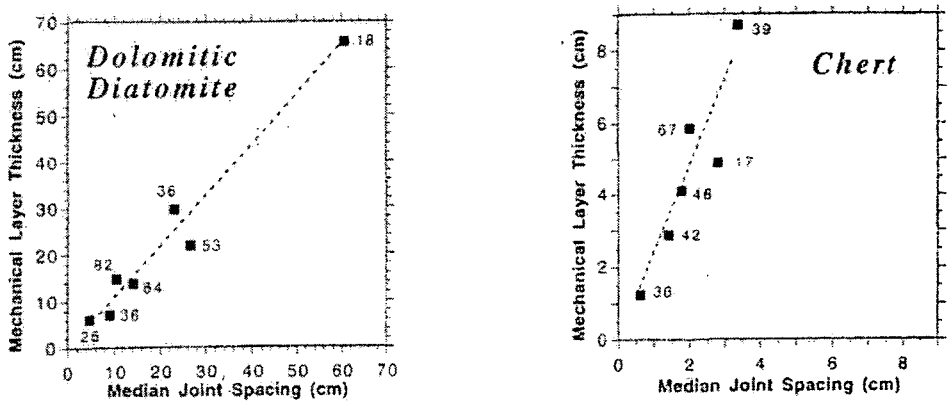

Figure 1.17b Graphs illustrating different FSI ratios for different lithologies
Chert has a steeper slope on the graph than diatomite, and therefore a higher Fracture Spacing Index (FSI)
(numbers next to data points refer to total number of spacing datapoints taken in that bed to calculate median value)
(after Gross et al., 1995)

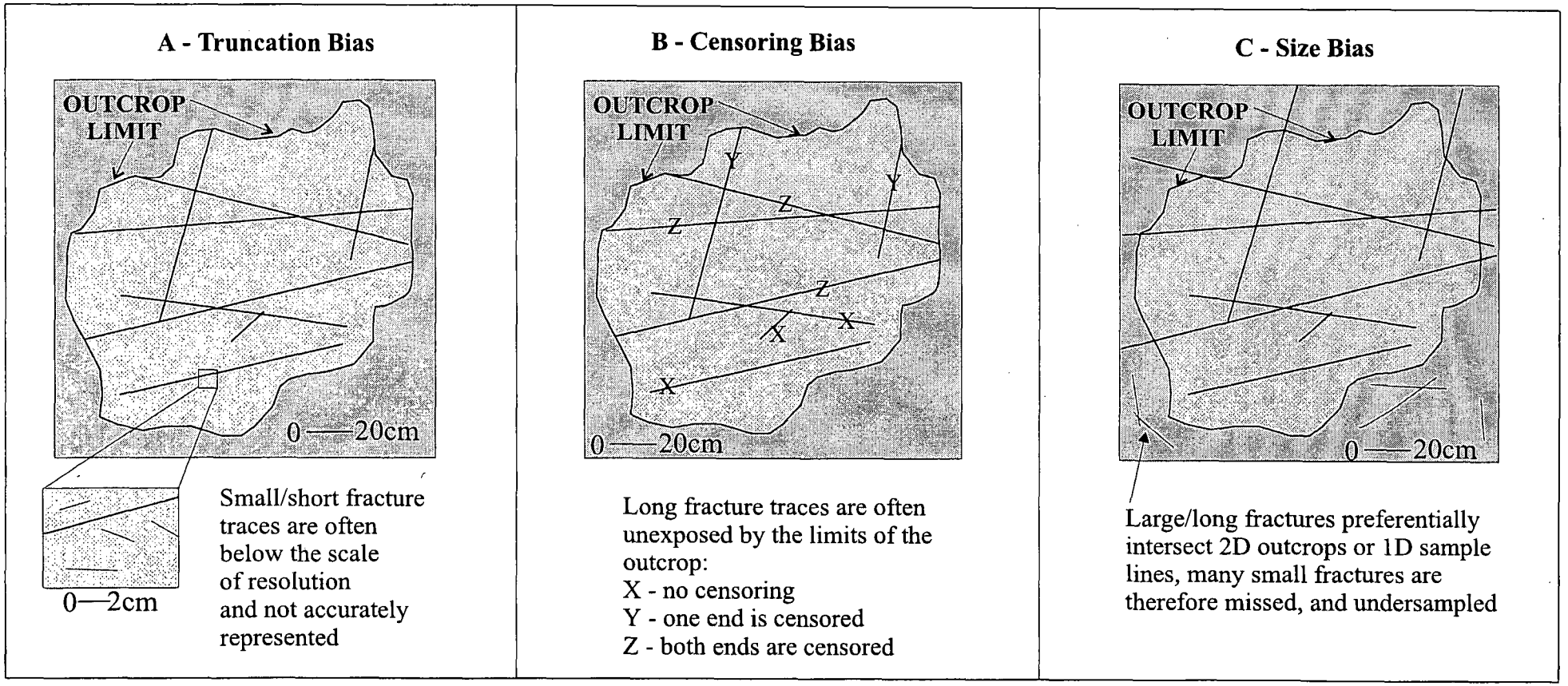

Figure 1.18 Schematic diagram to illustrate the three main biases that occur when measuring fracture trace lengths

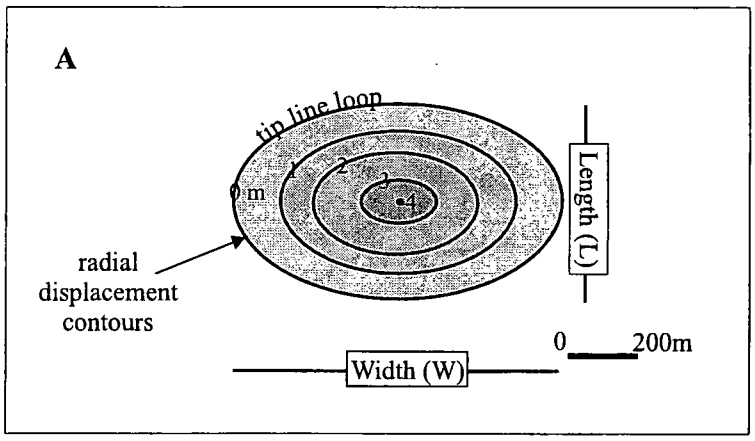

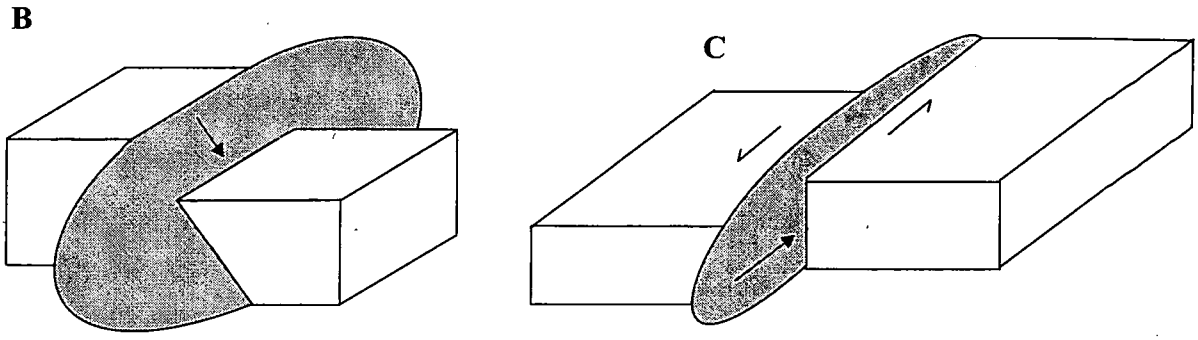

Figure 1.19
A - Schematic displacement diagram for a simple fault, viewed normal to fault surface (after Barnett et al., 1987)
B - Schematic displacement diagram for a dip-slip fault, displacement is parallel to the short axis of the elipse
C - Schematic diagram for a strike-slip fault, displacement is parallel to the long axis of the elipse

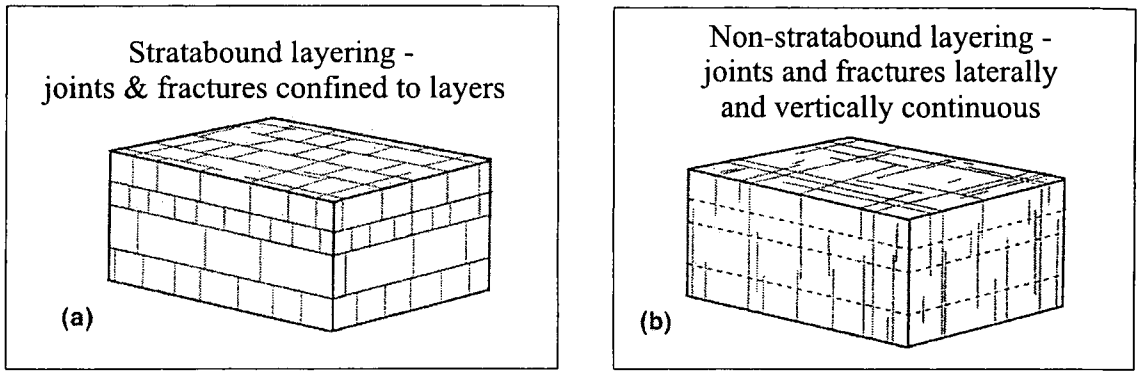

Figure 1.20 Two end members of layering - (a) stratabound (b) non-stratabound (after Odling et al., 1999)

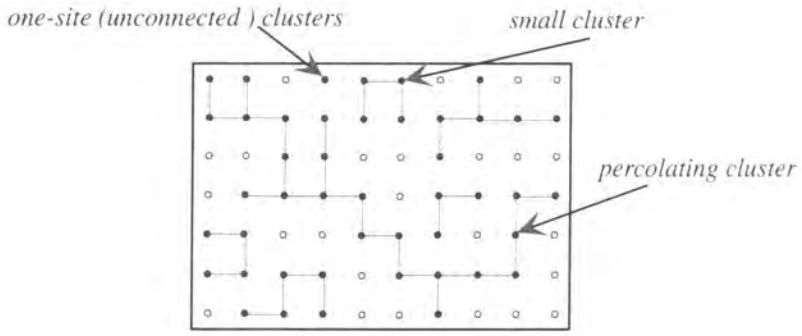

Figure 1.21 Percolation theory illustrated by a finite, regular lattice composed of points/sites. Points/sites can be connected to forma a cluster or be unconnected. The percolating cluster intersects all four sides of the sample area (after Berkowitz & Balberg, 1993)

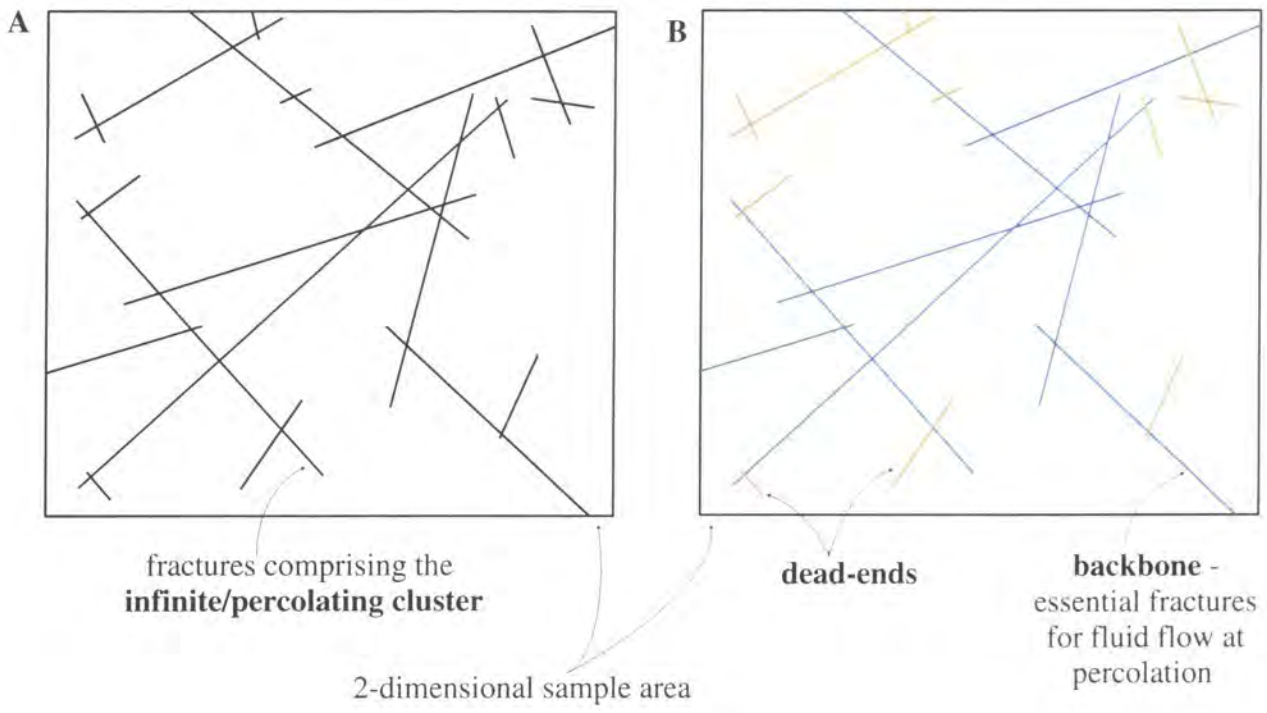

Figure 1.22 Fracture cluster terminology

A - the infinite or percolating cluster, intersecting all sides of the sample area, pc = 1

B - the backbone of the infinite cluster is shown in blue, and in orange are the dead-ends

A

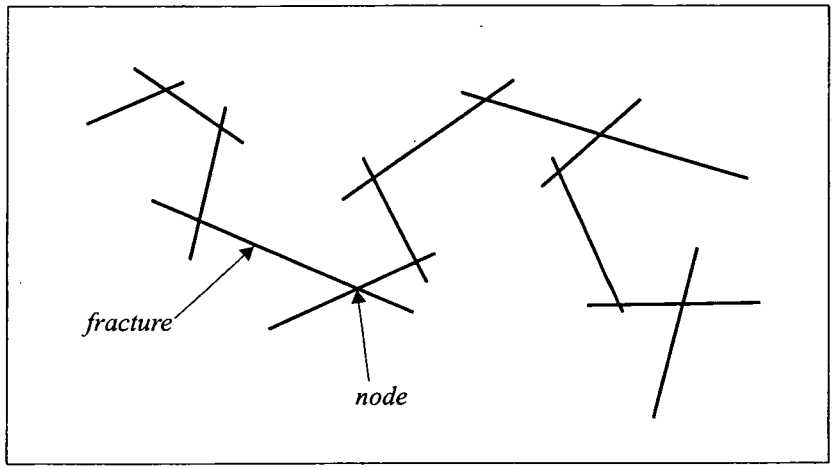

no. fractures (x) = 12
no. nodes (y) = 11

$y = (x - 1)$

Minimum cluster connectivity - as another fracture is added to the cluster, only one more node is created.

B

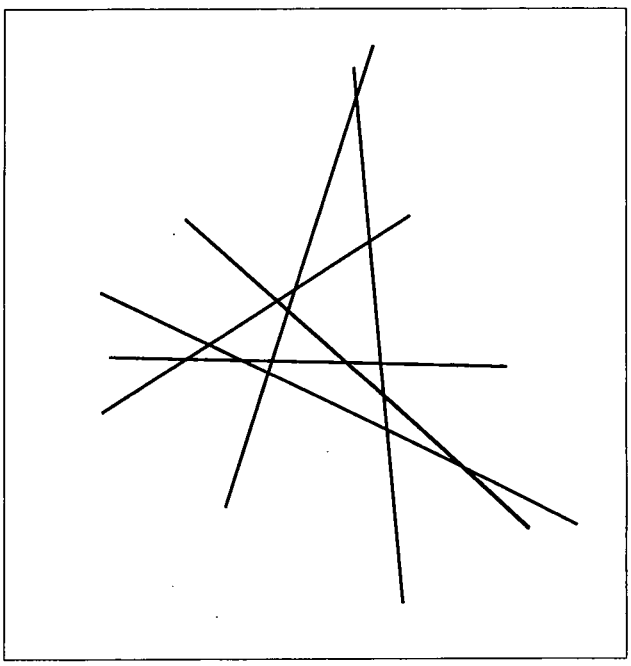

no. fractures (x) = 6
no. nodes (y) = 15

$$y = \frac{x(x - 1)}{2}$$

Maximum cluster connectivity - as another fracture is added to the cluster, it intersects with every other fracture.

Figure 1.23 Fracture cluster connectivity
A - minimum connectivity
B - maximum connectivity

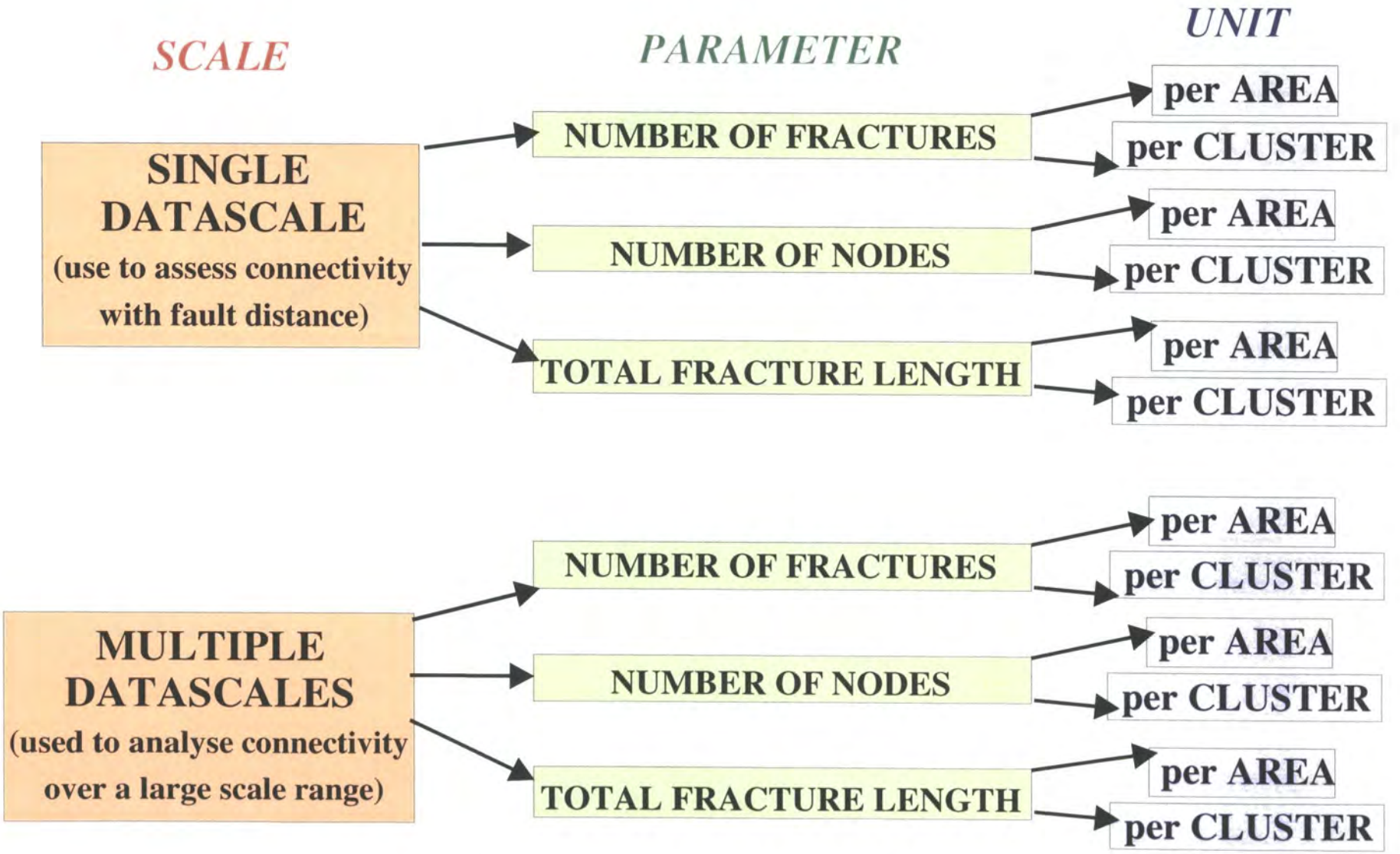

Figure 1.24 Flow chart illustrating measures of **fracture density** (number of fractures), **fracture intensity** (fracture length) fracture network **connectivity** (number of nodes)

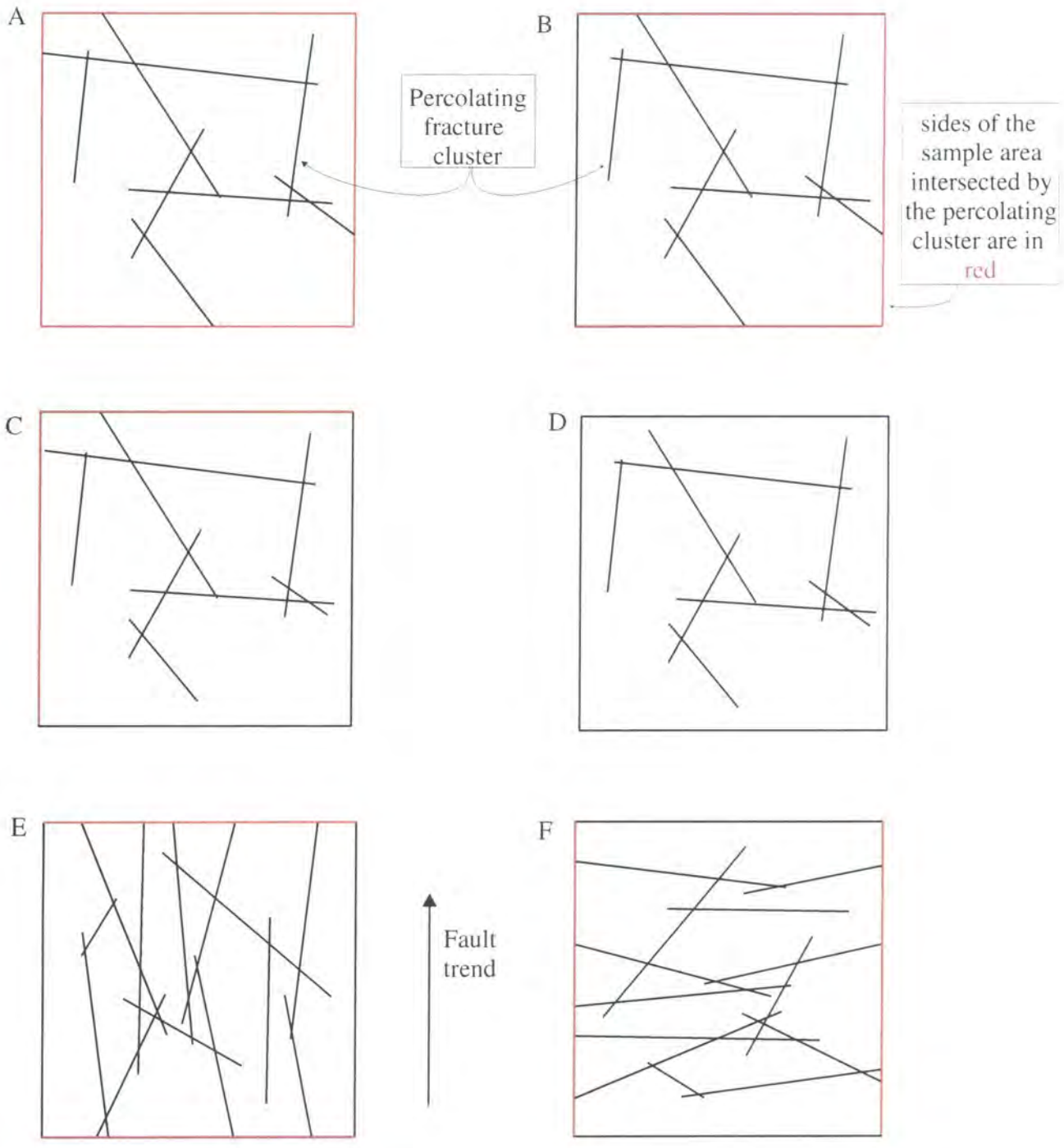

Figure 1.25
Percolation threshold as a relative measure of percolation using a 4 sided 2-dimensional sample area

A - When *pc* = 1, all 4 sides of the sample area are intersected by the percolating cluster
B - When *pc* = 0.75, 3 sides of the sample area are intersected by the percolating cluster
C - When *pc* = 0.5, 2 sides of the sample area are intersected by the percolating cluster
D - When *pc* = 0.25, 1 side of the sample area is intersected by the percolating cluster

When pc = 0.5, and the orientation of the main fault is known, connectivity can be assessed relative to the fault:
E - the fractures of the percolating cluster intersect 2 sides, connectivity is *parallel* to the fault trend
F - the fractures of the percolating cluster intersect 2 sides, connectivity is *perpendicular* to the fault trend

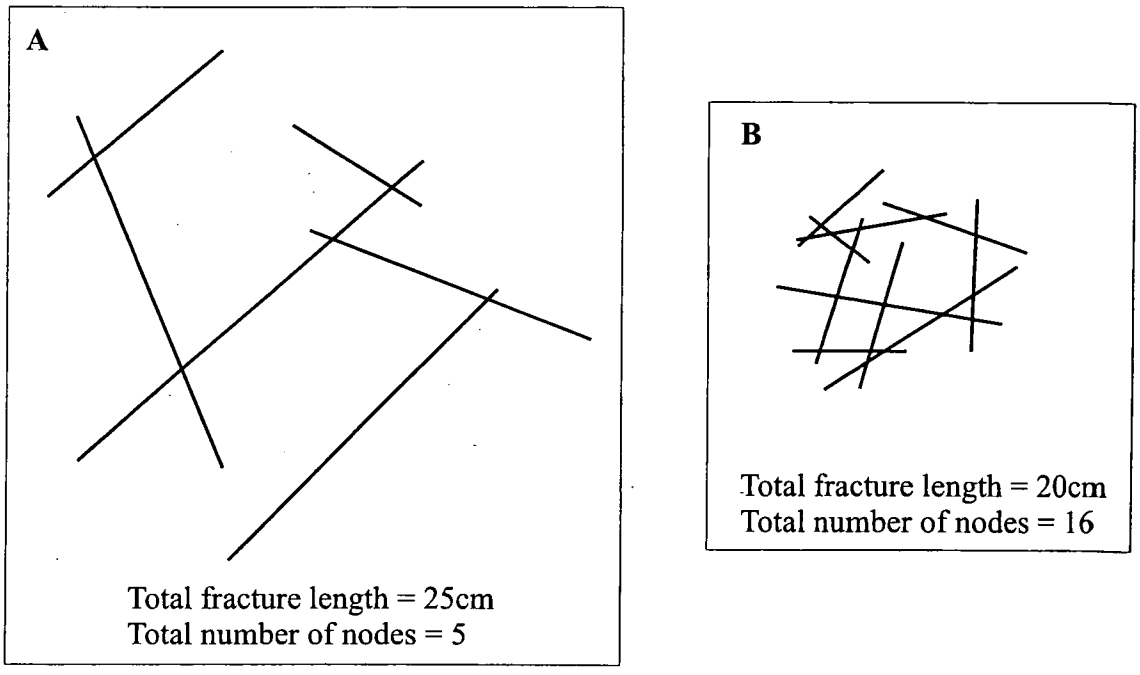

Figure 1.26 Schematic diagram illustrating the relationship between cluster length and connectivity, showing that a long fracture cluster is not necessarily better connected than a short fracture cluster. Cluster A is longer but has less intersections than cluster B which is 5cm shorter

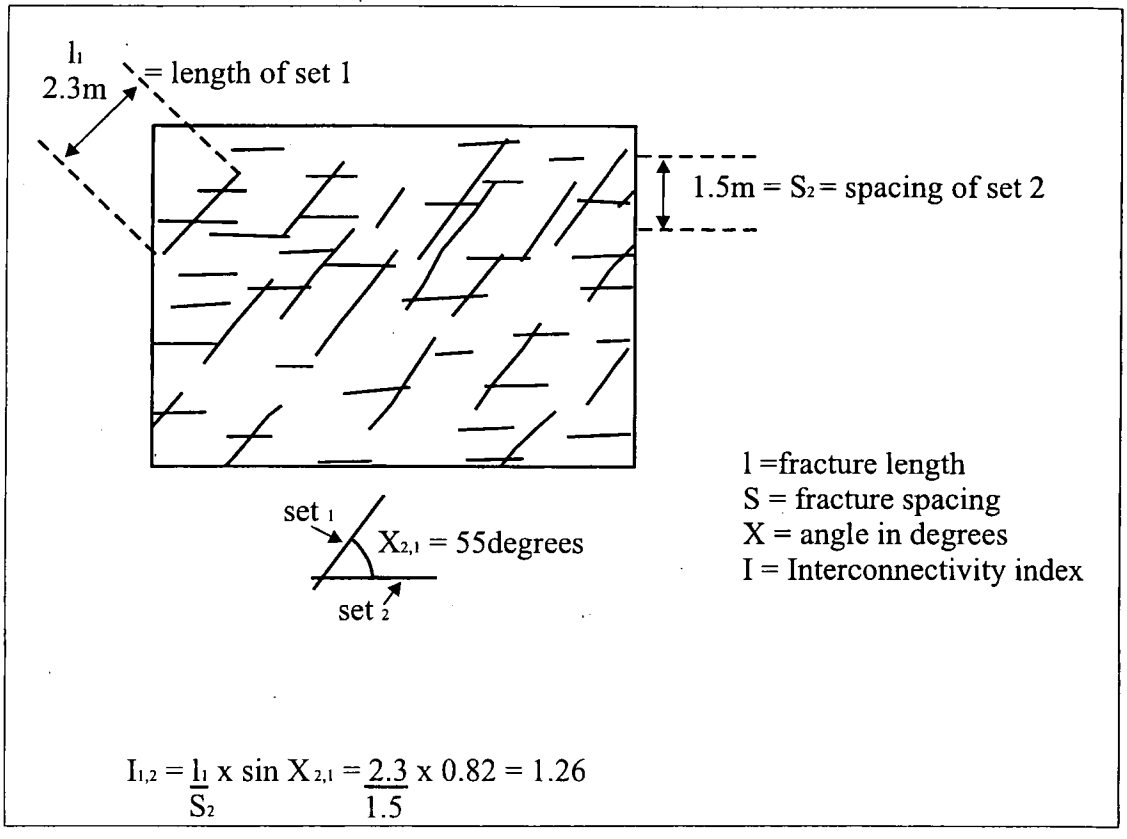

Figure 1.27 Diagram to illustrate the interconnectivity index (ICI) proposed by Rouleau & Gale (1985) which can be used to measure the degree of connectivity between two fracture sets (set 1 & set 2). See text for explanation of equation.

A

Ammonite diameter (cm)			
3.2	3.1	3.2	3.3
3.6	3.2	3.3	3.5
3.4	3.6	3.9	3.5
3.8	3.2	3	3.9
3.7	3.1	3.4	3.4
3.8	3.5	2.9	3.3
2.9	3.7	3.4	3.3
3.7	3.6	3.5	3.6
2.9	3.9	2.9	4
3.7	3.7	3.1	3.4

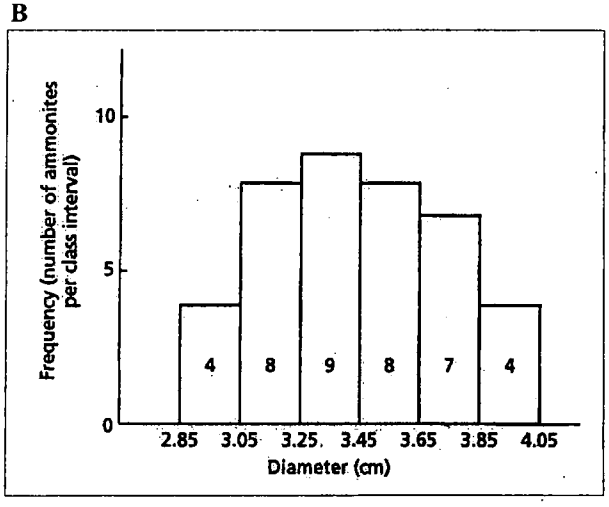

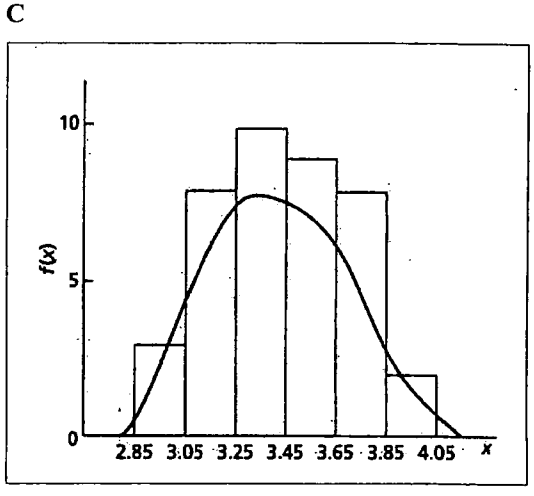

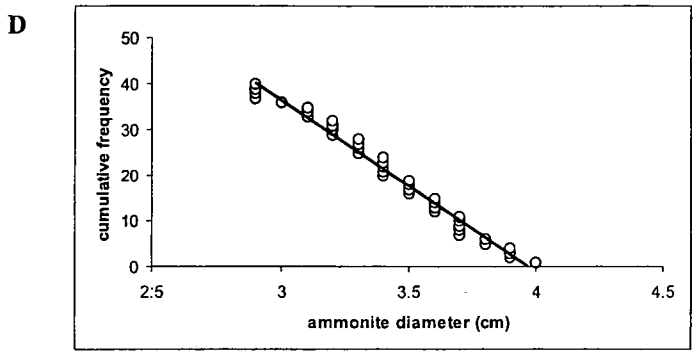

Figure 1.28 Methods used to analyse the best-fit statistical distribution
A - Dataset used to create plots in B, C & D
B - histogram
C - probability density function superimposed onto histogram
D - cumulative density function, both x & y axes are plotted as linear scales
This dataset of ammonite diameters is best described by a normal distribution
(A, B & C = after Swan & Sandilands 1995)

A

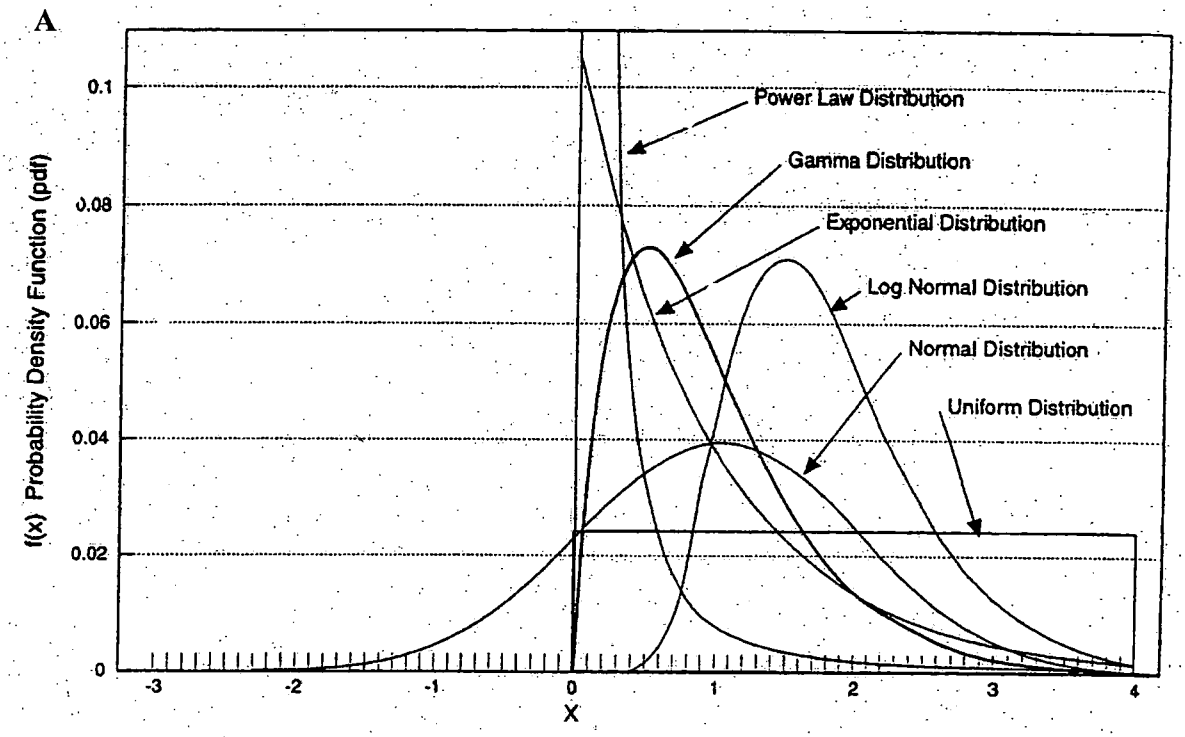

B

	Statistical distribution					
Parameter	**Uniform**	**Normal**	**Log-normal**	**Exponential**	**Power-law**	**Gamma**
Mean	1	1	1	1	n/a	1
standard deviation	1	1	1	1	n/a	1
Minimum possible value	0	$-\infty$	0	0	0	0
Maximum possible value	∞	∞	∞	∞	∞	∞

Figure 1.29 **A** - probability density functions for Uniform, Normal, Log-normal, Exponential, Power-law and Gamma distributions
B - main parameters for the probability density functions illustrated in A (after Dershowitz et al., 1995)

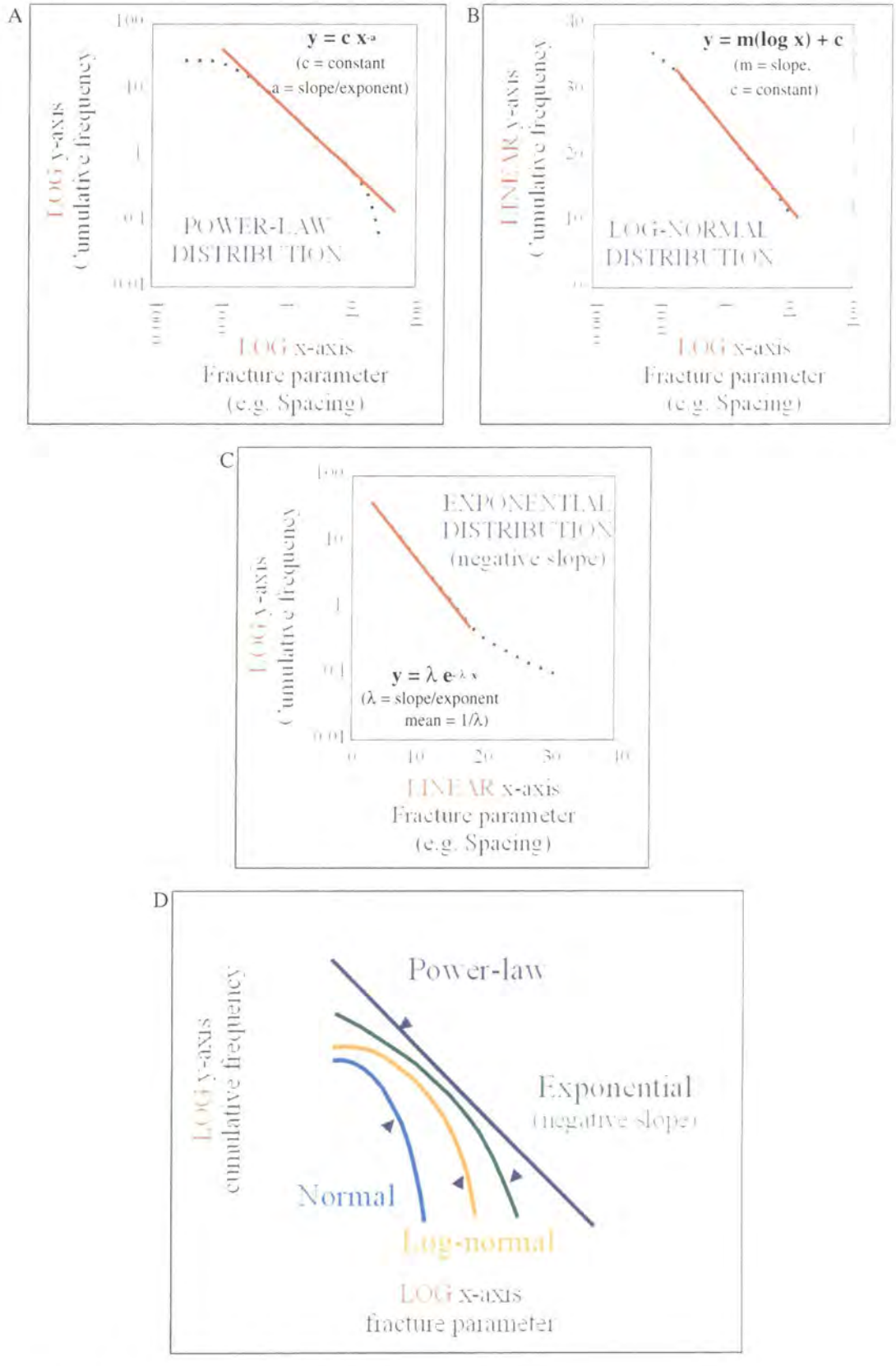

Figure 1.30 Cumulative frequency distributions for

A Power-law distribution (x & y axes both logarithmic)

B Log-normal distribution (x-axis logarithmic, y-axis linear)

C Exponential distribution (x-axis linear, y-axis logarithmic)

D Cumulative frequency distributions for Power-law, Log-normal, Exponential and Normal distributions, all plotted on logarithmic x & y axes.

NB, dotted lines are data points that do not lie on the best-fit line, (due to undersampling for example)

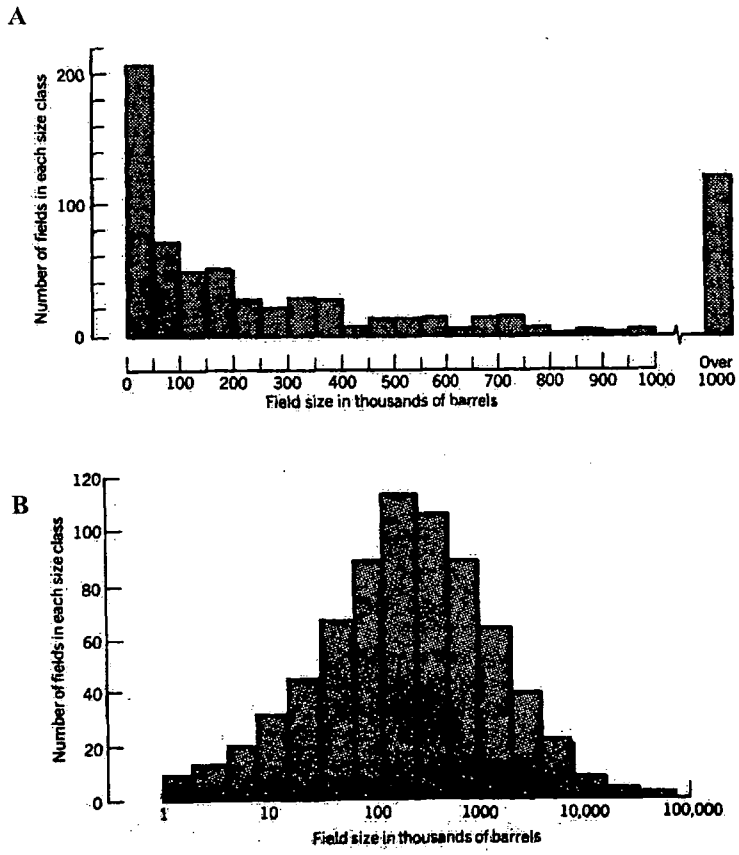

Figure 1.31 Histogram of oil field sizes, discovered in the Denver Basin, USA in 1969
A - with x-axis plotted as a linear scale
B - with x-axis plotted as a logarithmic scale
This data set is best described by a log normal distribution.
(After Davis, 1986))

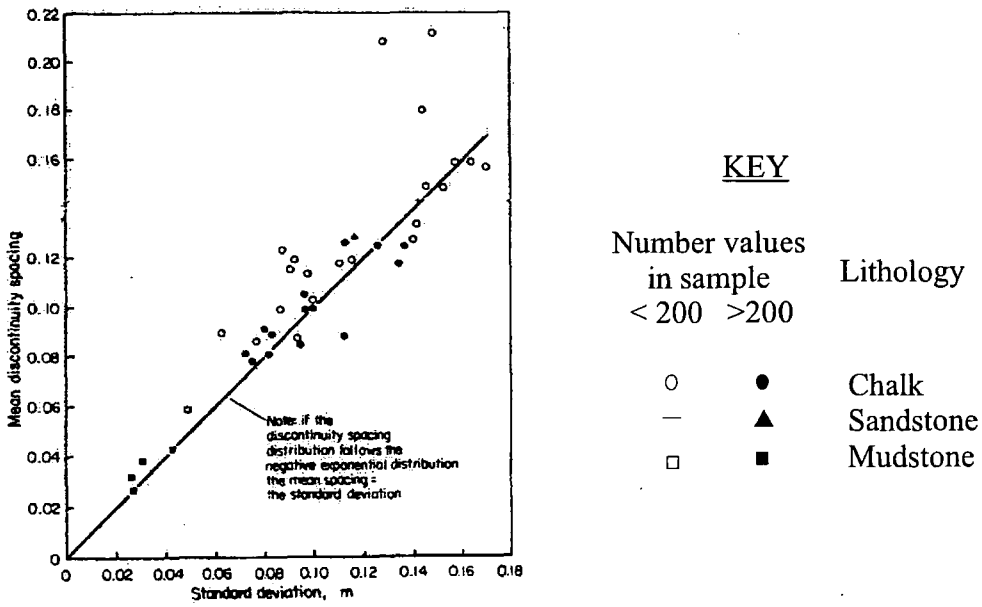

Figure 1.32 Mean fracture spacing and standard deviation measured for three lithologies, chalk, sandstone and mudstone.
There is a good correspondence between the mean and standard deviation values, suggesting the datasets are best described by an exponential distribution (After Priest & Hudson 1976)

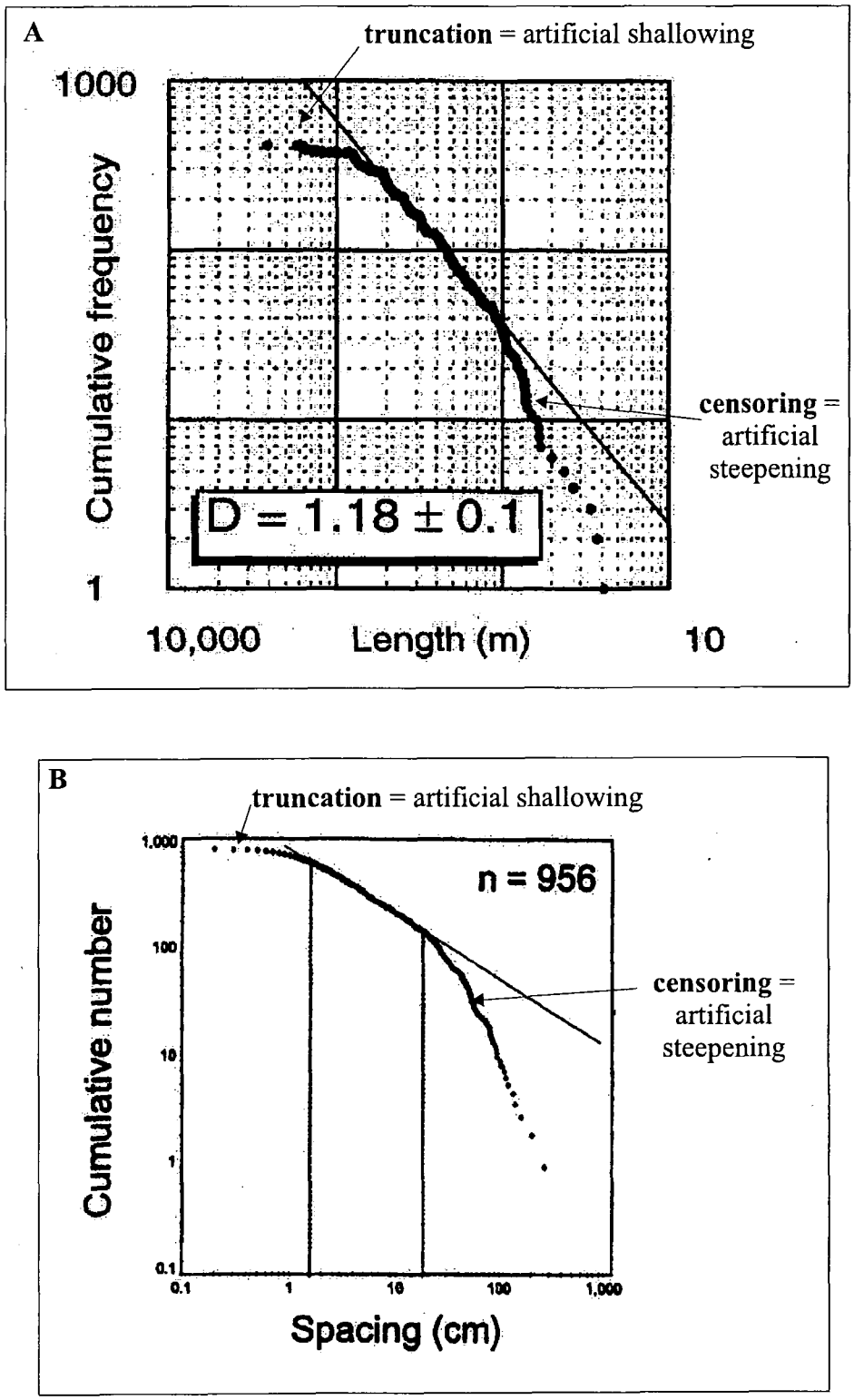

Figure 1.33 Graphs illustrating deviation of a power-law cumulative frequency distribution caused by censoring and truncation

A - power-law cumulative frequency graph of fault length, D = power-law exponent (after Pickering et al., 1997)

B - power-law cumulative frequency graph of fault spacing, exponent = 0.63 (after Knott et al., 1996)

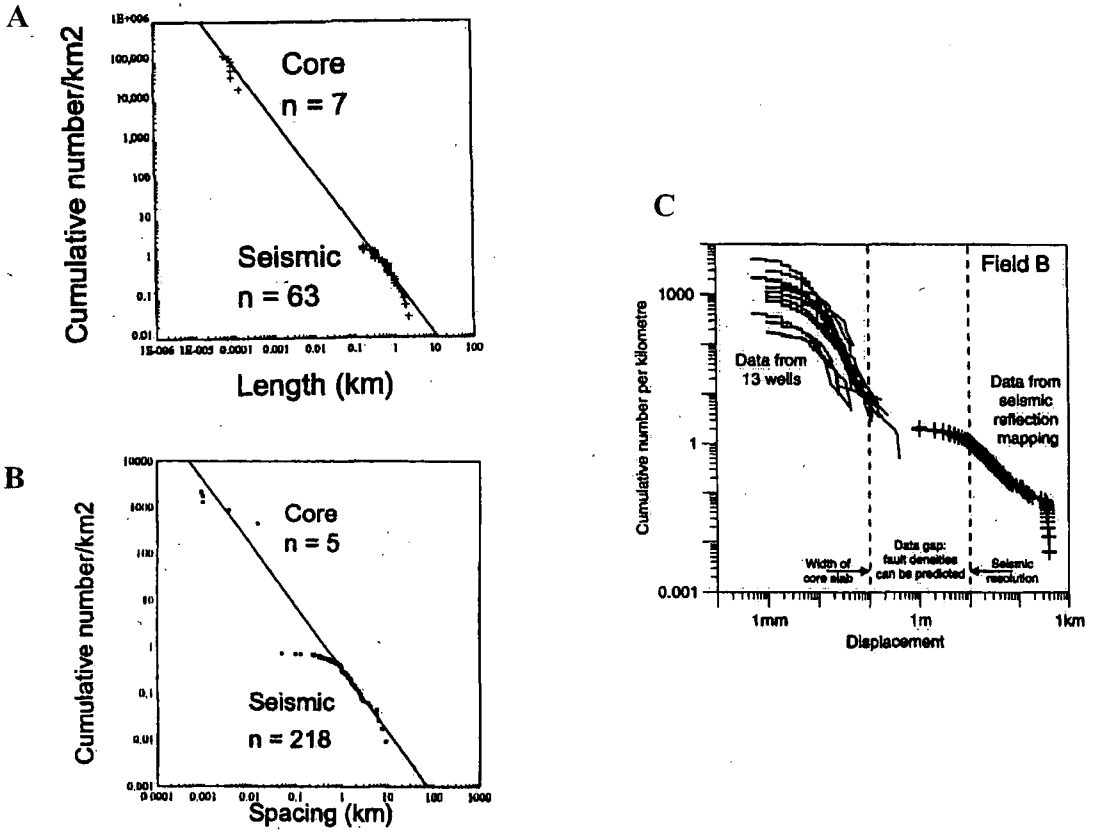

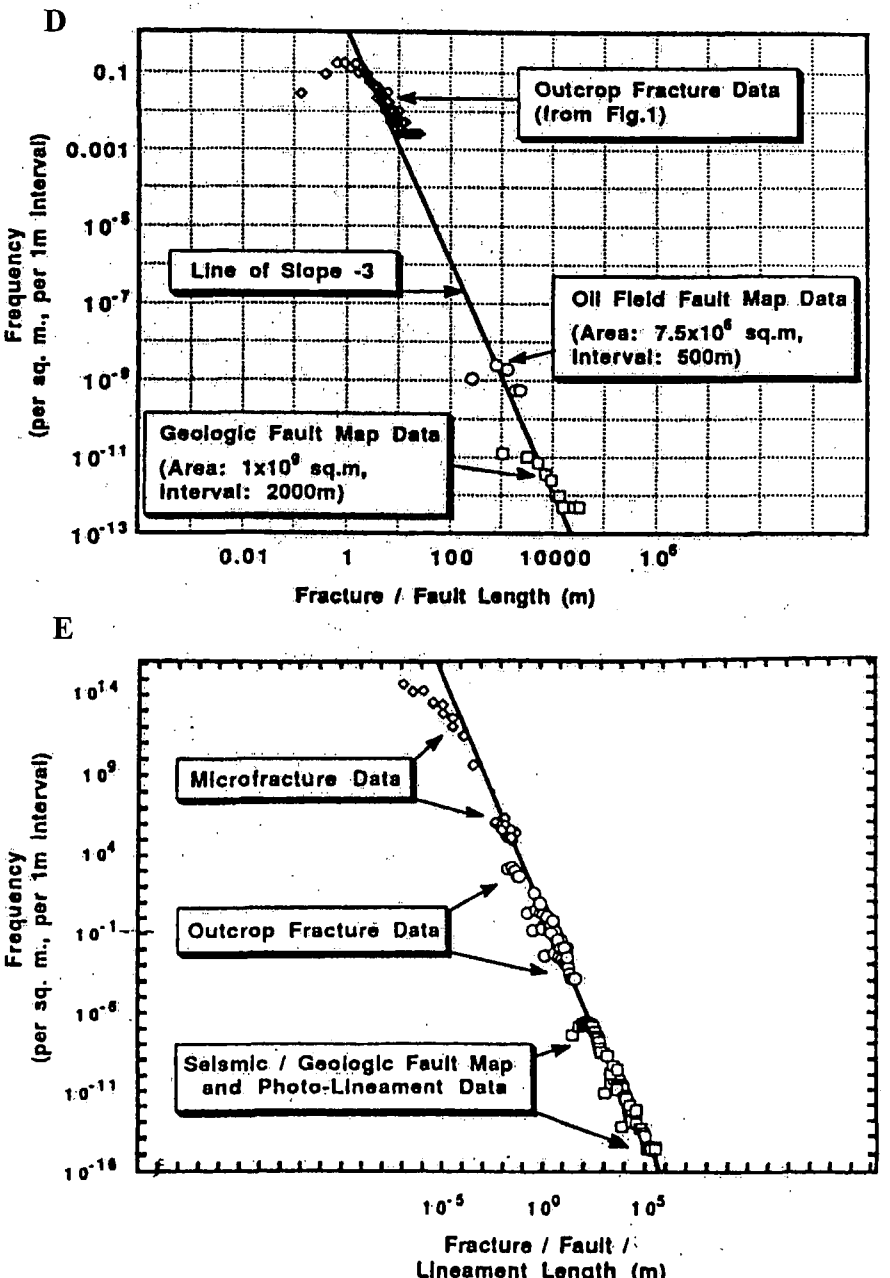

Figure 1.34 Graphs illustrating how power-law relationships can be extrapolated between data sets of different scales

A - power-law extrapolation for fault length data sets (after Knott et al., 1996)

B - power-law extrapolation of fault spacing data sets (after Knott et al., 1996)

C - power-law extrapolation for fault displacement data sets (after Needham et al., 1996)

D & **E** - power-law extrapolation of fault/fracture length data sets (after Heffer & Bevan 1990)

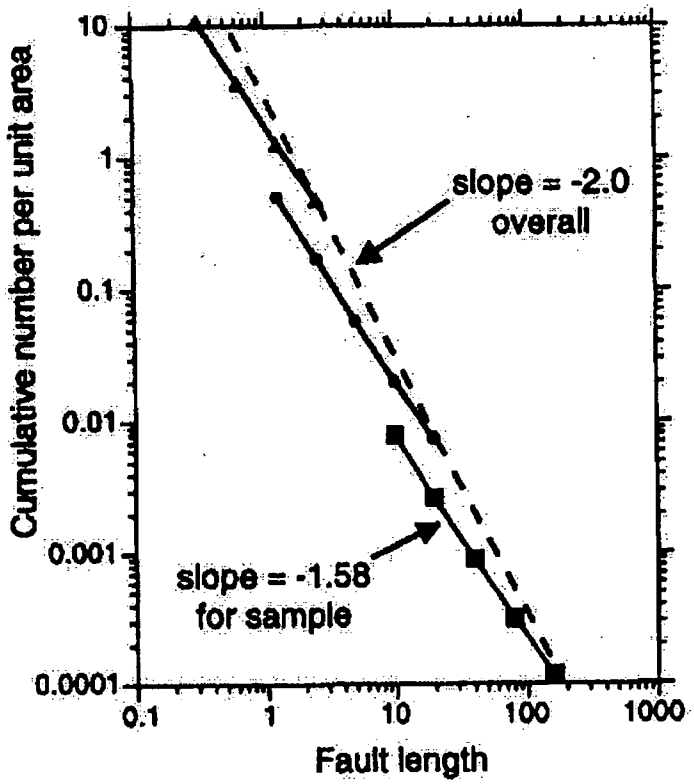

Figure 1.35 Graph to show that the slopes/exponent for amalgamated and extrapolated data scales may not accurately reflect the exponents of the individual data sets, because the individual data sets may be offset from each other.
(after Yielding et al., 1996)

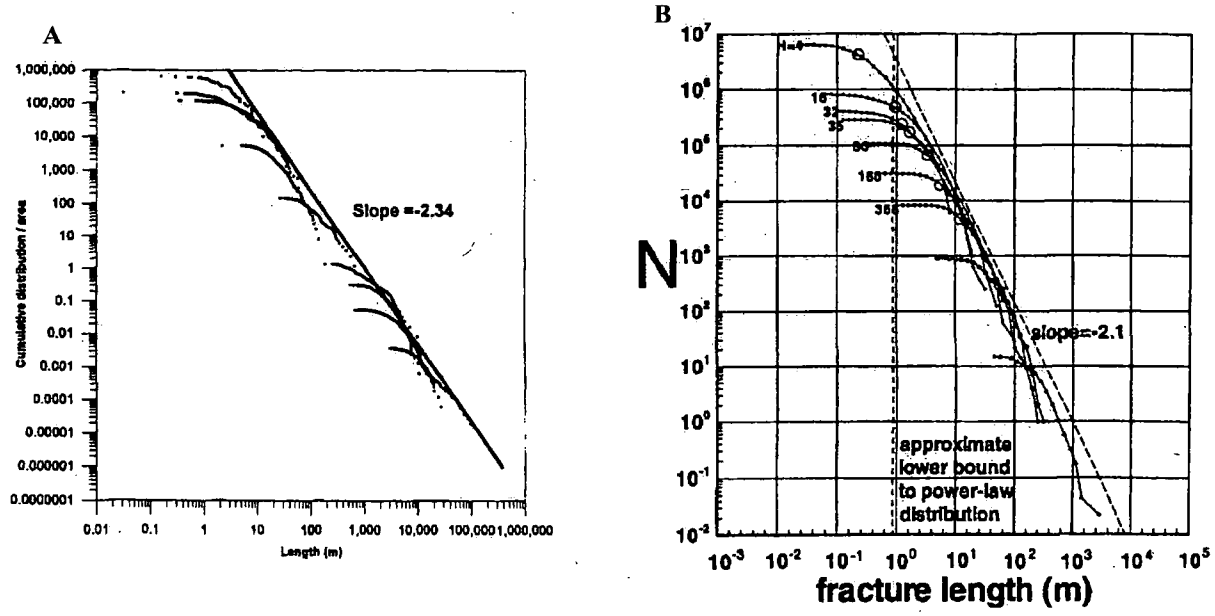

Figure 1.36 Graphs illustrating combined data sets with slopes > 2, suggesting that the data do not indicate strict self-similarity.
(**A** - after Castaing et al., 1996)
(**B** - after Odling 1997)

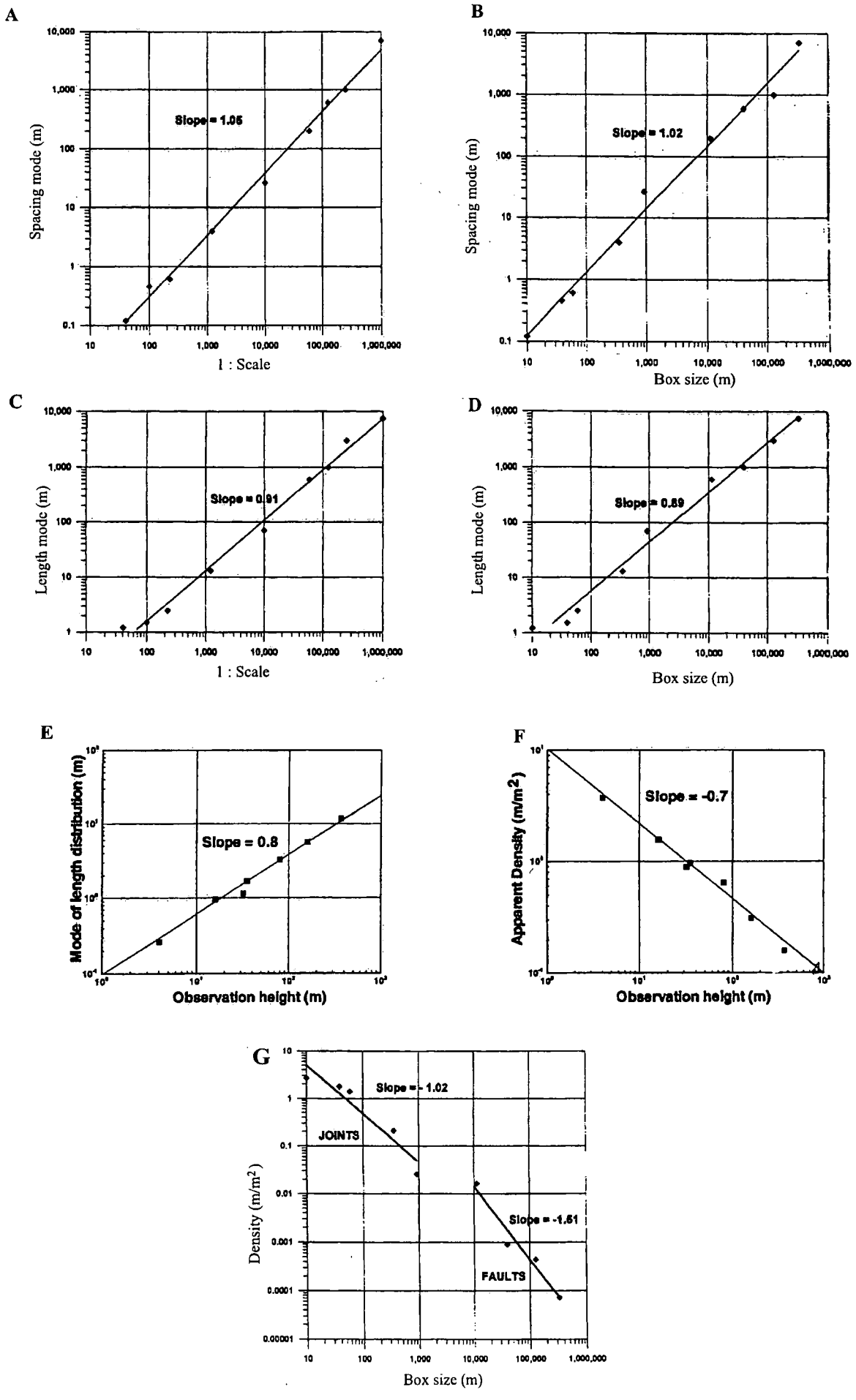

Figure 1.37 Plots to test self-similarity between data sets of different sample ranges
See text for explanation
(**A, B, C, D, G** after Castaing et al., 1996,)
(**E, F** after Odling 1997, where observation height is equivalent to data scale)

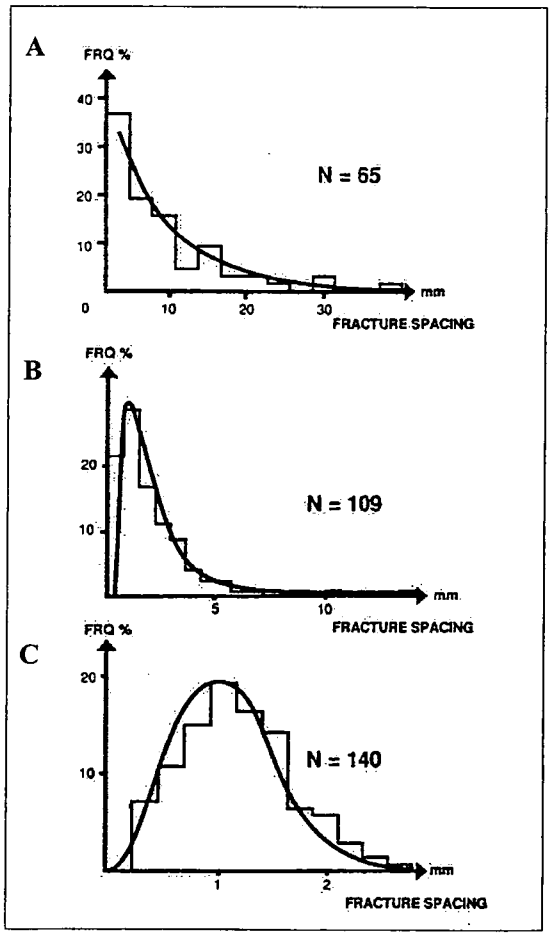

Figure 1.38 Histograms and probability density functions of spacing distributions at 3 stages of an analogue model (3 different magnitudes of strain) illustrating the evolution from best-fitting exponential to normal distributions

A - low fracture density, early stage in the fracture set development the spacings are best described by an exponential distribution

B - intermediate fracture density, the spacings are best described by a log-normal distribution

C - high fracture density, late stage in fracture set development, the fracture spacings are best described by a normal distribution

(after Rives et al., 1992)

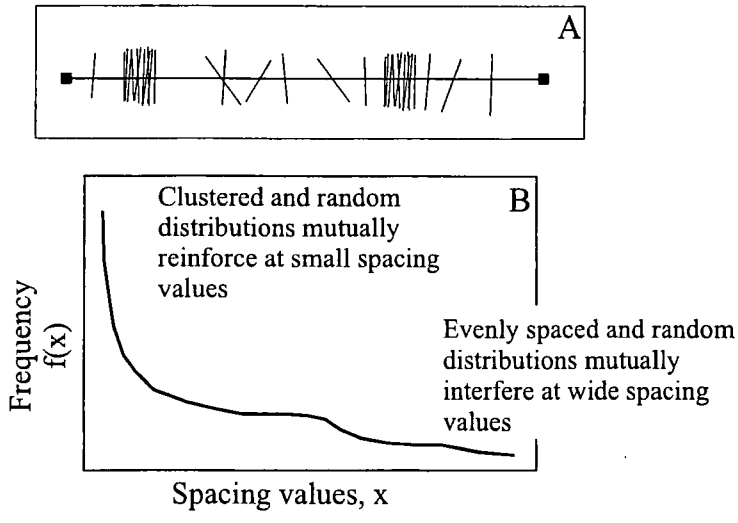

Figure 1.39 In geologically complex rocks it is likely that the evenly spaced (normal), clustered, and random (exponential) distributions will combine (**A**) resulting in a distribution shown in **B**, which is similar to an exponential distribution (after Priest & Hudson 1976)

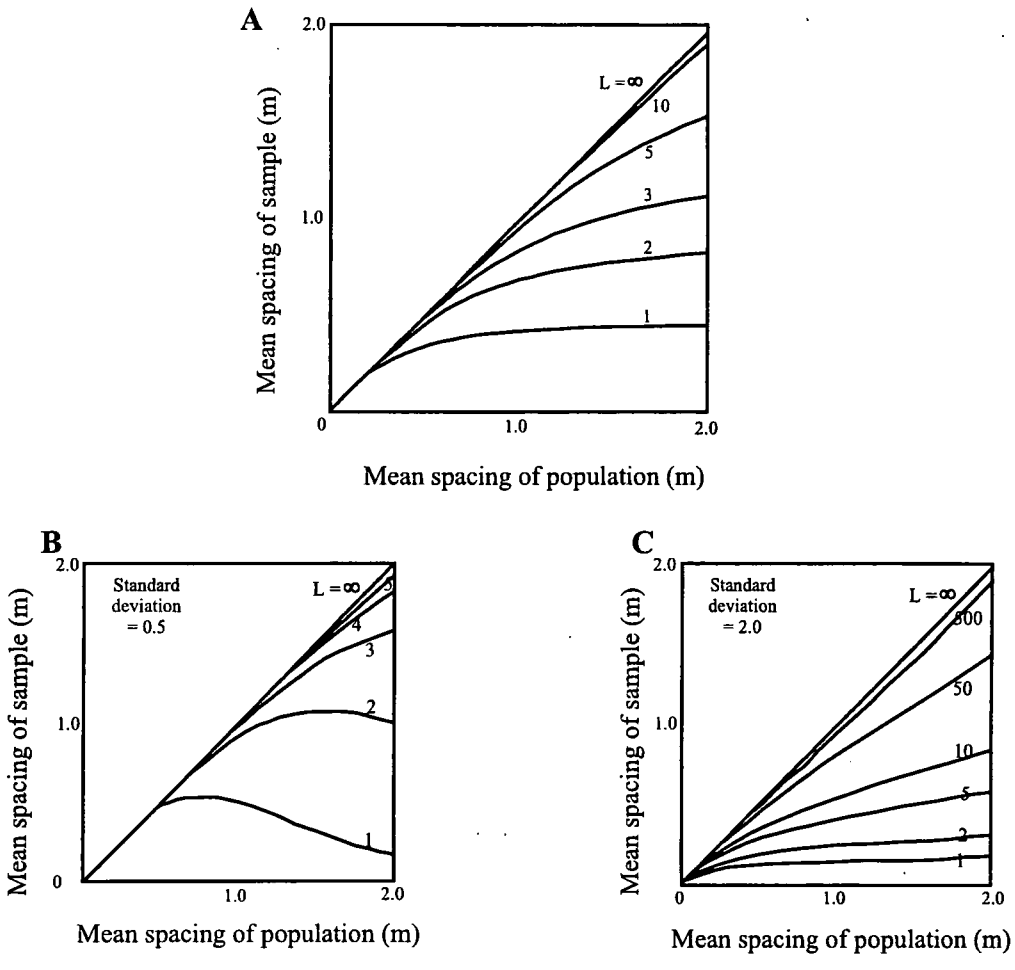

Figure 1.40 Relationship between the mean spacing of the population and the mean spacing from a finite 1-dimensional transect (sample) illustrating the errors for different transect lengths (L, measured in metres)
A - exponential distribution with negative slope
B & **C** - log-normal distributions with different standard deviations
(after Sen & Kazi, 1984)

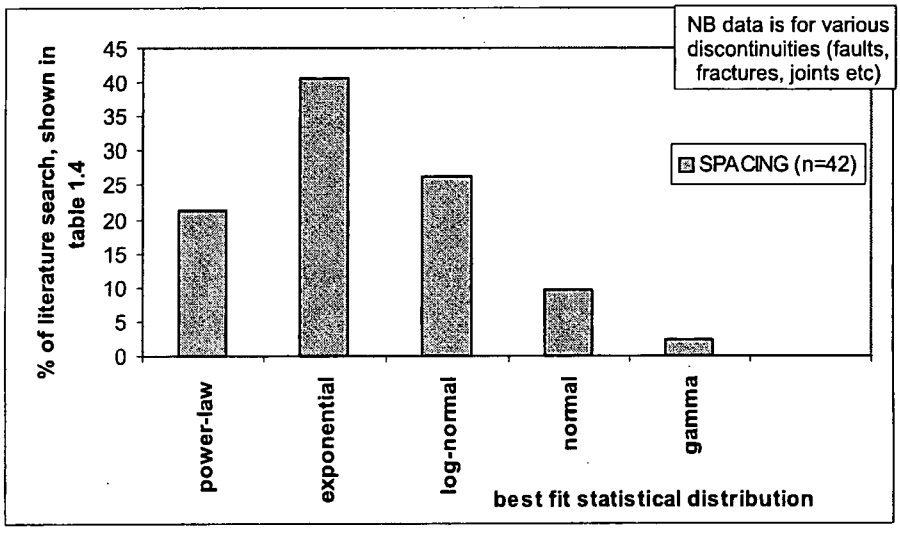

Figure 1.41 Graph illustrating the various distributions used to describe discontinuity spacing in the literature from Table 1.4 (includes fractures, joints and faults)

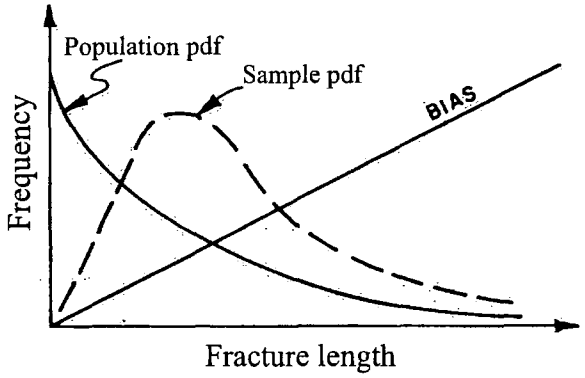

Figure 1.42 Diagram illustrating how an exponential distribution (the probability density function, pdf for the population) can be affected by linear bias, and transformed into a log-normal distribution (illustrated by the sample pdf)
(after Baecher 1983)

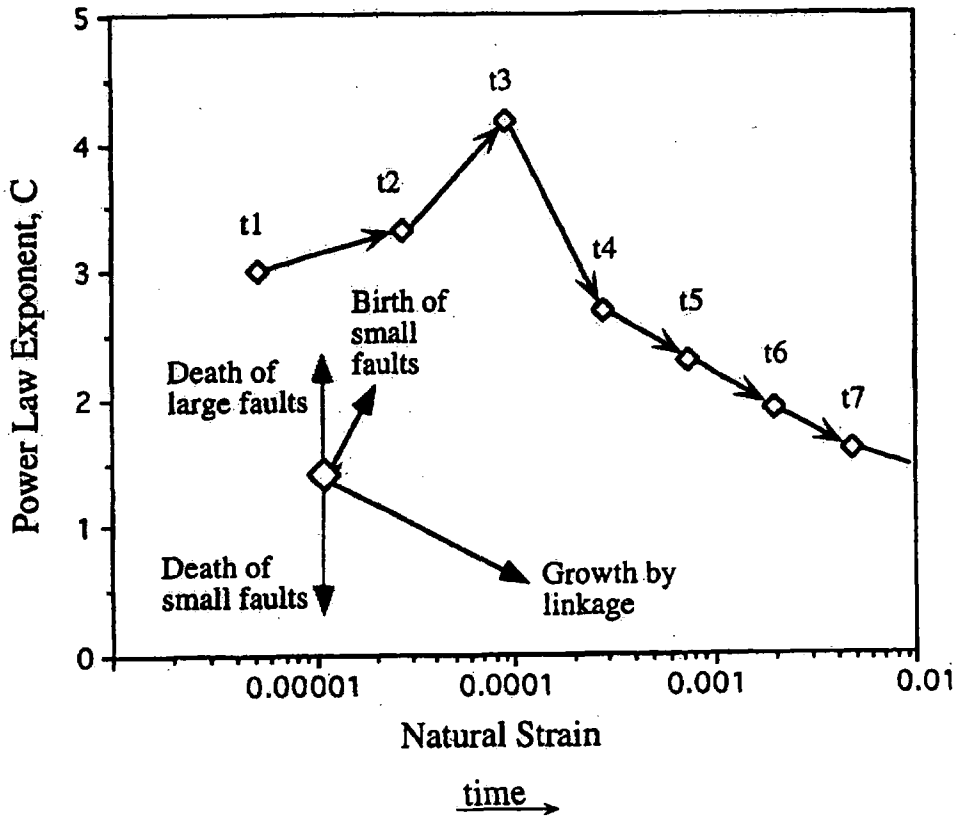

Figure 1.43 Diagram illustrating a decrease of the power-law exponent (C) over time as strain increases. Also shown are the processes which govern the development of the power-law distribution
(after Cladouhos & Marrett 1996)

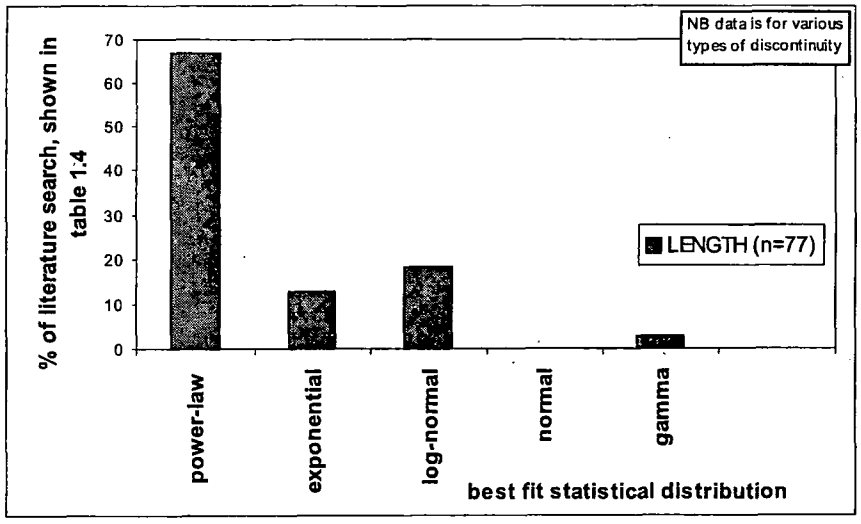

Figure 1.44 Graph illustrating the various distributions used to describe discontinuity length in the literature from Table 1.4 (includes fractures, joints and faults)

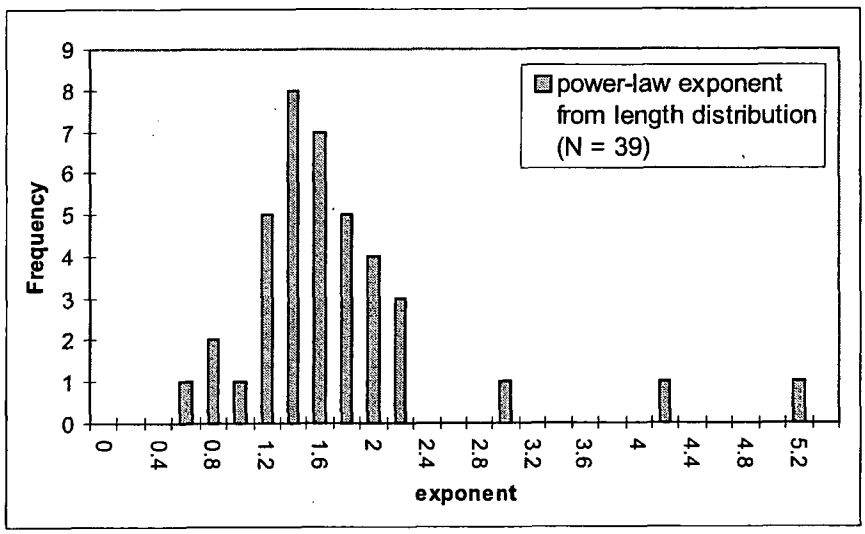

Figure 1.45 Graph illustrating the range of power-law exponents used to describe discontinuity length in the literature from Table 1.4 (includes fractures, joints and faults)

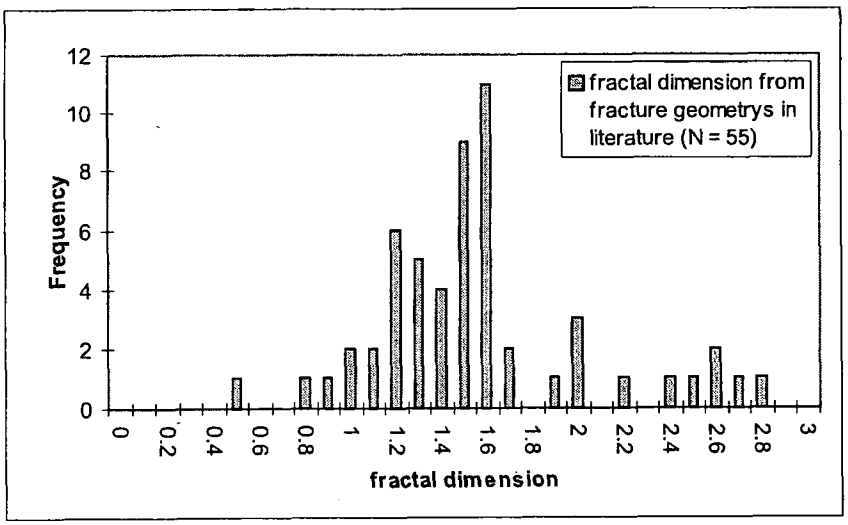

Figure 1.46 Graph illustrating the range of fractal dimensions reported by Bonnet et al., (2001), after their comprehensive literature review.

A

Procedure for Kolmogorov-Smirnov analysis

1. Sort sample values into descending order
2. Normalised cumulative frequency values by dividing by total number of sample values (n)
3. Plot best fit line for sample data which gives the theoretical distribution
4. Find biggest vertical difference between sample and theoretical distributions = D
5. Use (n) to find the critical value of D
6. Compare D and Dcritical and decide whether to accept or reject the null hypothesis

B

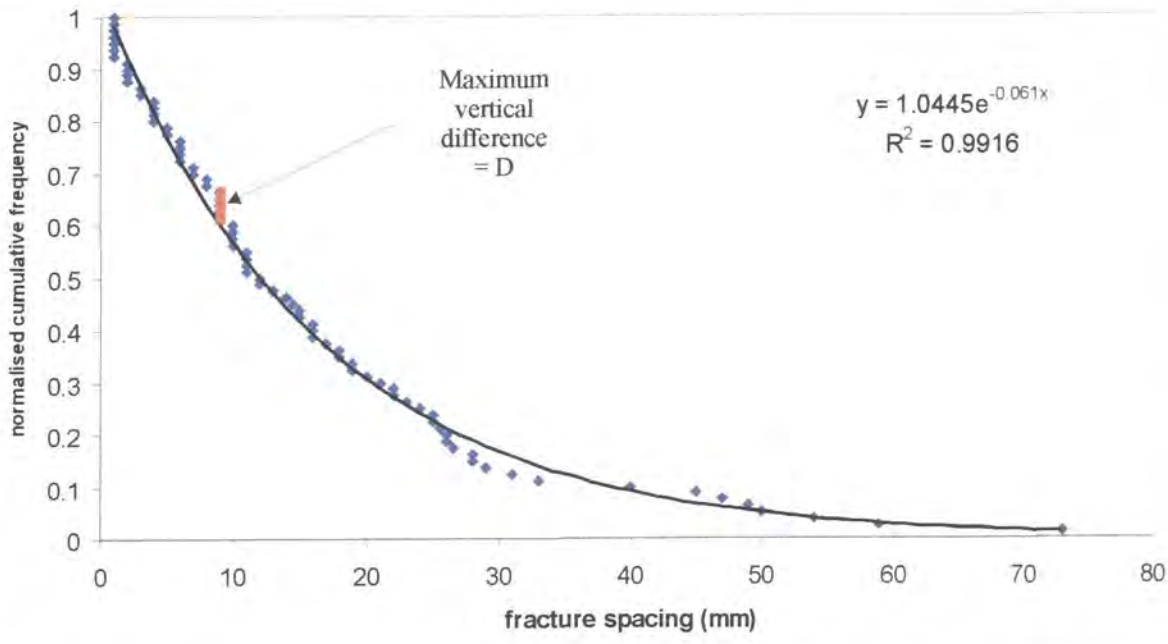

cumulative frequency distribution for fracture spacing values (the sample)

cumulative frequency distribution for theoretical distribution, in this case an exponential distribution (see equation)

largest vertical deviation between sample and theoretical cumulative frequency distributions = **D value**

C

Kolmogorov-Smirnov results for the example shown in the above graph

n = 80
D = 0.058695
Dcritical at 95% confidence level = 0.15205

therefore D < Dcritical, so accept null hypothesis

the sample data comes from the same statistical distribution as the theoretical data - an exponential distribution

Figure 1.47 The Kolmogorov-Smirnov test
A - procedure for testing the goodness of fit of a sample distribution to a theoretical distribution
B - example of Kolmogorov-Smirnov test for a fracture spacing data set
C - results of test illustrated in B

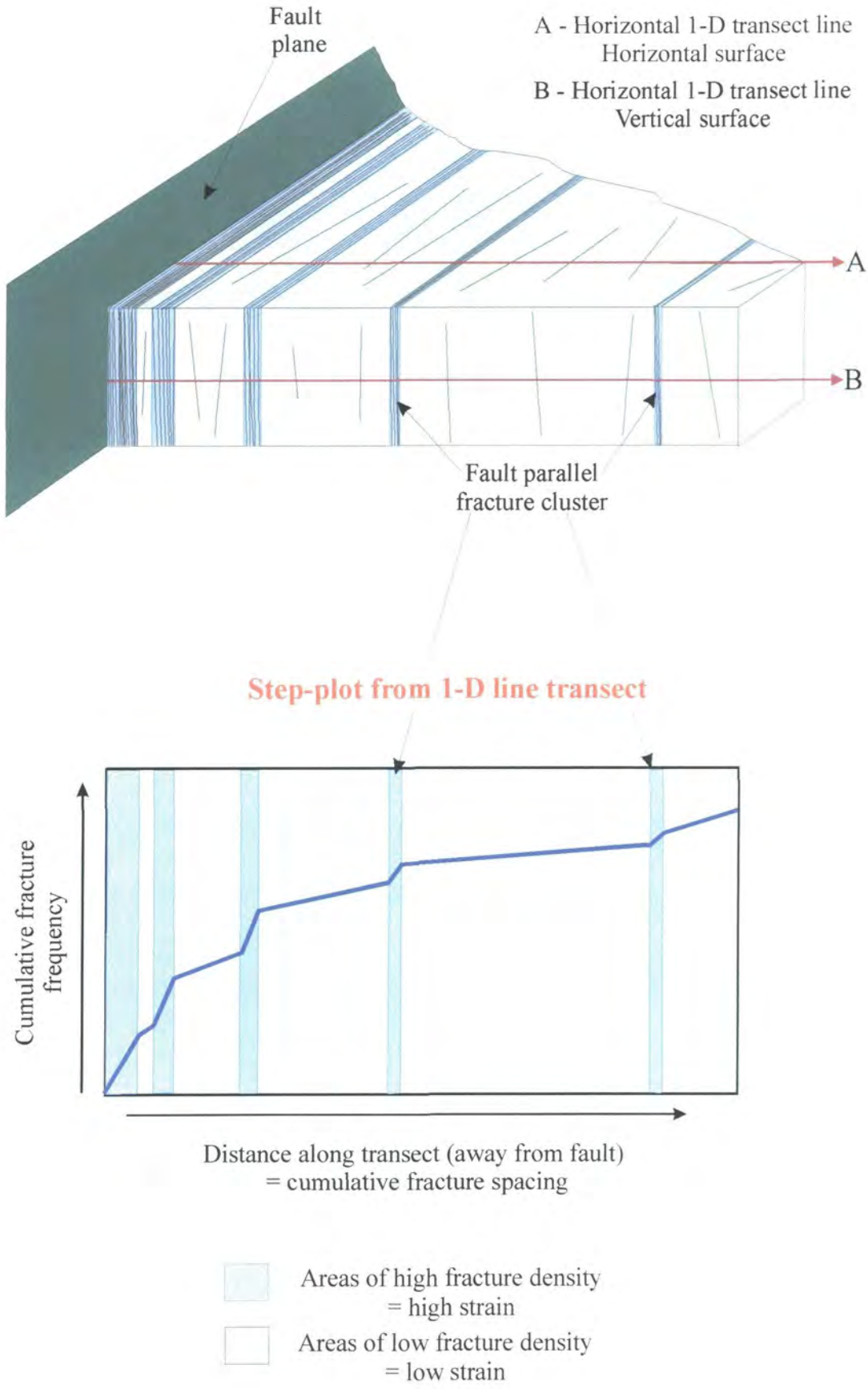

Figure 1.48 Schematic representation of a step plot from a 1-dimensional line transect reflecting the change in fracture density (fracture spacing) away from a fault

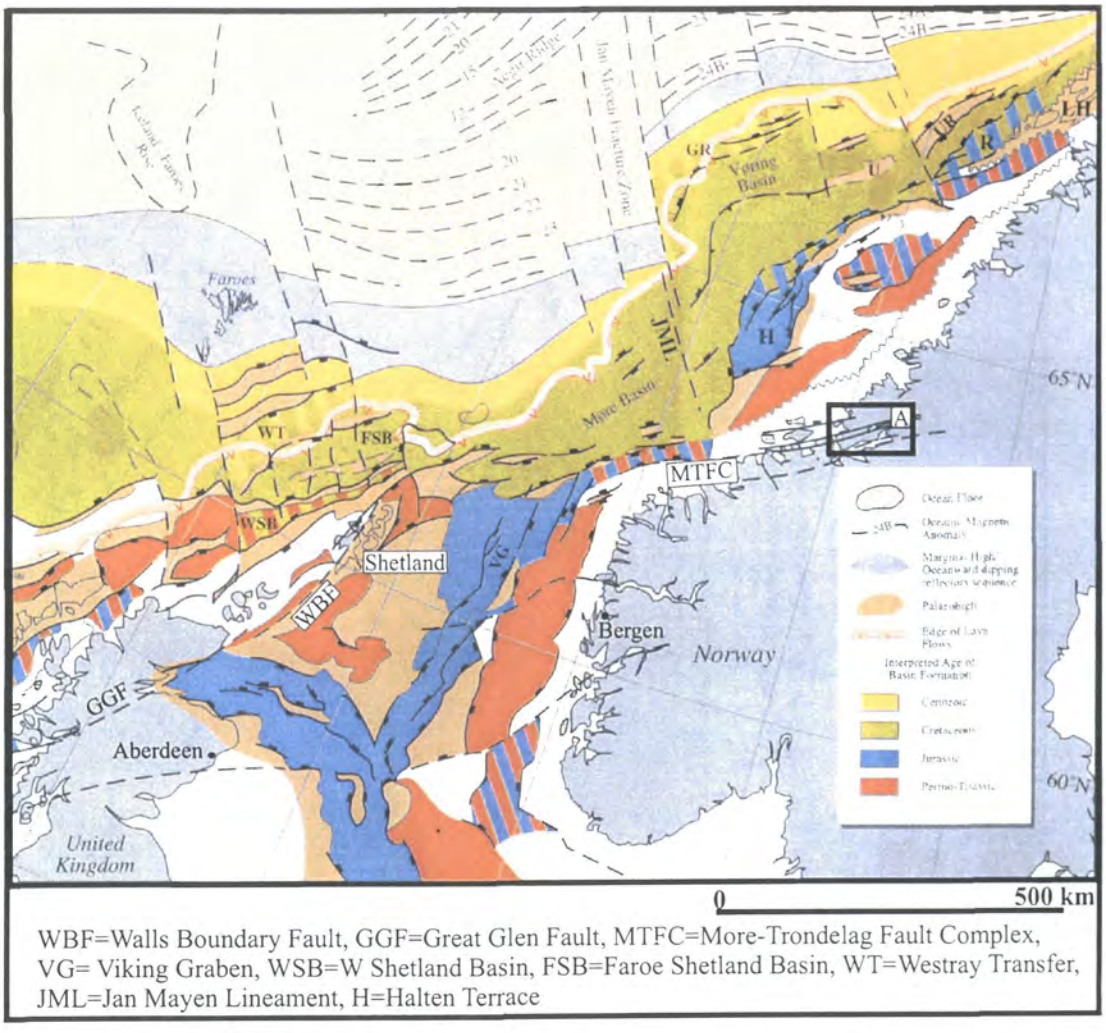

Figure 2.1 Map to show the location of the Fosen Peninsula (A) and the major offshore basins of the NE Atlantic margin. (after Watts 2001, adapted from Dore et al., 1997).

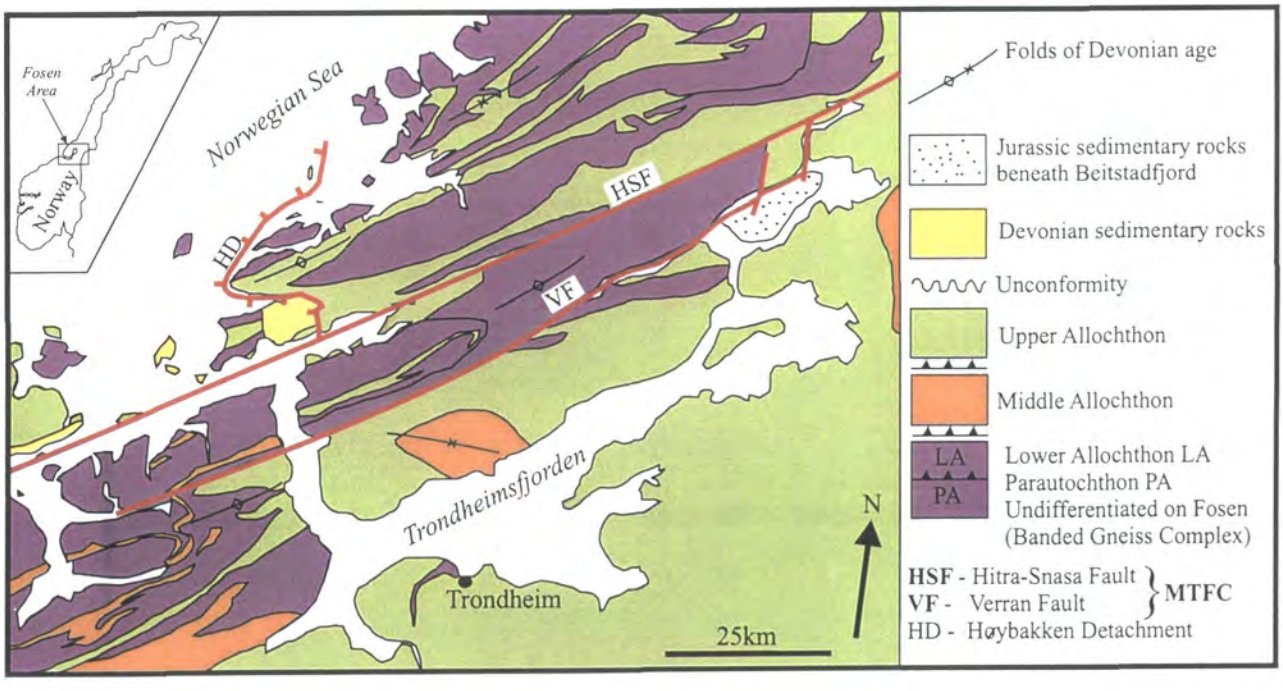

Figure 2.2 Simplified geological map of the Fosen area, Central Norway. (after Watts 2001)

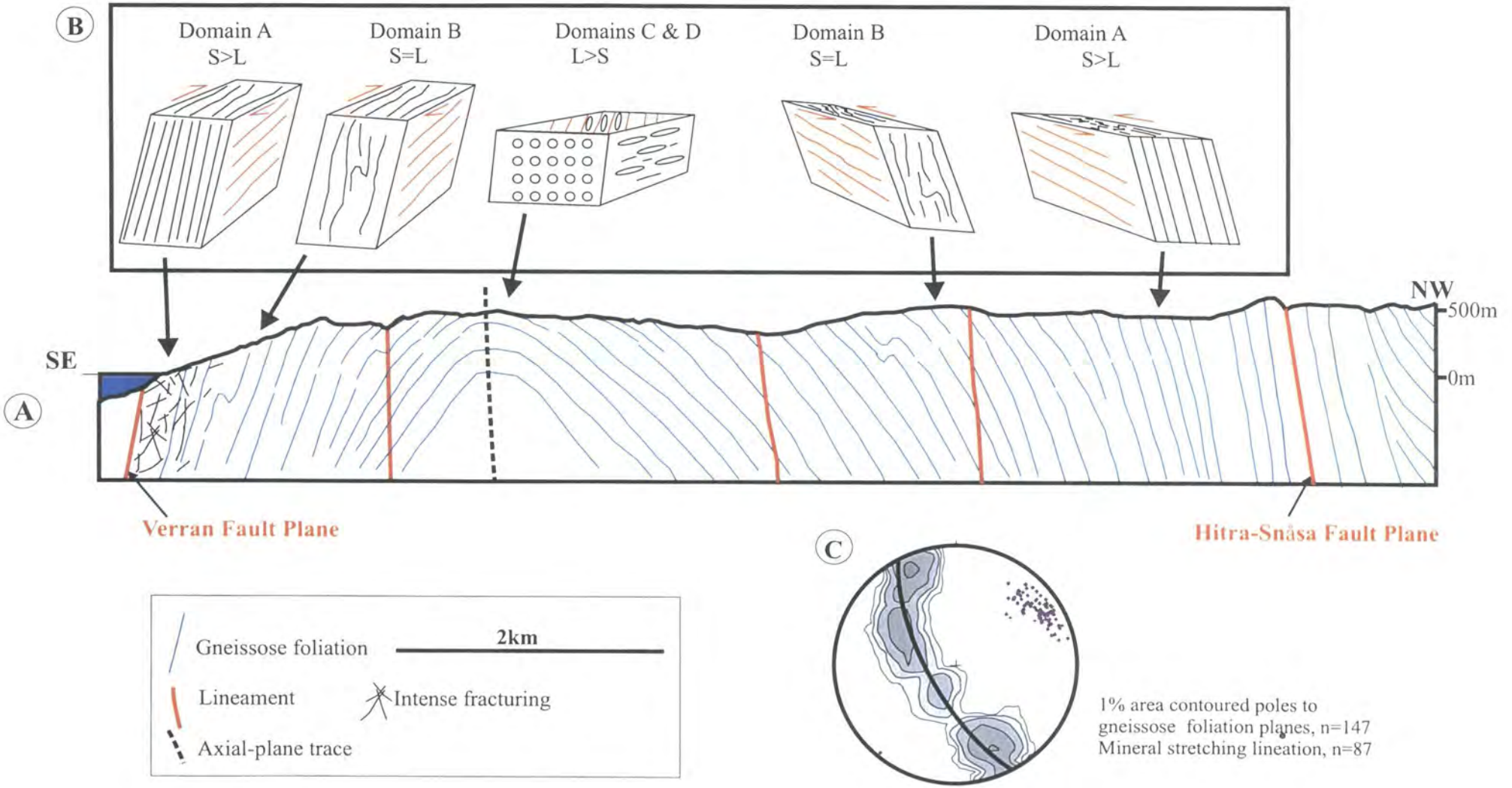

Figure 2.3 (**A**) Cross-section across the MTFC illustrating VF and HSF on opposite limbs of a regional fold. (**B**) Schematic diagrams to illustrate tectonite fabrics in structural domains around fold. (**C**) Stereographic projection to show gneissose foliation and mineral stretching lineation. (after Watts 2001)

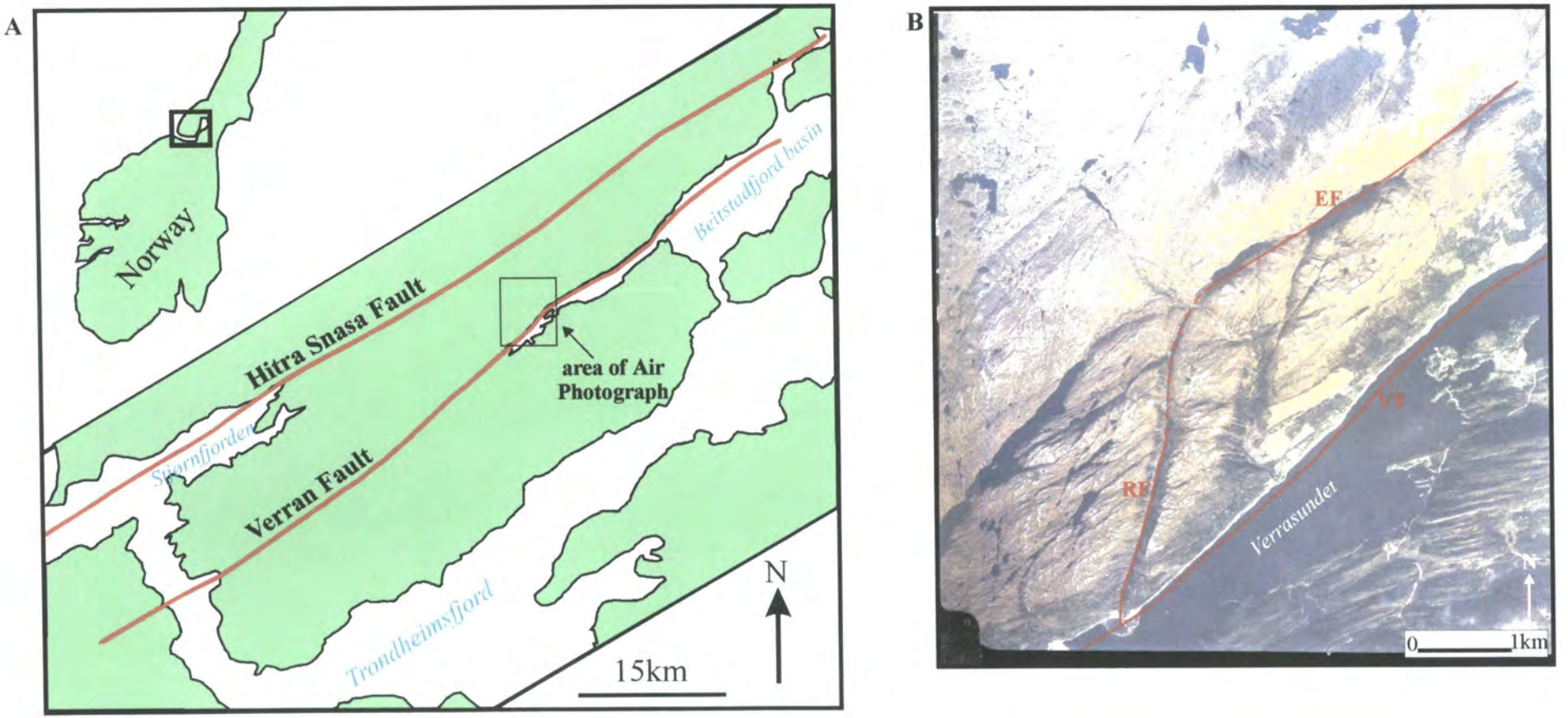

Figure 2.4 (**A**) - Location of the two main bounding faults within the MTFC (VF and HSF) on the Fosen Peninsula
(**B**) - Air Photograph showing part of the Verran Fault Zone, with the locations of the Rautingdalen and Elvdalen Faults

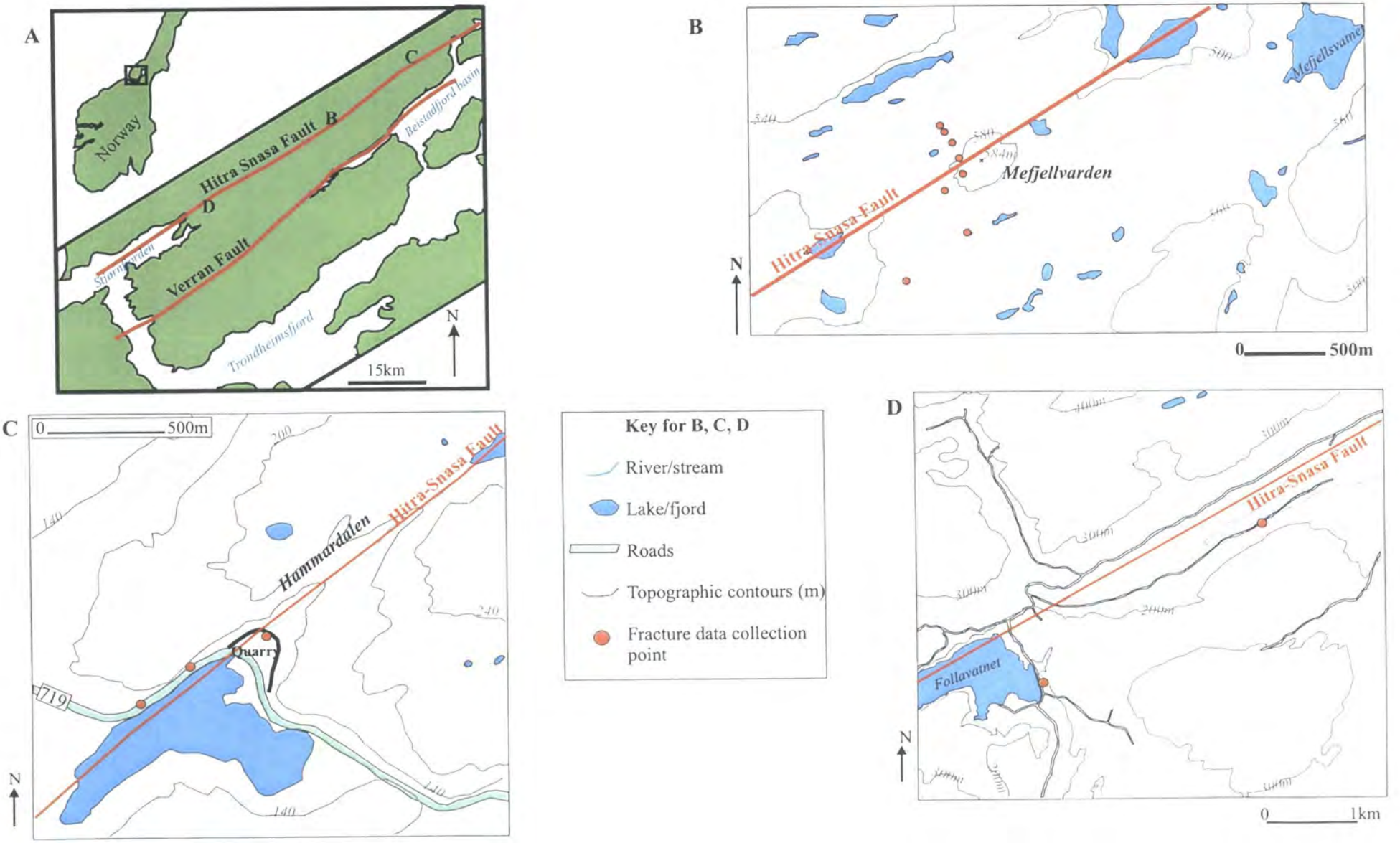

Figure 2.5 HSFZ localities.
A - Map of Fosen showing locations of B, C and D
B - Mefjellet section, **C** - Hammardalen quarry and 719 road cut, **D** - Follavatnet section

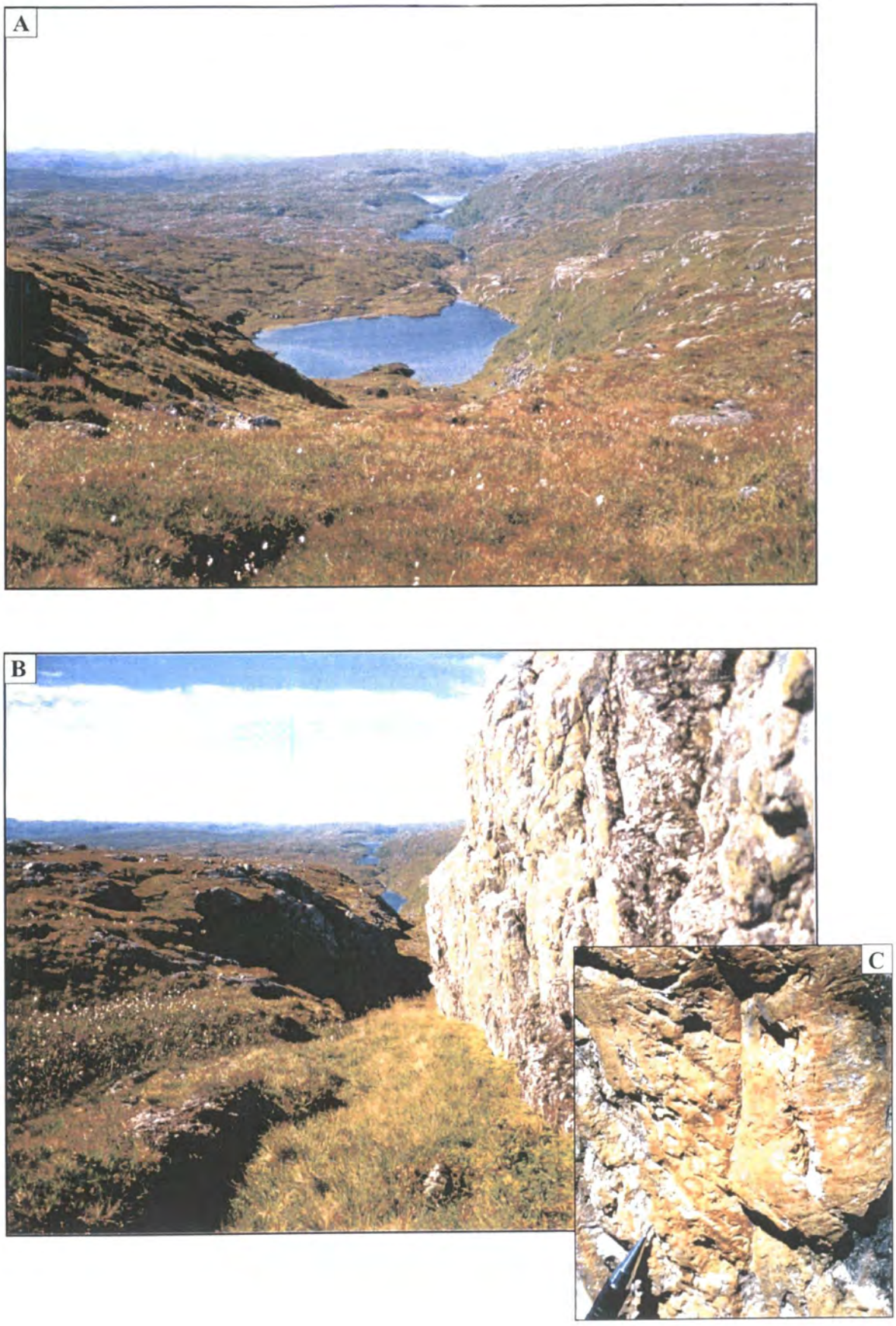

Figure 2.6 Photographs taken from the HSFZ at the Mefjellet section
A - Alignment of lakes along the trace of the HSFP, photograph looking SW
B - Exposure of the HSFP in the foreground, with alignment of lakes along HSFP trace in background. Photograph looking SW.
C - Slickenside lineation observed on the HSFP (shown in B). Photograph looking NW

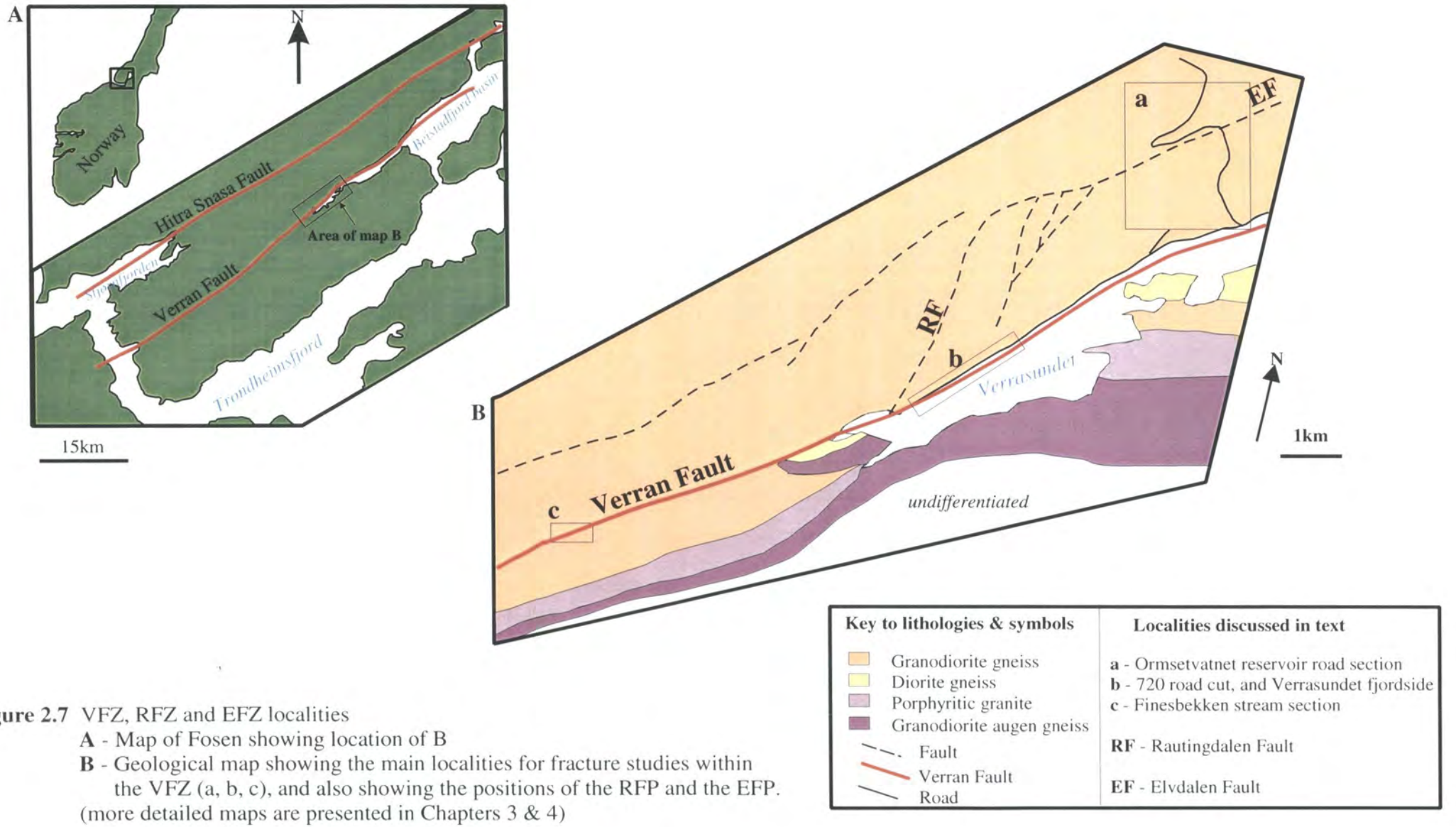

Figure 2.7 VFZ, RFZ and EFZ localities
A - Map of Fosen showing location of B
B - Geological map showing the main localities for fracture studies within the VFZ (a, b, c), and also showing the positions of the RFP and the EFP.
(more detailed maps are presented in Chapters 3 & 4)

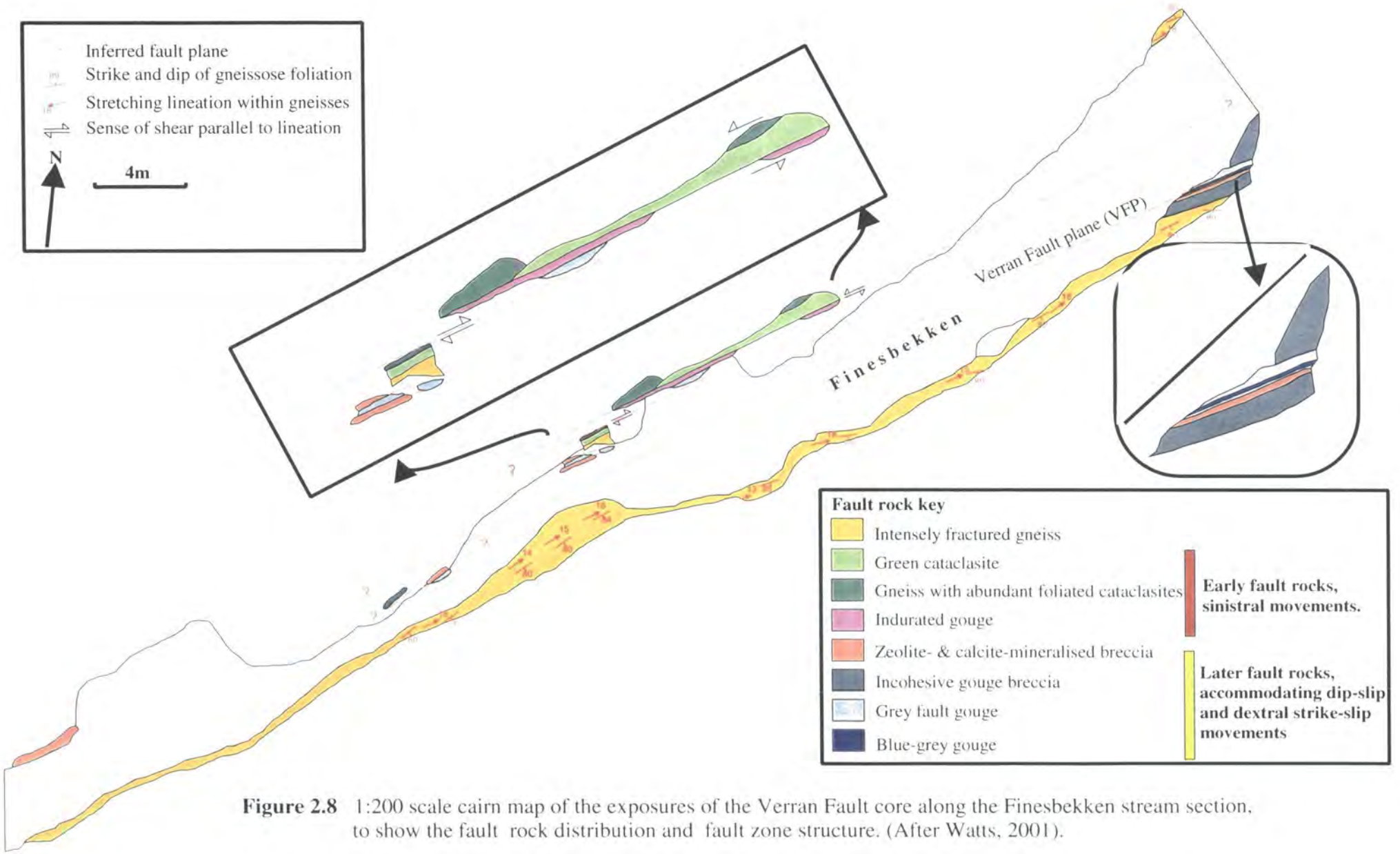

Figure 2.8 1:200 scale cairn map of the exposures of the Verran Fault core along the Finesbekken stream section, to show the fault rock distribution and fault zone structure. (After Watts, 2001).

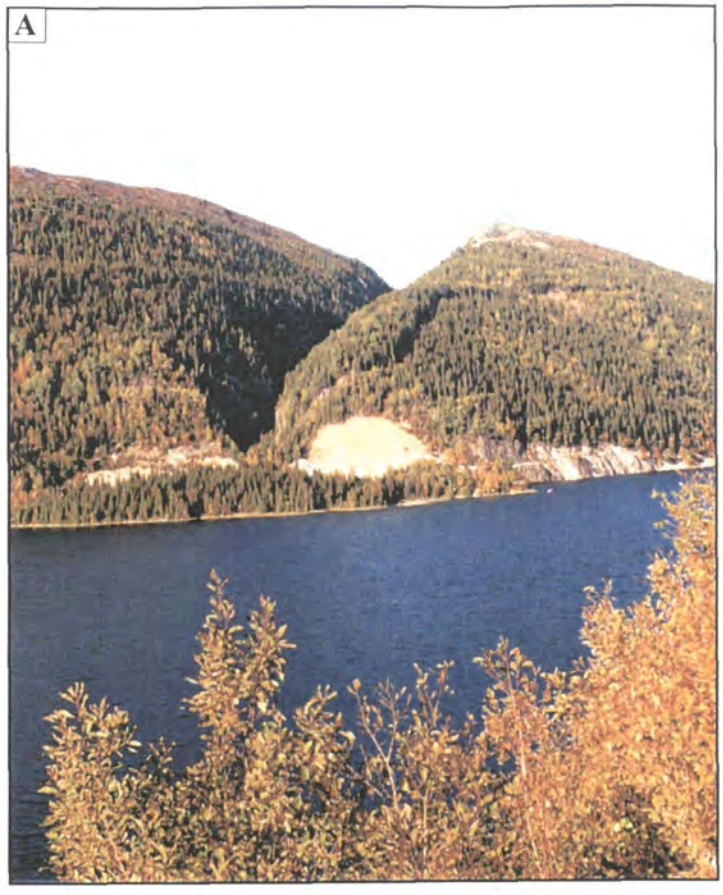

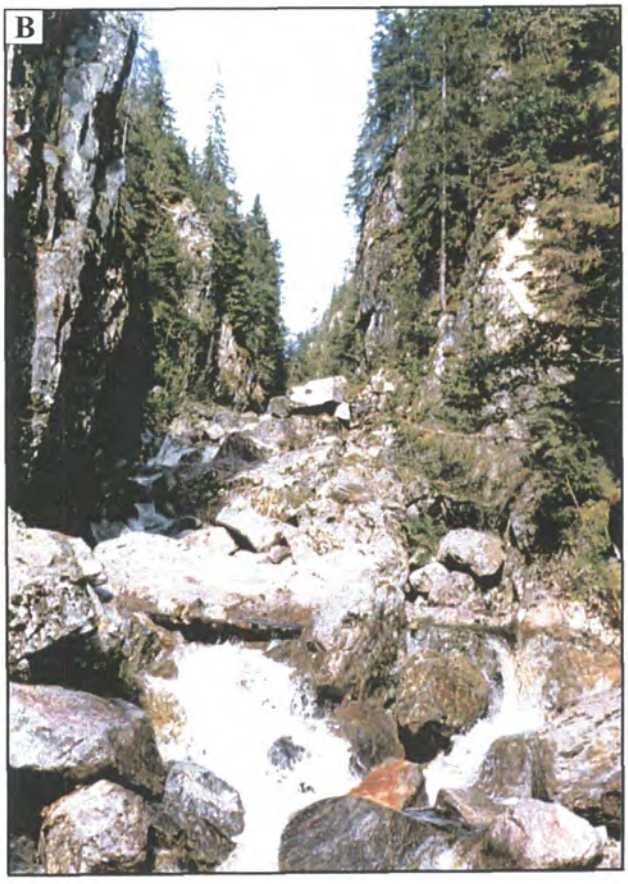

Figure 2.9 Photographs from the RFZ.
A - The Rautingdalen gorge, photograph looking N, gorge trends NNE-SSW
B - Inside the steep-sided, 10m wide Rautingdalen gorge, photograph looking NNE
C - Recent rock fall towards the northern end of the Rautingdalen gorge. Photograph looking SW

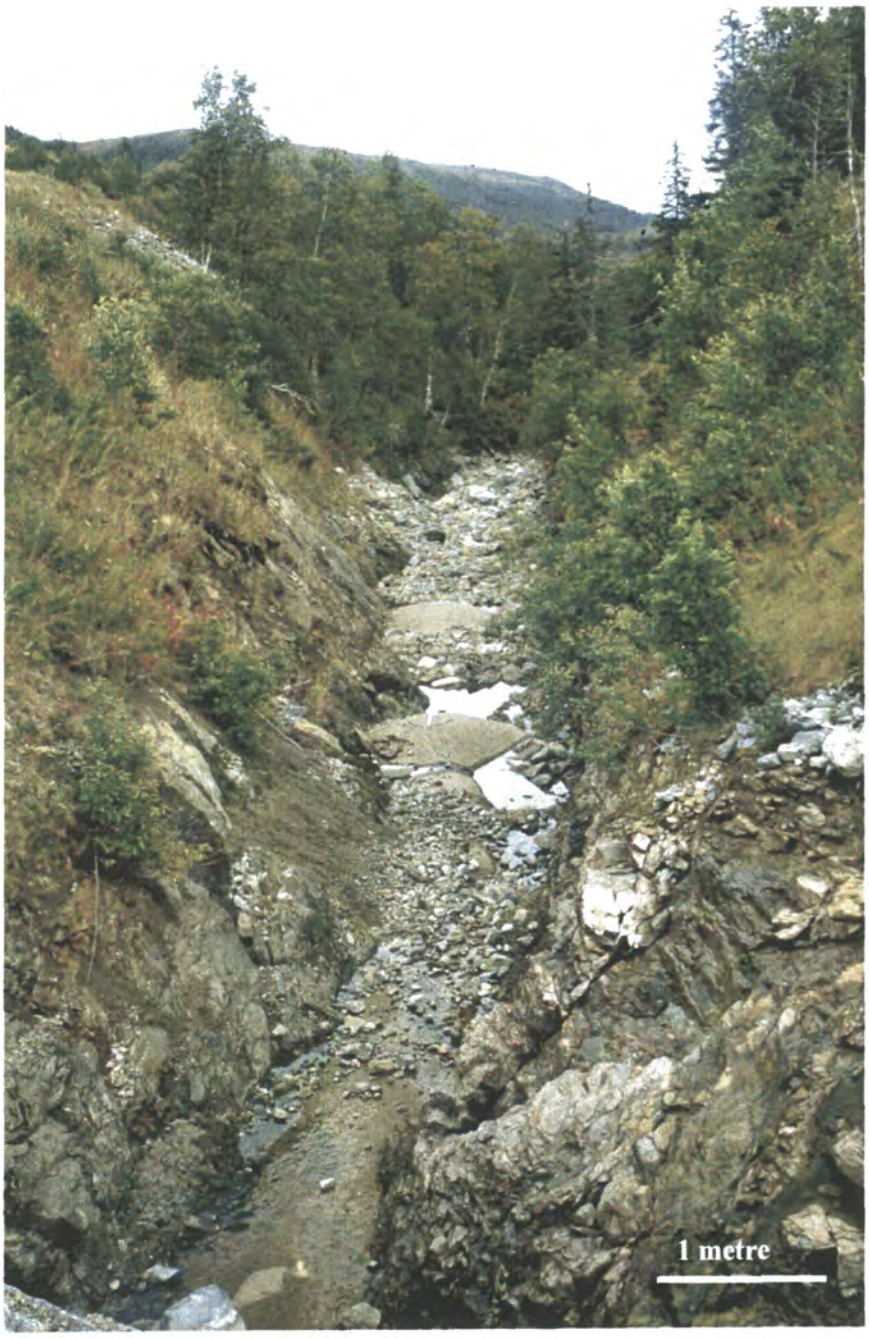

Figure 2.10 Exposures of the Elvdalen Fault zone along a dried up stream-bed adjacent to a Hydro station along the road to the Ormsetvatnet reservoir. The stream bed marks the trace of the EFP which is unexposed at this locality. (photograph looking NE)

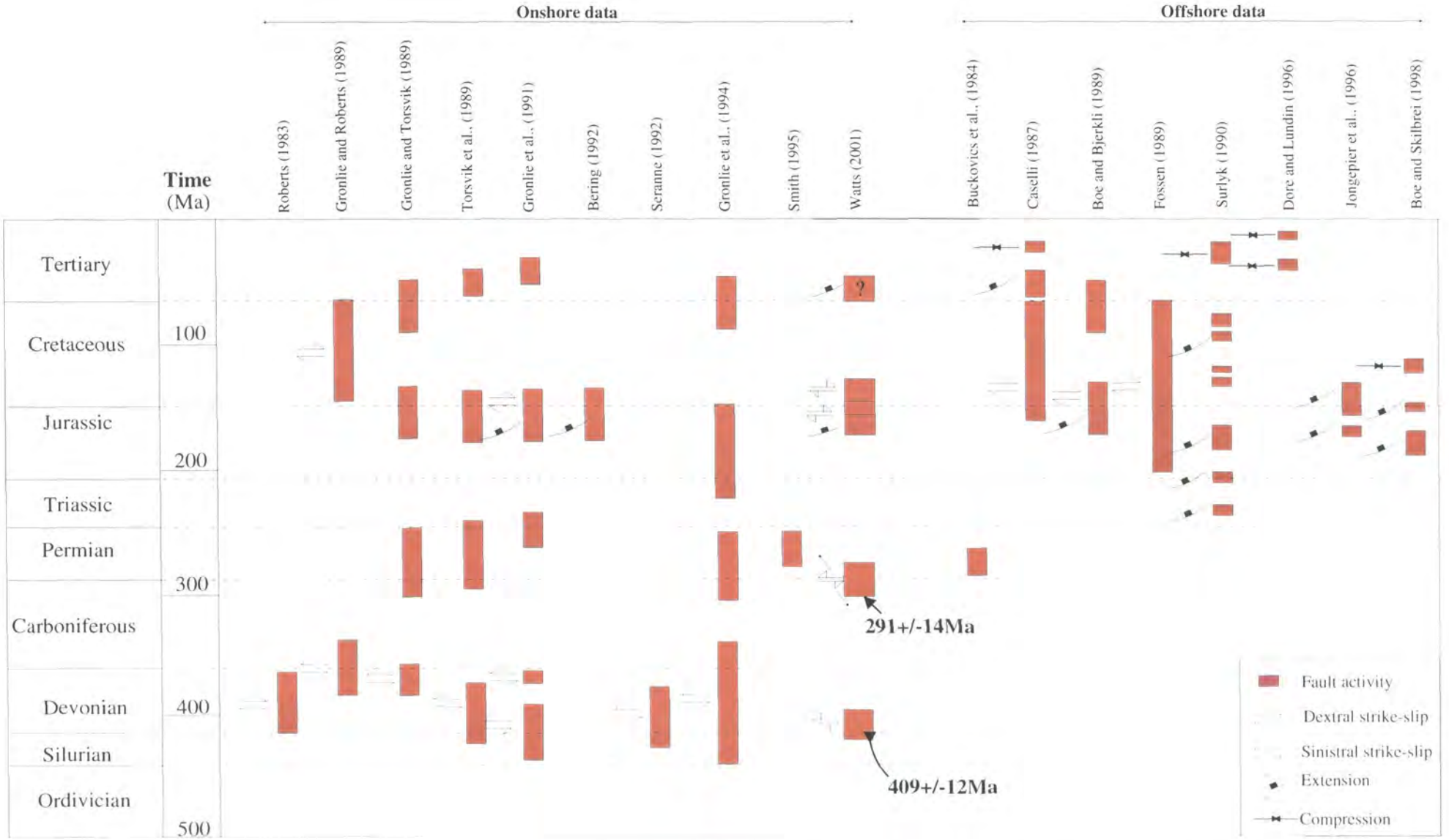

Figure 2.11 Summary of kinematic events suggested for the MTFC, taken from onshore and offshore publications. (adapted from Watts 2001) (NB kinematic symbols are positioned to the LEFT of the red fault activity boxes. Red boxes with no associated kinematics represent periods of fault activity but with no identified kinematics.)

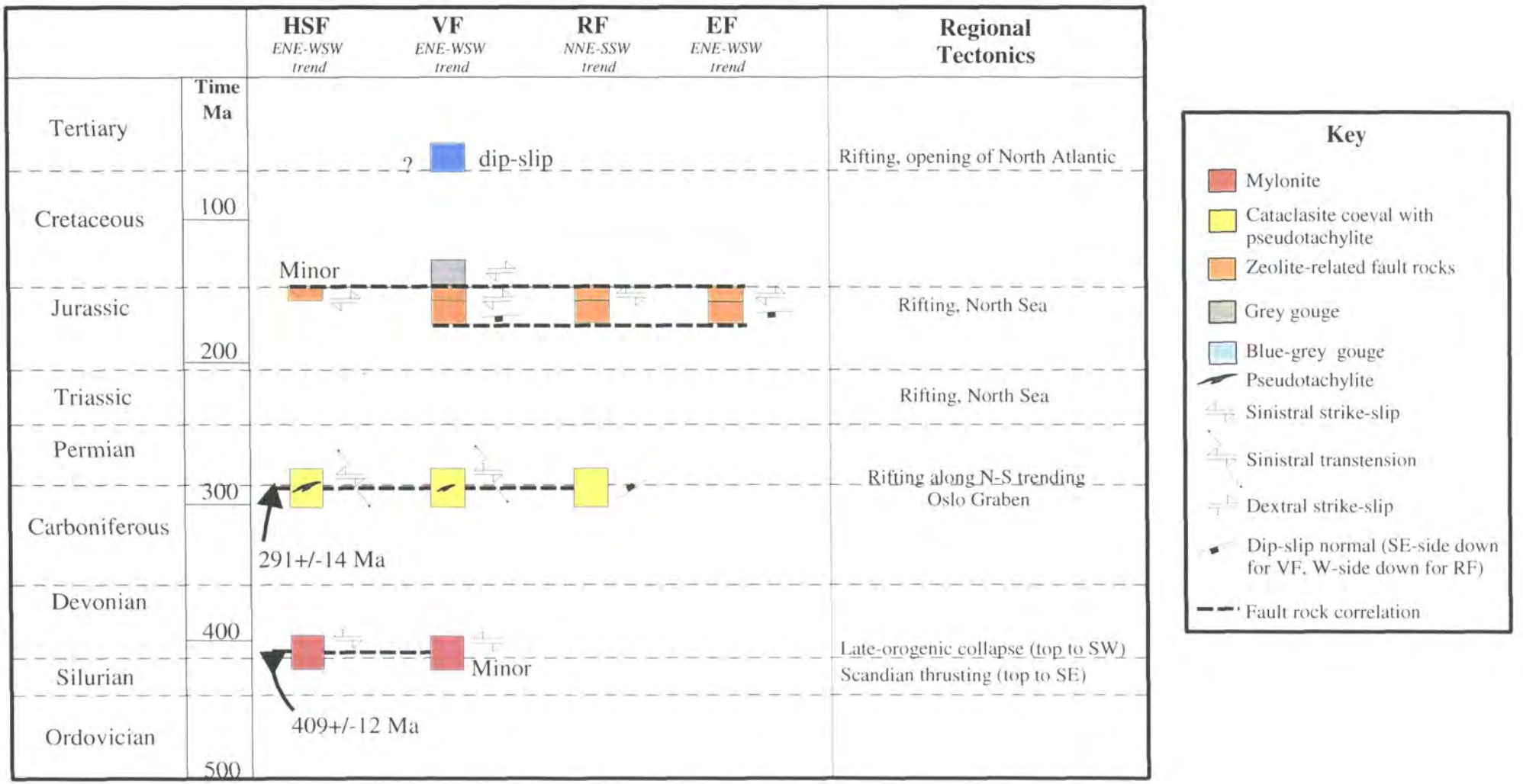

Figure 2.12 Time diagram to show fault rock correlation, kinematic evolution and timing for the HSF, VF, RF and EF within the MTFC. Kinematic symbols are positioned to the RIGHT of the coloured fault activity box. (Adapted from Watts, 2001)

		Stereonet							
		A	B	C	D	E	F	G	H
	Place	VFC	Fjordside	720 Road	Res. Road	Res. Road	Res. Road	Res. Road	Res. Road
	Locality	130, 139. 161	47, 137	48	28a, 164	28b, 157	133	132a	138
	Distance to VFP	< 20m	20 – 30m	100 – 150m	~450m	~500m	~1300m	~1930m	~2250m
	no. data points	365	350	372	300	278	137	90	103
mean girdles to fracture orientations	RED (ENE-WSW, parallel to MTFC trend)	047/ 75SE	050/ 75 SE	068/ 67 SE	055/ 65 SE	056/ 71 SE	051/ 54 SE	-	-
	GREEN (E-W to ESE-WNW)	095/ 28 N	090/ 49 N	070/ 45 N	091/ 72 N	098/ 64 N	090/ 61 N	-	-
	BLUE (NNW-SSE)	150/ 73 W	155/ 76 W	159/ 70 W	151/ 76 W	152/ 79 W	131/ 84 NE	016/ 34 E	020/ 35 E-
	ORANGE (N-S)	172/ 57 W	005/ 81 E	178/ 87 E	174/ 79 W	175/ 78 W	-	-	-

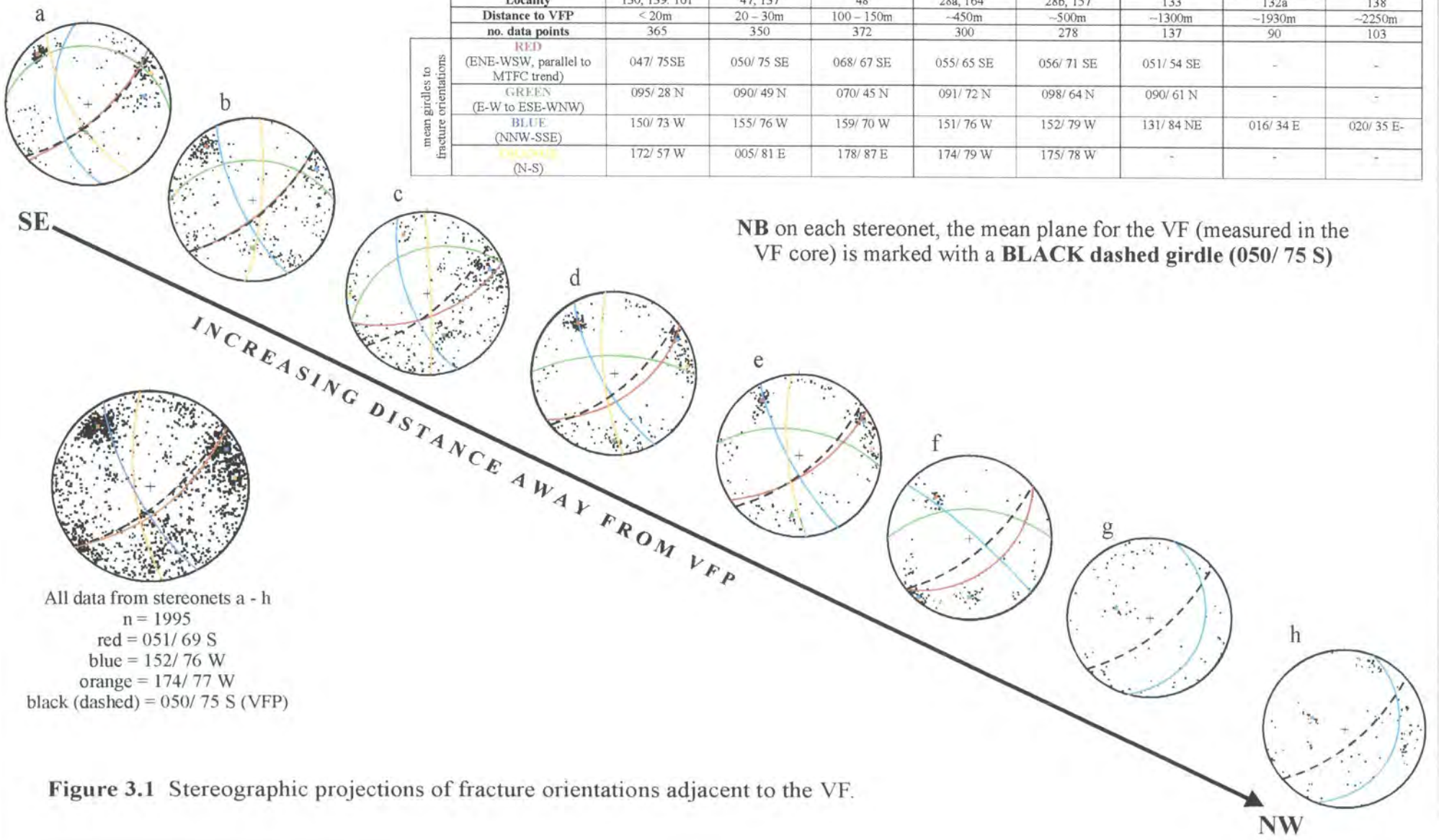

Figure 3.1 Stereographic projections of fracture orientations adjacent to the VF.

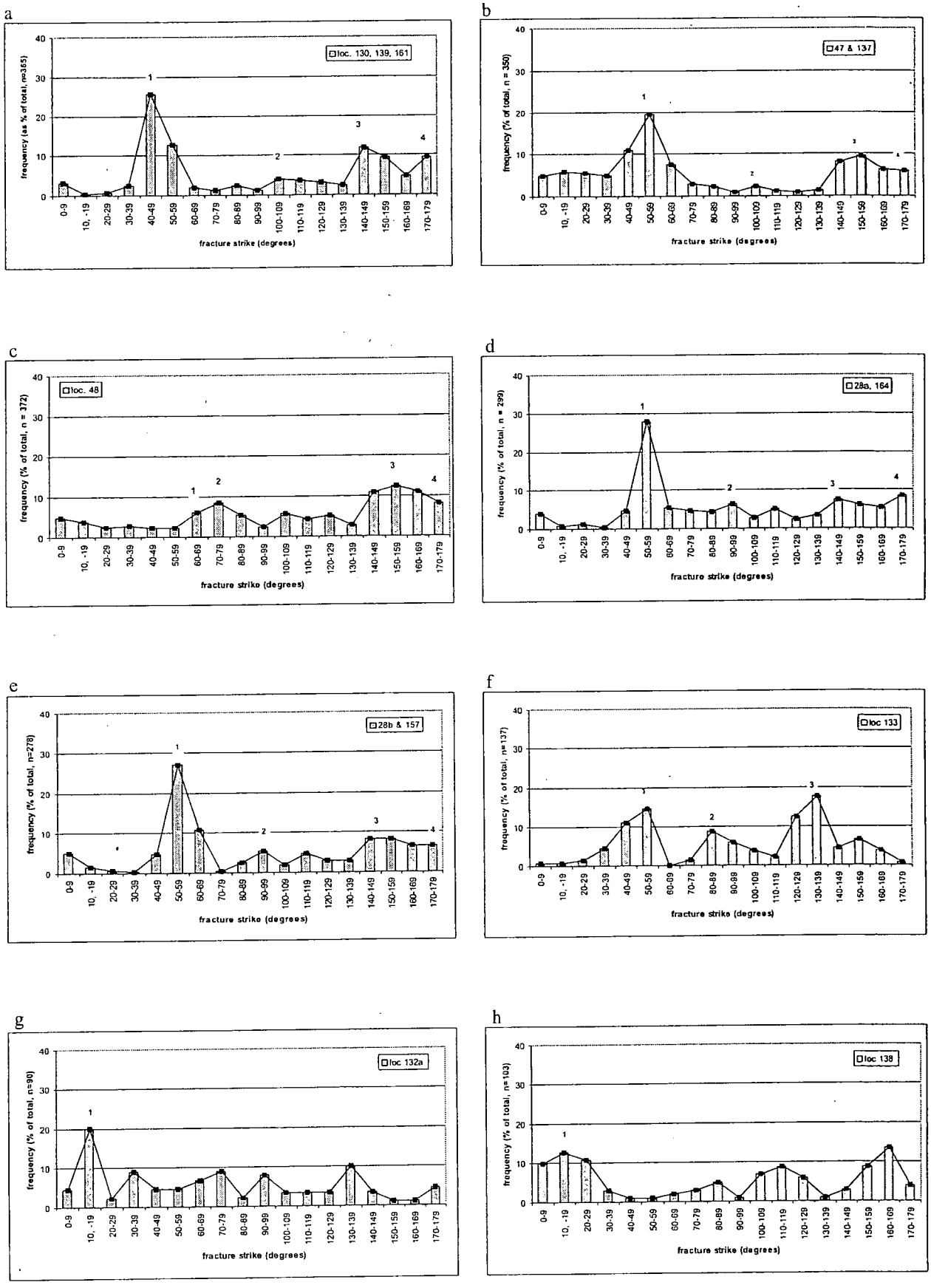

Figure 3.2 Von-Mises diagrams created for the same data illustrated in **Figure 3.1** (1 = red girdles in **Fig. 3.1**, 2 = green girdles, 3 = blue girdles, 4 = orange girdles)

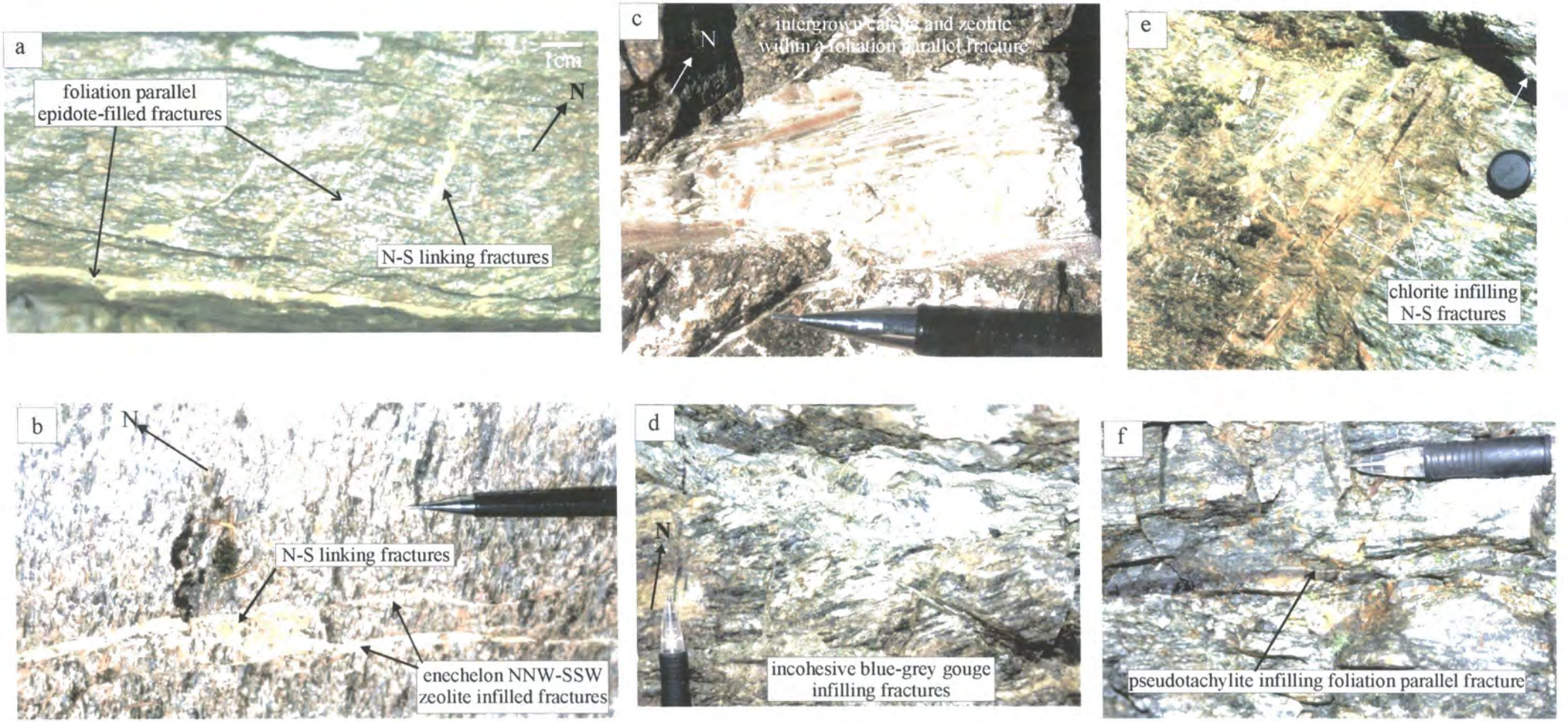

Figure 3.3 Fracture infills observed in the field adjacent to the VF. (All photographs are plan view).

a - epidote cataclastite
b - zeolite
c - zeolite & calcite
d - incohesive gouge
e - chlorite
f - pseudotachylite

(a, d & f = from Verran Fault Core (Finesbekken stream section), b = from Road to Ormsvatnert reservoir c = from Verrasundet fjordside, e = from 720 Road section)

A

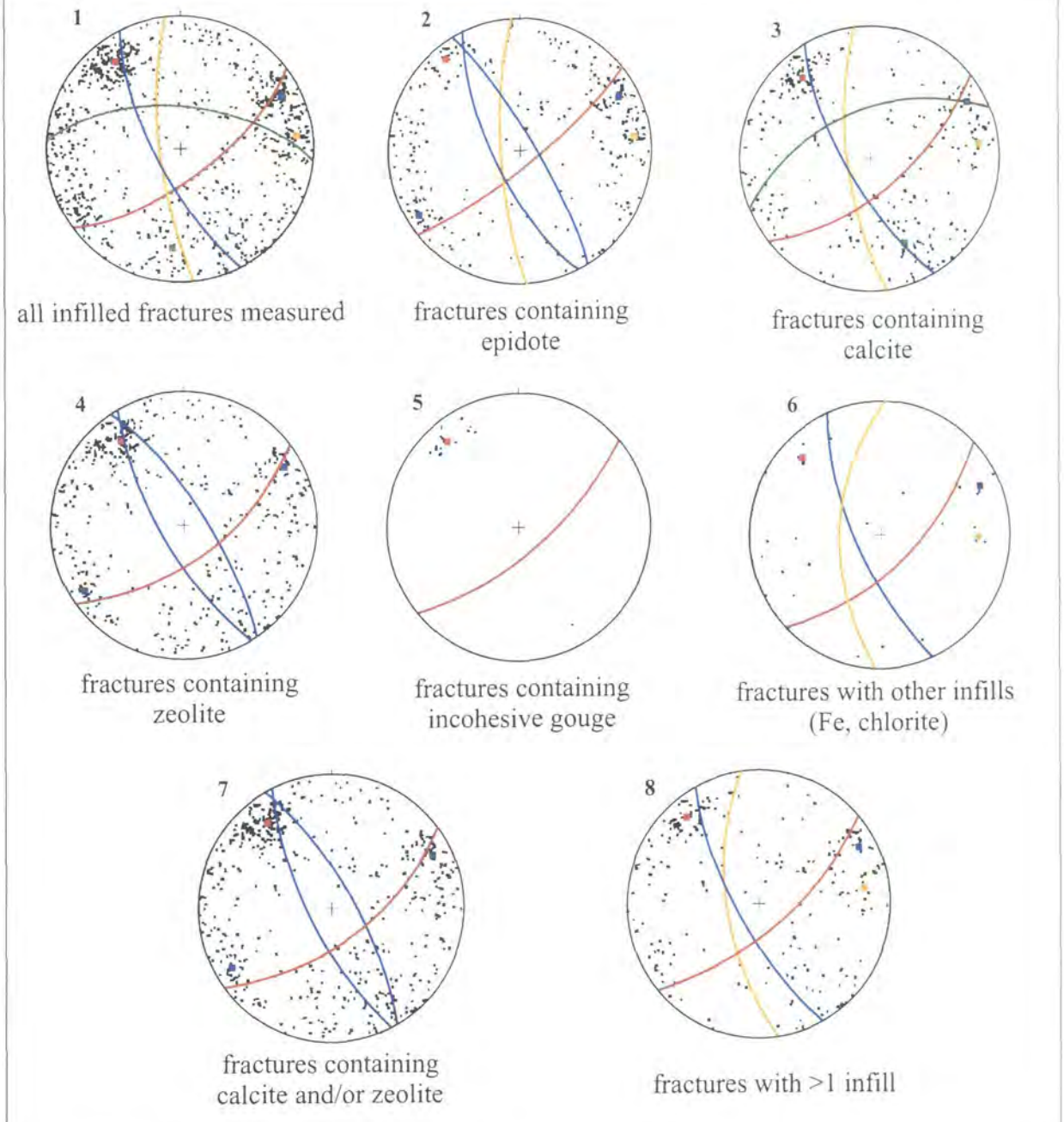

Stereonet	1	2	3	4	5	6	7	8
Description of data	All infilled fractures measured adjacent to VF.	fractures containing epidote/ epidote cataclasite	fractures containing calcite	fractures containing zeolite	fractures containing incohesive fault gouge	fractures with other infills (Fe. chlorite, pseudotachylite)	fractures containing calcite and/or zeolite	fractures with >1 infilling material
number of data points	824	291	279	481	17	28	566	249
Mean girdles to fracture orientation clusters: RED (~ENE-WSW)	053/ 70 S	051/ 80 S	051/ 69 S	054/ 68 S	050/ 73 S	046/ 70 S	054/ 68 S	050/ 73 S
GREEN (~E-W)	095/ 64 N	-	070/ 60 N	-	-	-	-	-
BLUE (~NNW-SSE)	153/ 75 W	154/ 73 W & 149/ 81 E	150/ 74 W	150/ 76 W & 147/ 77 E	-	156/ 74 W	153/ 76 W & 150/ 76 E	151/ 76 W & 153/ 75 E
ORANGE (~N-S)	174/ 78 W	177/ 73 W	173/ 75 W	-	-	002/ 64 W	-	174/ 79 W

Figure 3.4 Filled-fractures adjacent to the VFP.

A - Stereographic projections of fractures with identifiable infills adjacent to the VFP

B - The percentages of filled-fractures observed at different distances from the VFP

(continued on next page)

B

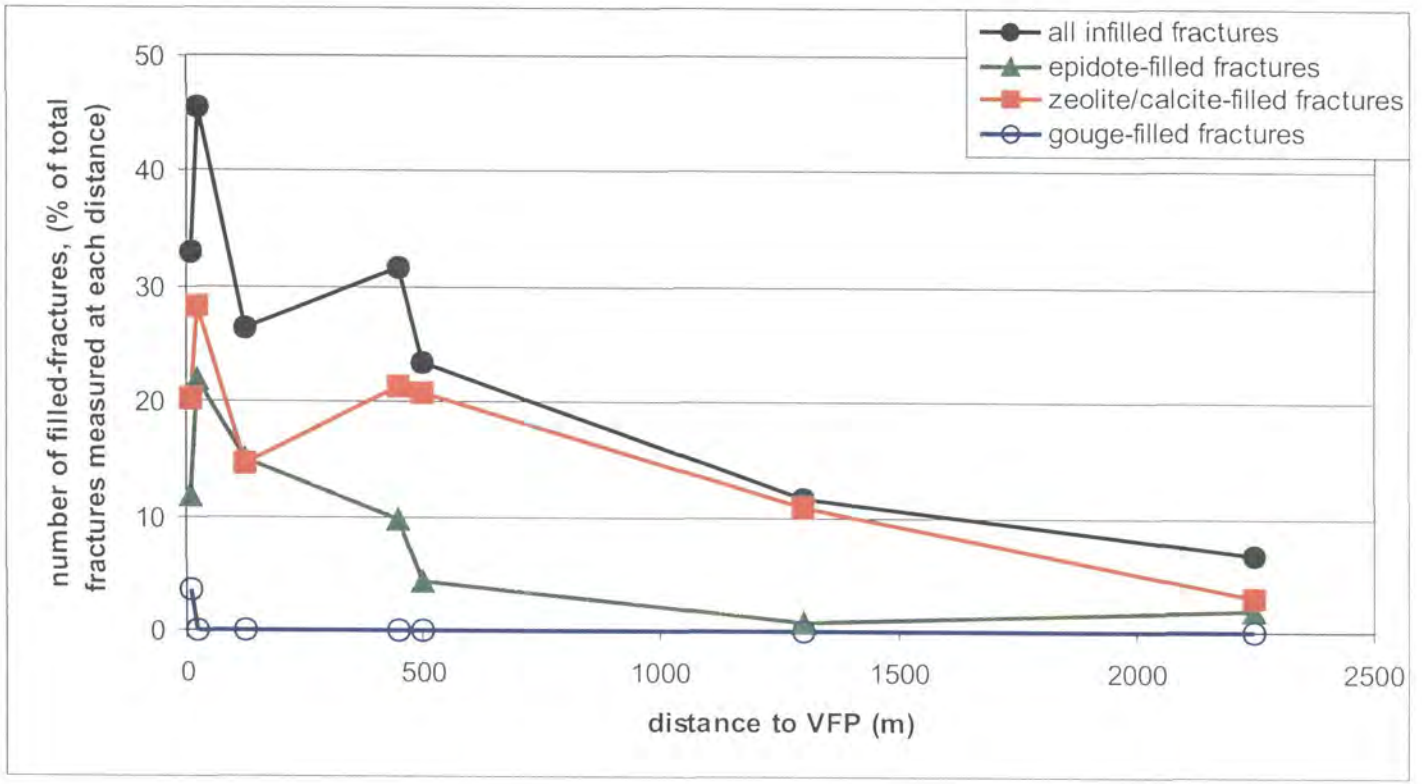

Figure 3.4 Filled-fractures adjacent to the VFP.
A - Stereographic projections of fractures with identifiable infills adjacent to the VFP
B - The percentages of filled-fractures observed at different distances from the VFP
(continued from previous page)

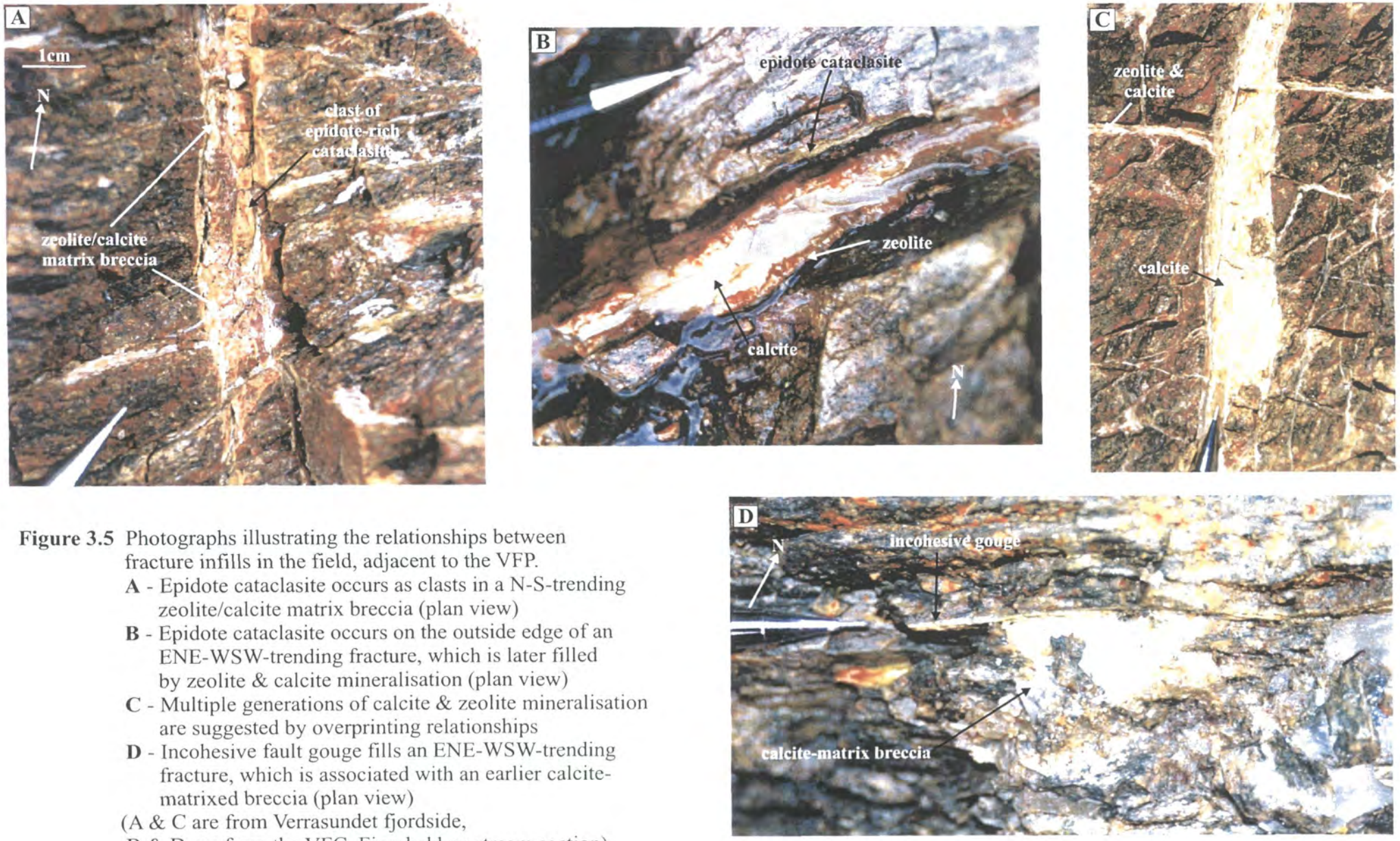

Figure 3.5 Photographs illustrating the relationships between fracture infills in the field, adjacent to the VFP.

A - Epidote cataclasite occurs as clasts in a N-S-trending zeolite/calcite matrix breccia (plan view)

B - Epidote cataclasite occurs on the outside edge of an ENE-WSW-trending fracture, which is later filled by zeolite & calcite mineralisation (plan view)

C - Multiple generations of calcite & zeolite mineralisation are suggested by overprinting relationships

D - Incohesive fault gouge fills an ENE-WSW-trending fracture, which is associated with an earlier calcite-matrixed breccia (plan view)

(A & C are from Verrasundet fjordside,
B & D are from the VFC, Finesbekken stream section)

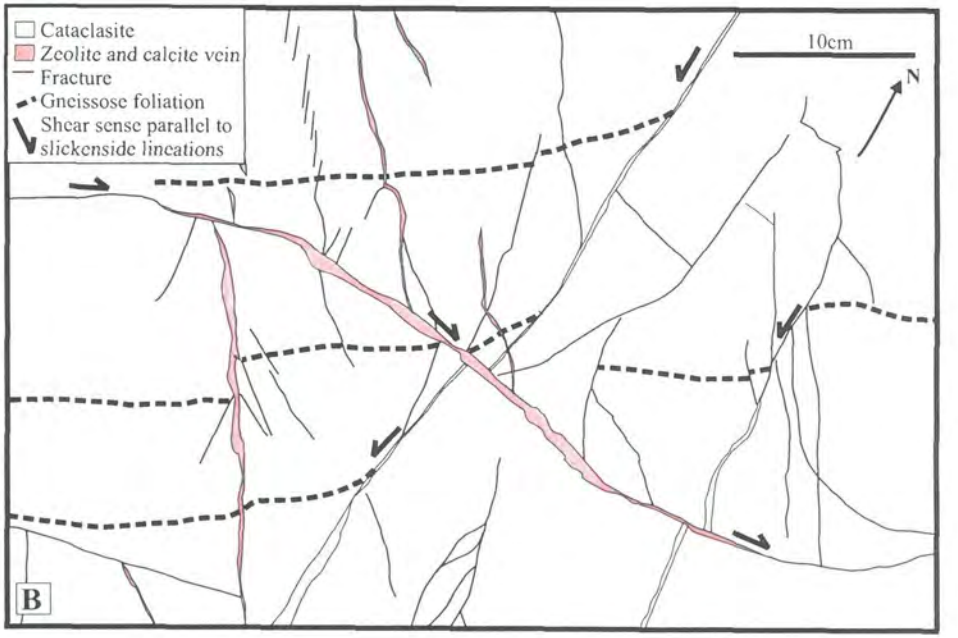

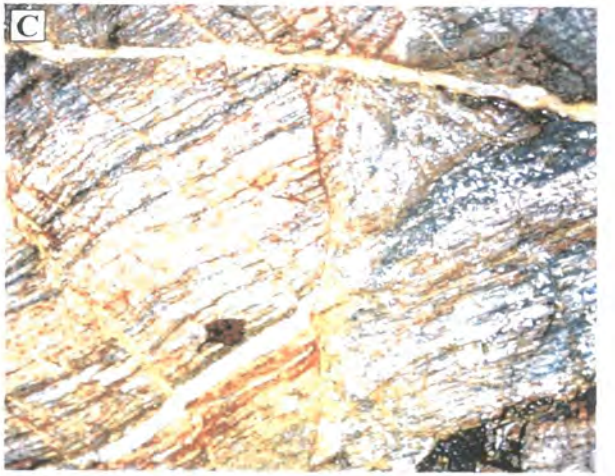

Figure 3.6 Photographs illustrating kinematics associated with fracture infills (taken along the road to Ormsetvatnet Reservoir)

A - NNE-SSW-trending fractures filled with millimetre-thick epidote-rich cataclasites offset the gneissose foliation by 3cm to 2m in a sinistral sense, and are interpreted as R-type Riedel shears. ENE-WSW-trending zeolite and calcite veins offset the earlier-formed cataclasites by 1cm to 4cm in a dextral sense. (White box illustrates area of **C**). (Plan view).

B - sketch of photograph in **A**

C - enlargement of part of photograph in **A** (area of white box)

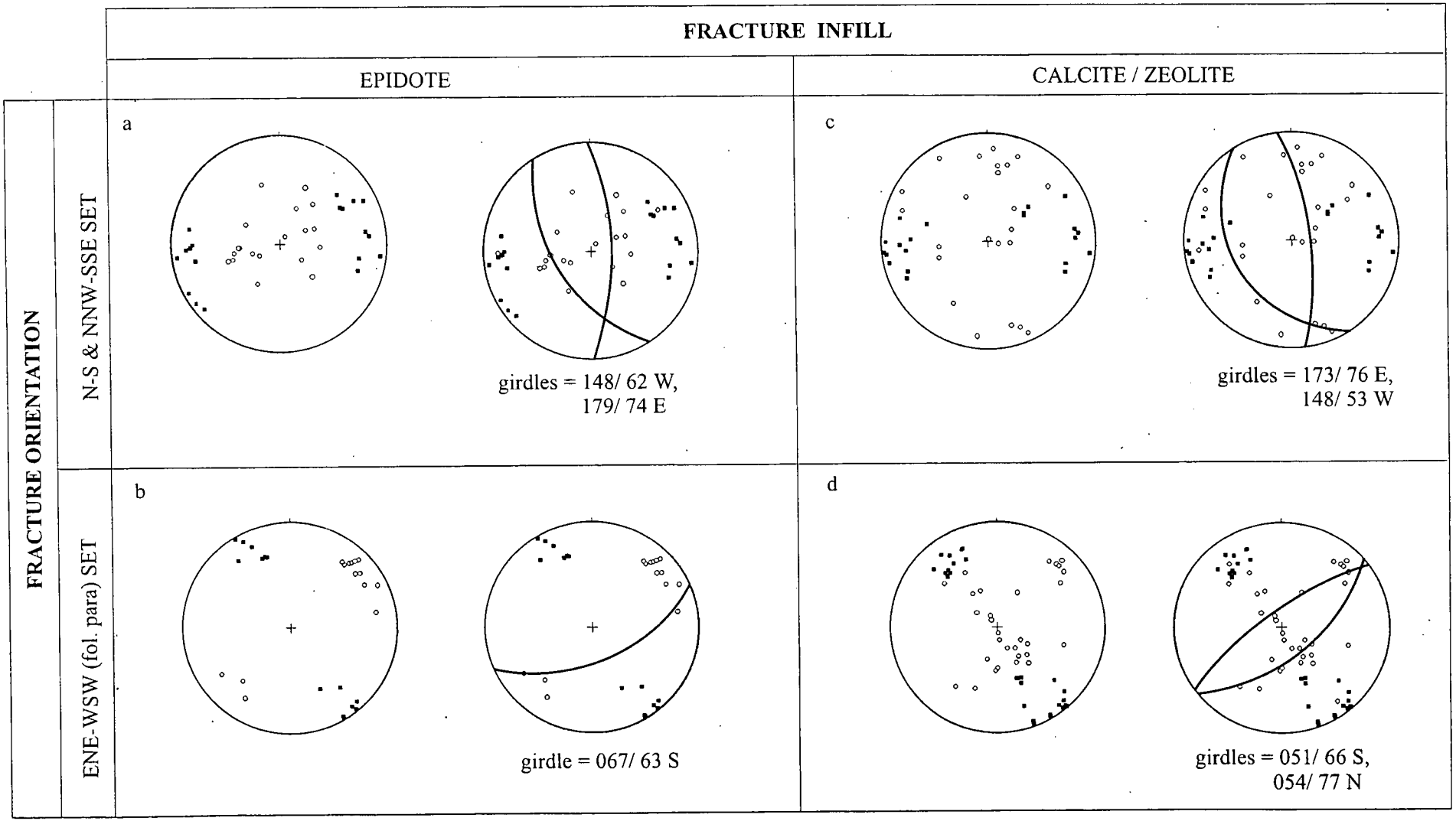

Figure 3.7 Stereographic projections of infilled fractures with slickenfibre lineation data
Black squares = fracture planes plotted as poles with mean girdles.
Open circles = slickenfibre lineations

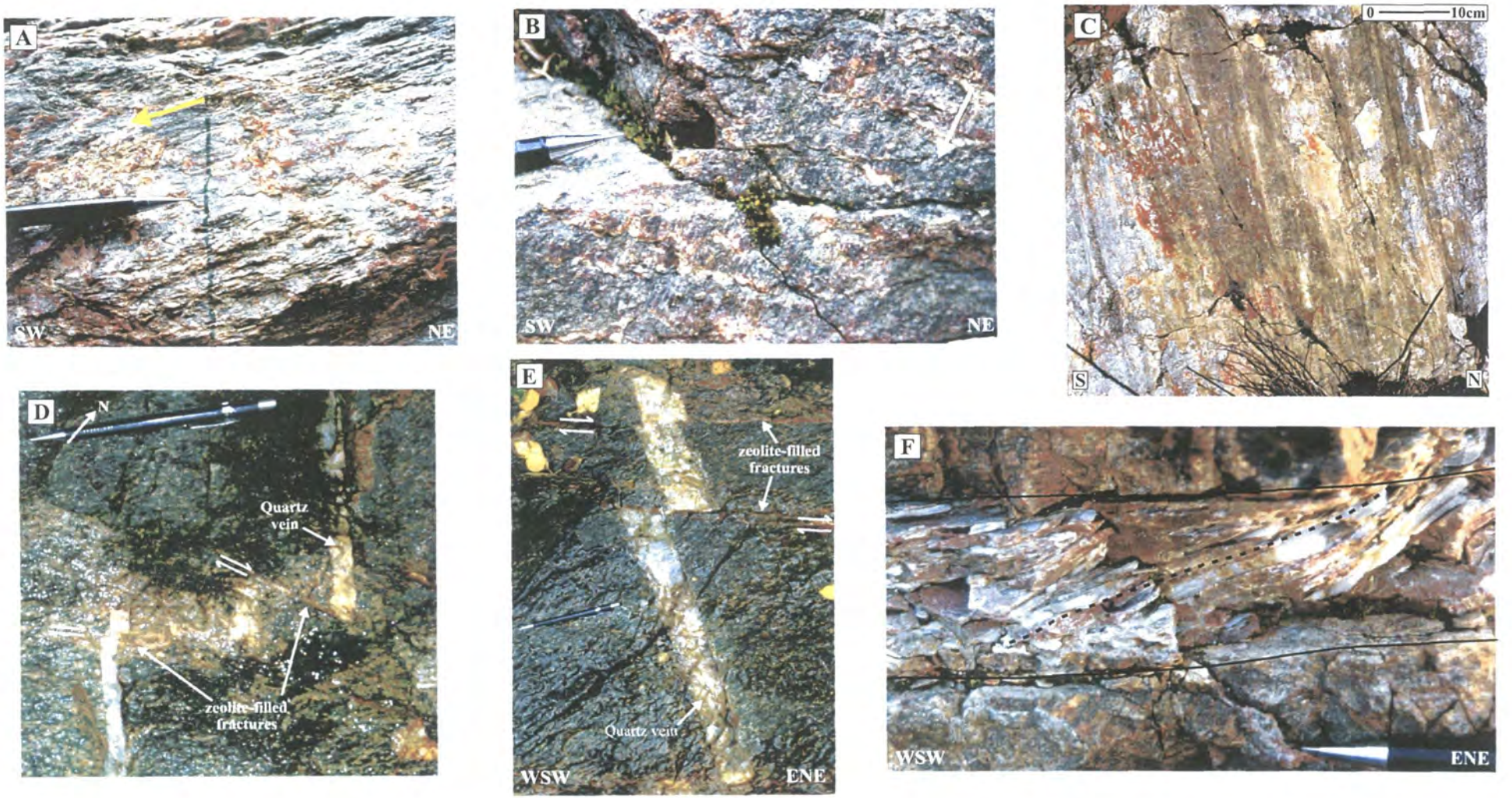

Figure 3.8 Photographs of kinematic indicators associated with zeolite/calcite-filled fractures.
A, B, C - zeolite/calcite slickenfibre lineations observed on fracture surfaces trending ENE-WSW (**A**, **B**) and N-S (**C**). (All cross-section view).
D, E - ENE-WSW and E-W trending zeolite-filled fractures offset quartz veins in a dextral sense (plan view).
F - Fibrous infill of intergrown zeolite & calcite within a fracture orientated ENE-WSW suggesting dextral sense of shear (plan view).
(A, B, D & E = from Ormsetvatnet reservoir road, C = from 720 Road section, F = from Verrasundet fjordside)

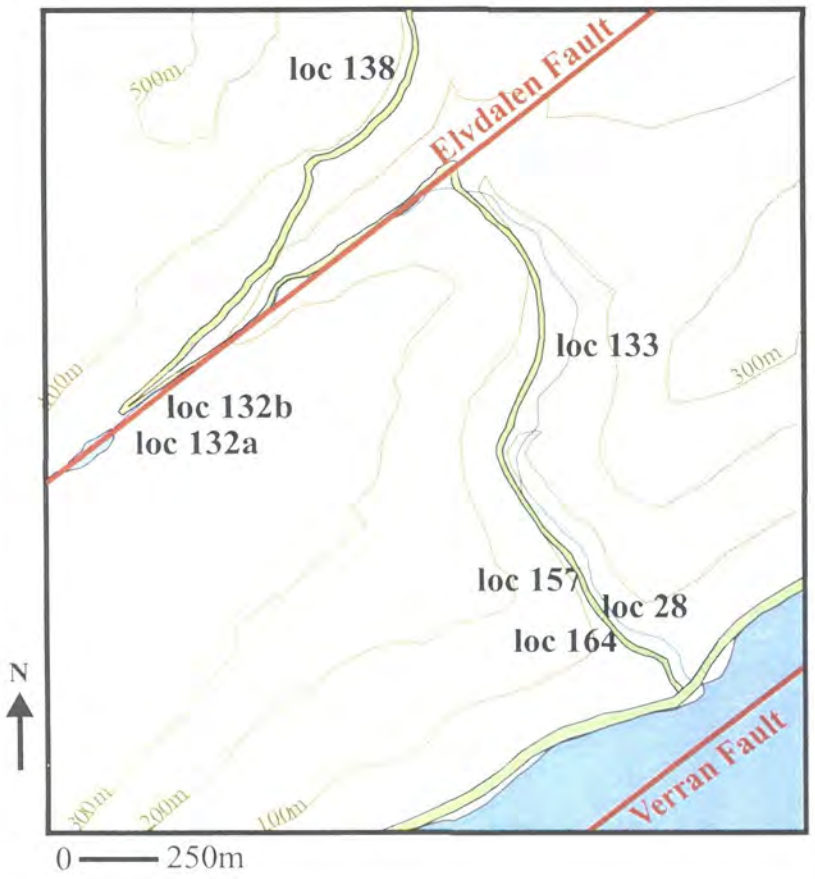

Figure 3.9 Spacing 's' cumulative frequency plots from the Reservoir Road section (VF). (Map contours are in metres)

BLUE data sets = transects carried out parallel to the trend of the VF
RED data sets = transects carried out perpendicular to the trend of the VF
GREEN data sets = vertical transects
(legends on each graph record the locality number, transect number and transect orientation)

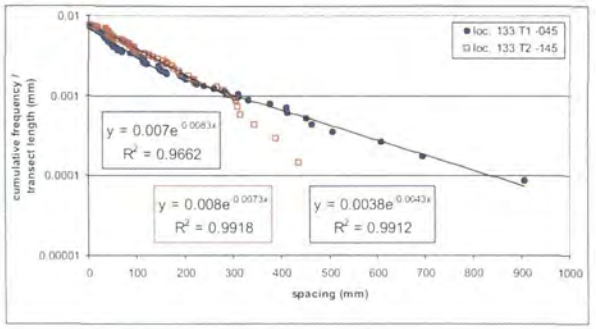

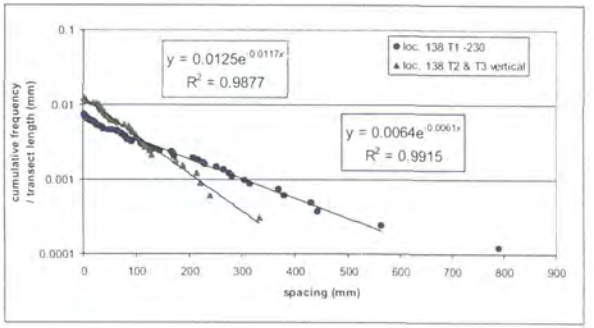

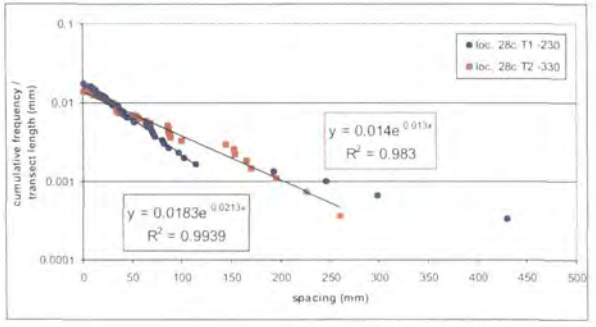

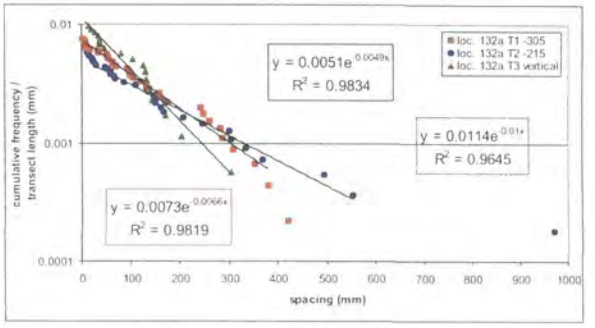

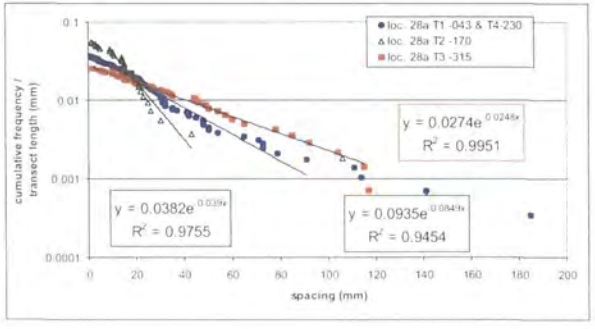

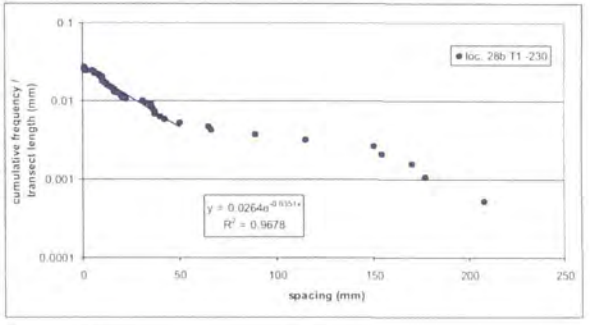

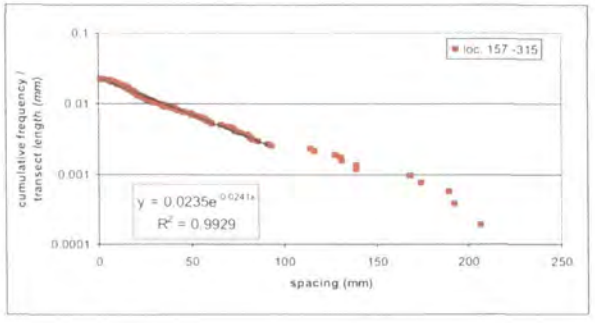

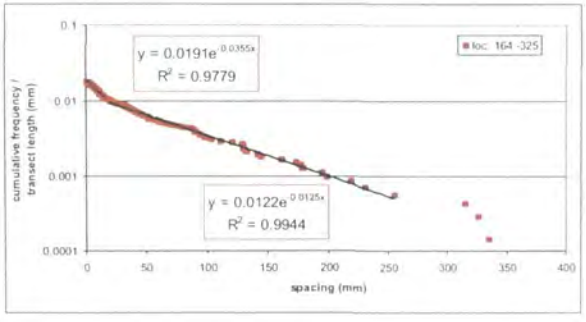

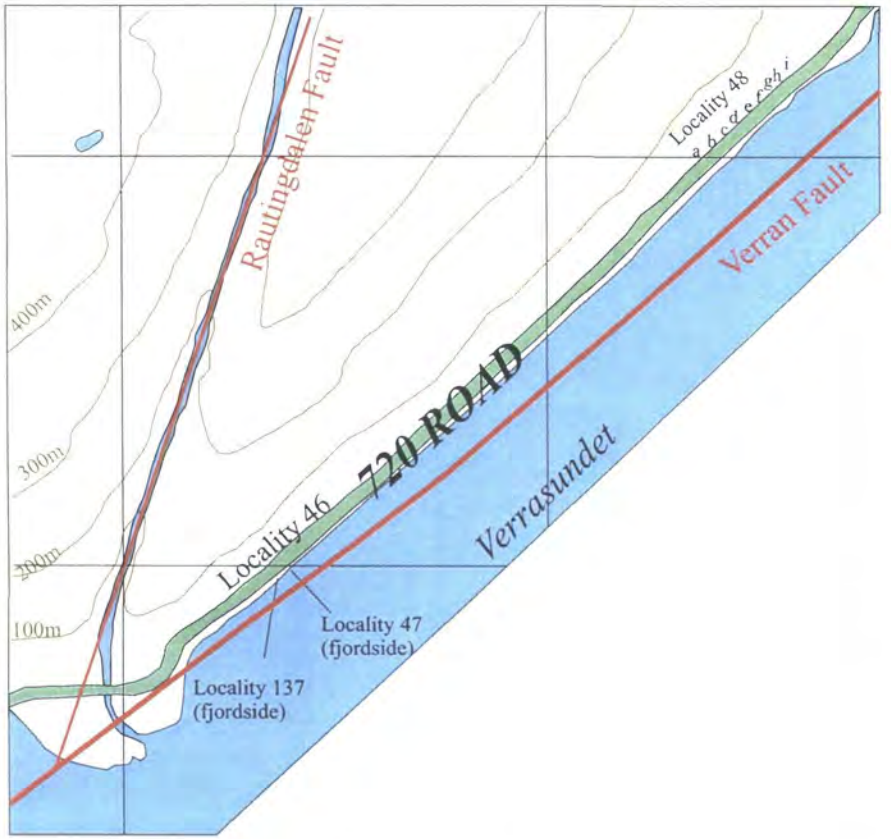

Figure 3.10 Spacing 'v' cumulative frequency plots for localities from the 720 road section (VF) (46, 48b, 48g, 48h, 48i) and Verrasundet fjordside (47 & 137).
(Map contours are in metres)

BLUE data sets = transects carried out parallel to the trend of the VF
RED data sets = transects carried out perpendicular to the trend of the VF
GREEN data sets = vertical transects
(legends on each graph record the locality number, transect number and transect orientation)

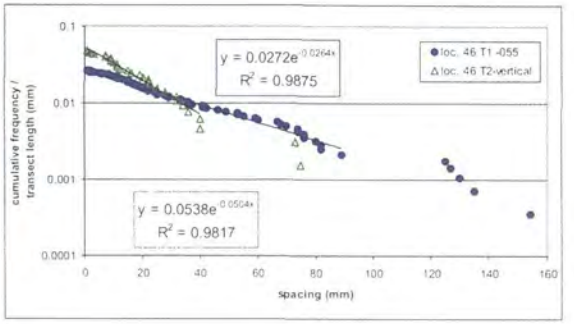

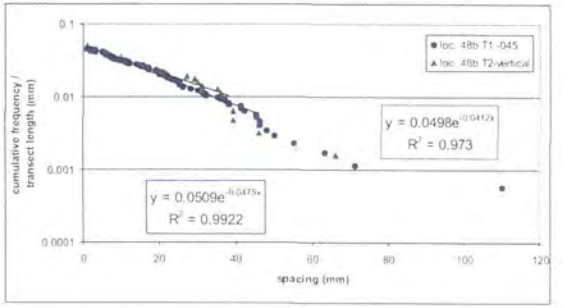

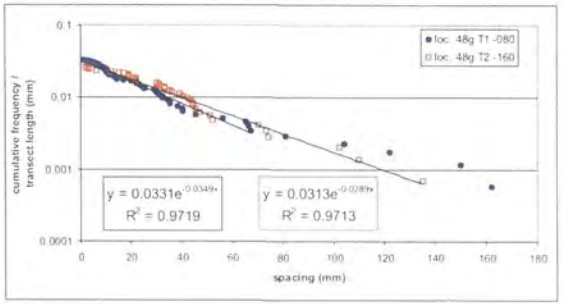

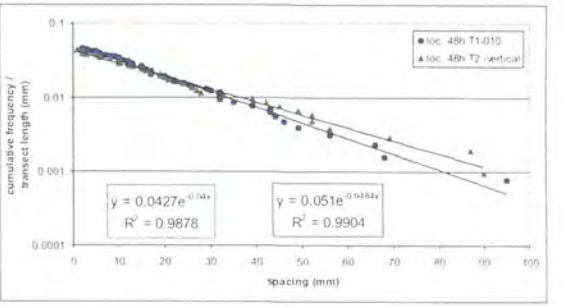

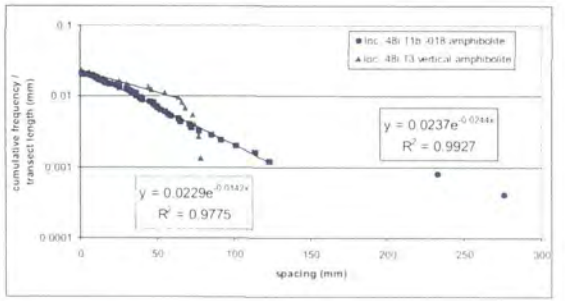

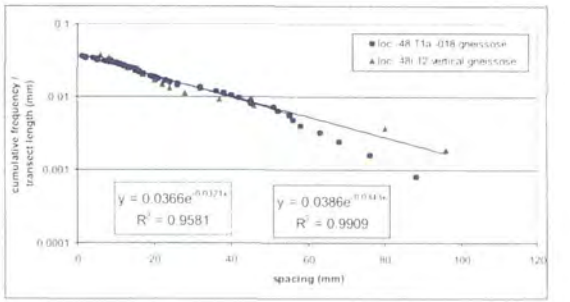

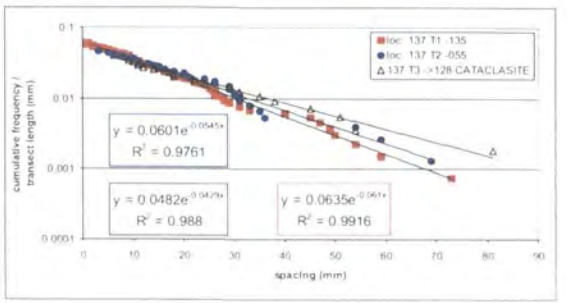

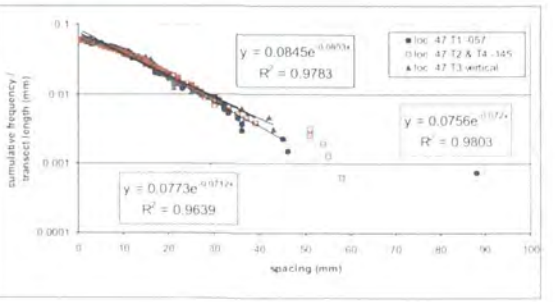

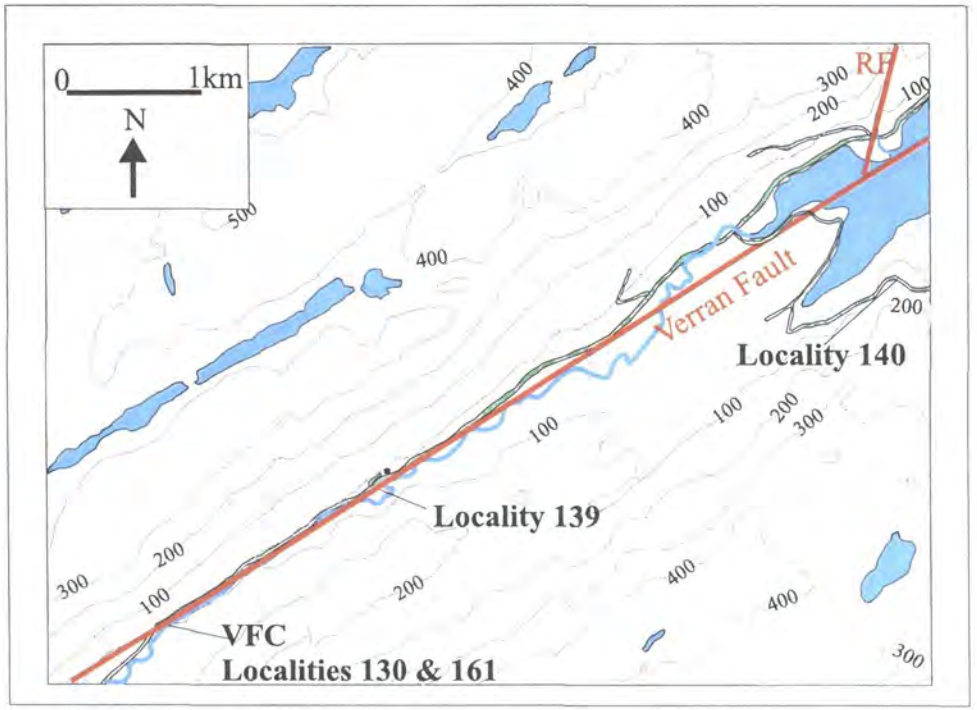

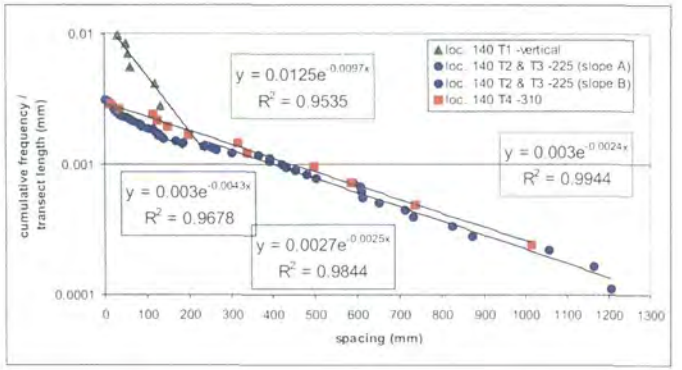

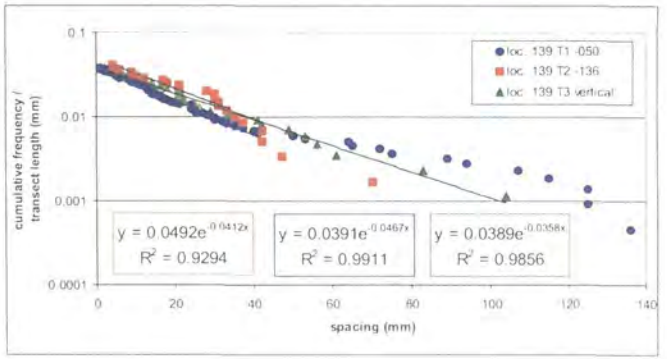

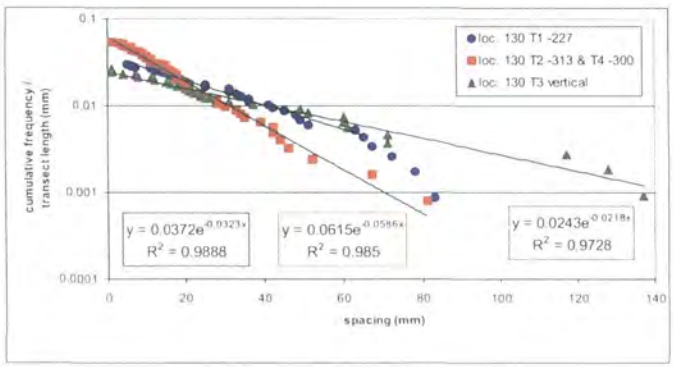

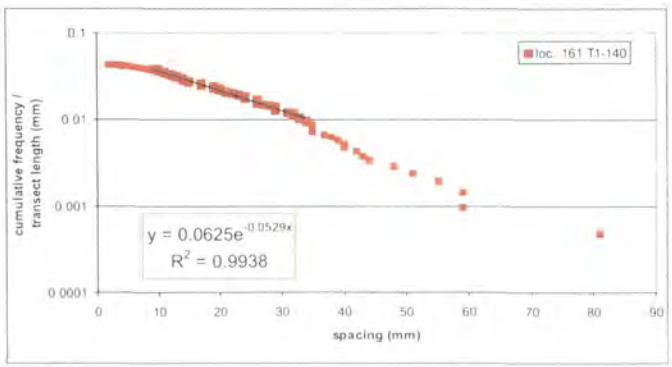

BLUE data sets = transects carried out parallel to the trend of the VF
RED data sets = transects carried out perpendicular to VF trend
GREEN data sets = vertical transects
(legends on each graph record the locality number, transect number and transect orientation)

Figure 3.11 Spacing 'v' cumulative frequency plots for localites from the Verran Fault Core (loc. 130 & 161) and road section (loc. 139); and the Verrabotn Road (loc. 140). (Map contours are in metres)

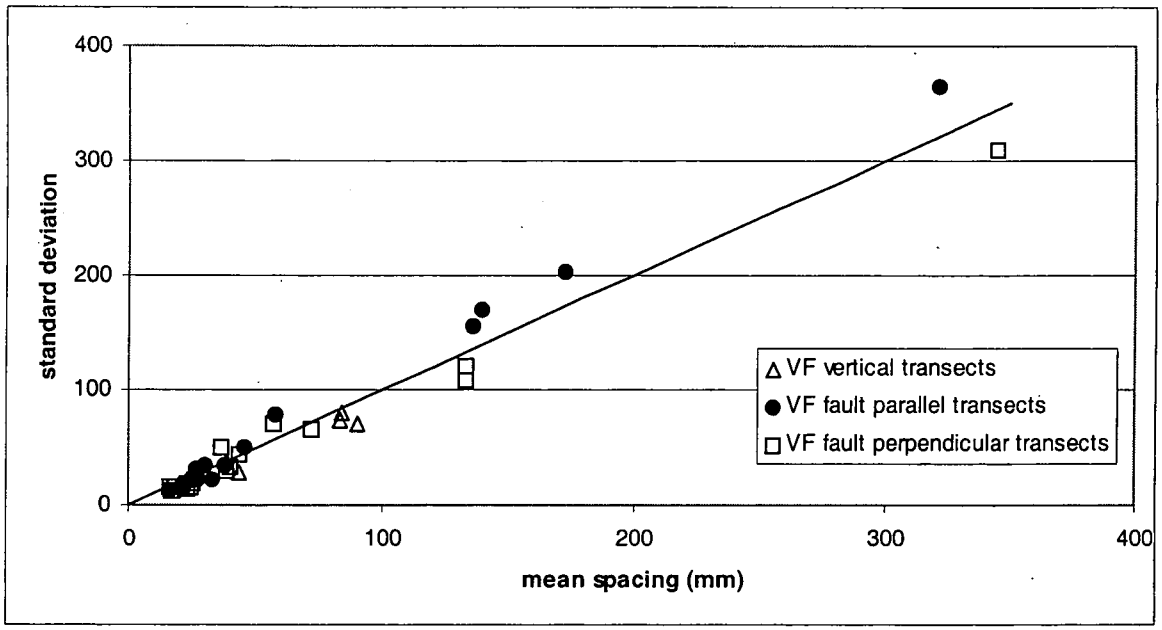

Figure 3.12 Mean 'v' standard deviation plot for VF data

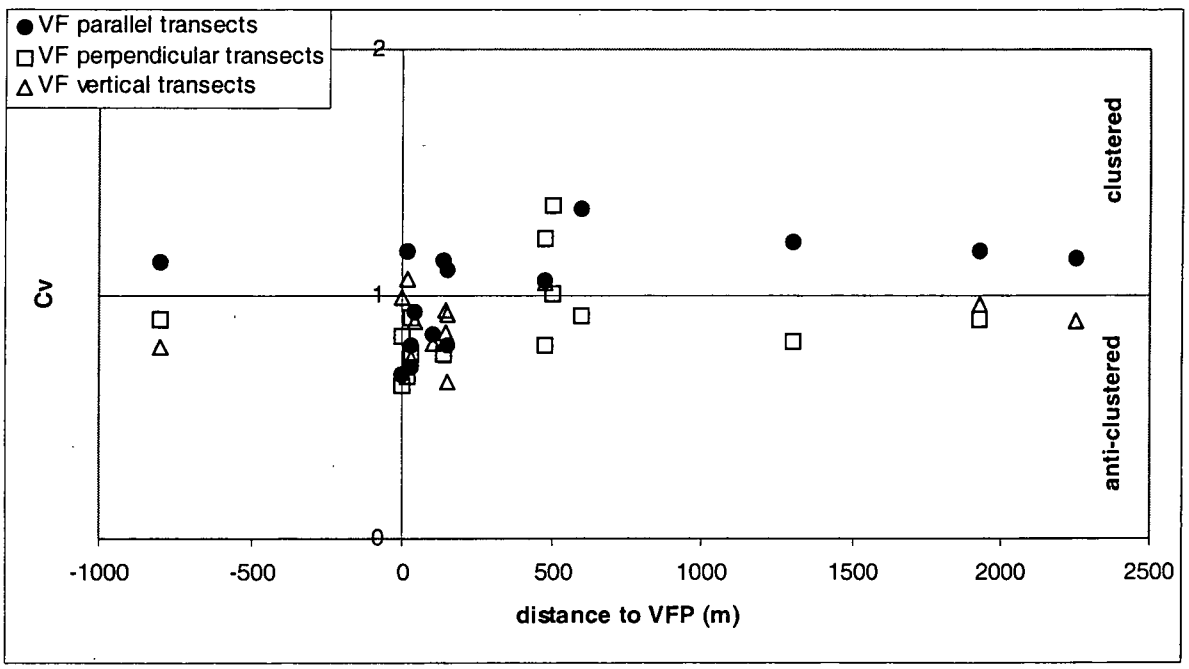

Figure 3.13 Co-efficient of variation 'v' distance plot for VF data

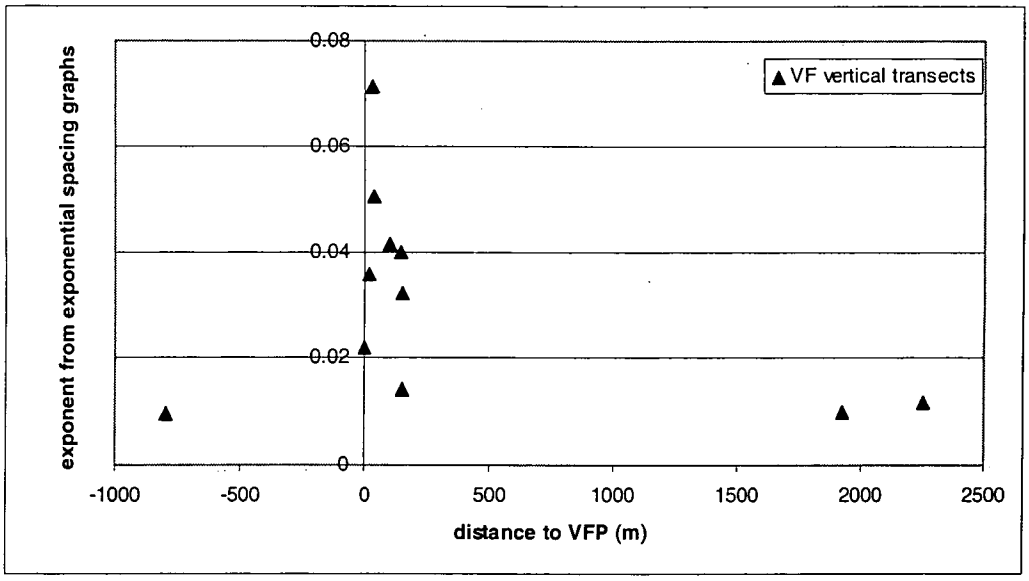

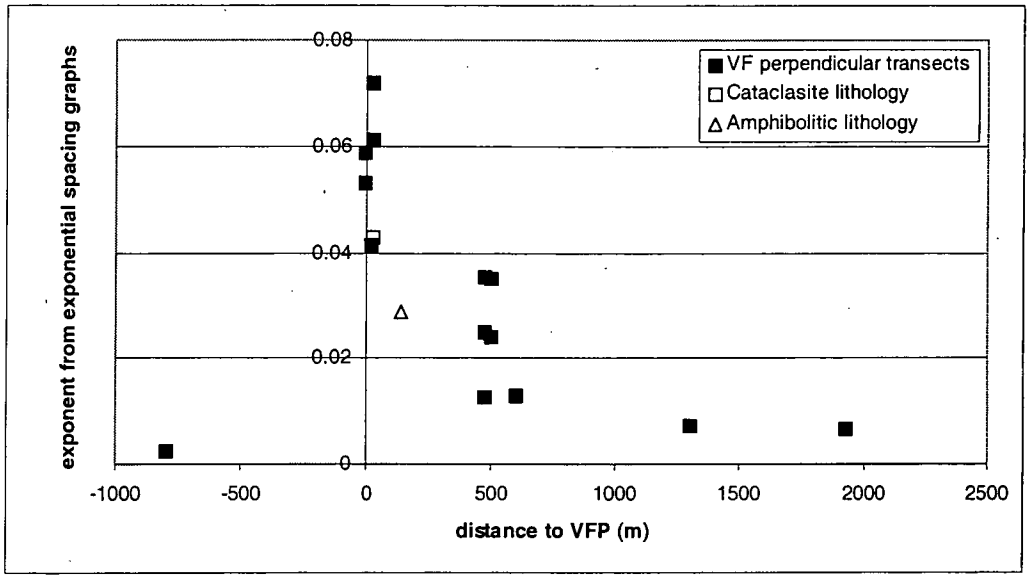

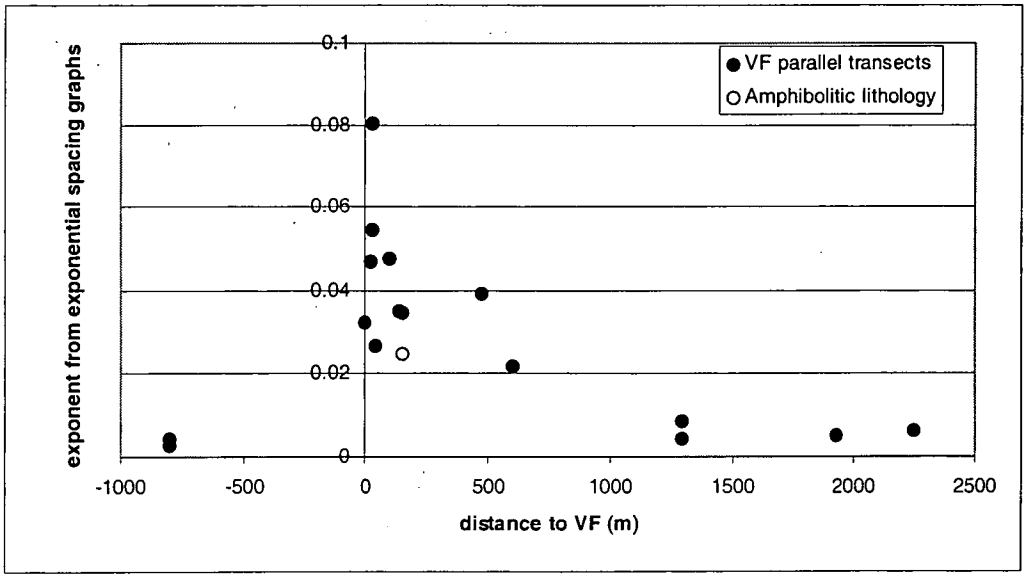

Figure 3.14 Exponential exponent data (from graphs plotted in **Figures 3.9, 3.10, & 3.11**) 'v' perpendicular distance to VFP.

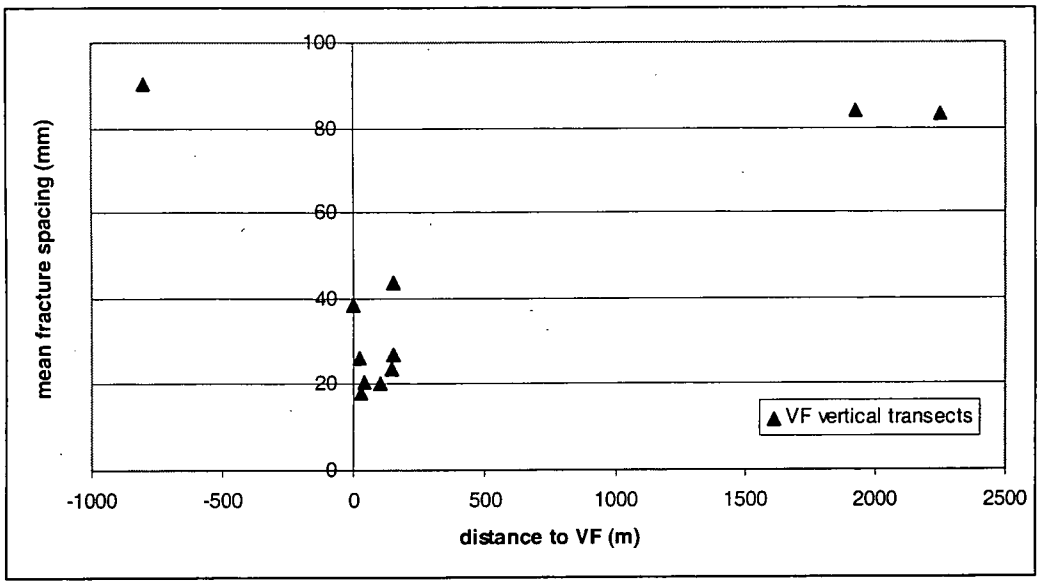

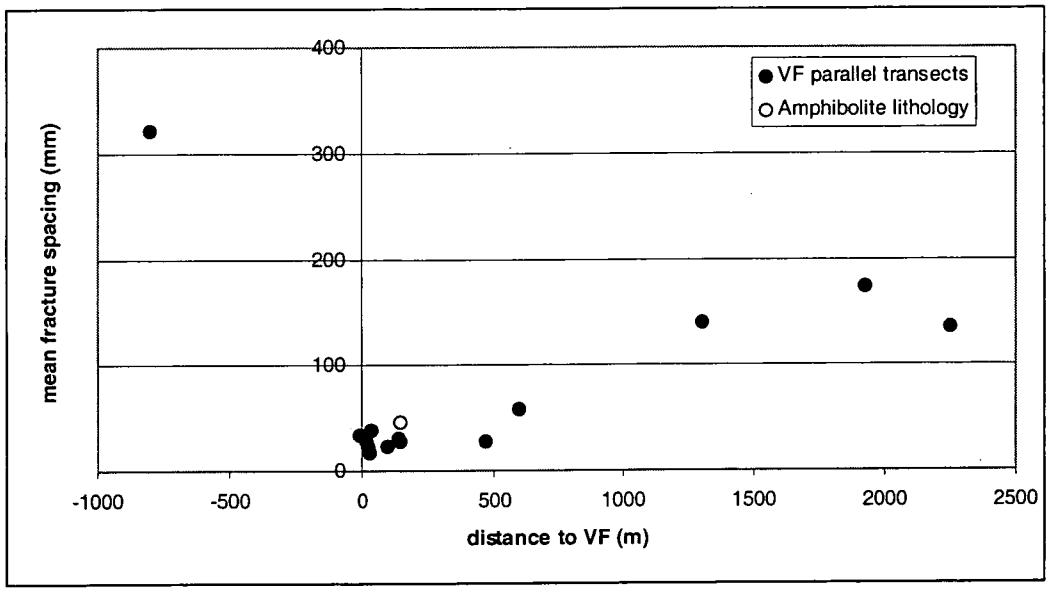

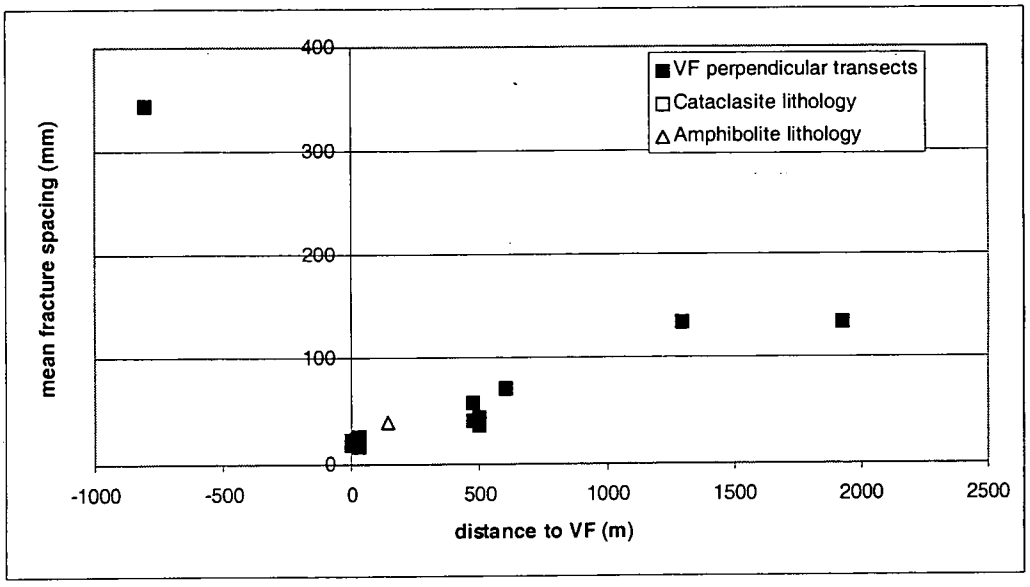

Figure 3.15 Mean fracture spacing 'v' perpendicular distance to VFP for all three transect orientations.

A

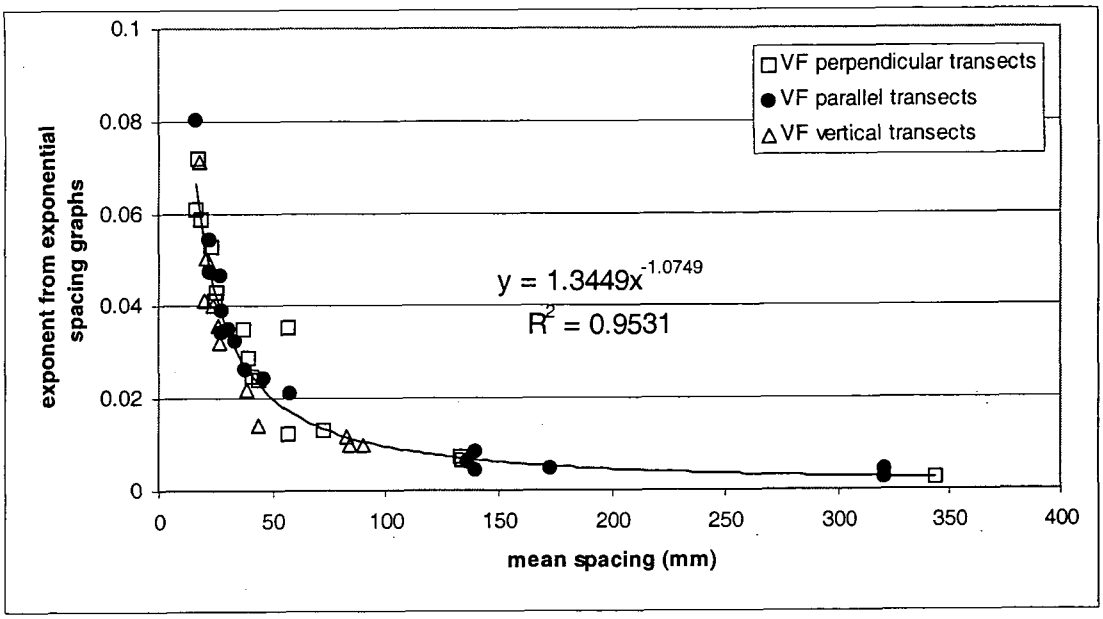

B

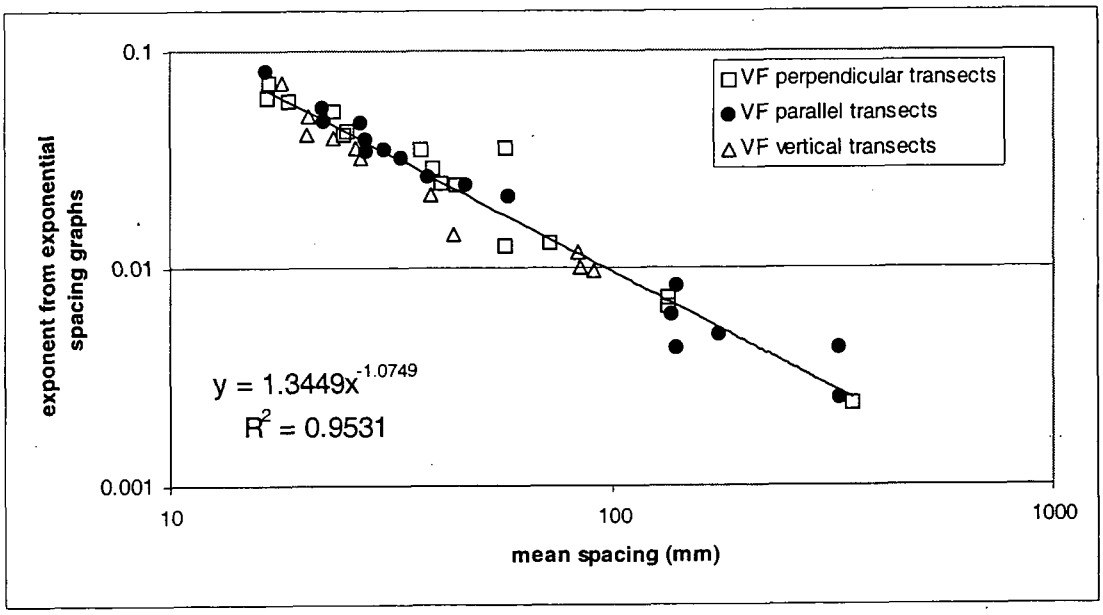

Figure 3.16 Mean fracture spacing 'v' exponential exponent value for data collected adjacent to the VFP.
A – data plotted on linear axes
B – data plotted on logarithmic axes

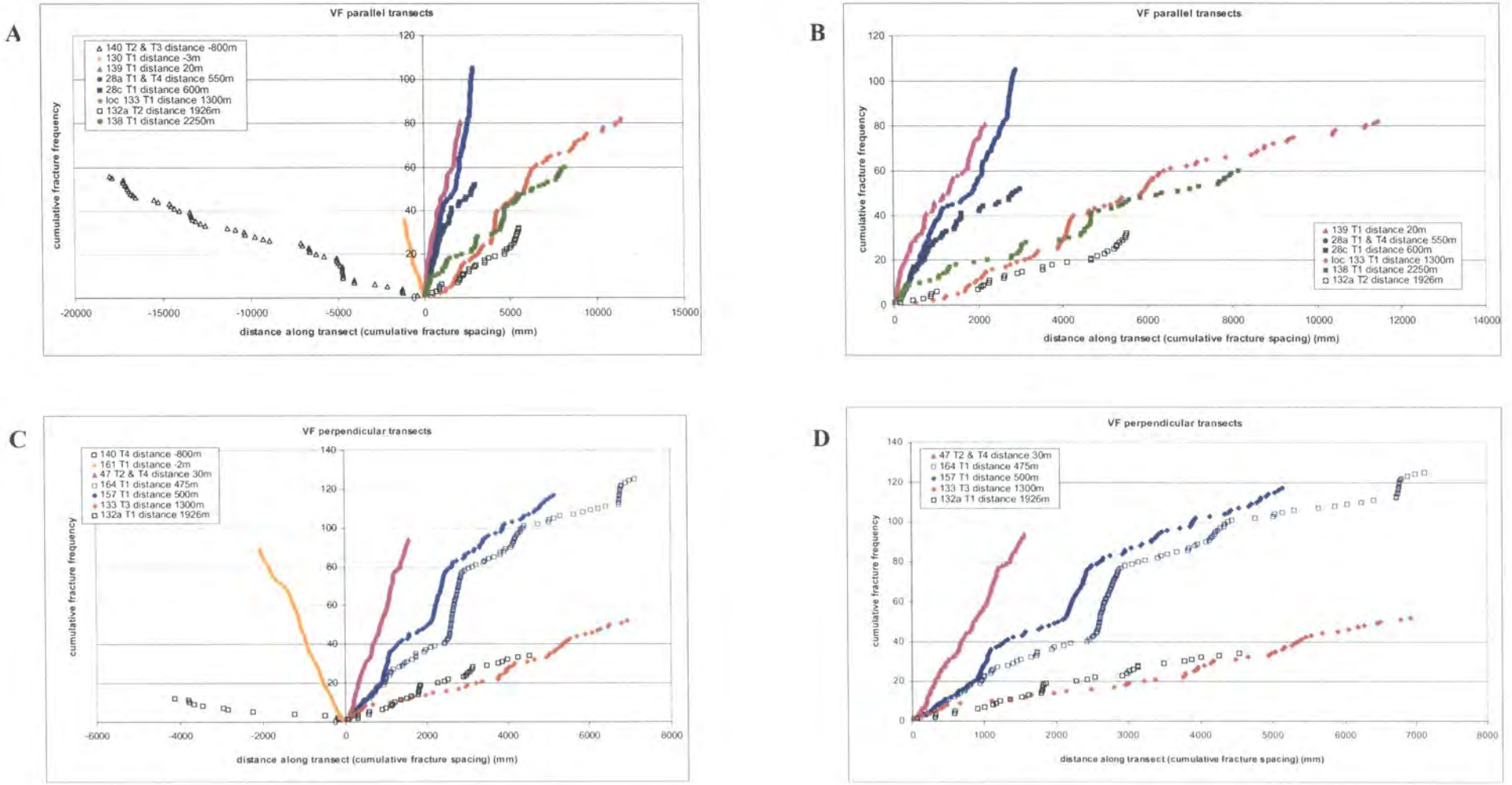

Figure 3.17 Cumulative fracture frequency 'v' distance along 1-dimensional transects orientated both parallel and perpendicular to the VF trend (negative distances represent localities south of the VFP, positive distances represent localities north of the VFP).

A – all transects orientated parallel to the MTFC trend.

B – transects orientated parallel to the MTFC from localities to the NW of the VFP.

C – all transects orientated perpendicular to the MTFC trend.

D – transects orientated perpendicular to the MTFC from localities to the NW of the VFP.

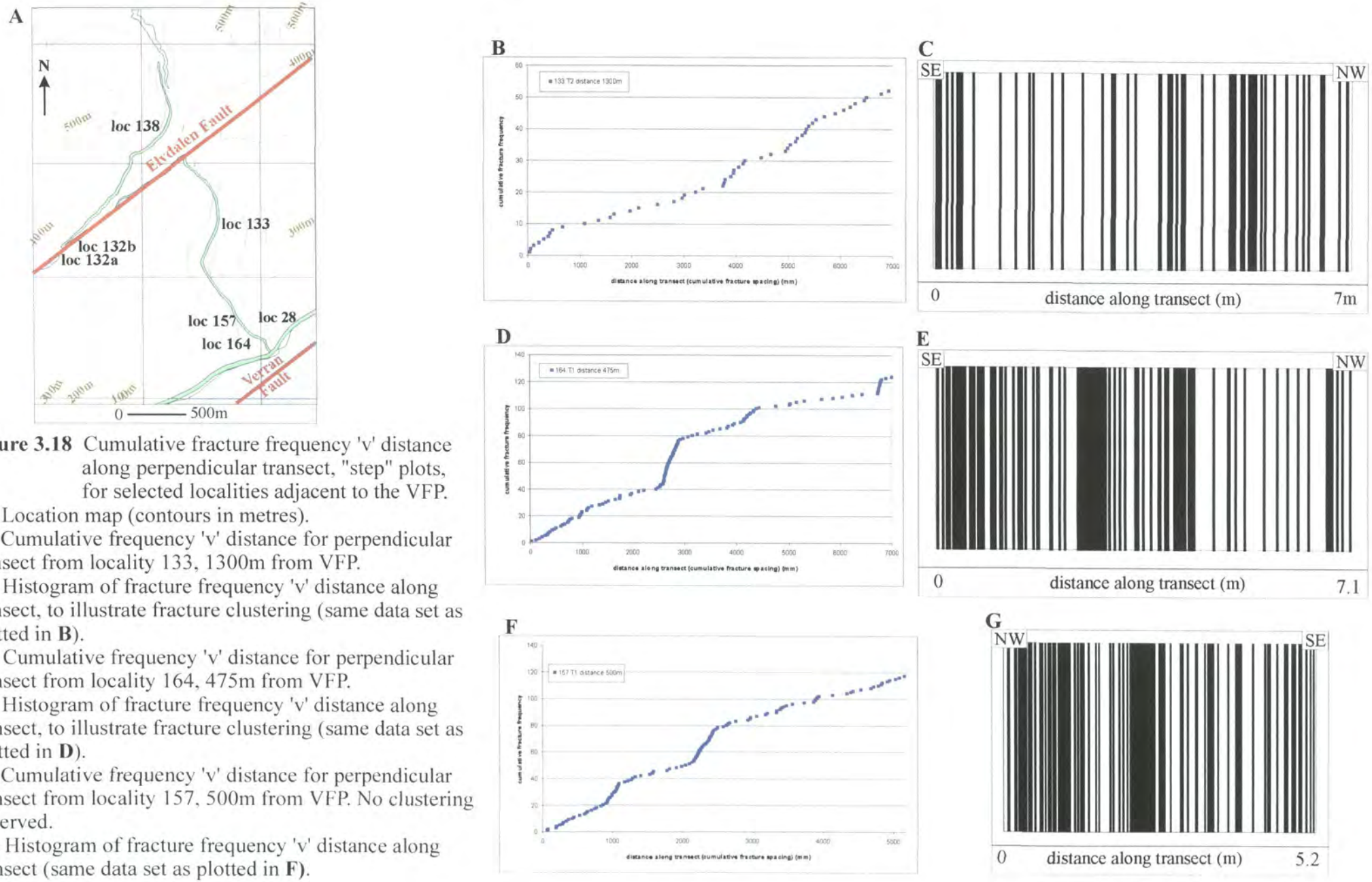

Figure 3.18 Cumulative fracture frequency 'v' distance along perpendicular transect, "step" plots, for selected localities adjacent to the VFP.

A - Location map (contours in metres).

B - Cumulative frequency 'v' distance for perpendicular transect from locality 133, 1300m from VFP.

C - Histogram of fracture frequency 'v' distance along transect, to illustrate fracture clustering (same data set as plotted in **B**).

D - Cumulative frequency 'v' distance for perpendicular transect from locality 164, 475m from VFP.

E - Histogram of fracture frequency 'v' distance along transect, to illustrate fracture clustering (same data set as plotted in **D**).

F - Cumulative frequency 'v' distance for perpendicular transect from locality 157, 500m from VFP. No clustering observed.

G - Histogram of fracture frequency 'v' distance along transect (same data set as plotted in **F**).

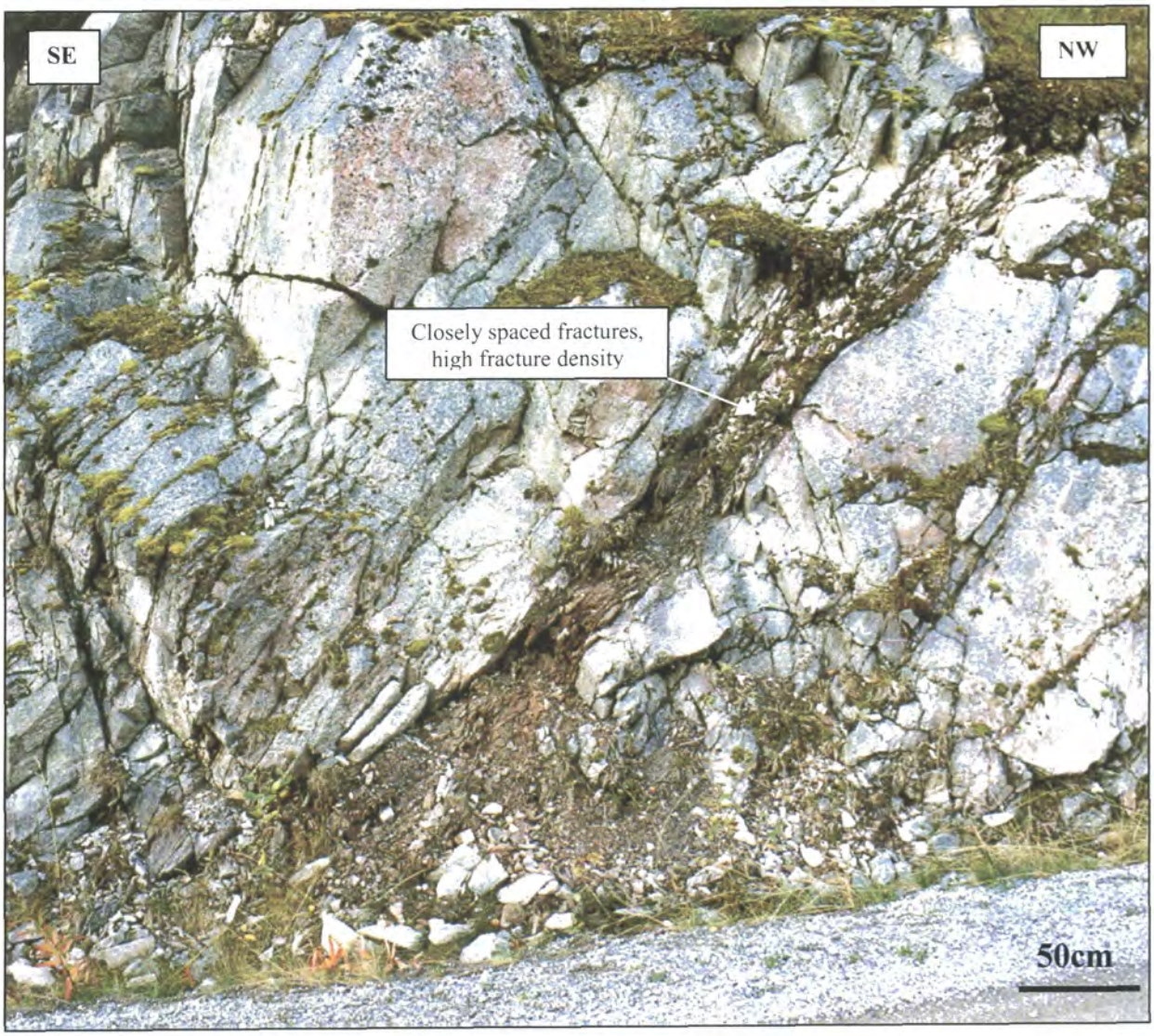

Figure 3.19 ENE-WSW trending zone of closely spaced fractures and high fracture density ~ 500m from VFP. This zone corresponds to a relatively steep slope on the step plot from locality 157 illustrated in **Figure 3.17 c & d and Figure 3.18 f & g**. Pink coloration is due to zeolite and calcite mineralisation. (cross-section view)

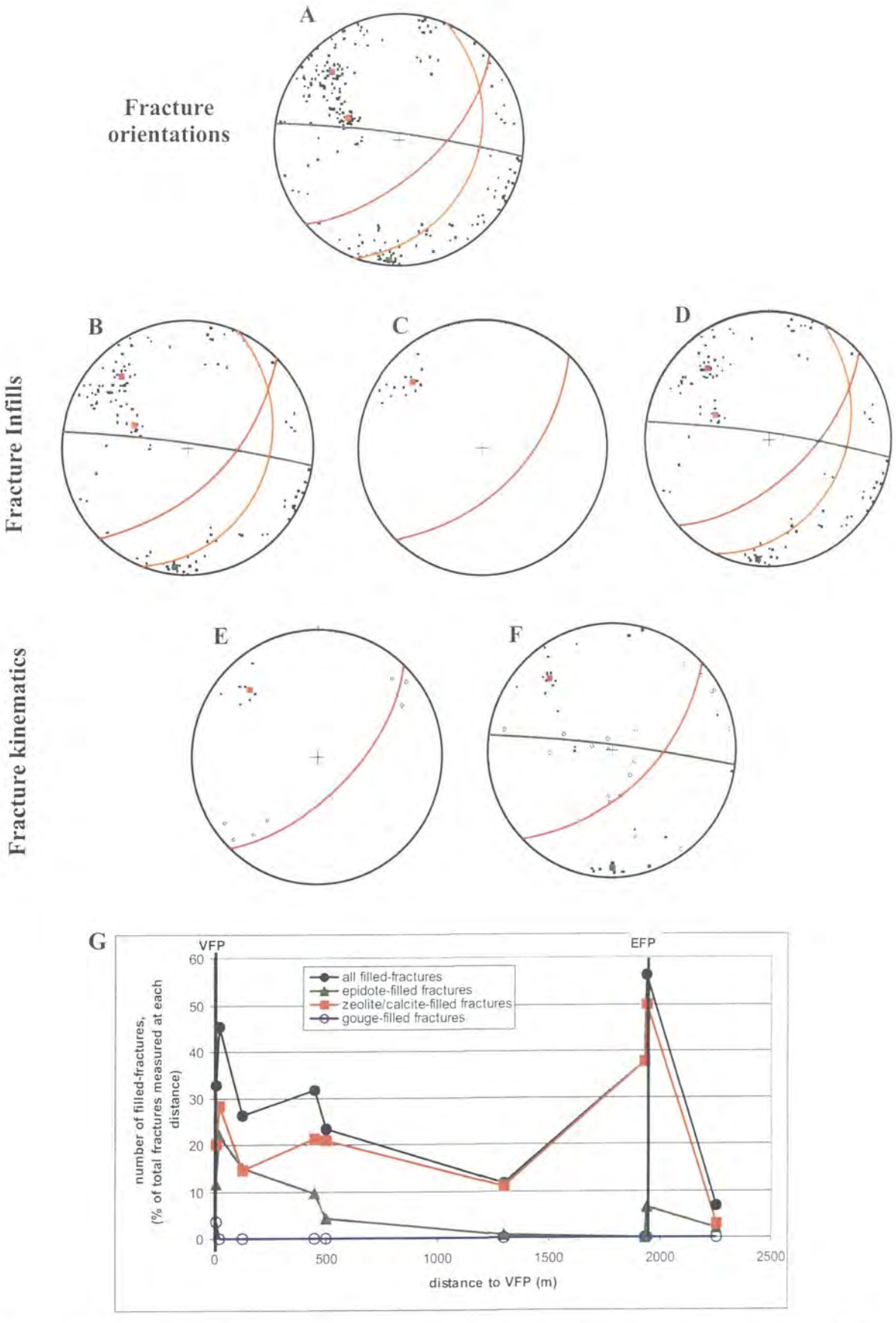

Figure 3.20 Fracture orientations, infills and kinematics data collected adjacent to the EFP (all stereonets are plotted as poles to fracture planes)

A - All fracture orientations measeured adjacent to the EFP. n = 212, mean girdles = 027/ 37 E, 048/ 67 S, 098/ 86 N
B - All filled-fractures adjacent to the EFP. n = 119, mean girdles = 022/ 36 E, 045/ 65 S, 098/ 87 N
C - All fractures filled with epidote-cataclasite adjacent to the EFP. n = 14, mean girdle = 044/ 66 E
D - All fractures filled with zeolite/calcite adjacent to the EFP. n = 106, mean girdles = 026/ 38 E, 047/ 65 S, 098/ 86 N
E - Fractures filled with epidote-cataclasite with slickenfibre lineations. n = 7, mean girdle = 044/ 66 E
F - Fractures filled with zeolite/calcite with slickenfibre lineations. n = 29, mean girdles = 046/ 64 S, 097/ 86 N
G - Distribution of filled-fractures adjacent to the EFP and the VFP

Figure 3.21 Photographs illustrating infilled fractures and kinematic indicators adjacent to the EFP (all from road to Ormsetvatnet reservoir).
A - zeolite mineralisation on a partially exposed fracture surface (plan view).
B - Zeolite veins displaced by zeolite-filled fractures displaying dextral strike-slip (plan view).
C - Dip-slip zeolite slickenfibres (white arrow) on an E-W trending fracture plane (cross-section view).
D - Dip-slip/oblique zeolite slickenfibres (white arrow) on an ENE-WSW trending fracture plane (cross-section view).

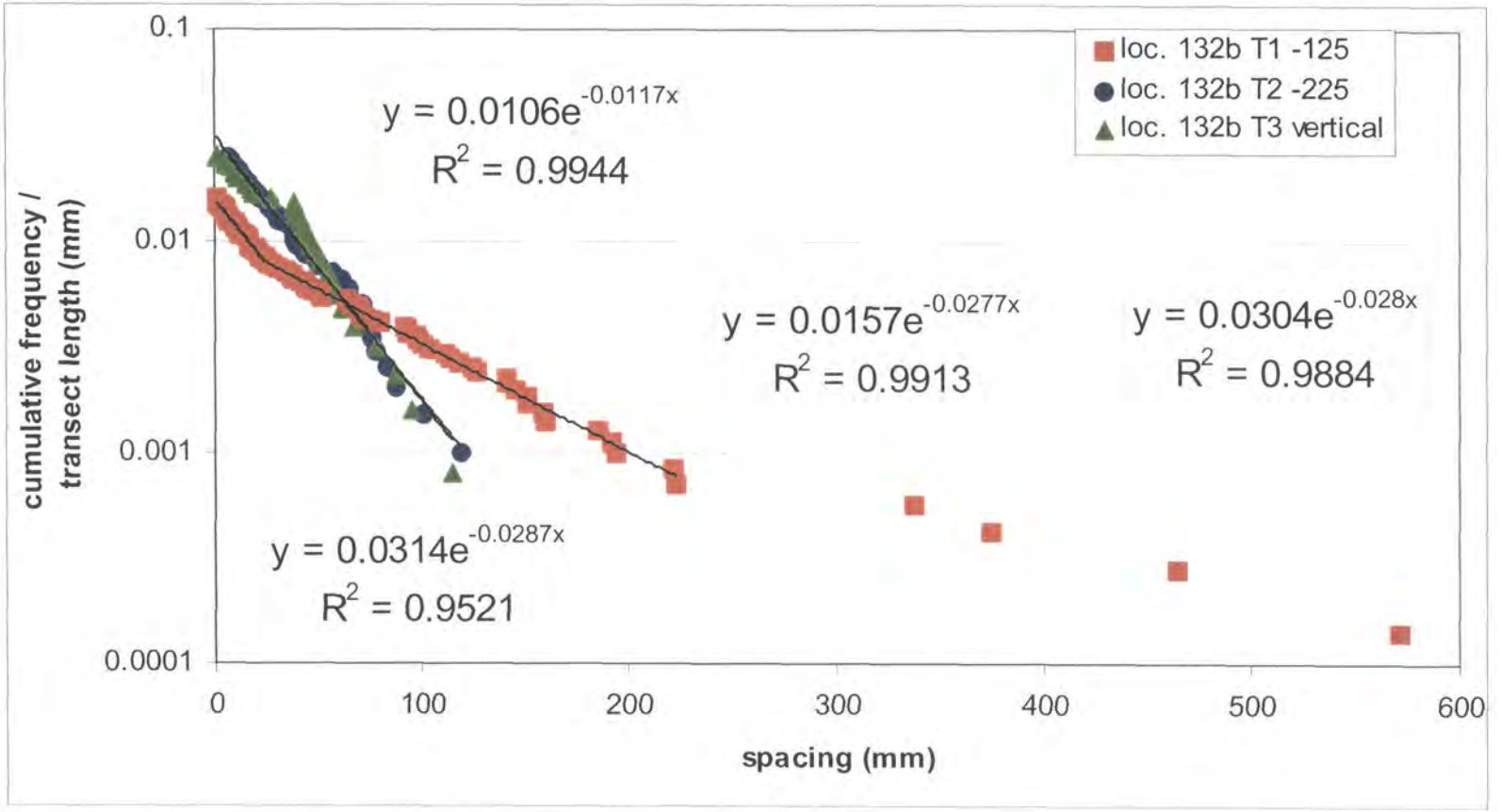

Figure 3.22 Spacing 'v' cumulative frequency plot for locality 132b, 1m SW of the EFP (transect orientated parallel to EF trend shows 2 slopes, ∴ 2 equations shown)

BLUE data set = transect orientated parallel to the trend of the EFP
RED data set = transect orientated perpendicular to the trend of the EFP
GREEN data set = vertical transect

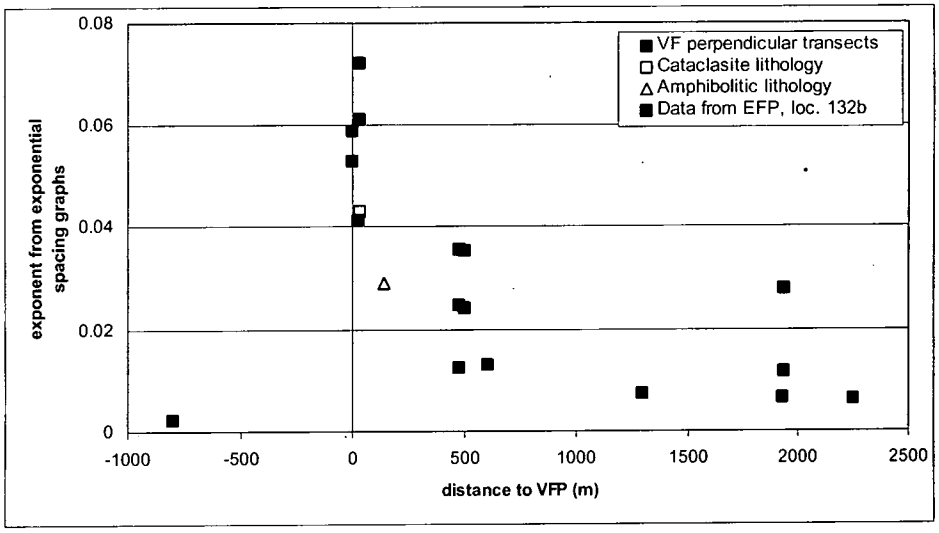

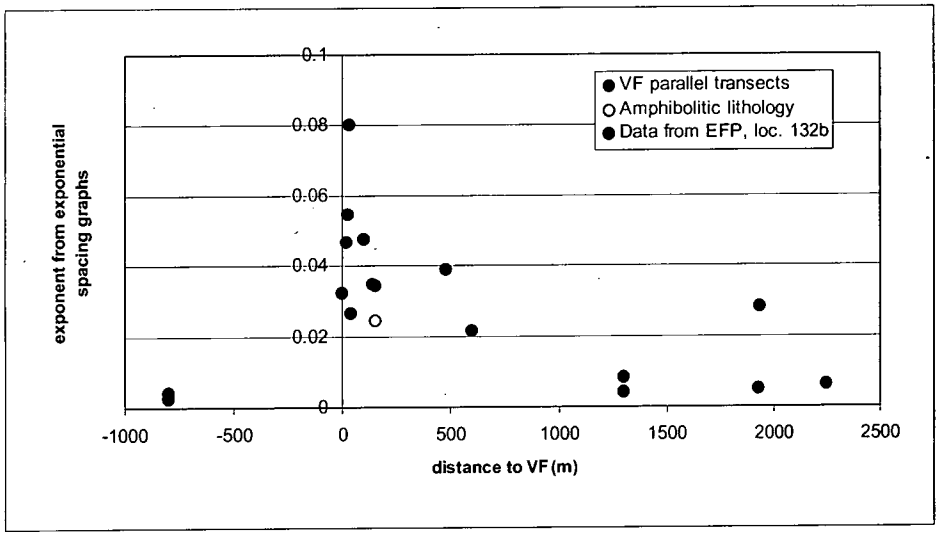

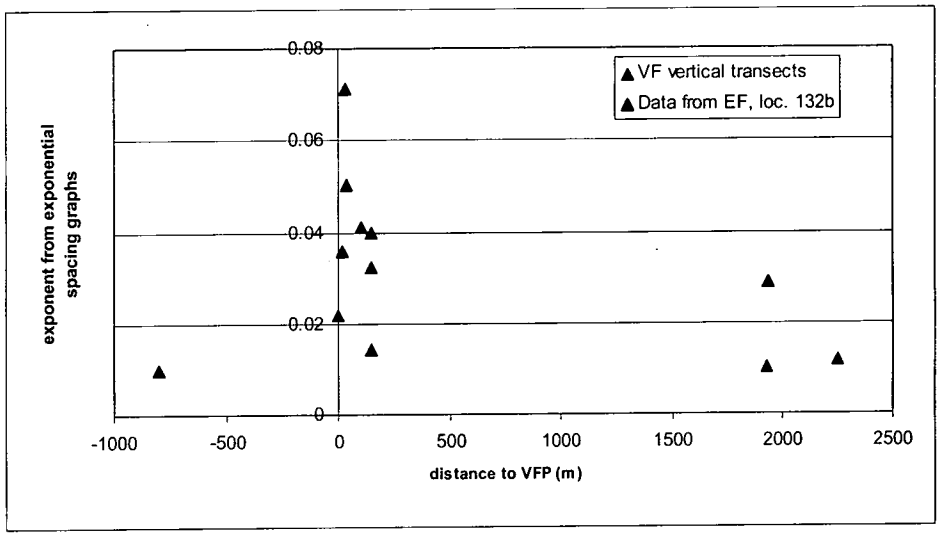

Figure 3.23 Exponential exponent data 'v' distance to VFP for data collected adjacent to the EFP and the VFP.

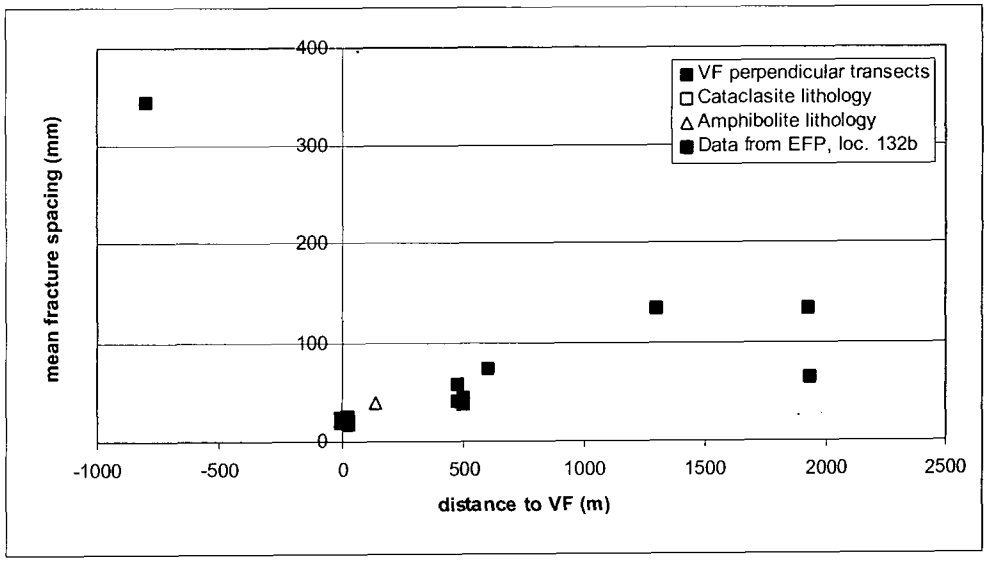

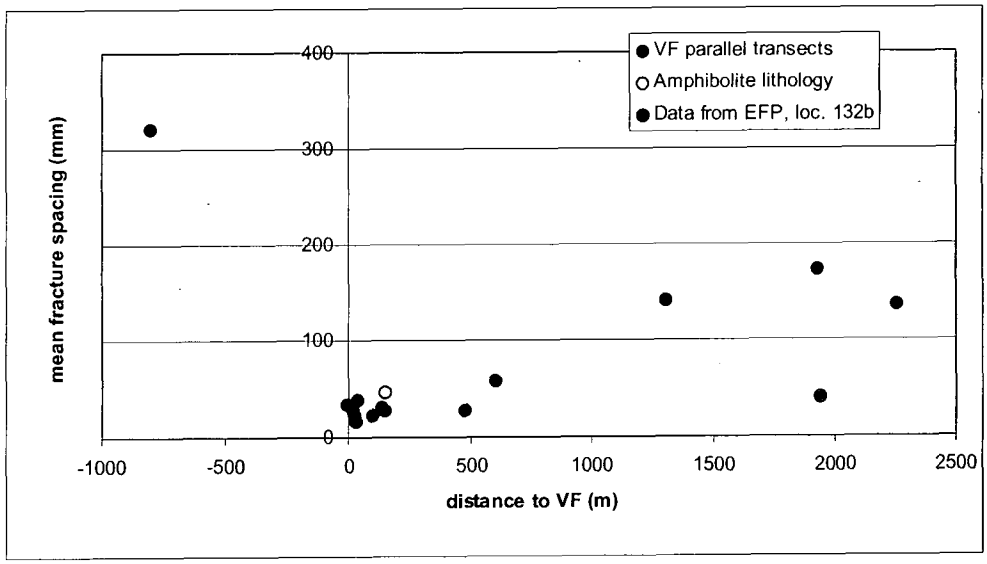

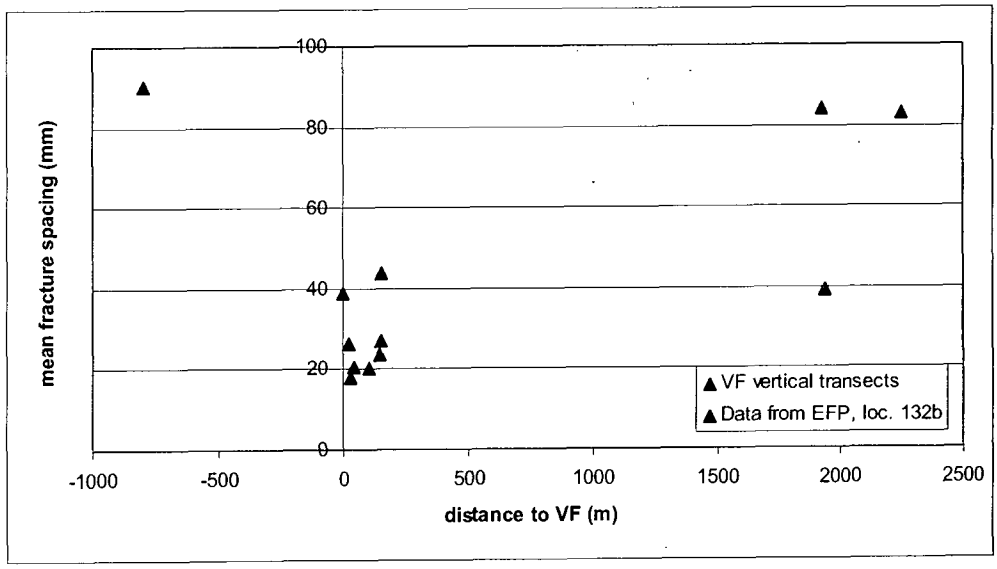

Figure 3.24 Mean spacing 'v' distance to VFP for data collected adjacent to the EFP and the VFP.

A

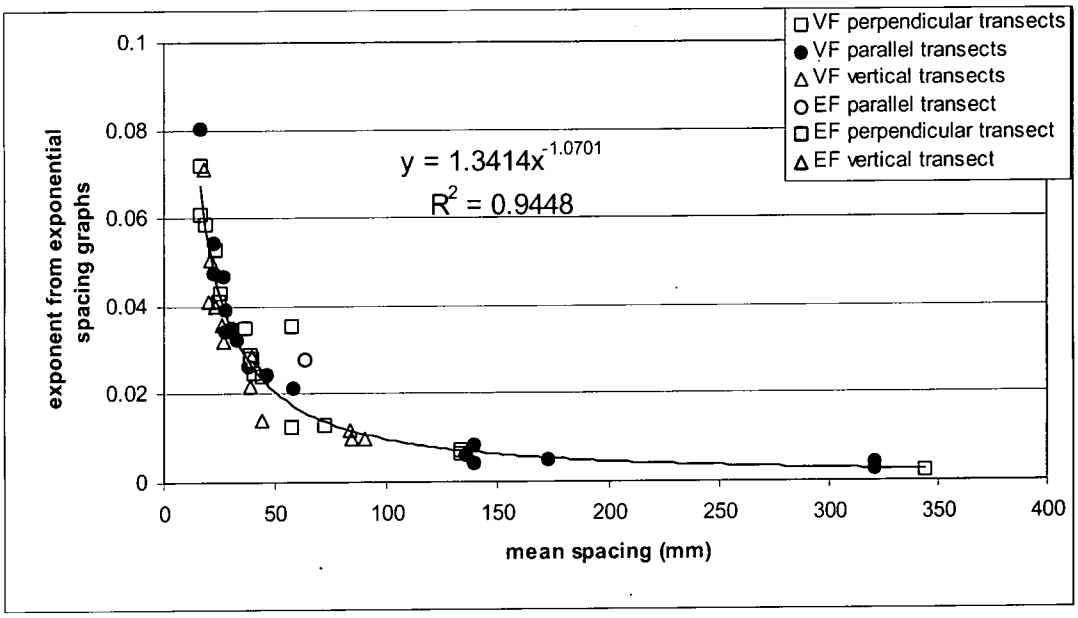

B

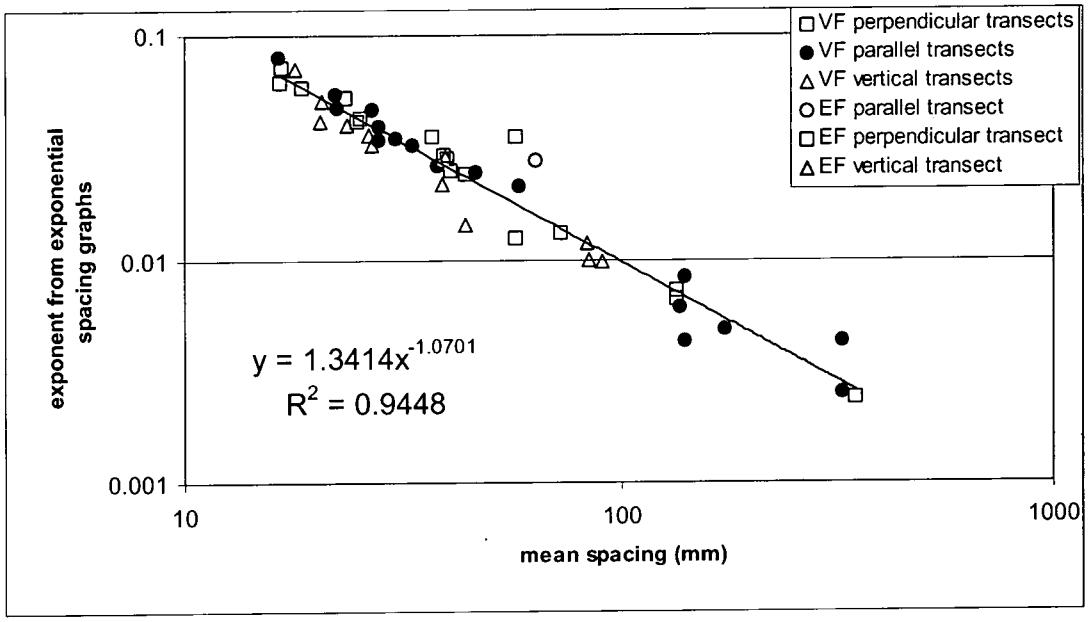

Figure 3.25 Mean fracture spacing 'v' exponent from exponential spacing graphs
A – data plotted on linear axes
B – data plotted on logarithmic axes

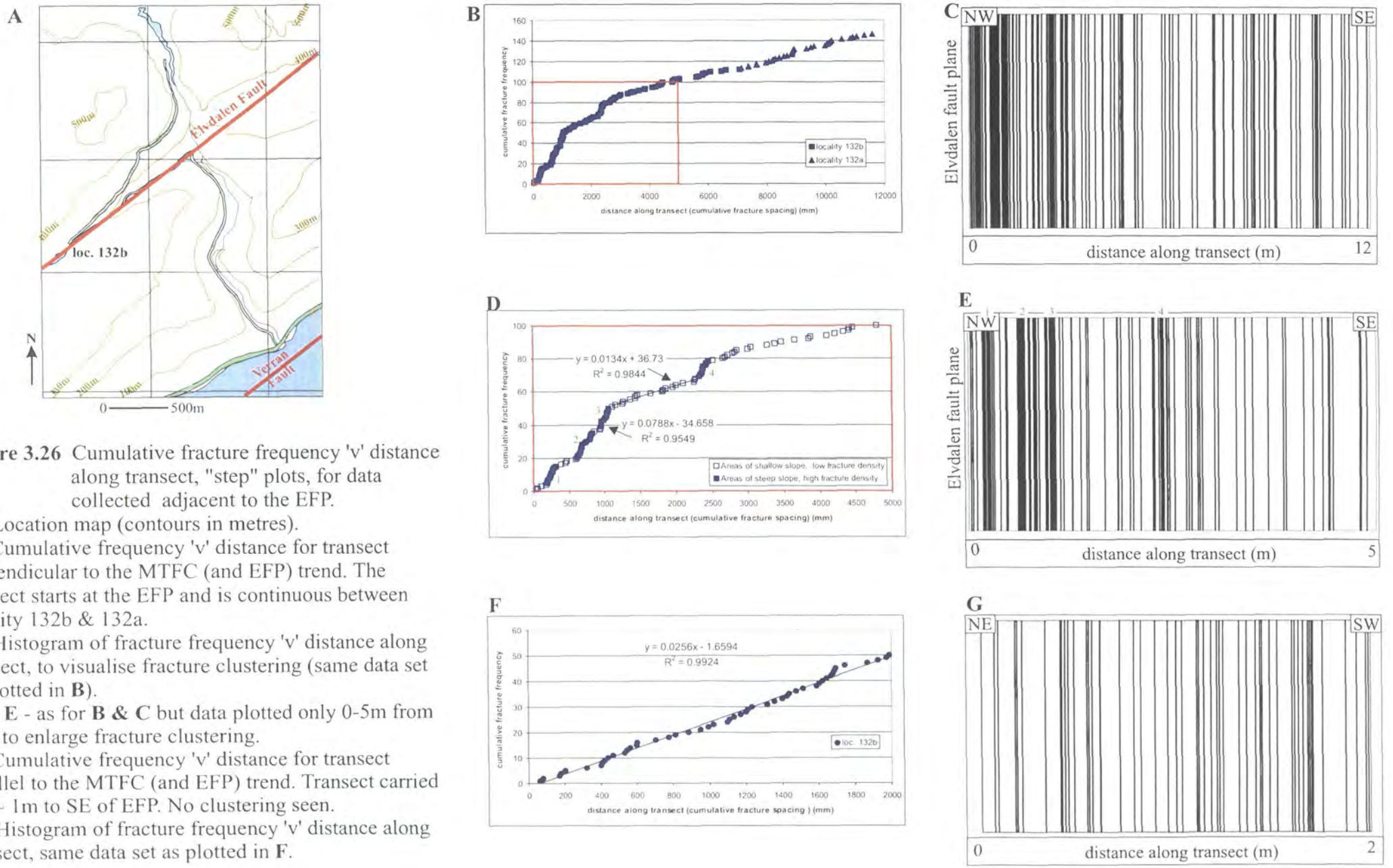

Figure 3.26 Cumulative fracture frequency 'v' distance along transect, "step" plots, for data collected adjacent to the EFP.

A - Location map (contours in metres).

B - Cumulative frequency 'v' distance for transect perpendicular to the MTFC (and EFP) trend. The transect starts at the EFP and is continuous between locality 132b & 132a.

C - Histogram of fracture frequency 'v' distance along transect, to visualise fracture clustering (same data set as plotted in **B**).

D & E - as for **B & C** but data plotted only 0-5m from EFP to enlarge fracture clustering.

F - Cumulative frequency 'v' distance for transect parallel to the MTFC (and EFP) trend. Transect carried out ~ 1m to SE of EFP. No clustering seen.

G - Histogram of fracture frequency 'v' distance along transect, same data set as plotted in **F**.

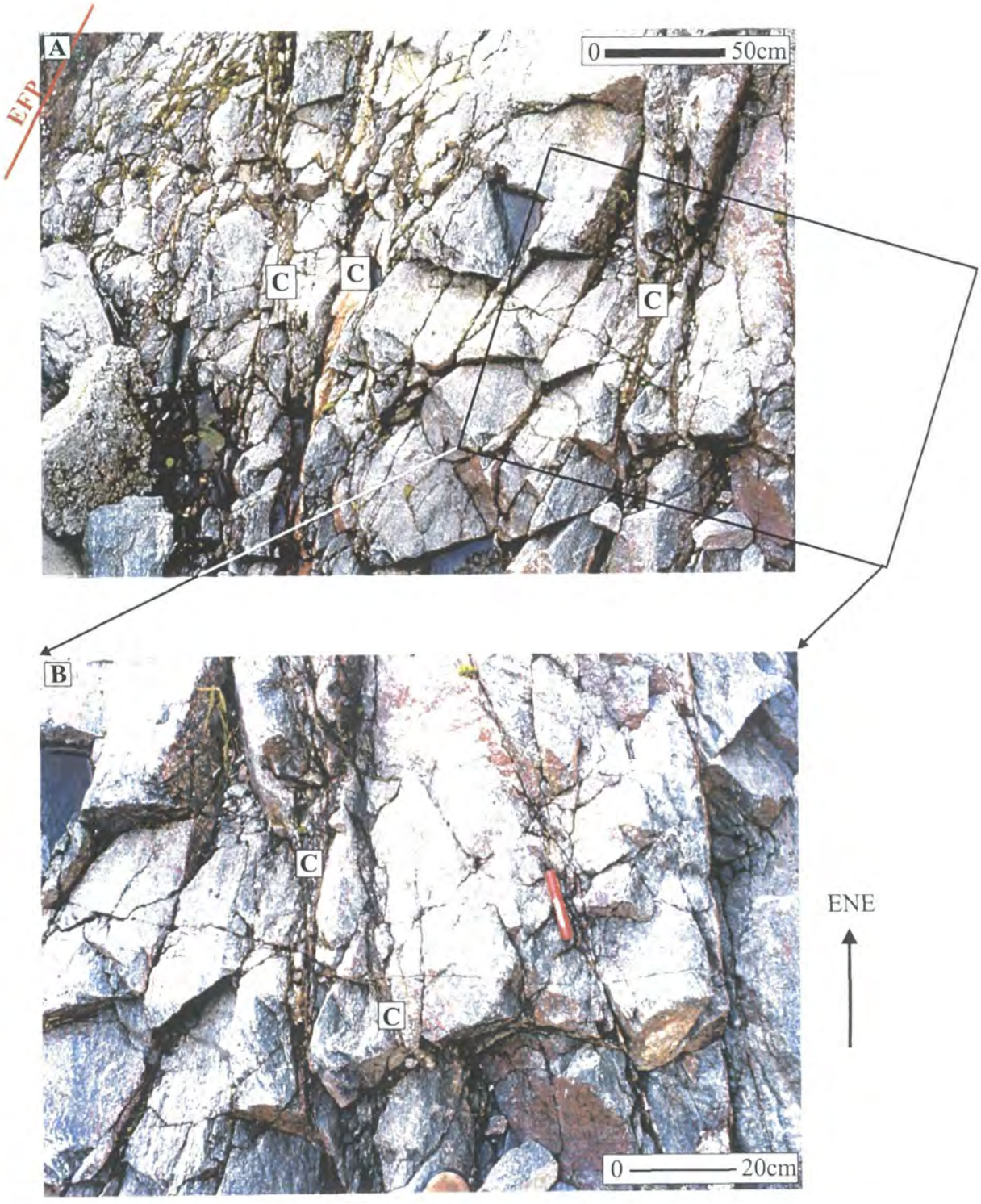

Figure 3.27 Photographs illustrating fracture density adjacent to the EFP (both plan view)
A - Illustrates increased fracture density towards EFP (top left-hand corner of photo) (C) = cluster of fractures parallel to EFP and MTFC trend. Orange colouration is zeolite mineralisation
B - Enlarged view of fault parallel fracture clusters (C). Red/orange colouration is zeolite mineralisation.

1

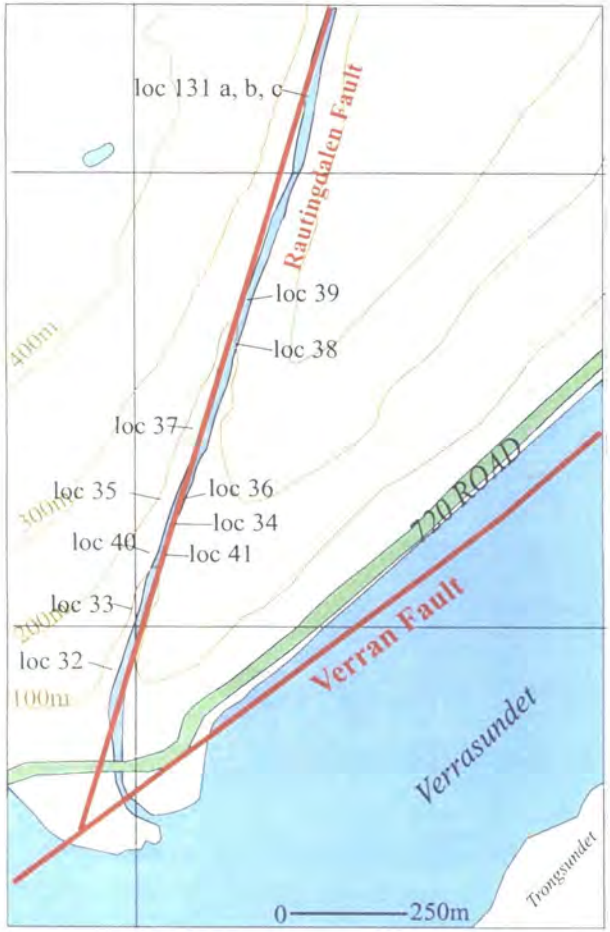

2

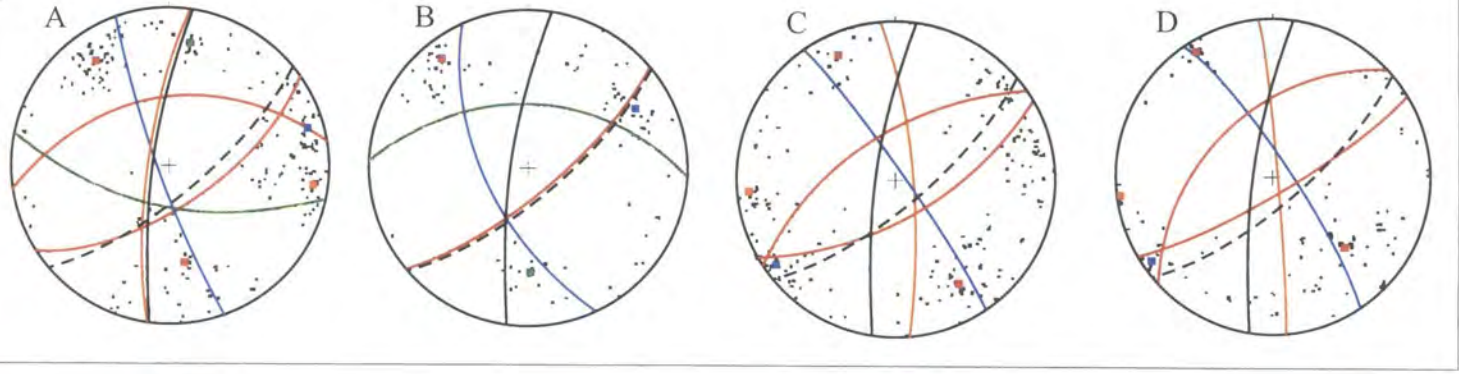

3

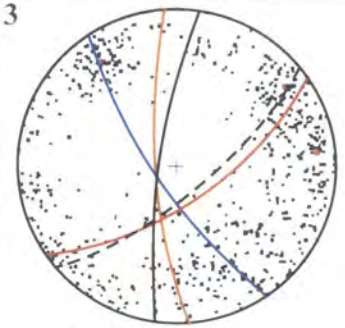

all fracture data, RF, (n = 622)
red = 055/ 70 S
blue = 146/ 79 W
orange = 176/ 79 W

4

		A	B	C	D
	Place	Rautingdalen	Rautingdalen	Rautingdalen	Rautingdalen
	Locality	32	33	131a&b	131c
	Distance to RFP	2	5	1	0.5
	Distance to VFP	235-265	315	1000	1000
	no. data points	236	96	188	102
	lithology	gneiss	gneiss	gneiss	cataclasite
mean girdles to fracture orientations	**RED** (ENE-WSW)	056/ 68 S 079/ 55 N	050/ 76 S	060/ 70 S 056/ 67 N	059/ 81 S 047/ 56 N
	BLUE (NNW-SSE)	158/ 84 W	155/ 67 W	145/ 85 E	146/ 81 E
	ORANGE (N-S)	008/ 79 W	-	175/ 81 E	175/ 88 E
	GREEN (E-W to ESE-WNW)	102/ 69 S	092/ 57 N	-	-

NB on each stereonet, the mean plane for the **VFP** is marked with a **black dashed girdle (050/ 75 S)**, and the mean plane for the **RFP** is marked with a **black girdle (008/ 81 W)**

Figure 3.28 Fracture orientations adjacent to the Rautingdalen Fault
1 - map of localities (contours are in metres)
2 - stereographic projections of fracture orientations from each locality
3 - all fracture orientations measured adjacent to the RFP
4 - table of fracture orientation data from stereonets A, B, C and D

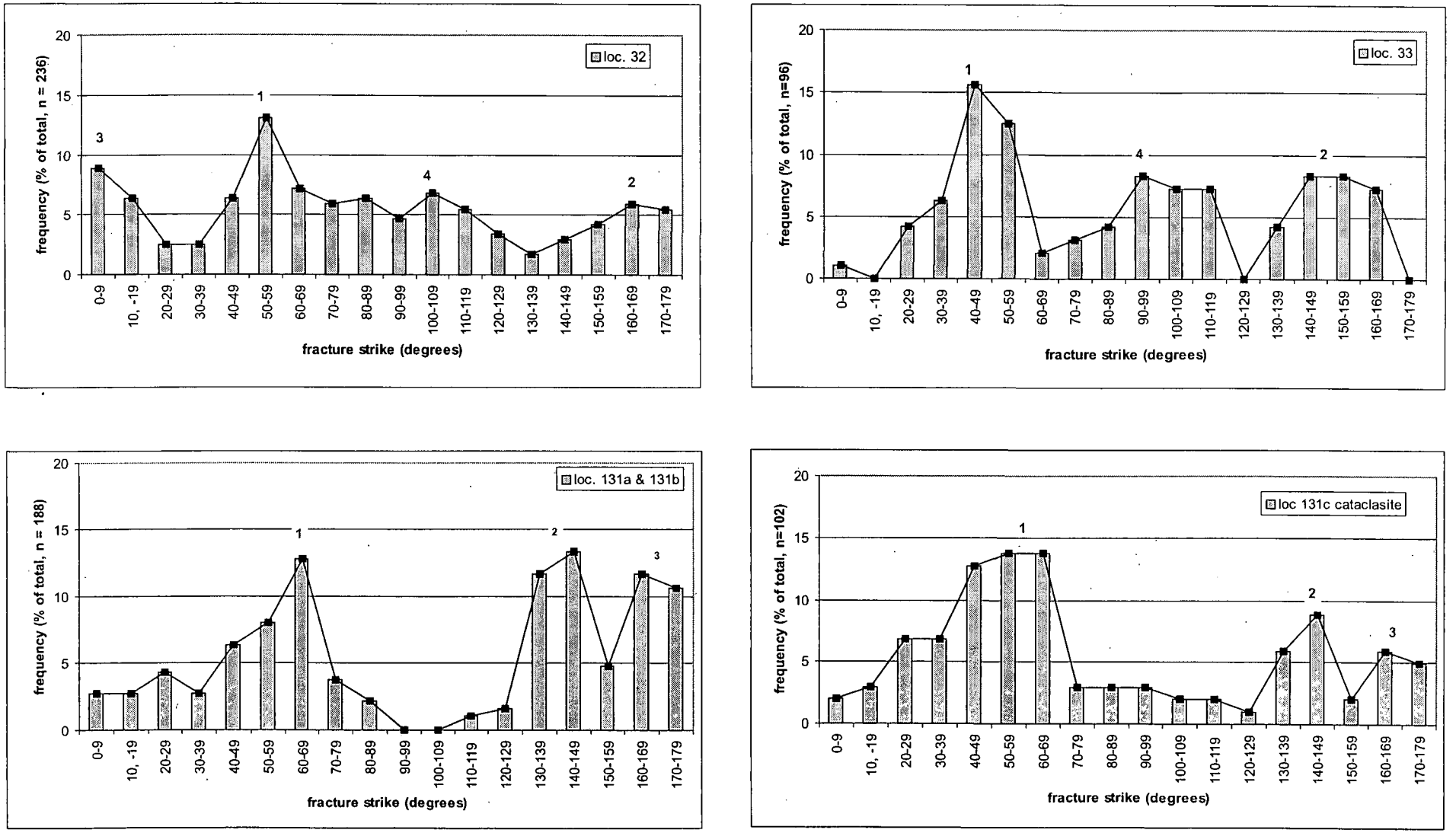

Figure 3.29 Von Mises diagrams for the same data plotted as stereonets in **Figure 3.28**.
(1 = red mean fracture girdle, 2 = blue girdle, 3 = orange girdle, 4 = green girdle

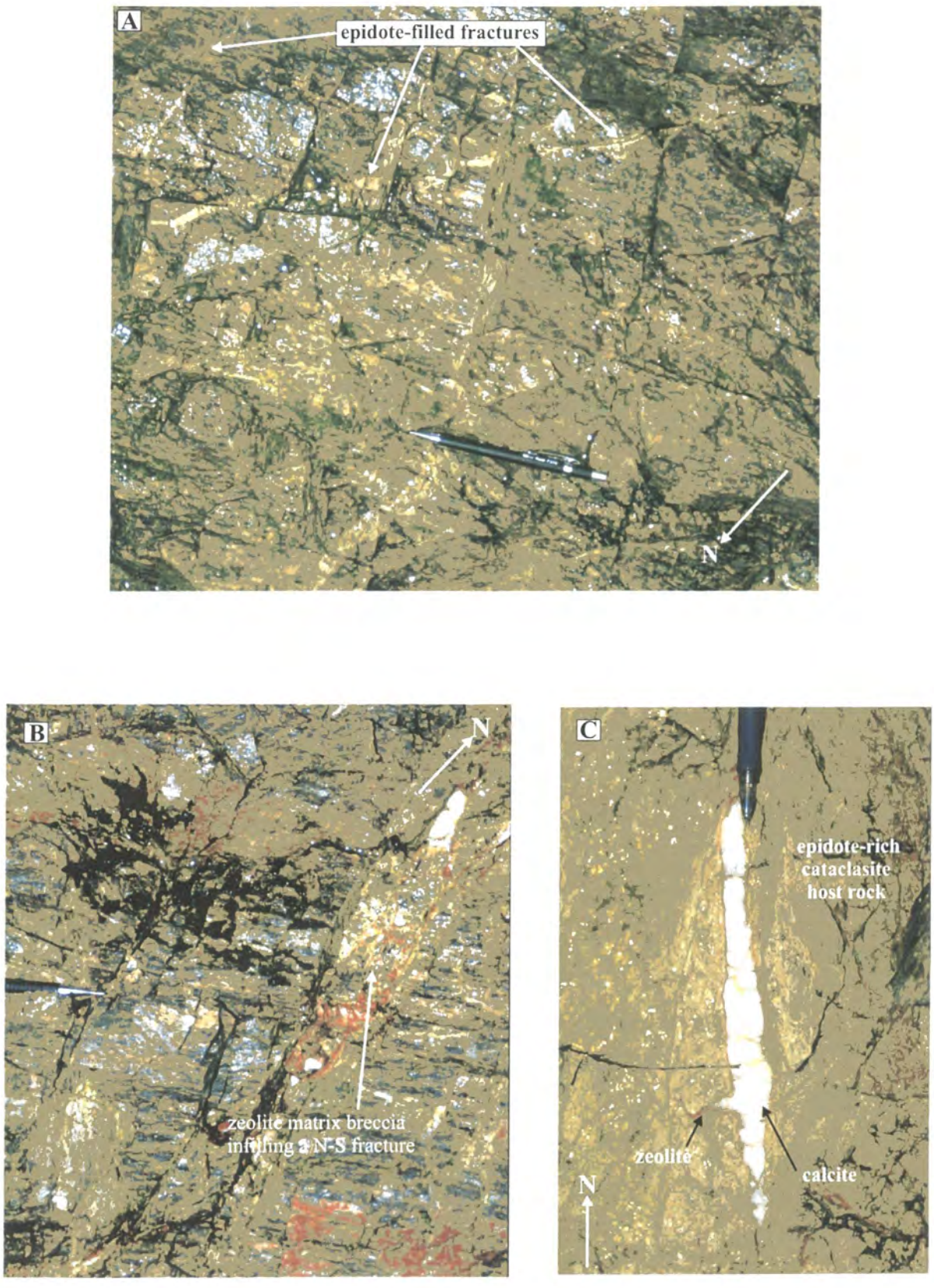

Figure 3.30 Photographs illustrating examples of infilled fractures observed adjacent to the RFP in the Rautingdalen Gorge.
A - epidote-filled fractures
B - zeolite matrixed breccia
C - zeolite and calcite mineralisation

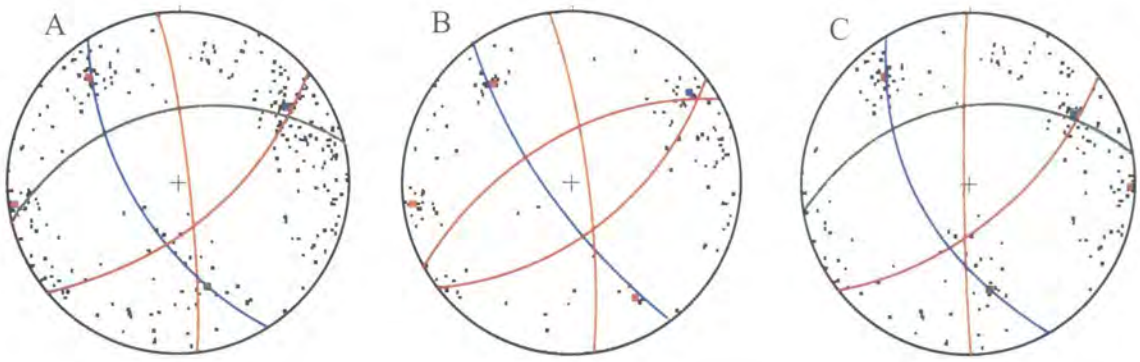

	STEREONET	A	B	C
	Description of data	All infilled fractures measured adjacent to RF	fractures containing epidote/ epidote cataclasite	fractures containing calcite and/or zeolite
	number of data points plotted	278	109	180
Mean girdles to fracture orientation clusters	**RED** (foliation parallel set)	050/ 69 S	052/ 65 S 060/ 68 N	051/ 70 S
	BLUE (NNW-SSE)	148/ 68 W	144/ 78 W	150/ 65 W
	ORANGE (N-S)	173/ 85 E	172/ 82 E	179/ 88 W
	GREEN (E-W TO ESE-WNW)	080/ 59 N	-	080/ 52 N 104/ 66 S

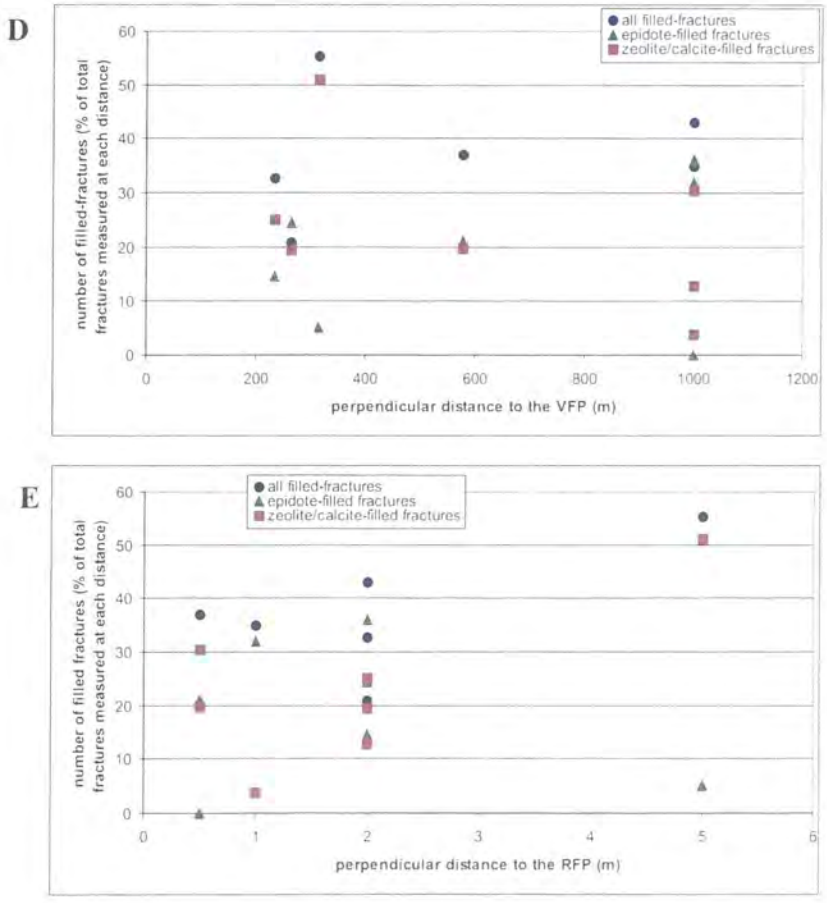

Figure 3.31 Infilled fractures adjacent to the RFP.
A - stereonet of all filled-fractures (poles to planes)
B - stereonet of all epidote-filled fractures (poles to planes)
C - stereonet of all zeolite/calcite-filled fractures (poles to planes)
D - percentage of filled fractures 'v' perpendicular distance to the VFP
E - percentage of filled fractures 'v' perpendicular distance to the RFP

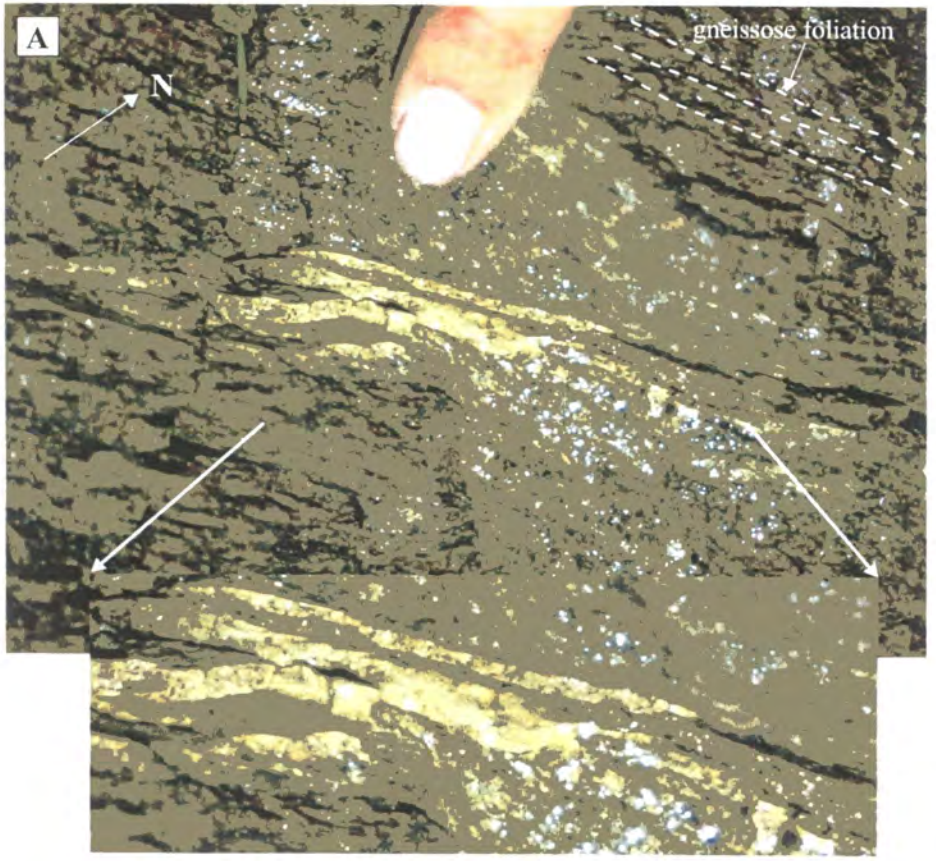

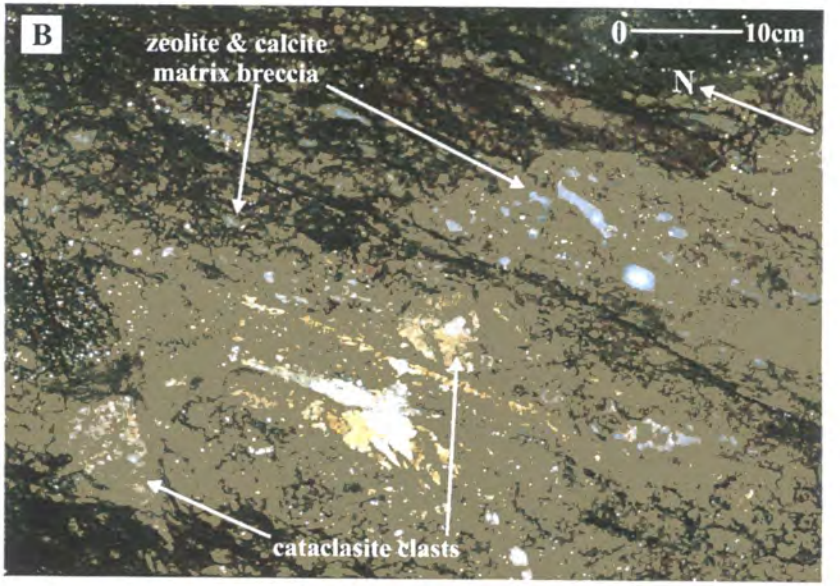

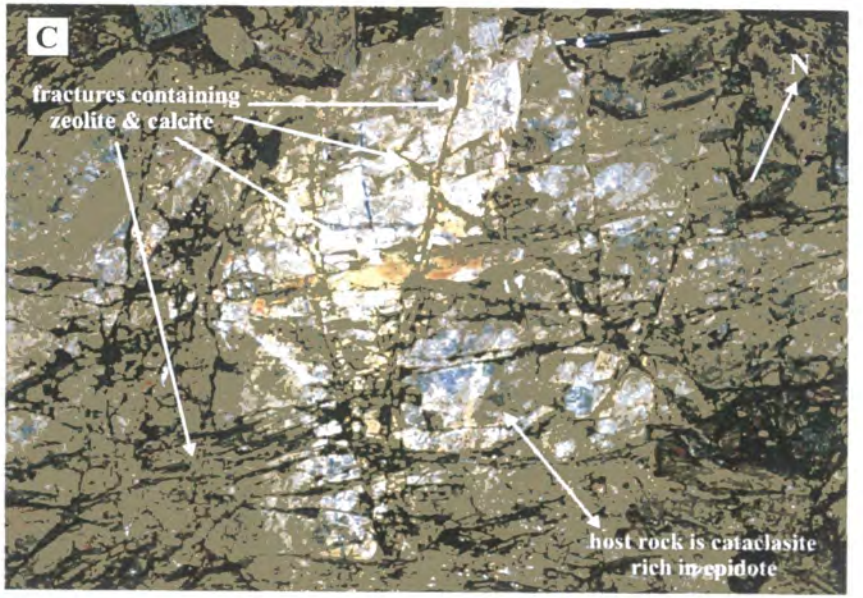

Figure 3.32 Photographs illustrating the relationship between epidote-rich cataclasite and zeolite/calcite mineralisation adjacent to the RFP (within the Rautingdalen gorge)

A - Fracture filled with early epidote cataclasite and later zeolite mineralisation (pink-orange colour) (plan view).

B - Zeolite & calcite matrix breccia containing clasts of epidote-rich cataclasite (plan view).

C - Fractures containing zeolite & calcite cross-cutting epidote-rich cataclasite (cross-section view).

A

Fractures filled with epidote displaying slickenfibre lineations

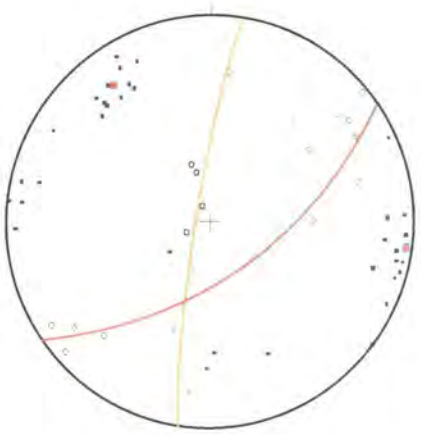

Number of fractures (black squares) = 26
Number of lineations (open circles) = 26

Mean fracture planes (girdles) =
052/ 67 S (RED)
007/ 85 W (ORANGE)

B

Fractures filled with zeolite displaying slickenfibre lineations

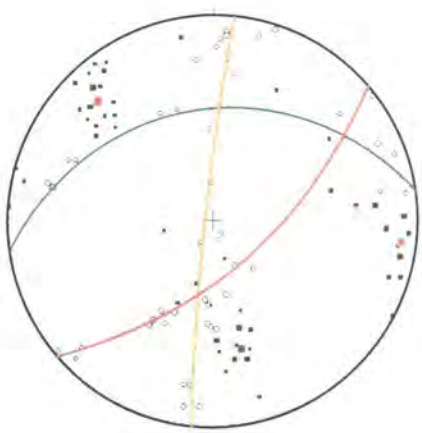

Number of fractures (black squares) = 27
Number of lineations (open circles) = 27

Mean fracture planes (girdles) =
049/ 70 N (RED)
006/ 87 W (ORANGE)
085/ 45 N (GREEN)

Figure 3.33 Infilled fractures with slickenfibre lineations adjacent to the RFP.
A - fractures containing epidote-rich cataclasite
B - fractures containing zeolite/calcite mineralisation

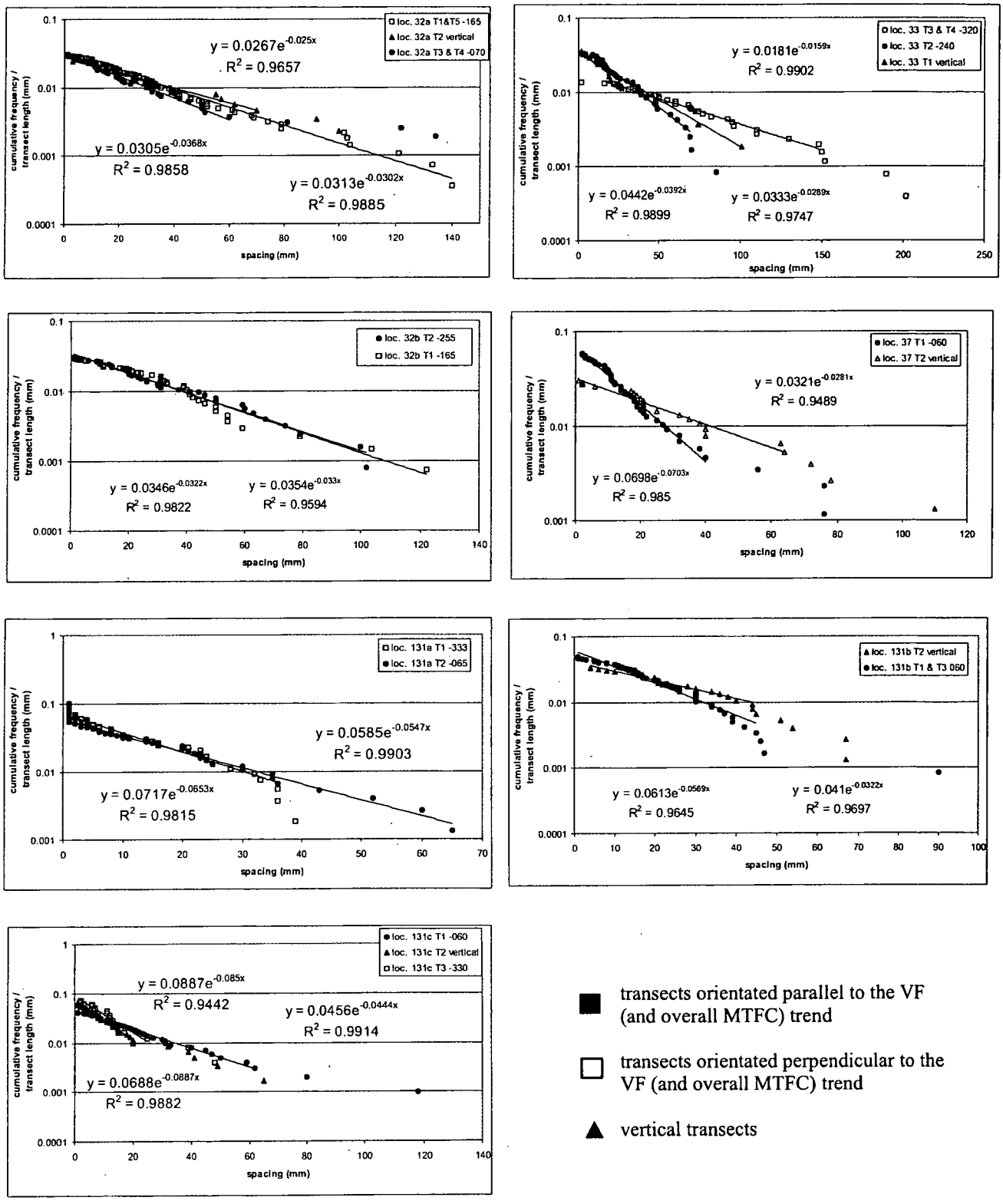

Figure 3.34 Spacing 'v' cumulative frequency plots for localities adjacent to the RFP.

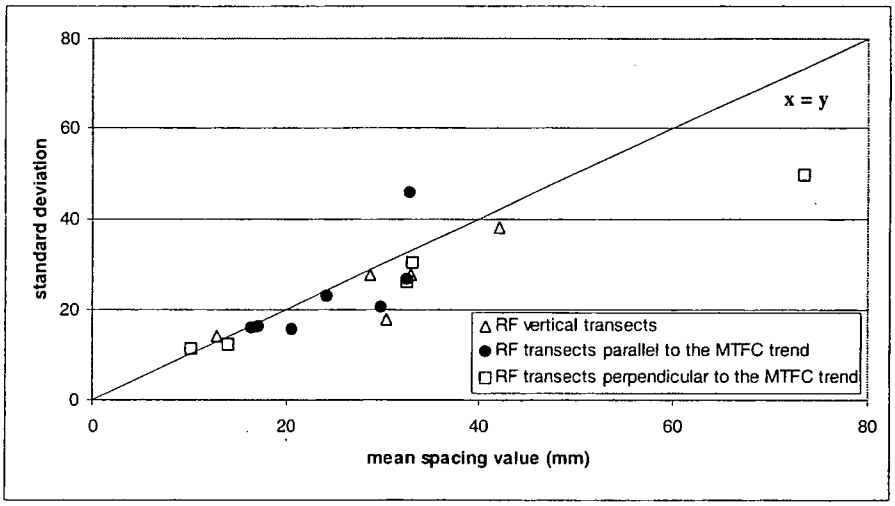

Figure 3.35 Mean spacing 'v' standard deviation for data collected adjacent to the RFP.

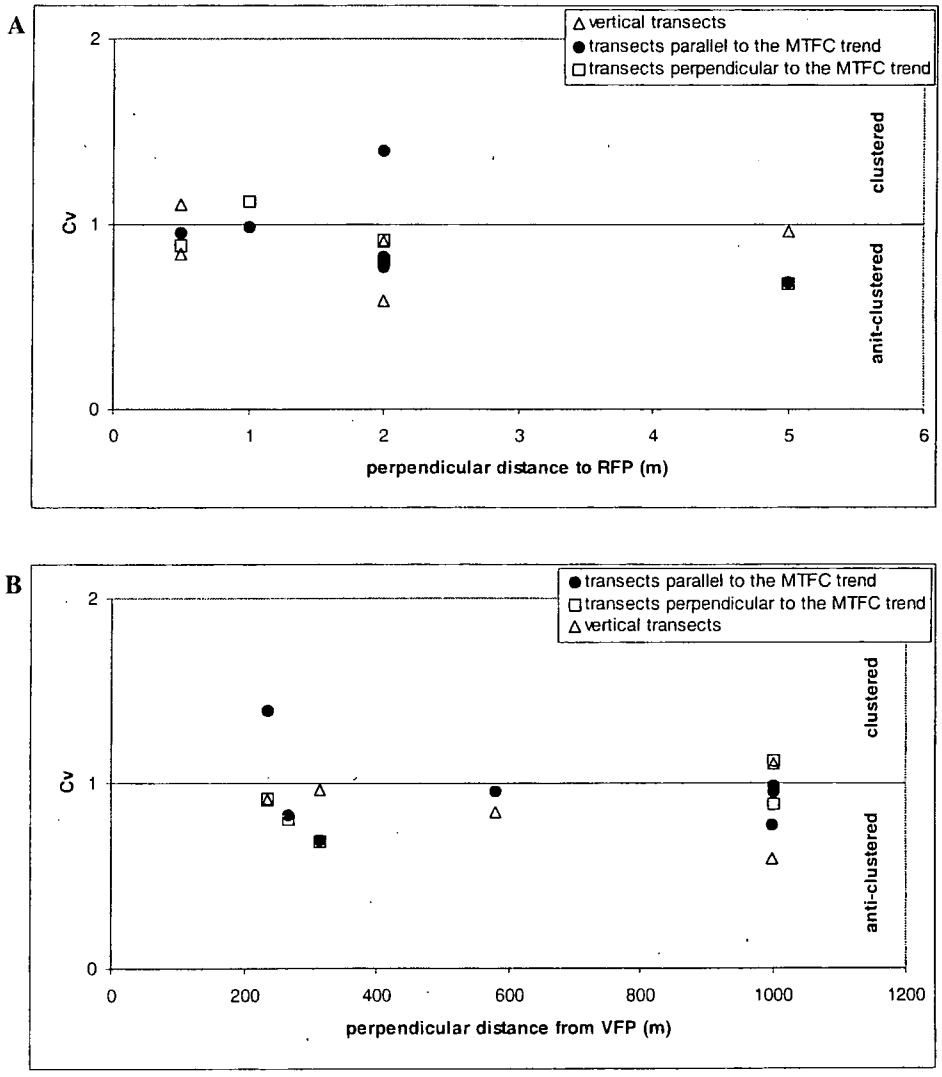

Figure 3.36 **A** - Co-efficient of variation (Cv) 'v' distance to RFP to illustrate the change in Cv with perpendicular distance to the RFP.
B - Co-efficient of variation (Cv) 'v' distance to VFP to illustrate the change in Cv along the strike of the RFP.

A

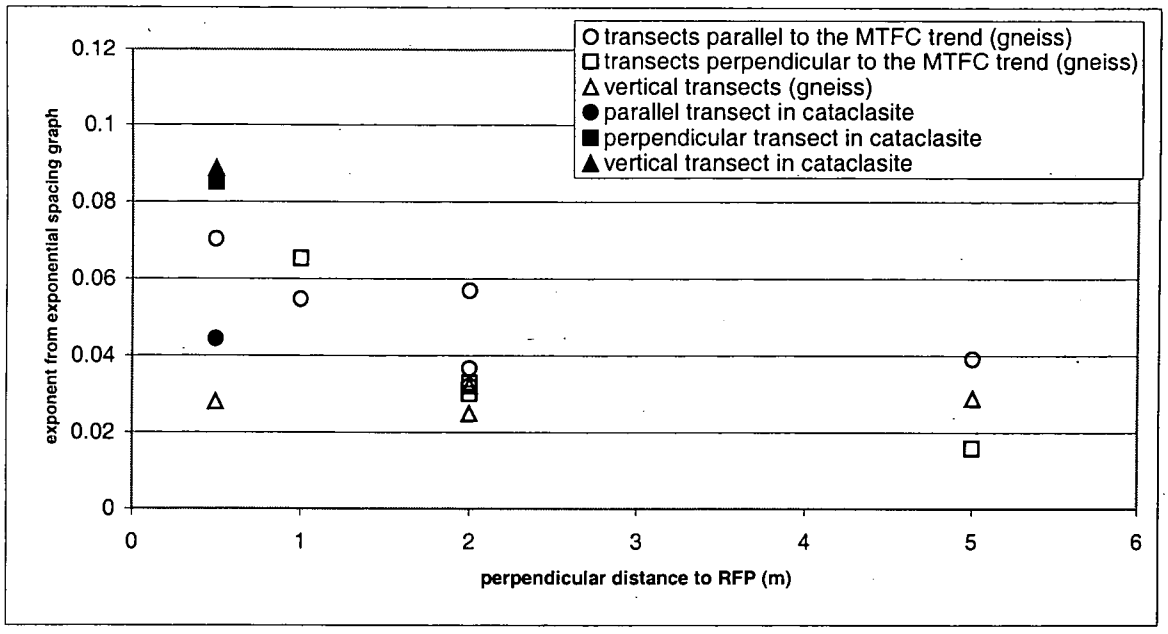

B

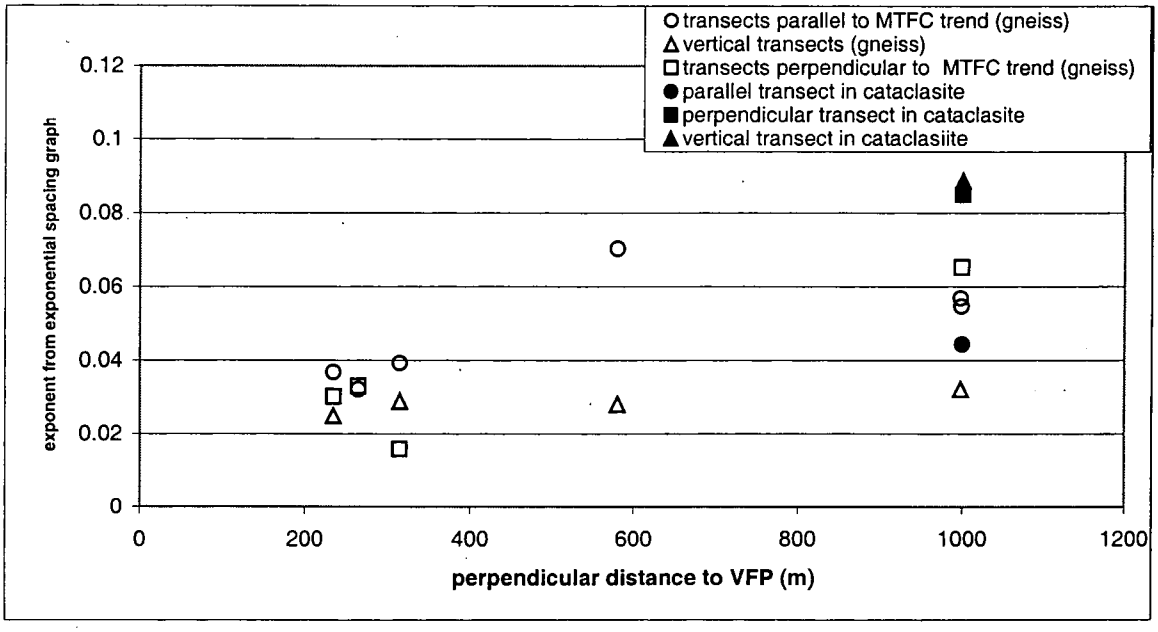

Figure 3.37 **A** – exponent from exponential spacing graphs (**Figure 3.34**) 'v' perpendicular distance to RFP.
B - exponent from exponential spacing graphs (**Figure 3.34**) 'v' perpendicular distance to VFP to illustrate change along strike of the RFP.

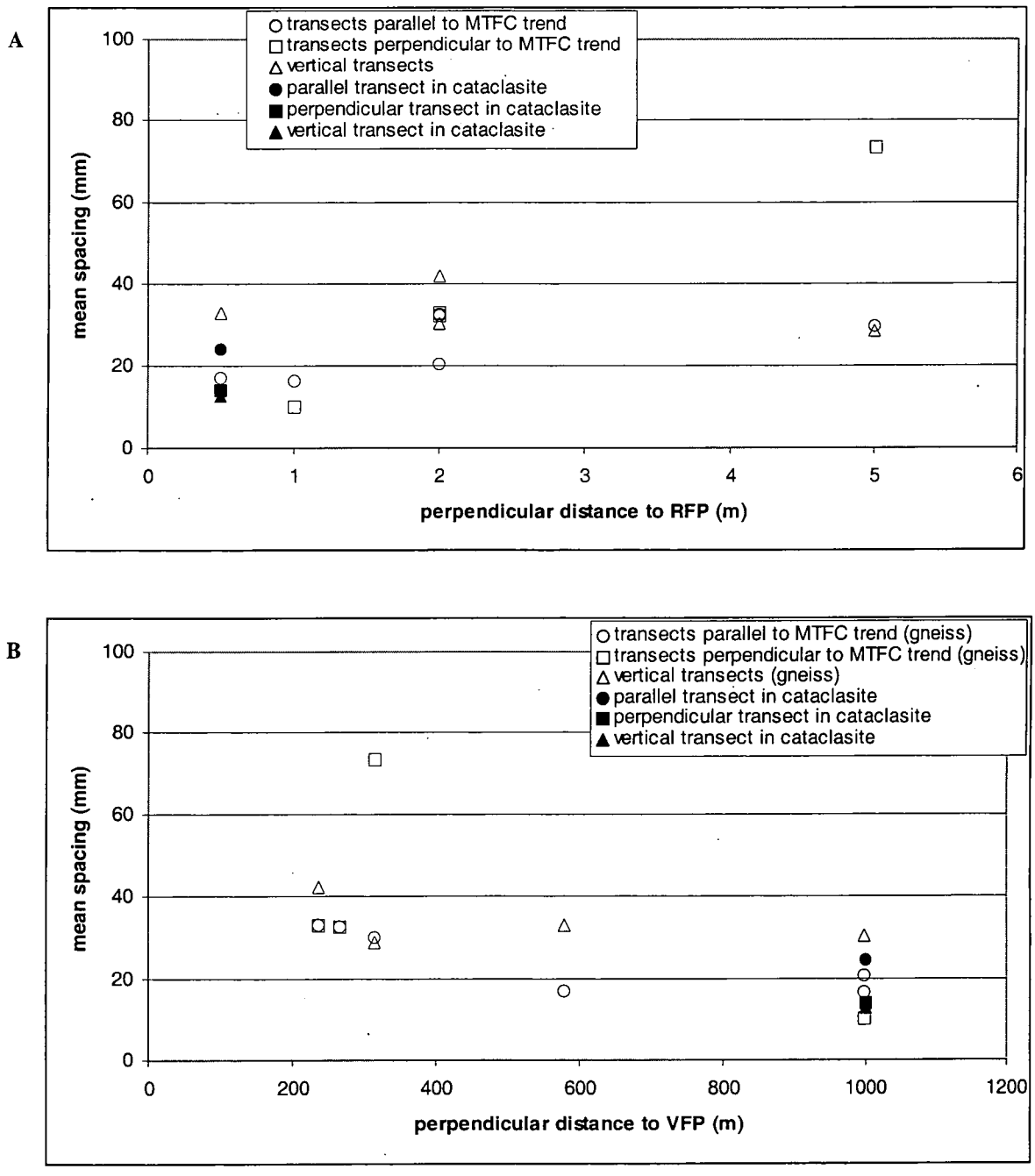

Figure 3.38 **A** – mean spacing 'v' perpendicular distance to RFP
B – mean spacing 'v' perpendicular distance to VFP (illustrates changes along the strike of RFP)

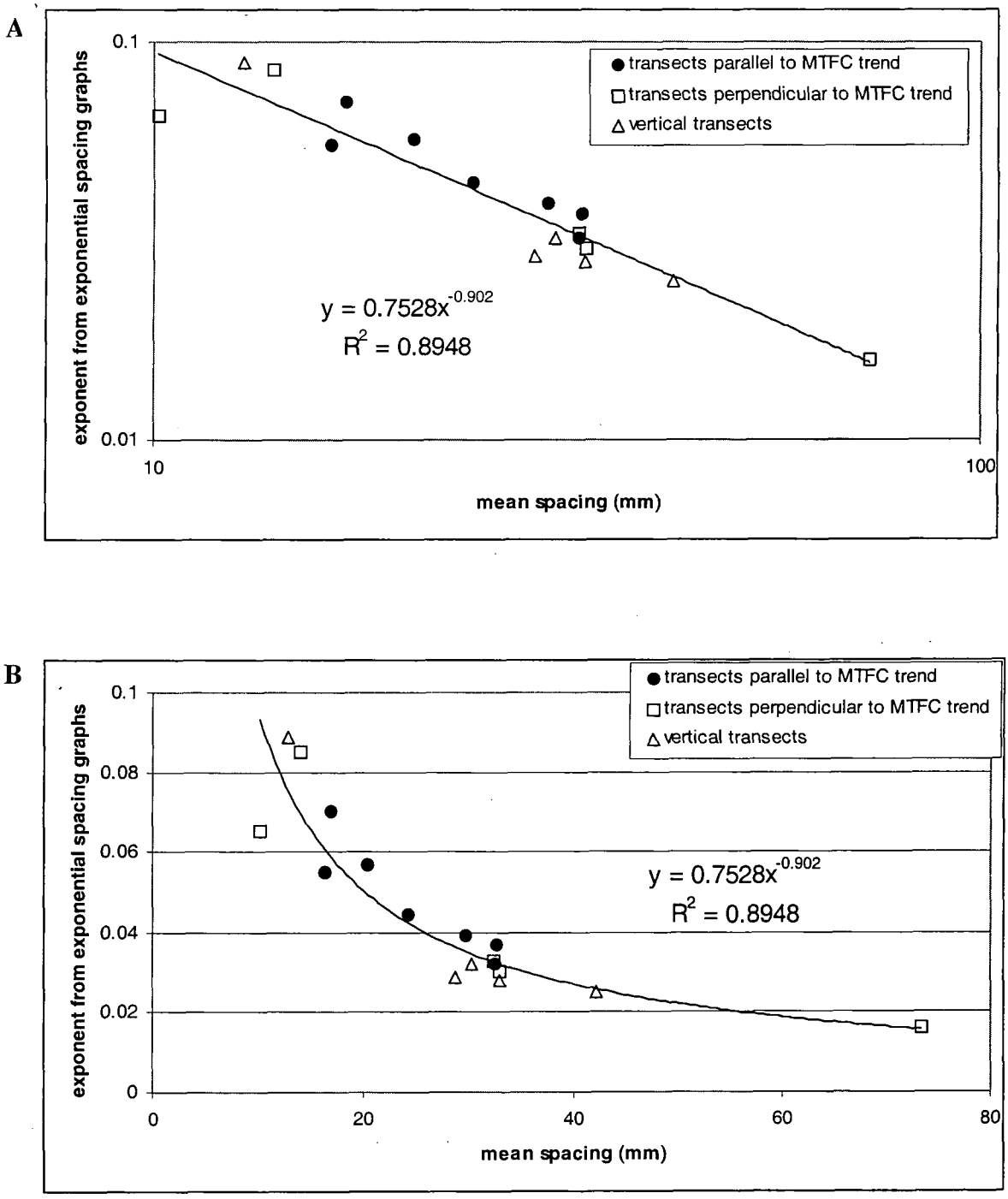

Figure 3.39 Mean spacing 'v' exponent from exponential spacing graphs plotted on both logarithmic axes (**A**) and linear axes (**B**) for data collected adjacent to the RFP.

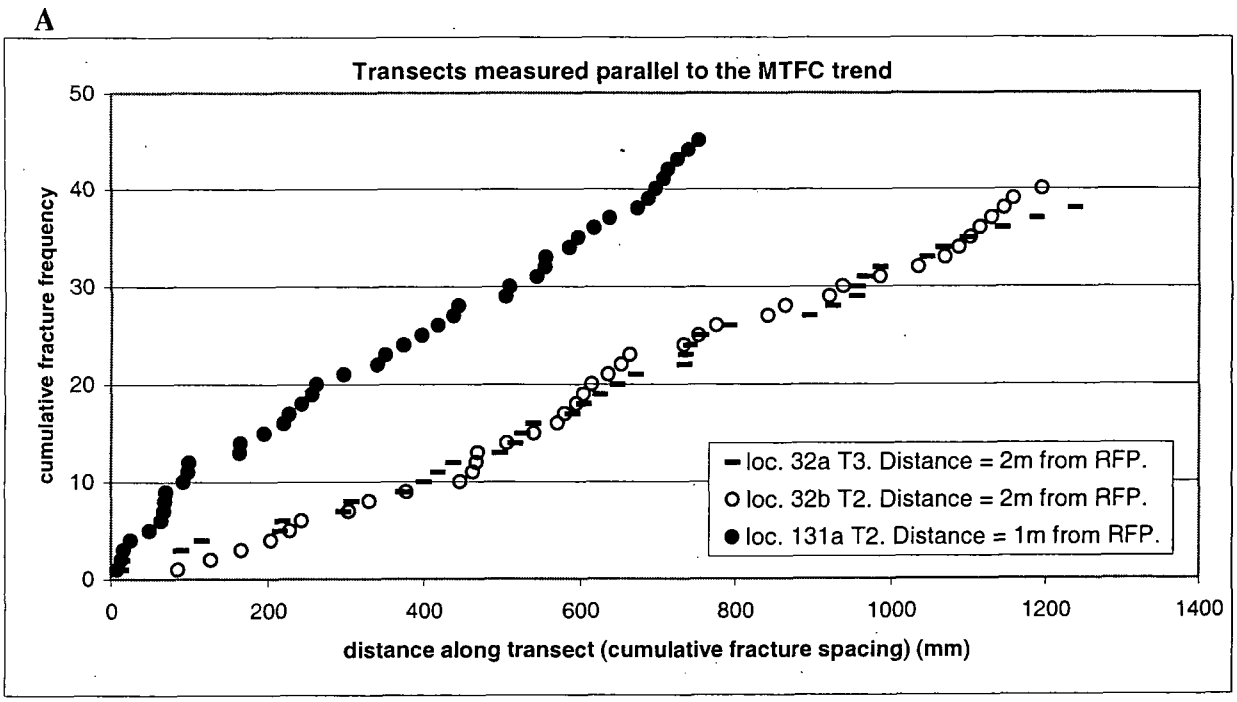

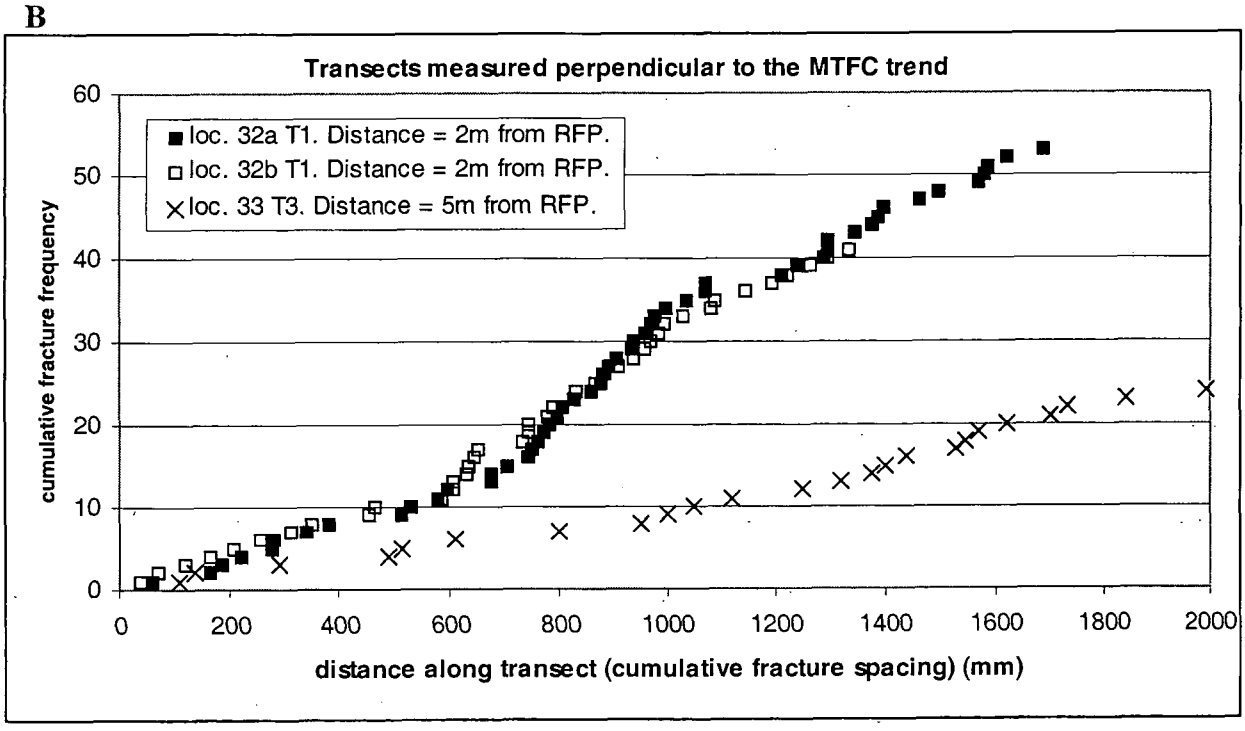

Figure 3.40 Plots of cumulative fracture frequency 'v' distance along 1-dimensional transect for data collected adjacent to the RFP.
A – transects measured parallel to the MTFC trend
B – transects measured perpendicular to the MTFC trend

		Stereonets from data collected NW of the HSFP					
		A	B	C	D	E	F
	Place	Mefjellet	Hammardalen/ 719 Road	Hammardalen/ 719 Road	Mefjellet	Mefjellet	Mefjellet
	Locality	145	136	148	158	160	159
	Distance to HSFP	8m	35m	50m	100m	215m	250m
	no. data points	104	170	147	106	96	84
mean girdles to fracture orientations	RED (ENE-WSW)	060/ 70 N	058/ 56 N	057/ 60 N	061/ 70 N	060/ 71 N	060/ 74 N
	BLUE (NNW-SSE)	159/ 80 W	148/ 86 W	162/ 85 E	146/ 74 W	151/ 82 W	156/ 78 W
	ORANGE (N-S)	174/ 87 E	171/ 87 W	012/ 16 W	179/ 86 W	171/ 83 W	178/ 83 W
	GREEN (E-W to ESE-WNW)	-	116/ 81 S	112/ 82 S	-	-	-

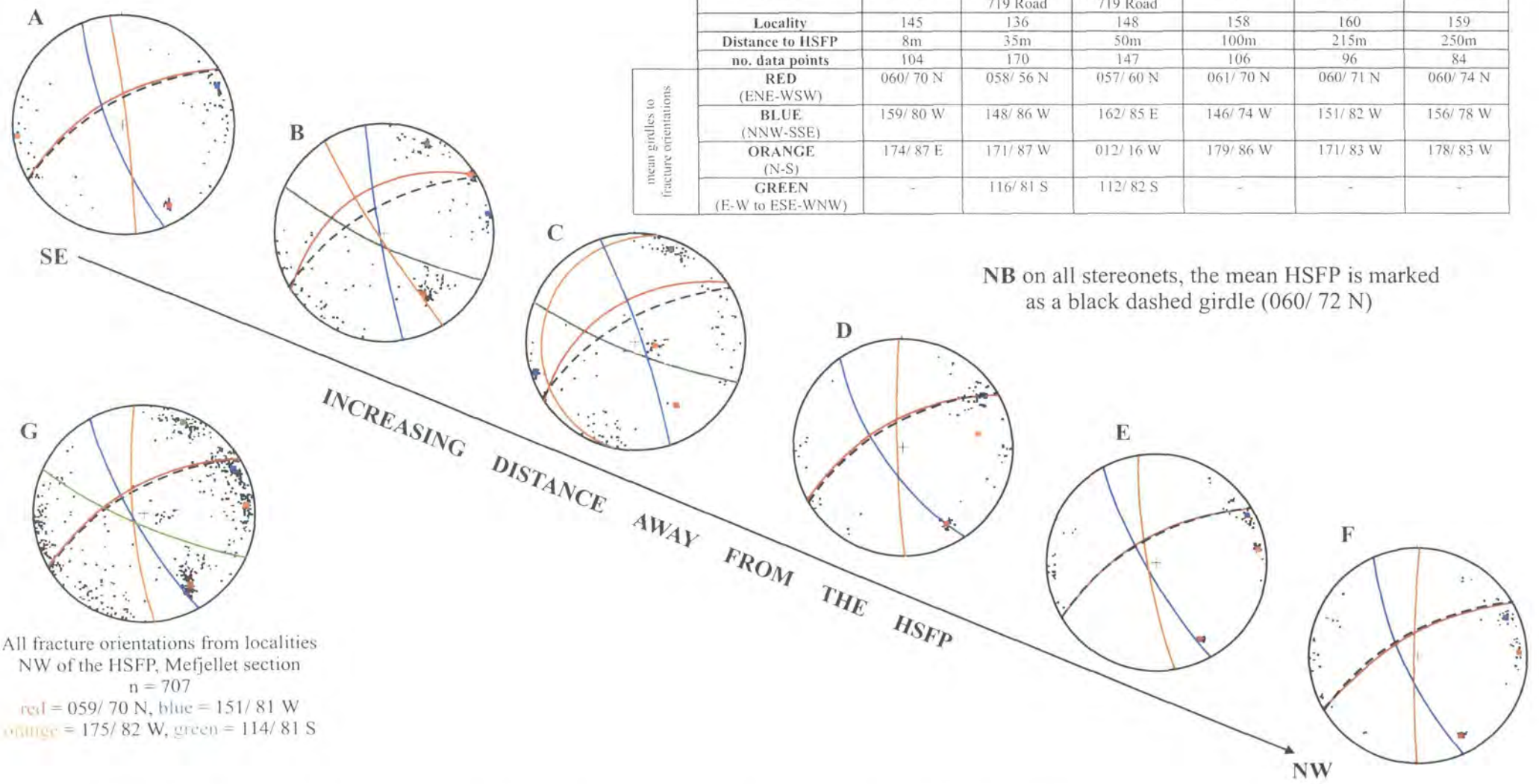

Figure 3.41 Stereographic projections of fracture orientations from localities to the NW of the HSFP.

		Stereonets from data collected SE of the HSFP						
		A	B	C	D	E	F	G
	Place	Mefjellet	Hammardalen/ 719 Road	Mefjellet	near Follavatnet	Mefjellet	Mefjellet	near Follavatnet
	Locality	144	135	143	147	141	142	146
	Distance to HSFP	15m	20m	81m	150m	360m	375m	700m
	no. data points	141	157	167	75	72	104	119
mean girdles to fracture orientations	RED (ENE-WSW)	062/ 72 N	045/ 70 N	060/ 72 N	058/ 58 S	048/ 71 N	062/ 71 N	063/ 48 S
	BLUE (NNW-SSE)	157/ 85 W	157/ 78 W	151/ 86 W	150/ 78 E	-	160/ 80 E	147/ 77 E
	ORANGE (N-S)	013/ 70 E	009/ 37 E	175/ 85 W	-	177/ 88 W	-	010/ 74 W
	GREEN (E-W to ESE-WNW)	-	121/ 80 S	123/ 84 N	110/ 54 S	-	-	-

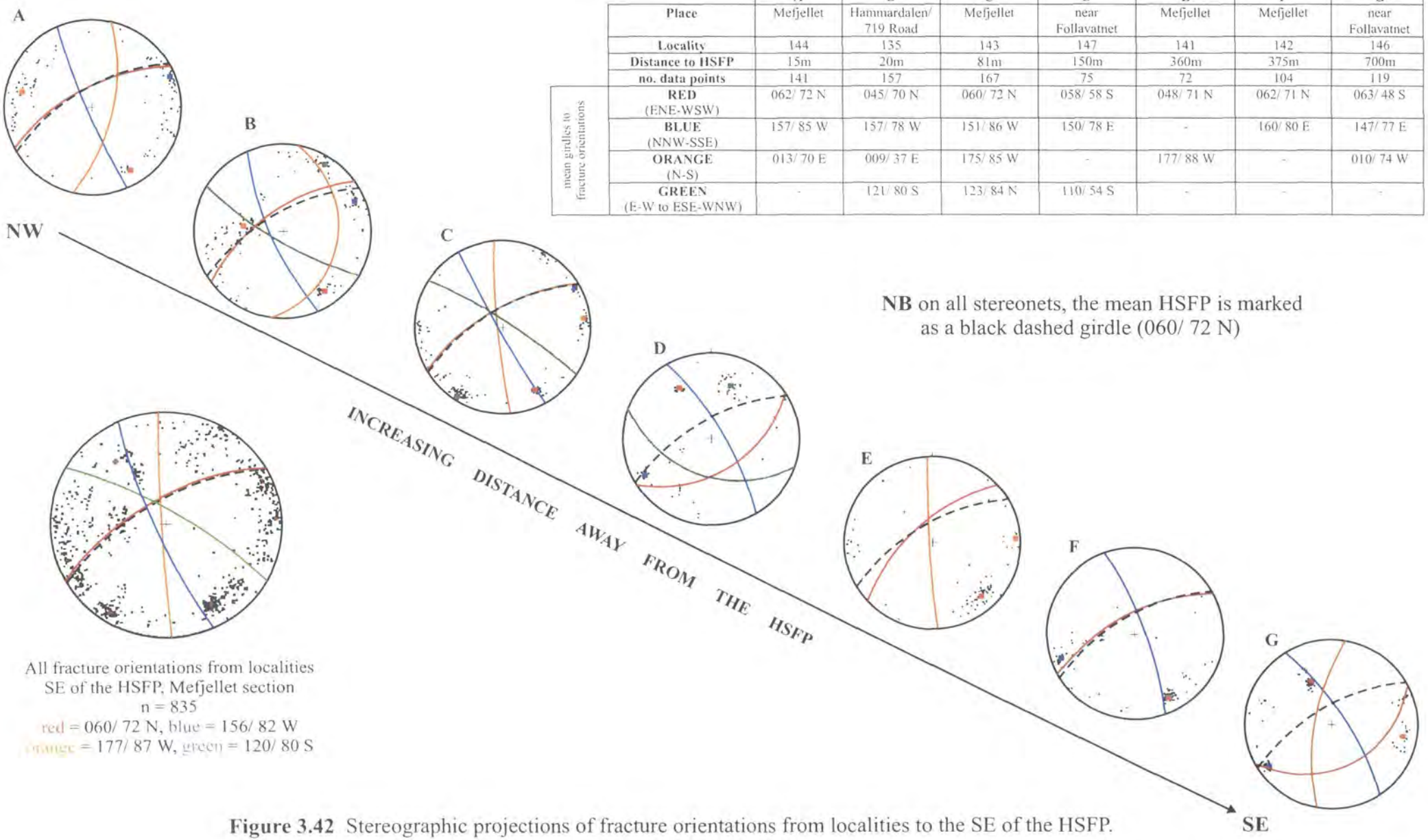

Figure 3.42 Stereographic projections of fracture orientations from localities to the SE of the HSFP.

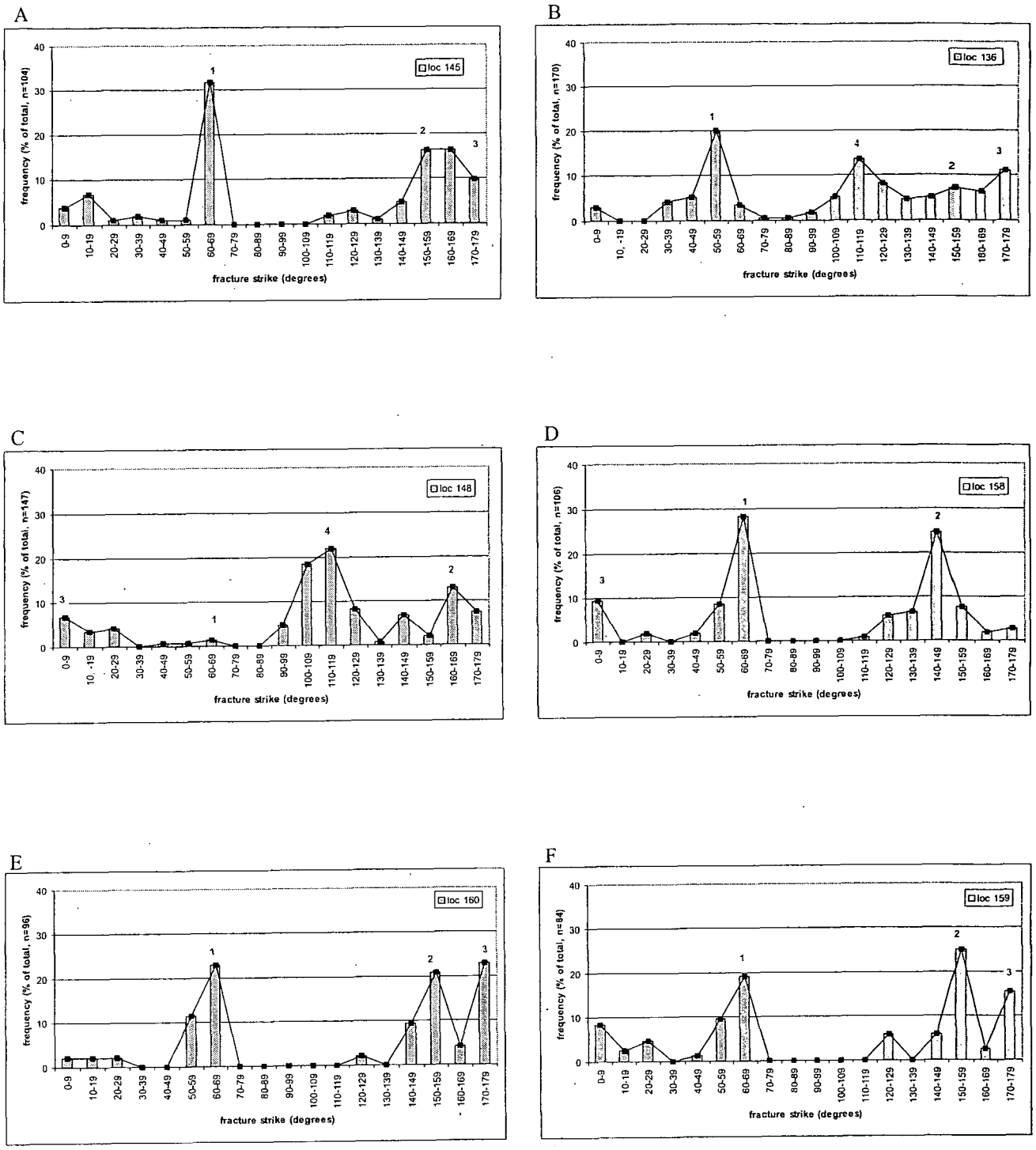

Figure 3.43 Von Mises diagrams created for fracture data sets collected NW of the HSFP (same data sets as stereonets illustrated in **Figure 3.41**)
Numbers on each plot correspond to the mean fracture orientations in **Figure 3.41**, 1 = red girdles, 2 = blue girdles, 3 = orange girdles, 4 = green girdles.

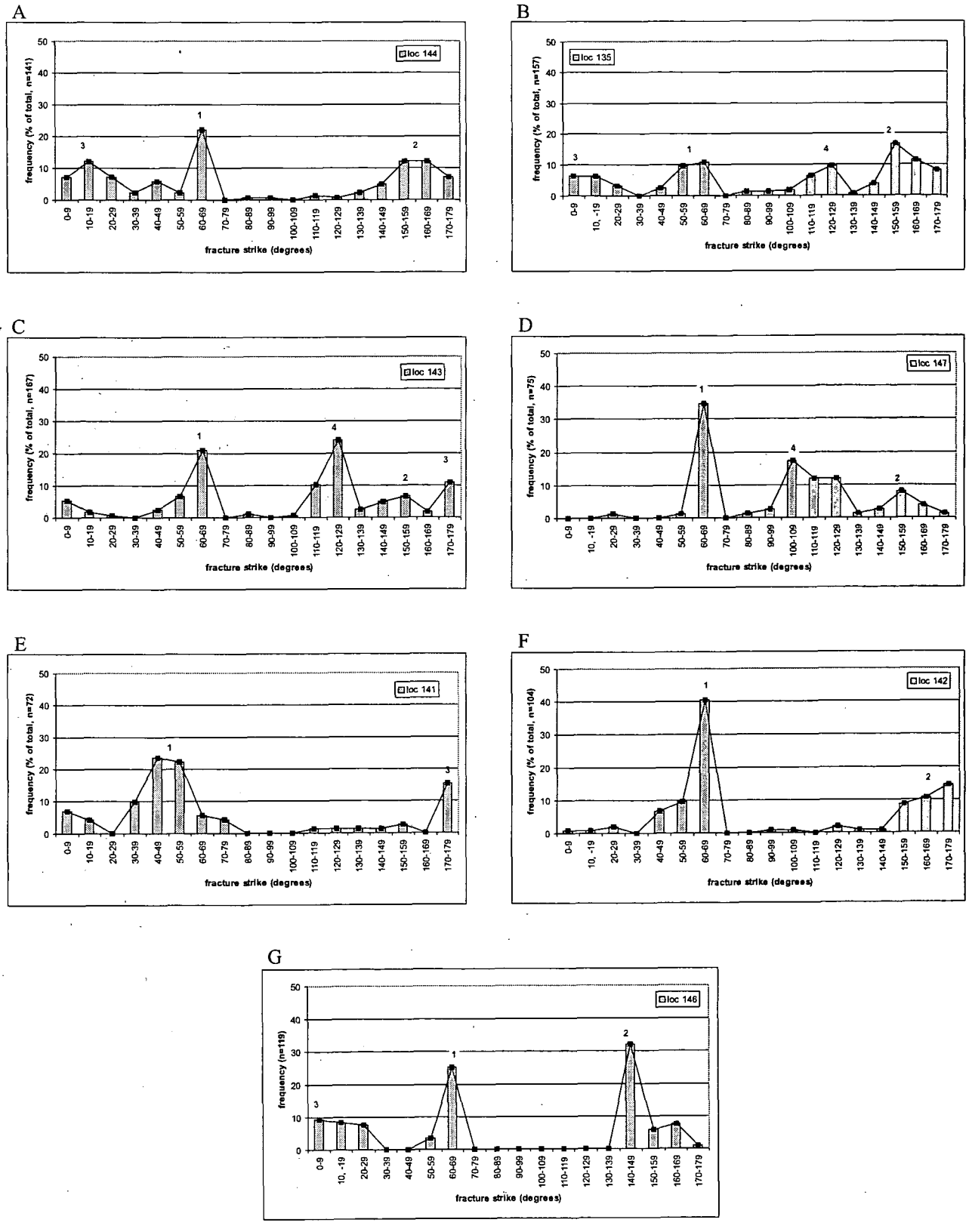

Figure 3.44 Von Mises diagrams created for fracture data sets collected SE of the HSFP (same data sets as stereonets illustrated in **Figure 3.42**)
Numbers on each plot correspond to the mean fracture orientations in **Figure 3.42**, 1 = red girdles, 2 = blue girdles, 3 = orange girdles, 4 = green girdles.

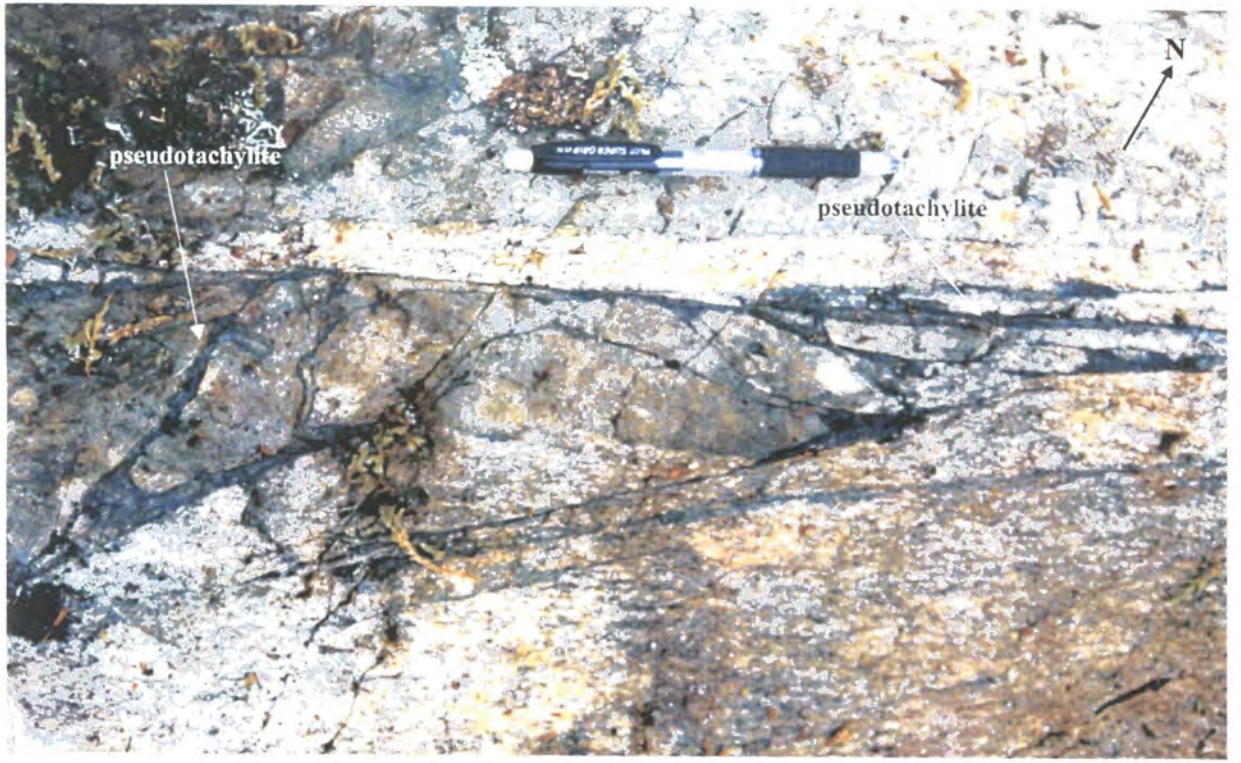

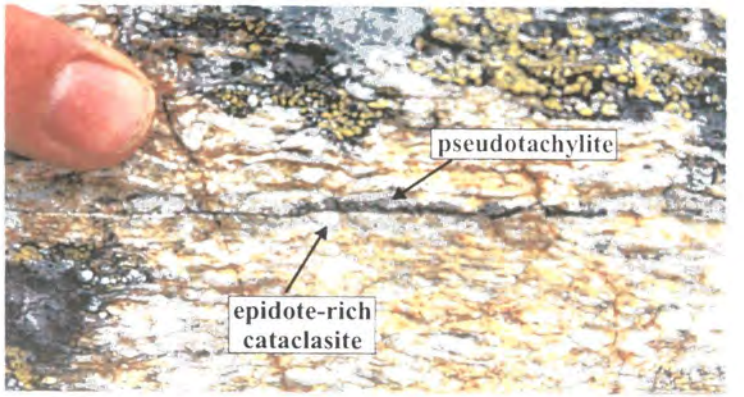

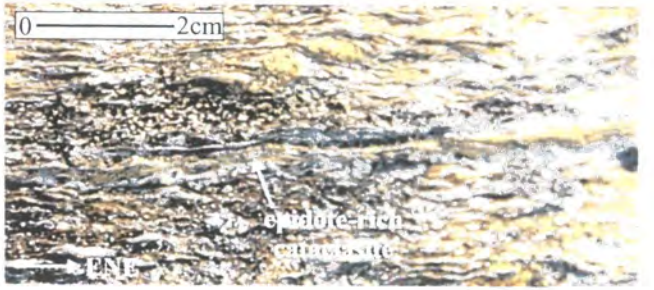

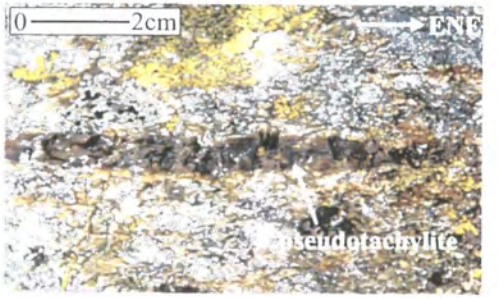

Figure 3.45 Photographs illustrating fractures infilled by coeval epidote-rich cataclasite and pseudotachylite, from the Mefjellet section
(All plan view)

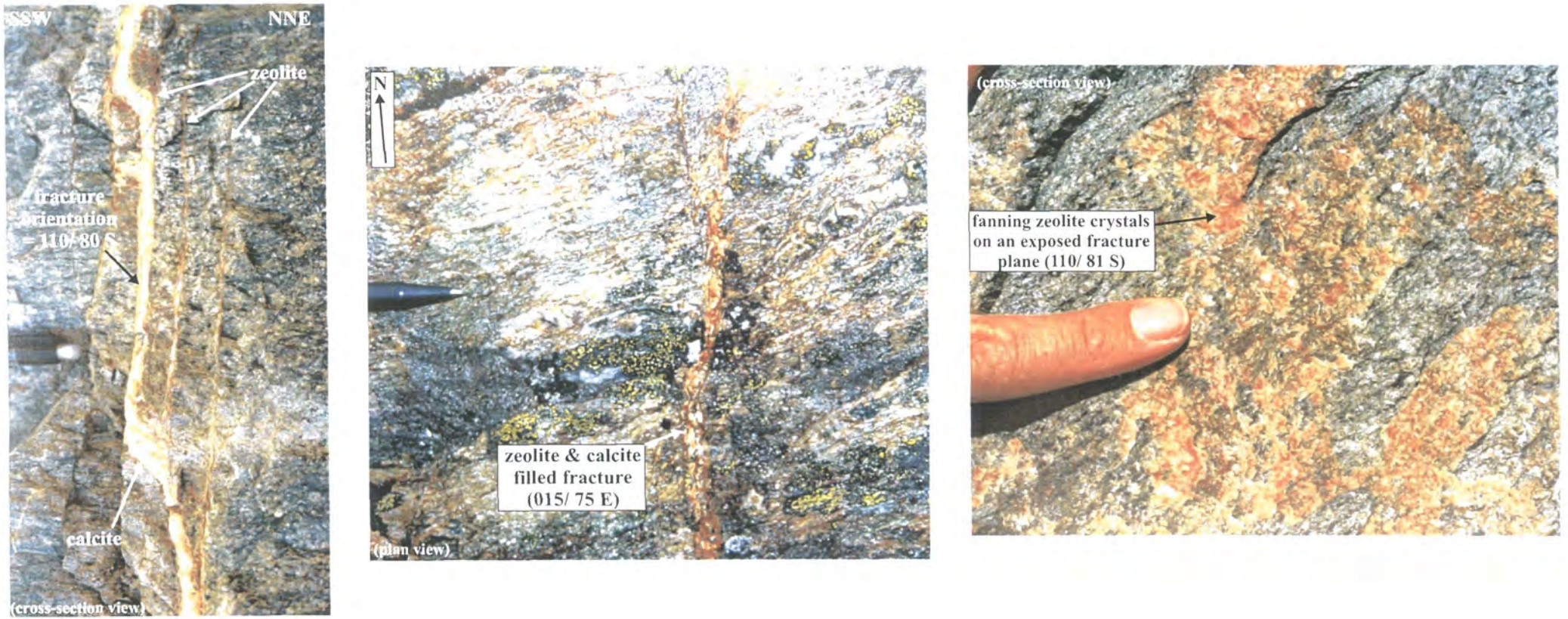

Figure 3.46 Zeolite & calcite-filled fractures observed adjacent to the HSFP, from the Hammardalen quarry & 719 road cut localities.

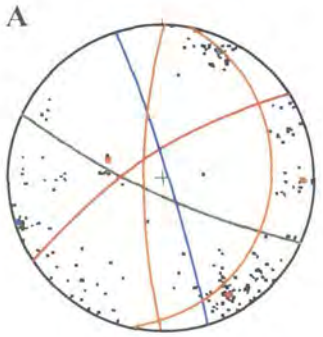

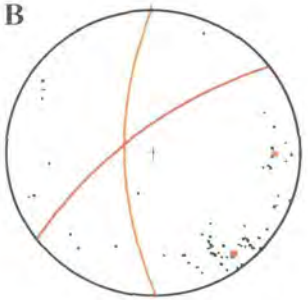

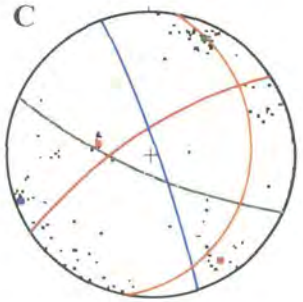

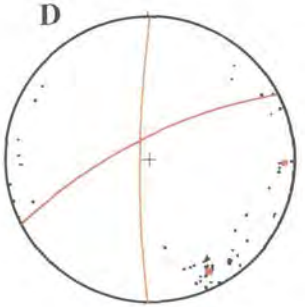

		Stereonet			
		A	B	C	D
	Description of data	All infilled fractures measured adjacent to HSF	fractures containing epidote/ epidote cataclasite	fractures containing calcite and/or zeolite	fractures containing pseudotachylite
	number of data points plotted	276	75	163	74
Mean girdles to fracture orientation clusters	RED (foliation parallel set)	057/ 77 N	053/ 77 N	057/ 77 N	063/ 78 N
	BLUE (NNW-SSE)	163/ 87 E	-	161/ 86 E	-
	ORANGE (N-S)	011/ 29 E & 001/ 80 W	000/ 74 W	011/ 29 E	001/ 85 W
	GREEN (E-W to ESE-WNW)	115/ 81 S	-	114/ 79 S	-

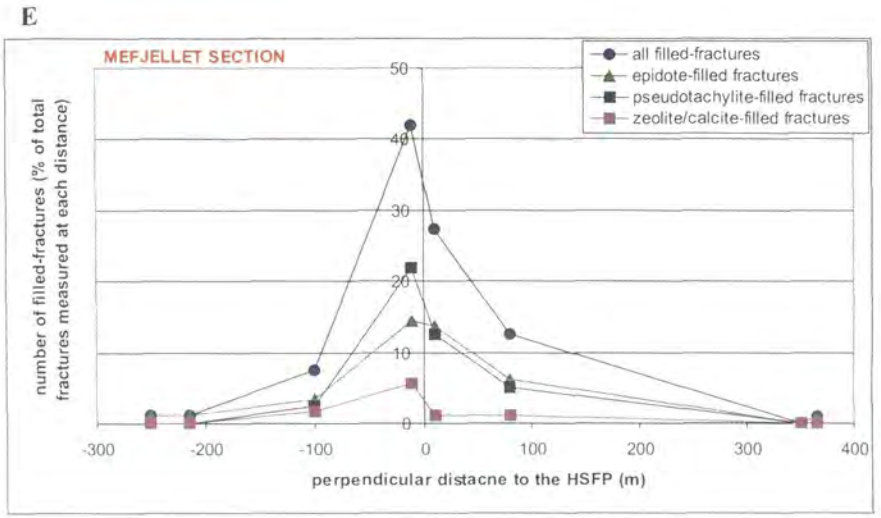

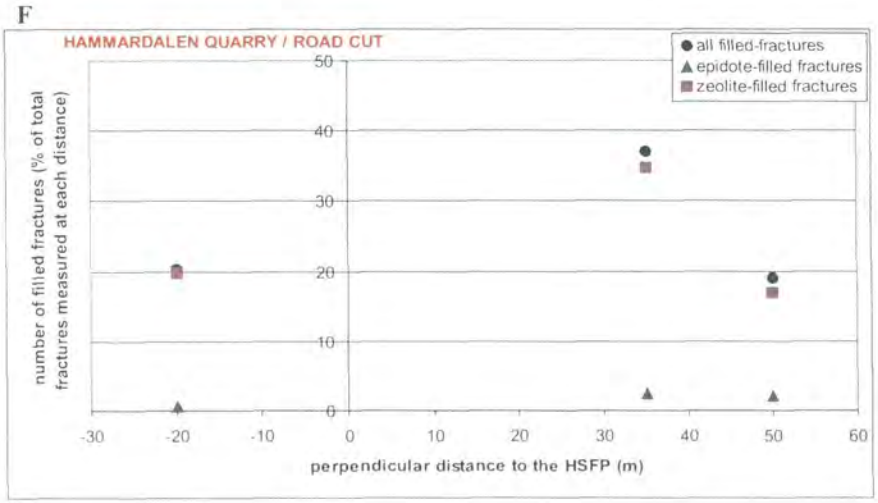

Figure 3.47 Infilled fractures observed adjacent to the HSFP.
A - D = stereonets (poles to fracture planes) of filled-fractures adjacent to the HSFP. Details are presented in the table
E & F = Percentage of filled-fractures at different distances to the HSFP, from Mefjellet (E) and the Hammardalen quarry / 719 road (F)

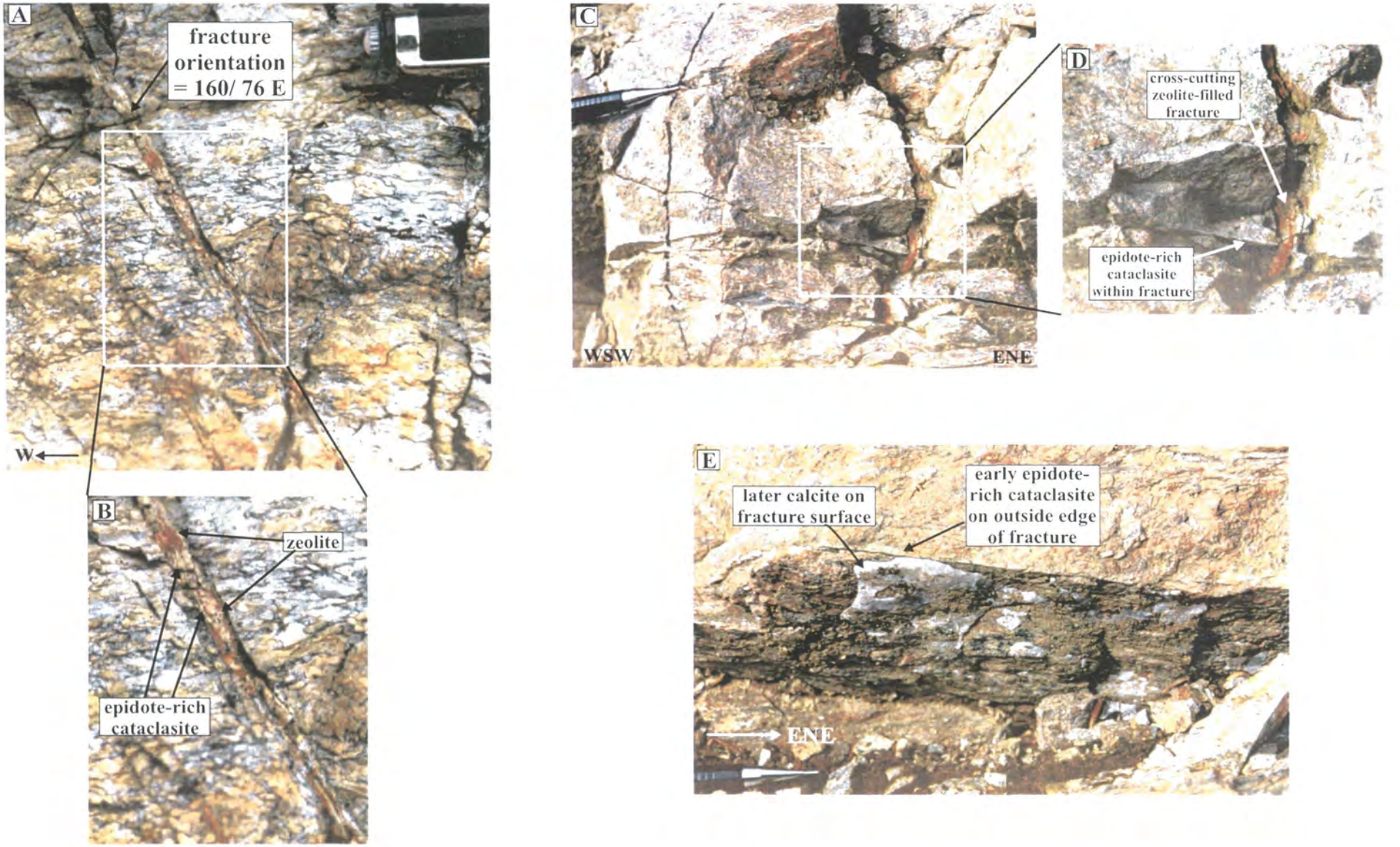

Figure 3.48 Fractures filled with early epidote cataclasite and later zeolite/calcite mineralisation adjacent to the HSFP from the Hammardalen quarry and 719 road cut localities. (All cross-section view)

Fractures filled with epidote displaying slickenfibre lineations

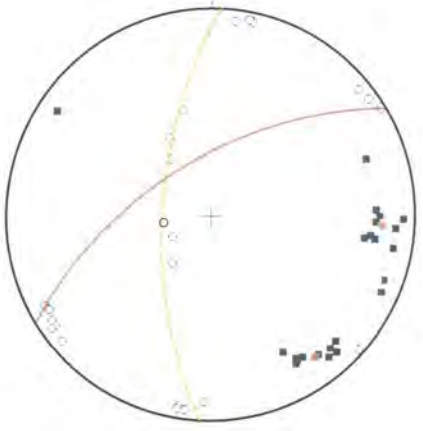

Number of fractures (black squares) = 25
Number of lineations (open circles) = 25

Mean fracture planes (girdles) =
059/ 68 N (RED),
003/ 70 W (ORANGE),

Fractures filled with zeolite displaying slickenfibre lineations

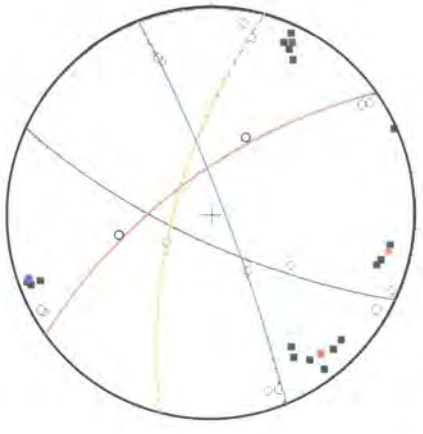

Number of fractures (black squares) = 17
Number of lineations (open circles) = 17

Mean fracture planes (girdles) =
054/ 74 N (RED),
015/ 75 W (ORANGE)
159/ 85 E (BLUE)
115/ 79 S (GREEN),

Figure 3.49 Fractures displaying slickenfibre lineations adjacent to the HSFP

Figure 3.50 Slickenfibre lineations observed on fracture planes adjacent to the HSFP
A - ENE-WSW trending fracture with shallowly plunging epidote slickenfibres
B - N-S trending fracture with steeply plunging zeolite slickenfibres

Figure 3.51 Fractures filled with epidote-rich cataclasite offsetting quartz veins with a sinistral sense of shear from the Mefjellet section, adjacent to the HSF.
(all plan view)

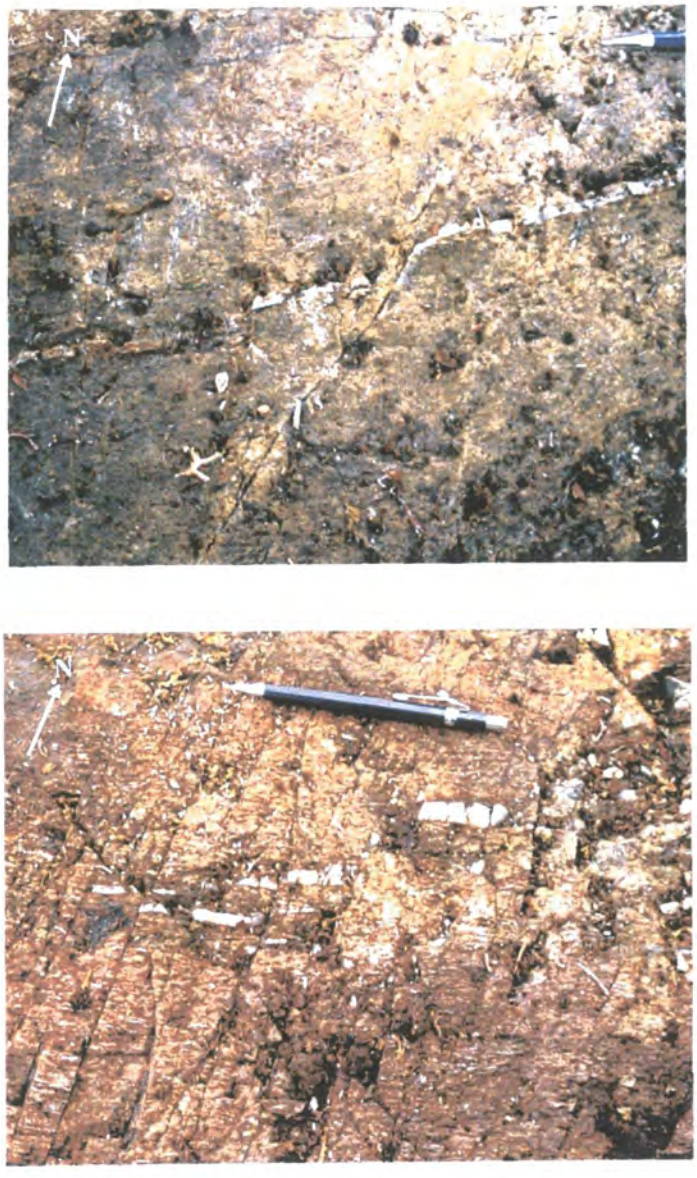

Figure 3.52 N-S trending pseudotachylite-filled fractures offsetting quartz veins with a sinistral sense (from Mefjellet section, adjacent to the HSF) (plan view).

Figure 3.53 Zeolite-filled fractures offsetting a quartz vein in a dextral sense (from Mefjellet section, photograph = plan view).
Fracture A = 046/ 86 SE

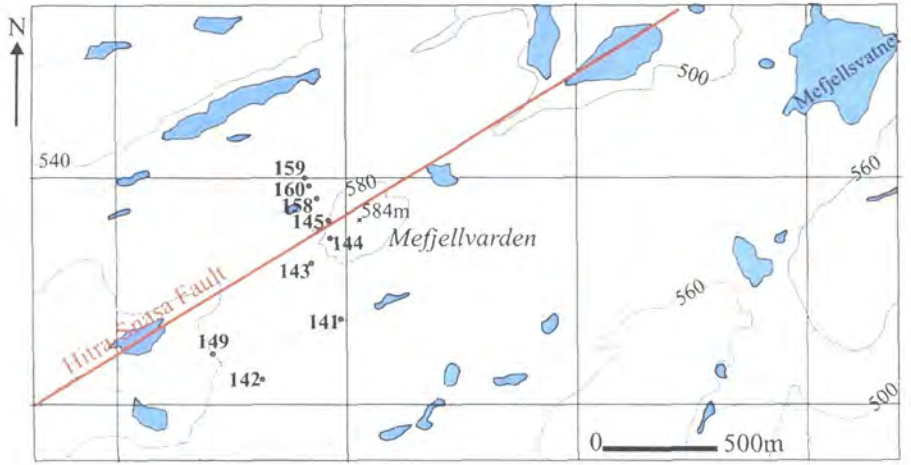

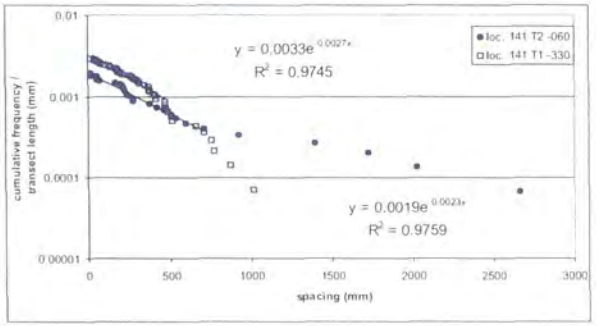

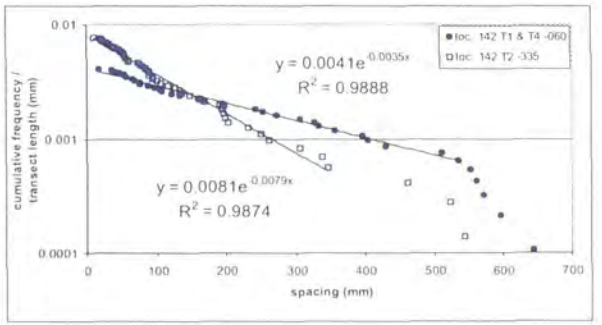

Figure 3.54 Spacing 'v' cumulative frequency plots for localities from the Mefjellet section, HSF.
(map contours are in metres)
(graph legends display locality number, transect number and transect orientation)

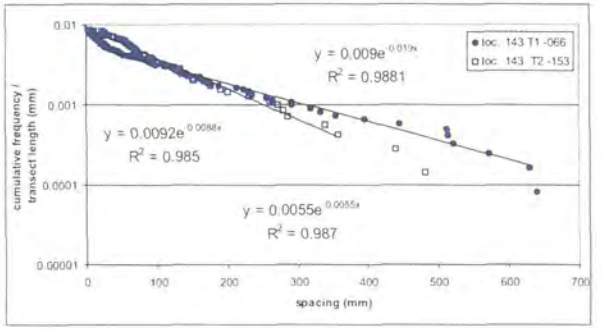

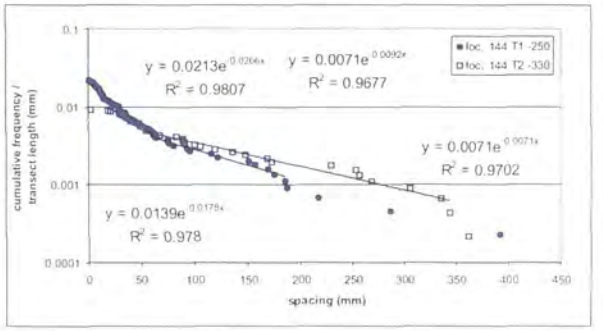

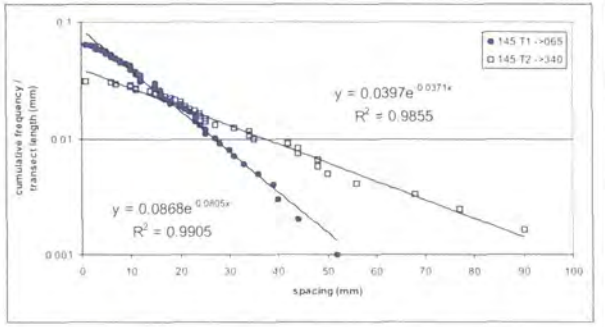

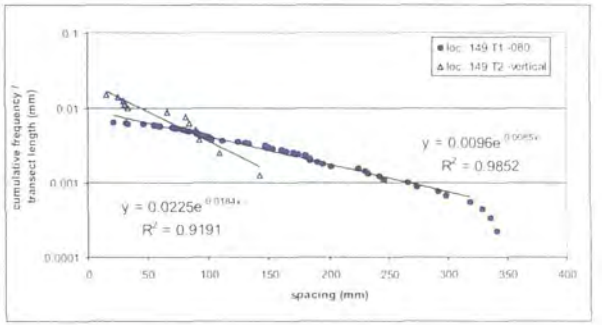

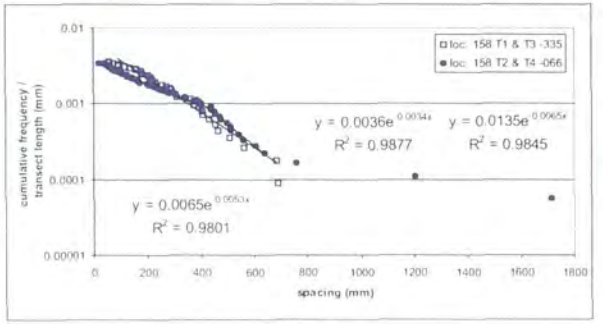

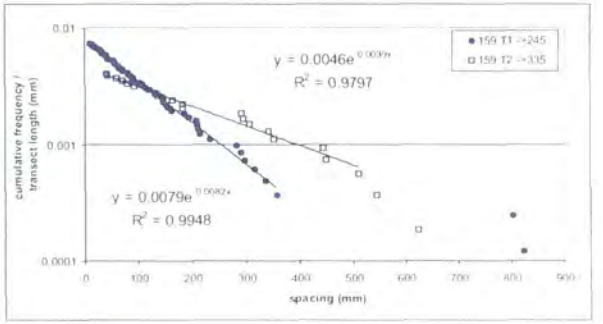

Key to data set symbols

- transects orientated parallel to the HSF (and overall MTFC) trend
- transects orientated perpendicular to the HSF (and overall MTFC) trend
- vertical transects

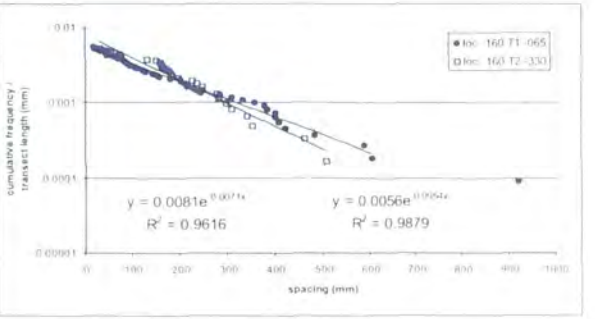

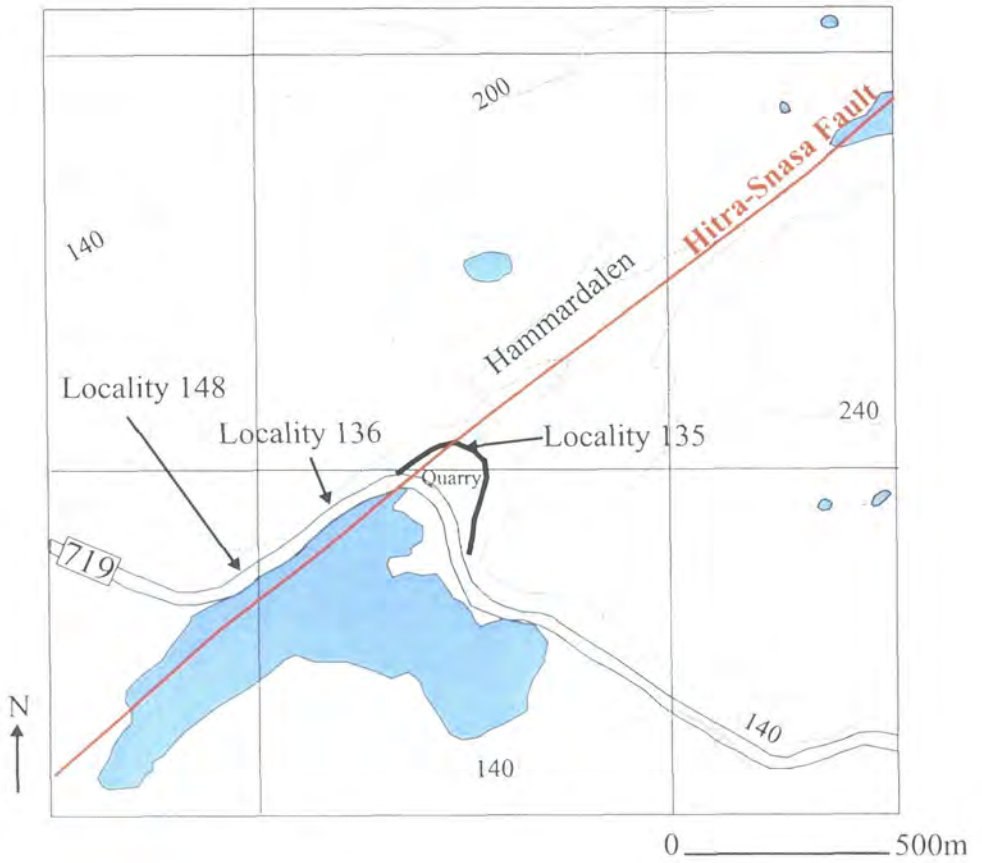

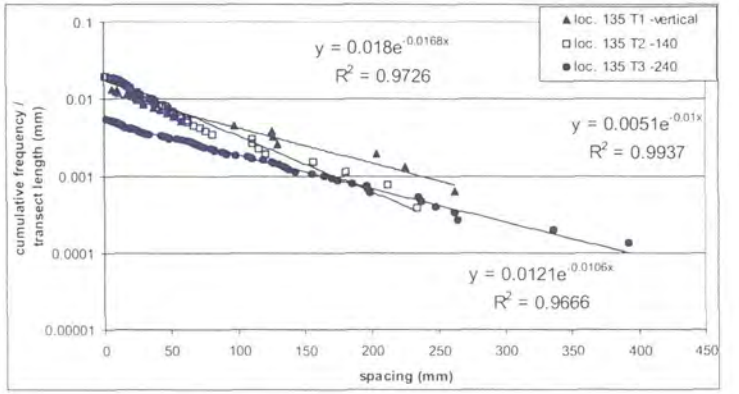

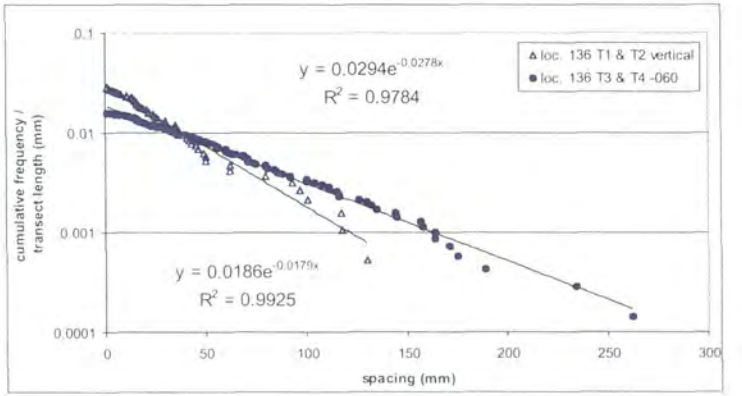

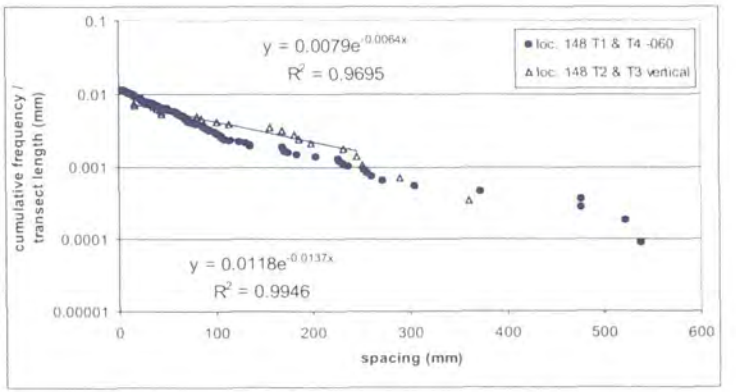

Figure 3.55 Spacing 'v' cumulative frequency plots for localities from the Hammardalen Quarry & 719 road section.
(map contours are in metres)
(graph legends display locality number, transect number and transect orientation)

Key to data set symbols

■ transects orientated parallel to the HSF (and overall MTFC) trend

□ transects orientated perpendicular to the HSF (and overall MTFC) trend

▲ vertical transects

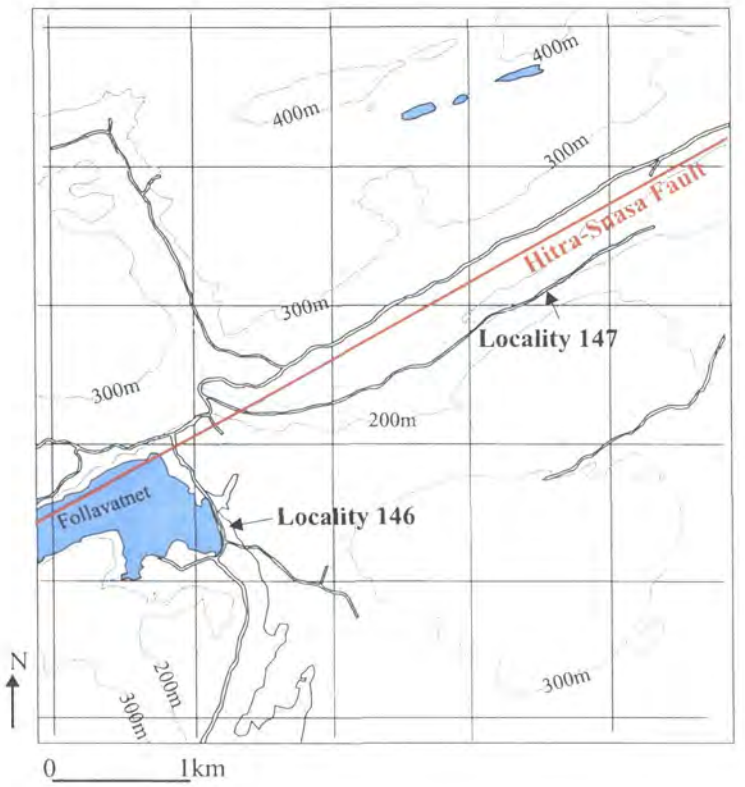

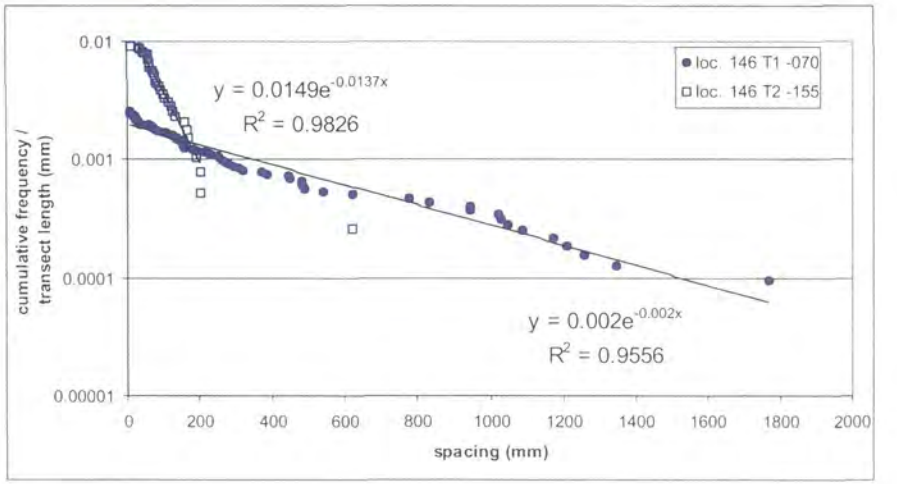

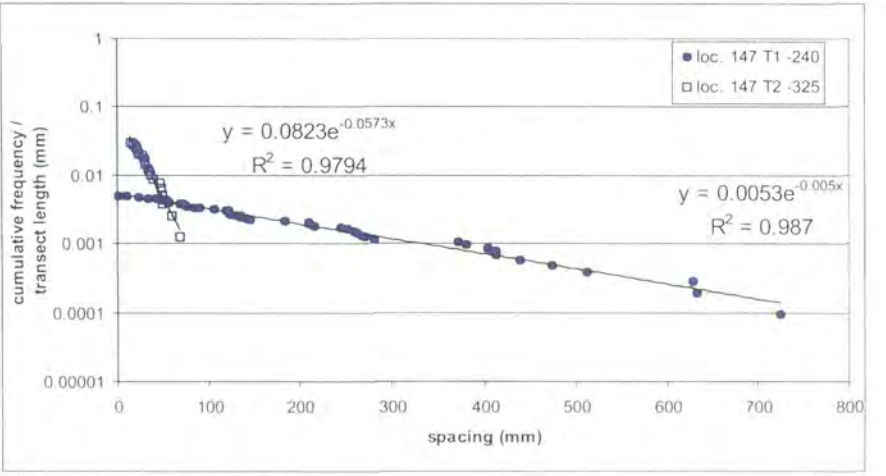

Figure 3.56 Spacing 'v' cumulative frequency plots for localities near Follavatnet.
(map contours are in metres)
(graph legends display locality number, transect number and transect orientation)

Key to data set symbols

- transects orientated parallel to the HSF (and overall MTFC) trend
- transects orientated perpendicular to the HSF (and overall MTFC) trend
- vertical transects

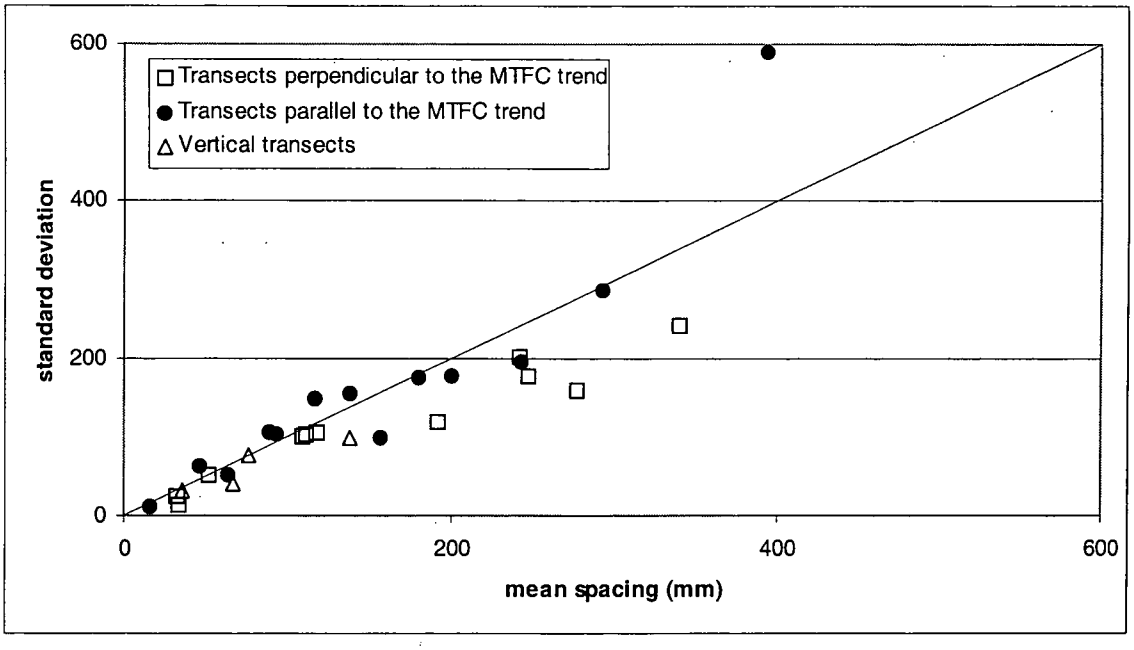

Figure 3.57 Mean spacing 'v' standard deviation plot for HSF data.

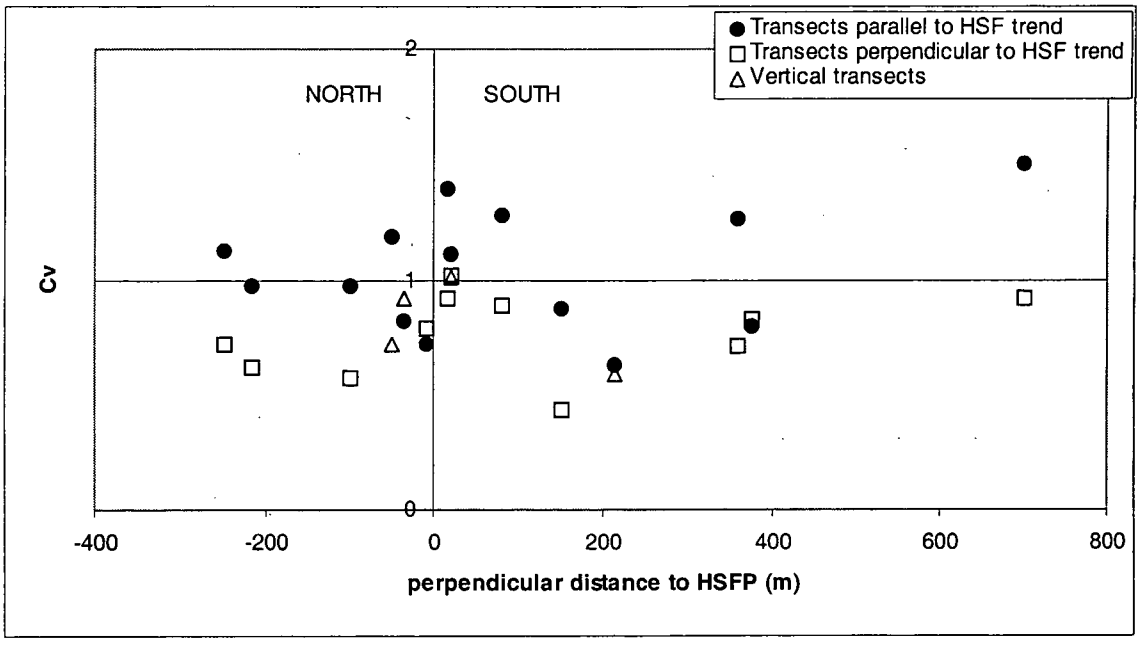

Figure 3.58 Co-efficient of variation 'v' distance plot for HSF data.

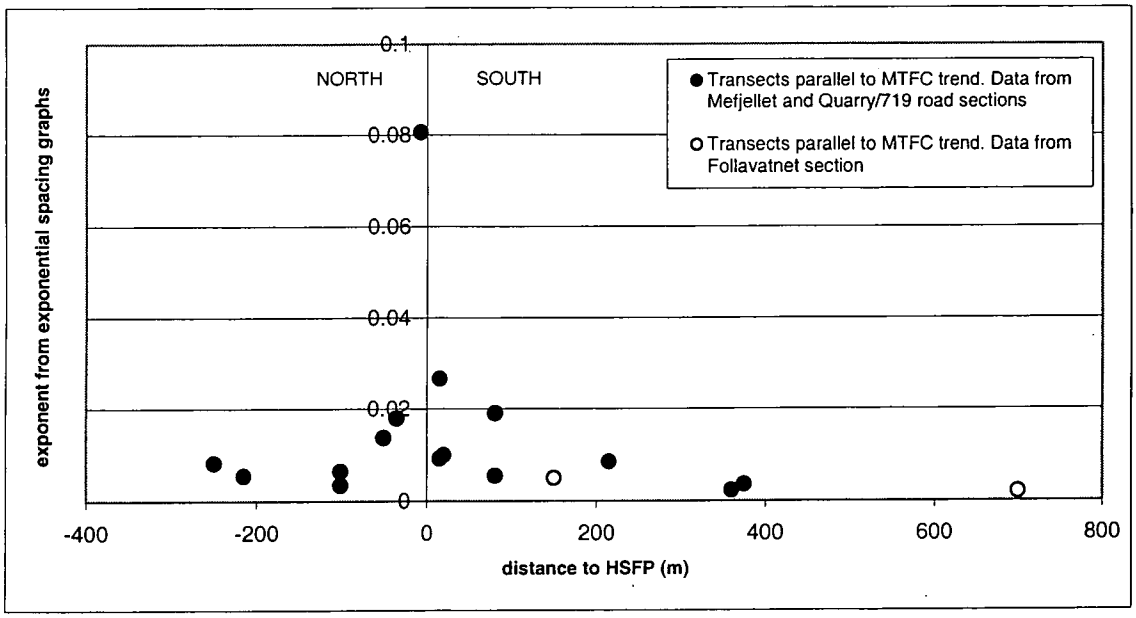

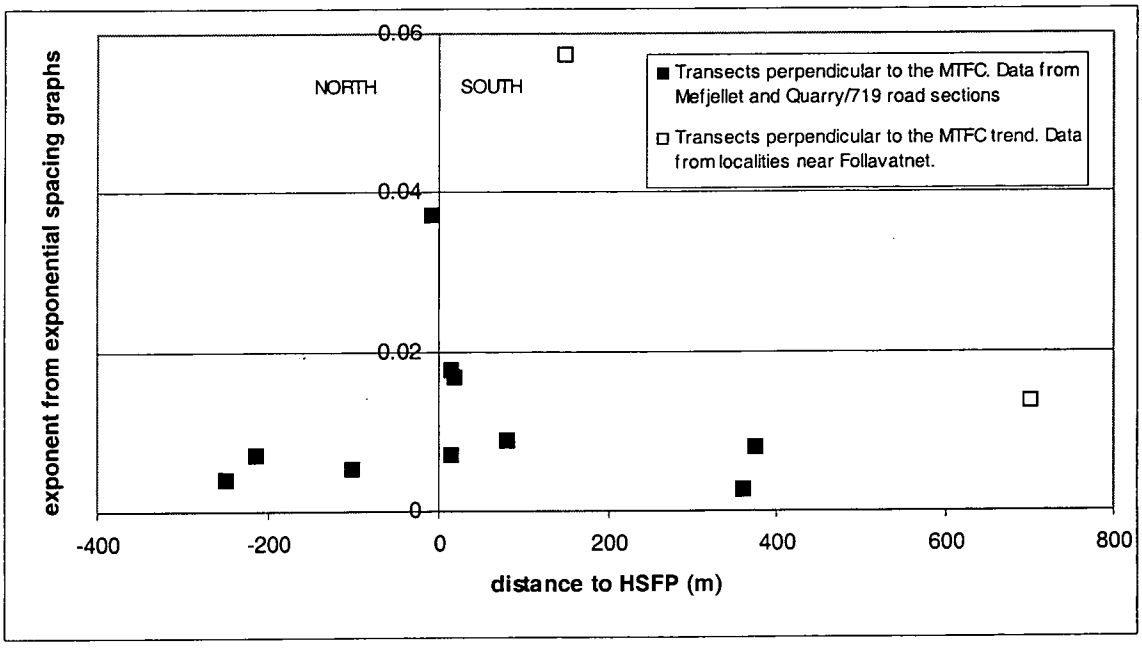

Figure 3.59 Exponential exponent values (from graphs plotted in **Figure 3.54, Figure 3.55 & Figure 3.56**) 'v' distance to HSFP.

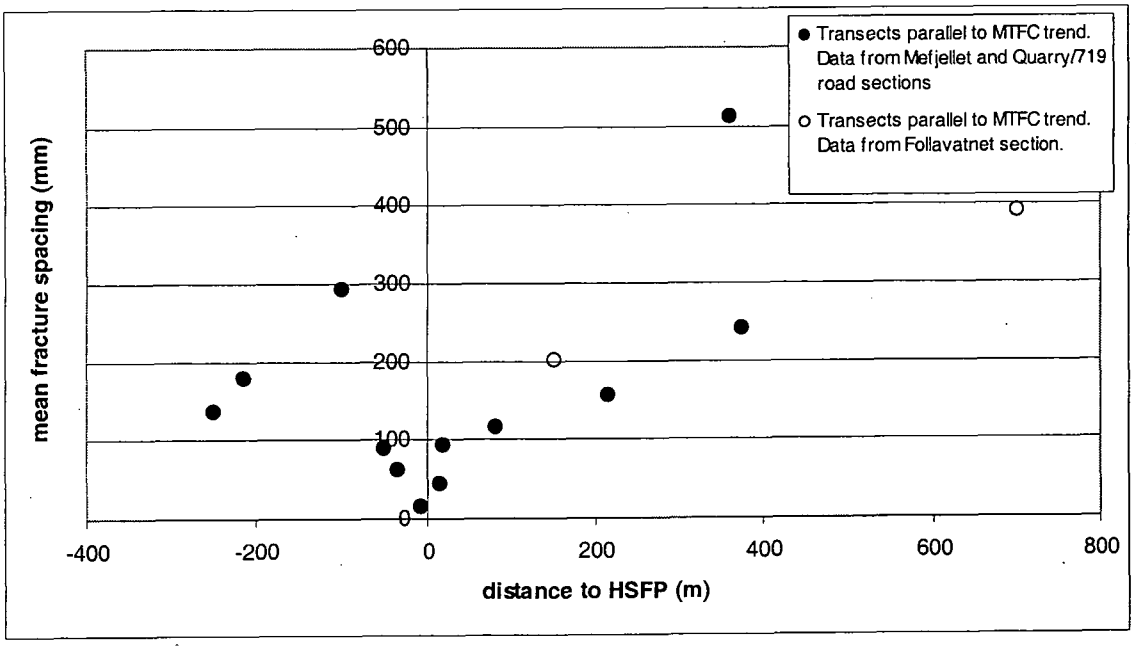

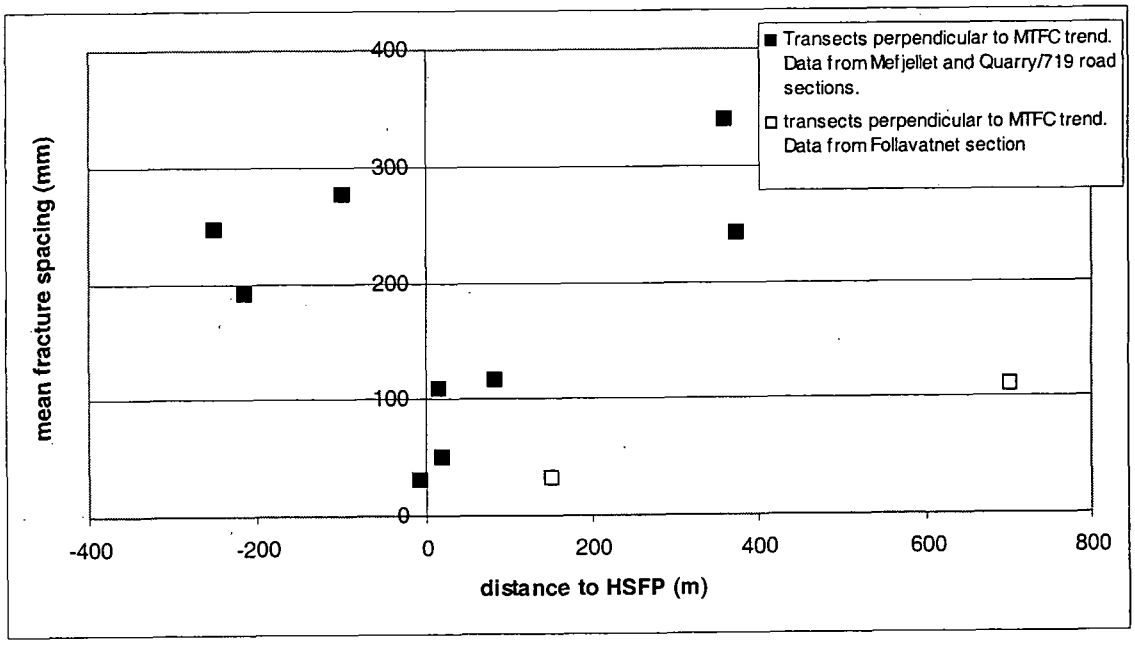

Figure 3.60 Mean fracture spacing 'v' distance to HSFP.

A

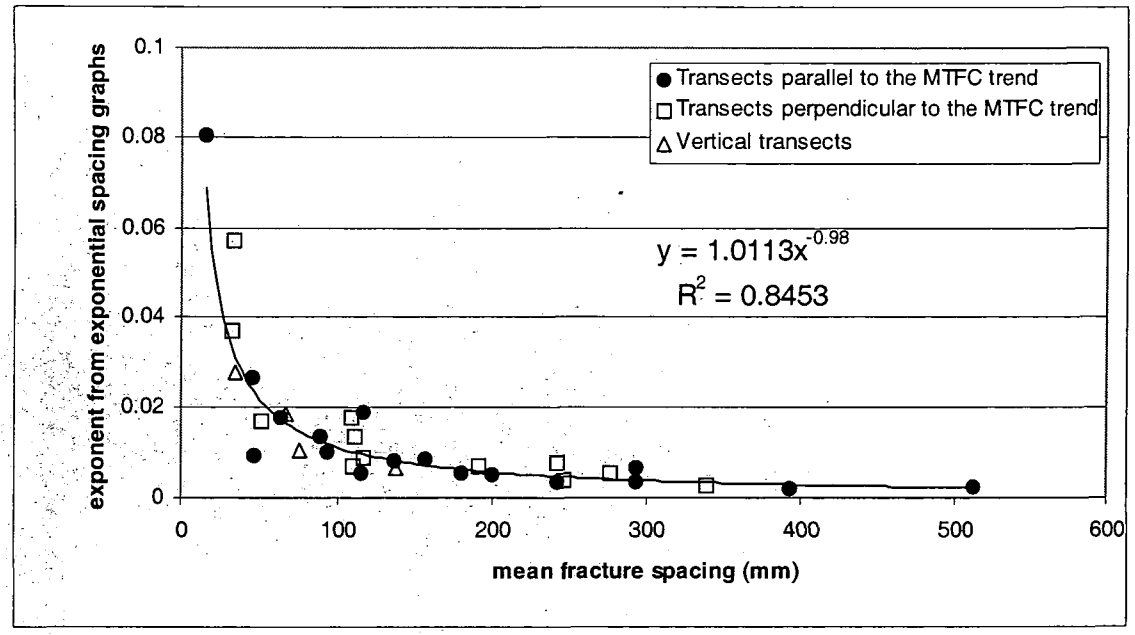

B

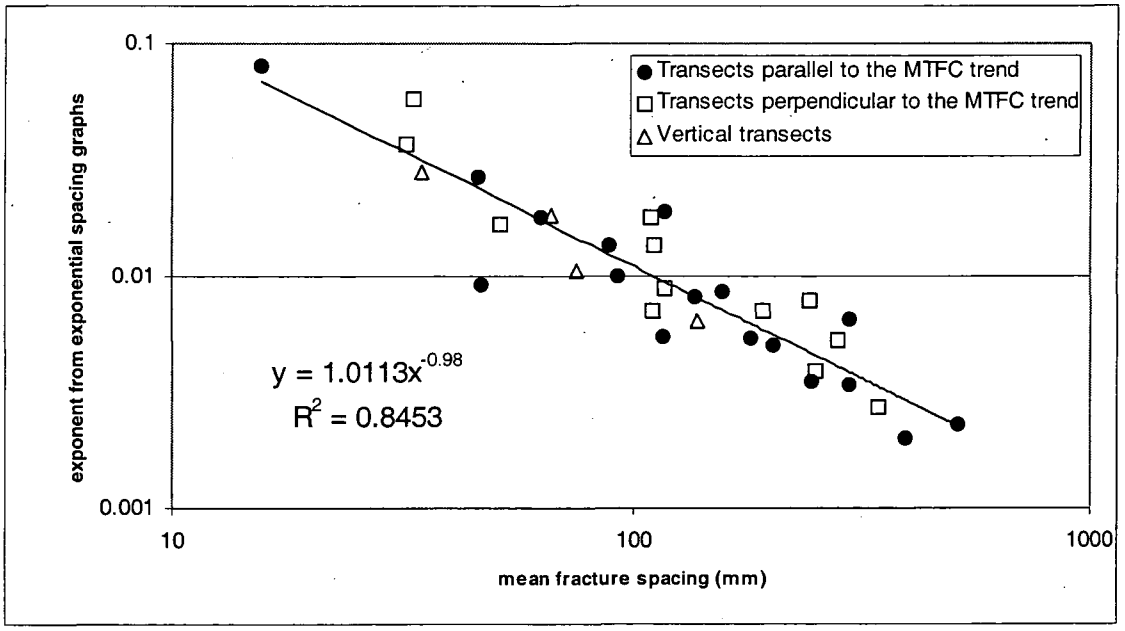

Figure 3.61 Mean fracture spacing 'v' exponential exponent value, HSF data.
A – data plotted on linear axes
B – data plotted on logarithmic axes

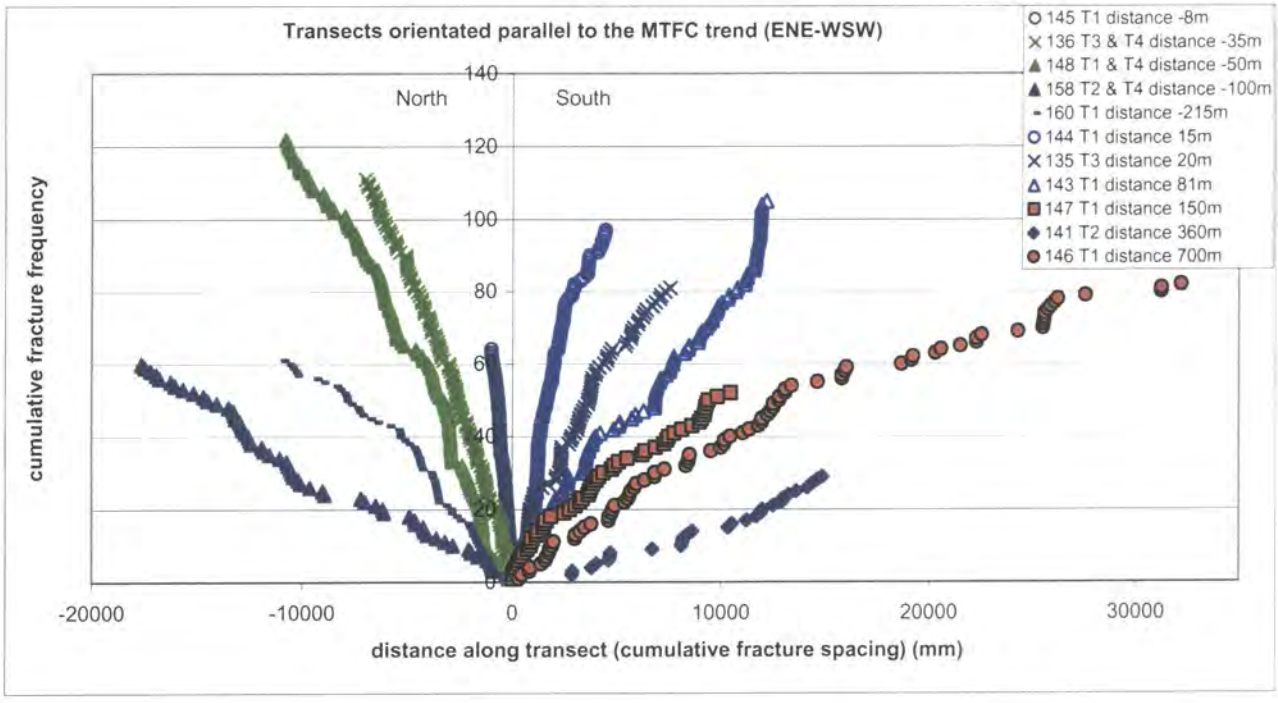

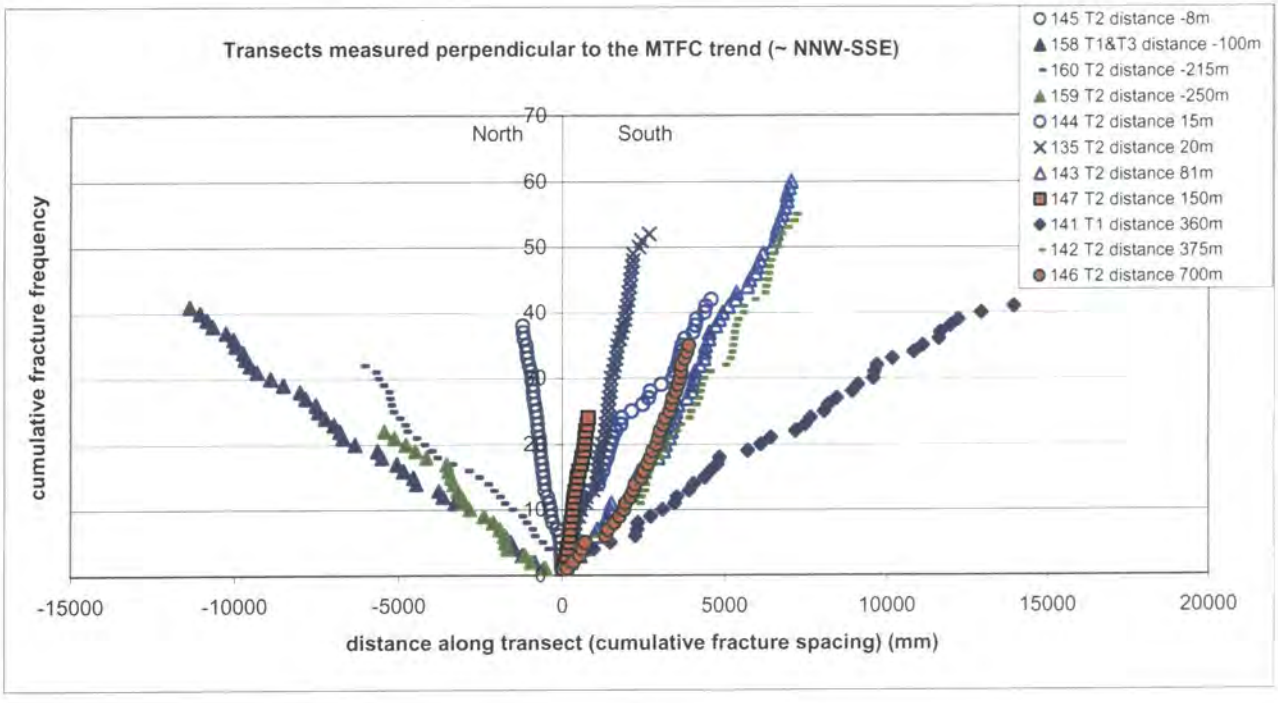

Figure 3.62 Cumulative frequency 'v' distance along 1-dimensional line transects both **A** - parallel and **B** -perpendicular to the MTFC trend.
Negative distances represent localities NW of the HSFP positive distances represent localities SE of the HSFP.

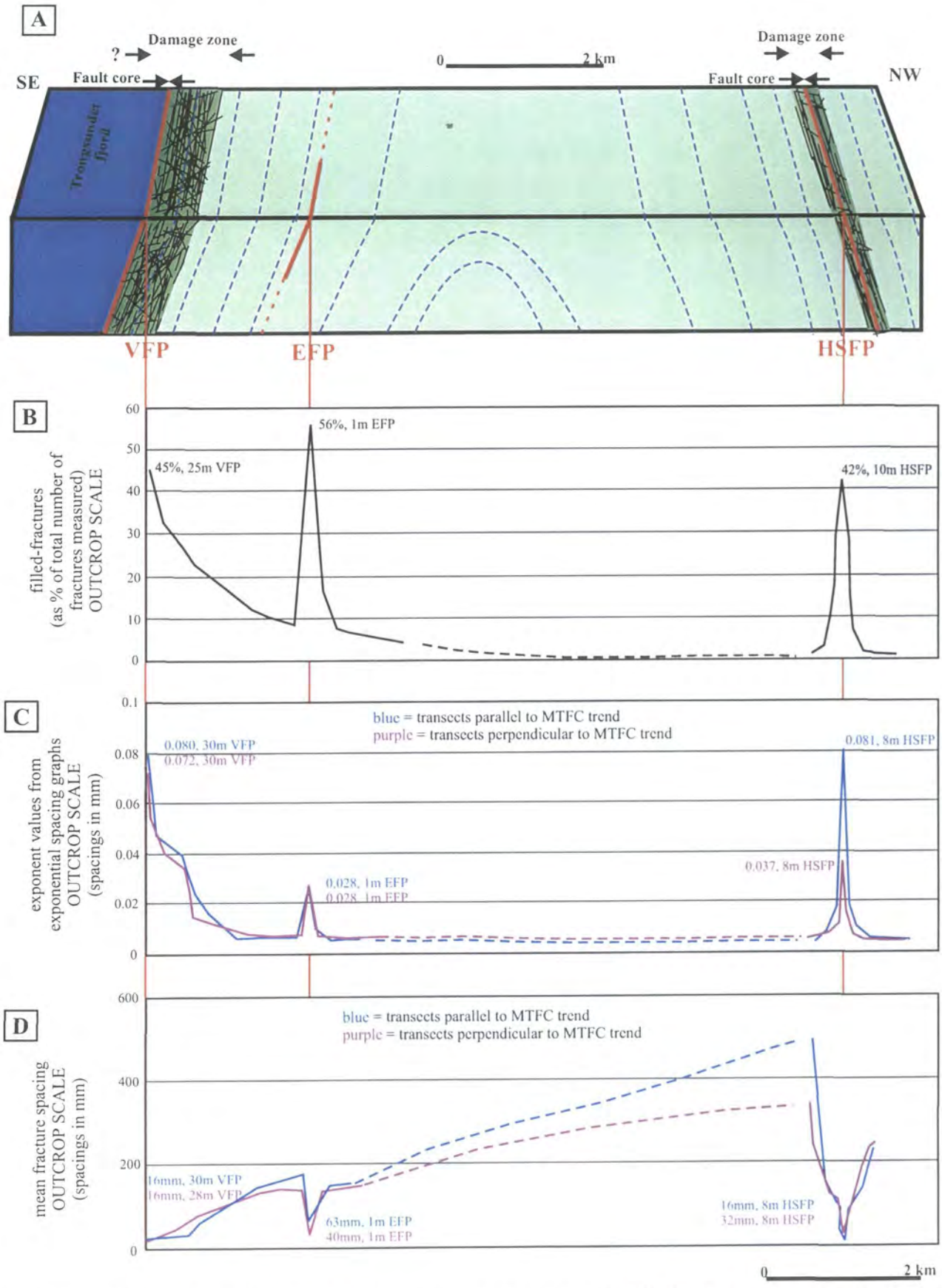

Figure 3.63 Variation in fracture parameters adjacent to the VF, HSF and EF within the MTFC. measured along 1-D line transects

A = representative cross-section across the MTFC

B = plot of filled-fractures

C = exponential exponent plots

D = mean spacing plots

(C & D show data for transects orientated both parallel & perpendicular to the MTFC trend)

dashed line = interpreted, no data points

numbers adjacent to peaks = absolute peak value and distance that data was collected from fault plane (VF, EF or HSF)

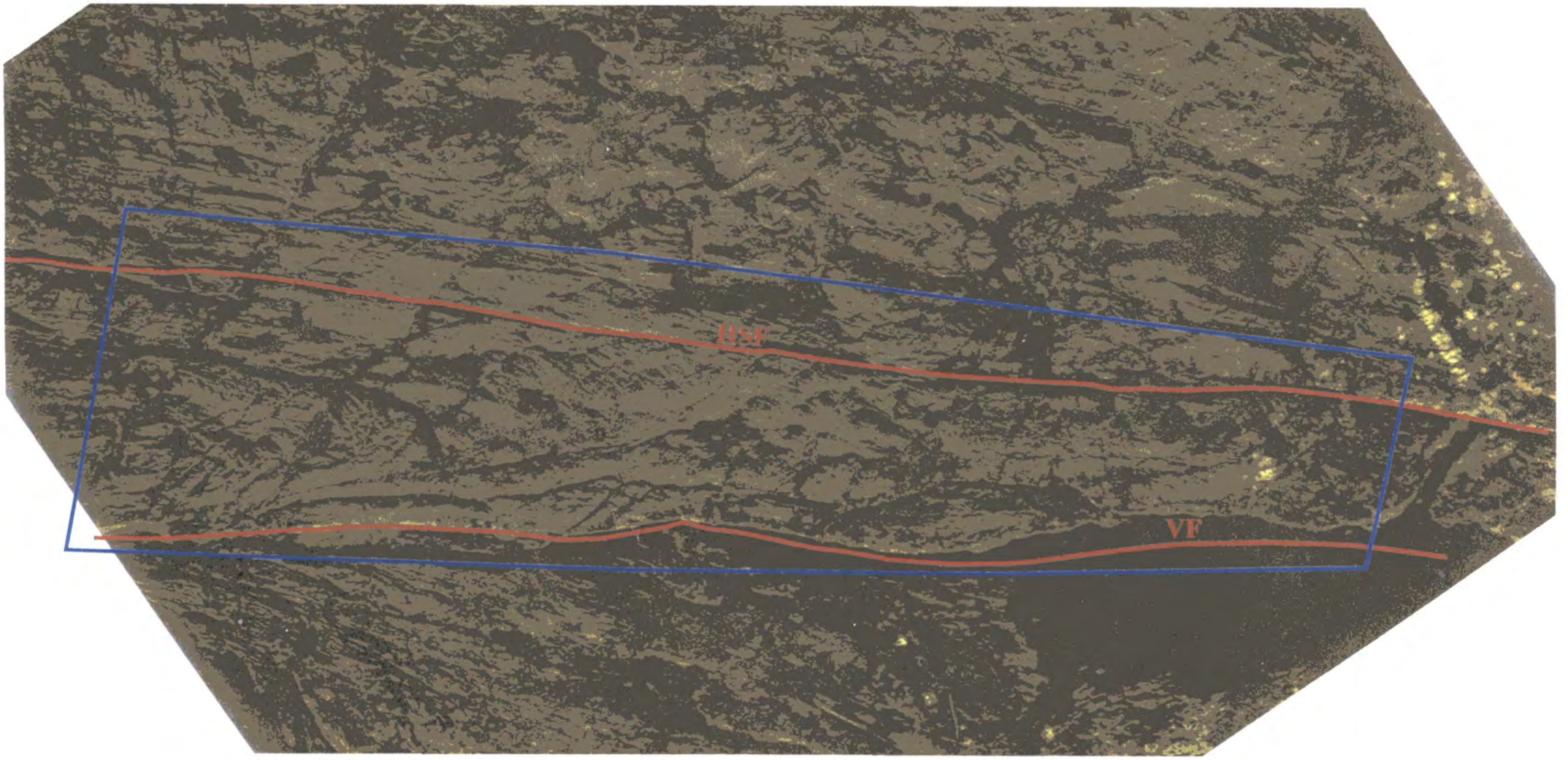

Figure 4.1 Landsat (thematic mapper) image over part of the MTFC used in this study.
Blue box = area of interpretation presented in Figure 4.2,
Red lines = 2 main fault strands within the MTFC (**VF** = Verran Fault, **HSF** = Hitra-Snasa Fault)

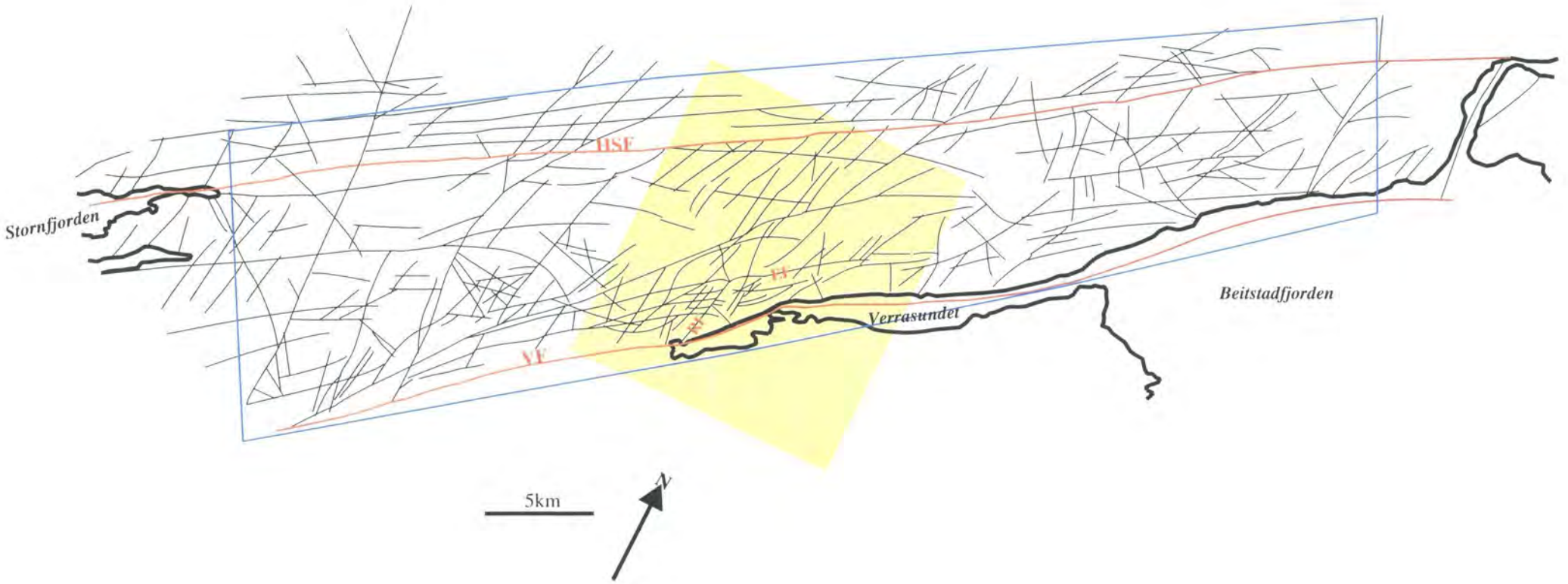

Figure 4.2 Landsat interpretation of faults/fractures within the area of the MTFC used in this study.
The mainfaults within the MTFC are indicated in red. **VF** = Verran Fault, **HSF** = Hitra-Snasa Fault, **RF** = Rautingdalen Faults, **EF** = Elvdalen Fault.
The blue box indicates the sample area used to calculate fracture parameters from the Landsat in this study.
The green box illustrates the area of the Air Photograph presented in **Figures 4.6 & 4.7**, and used in this study.
The yellow box illustrates the area of the map presented in **Figure 4.8**, which represents the area where thin section and outcrop data sets were collected

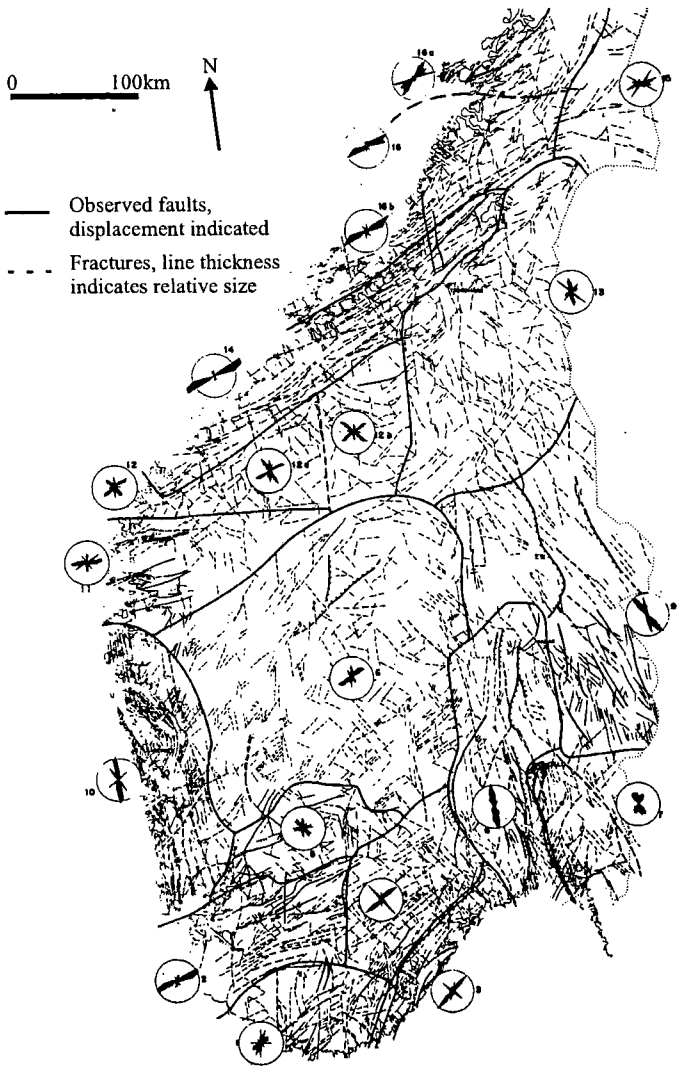

Figure 4.3a Lineament analysis of satellite data set, onshore Norway after Ramberg et al., 1997.
The interpretation is divided into sub-areas each with individual rose diagrams. MTFC lies in sub-area 14.

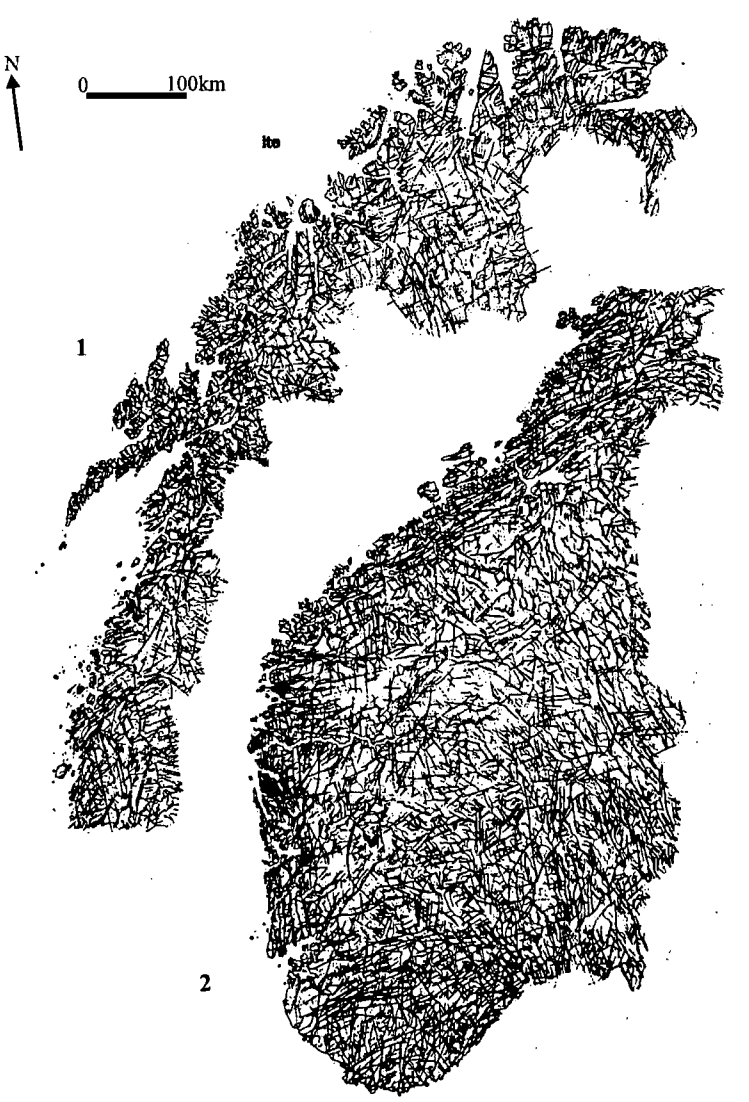

Figure 4.3b Lineament analysis of satellite data set, onshore Norway after Gabrielsen & Ramberg, 1979.
1 - Northern Norway, **2** - Central and southern Norway

Figure 4.4 Interpretation of satellite image over the MTFC and surrounding area, Central Norway. The two main strands of the MTFC are indicated in red, **VF** = Verran Fault, **HSF** = Hitra-Snasa Fault. (after Rinstad & Gronlie, 1986)

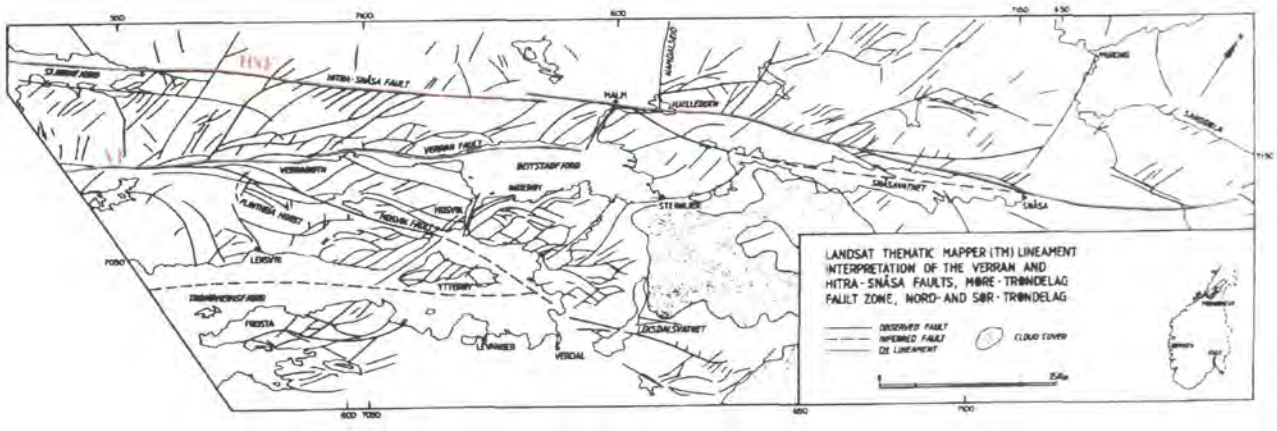

Figure 4.5 Interpretation of satellite image over the area of the MTFC, Central Norway. The two main strands of the MTFC are indicated in red, **VF** = Verran Fault, **HSF** = Hitra-Snasa Fault. (after Gronlie & Roberts, 1989)

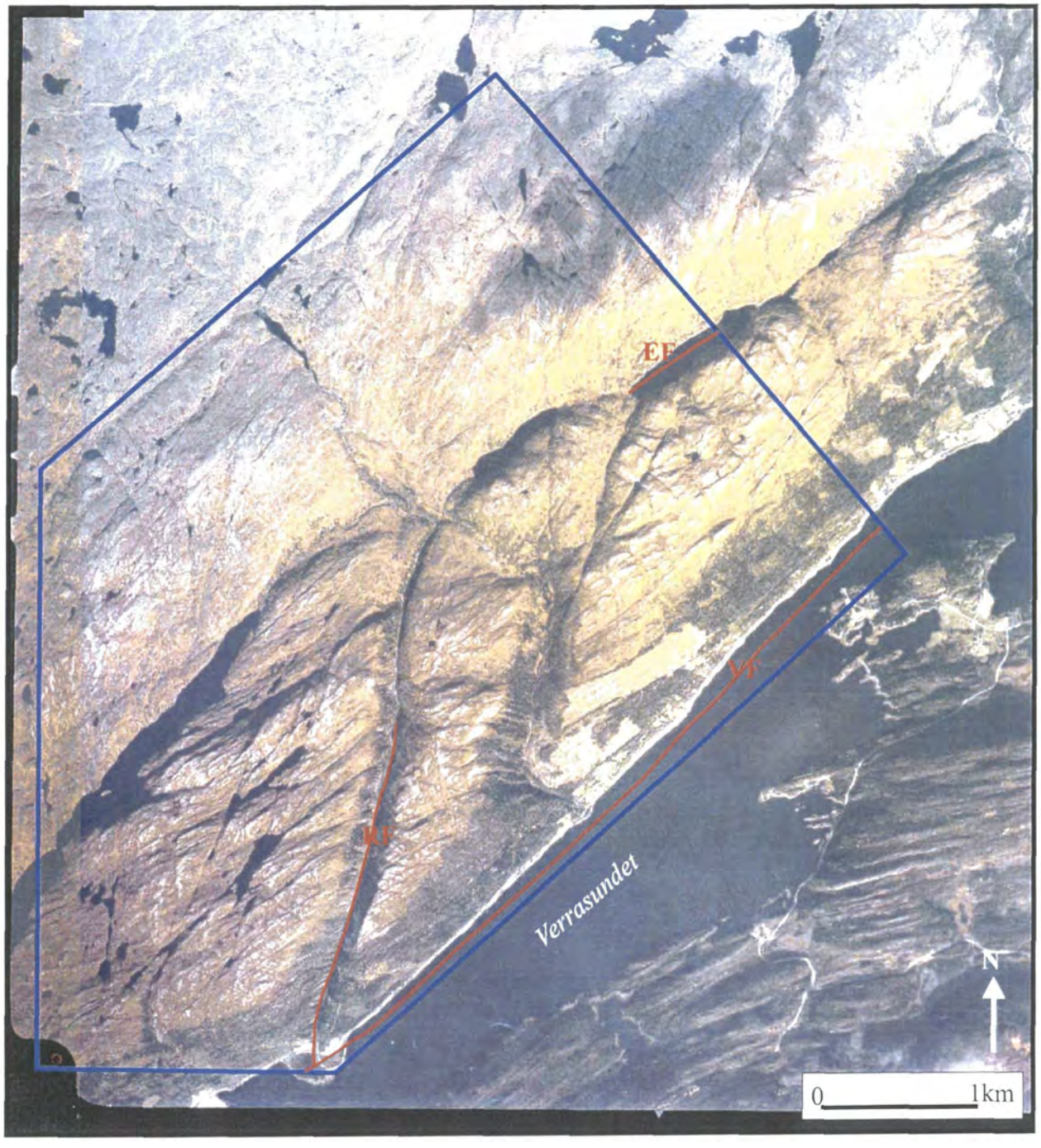

Figure 4.6 Air photograph over part of the MTFC used in this study for fault/fracture interpretation.
Blue box = area of interpretation presented in **Figure 4.7**
Red lines = main faults within the MTFC
(VF = Verran fault, RF = Rautingdalen Fault, EF = Elvdalen Fault)

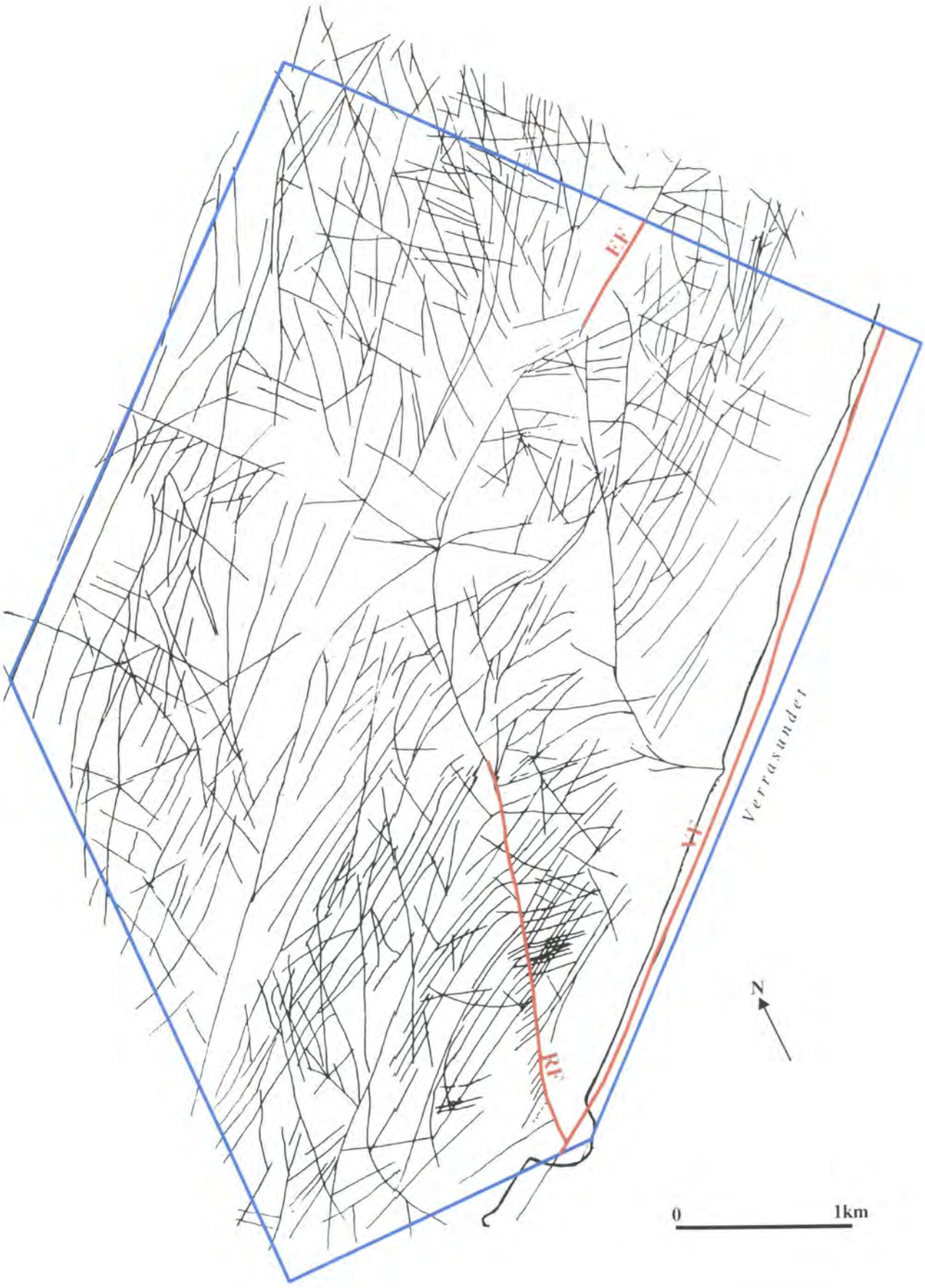

Figure 4.7 Air photograph interpretation of fractures/faults over part of the MTFC used in this study. **VF** = Verran Fault, **RF** = Rautingdalen Fault, **EF** = Elvdalen Fault.
The blue box indicates the sample area used to calculate fracture parameters in this study.

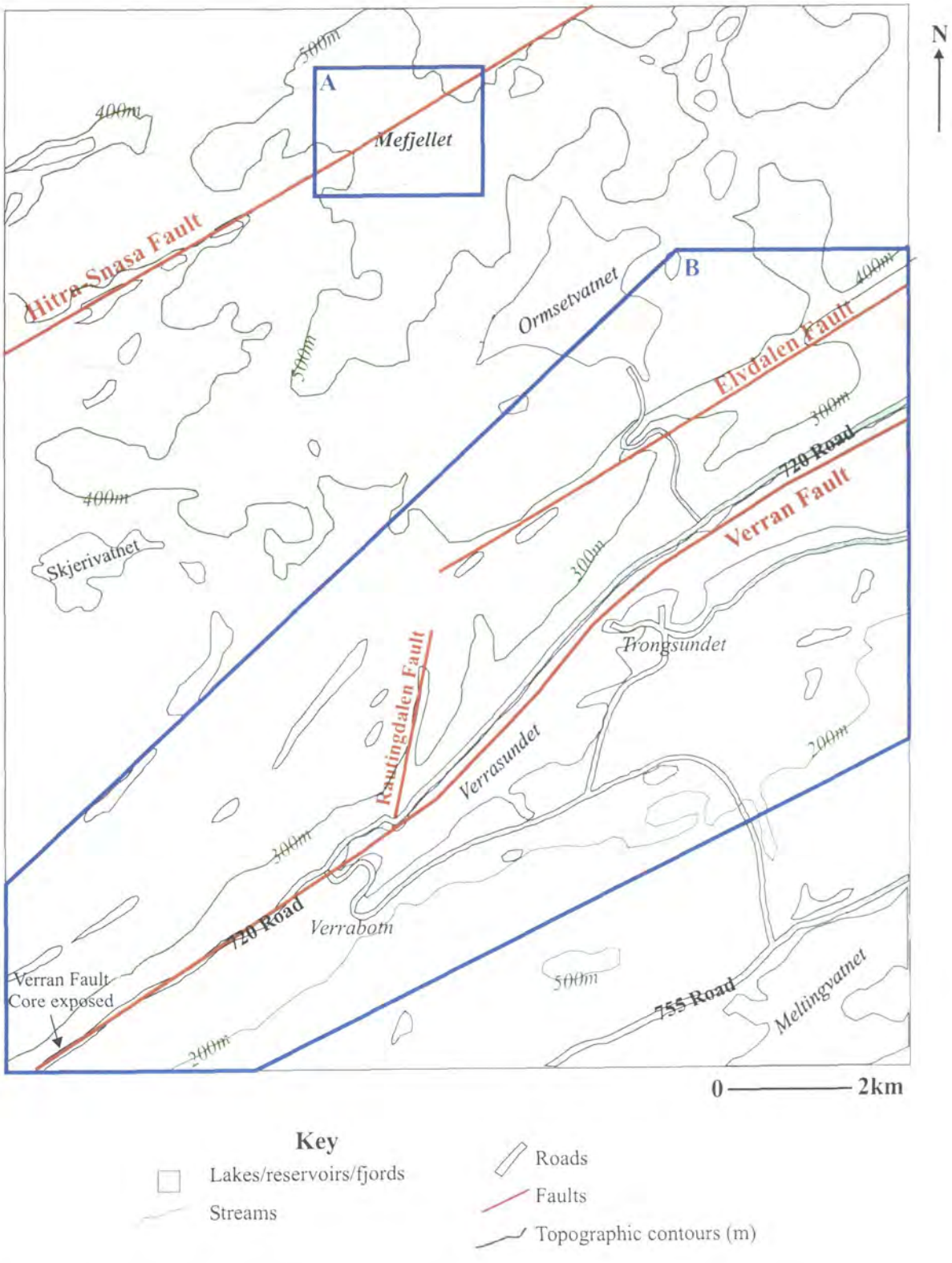

Figure 4.8 Map illustrating the areas studied for 2-dimensional fracture attribute analysis from the MTFC. (The area of this map is illustrated in **Figure 4.2**.) Blue box **A** illustrates the areas for **Figure 9a & Figure 11a**, HSF localities Blue box **B** illustrates the areas for **Figure 9b & Figure 11b**, VF and EF localities

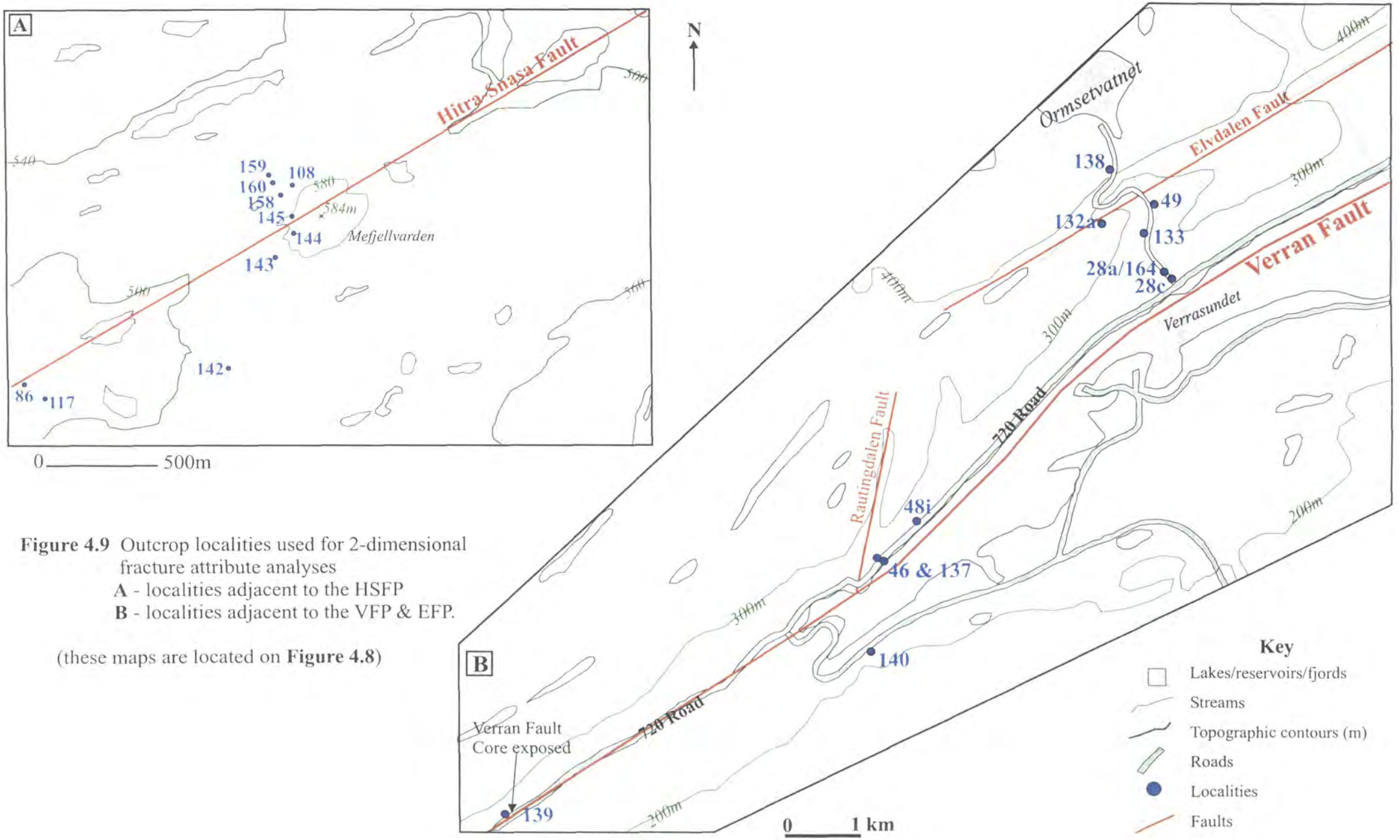

Figure 4.9 Outcrop localities used for 2-dimensional fracture attribute analyses
A - localities adjacent to the HSFP
B - localities adjacent to the VFP & EFP.

(these maps are located on **Figure 4.8**)

A

locality 132a

B

locality 132b

C

locality 86

D

locality 144

E

locality 117

F

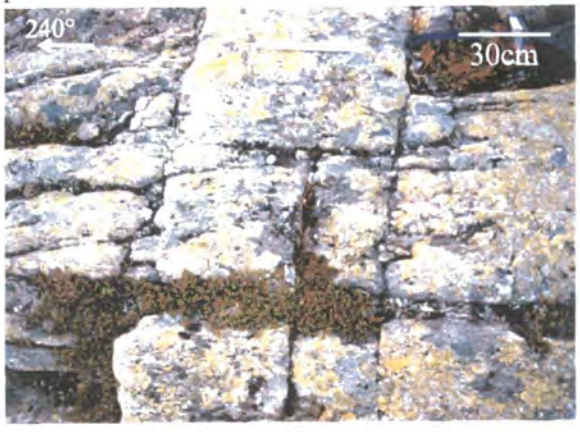

locality 142

G

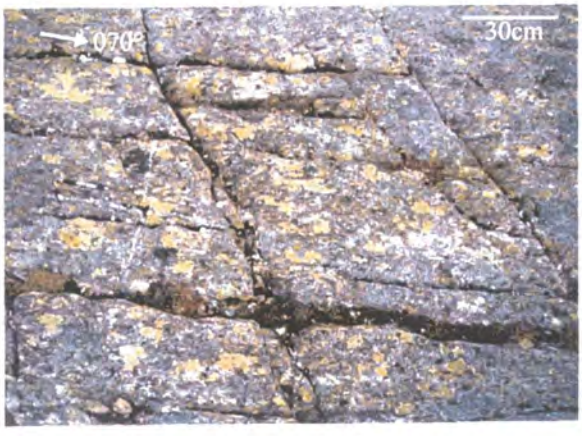

locality 143

Figure 4.10 Outcrop data sets used for the analysis of fracture attributes in 2-D.
A & B = data sets adjacent to EF
C - L = data sets adjacent to HSF
M - Z = data sets adjacent to VF
(see Table 4.1 for details)

(continued on next 3 pages)

H

locality 108

I

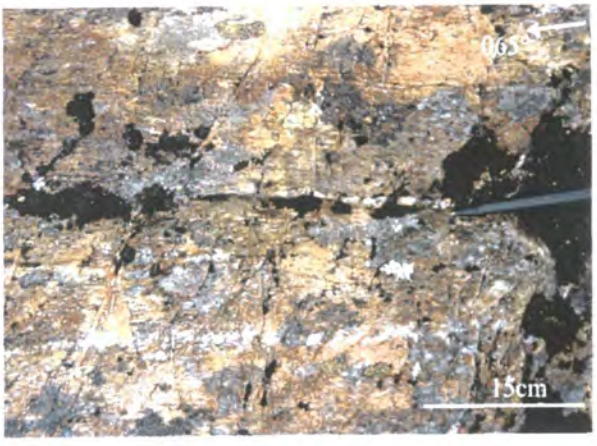

locality 145

J

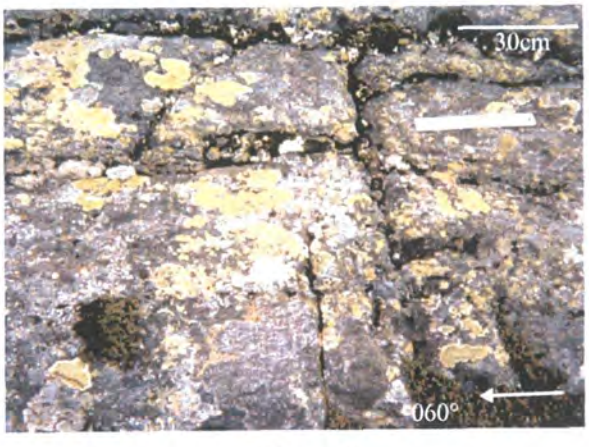

locality 159

K

locality 159

L

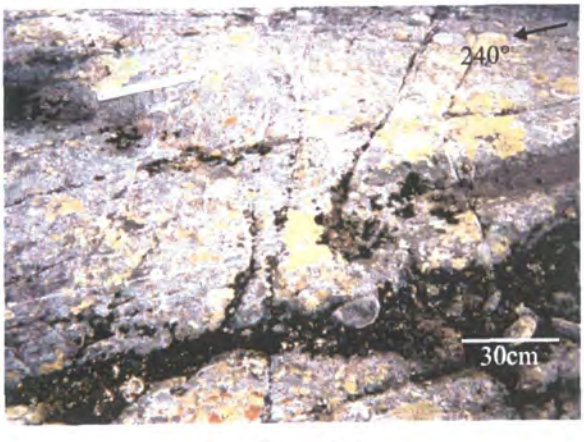

locality 160

Figure 4.10 Outcrop data sets used for the analysis of fracture attributes in 2-D.
A & B = data sets adjacent to EF
C - L = data sets adjacent to HSF
M - Z = data sets adjacent to VF
(see Table 4.1 for details)
(continued from previous page, & on next 2 pages)

M

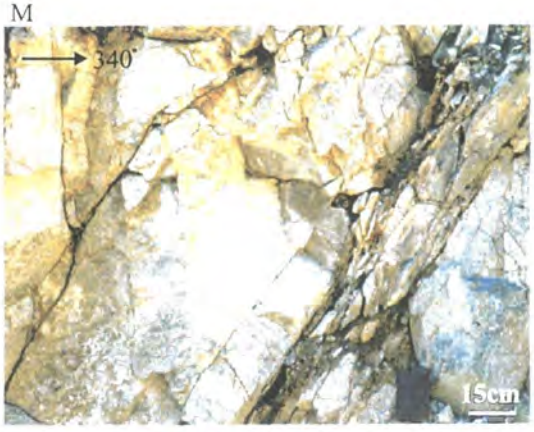

locality 28a/164 photo 1

N

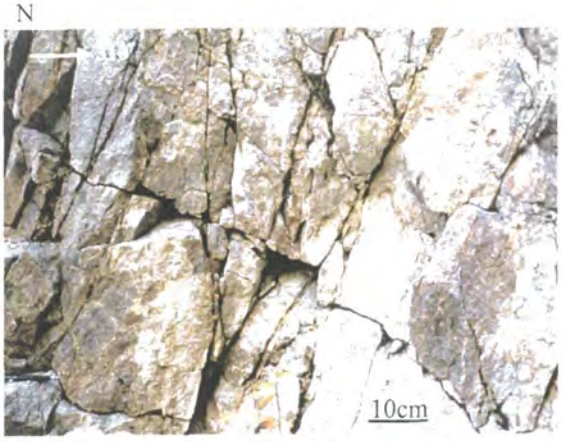

locality 28a/164 photo 2

O

locality 28c photo 1

P

locality 28c photo 2

Q

locality 49

R

locality 133

S

locality 138

Figure 4.10 Outcrop data sets used for the analysis of fracture attributes in 2-D.
A & B = data sets adjacent to EF
C - L = data sets adjacent to HSF
M - Z = data sets adjacent to VF
(see Table 4.1 for details)

(continued from previous 2 pages, & on next page)

T

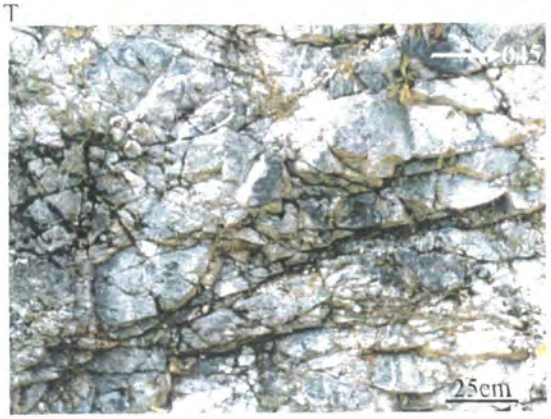

locality 46

U

locality 137

V

locality 48i (gneiss)

W

locality 48i (amphibolite)

X

locality 139 photo 1

Y

locality 139 photo 2

Z

locality 140

Figure 4.10 Outcrop data sets used for the analysis of fracture attributes in 2-D.
A & B = data sets adjacent to EF
C - L = data sets adjacent to HSF
M - Z = data sets adjacent to VF
(see Table 4.1 for details)

(continued from previous 3 pages)

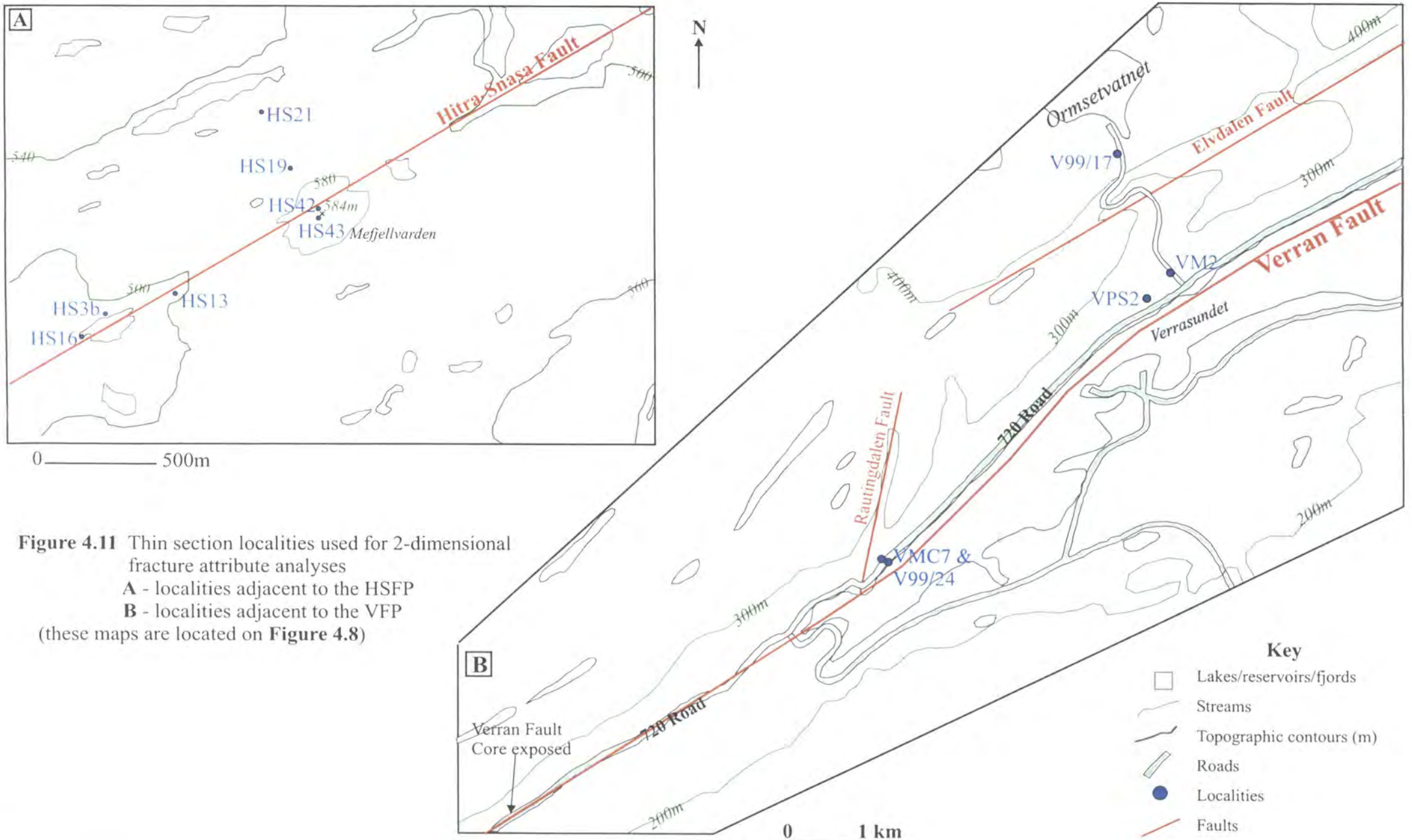

Figure 4.11 Thin section localities used for 2-dimensional fracture attribute analyses
A - localities adjacent to the HSFP
B - localities adjacent to the VFP
(these maps are located on **Figure 4.8**)

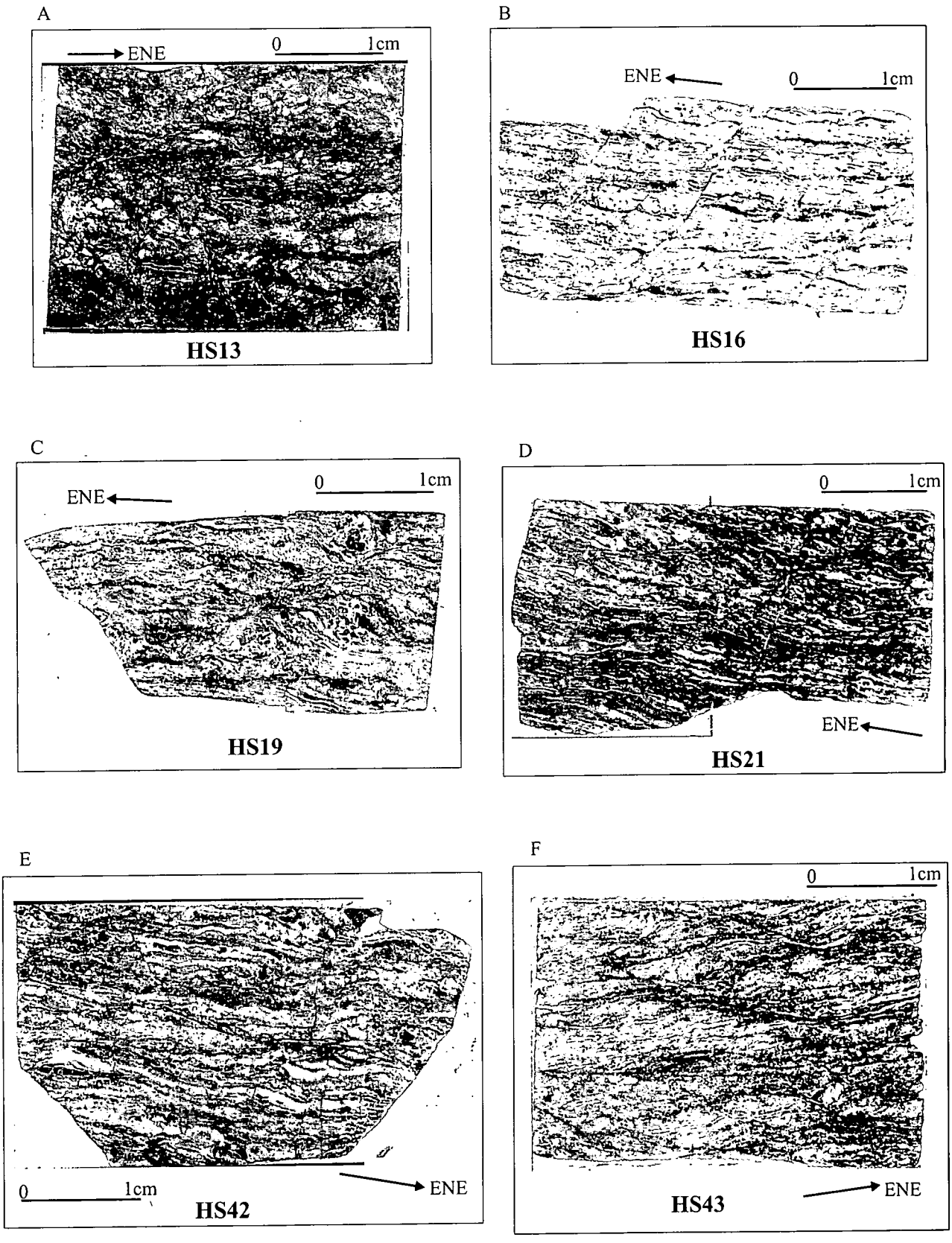

Figure 4.12 Thin-section data sets used to analyse fracture attributes.
A - F = data sets adjacent to the HSFP
(unfortunately section HS3b which was also used is broken and unable to be photographed or scanned)
G - K = data sets adjacent to the VFP
(see Table 4.2 for details)

(continued on next page)

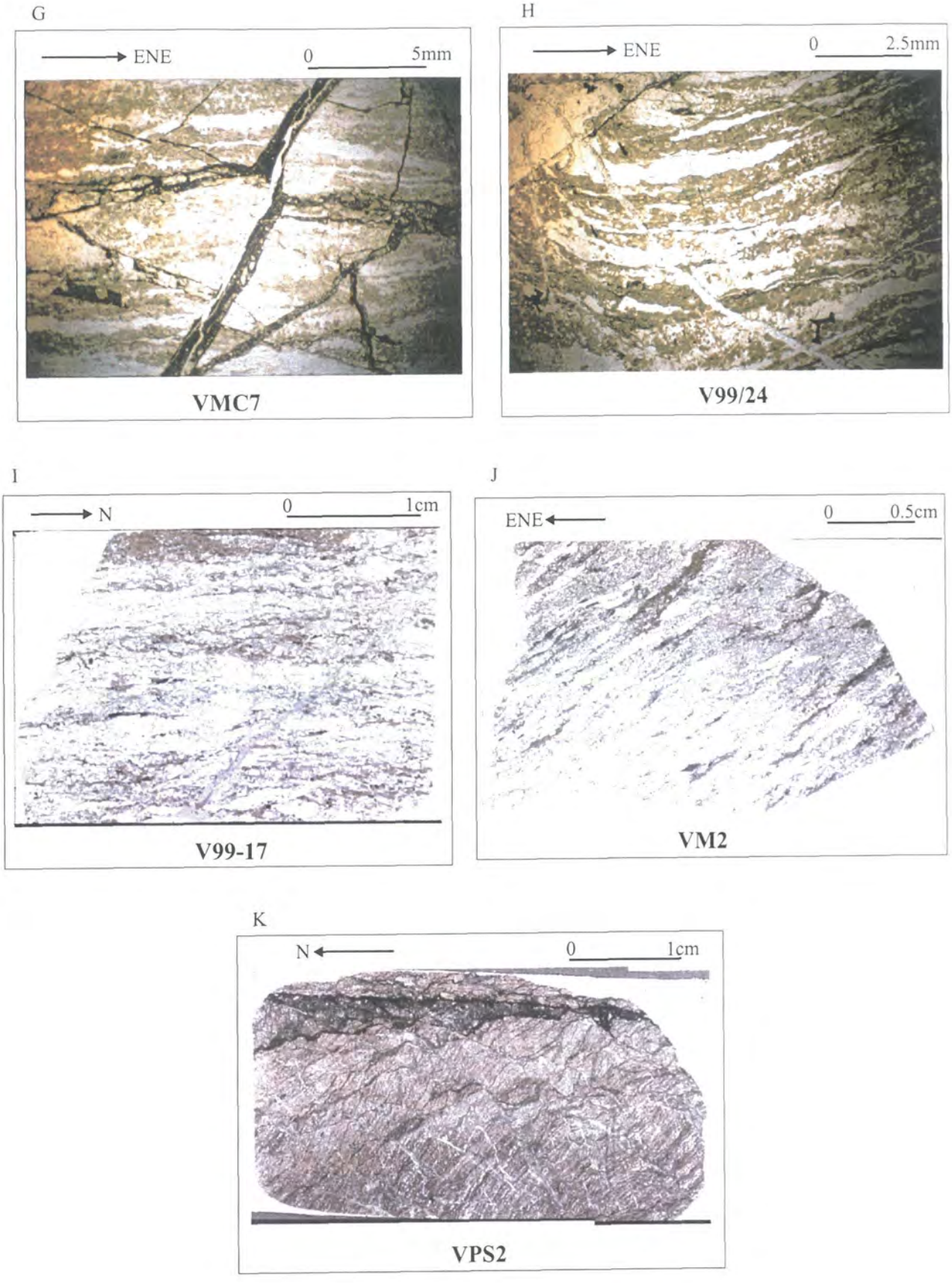

Figure 4.12 Thin-section data sets used to analyse fracture attributes.
A - F = data sets adjacent to the HSFP
G - K = data sets adjacent to the VFP
(G & H are only parts of the thin-section used, as the original sections are too large to scan)
(see Table 4.2 for details)

(continued from previous page)

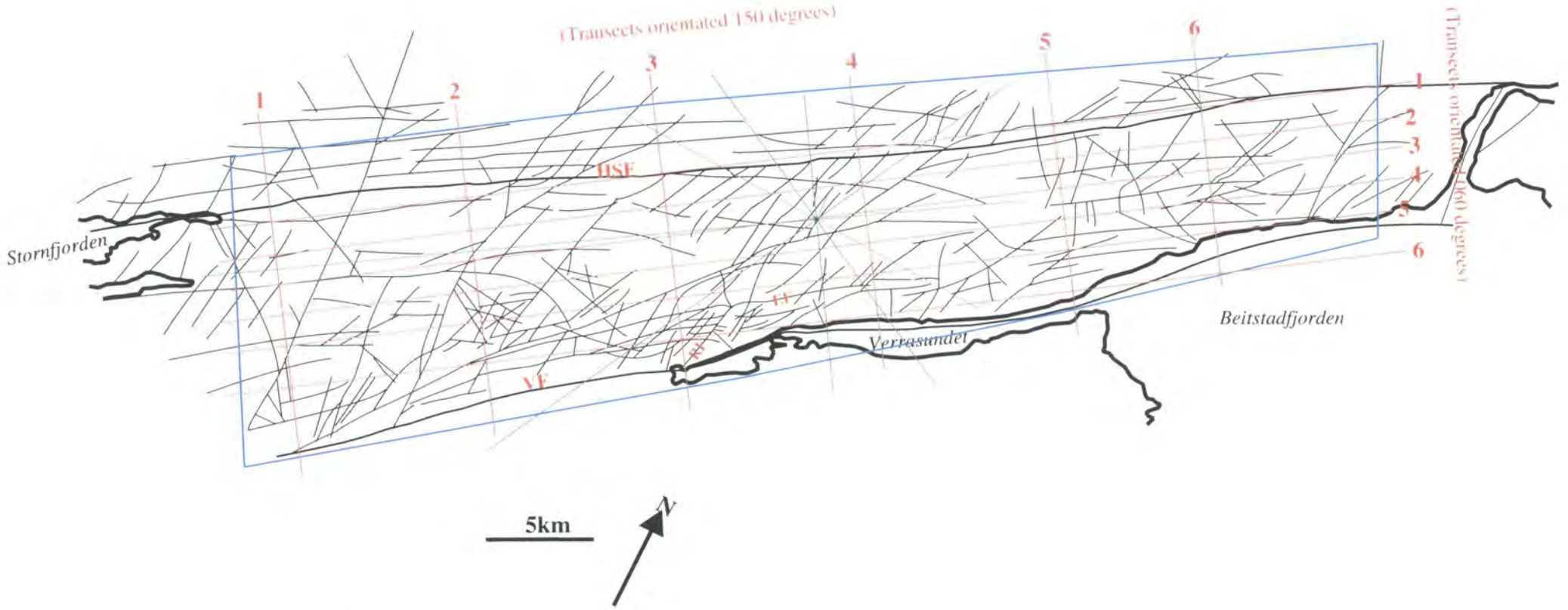

Figure 4.13 Landsat interpretation over the MTFC used in this study
VF = Verran Fault, **HSF** = Hitra-Snasa Fault, **EF** = Elvdalen Fault, **RF** = Rautingdalen Fault.
Blue box = sample area
Red lines = transects used to measure fracture spacings (6 x 060, parallel to MTFC trend, 6 x 150 perpendicular to MTFC trend)
Green lines = transects used to calculate mean spacing ellipse, (transects every 30 degrees across the Landsat interpretation)

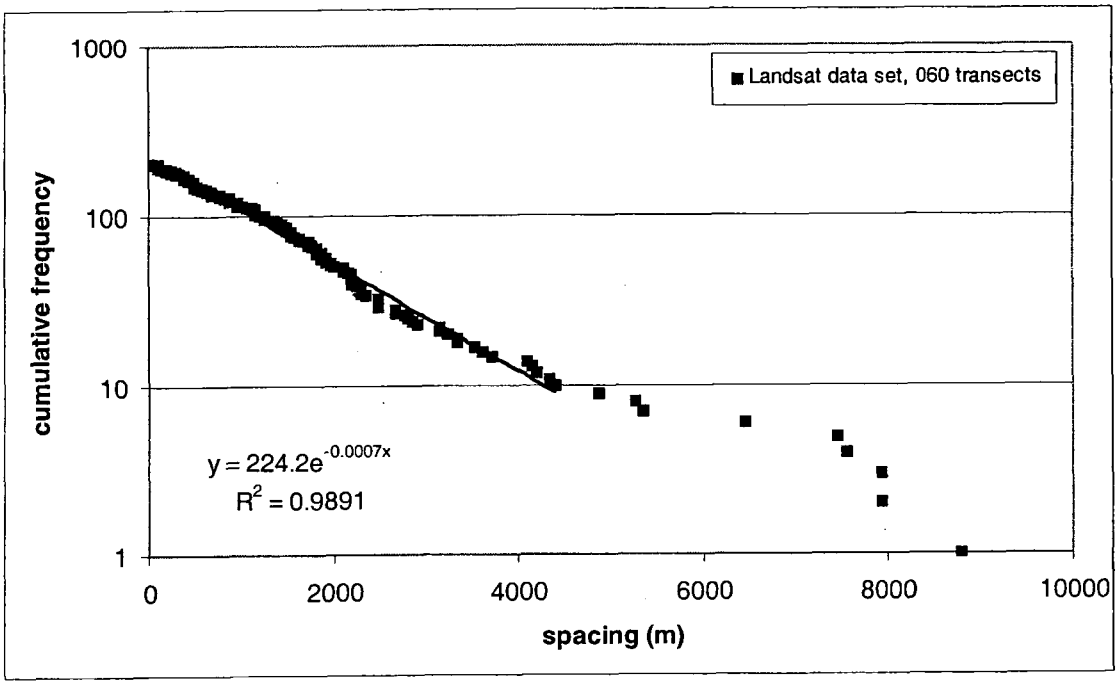

Figure 4.14 Cumulative frequency 'v' fracture spacing plot for transects orientated 060° across the Landsat™ image

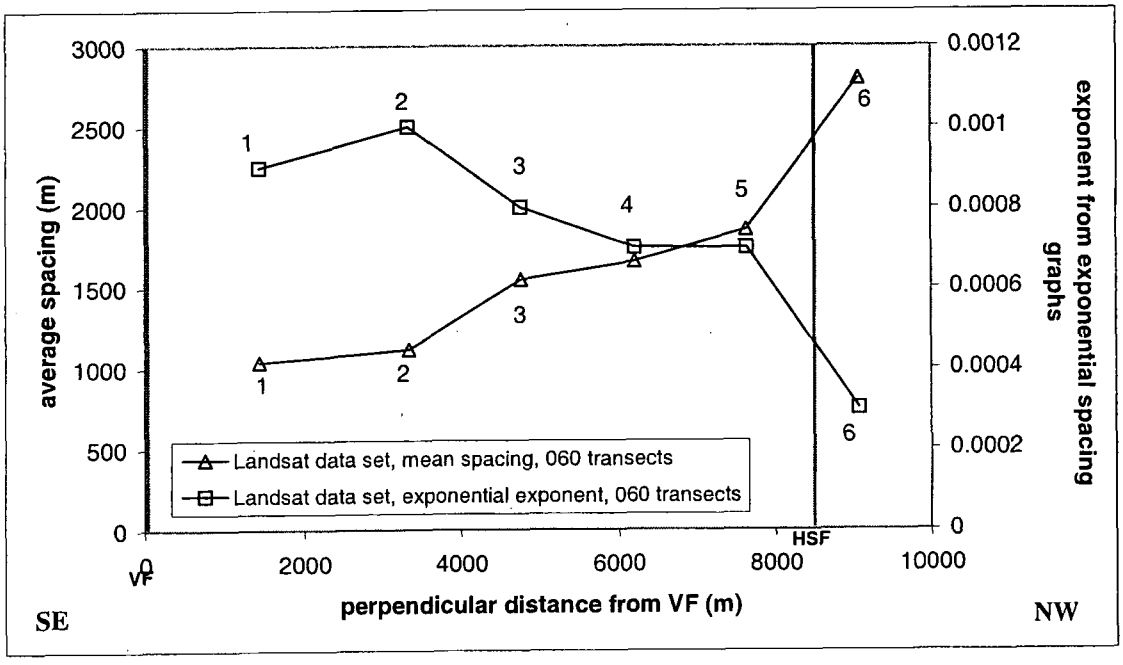

Figure 4.15 Exponent values from exponential spacing distributions and mean fracture spacing values from transects orientated 060° across the Landsat™ image (numbers indicate 060° transects from **Figure 4.13**)

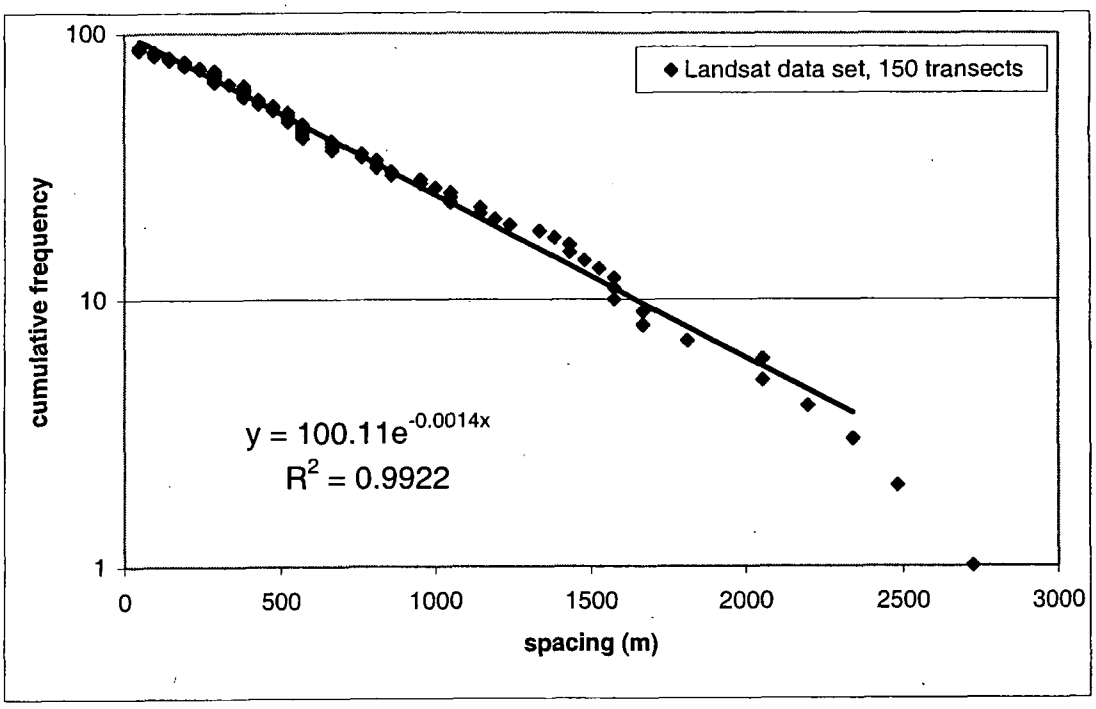

Figure 4.16 Cumulative frequency 'v' fracture spacing plot for transects orientated 150° across the Landsat™ image

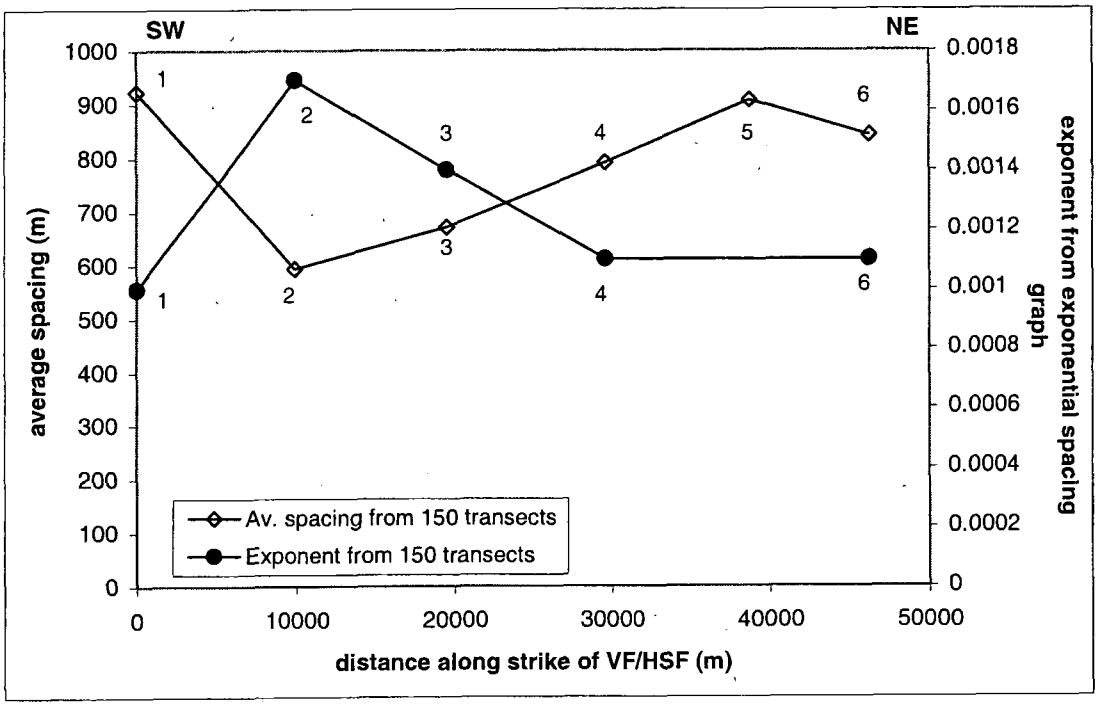

Figure 4.17 Exponent values from exponential spacing distributions and mean spacing values from transects orientated 150° across the Landsat™ image (numbers indicate 150° transects from **Figure 4.13**)

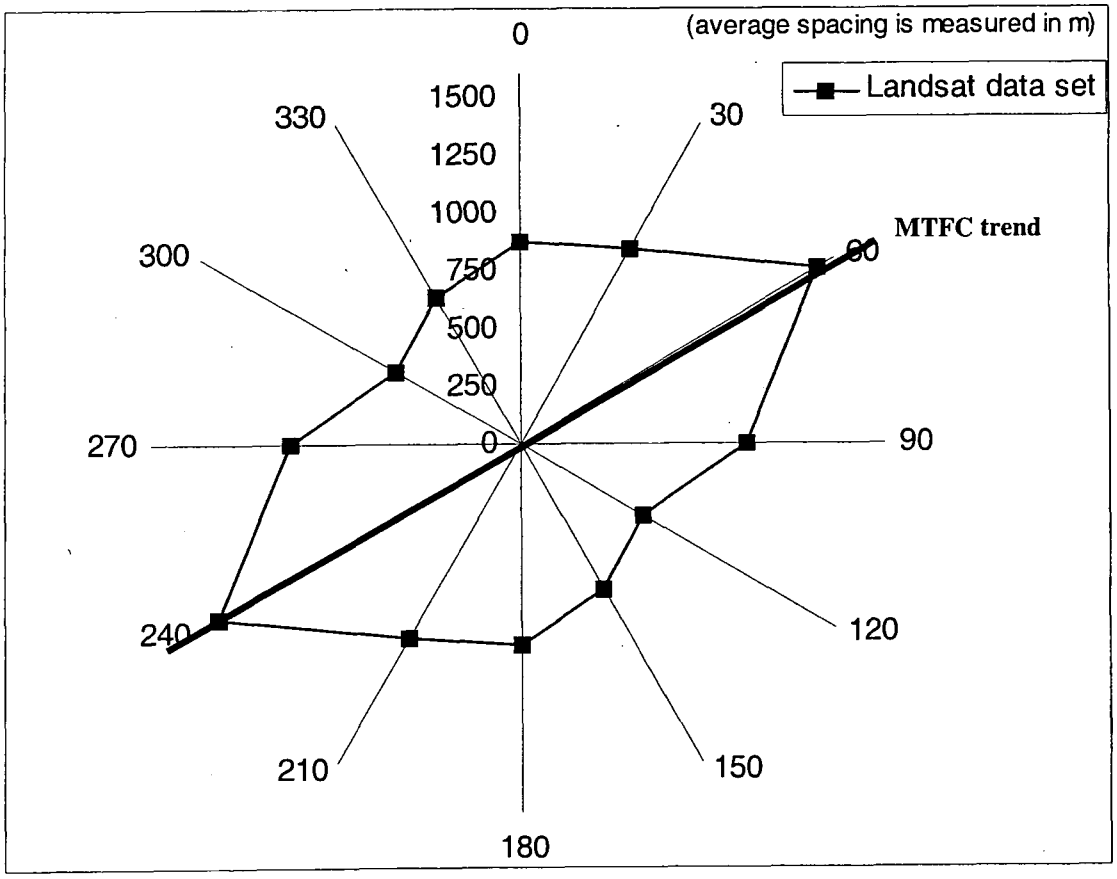

Figure 4.18 Mean spacing ellipse created from the Landsat™ image.

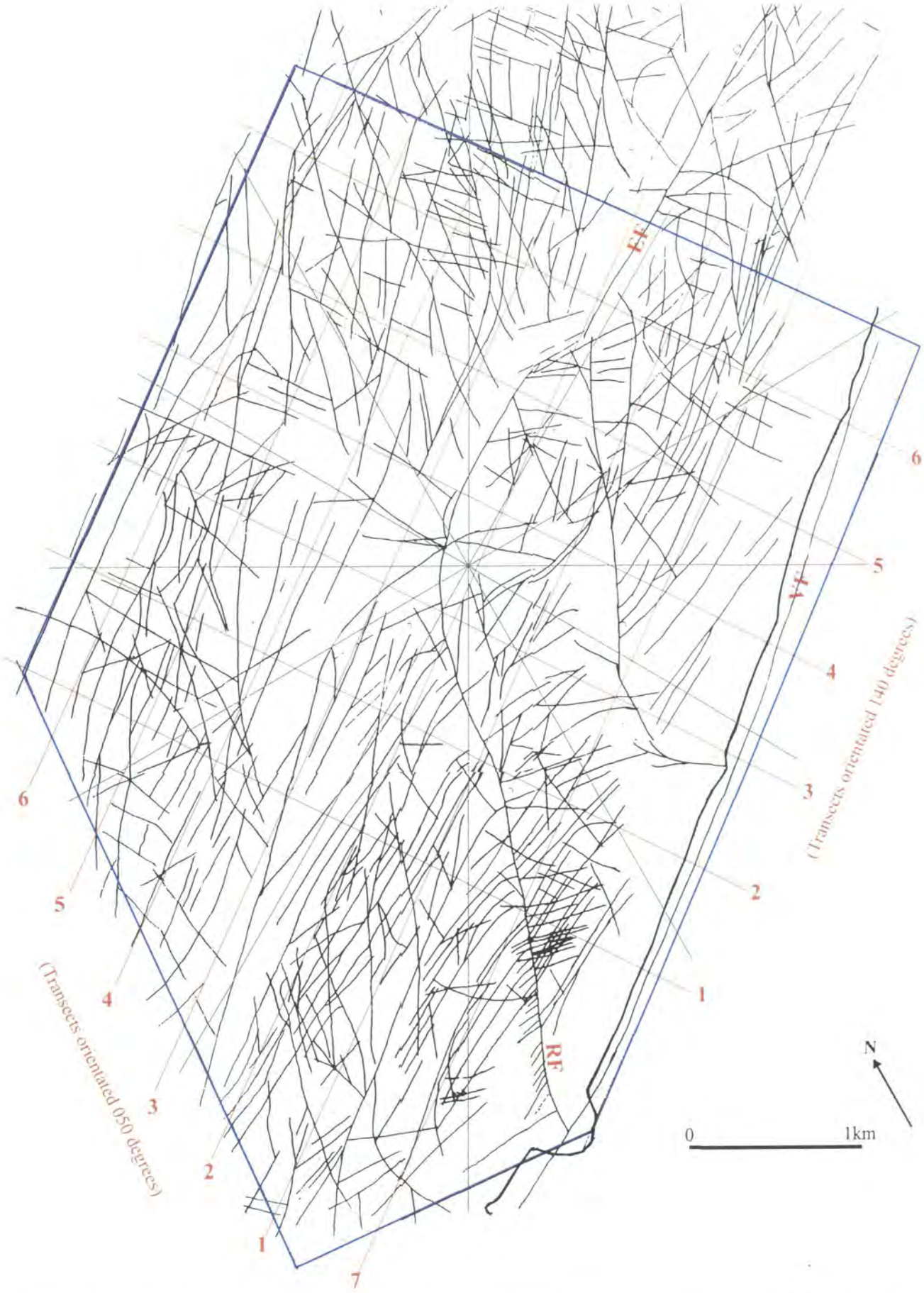

Figure 4.19 Air photograph interpretation over part of the MTFC used in this study, **VF** = Verran Fault, **EF** = Elvdalen Fault, **RF** = Rautingdalen Fault.
Blue box = sample area
Red lines = transects used to measure fracture spacings (6 x 050, parallel to MTFC trend, 6 x 140 perpendicular to MTFC trend)
Green lines = transects used to calculate mean spacing ellipse, (transects every 30 degrees across the Landsat interpretation)

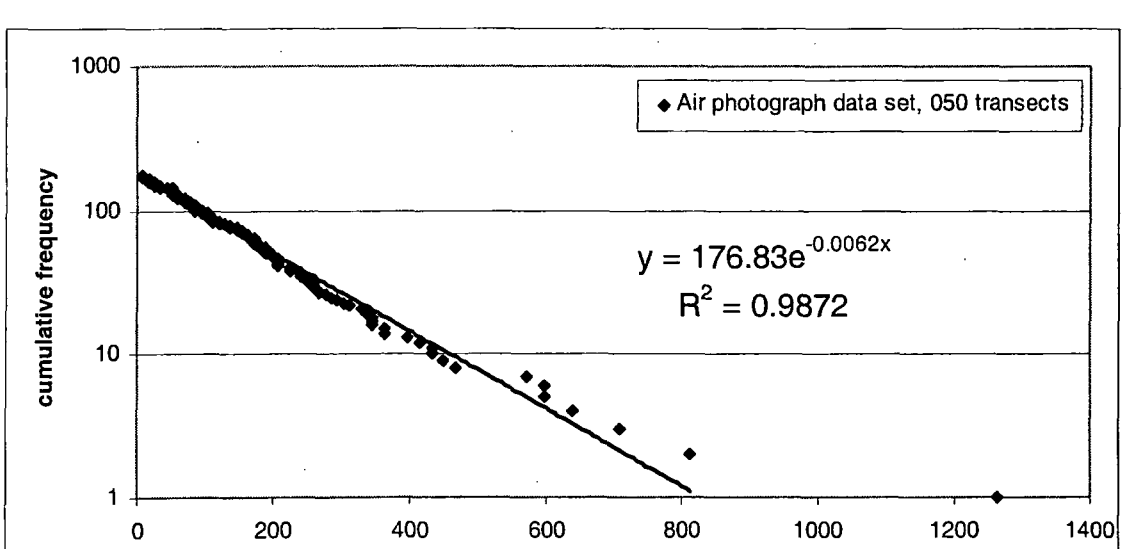

Figure 4.20 Cumulative frequency 'v' fracture spacing plot for transects orientated 050° across the air photograph data set

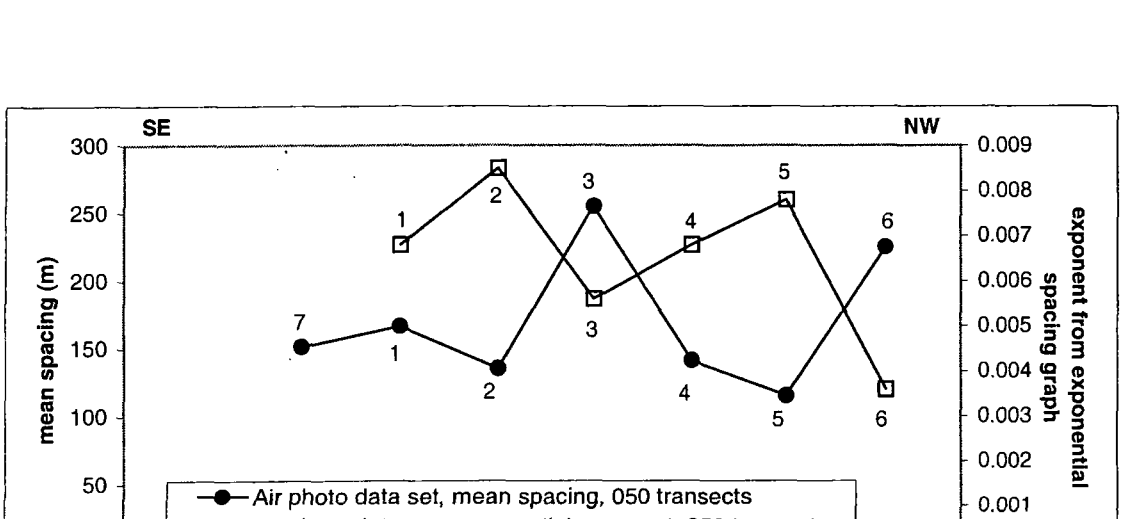

Figure 4.21 Exponent values from exponential spacing distributions and mean spacing values from transects orientated 050° across the air photograph data set (numbers indicate 050° transects from **Figure 4.19**)

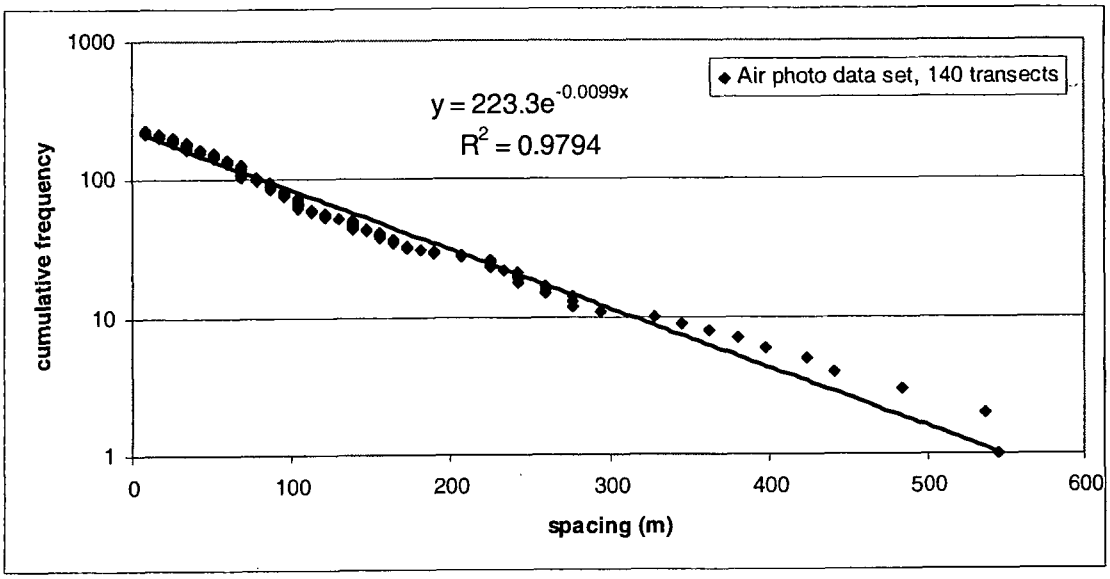

Figure 4.22 Cumulative frequency 'v' fracture spacing plot for transect orientated 140° across the air photograph data set

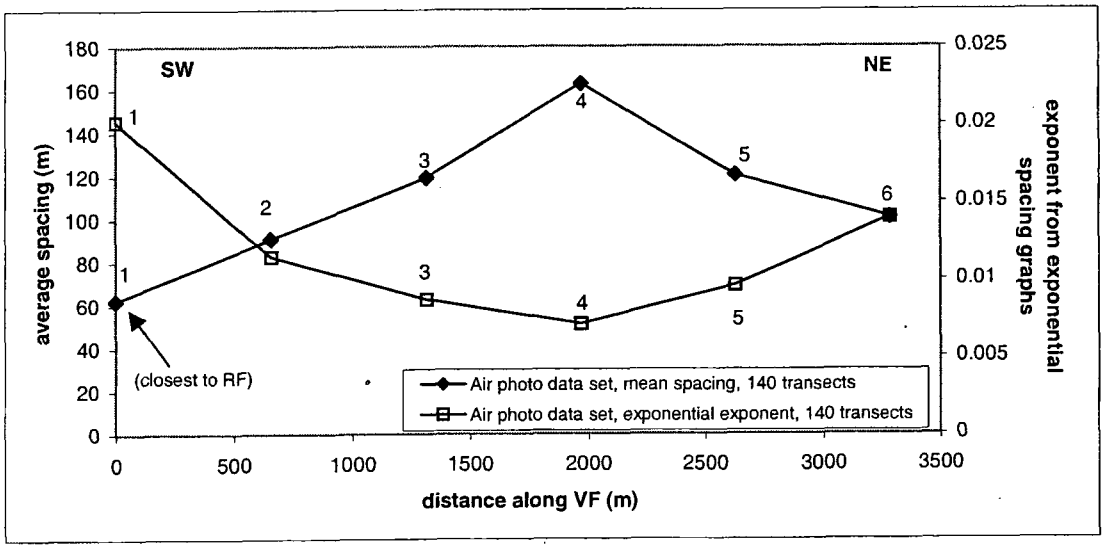

Figure 4.23 Exponent values from exponential spacing distributions and mean spacing values from transects orientated 140° across the air photograph data set (numbers indicate 140° transects from **Figure 4.19**)

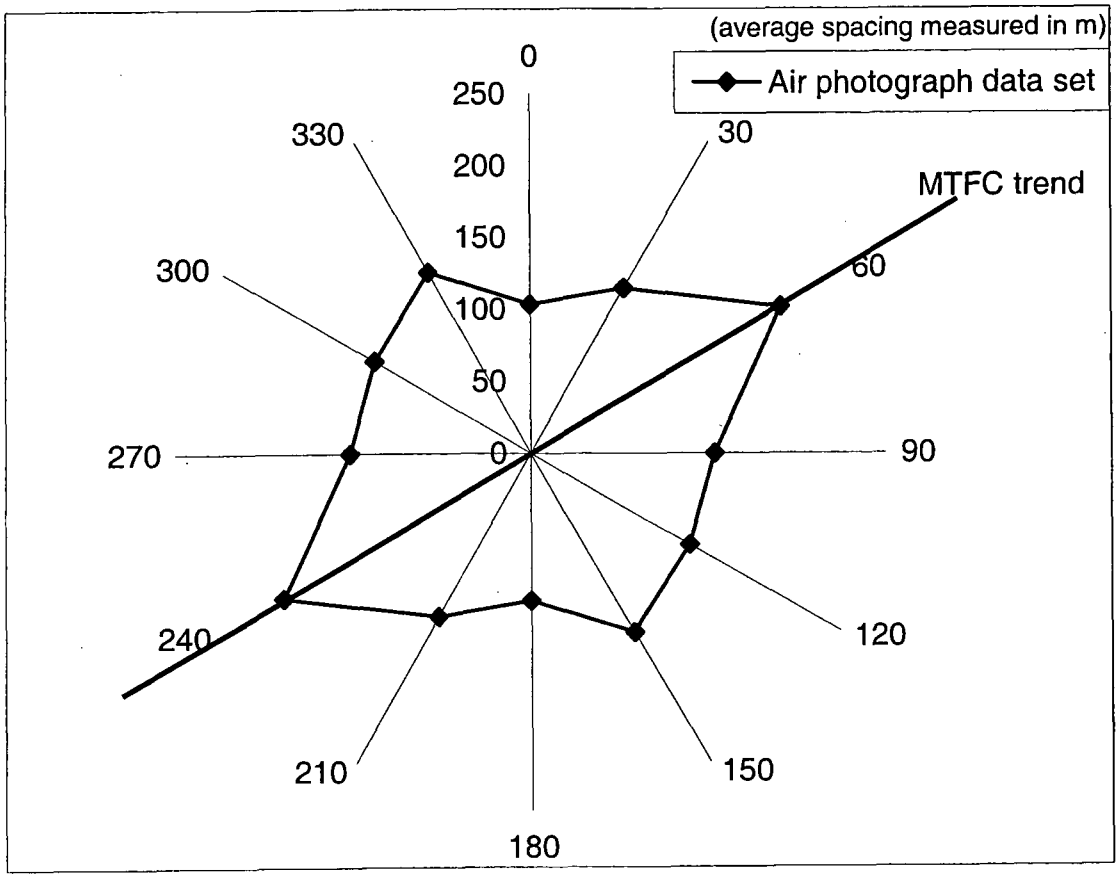

Figure 4.24 Mean spacing ellipse created from the Air Photograph data set.

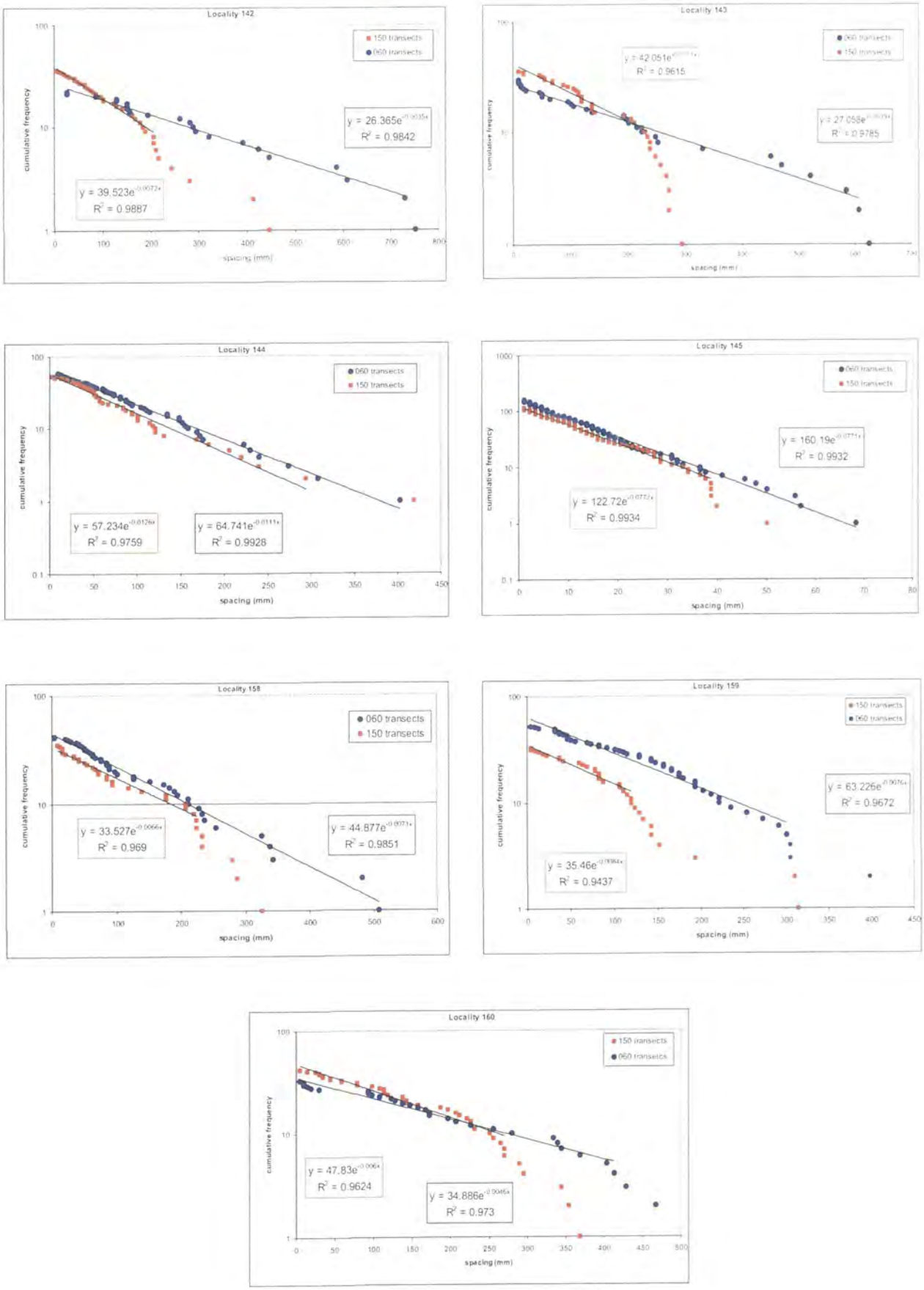

Figure 4.25 Cumulative frequency 'v' spacing plots for data sets collected at localities adjacent to the HSFP at outcrop scale.
BLUE data sets = transects orientated parallel to the HSF (and MTFC) trend
RED data sets = transects orientated perpendicular to the HSF and (MTFC) trend

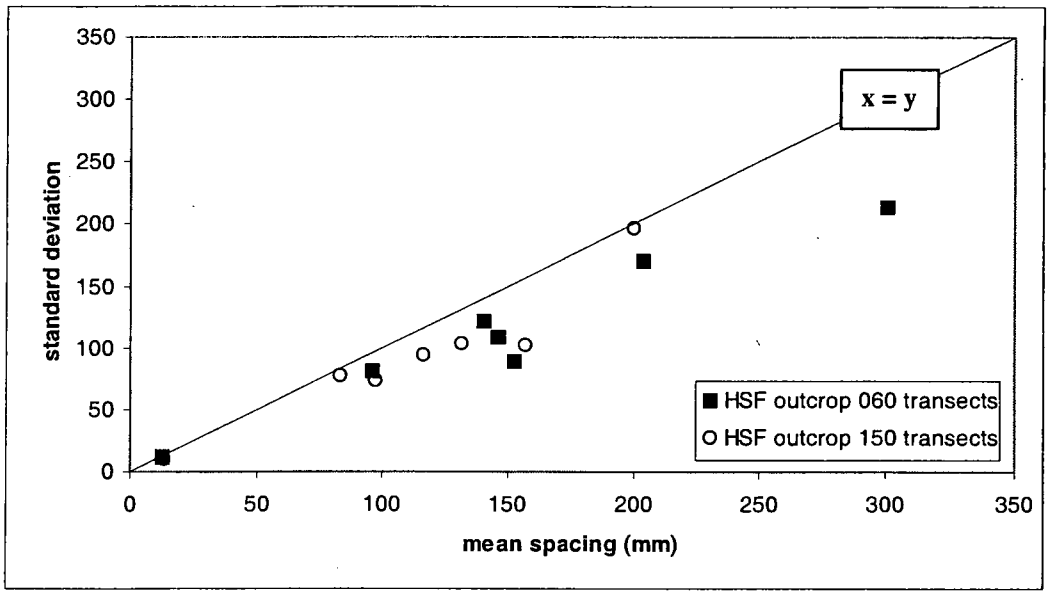

Figure 4.26 Mean fracture spacing 'v' standard deviation for data collected adjacent to the HSFP at outcrop scale.

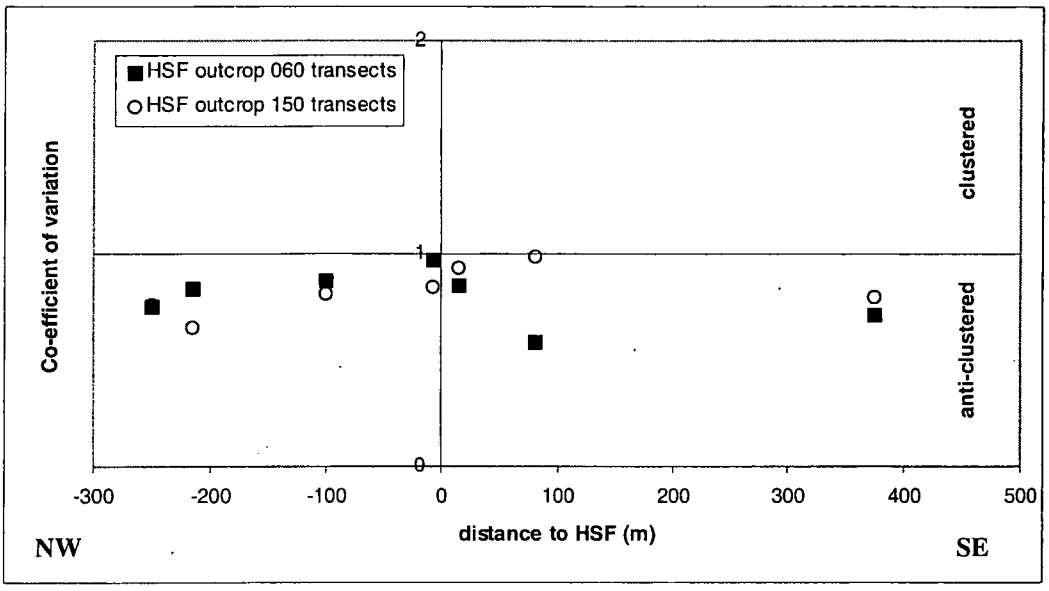

Figure 4.27 Co-efficient of variation 'v' perpendicular distance to the HSFP for all outcrop data collected from the HSF

a)

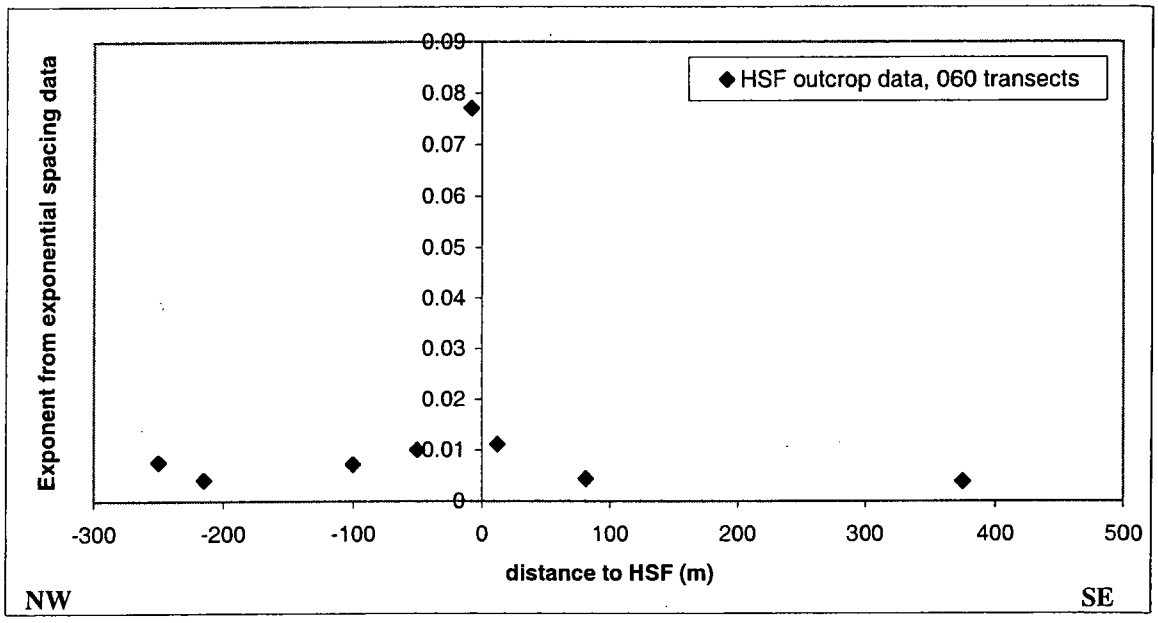

b)

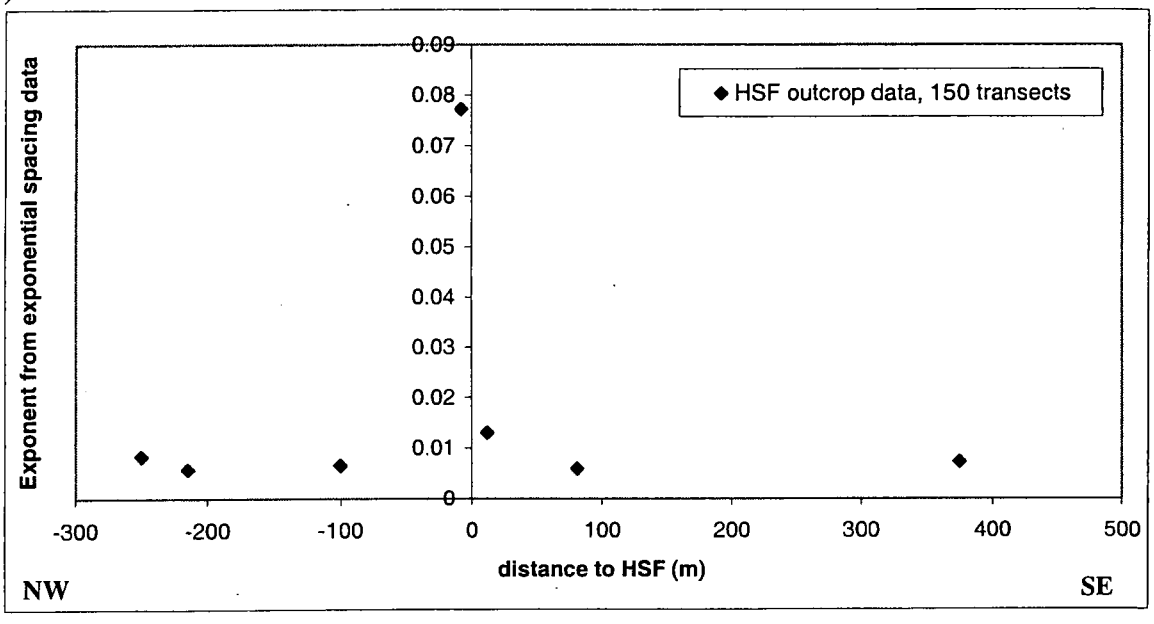

Figure 4.28 Exponent values from exponential spacing distributions 'v' perpendicular distance to the HSFP for **a**) transects orientated parallel to the MTFC trend, and **b**) transects orientated perpendicular to the MTFC trend.

a)

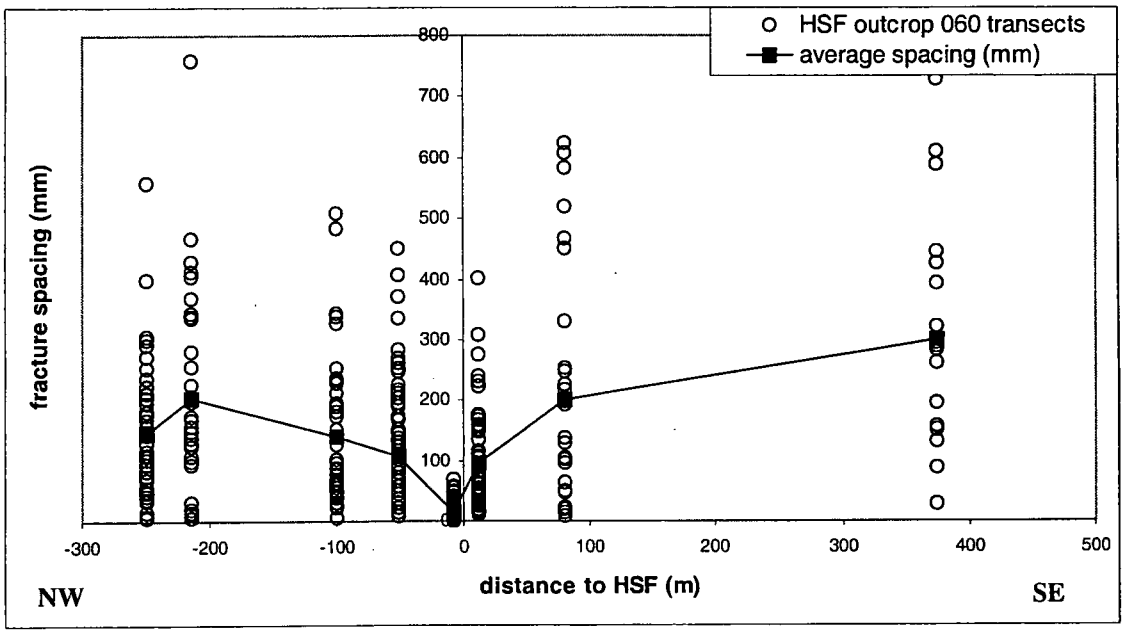

b)

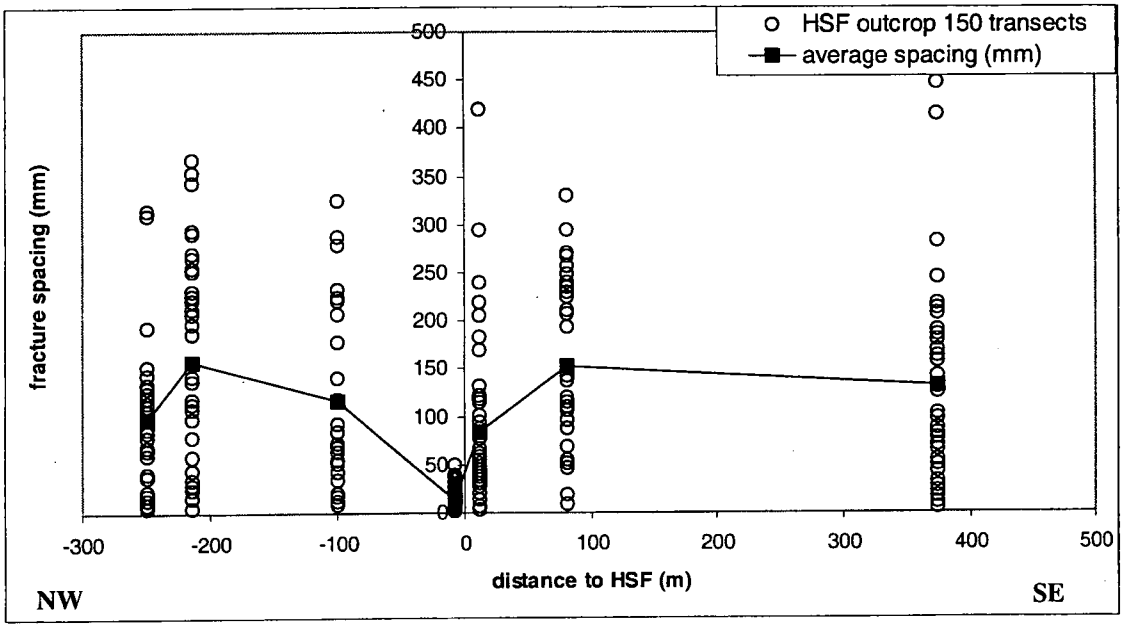

Figure 4.29 Mean spacing data from outcrop data sets, plotted with the range of spacing values, at various distances from the HSFP.
a) transects orientated parallel to the HSF (and MTFC) trend,
b) transects orientated parallel to the HSF (and MTFC) trend

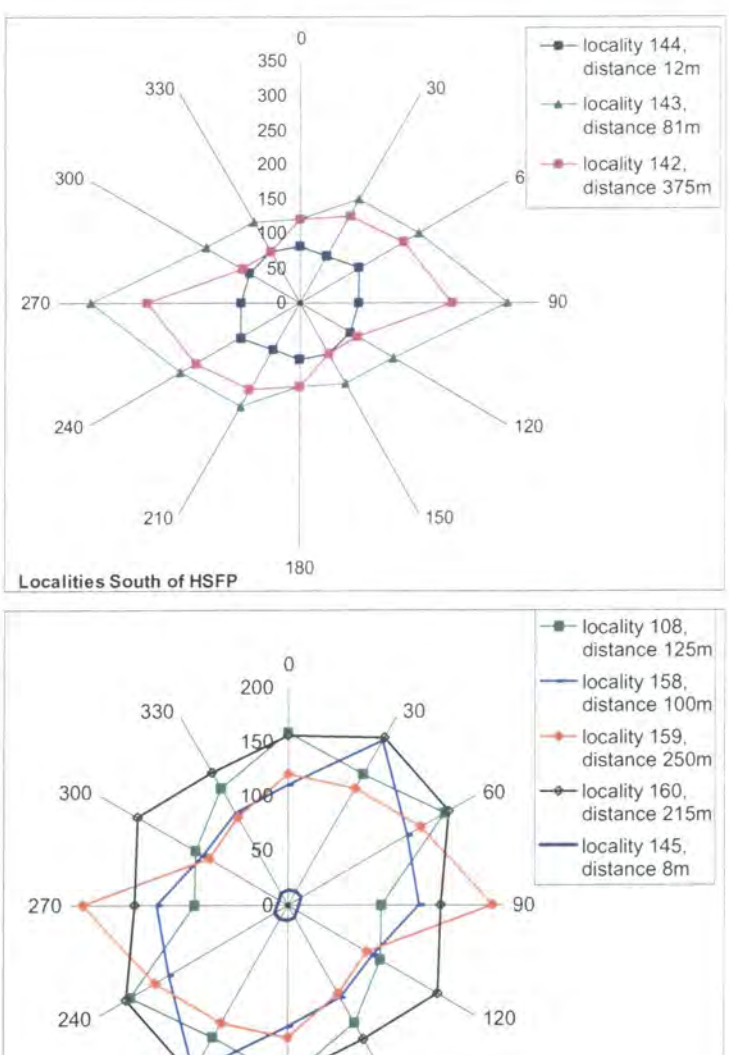

Figure 4.30 Mean spacing ellipses created for horizontal outcrop data sets adjacent to the HSFP. **a)** – localities south of the HSFP, **b)** – localities north of the HSFP.

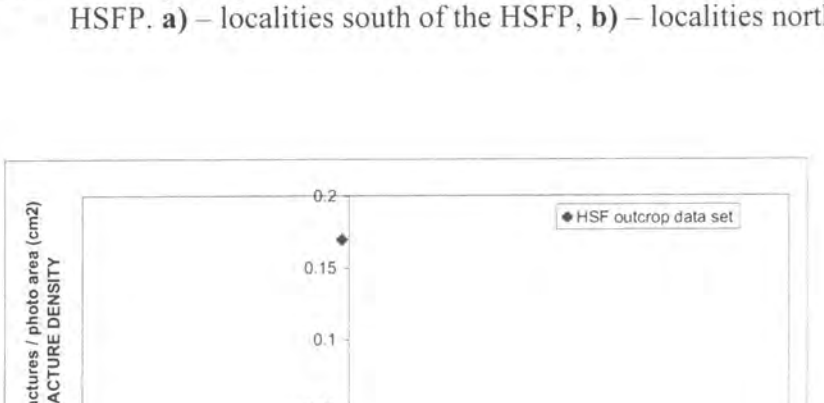

Figure 4.31 Fracture density (total number of fractures /cm²) 'v' perpendicular distance to the HSFP, for outcrop data sets collected adjacent to the HSFP

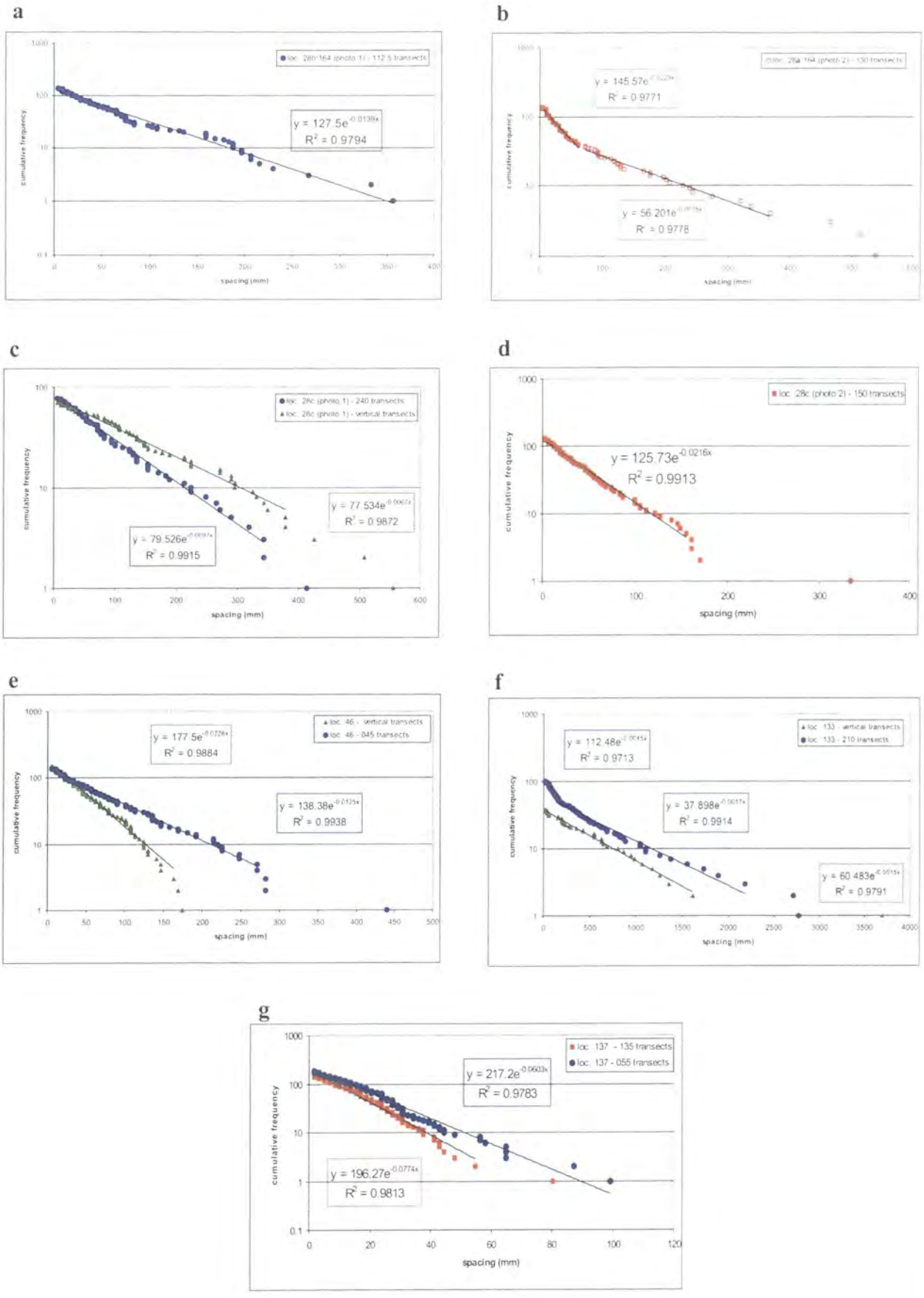

Figure 4.32 Cumulative frequency 'v' spacing plots for outcrop data sets collected adjacent to the VFP. Data measured from outcrop photographs.
BLUE data sets = transects orientated parallel to the VF (and MTFC) trend
RED data sets = transects orientated perpendicular to the VF (and MTFC) trend
GREEN data sets = vertical transects

(continued on next page)

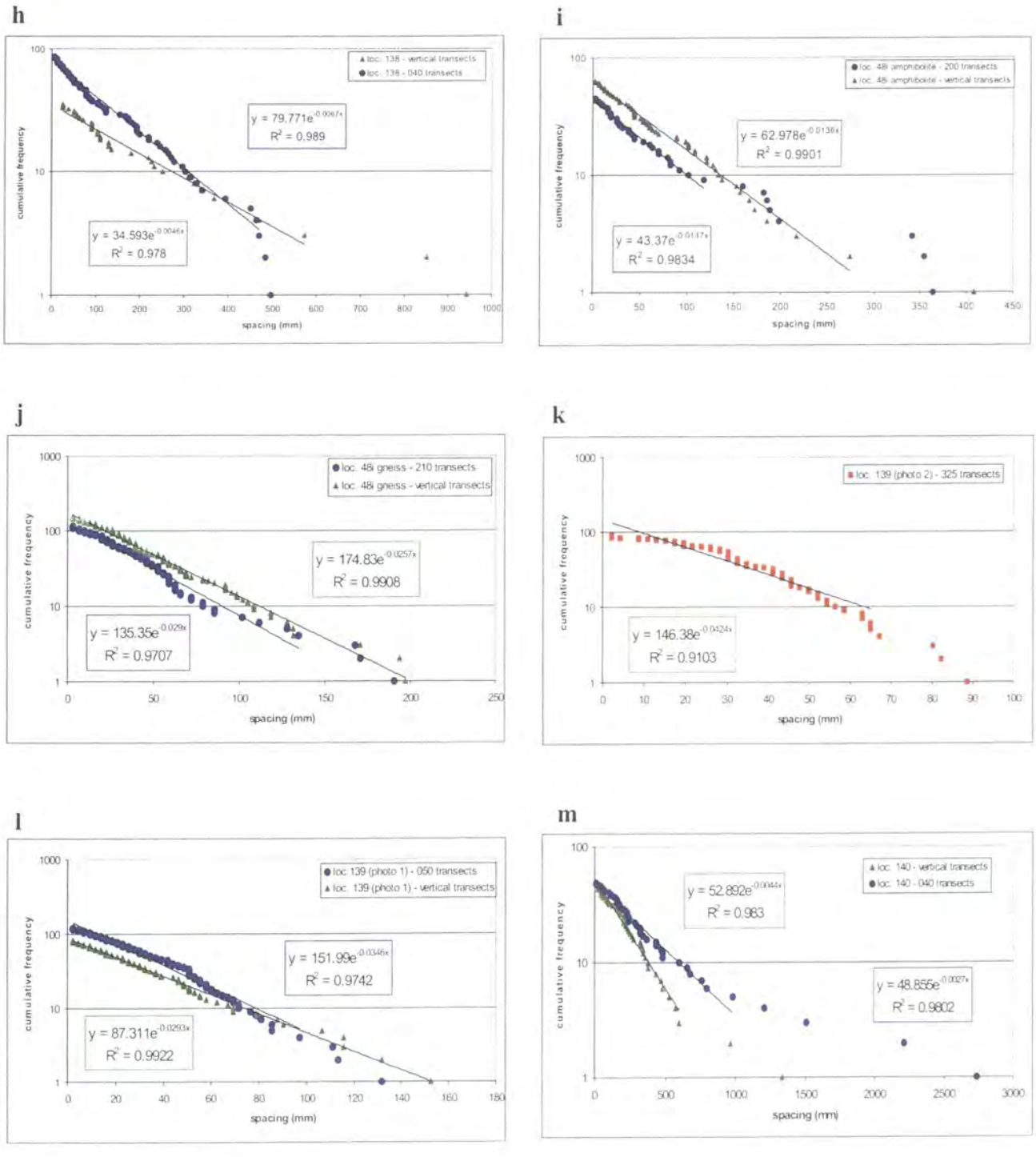

Figure 4.32 Cumulative frequency 'v' spacing plots for outcrop data sets collected adjacent to the VFP. Data measured from outcrop photographs.
BLUE data sets = transects orientated parallel to the VF (and MTFC) trend
RED data sets = transects orientated perpendicular to the VF (and MTFC) trend
GREEN data sets = vertical transects

(continued from previous page)

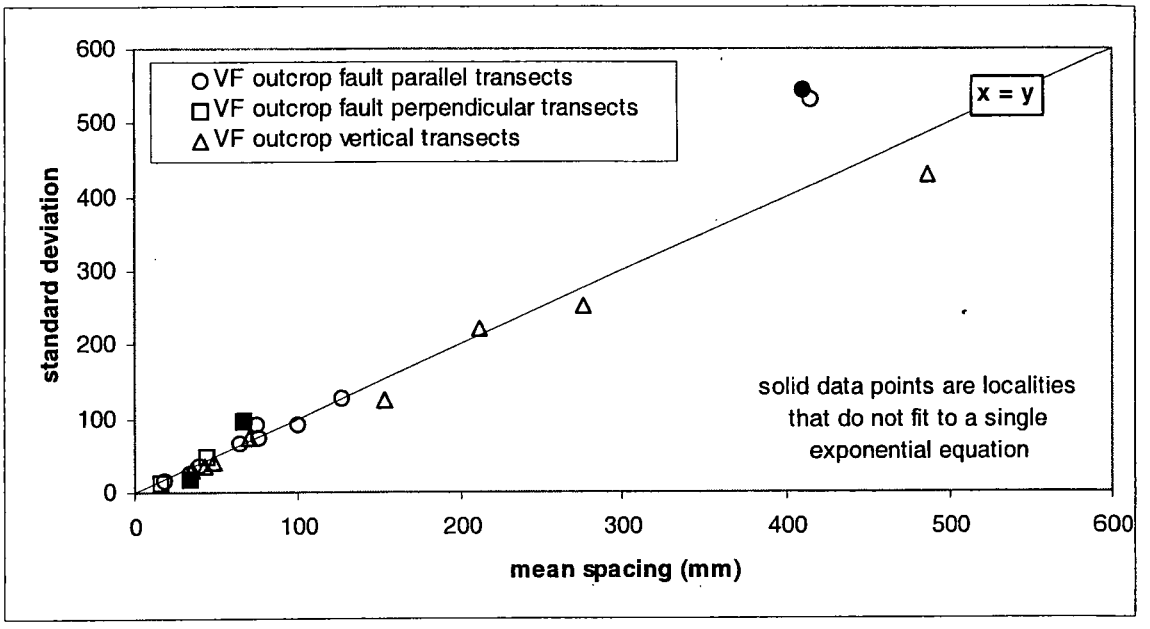

Figure 4.33 Mean fracture spacing 'v' standard deviation for data collected adjacent to the VFP at outcrop scale

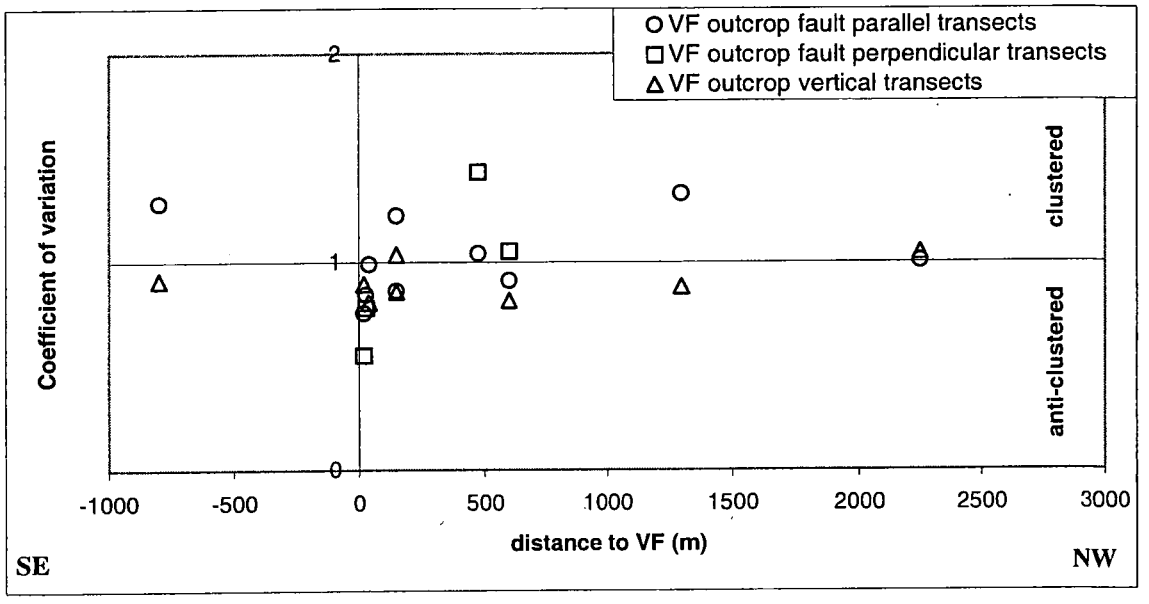

Figure 4.34 Co-efficient of variation 'v' perpendicular distance to the VFP for data collected at outcrop scale

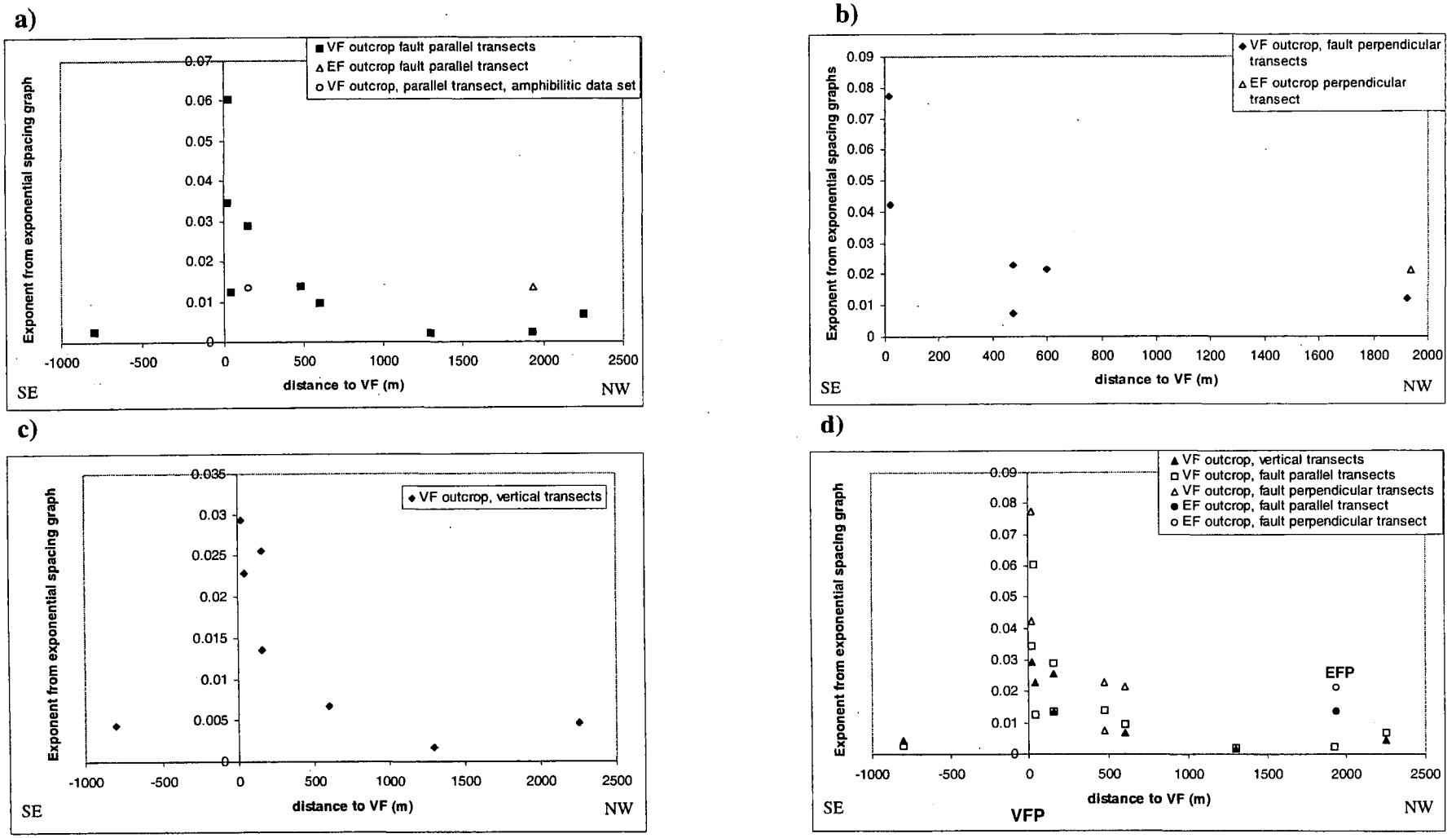

Figure 4.35 Exponent values from exponential spacing graphs plotted against the perpendicular distance to the VFP at outcrop scale. **a)** transects orientated parallel to the MTFC trend, **b)** transects orientated perpendicular to the MTFC trend, **c)** vertical transects, **d)** all transect data

a)

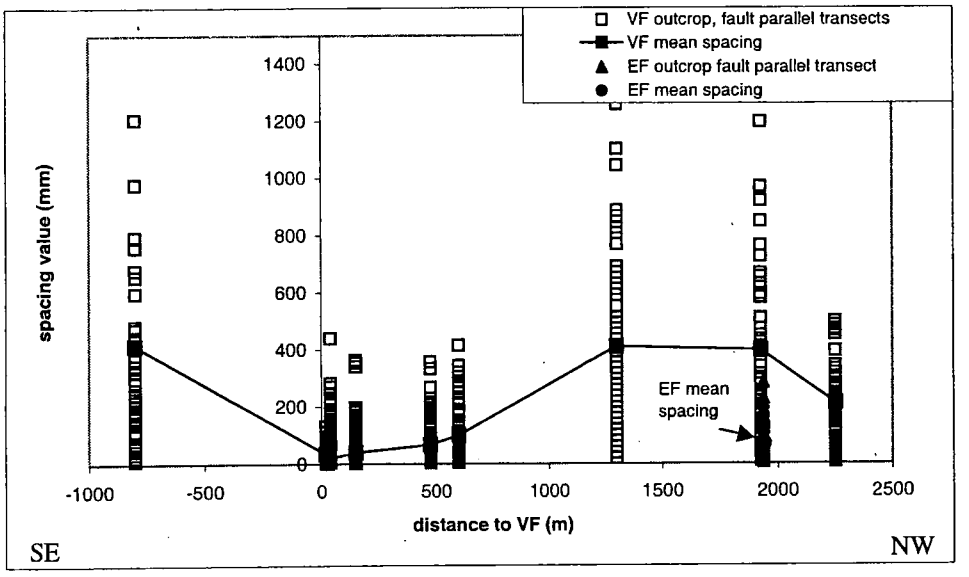

b)

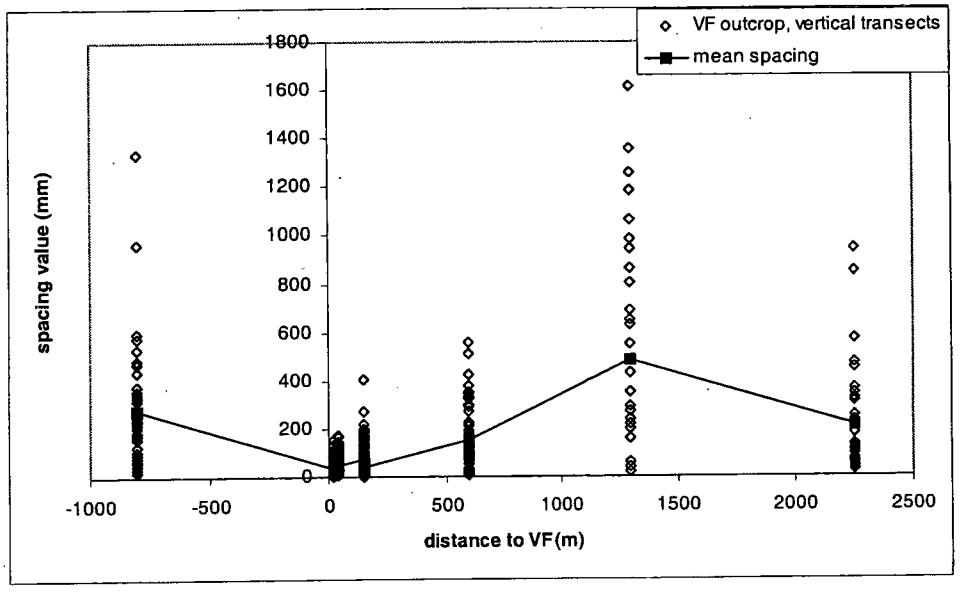

c)

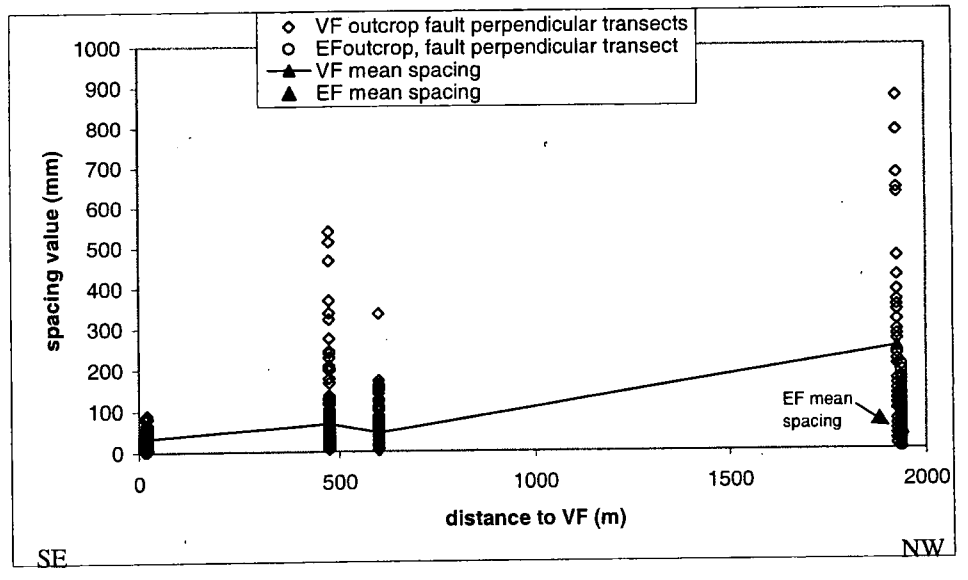

Figure 4.36 Mean spacing 'v' perpendicular distance to VFP from outcrop data sets
a) transects orientated parallel to the VF (and MTFC),
b) transects orientated perpendicular to the VF (and MTFC),
c) vertical transects.

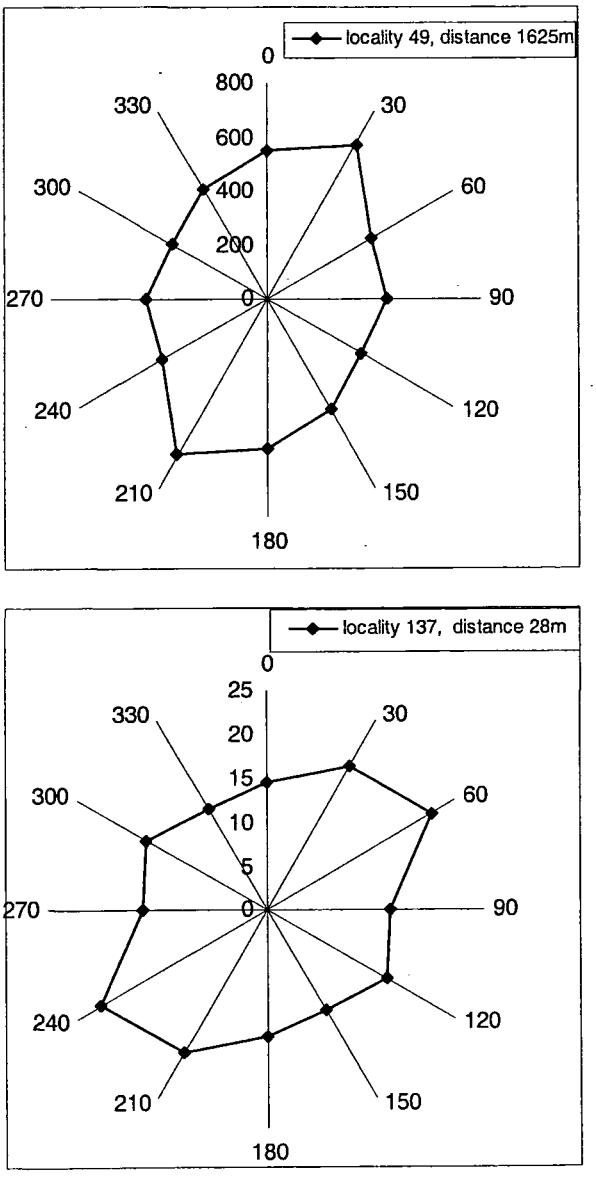

Figure 4.37 Mean spacing ellipses created for horizontal outcrop data sets adjacent to the VFP

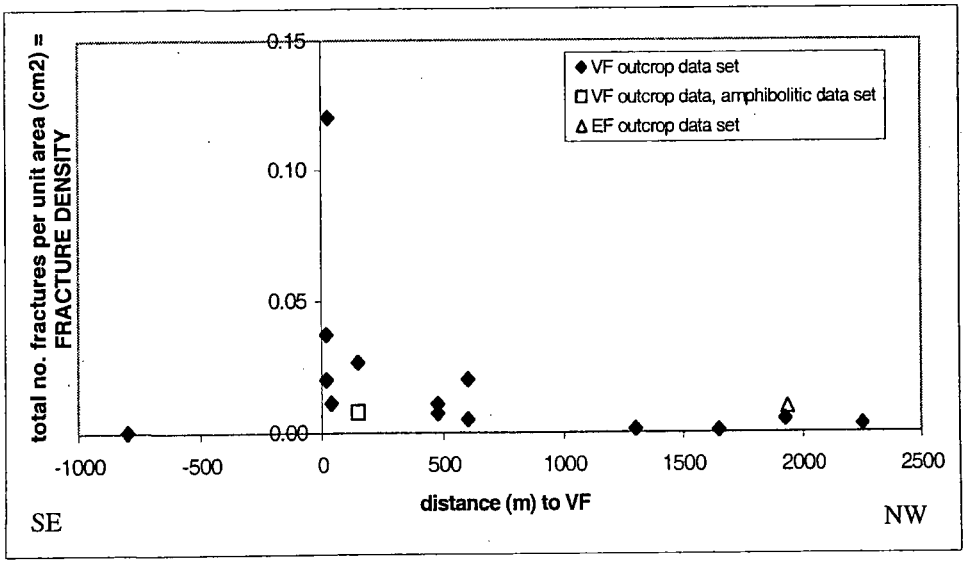

Figure 4.38 Fracture density 'v' perpendicular distance to the VFP for outcrop data sets

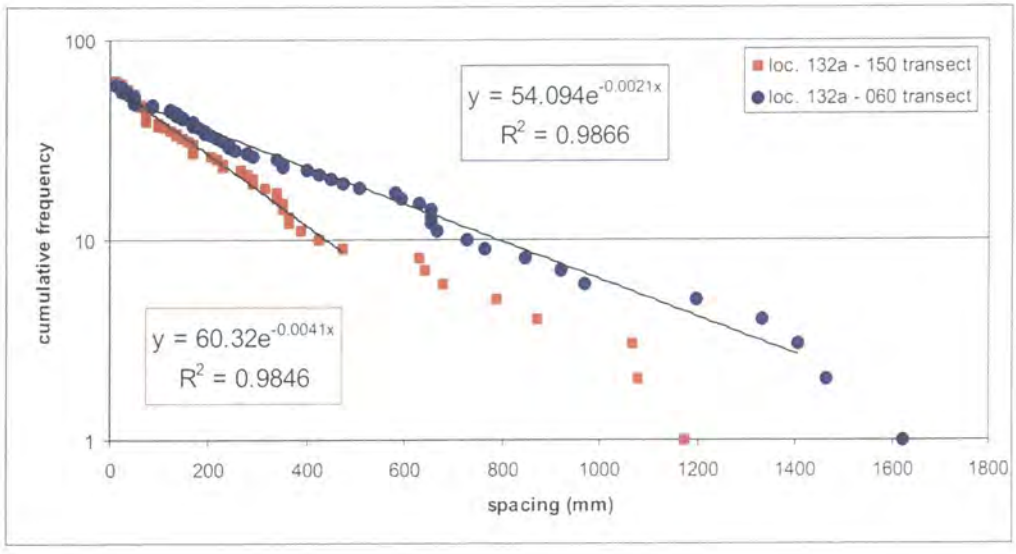

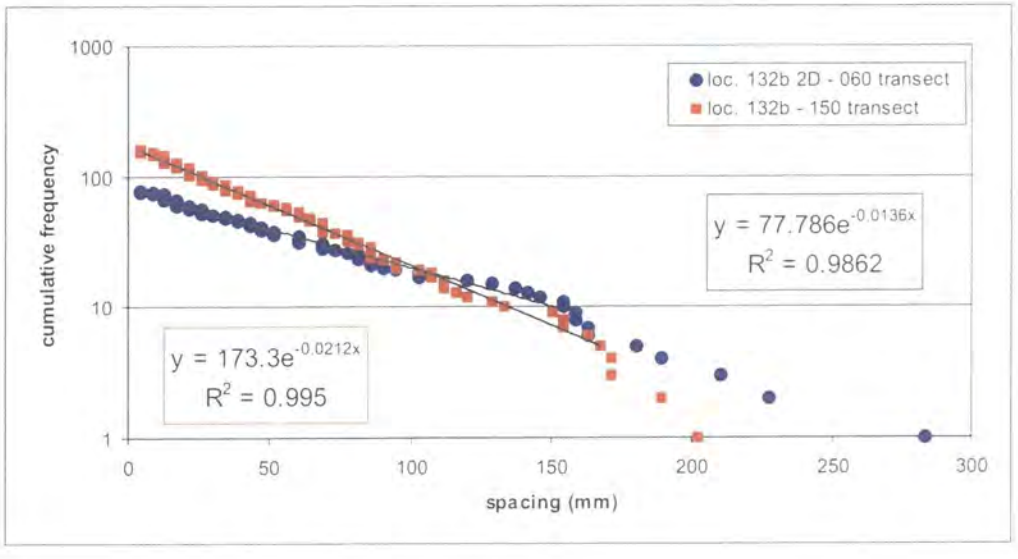

Figure 4.39 Cumulative frequency 'v' spacing plots for outcrop data sets collected adjacent to the EFP.
BLUE data sets = transects orientated parallel to the EF (and MTFC) trend
RED data sets = transects orientated perpendicular to the EF (and MTFC) trend

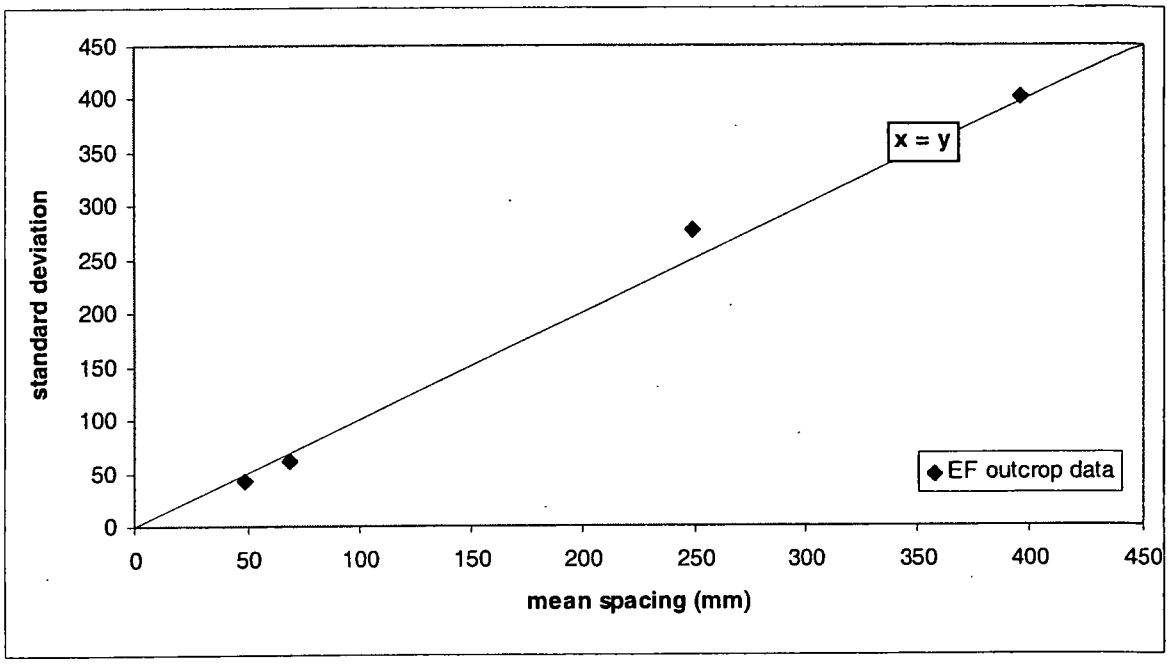

Figure 4.40 Mean spacing 'v' standard deviation for data collected adjacent to the EFP at outcrop scale

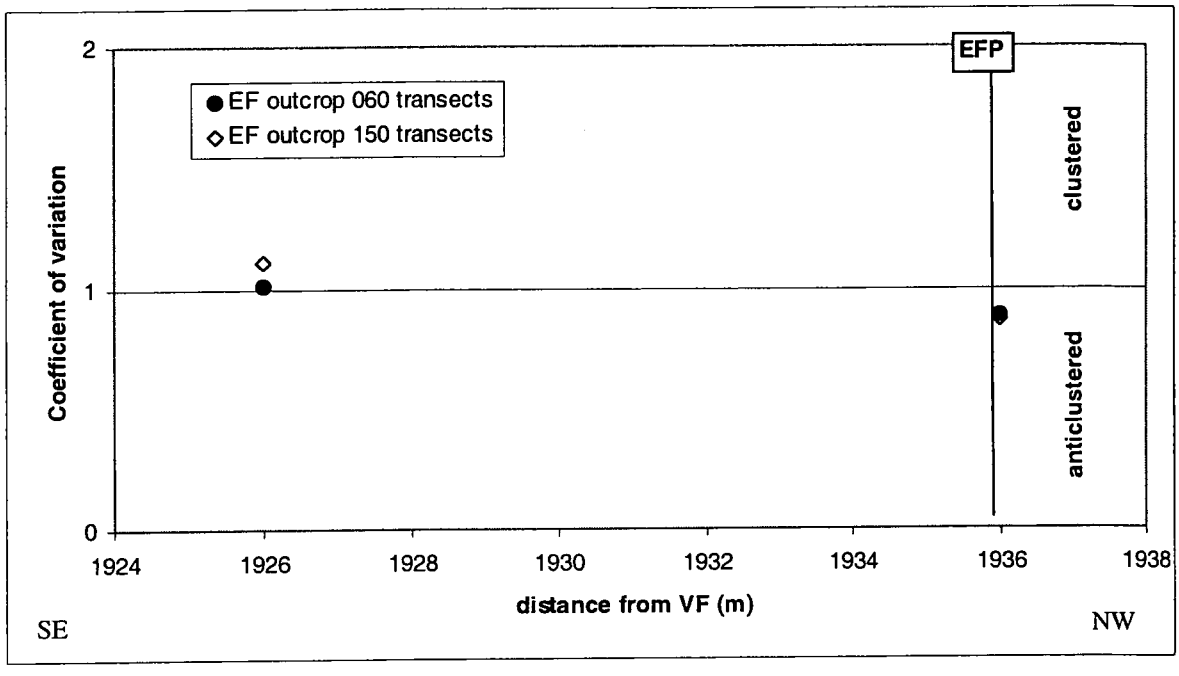

Figure 4.41 Co-efficient of variation 'v' perpendicular distance to the EFP for data collected at outcrop scale

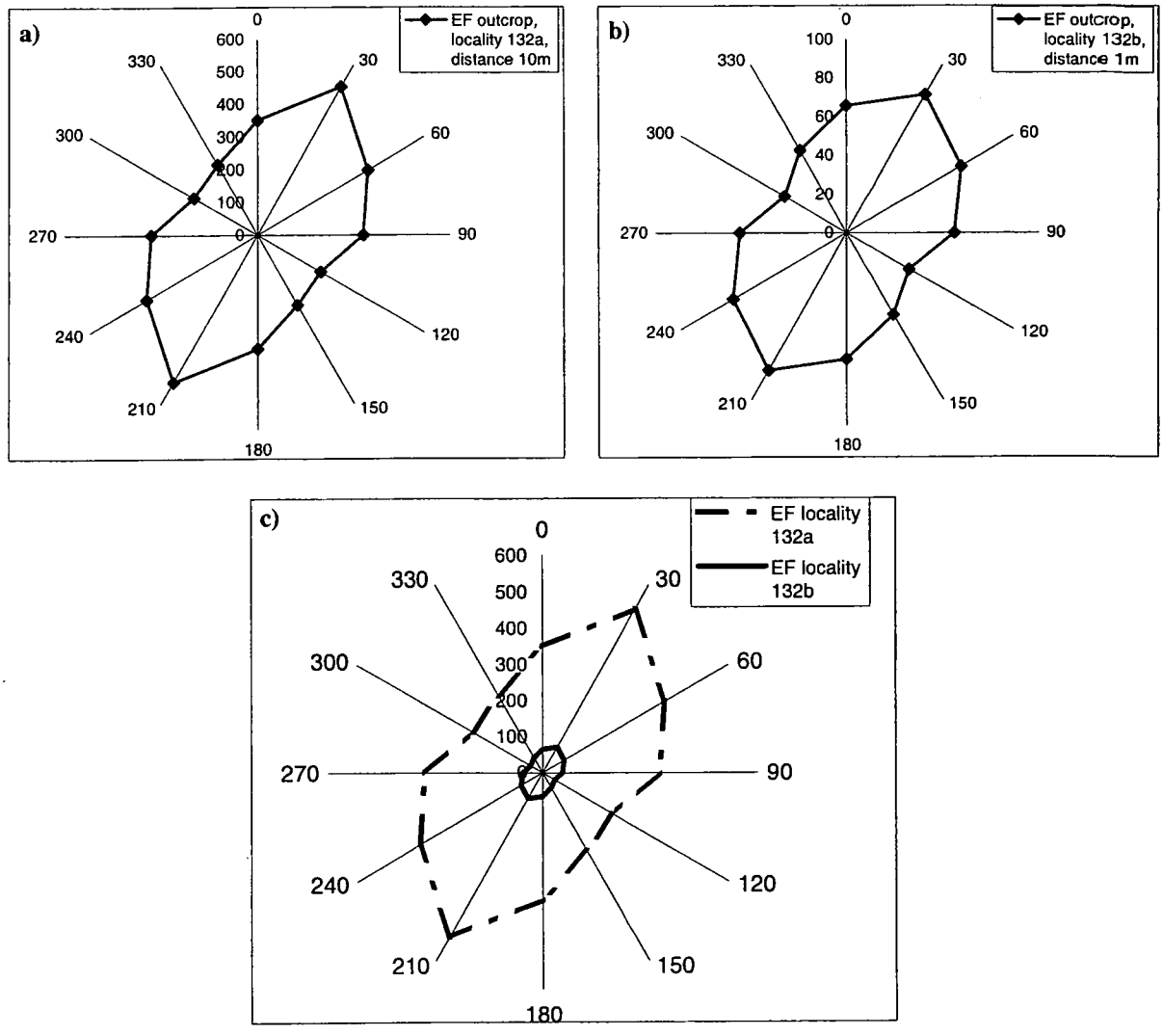

Figure 4.42 Mean spacing ellipses created for localities adjacent to the EFP.
a) locality 132a, 10m from EFP, **b)** locality 132b, 1m from EFP,
c) localities 132a & 132b plotted on the same axes to illustrate their relative sizes and shapes (all spacings measured in mm)

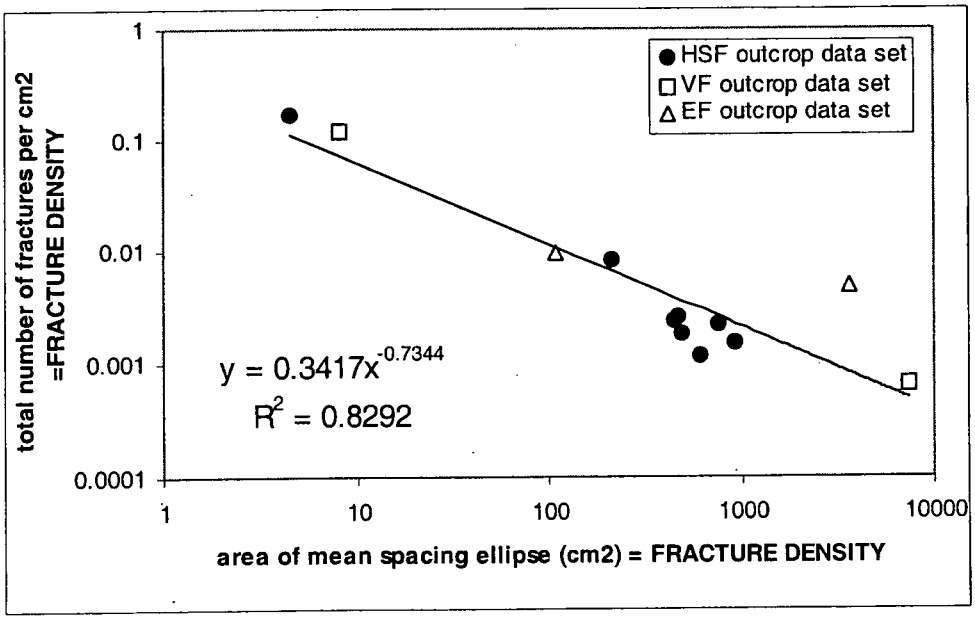

Figure 4.43 Fracture density plot for all data sets collected at outcrop scale

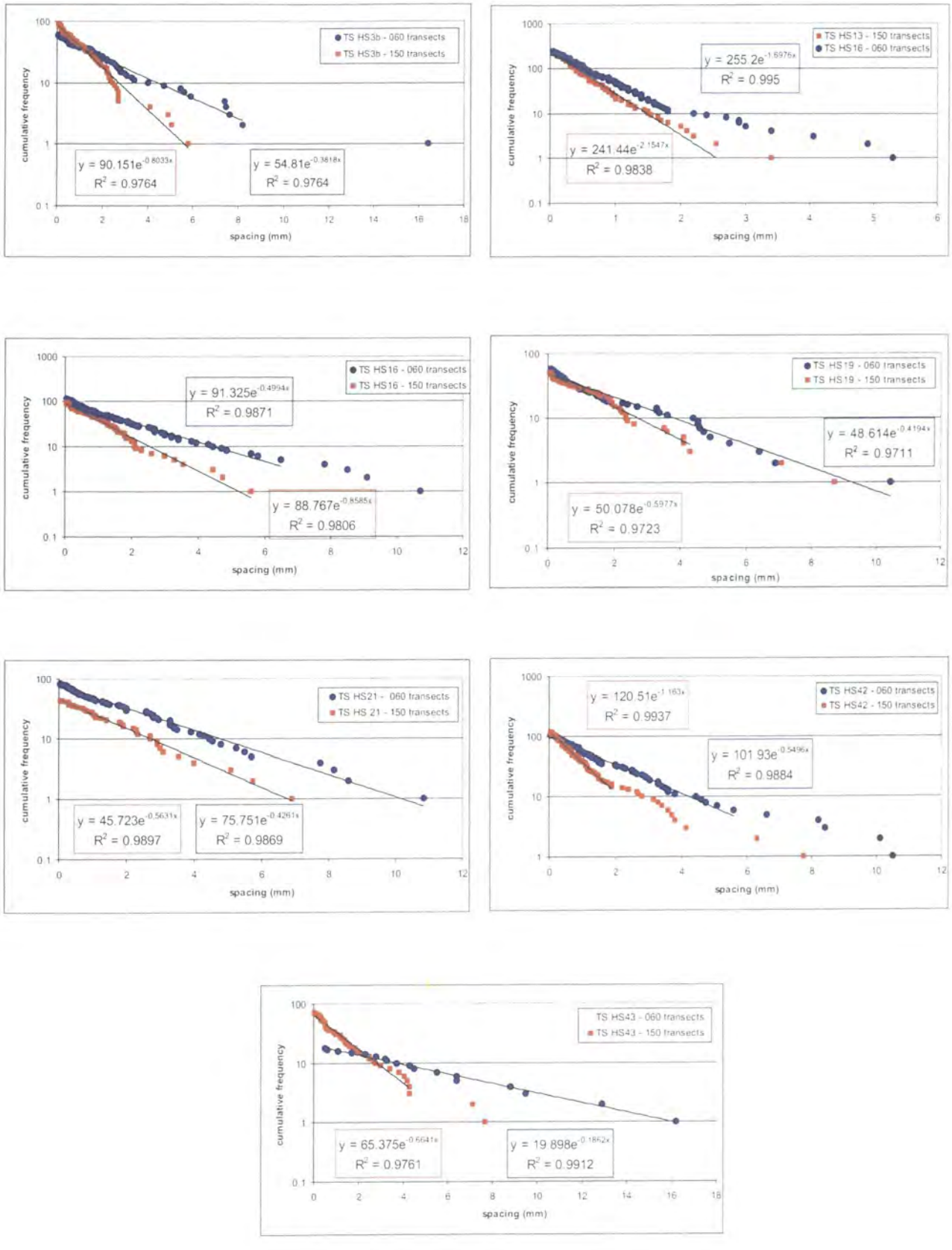

Figure 4.44 Cumulative frequency 'v' fracture spacing plots for thin section data sets collected adjacent to the HSFP
BLUE data sets = transects orientated parallel to the HSF (and MTFC) trend
RED data sets = transects orientated perpendicular to the HSF (and MTFC) trend

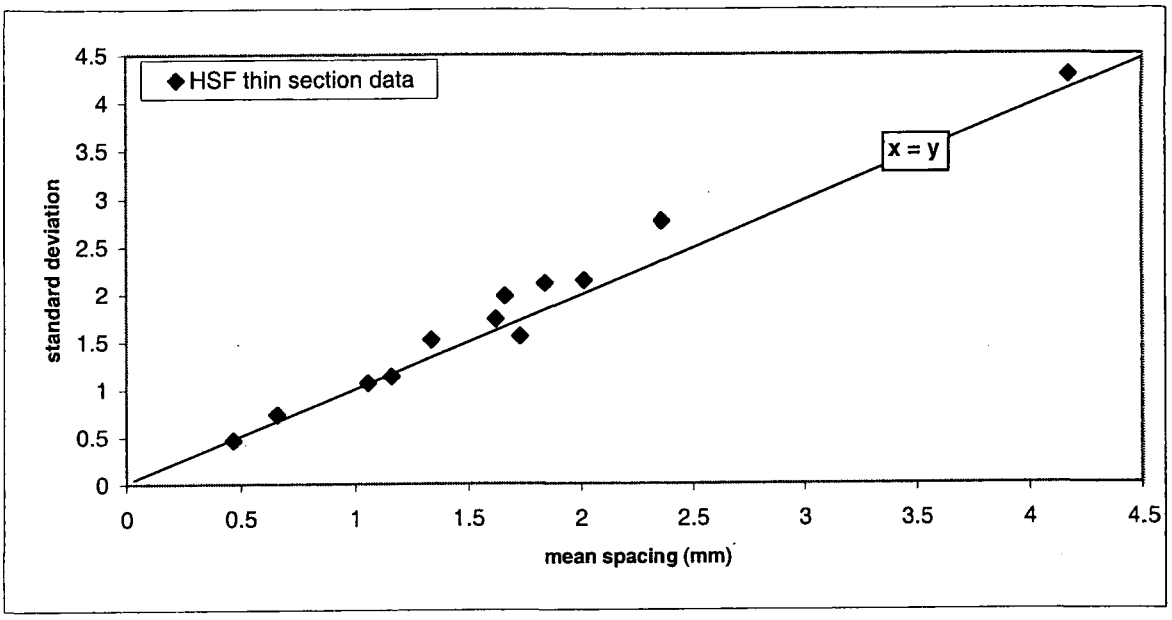

Figure 4.45 Mean spacing 'v' standard deviation for data sets collected at thin section scale adjacent to the HSFP

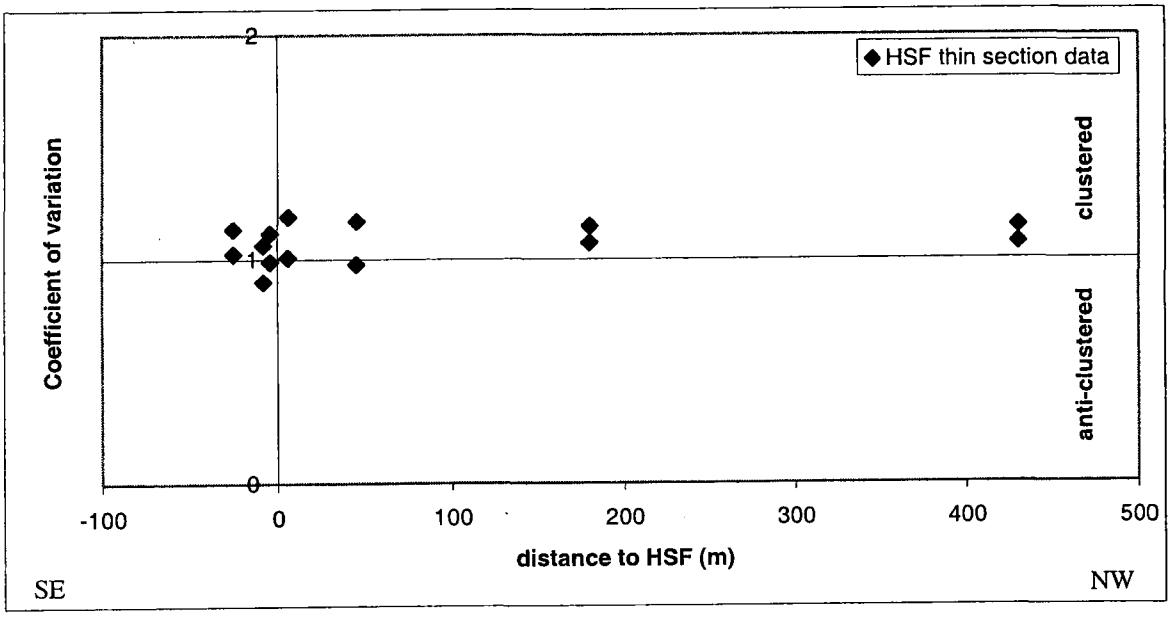

Figure 4.46 Co-efficient of variation 'v' perpendicular distance to the HSFP for data sets collected at thin section scale.

a)

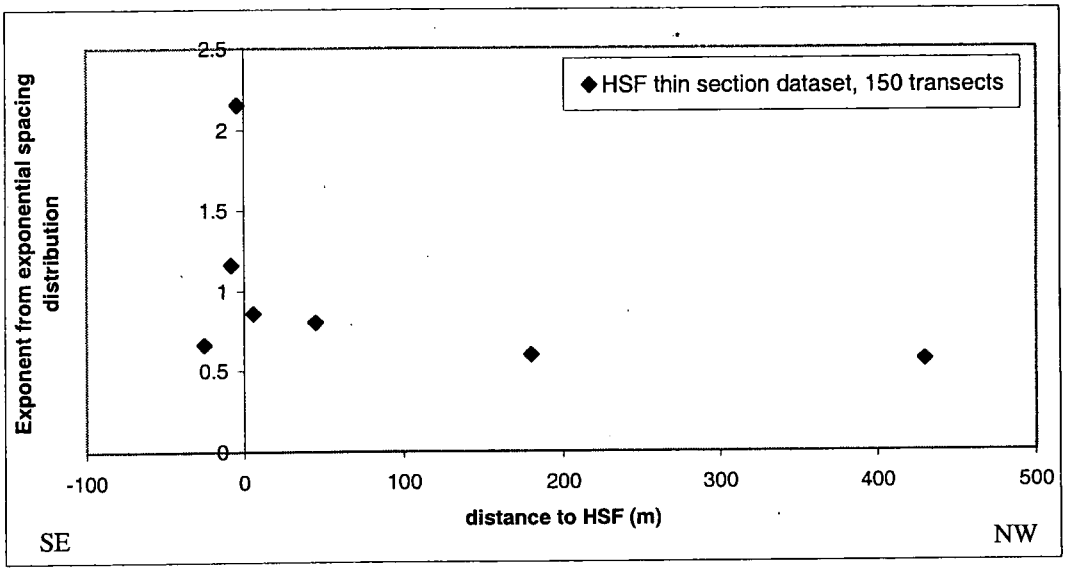

b)

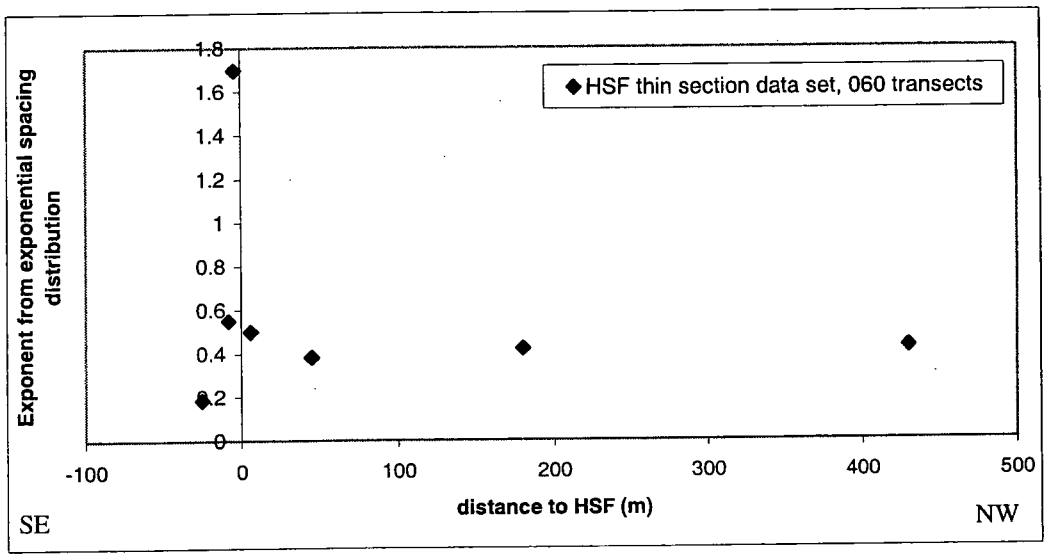

Figure 4.47 Exponent values from exponential spacing distributions 'v' perpendicular distance to the HSFP for data collected at thin section scale along **a)** transects orientated perpendicular to the MTFC trend (150°) and **b)** transects orientated parallel to the MTFC trend (060°).

a)

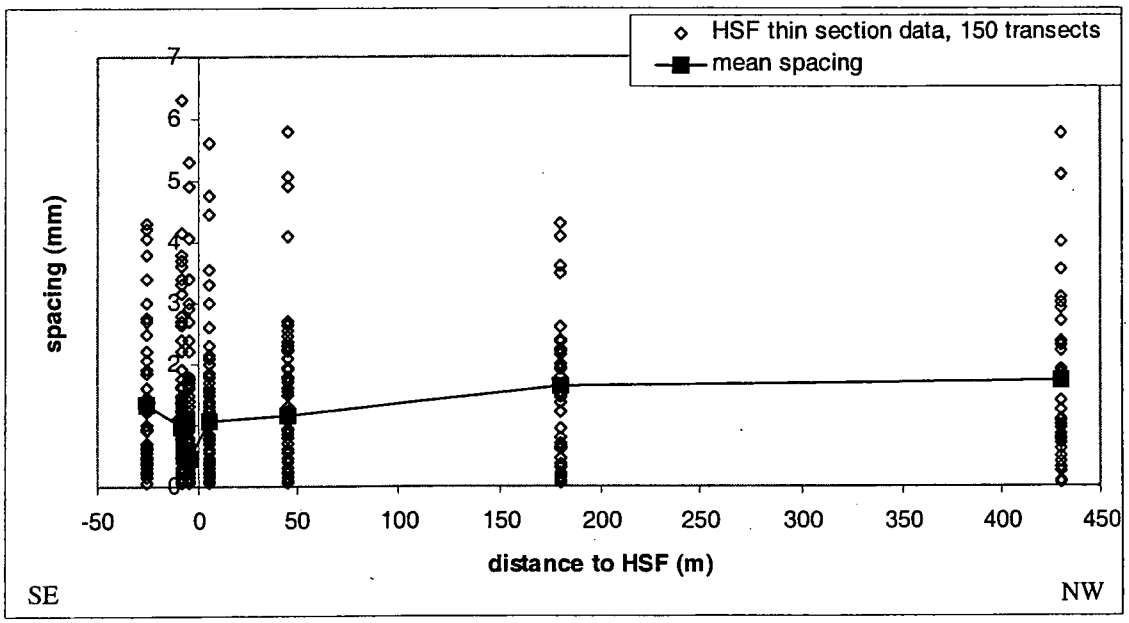

b)

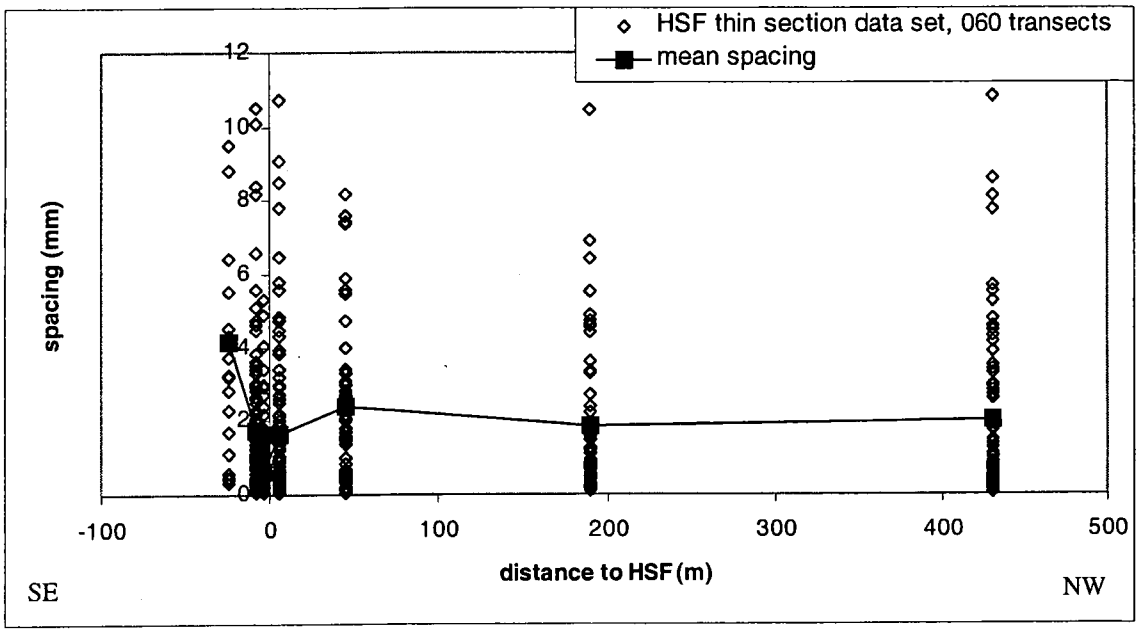

Figure 4.48 Mean fracture spacing and range of spacing values 'v' perpendicular distance to the HSFP at thin section scale for **a)** transects orientated perpendicular to the MTFC (150°) and **b)** for transects orientated parallel to the MTFC (060°)

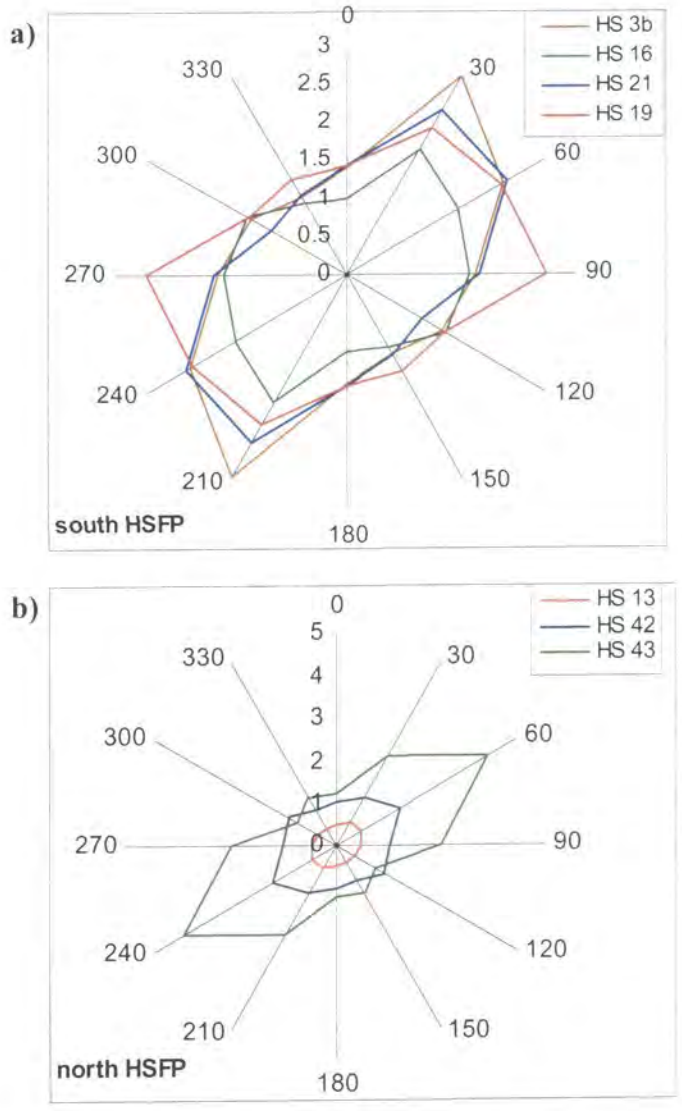

Figure 4.49 Mean spacing ellipses created for outcrop data sets adjacent to the HSFP at thin section scale. (Mean spacings are measured in mm.)
a) – localities south of the HSFP, **b)** – localities north of the HSFP

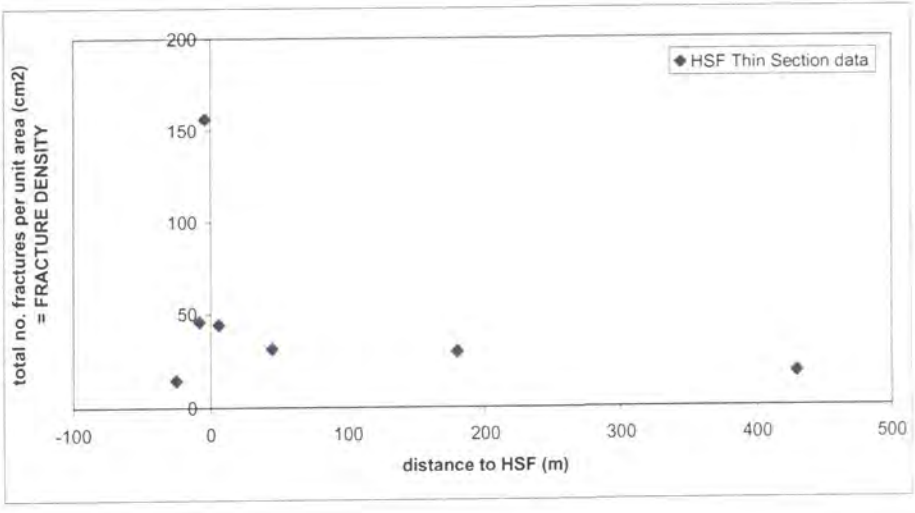

Figure 4.50 Fracture density (total number of fractures / cm^2) 'v' perpendicular distance to the HSFP, for thin section data sets adjacent to the HSFP

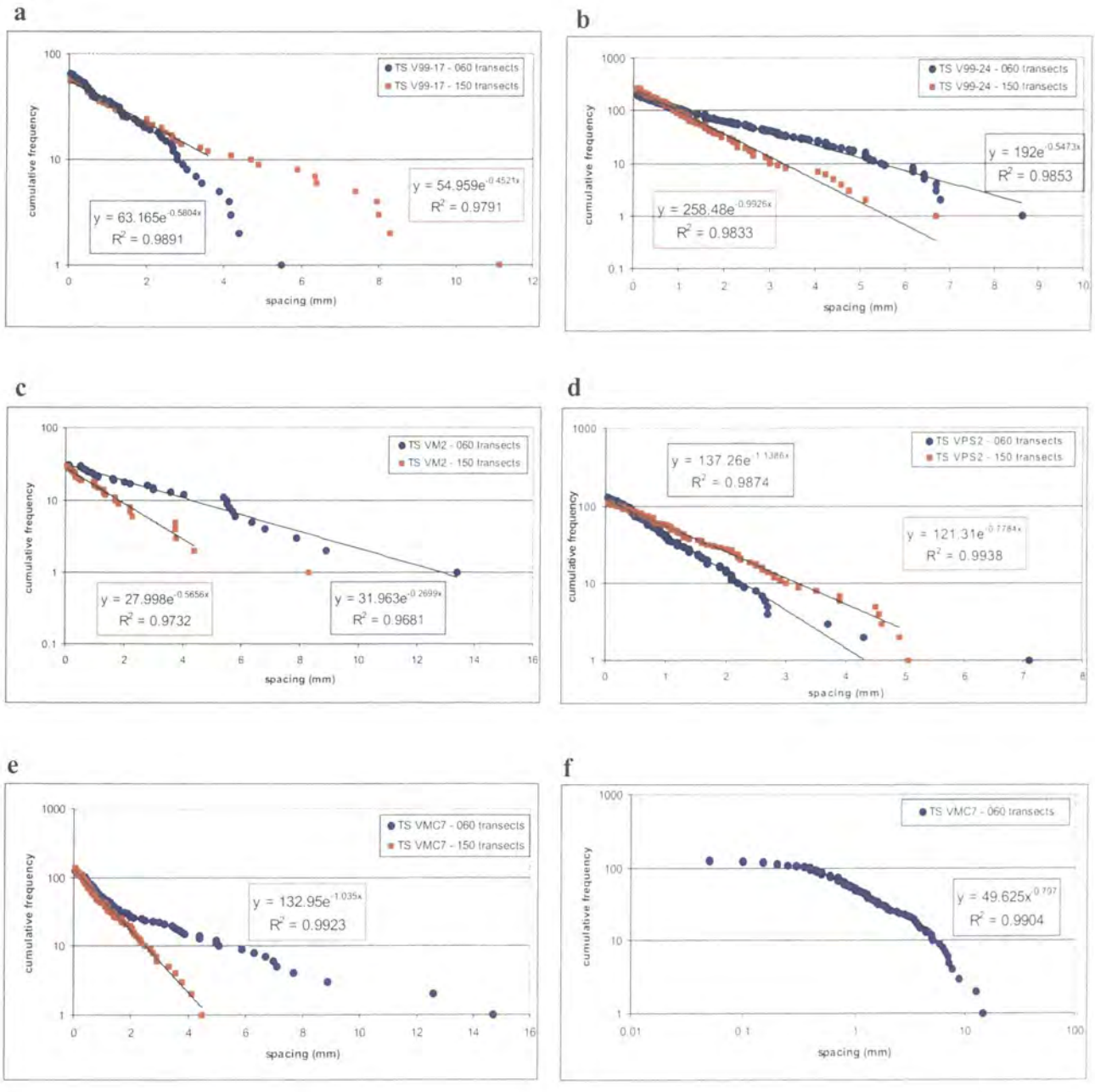

Figure 4.51 Cumulative frequency 'v' fracture spacing graphs for thin section data sets collected adjacent to the VFP
BLUE data sets = transects orientated parallel to the VF (and MTFC) trend
RED data sets = transects orientated perpendicular to the VF (and MTFC) trend

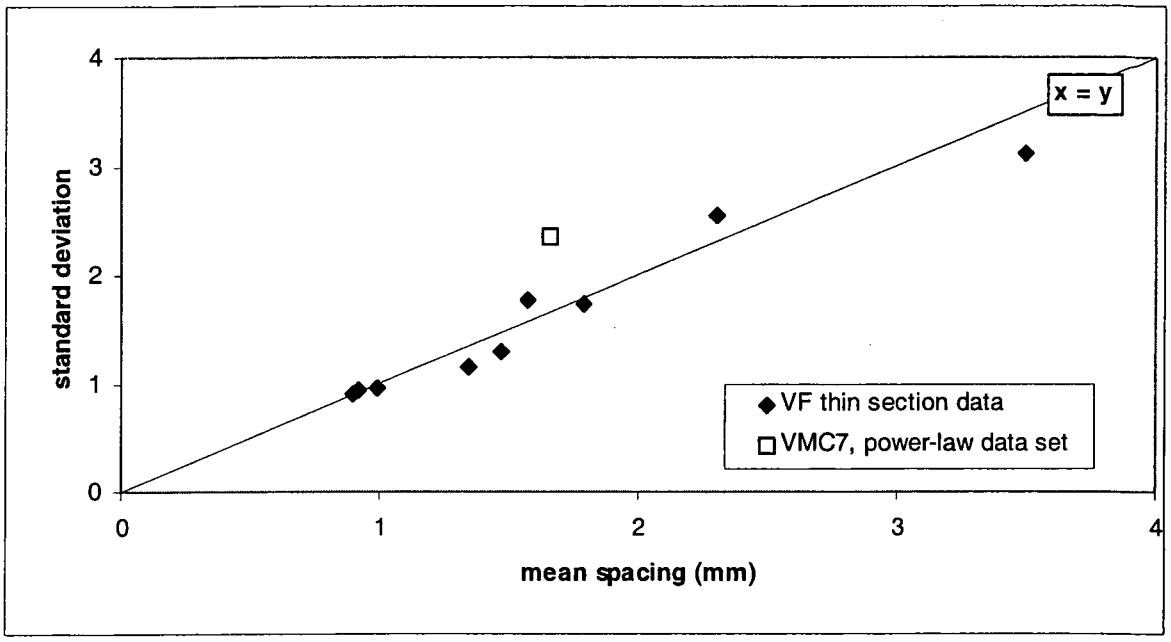

Figure 4.52 Mean fracture spacing 'v' standard deviation for thin section data sets collected adjacent to the VFP.

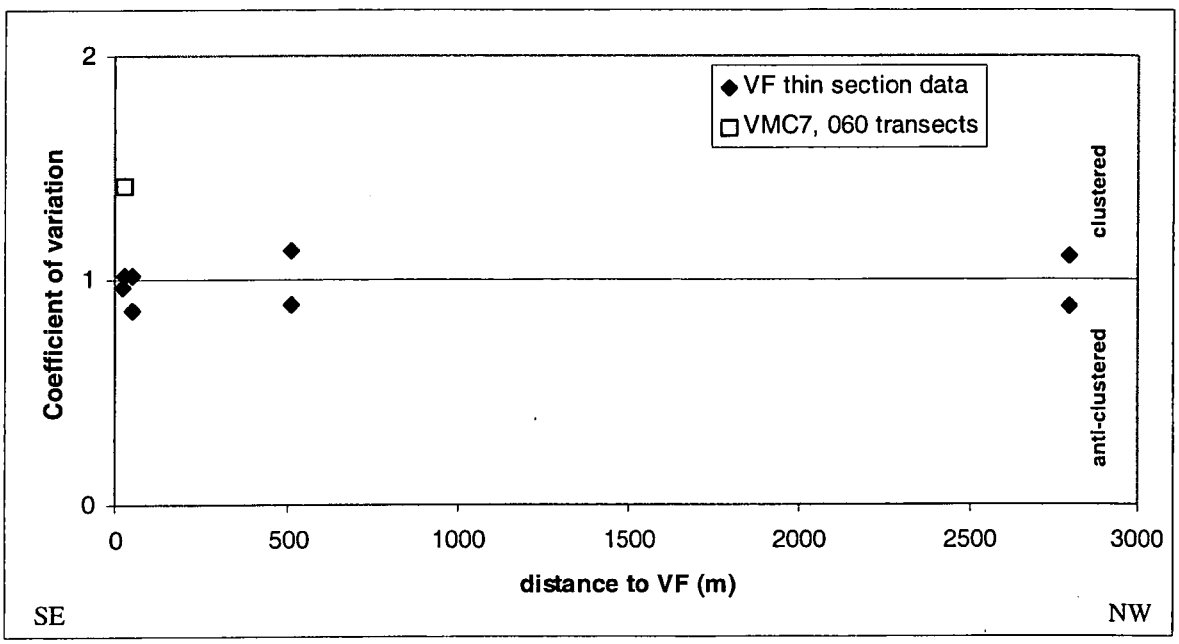

Figure 4.53 Co-efficient of variation 'v' perpendicular distance to the VFP, for thin section data sets

a)

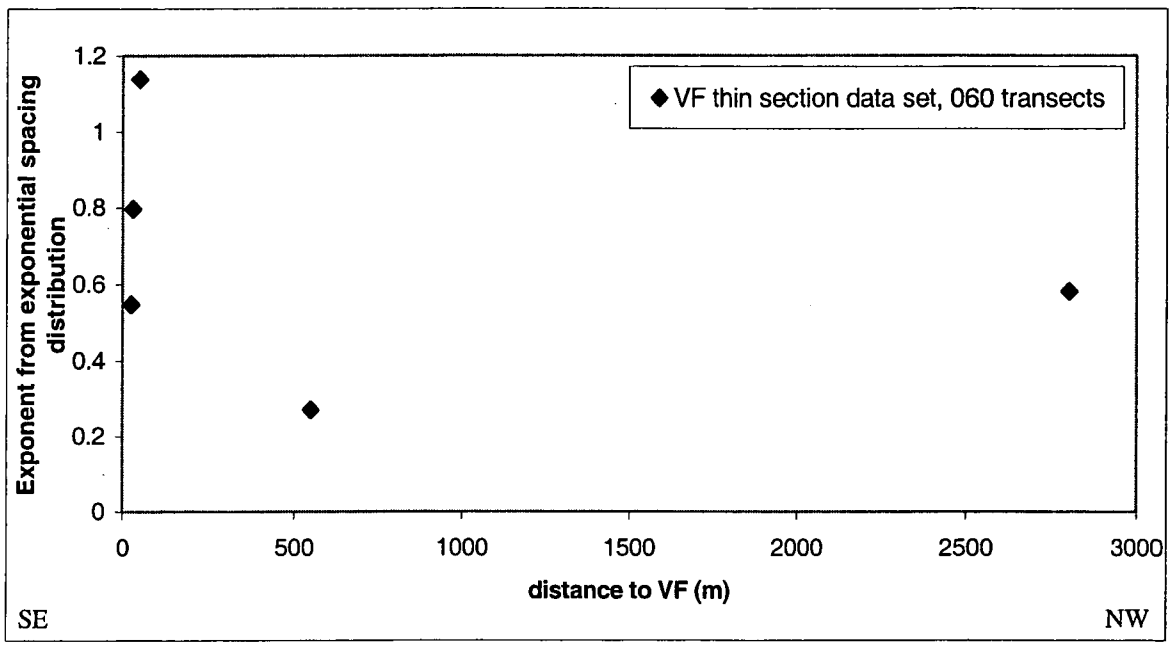

b)

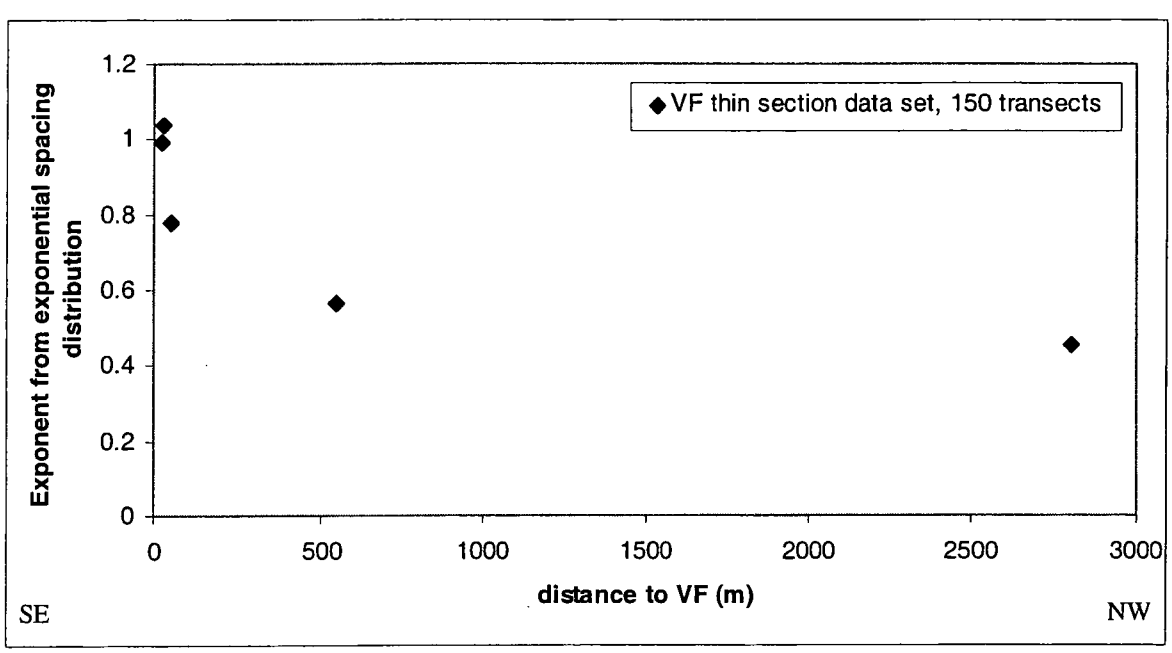

Figure 4.54 Exponent values from exponential spacing distributions 'v' perpendicular distance to the VFP, thin section data.
a) – transects orientated parallel to the MTFC trend (060°),
b) – transects orientated perpendicular to the MTFC trend (150°)

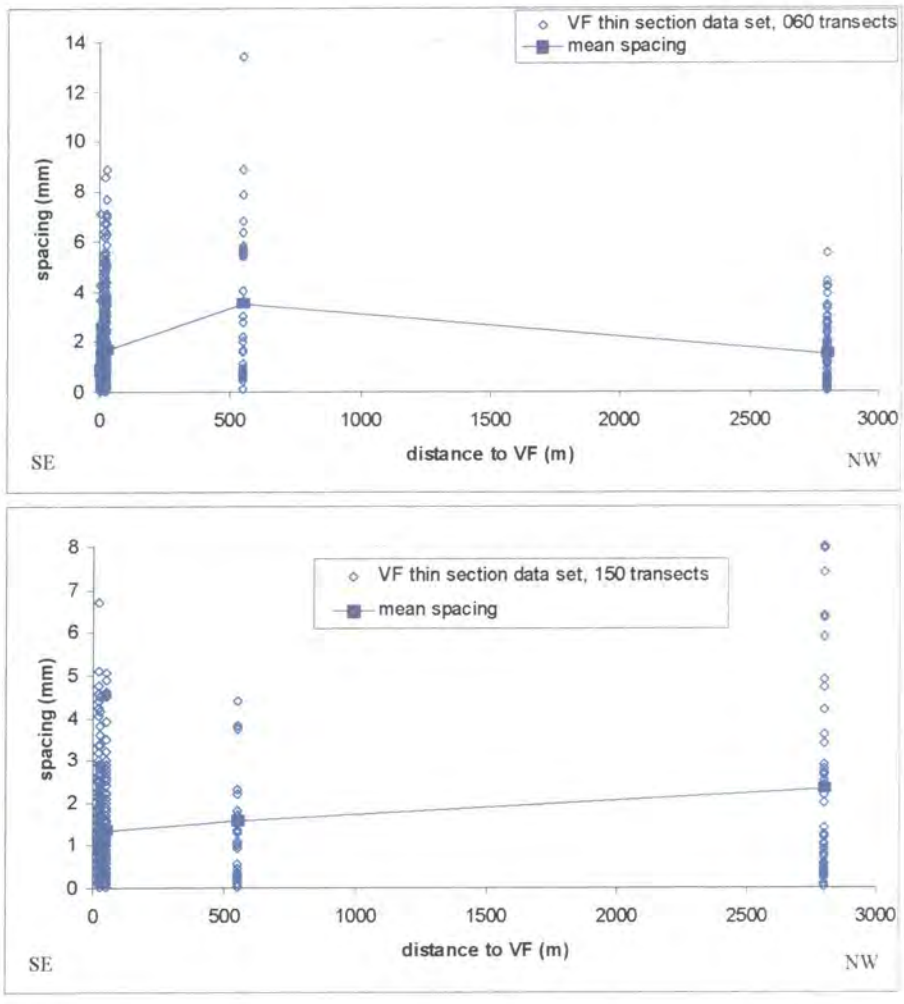

Figure 4.55 Mean spacing and range of spacing values 'v' perpendicular distance to the VFP, thin section data. **a)** – transects orientated parallel to the MTFC trend (060°), **b)** - transects orientated perpendicular to the MTFC trend (150°)

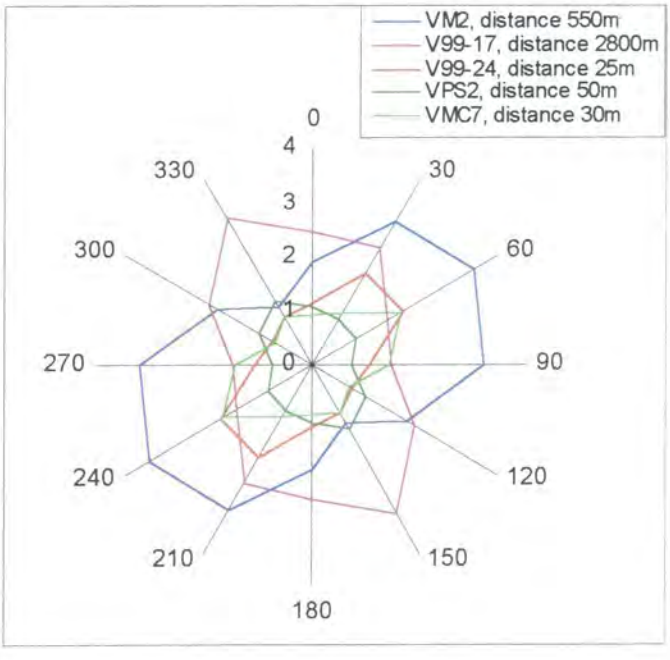

Figure 4.56 Mean spacing ellipses created for thin section data sets adjacent to the VFP. (Mean spacings are measured in mm.)

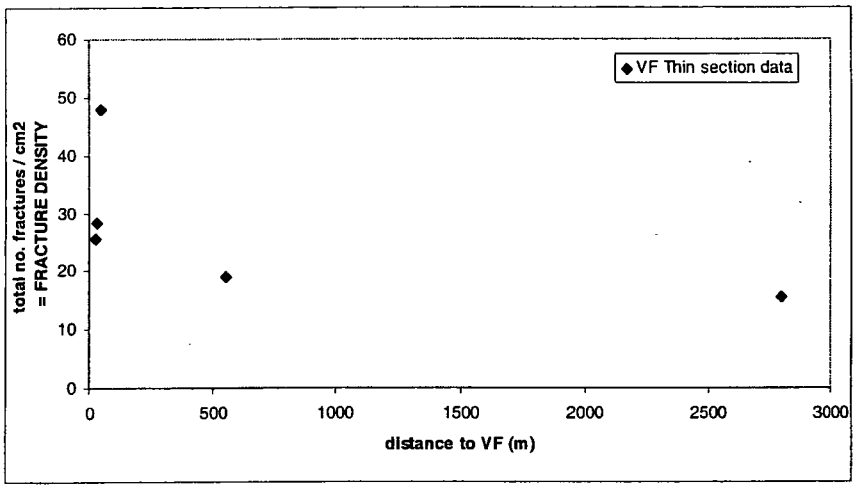

Figure 4.57 Fracture density 'v' perpendicular distance to the VFP for thin section data

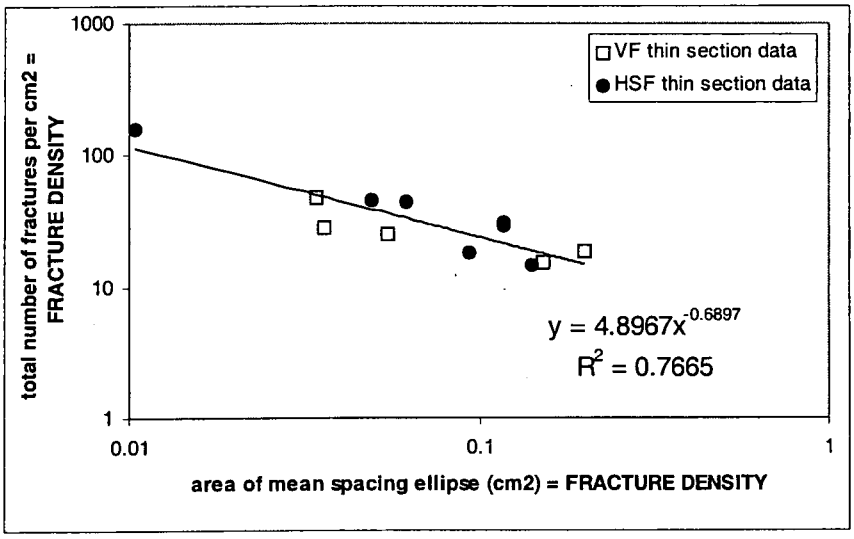

Figure 4.58 Fracture density plot for all data collected at thin section scale

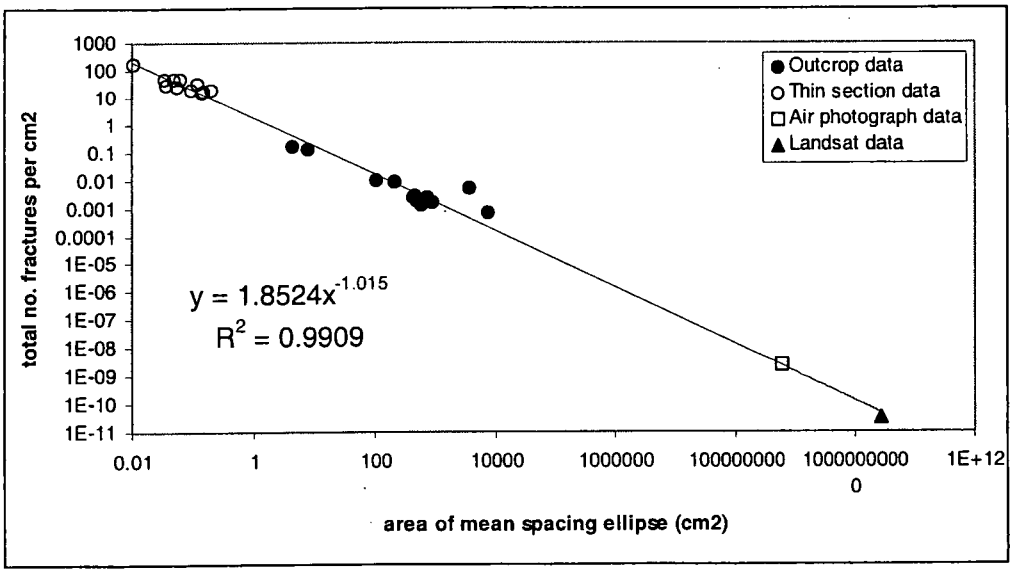

Figure 4.59 Fracture density plot for all data collected at the Landsat™ data set, the air photograph data set and all data from outcrop and thin section scales

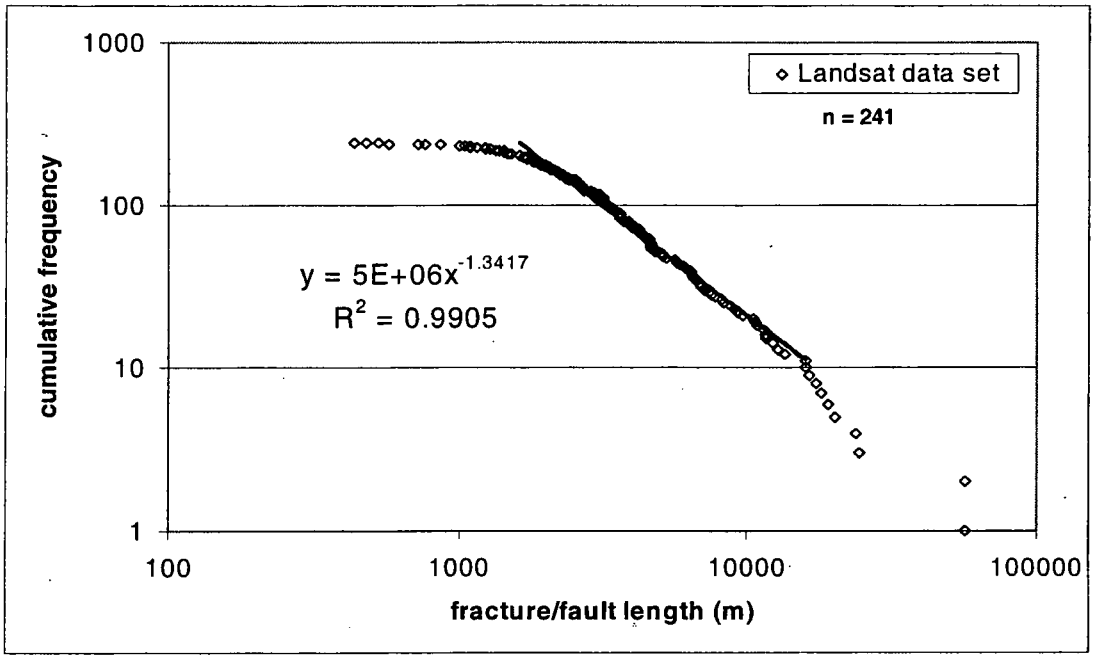

Figure 4.60 Plot of cumulative frequency 'v' fracture length for data collected from the Landsat™ image.

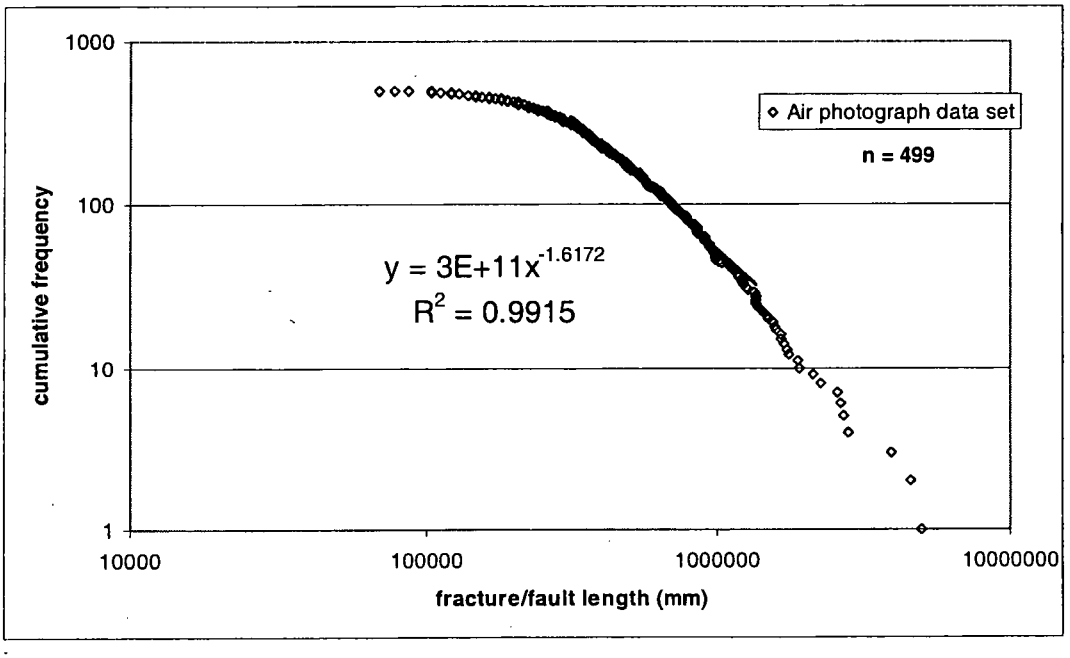

Figure 4.61 Plot of cumulative frequency 'v' fracture length for data collected from the air photograph data set.

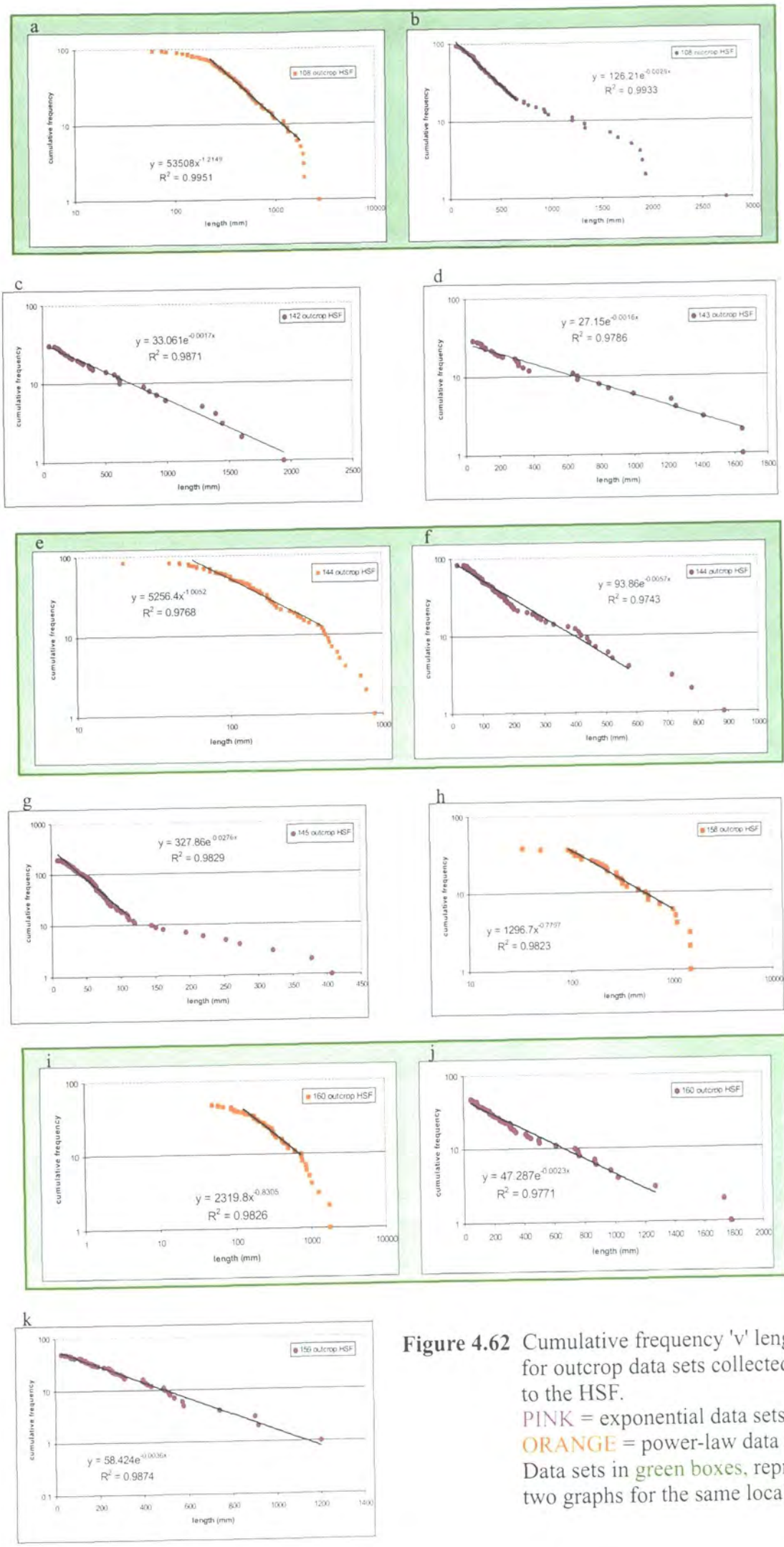

Figure 4.62 Cumulative frequency 'v' length plots for outcrop data sets collected adjacent to the HSF.
PINK = exponential data sets
ORANGE = power-law data sets
Data sets in green boxes, represent two graphs for the same locality

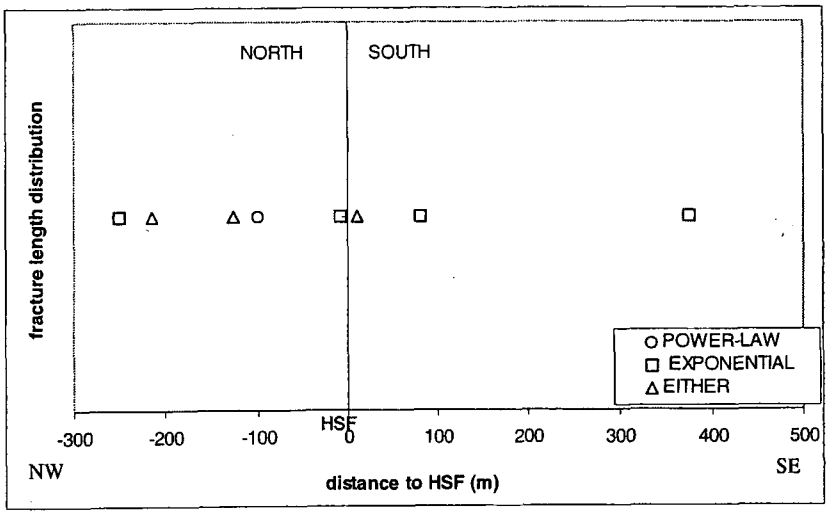

Figure 4.63 Graph illustrating the change in best-fitting fracture length distribution adjacent to the HSFP at outcrop scale

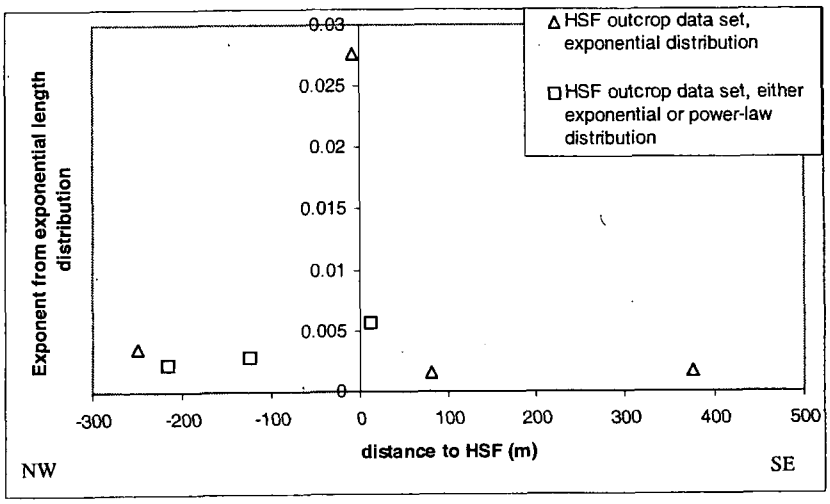

Figure 4.64 Exponent values from exponential fracture length distributions 'v' perpendicular distance to the HSFP, for outcrop data sets

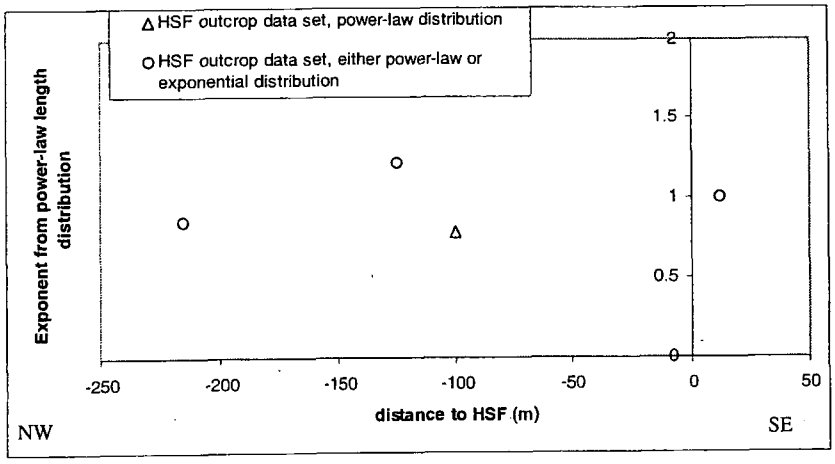

Figure 4.65 Exponent values from power-law fracture length distributions 'v' perpendicular distance to the HSFP, for outcrop data sets

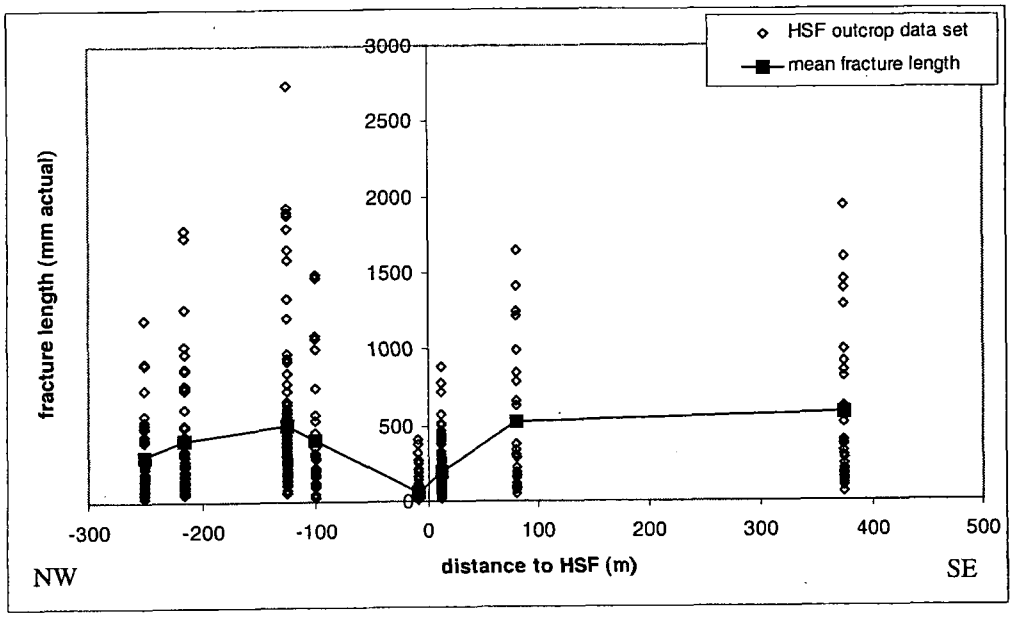

Figure 4.66 Mean fracture length and range of length values 'v' perpendicular distance to the HSFP, outcrop data sets

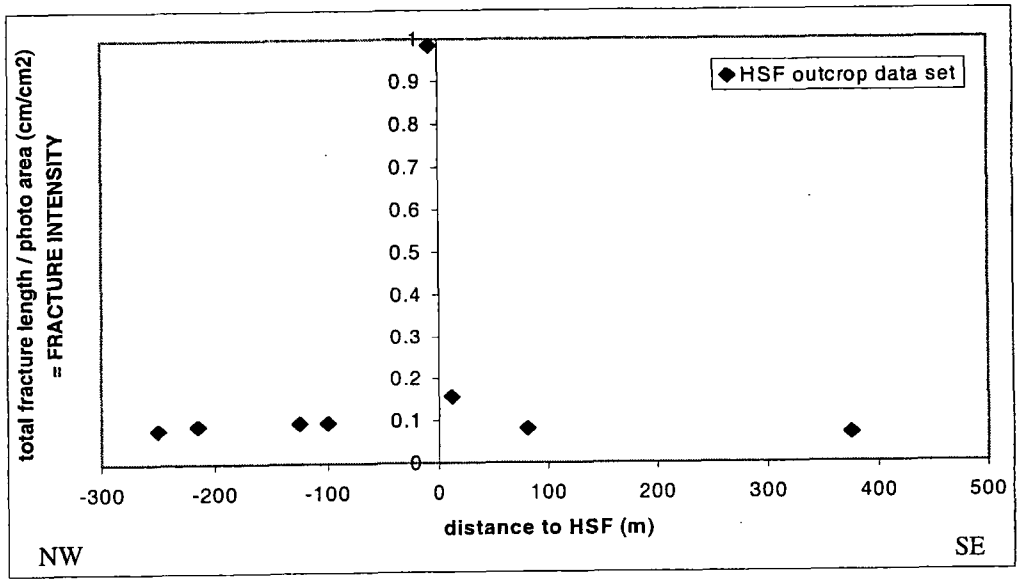

Figure 4.67 Fracture intensity 'v' perpendicular distance to the HSFP, outcrop data sets

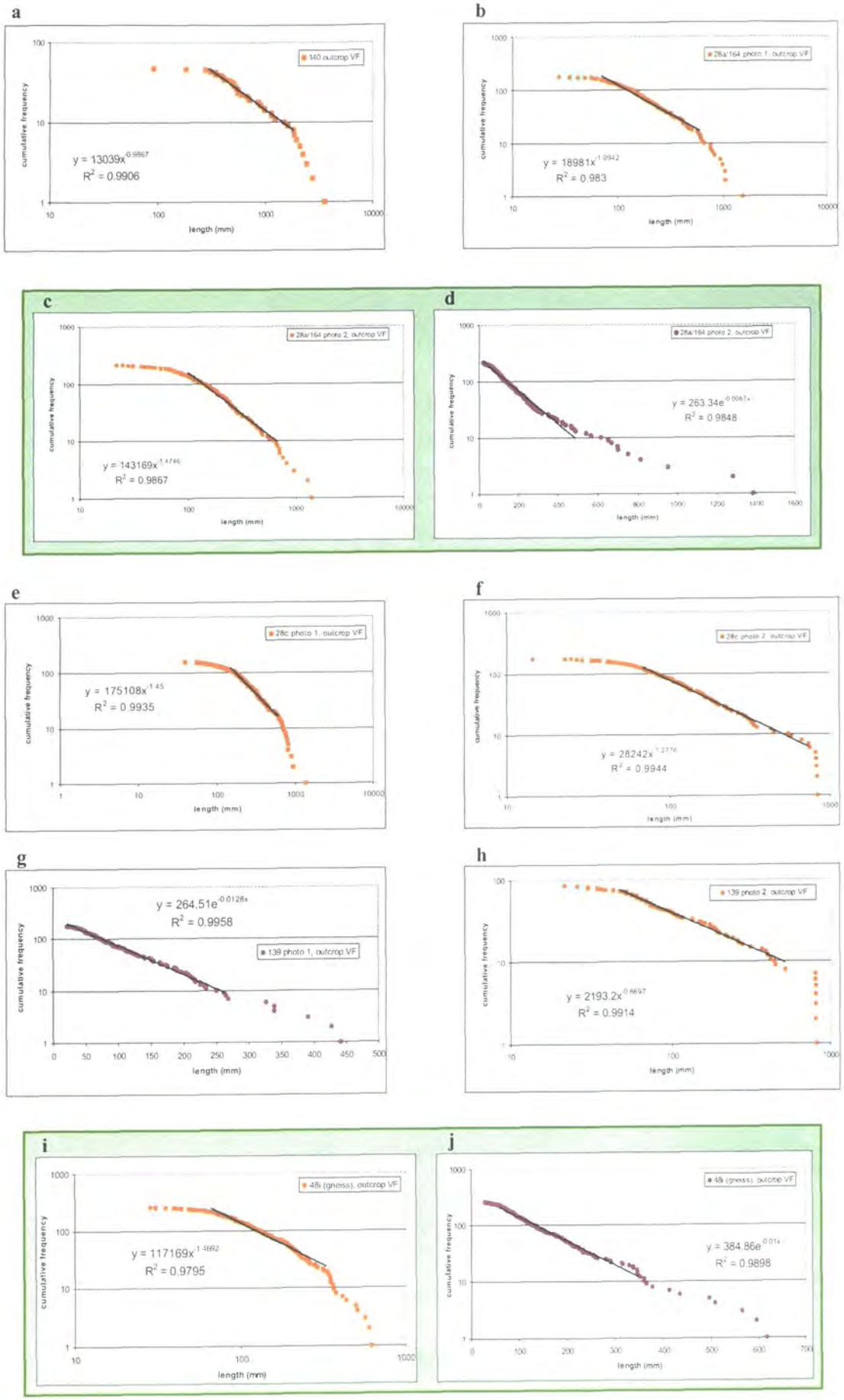

Figure 4.68 Cumulative frequency 'v' fracture length plots for outcrop data sets collected adjacent to the VFP
PINK = data sets best-fitted to an exponential distribution
ORANGE = data sets best-fitted to a power-law distribution
Data sets in green boxes represent two graphs for the same locality

(continued on next page)

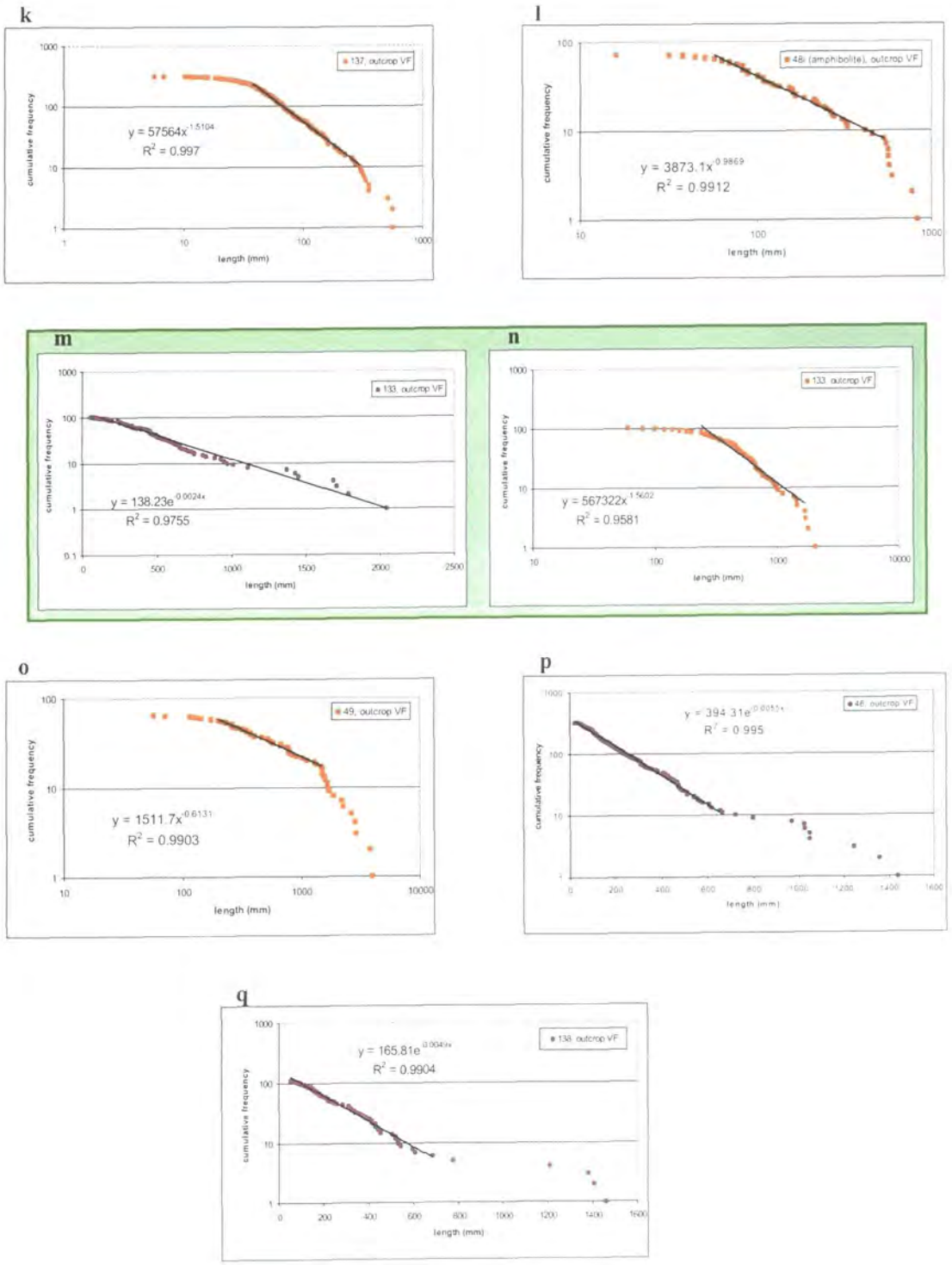

Figure 4.68 Cumulative frequency 'v' fracture length plots for outcrop data sets collected adjacent to the VFP
PINK = data sets best-fitted to an exponential distribution
ORANGE = data sets best-fitted to a power-law distribution
Data sets in green boxes represent two graphs for the same locality

(continued from previous page)

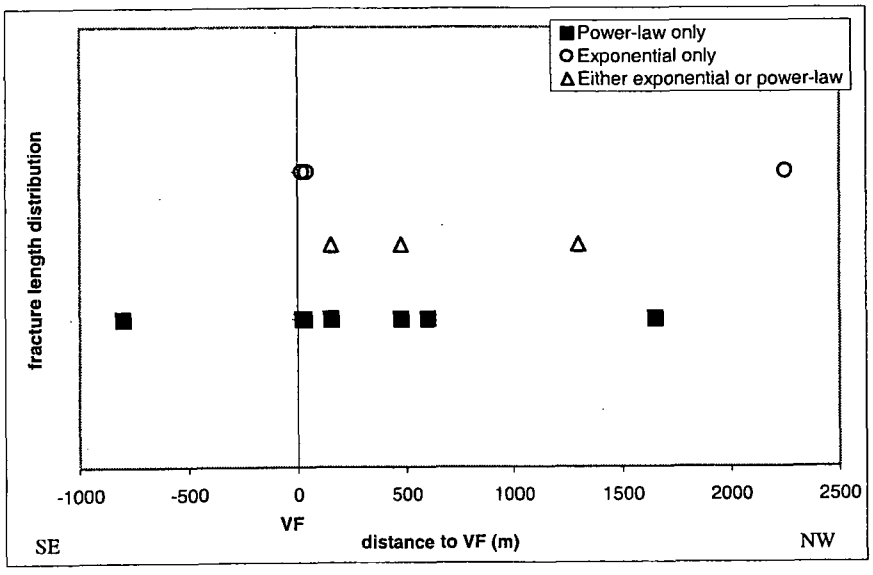

Figure 4.69 Best-fitting fracture length distributions at various distances from the VFP, for all outcrop data sets adjacent to the VFP and EFP

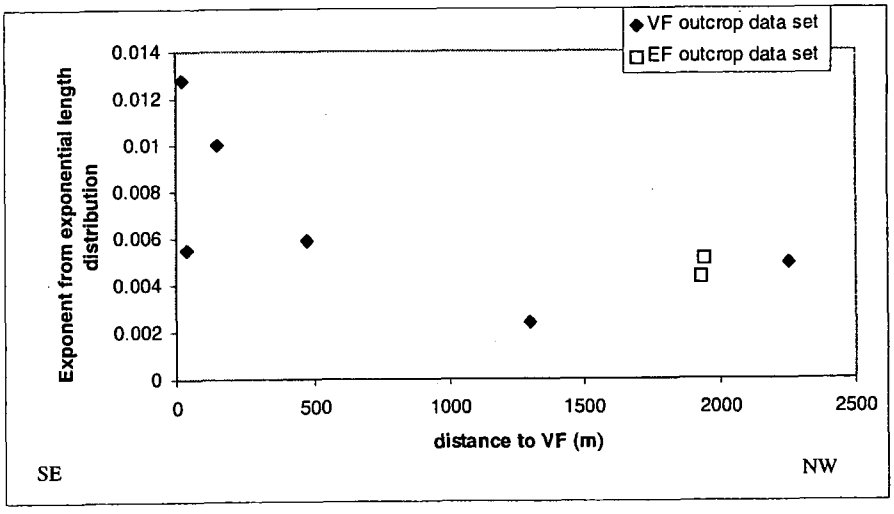

Figure 4.70 Exponents values from exponential length distributions plotted against the perpendicular distance to the VFP for outcrop data sets adjacent to the VFP & EFP.

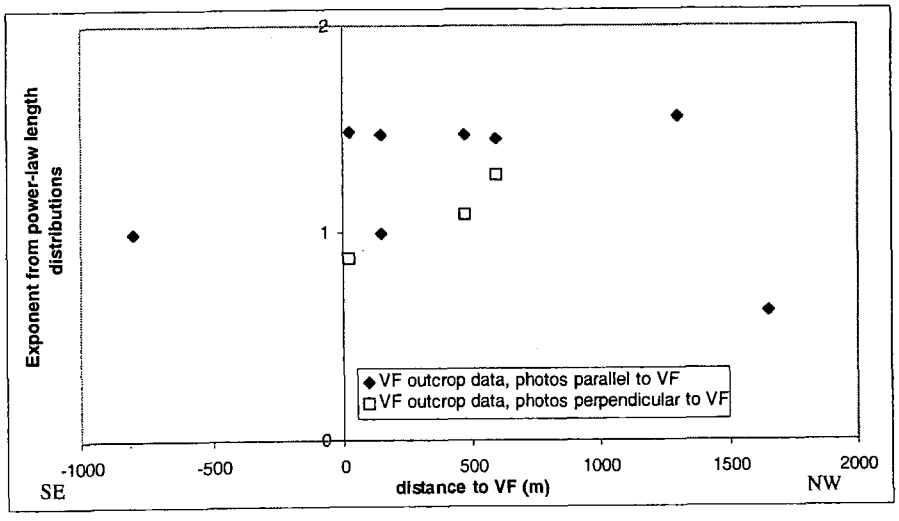

Figure 4.71 Exponent values from power-law length distributions plotted against the perpendicular distance to the VFP

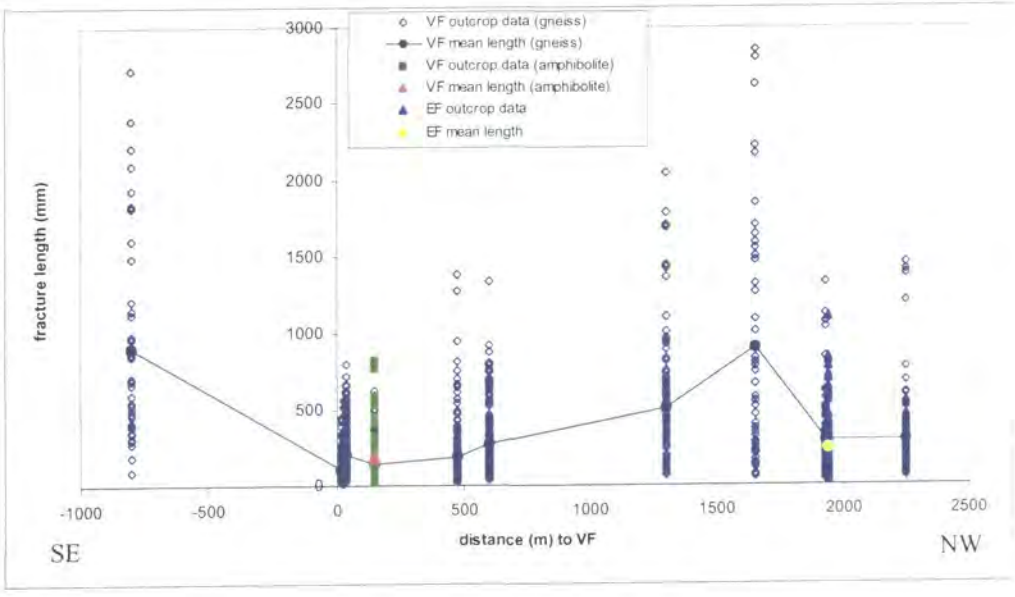

Figure 4.72 Mean fracture length and range of length values 'v' perpendicular distance to the VFP, outcrop data.

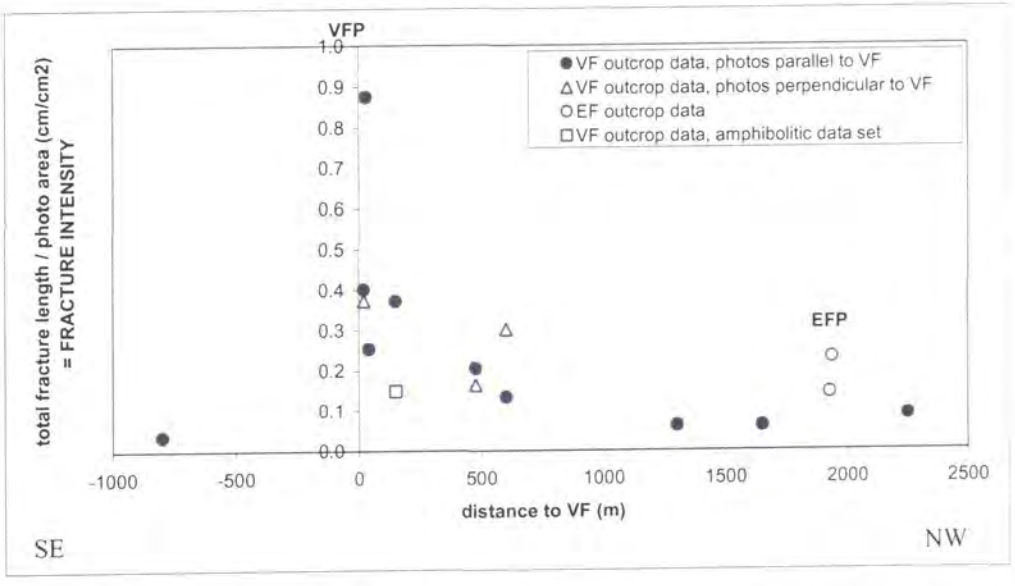

Figure 4.73 Fracture intensity 'v' perpendicular distance to the VFP, outcrop data.

a)

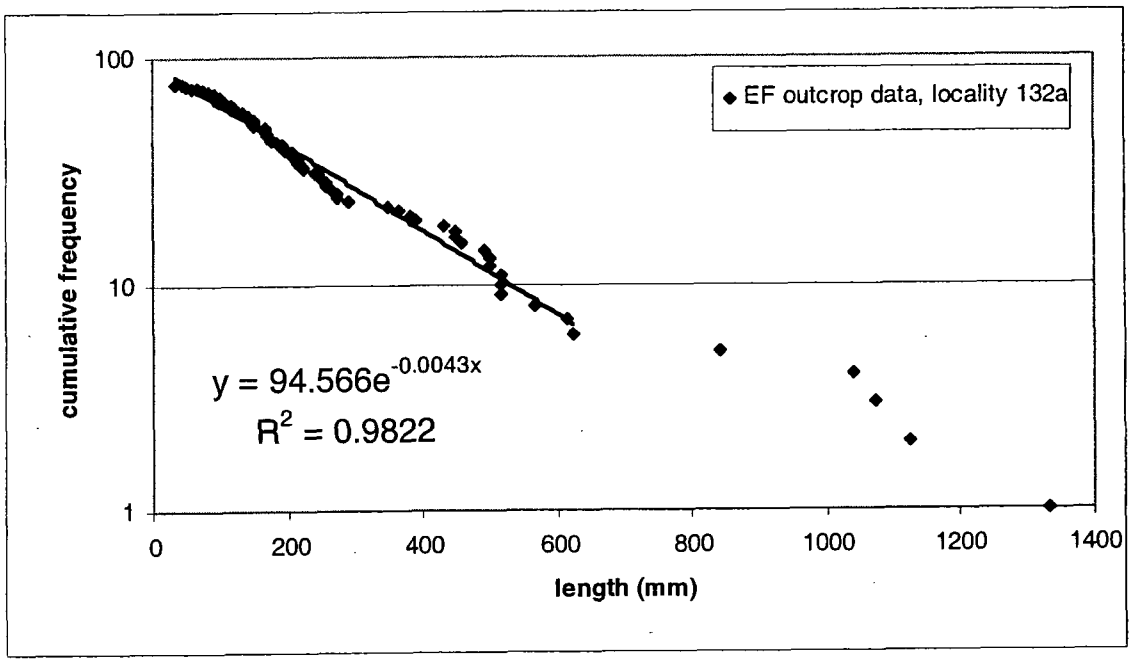

b)

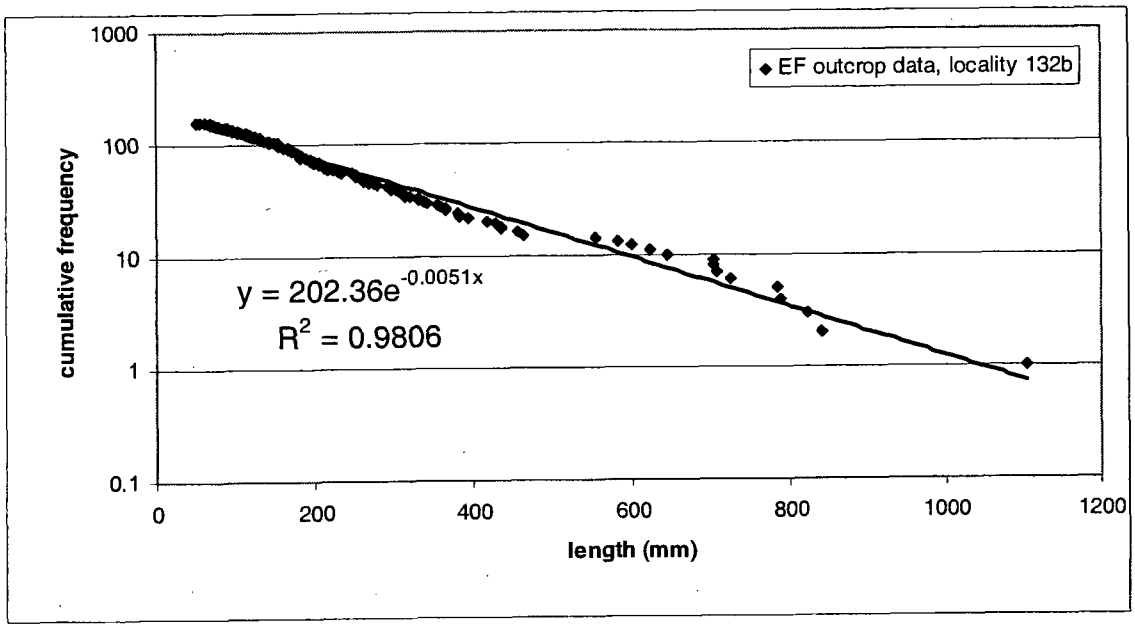

Figure 4.74 Cumulative frequency 'v' fracture length plots for **a)** locality 132a (10m from the EFP) and **b)** 132b (1m from the EFP)

a)

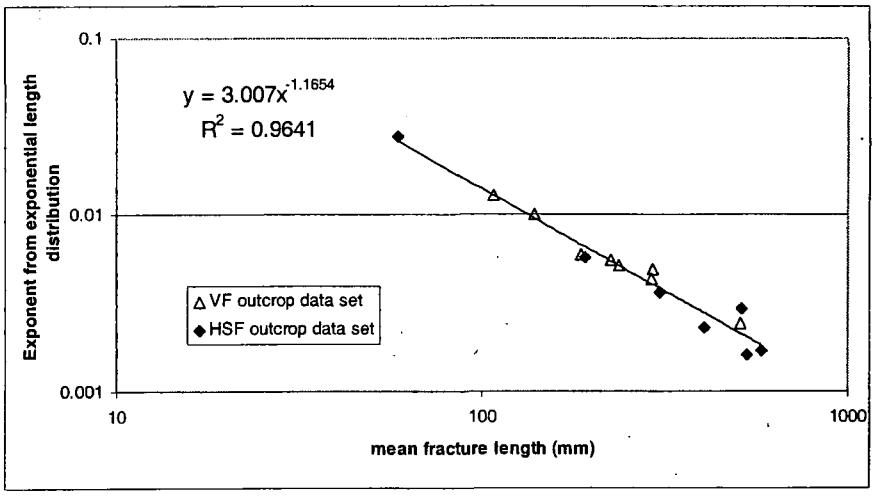

b)

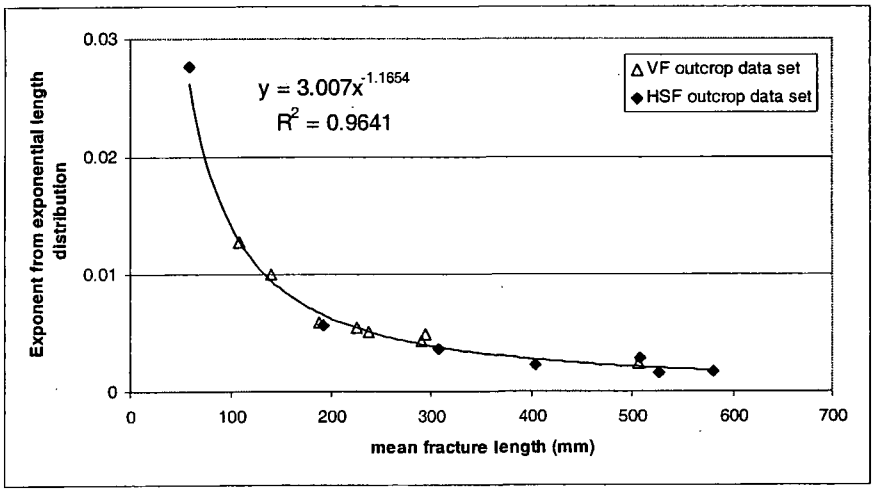

Figure 4.75 Exponent values from HSF & VF exponential length distributions 'v' mean length, outcrop data sets **a)** data plotted on logarithmic axes, **b)** data plotted on linear axes

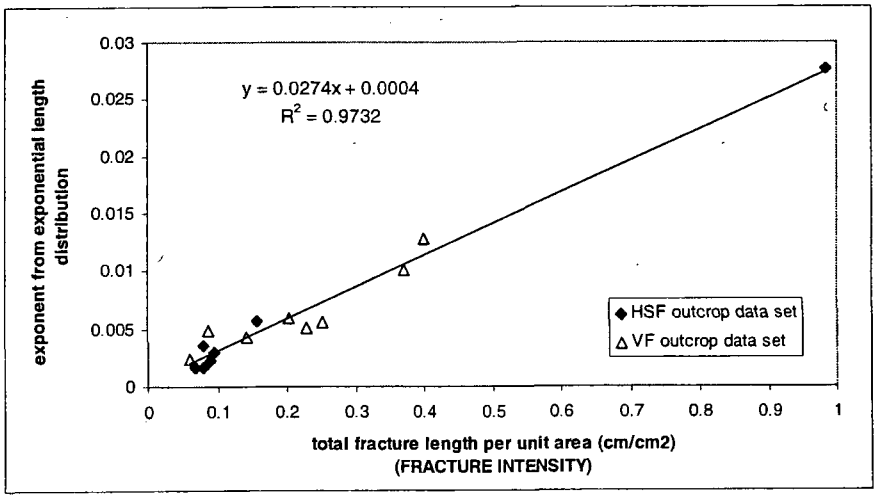

Figure 4.76 Exponent values from exponential length distributions 'v' fracture intensity for data collected adjacent to the VFP and HSFP at outcrop scale.

a)

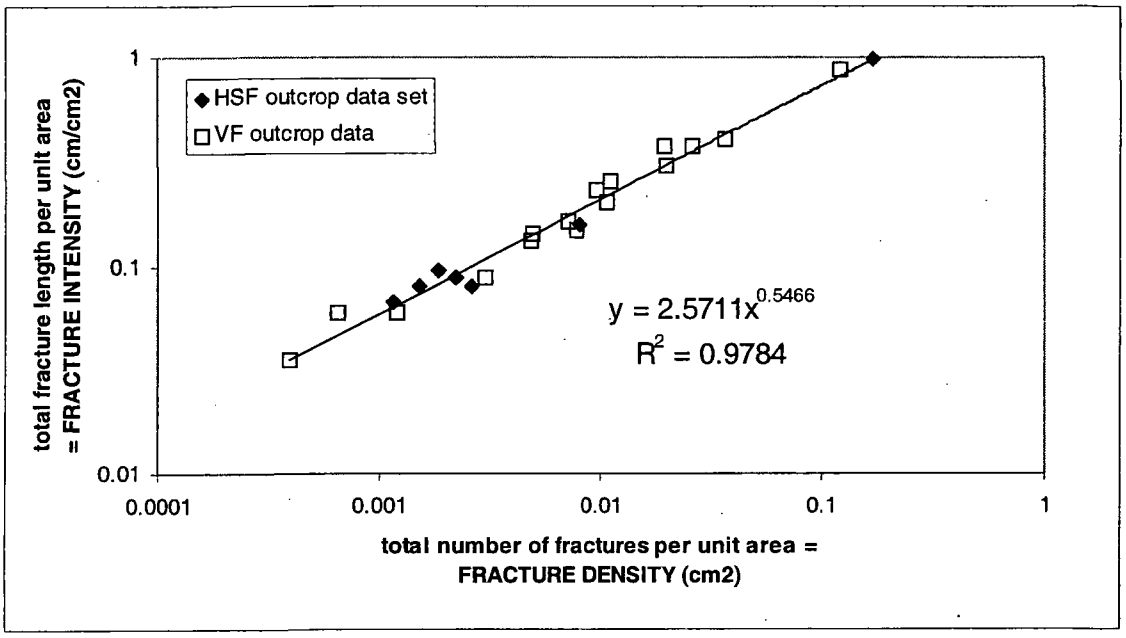

b)

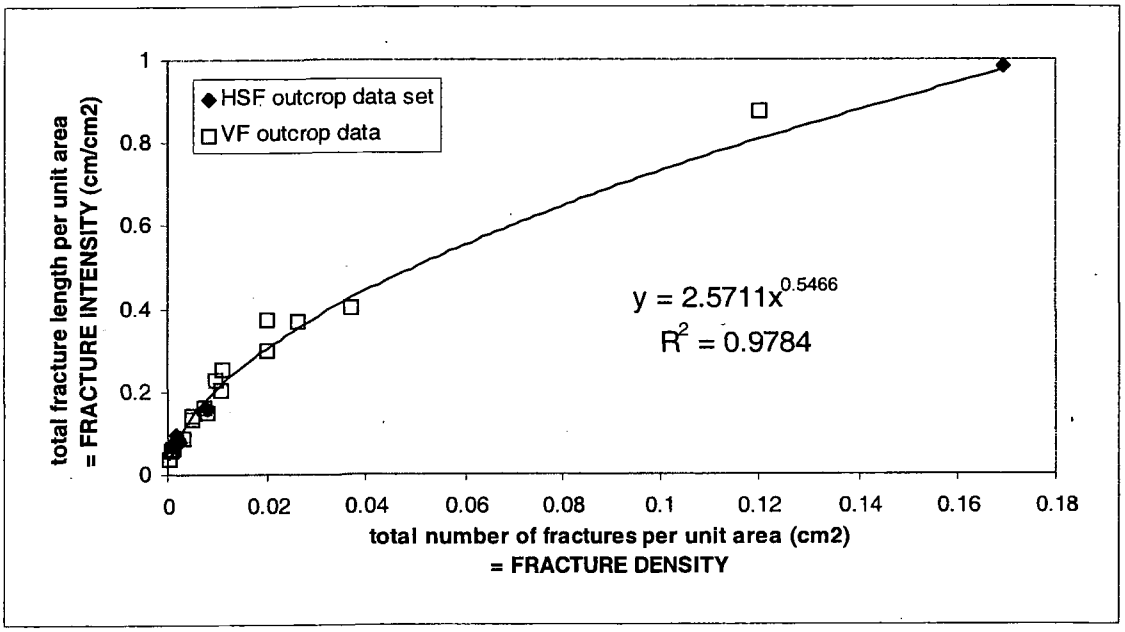

Figure 4.77 Fracture density 'v' fracture intensity for outcrop data sets measured adjacent to the VFP and the HSFP. **a)** data plotted on logarithmic axes, **b)** data plotted on linear axes

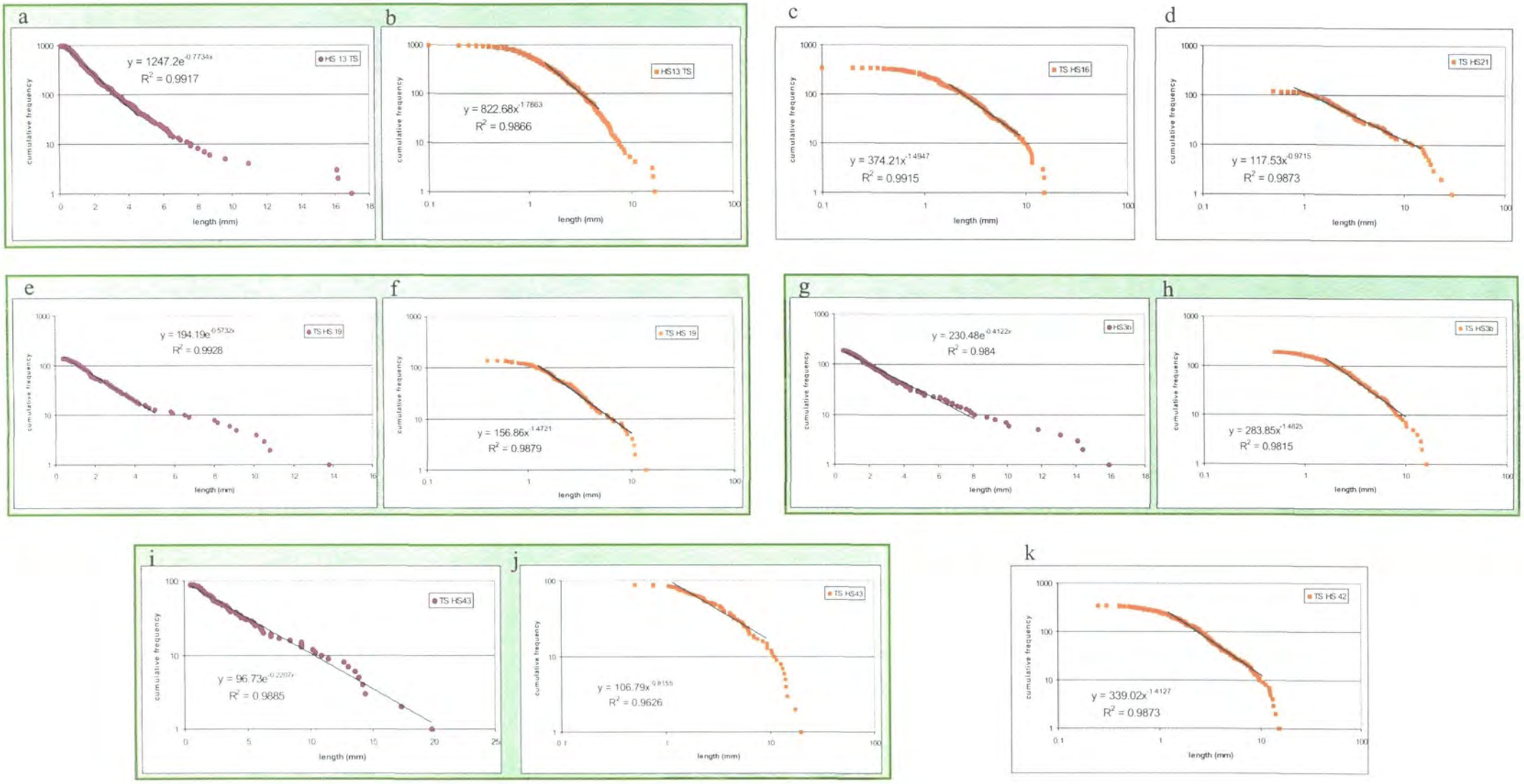

Figure 4.78 Cumulative frequency 'v' length plots for thin section data sets collected adjacent to the HSFP
PINK = data sets that can be fitted to an exponential distribution
ORANGE = data sets that can be fitted to a power-law distribution
Data sets in green boxes represent two graphs from the same locality

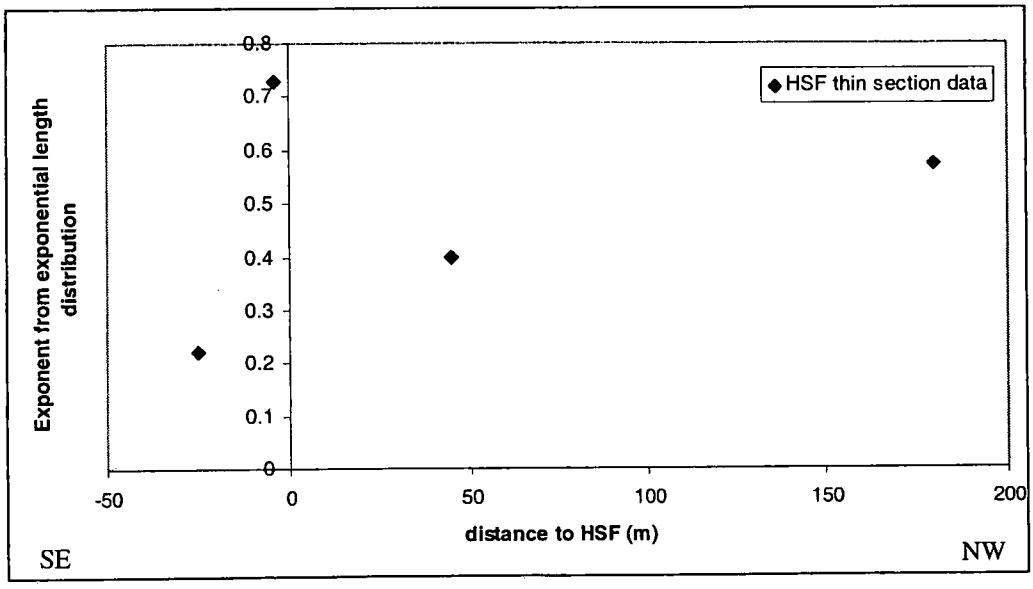

Figure 4.79 Exponential exponent values plotted against the perpendicular distance to the HSFP, for fracture length data sets collected at thin section scale

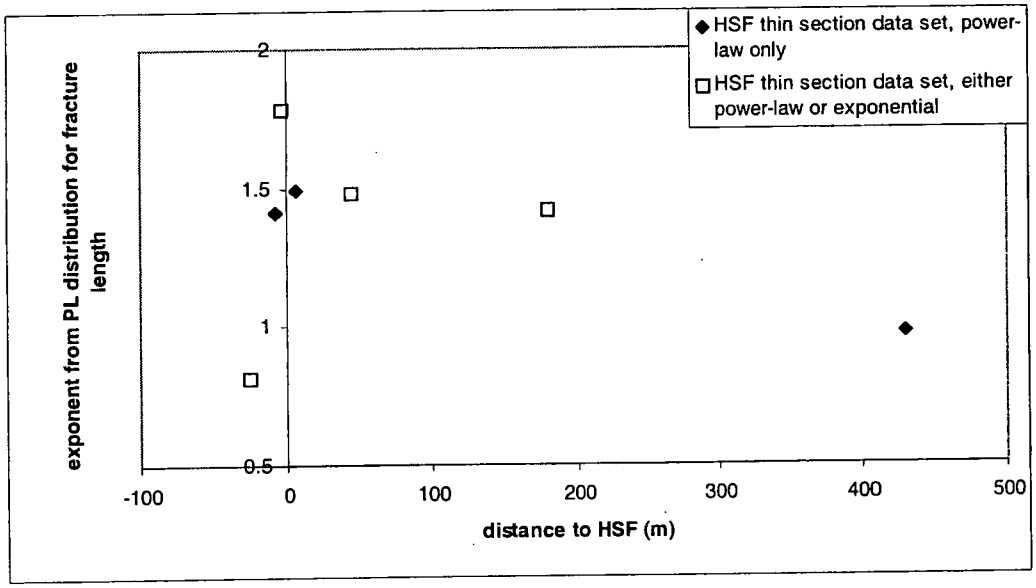

Figure 4.80 Exponent values from power-law fracture length distributions 'v' perpendicular distance to the HSFP, for data collected at thin section scale

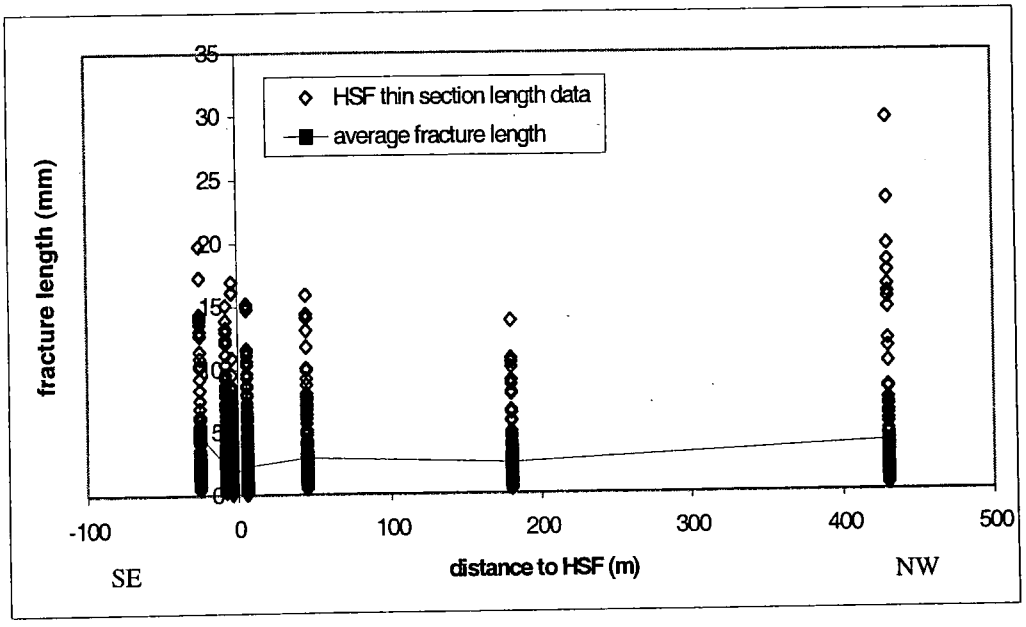

Figure 4.81 Mean fracture length data plotted with the range of fracture length values at various distances from the HSFP, for data collected at thin section scale

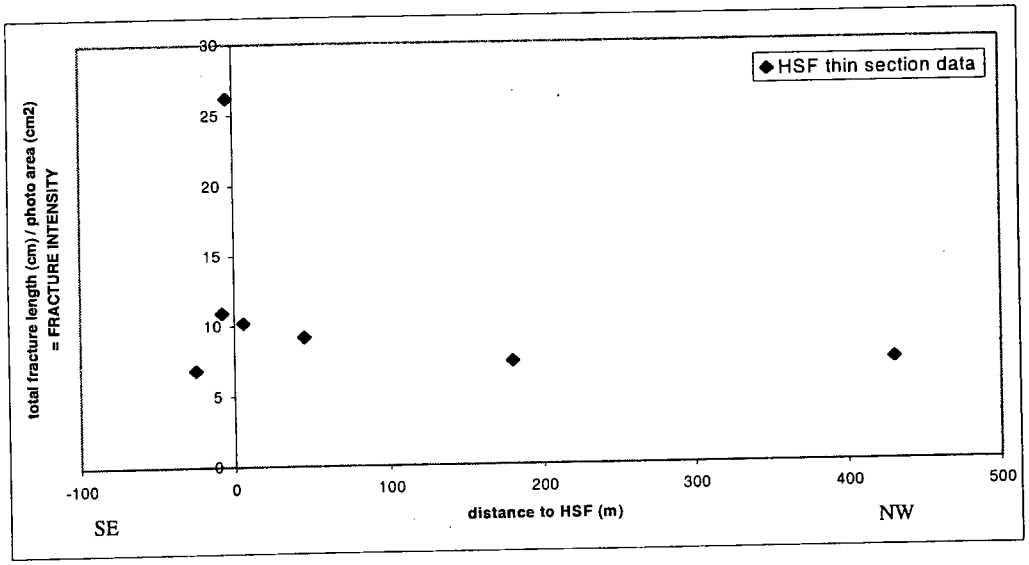

Figure 4.82 Fracture intensity values plotted against the perpendicular distance to the HSFP for data collected at thin section scale

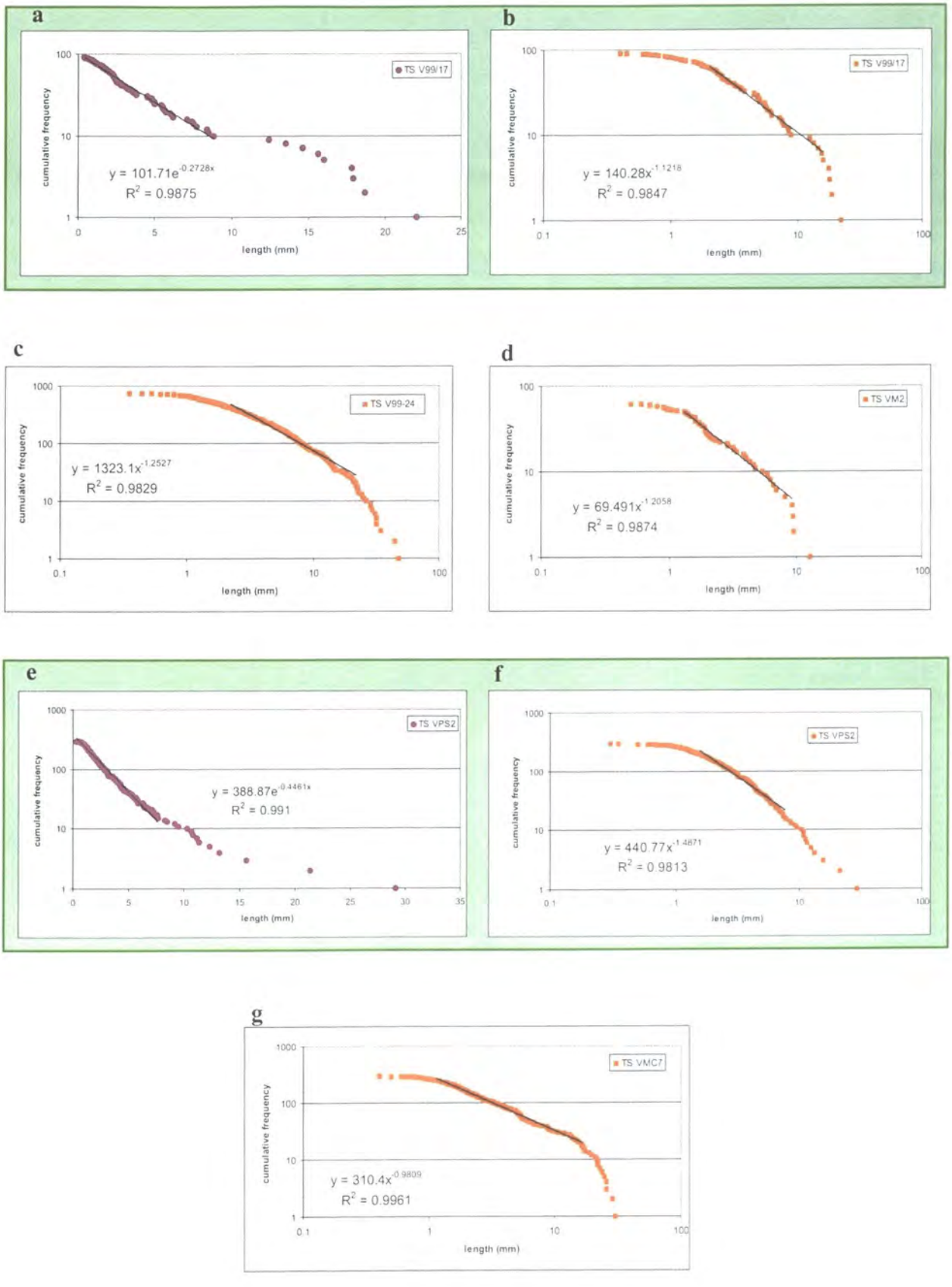

Figure 4.83 Cumulative frequency 'v' fracture length plots for thin section data sets collected adjacent to the VFP.
PINK data sets = best-fitted to an exponential distribution
ORANGE data sets = best-fitted to a power-law distribution
Data sets in green boxes, represent two graphs from the same locality

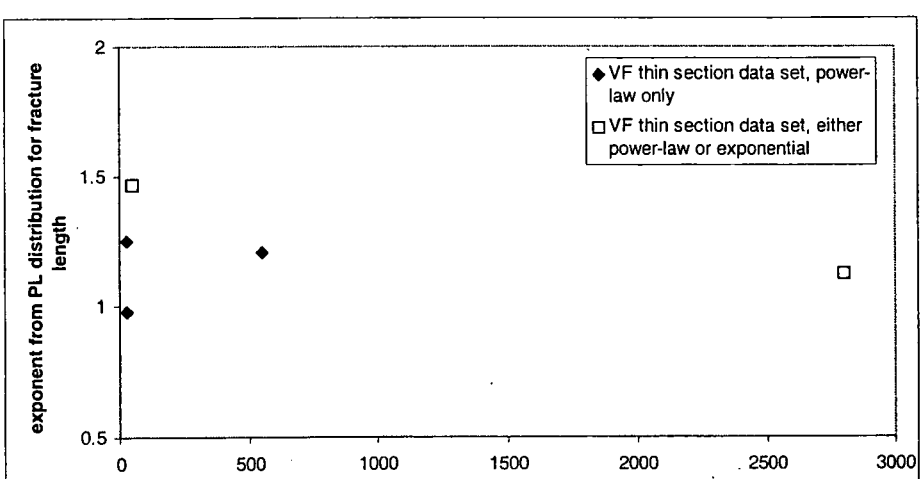

Figure 4.84 Exponent values from power-law (PL) length distributions 'v' perpendicular distance to the VFP, thin section data sets.

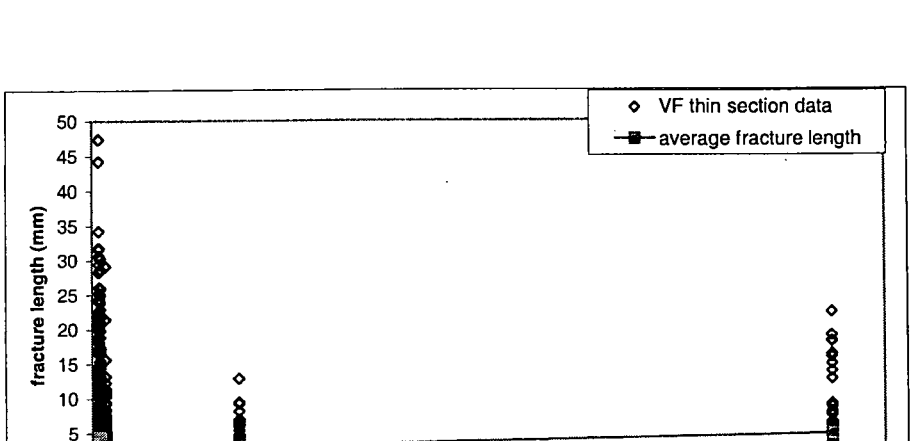

Figure 4.85 Mean fracture length and the ranges of fracture length values 'v' perpendicular distance to the VFP, thin section data sets

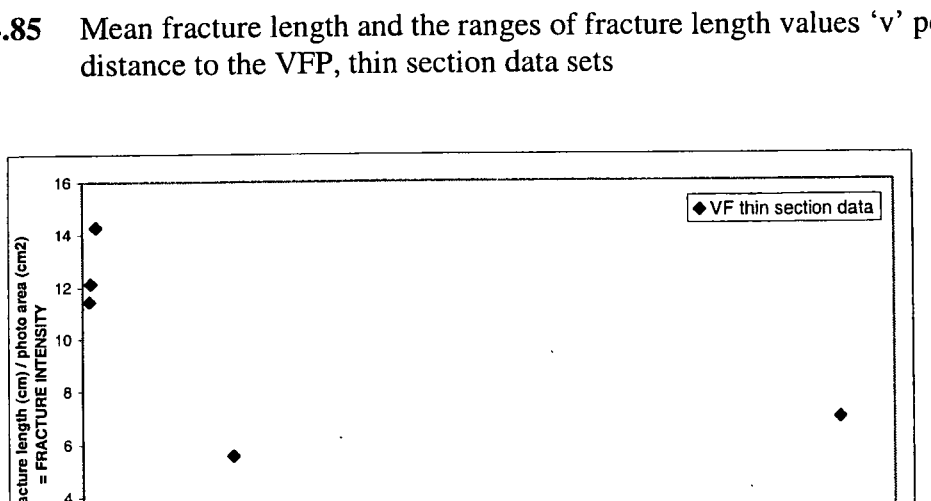

Figure 4.86 Fracture intensity 'v' perpendicular distance to the VFP, thin section data sets

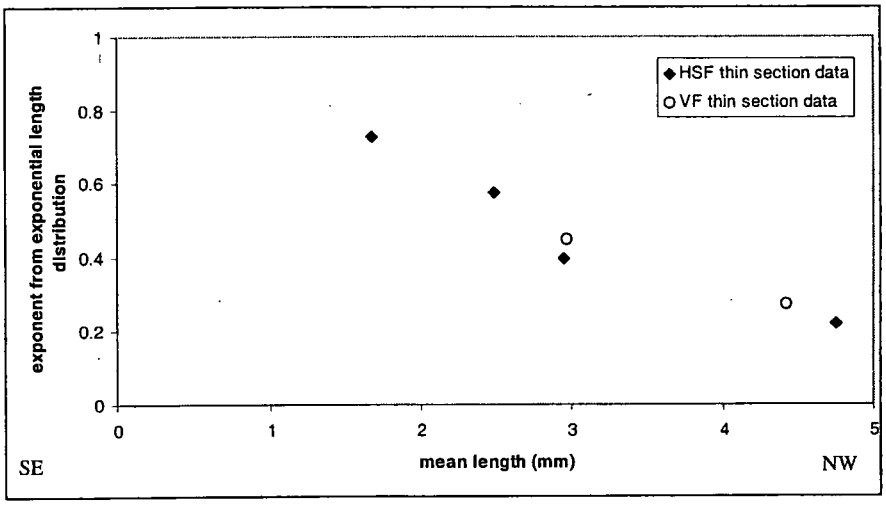

Figure 4.87 Exponent values from exponential length distributions 'v' mean length for data collected from thin sections adjacent to the HSFP and the VFP

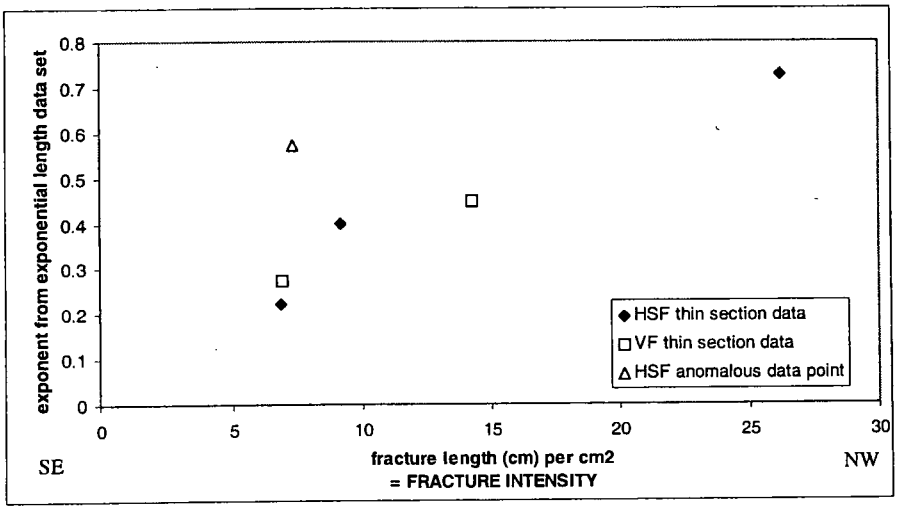

Figure 4.88 Exponent values from exponential length distributions 'v' fracture intensity for data collected from thin sections adjacent to the HSFP and the VFP

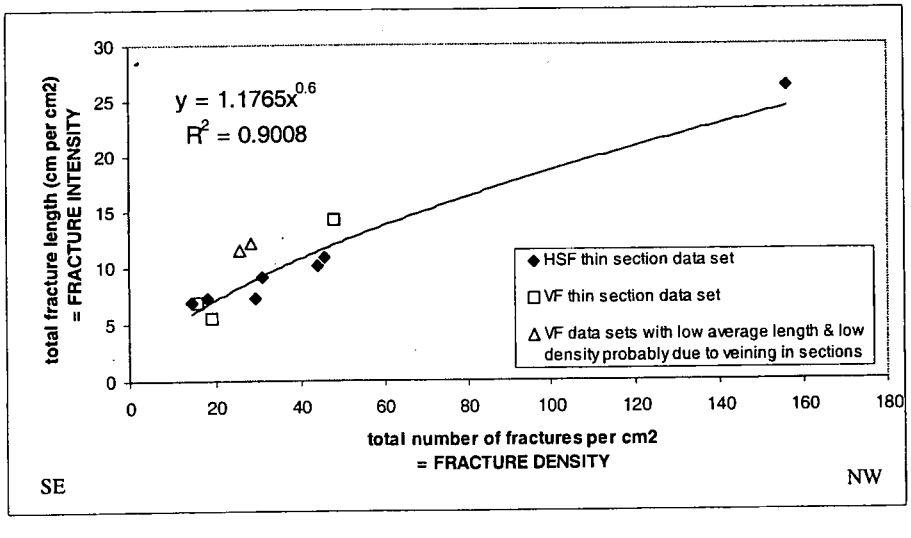

Figure 4.89 Fracture density 'v' fracture intensity for data collected adjacent to the HSFP and the VFP at thin section scale

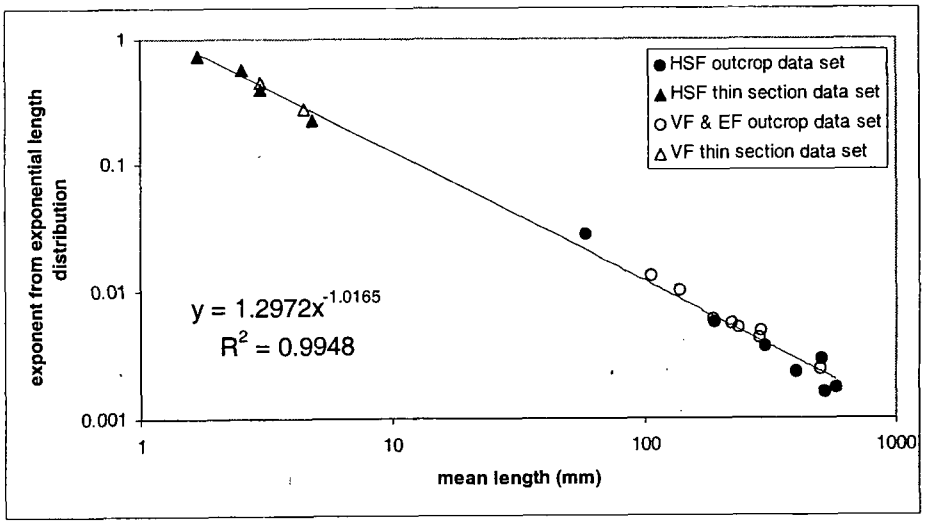

Figure 4.90 Exponent values from exponential length distributions 'v' mean fracture length values for thin section & outcrop data sets adjacent to HSFP, VFP & EFP

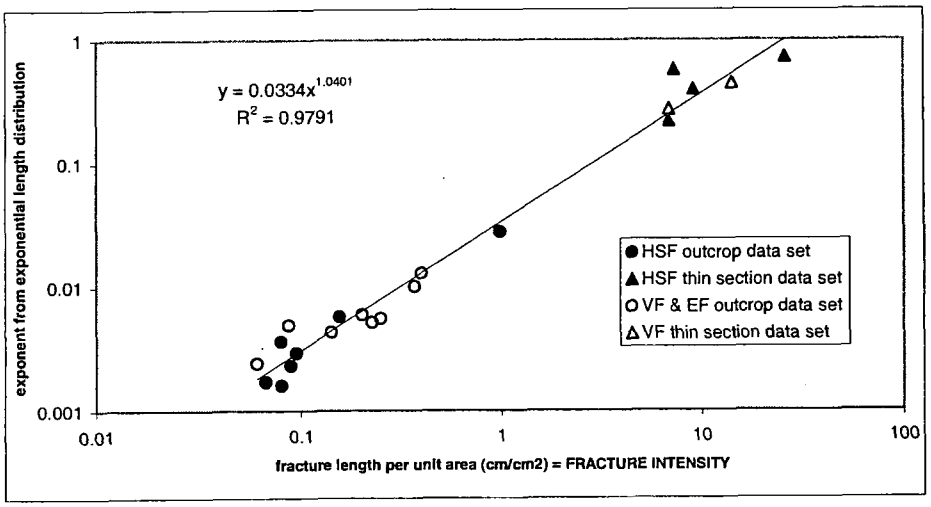

Figure 4.91 Exponent values from exponential length distributions 'v' fracture intensity for data from thin section and outcrop scales adjacent to the HSFP, VFP and EFP

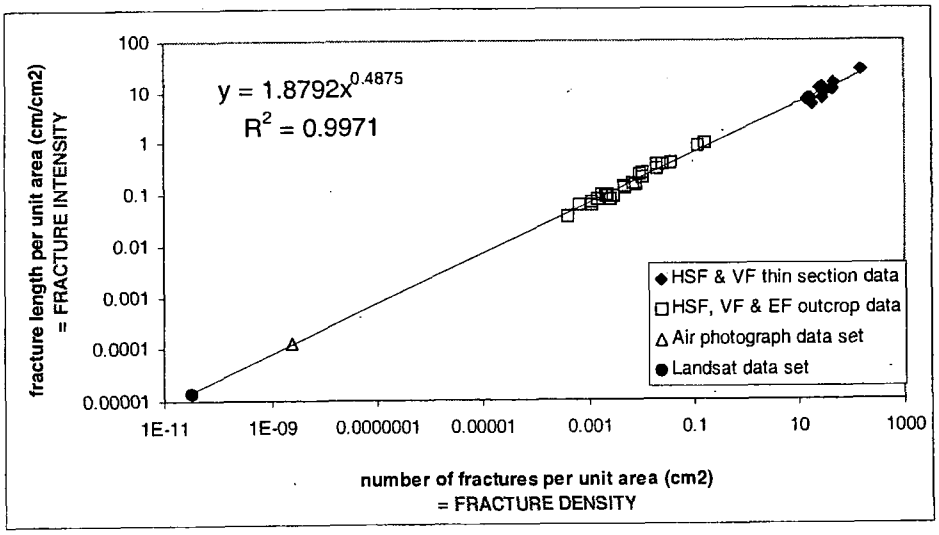

Figure 4.92 Fracture density 'v' fracture intensity values for data from thin section, outcrop, air photograph and Landsat data sets

a)

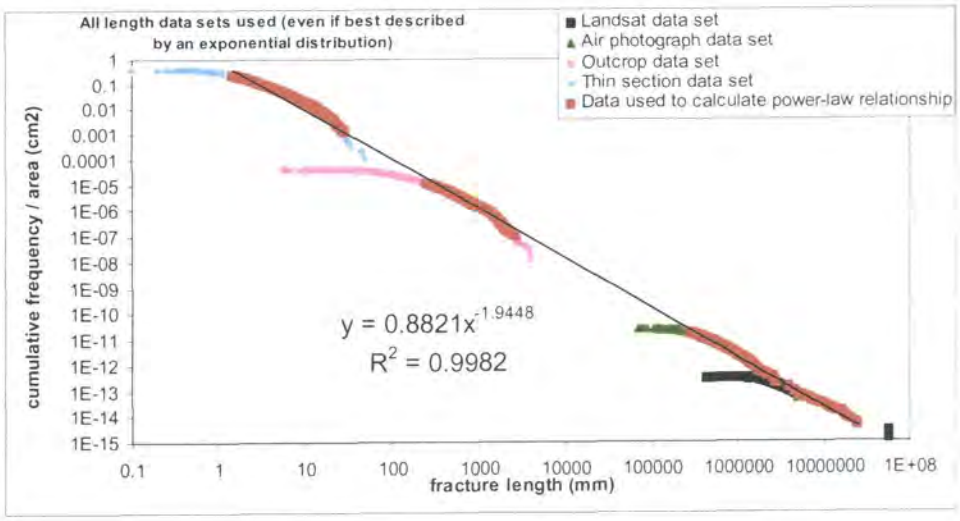

Data set	Total number of data points	Data points used for best-fit line
TOTAL	7515	3430
Landsat	241	48
Air Photo	499	337
Outcrop	3094	851
Thin section	3681	2194

(45.6% data points used for best-fit line)

b)

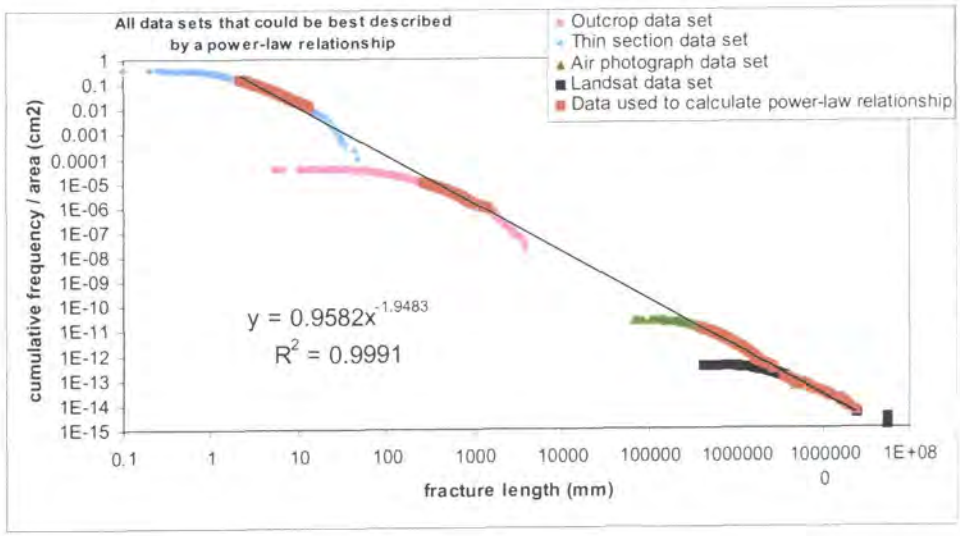

Data set	Total number of data points	Data points used for best-fit line
TOTAL	6355	2221
Landsat	241	81
Air Photo	499	233
Outcrop	1934	461
Thin section	3681	1446

(34.9% data points used for best-fit line)

c)

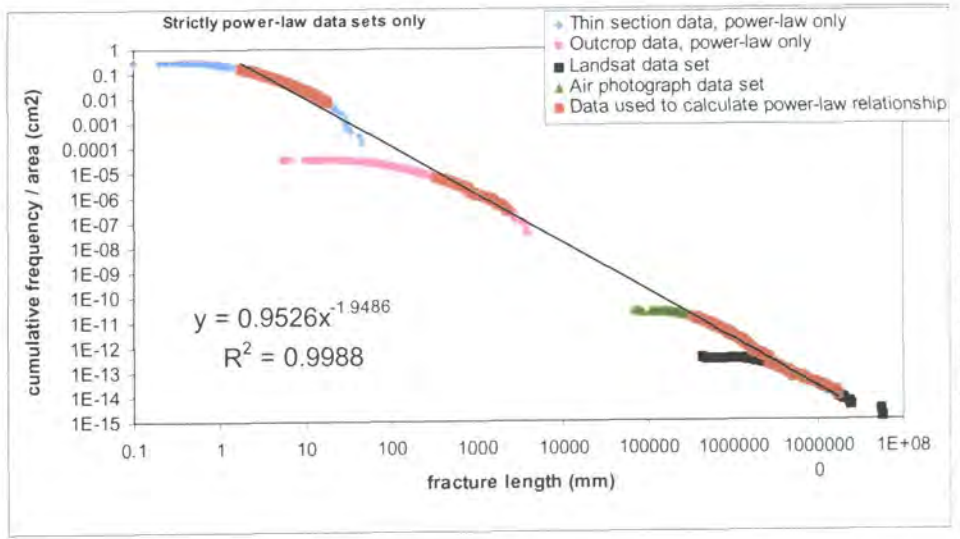

Data set	Total number of data points	Data points used for best-fit line
TOTAL	3742	1603
Landsat	241	129
Air Photo	499	280
Outcrop	1090	187
Thin section	1912	1007

(42.8% data points used for best-fit line)

Figure 4.93 Cumulative frequency 'v' fracture length plots for data from the Landsat™, air photograph, outcrop and thin section data sets. The best-fitting power-law relationship is calculated using different data, **a)** all individual data sets (power-law or exponential), **b)** all data sets that could be best-fitted to a power-law relationship, **c)** data sets that are best-fitted to a power-law relationship only. The tables adjacent to the graphs detail the number of data points used.

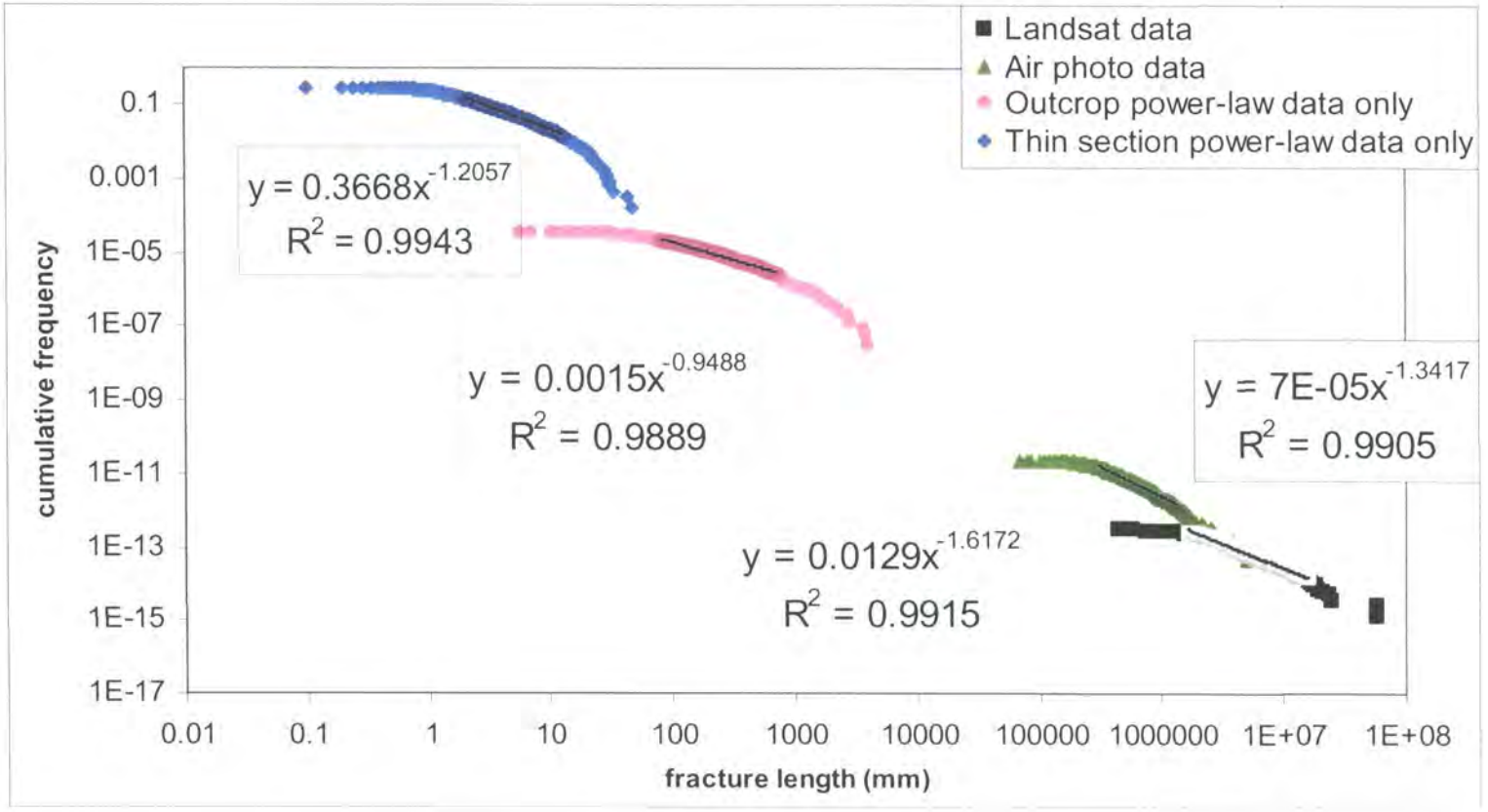

Figure 4.94 Fracture length 'v' cumulative frequency plot for data from the Landsat™ image, the air photograph, and data collected at outcrop and thin section scales.

a)

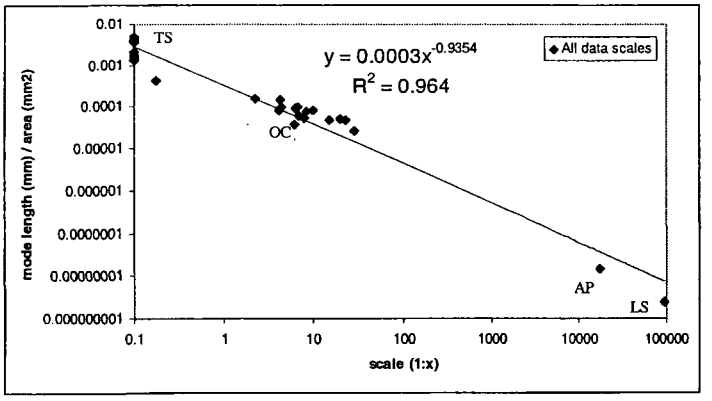

TS = thin section
OC = outcrop
AP = air photograph
LS = Landsat

b)

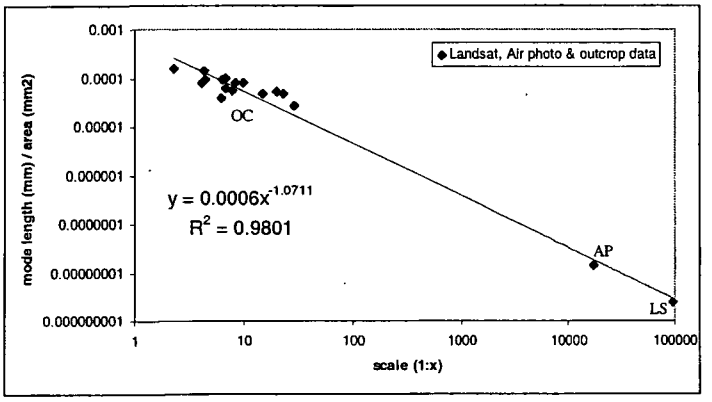

c)

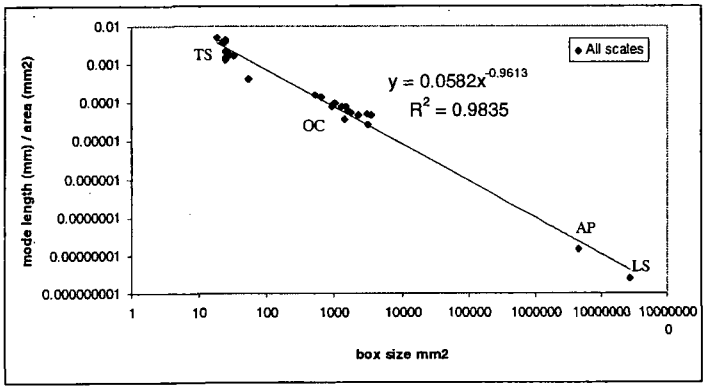

d)

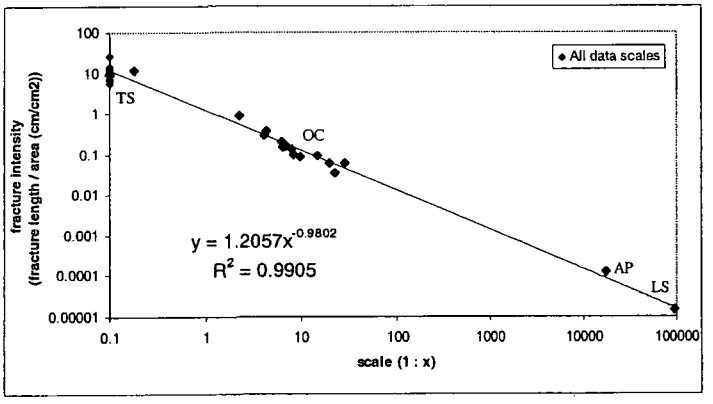

Figure 4.95 Plots to investigate fracture length scale-invariance within the data sets collected from the MTFC at all data scales.

a) Data scale 'v' normalised modal fracture length – all data scales
b) Data scale 'v' normalised modal fracture length –without thin section data
c) Box size (= √fracture map area) 'v' normalised modal fracture length
d) Data scale 'v' fracture intensity

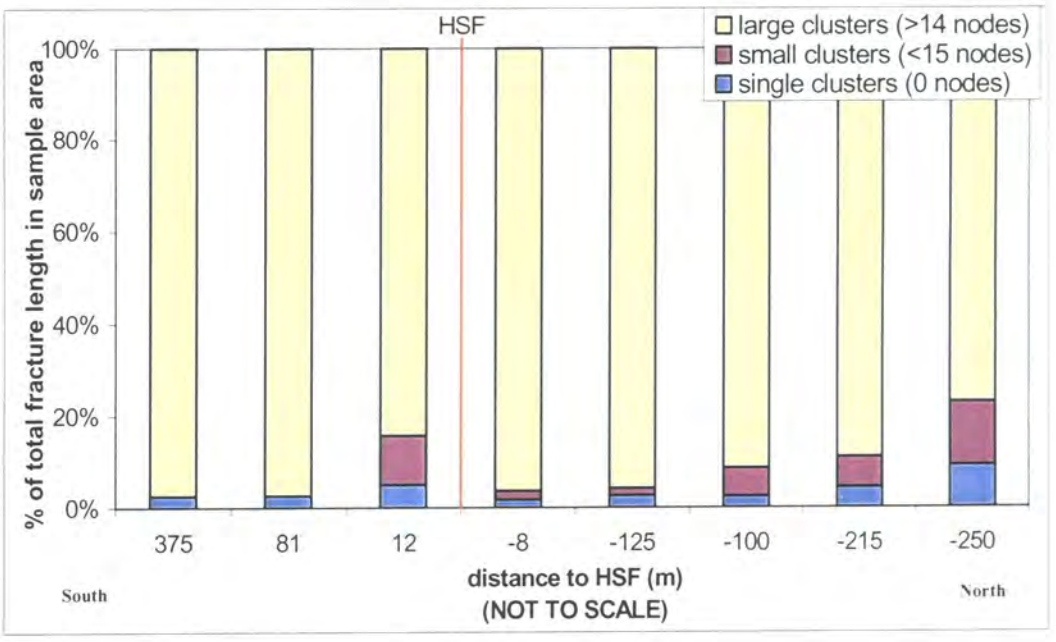

Figure 4.96 Relative percentages of total number of fractures contained in single, small and large clusters 'v' perpendicular distance to the HSFP, outcrop data set.

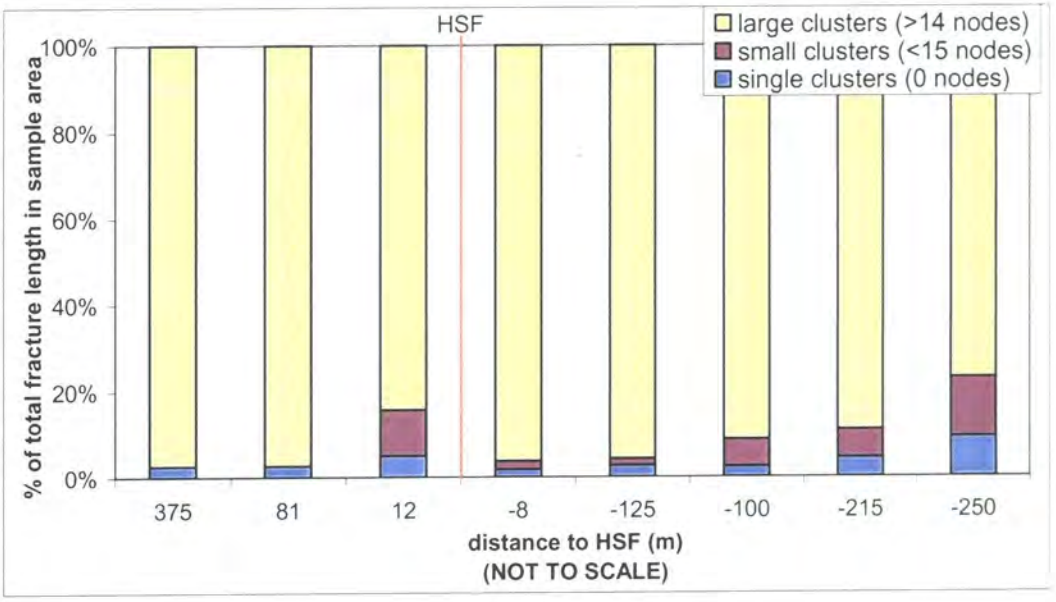

Figure 4.97 Relative percentages of the total fracture length contained in single, small and large clusters 'v' perpendicular distance to the HSFP. outcrop data set

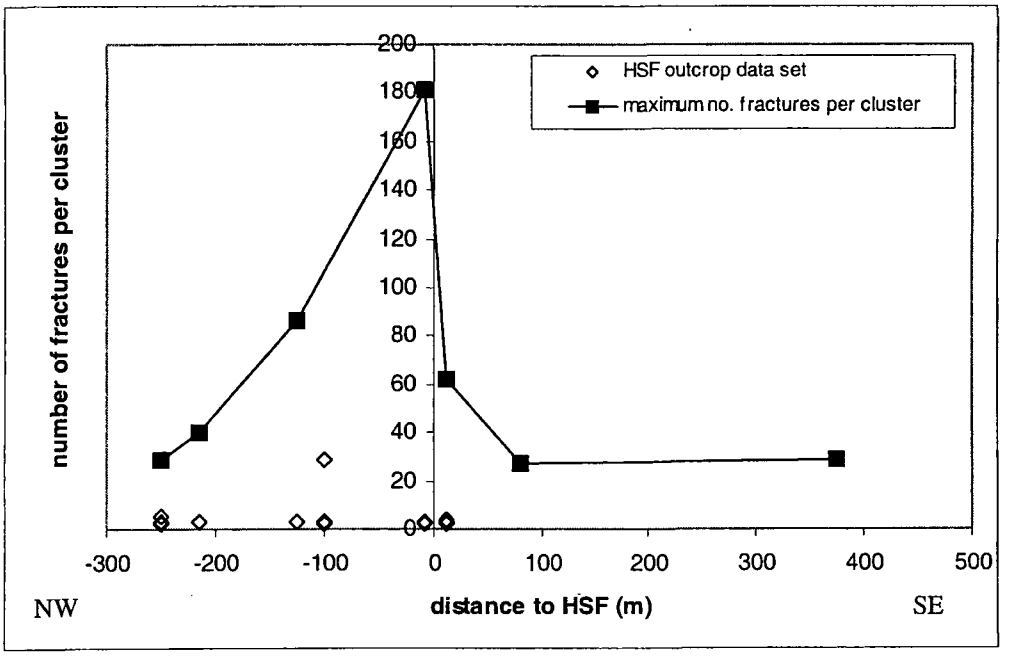

Figure 4.98 Total number of fractures per cluster 'v' perpendicular distance to the HSFP, outcrop data set. Black squares represent values from the largest cluster in each data set. In some data sets small clusters also occur, represented by open diamonds.

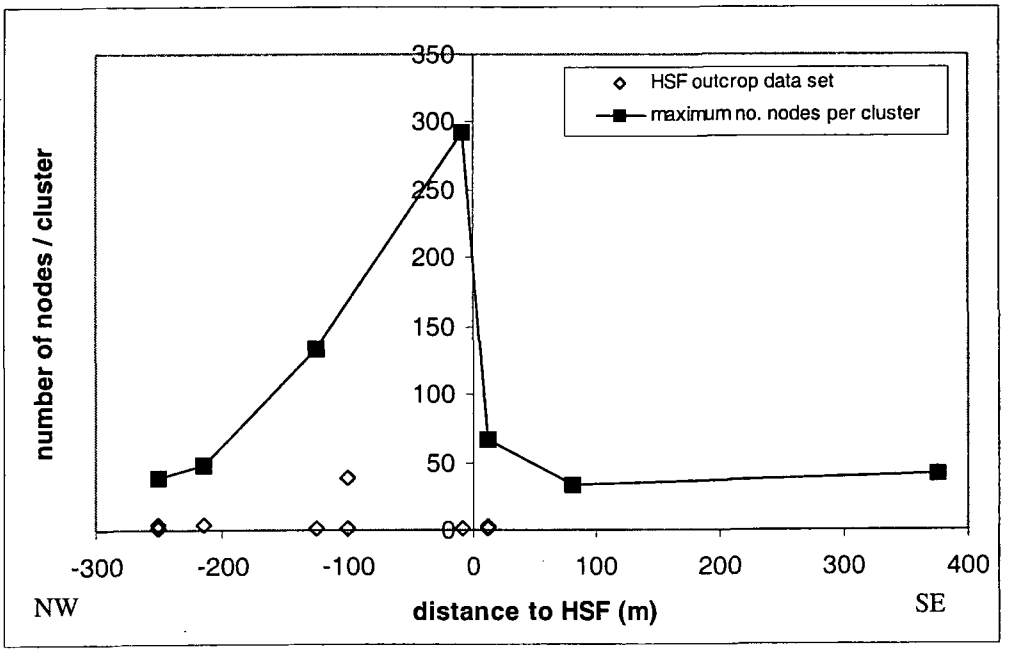

Figure 4.99 Total number of nodes per cluster 'v' perpendicular distance to the HSFP, outcrop data set. Black squares represent values from the largest cluster in each data set. In some data sets small clusters also occur, represented by open diamonds.

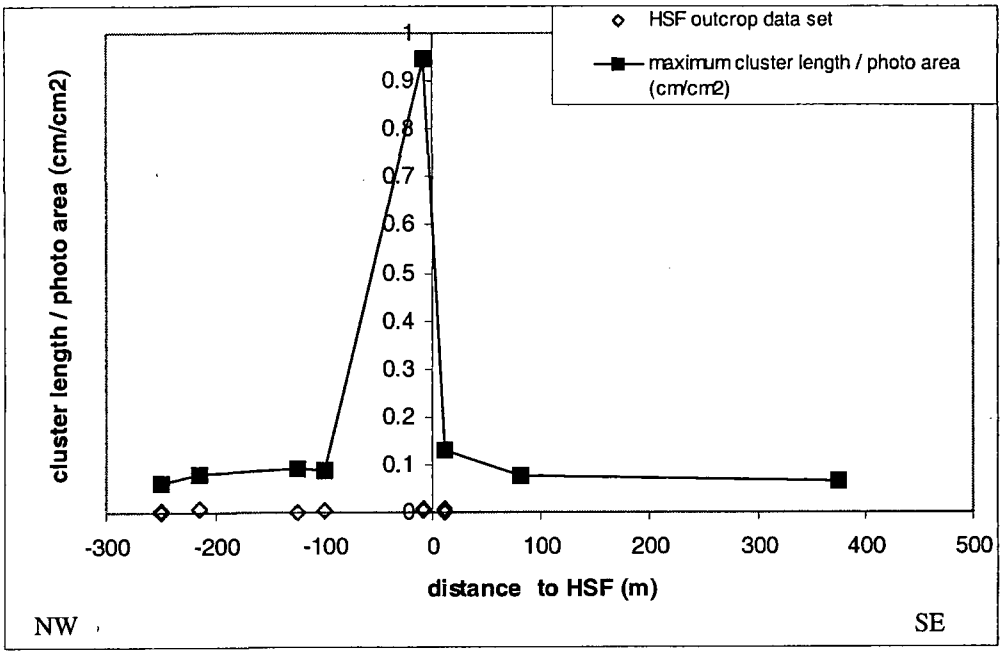

Figure 4.100 Total fracture cluster length (normalised for sample area) 'v' perpendicular distance to the HSFP, outcrop data set. Black squares represent values from the largest cluster in each data set. In some data sets small clusters also occur, represented by open diamonds.

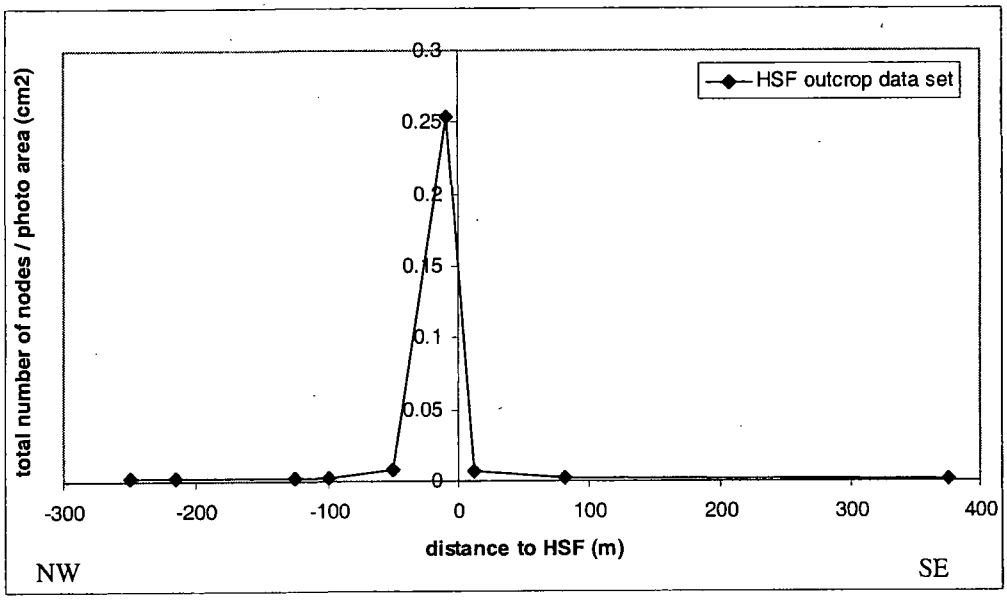

Figure 4.101 Total number of nodes per cm^2 'v' perpendicular distance to the HSFP, outcrop data set.

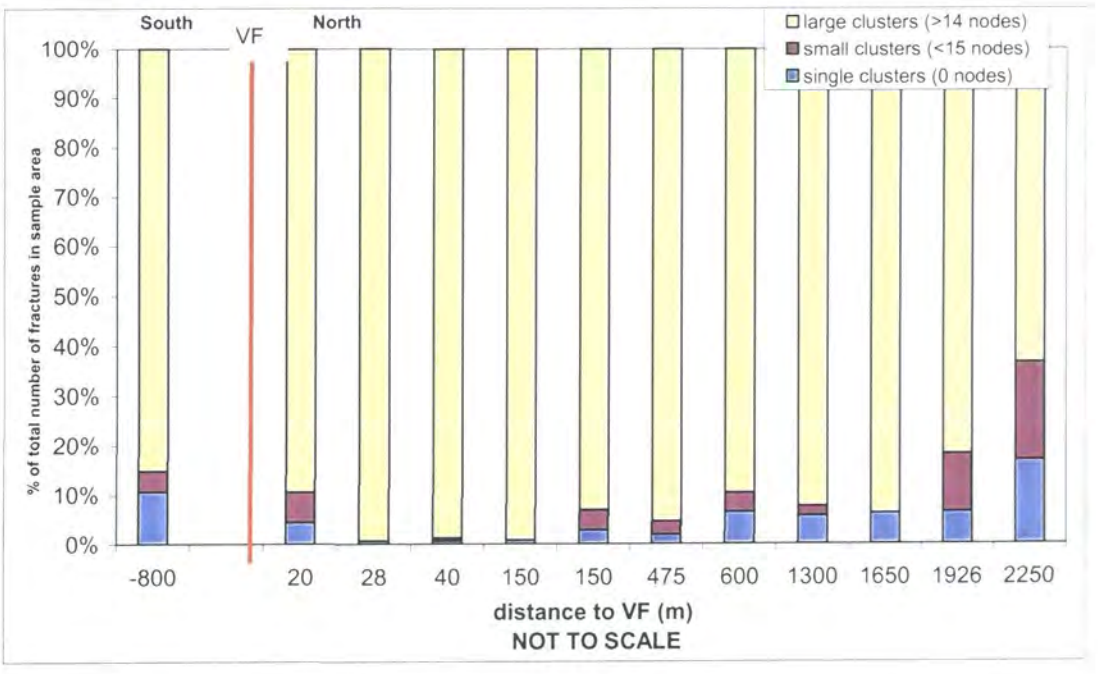

Figure 4.102 Relative percentages of total number of fractures contained in single, small and large clusters adjacent to the VFP, outcrop data set.

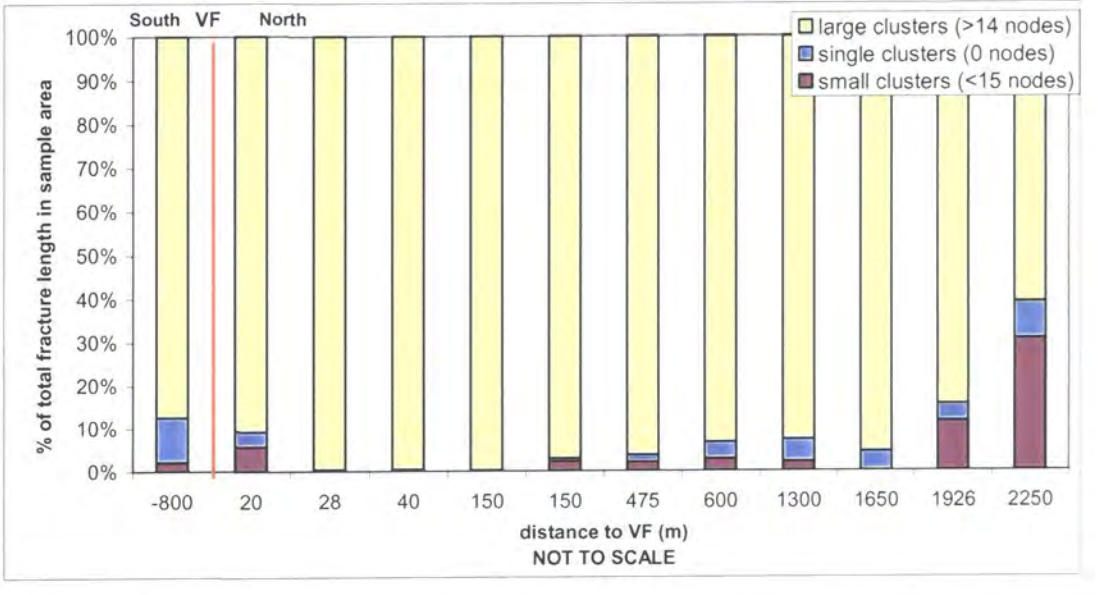

Figure 4.103 Relative percentages of total fracture length contained in single, small and large clusters adjacent to the VFP, outcrop data set.

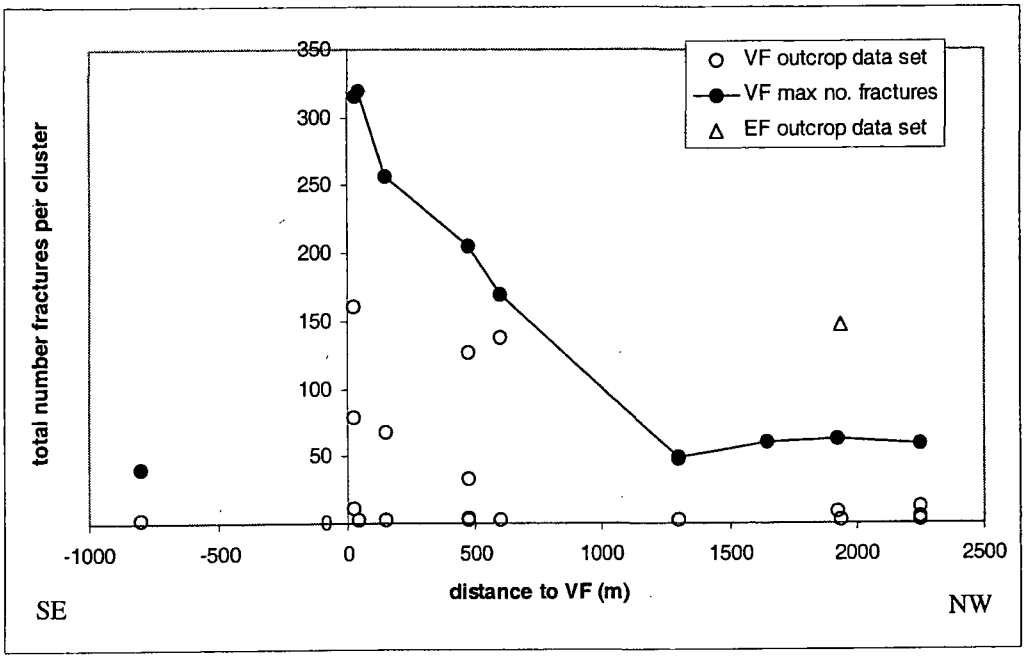

Figure 4.104 Total number of fractures per cluster 'v' perpendicular distance to the VFP, outcrop data set. Black circles represent values from the largest cluster in each VF data set. In some data sets small clusters also occur, represented by open circles.

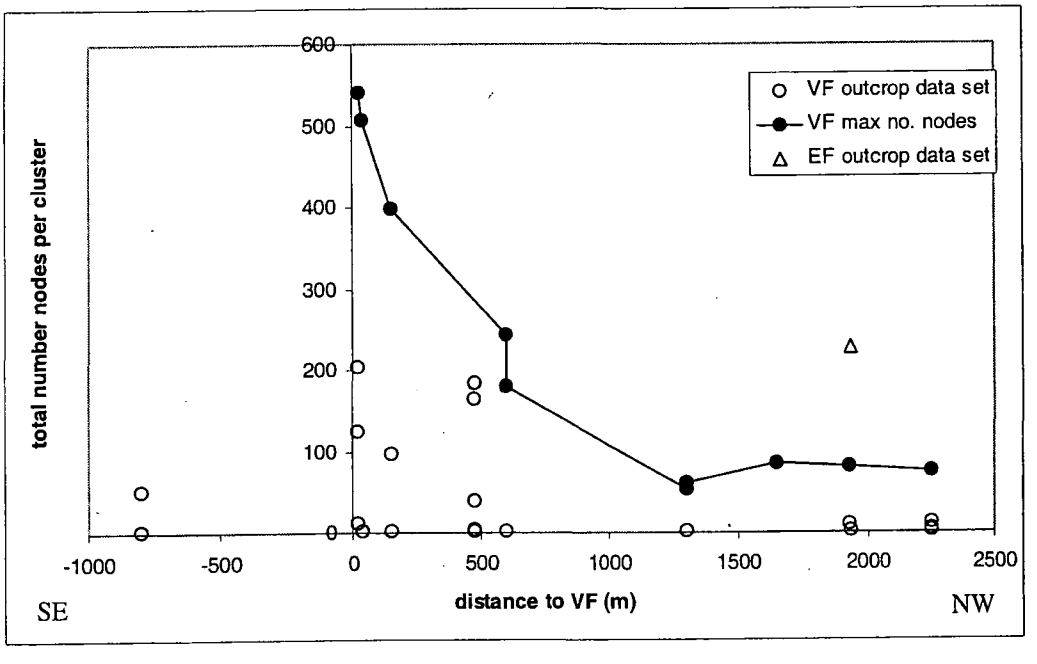

Figure 4.105 Total number of nodes per cluster 'v' perpendicular distance to the VFP, outcrop data set. Black circles represent values from the largest cluster in each VF data set. In some data sets small clusters also occur, represented by open circles.

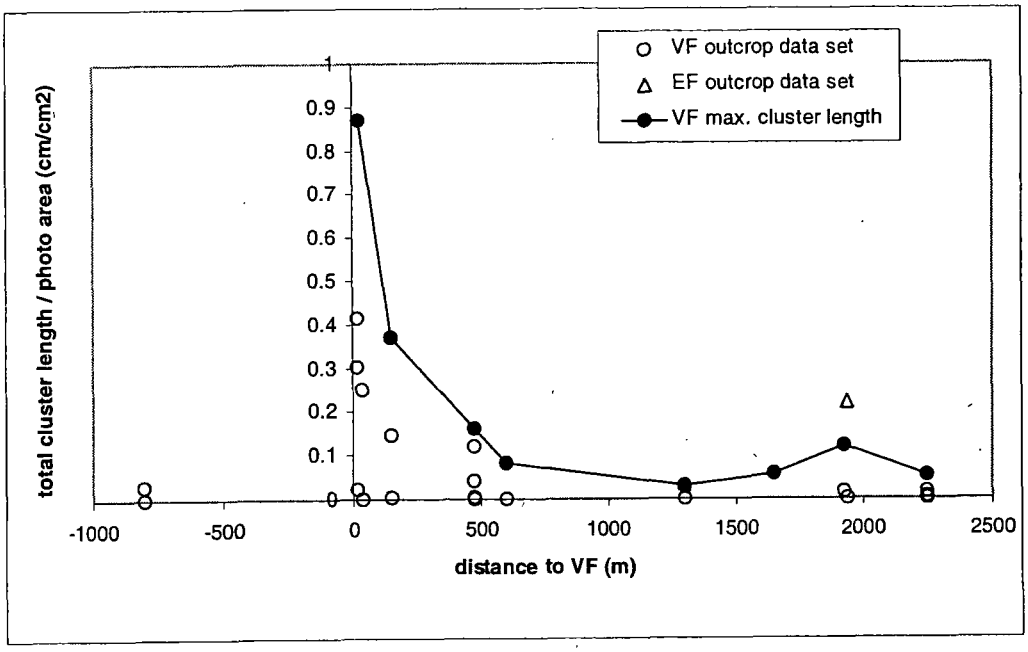

Figure 4.106 Total fracture cluster length (normalised for sample area) 'v' perpendicular distance to the VFP, outcrop data set. Black circles represent values from the largest cluster in each VF data set. In some data sets small clusters also occur, represented by open circles.

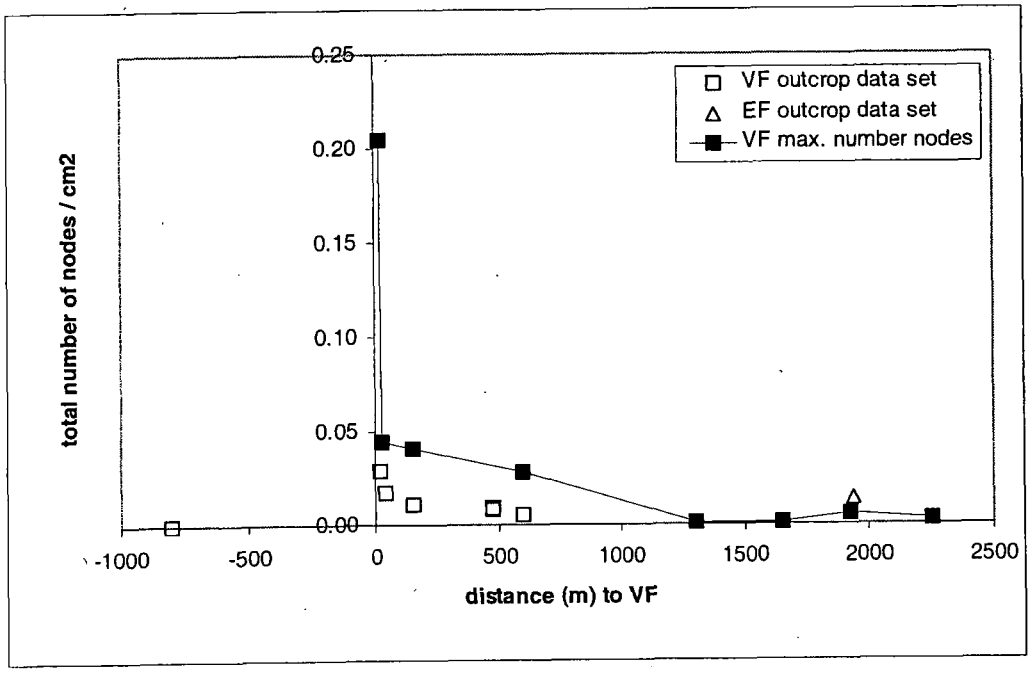

Figure 4.107 Total number of nodes per cm² 'v' perpendicular distance to the VFP, outcrop data set. Black circles represent values from the largest cluster in each VF data set. In some data sets small clusters also occur, represented by open circles.

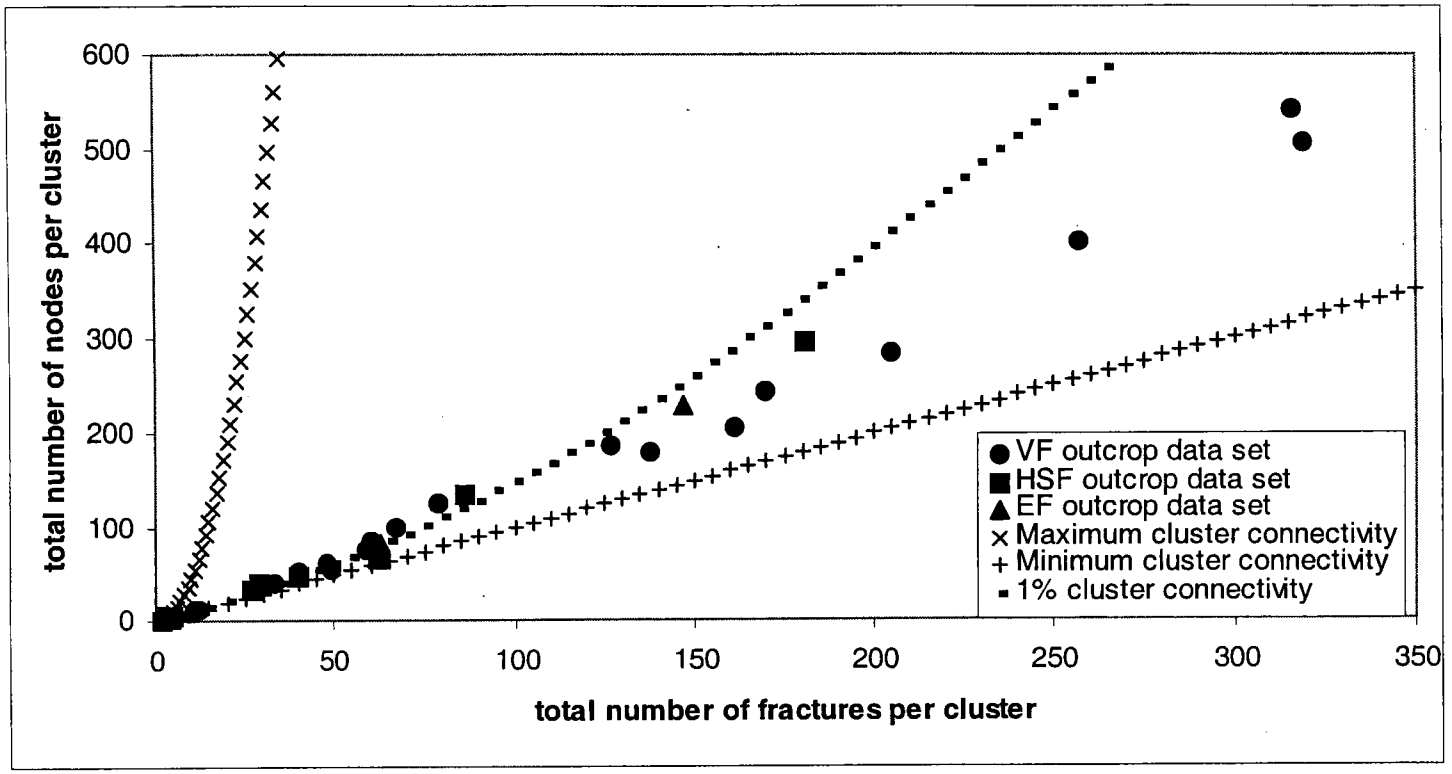

Figure 4.108 Total number of fractures per cluster 'v' total number of nodes per cluster for all outcrop data sets collected adjacent to the VFP, HSFP and EFP

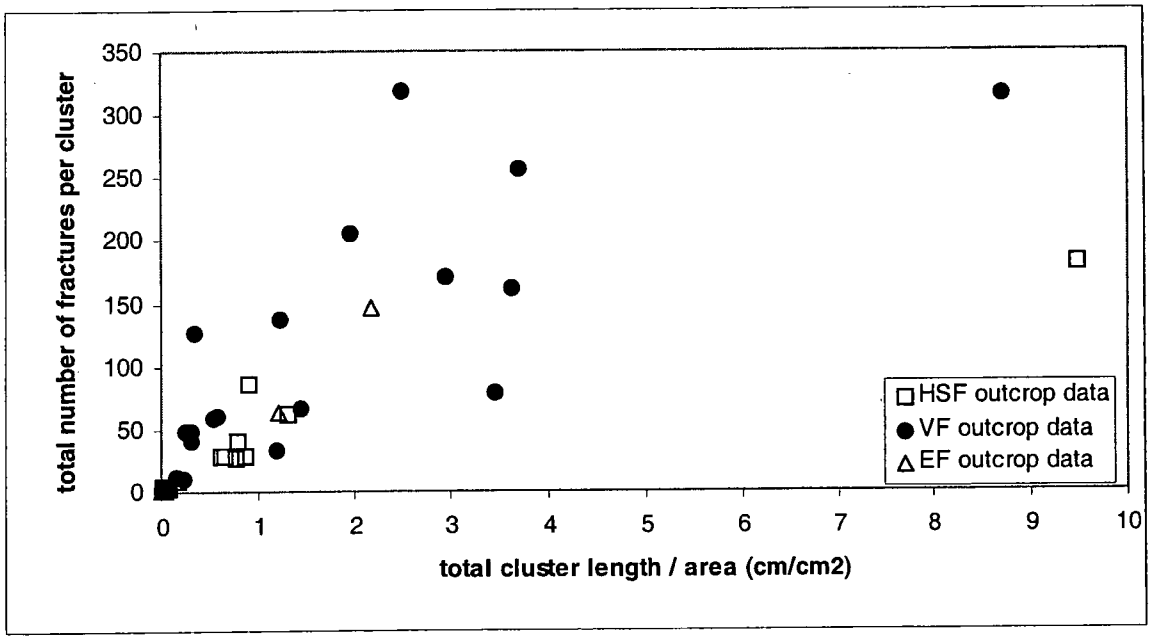

Figure 4.109 Total number of fractures per cluster 'v' total fracture cluster length (normalised for sample area) for all outcrop data sets collected adjacent to the HSFP, VFP and EFP.

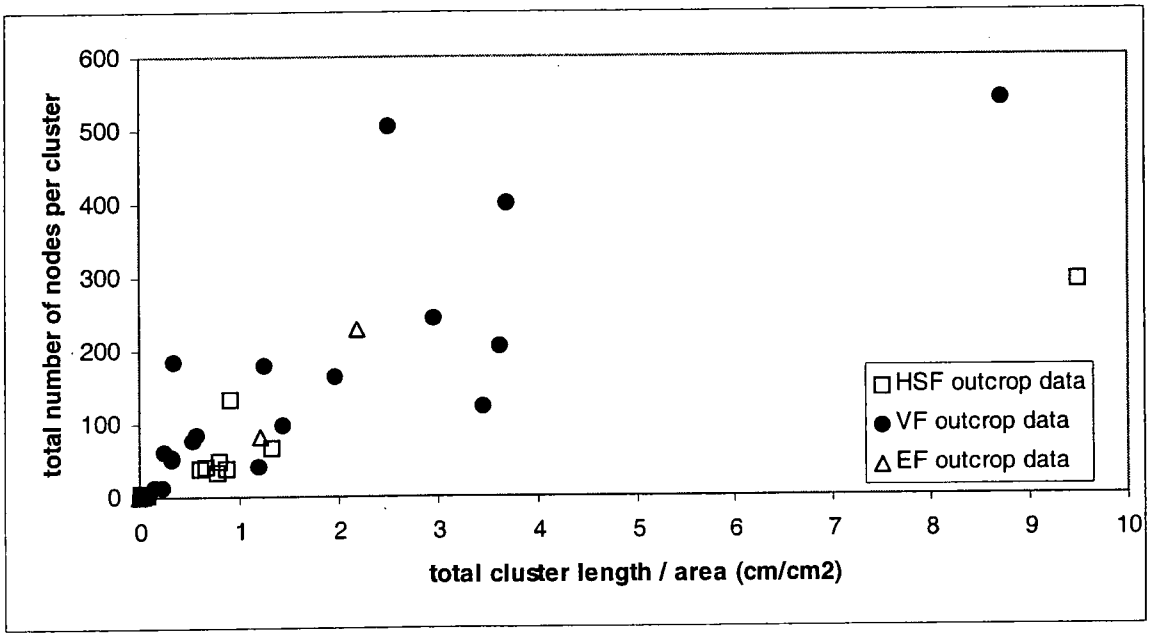

Figure 4.110 Total number of nodes per cluster 'v' total fracture cluster length (normalised for sample area) for all outcrop data sets collected adjacent to the HSFP, VFP and EFP.

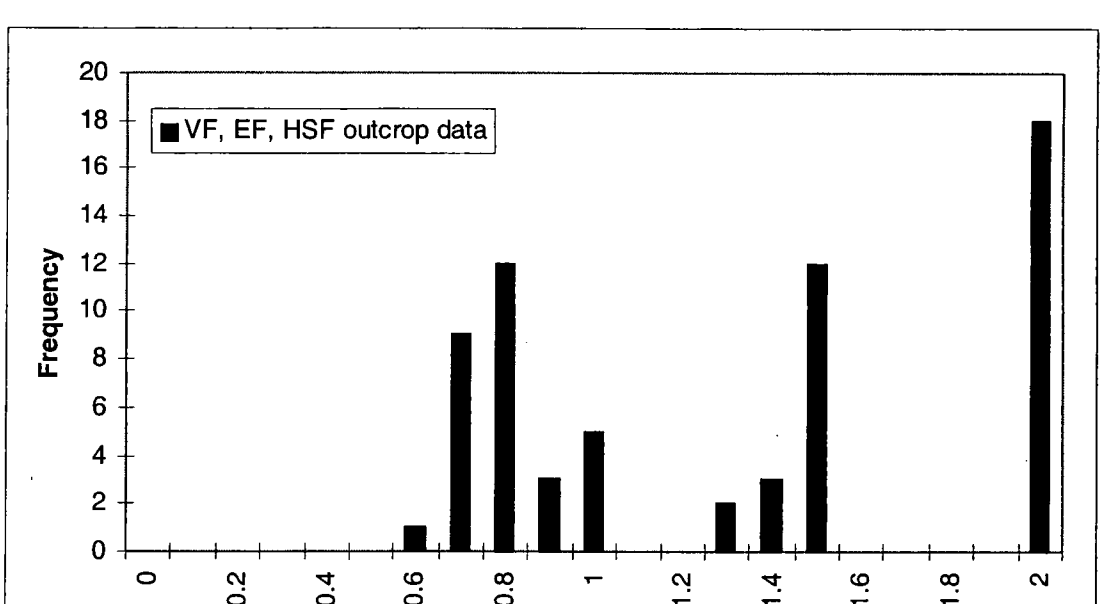

Figure 4.111 Histogram of the total number of fractures per node in a cluster for all outcrop data sets collected adjacent to the HSFP, VFP and EFP.

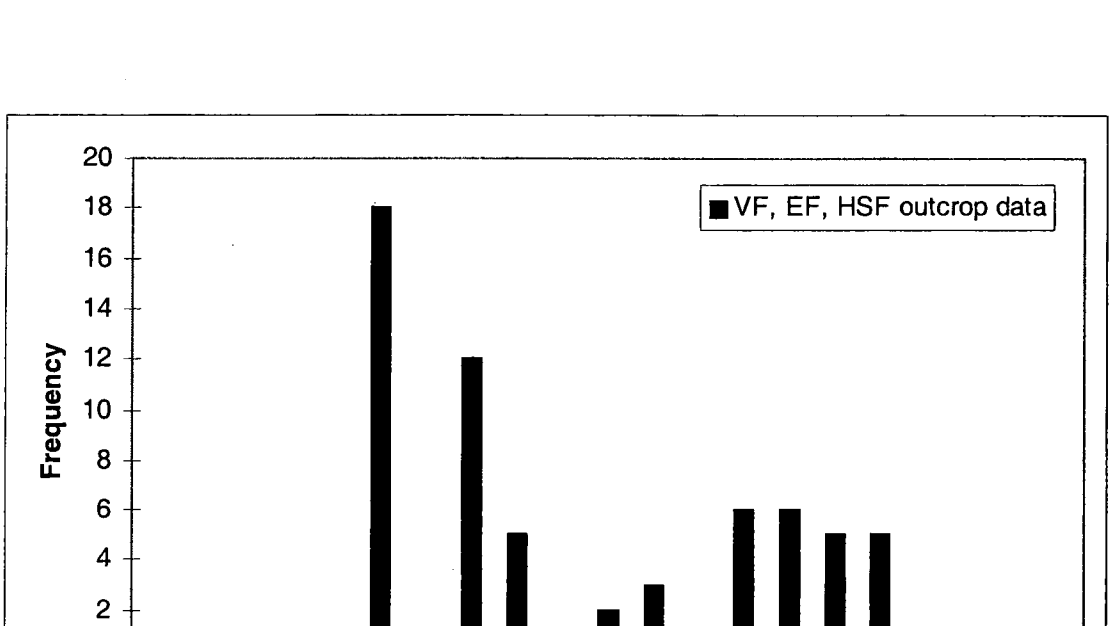

Figure 4.112 Histogram of the total number of nodes per fracture in a cluster for all outcrop data sets collected adjacent to the HSFP, VFP and EFP.

a)

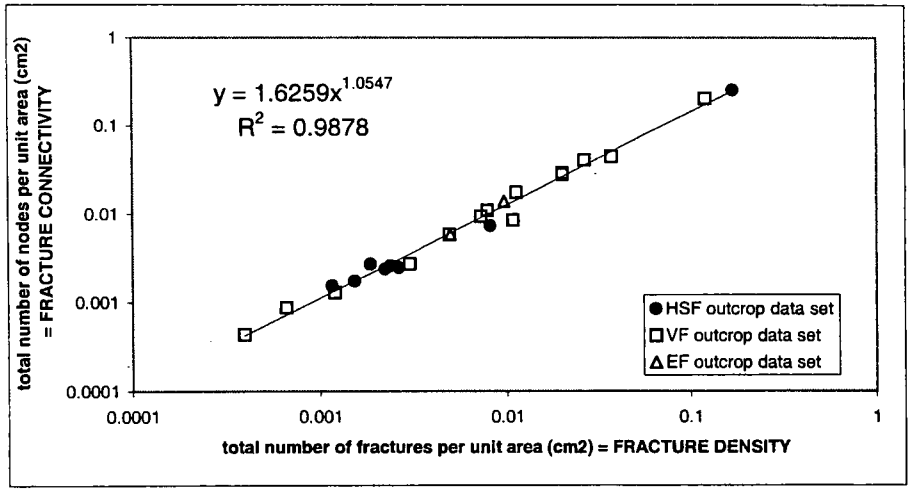

b)

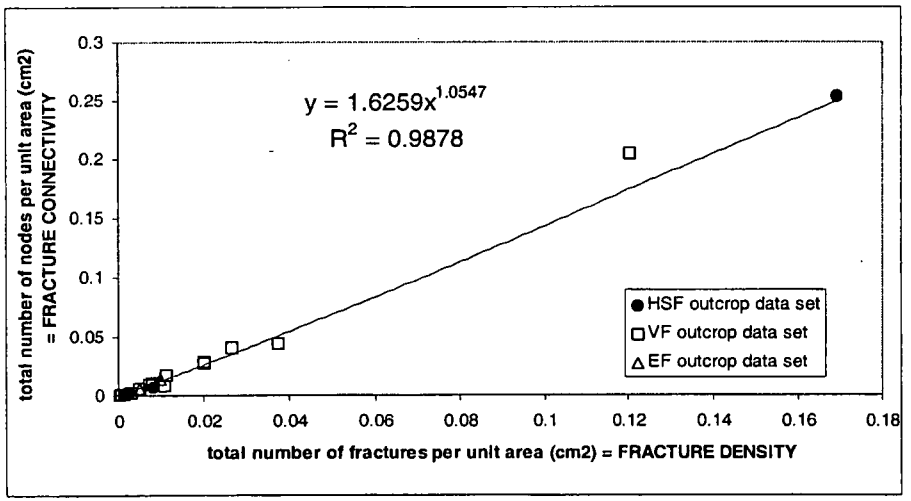

Figure 4.113 Fracture density 'v' fracture connectivity for all data sets collected at outcrop scale adjacent to the VFP, HSFP & EFP. **a)** data plotted on logarithmic axes, **b)** data plotted on linear axes.

a)

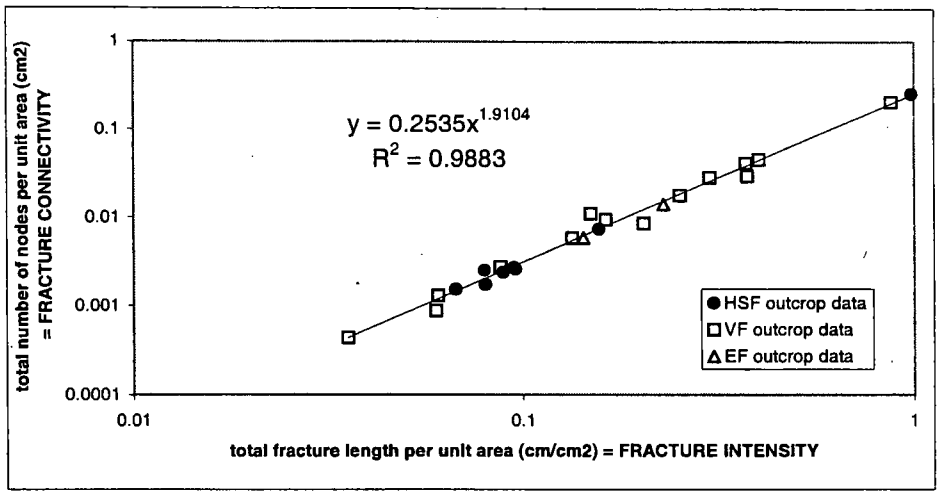

b)

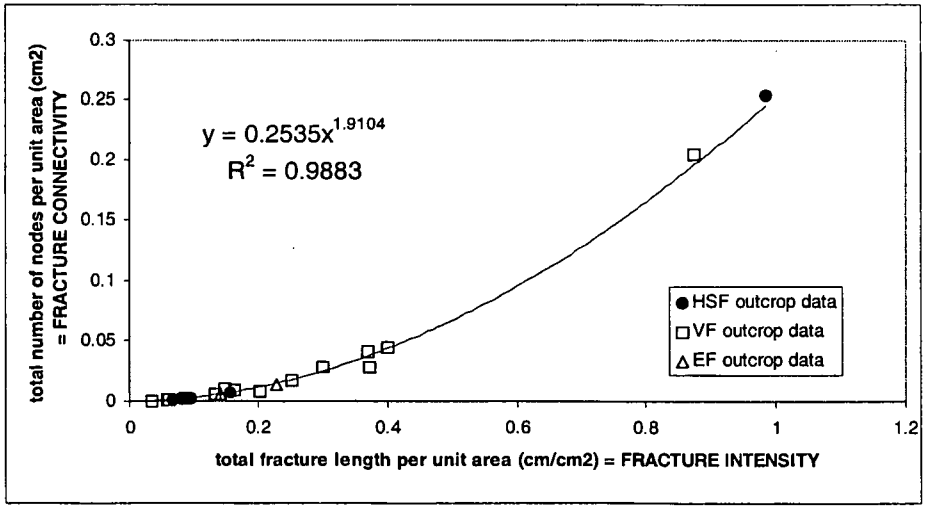

Figure 4.114 Fracture intensity 'v' fracture connectivity for all data sets collected at outcrop scale adjacent to the VFP, HSFP & EFP. **a)** data plotted on logarithmic axes, **b)** data plotted on linear axes.

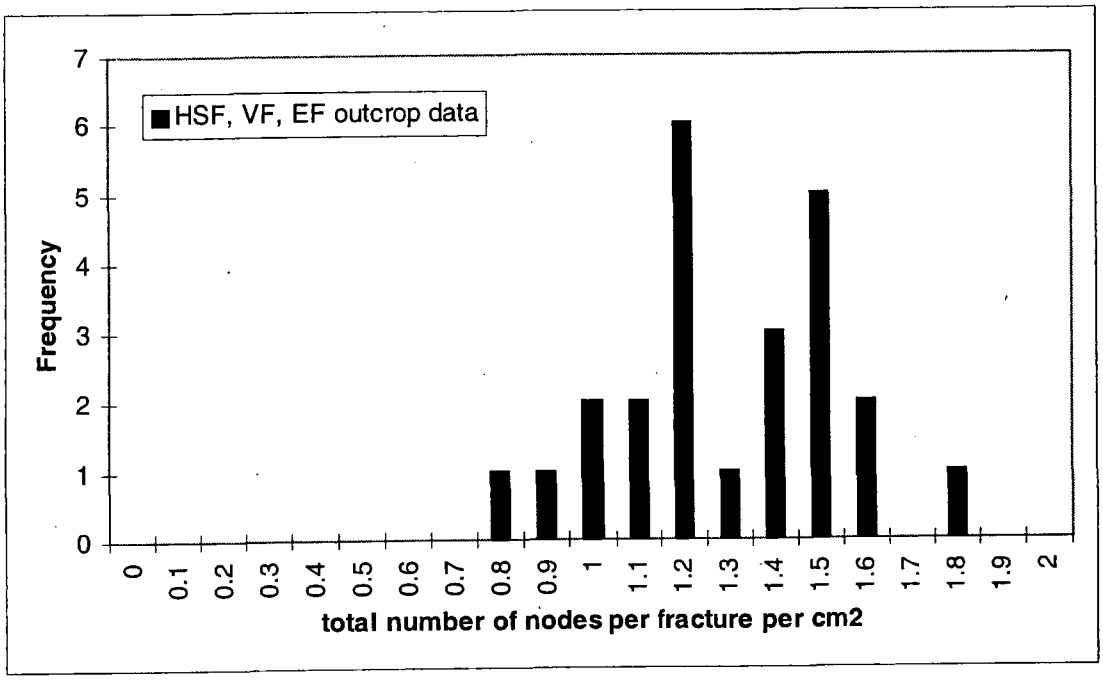

Figure 4.115 Histogram of the total number of nodes per fracture in a cm^2 for all outcrop data sets collected adjacent to the HSFP, VFP and EFP.

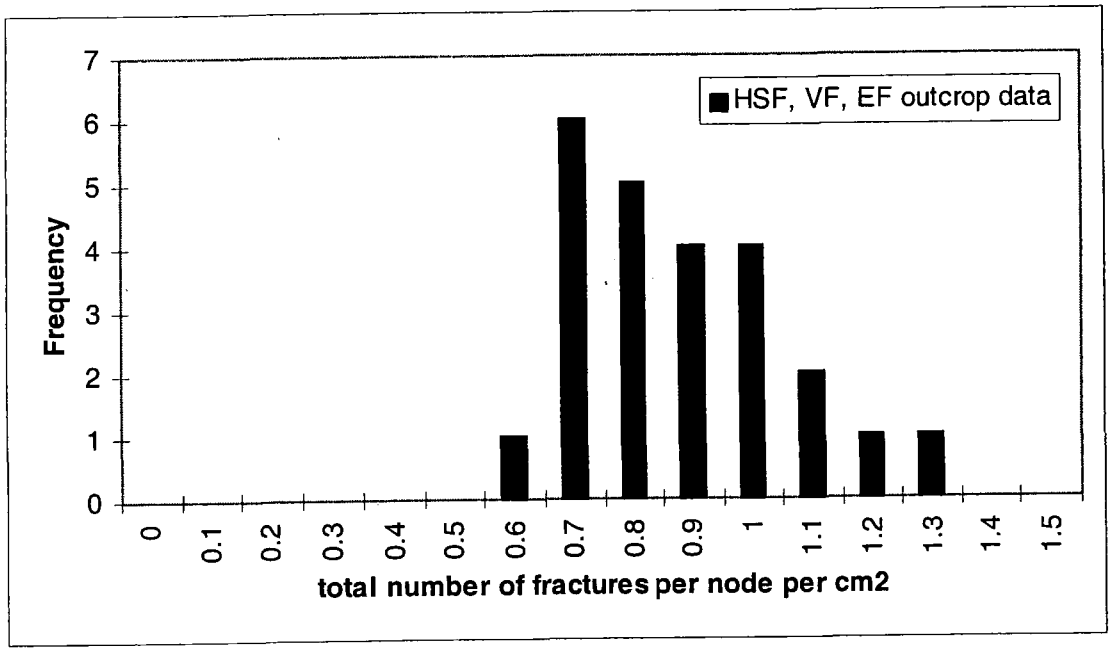

Figure 4.116 Histogram of the total number of fractures per node in a cm^2 for all outcrop data sets collected adjacent to the HSFP, VFP and EFP.

a)

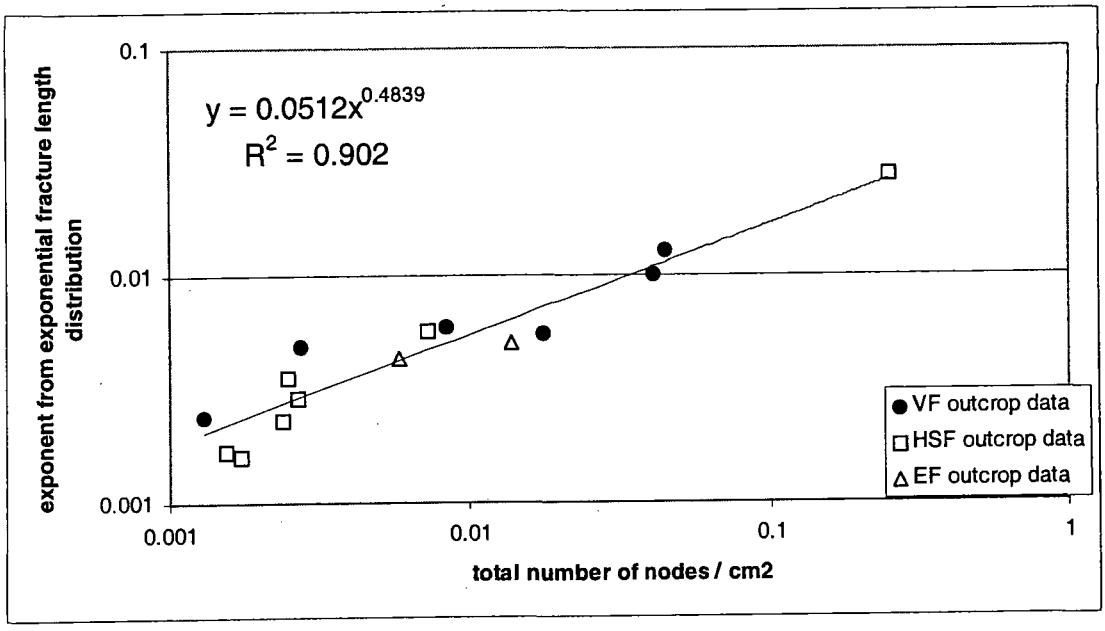

b)

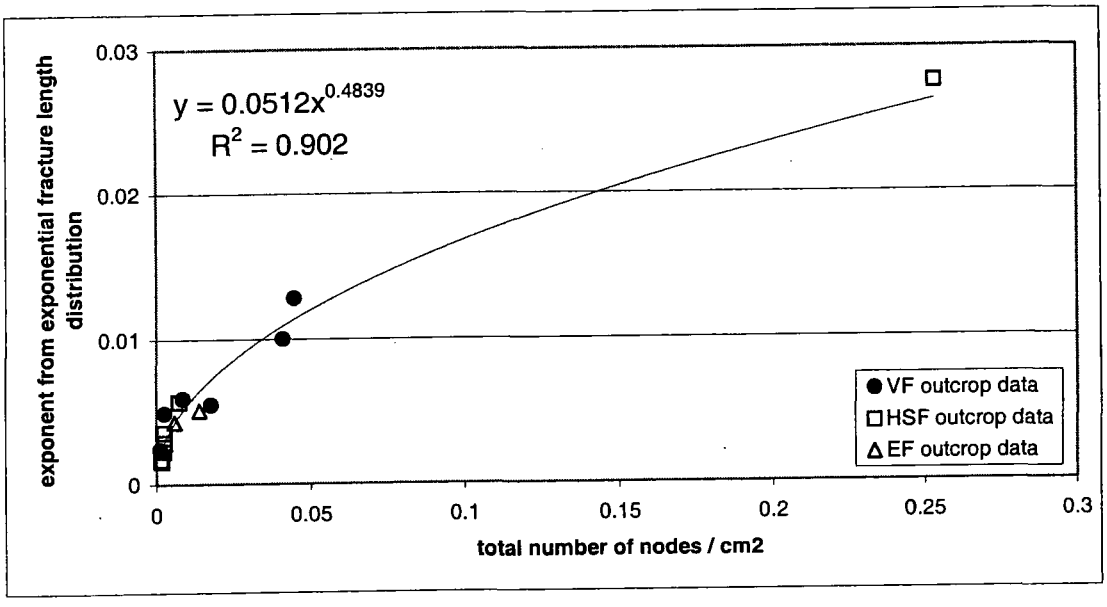

Figure 4.117 Exponent values from exponential fracture length distributions 'v' total number of nodes per cm² (connectivity).
a) data plotted on logarithmic axes
b) data plotted on linear axes

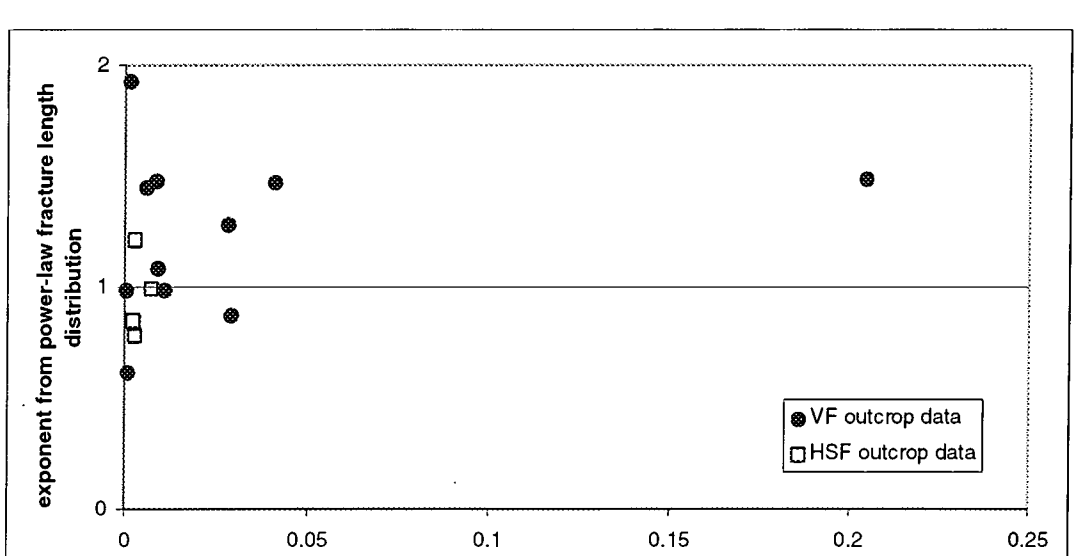

Figure 4.118 Exponent values from power-law fracture length distributions 'v' total number of nodes per cm² (connectivity), plotted on linear axes

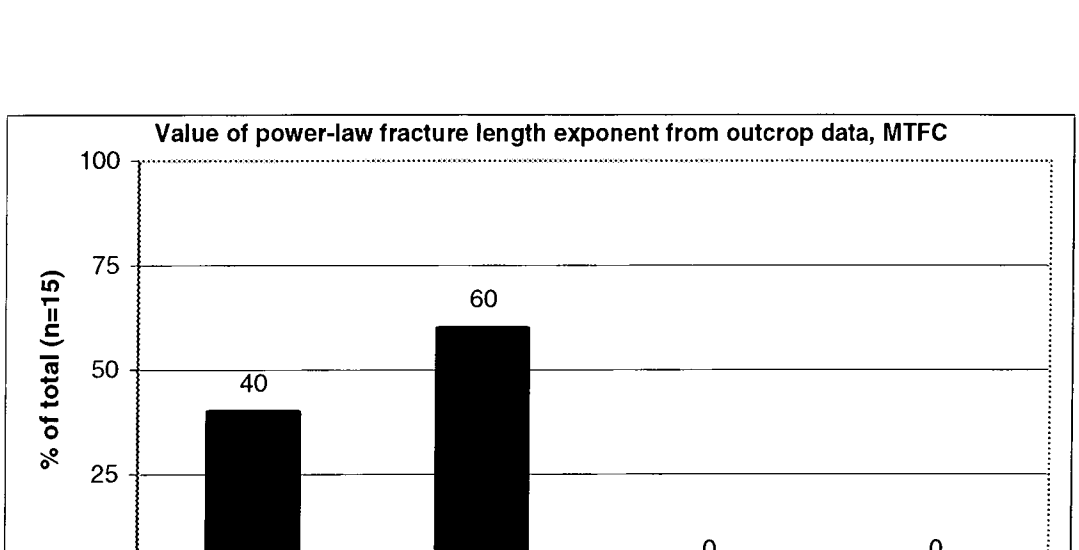

Figure 4.119 Histogram of power-law exponent values from fracture length data collected at outcrop scale adjacent to faults within the MTFC.

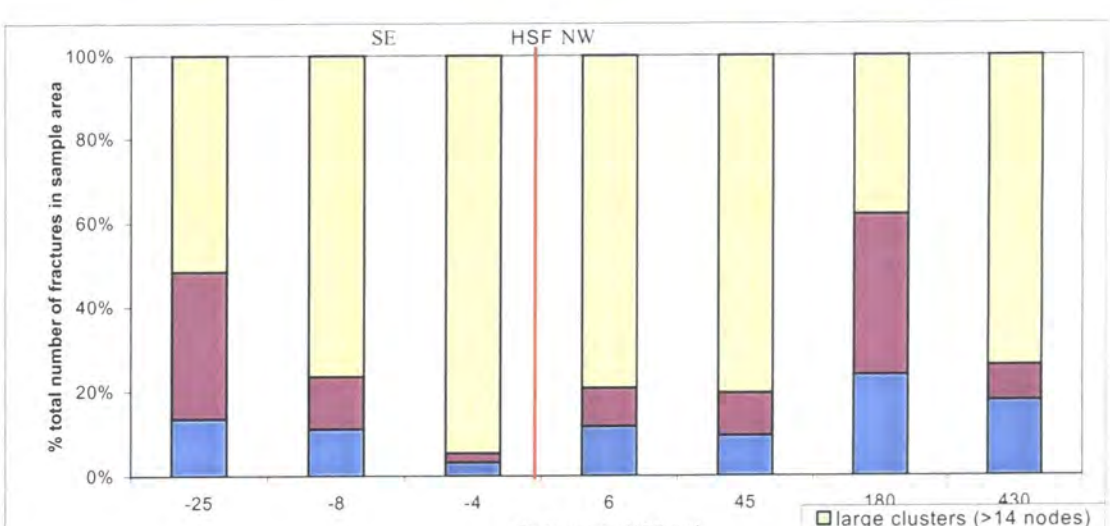

Figure 4.120 Relative percentages of total number of fractures contained in single, small and large clusters 'v' perpendicular distance to the HSFP, thin section data set.

Figure 4.121 Relative percentages of total fracture length contained in single, small and large clusters 'v' perpendicular distance to the HSFP, thin section data set.

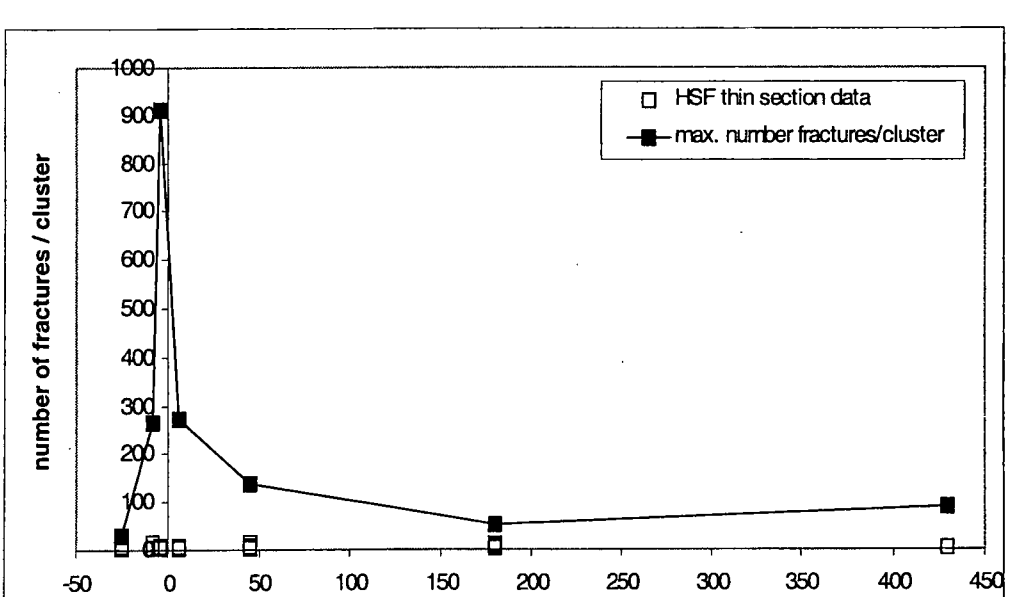

Figure 4.122 Total number of fractures per cluster 'v' perpendicular distance to the HSFP, thin section data set. Black squares represent values from the largest cluster in each data set. In some data sets small clusters also occur, represented by open squares.

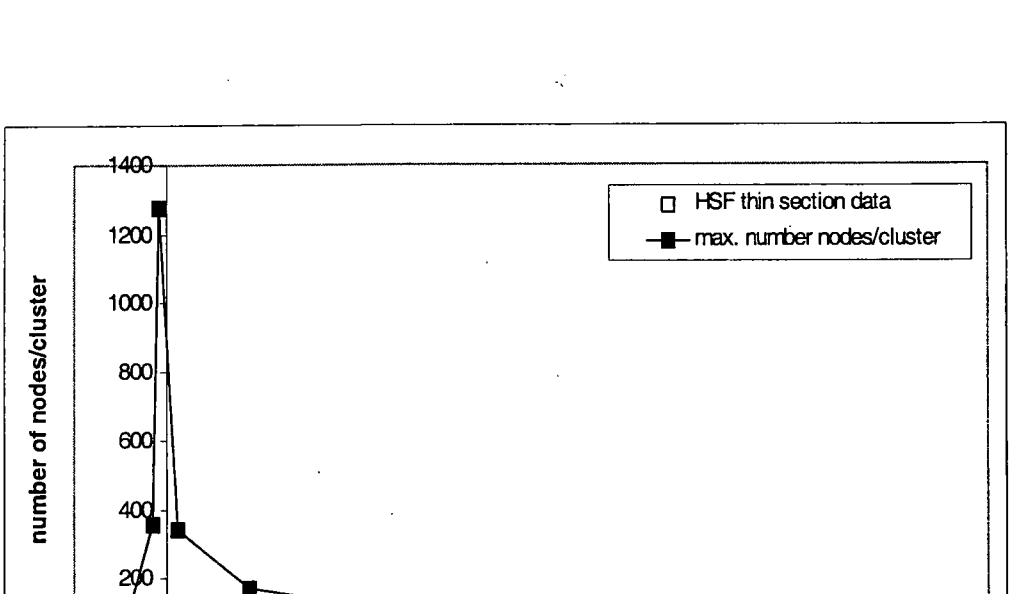

Figure 4.123 Total number of nodes per cluster 'v' perpendicular distance to the HSFP, thin section data set. Black squares represent values from the largest cluster in each data set. In some data sets small clusters also occur, represented by open squares.

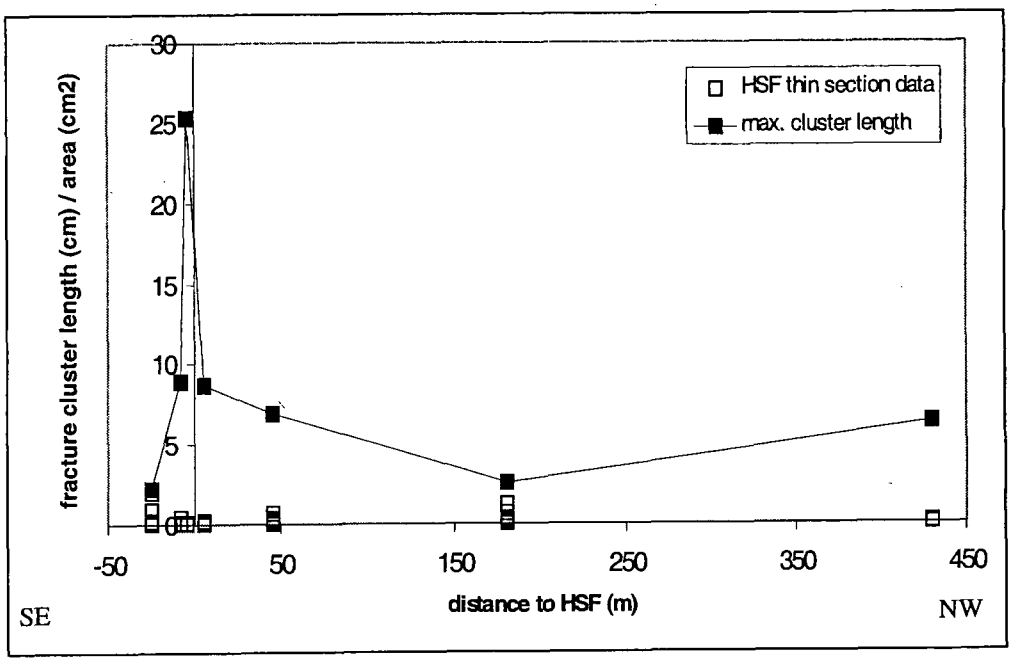

Figure 4.124 Total fracture cluster length (normalised for sample area) 'v' perpendicular distance to the HSFP, thin section data set. Black squares represent values from the largest cluster in each data set. In some data sets small clusters also occur, represented by open squares.

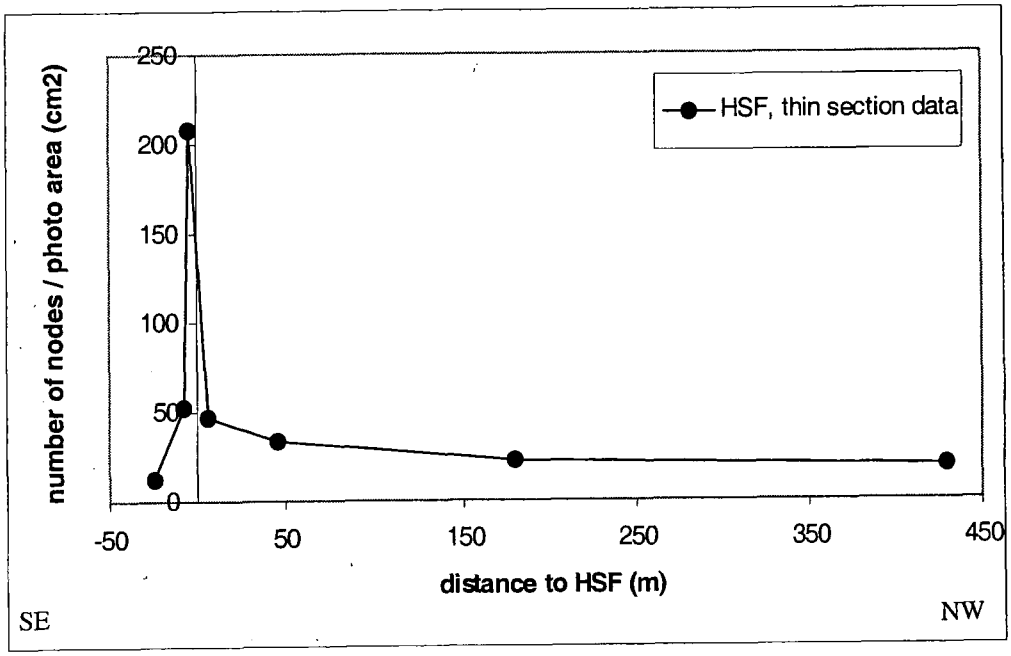

Figure 4.125 Total number of nodes per cm² 'v' perpendicular distance to the HSFP, thin section data set

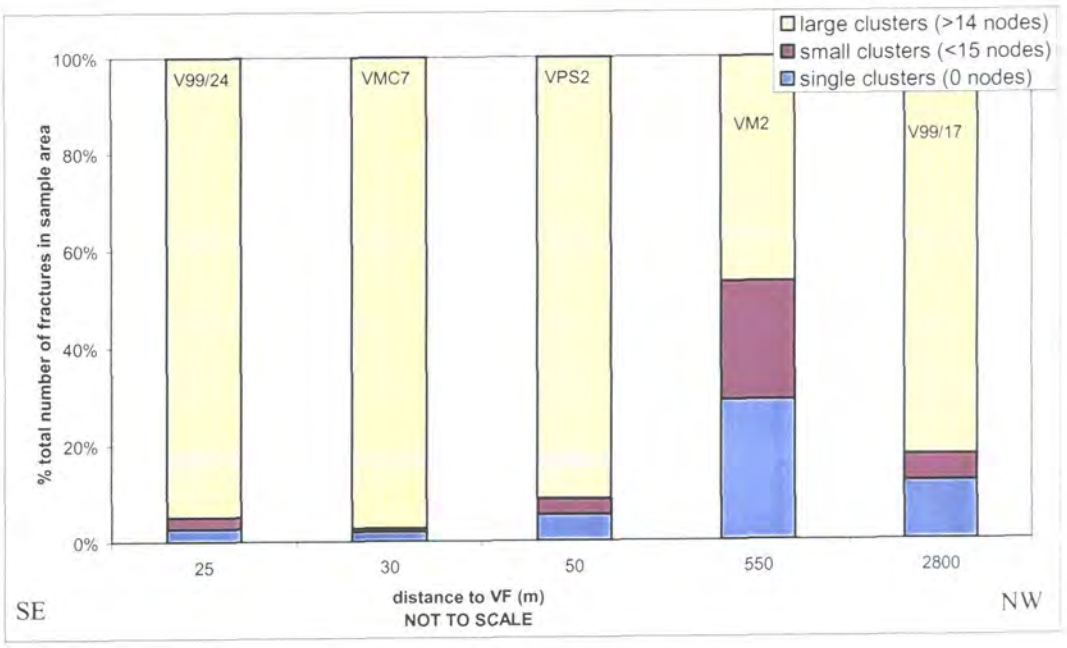

Figure 4.126 Relative percentages of total number of fractures contained in single, small and large clusters adjacent to the VFP, thin section data set

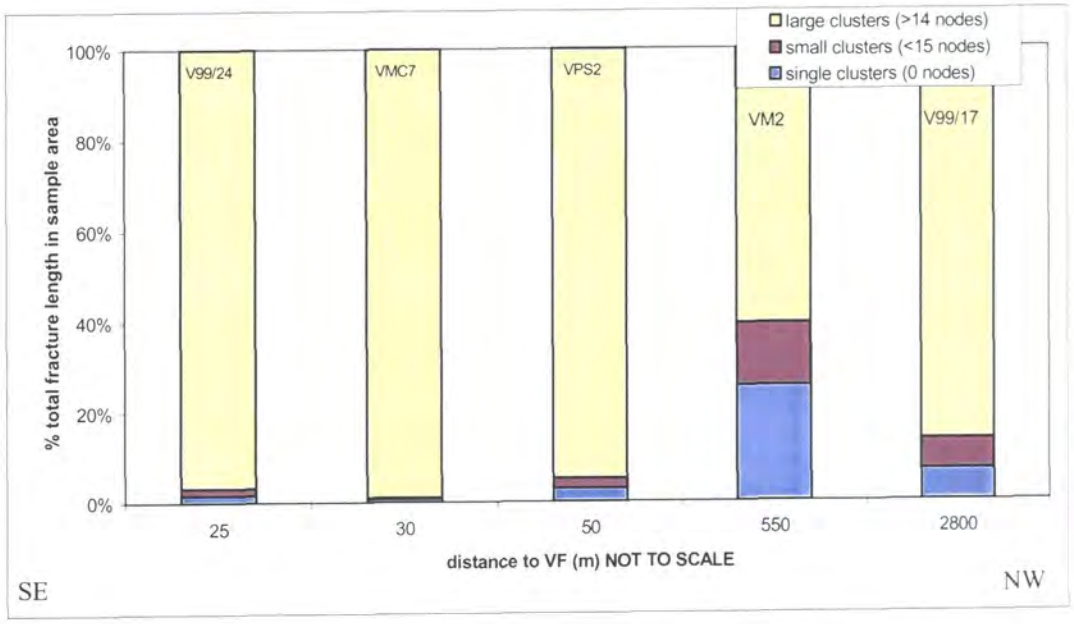

Figure 4.127 Relative percentages of total fracture length contained in single, small and large clusters adjacent to the VFP, thin section data set

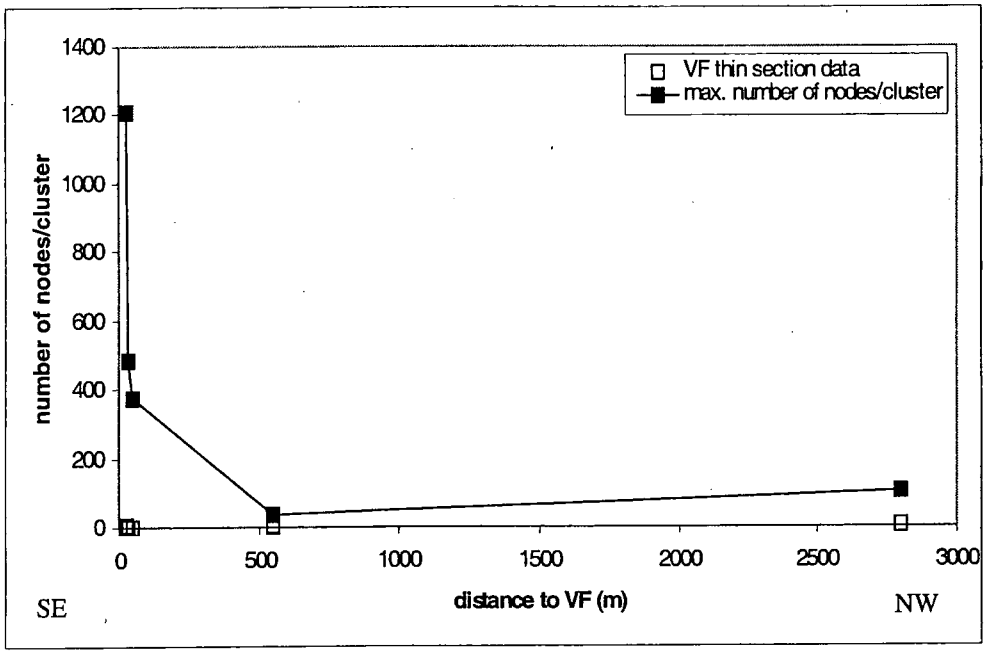

Figure 4.128 Total number of fractures per cluster 'v' perpendicular distance to the VFP, thin section data set. Black squares represent values from the largest cluster in each data set. In some data sets small clusters also occur, represented by open squares.

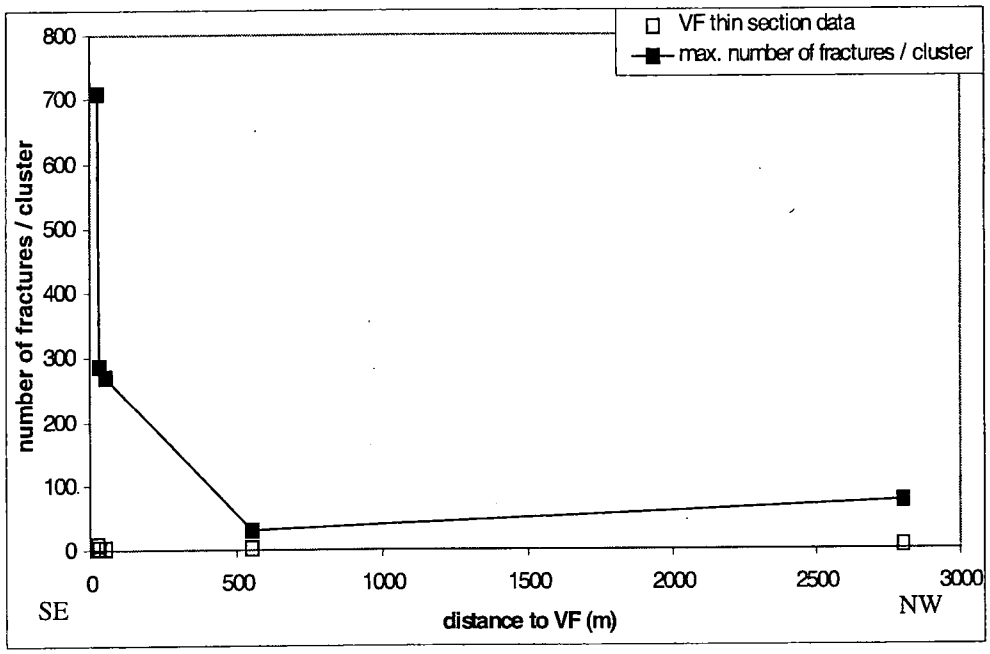

Figure 4.129 Total number of nodes per cluster 'v' perpendicular distance to the VFP, thin section data set. Black squares represent values from the largest cluster in each data set. In some data sets small clusters also occur, represented by open squares.

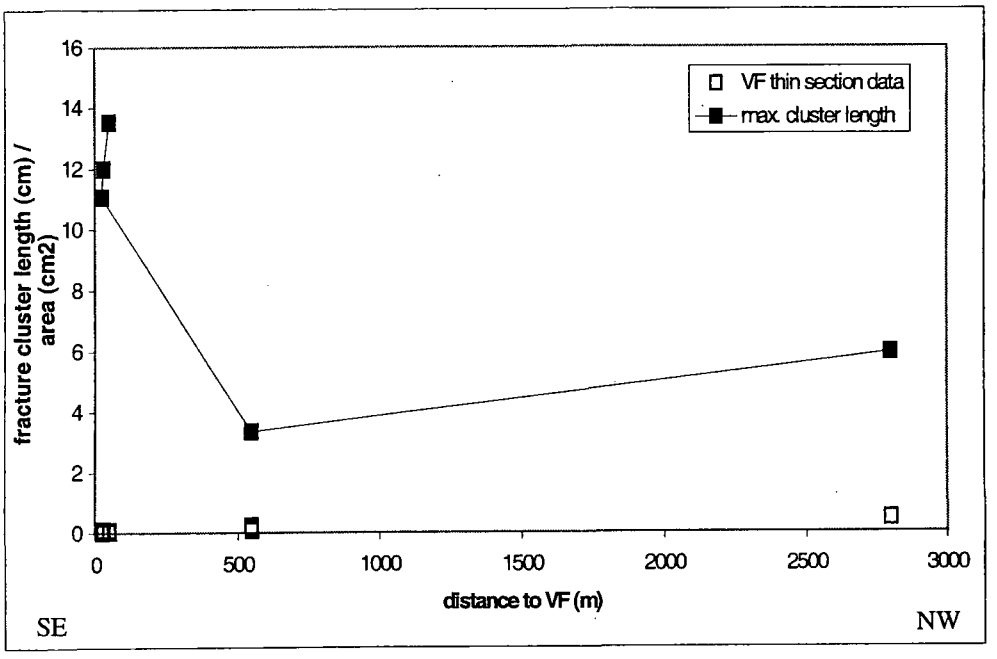

Figure 4.130 Total fracture cluster length (normalised for sample area) 'v' perpendicular distance to the VFP, thin section data set. Black squares represent values from the largest cluster in each data set. In some data sets small clusters also occur, represented by open squares.

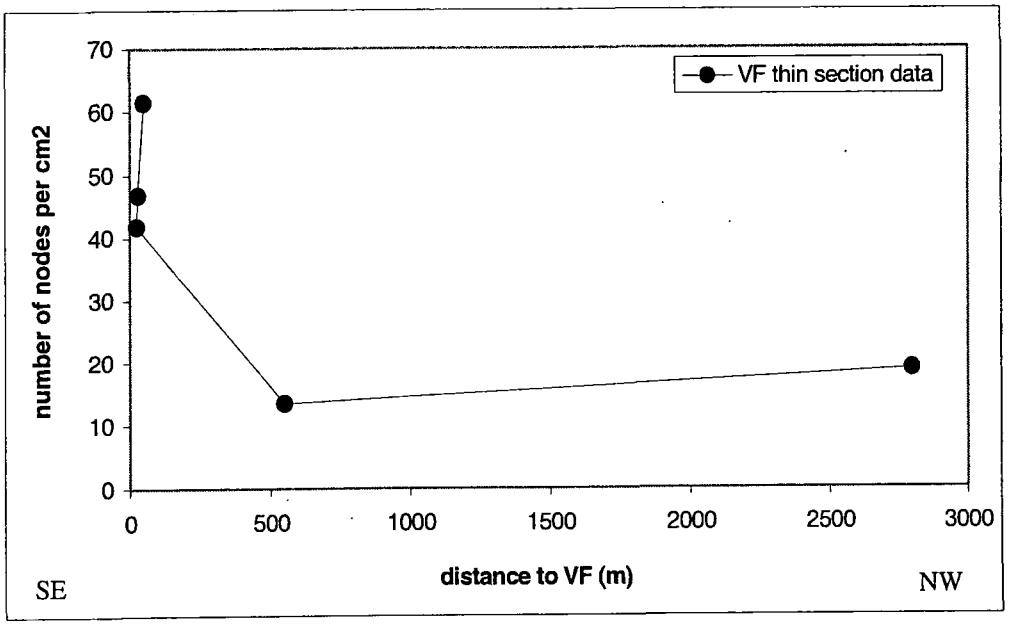

Figure 4.131 Total number of nodes per cm² 'v' perpendicular distance to the VFP, thin section data set

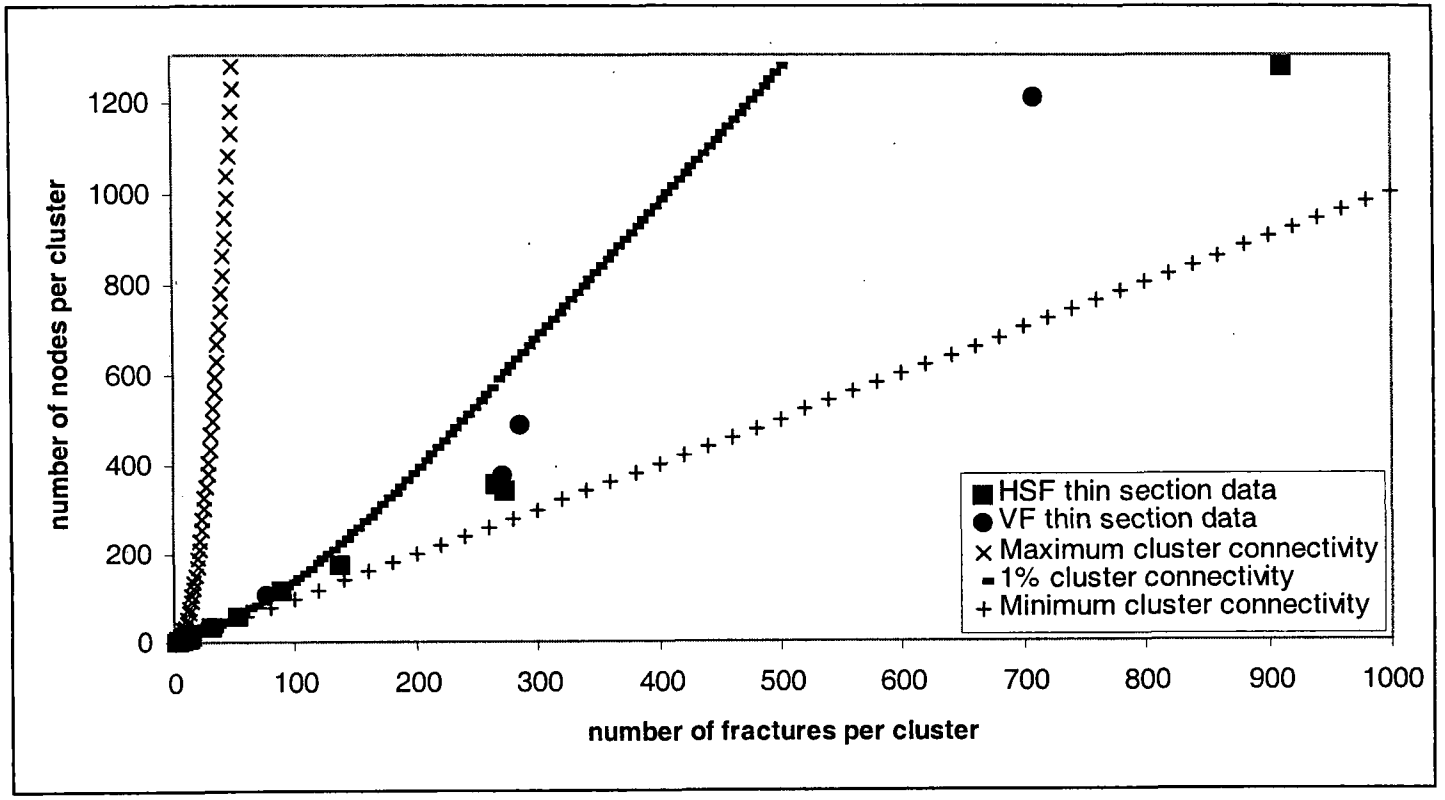

Figure 4.132 Total number of fractures per cluster 'v' total number of nodes per cluster for all thin section data sets collected adjacent to the VFP, HSFP and EFP

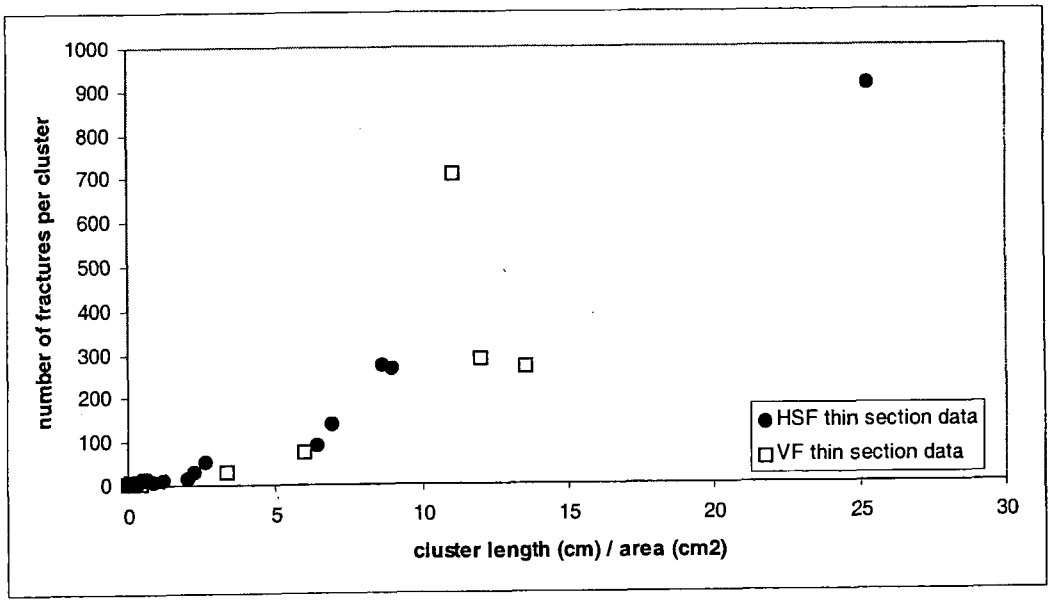

Figure 4.133 Total number of fractures per cluster 'v' total fracture cluster length (normalised for sample area), for thin section data sets collected adjacent to the VFP and the HSFP

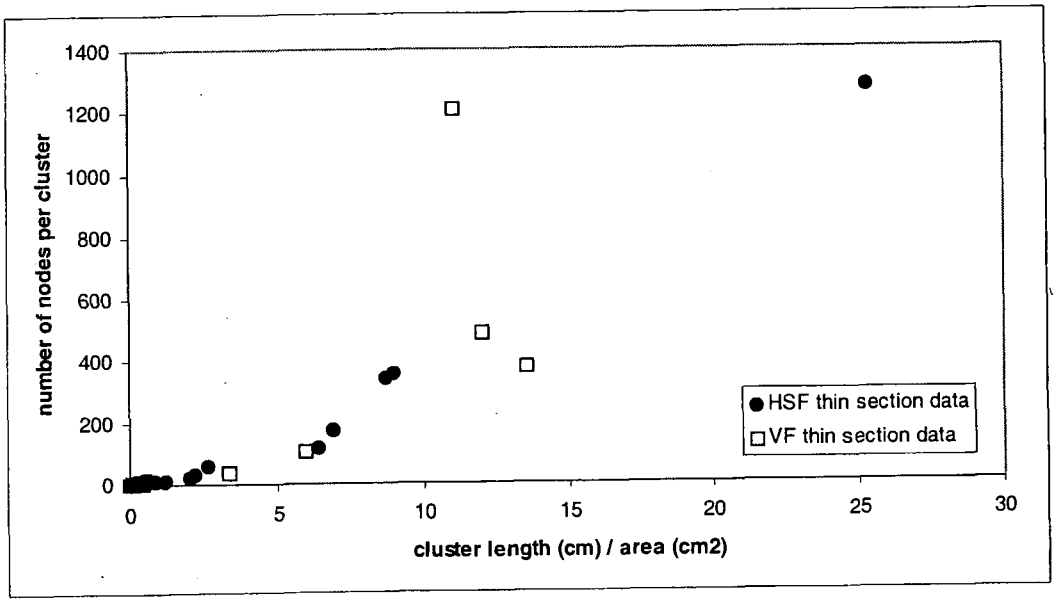

Figure 4.134 Total number of nodes per cluster 'v' total fracture cluster length (normalised for sample area), for thin section data sets collected adjacent to the VFP and the HSFP

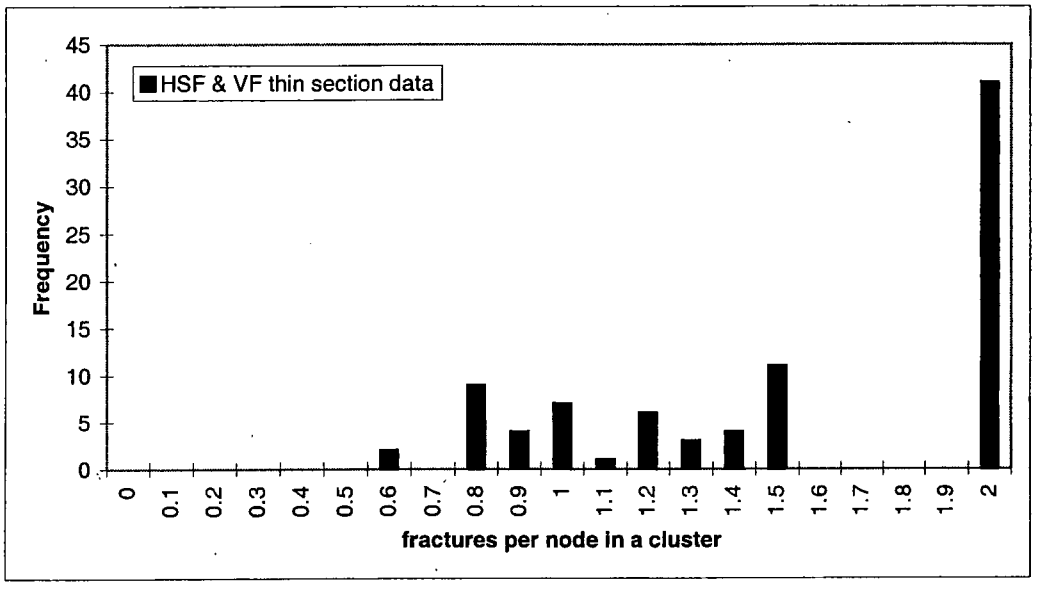

Figure 4.135 Histogram of the total number of fractures per node in a cluster for all thin section data sets collected adjacent to the HSFP and the VFP.

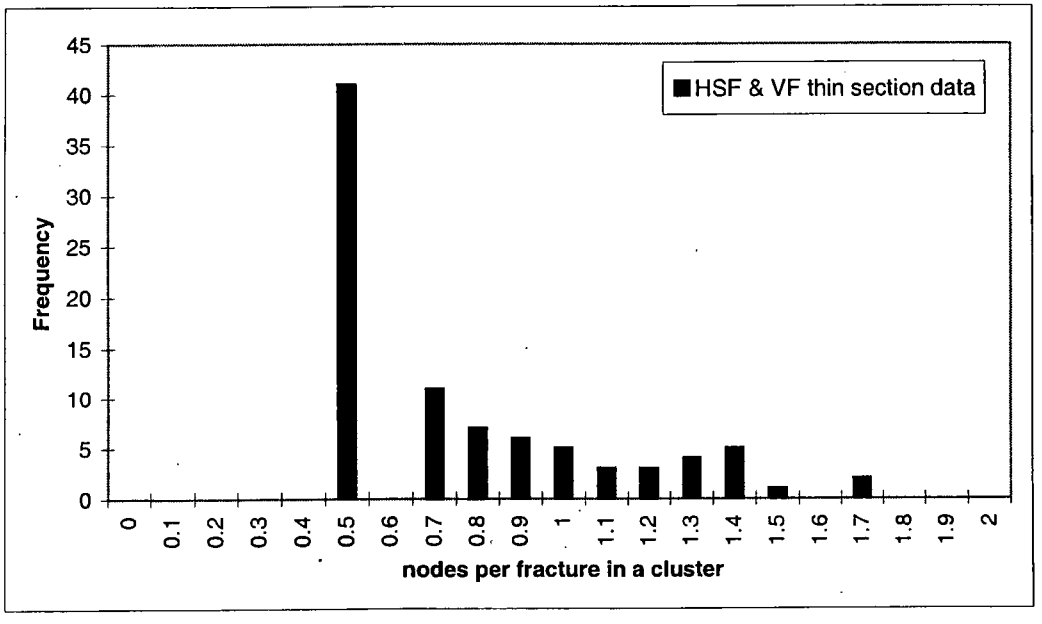

Figure 4.136 Histogram of the total number of nodes per fracture in a cluster for all thin section data sets collected adjacent to the HSFP and the VFP.

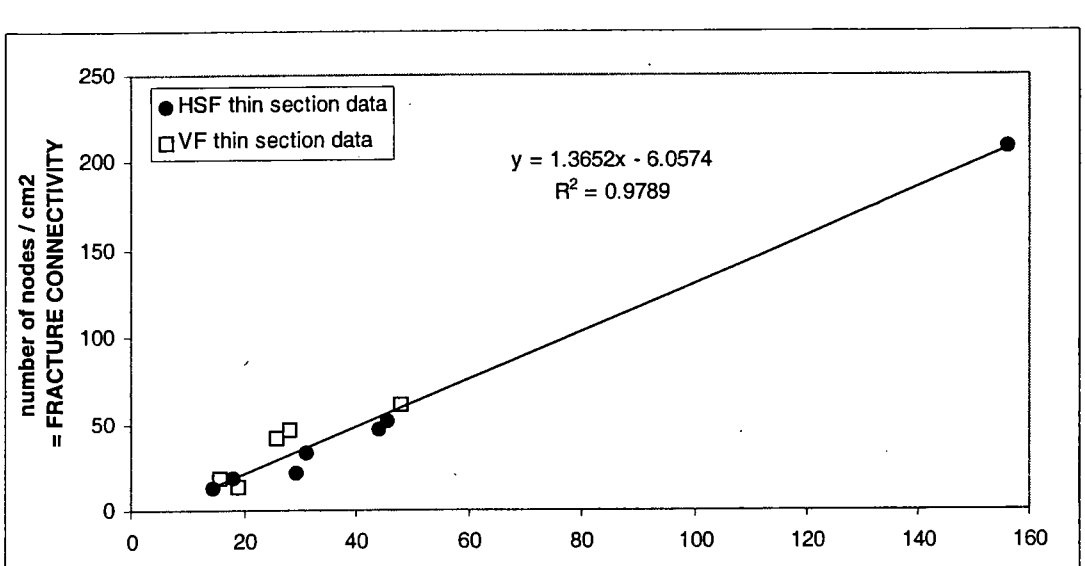

Figure 4.137 Total number of nodes per cm² (fracture connectivity) 'v' total number of fractures per cm² (fracture density) for all thin section data sets collected adjacent to the HSFP and the VFP

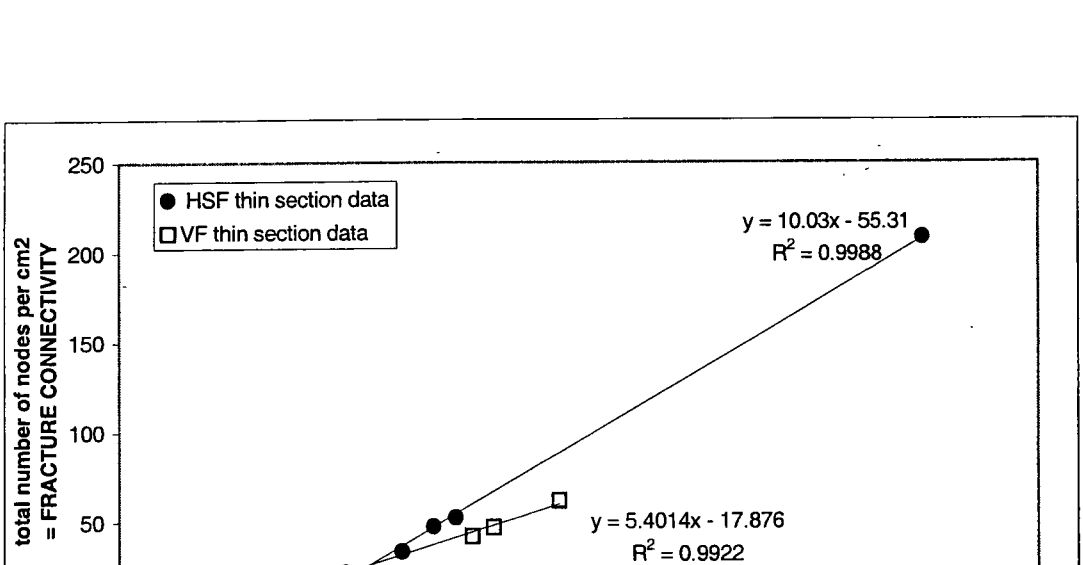

Figure 4.138 Total number of nodes per cm² (fracture connectivity) 'v' total fracture length per cm² (fracture intensity) for all thin section data sets collected adjacent to the HSFP and the VFP

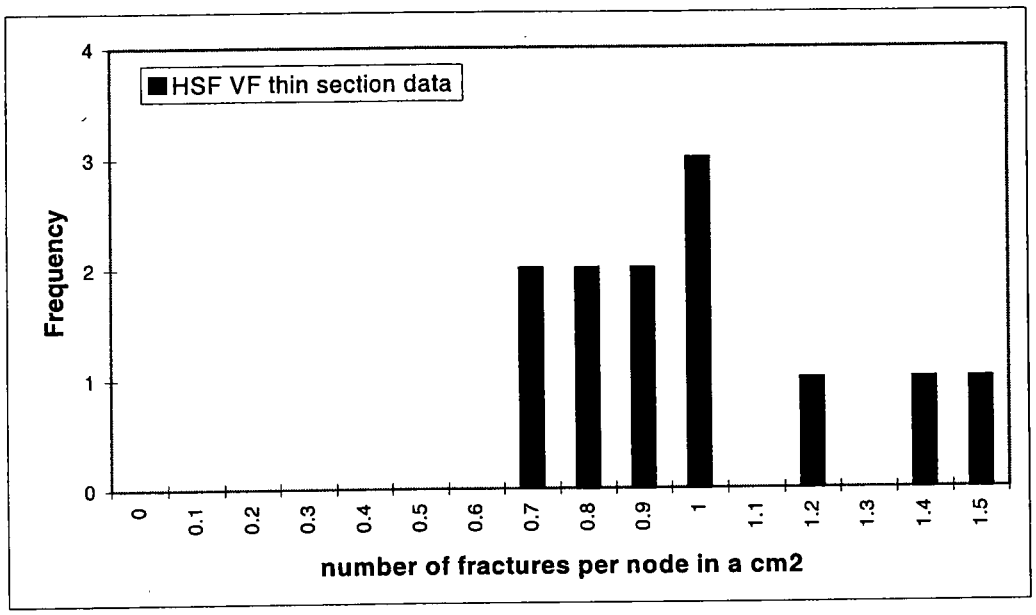

Figure 4.139 Histogram of the total number of fractures per node in a cm², for all thin section data sets adjacent to the VFP and the HSFP

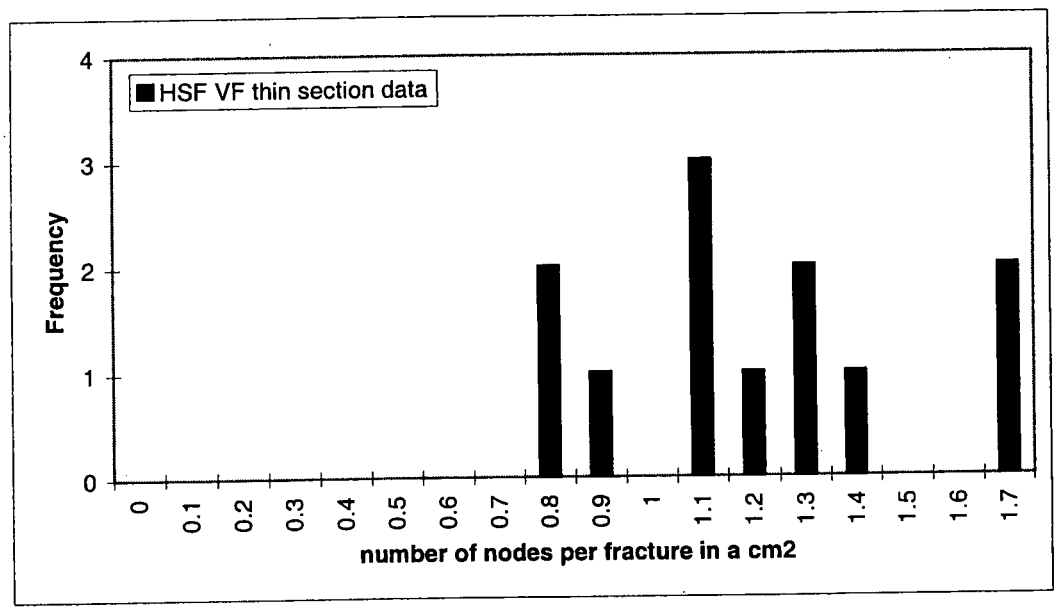

Figure 4.140 Histogram of the total number of nodes per fracture in a cm², for all thin section data sets adjacent to the VFP and the HSFP

a)

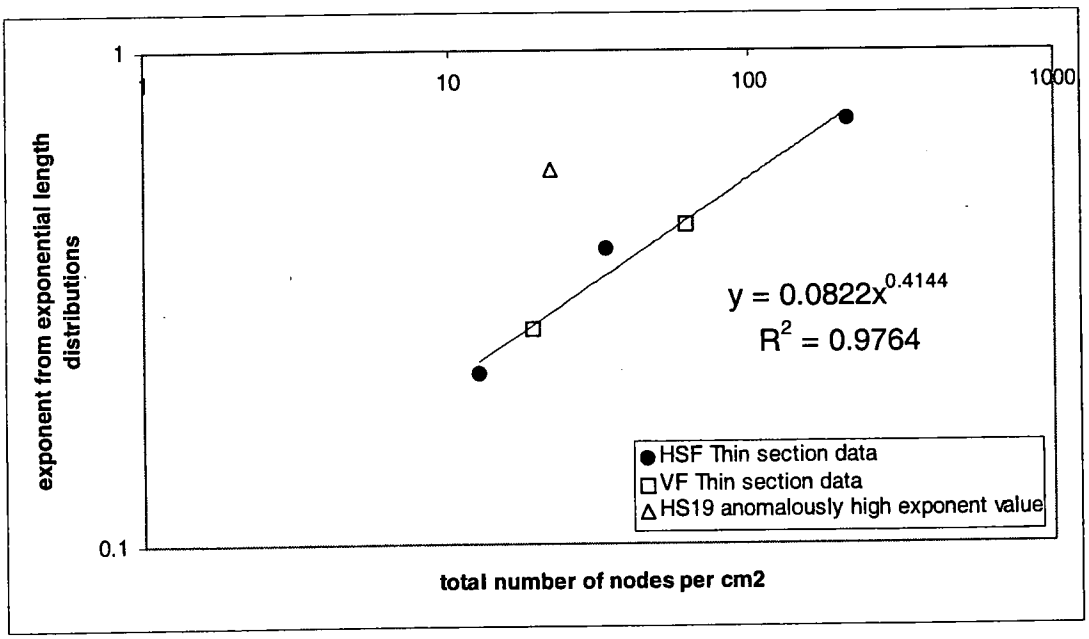

b)

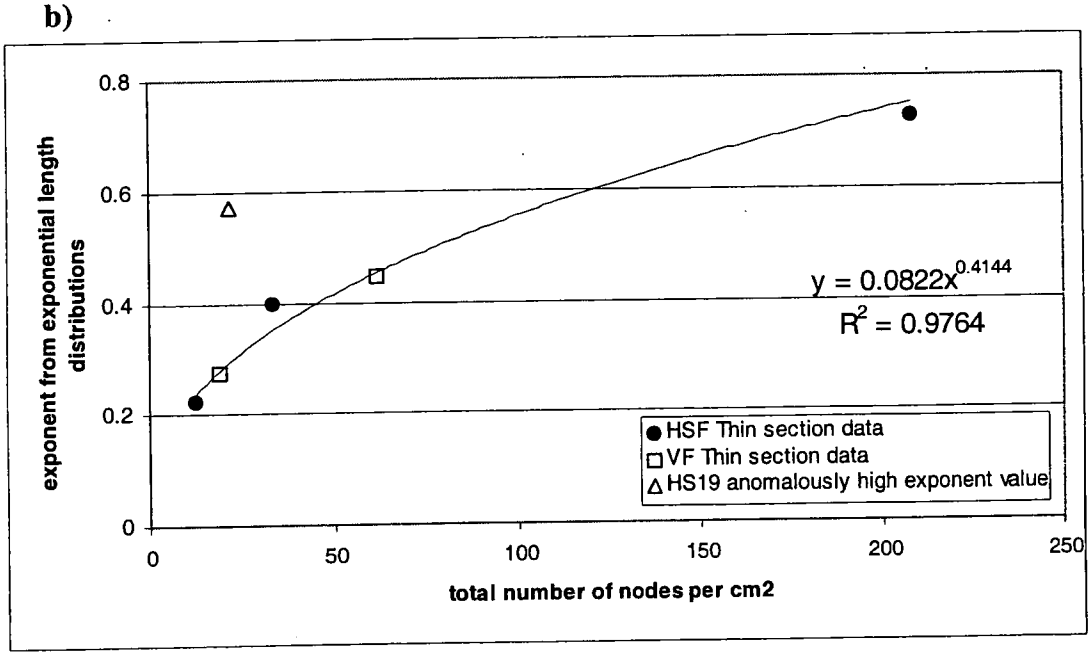

Figure 4.141 Exponent values from exponential fracture length distributions 'v' total number of nodes per cm².
a) data plotted on logarithmic axes, **b)** data plotted on linear axes

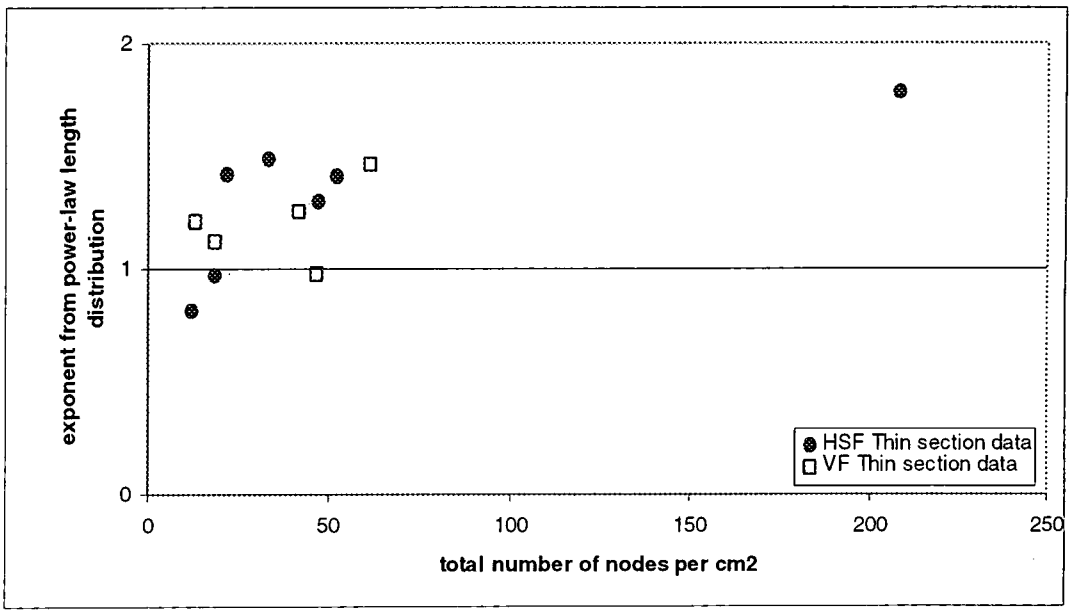

Figure 4.142 Exponent values from power-law fracture length distributions 'v' total number of nodes per cm²

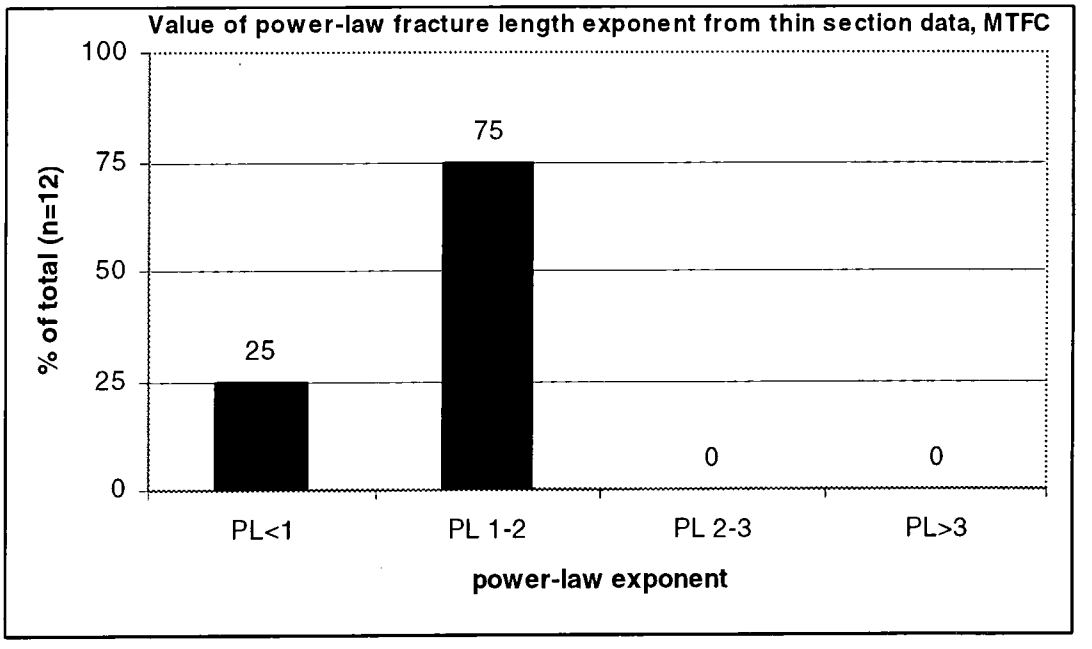

Figure 4.143 Histogram of power-law exponent values from the length data collected at thin section scale adjacent to faults within then MTFC

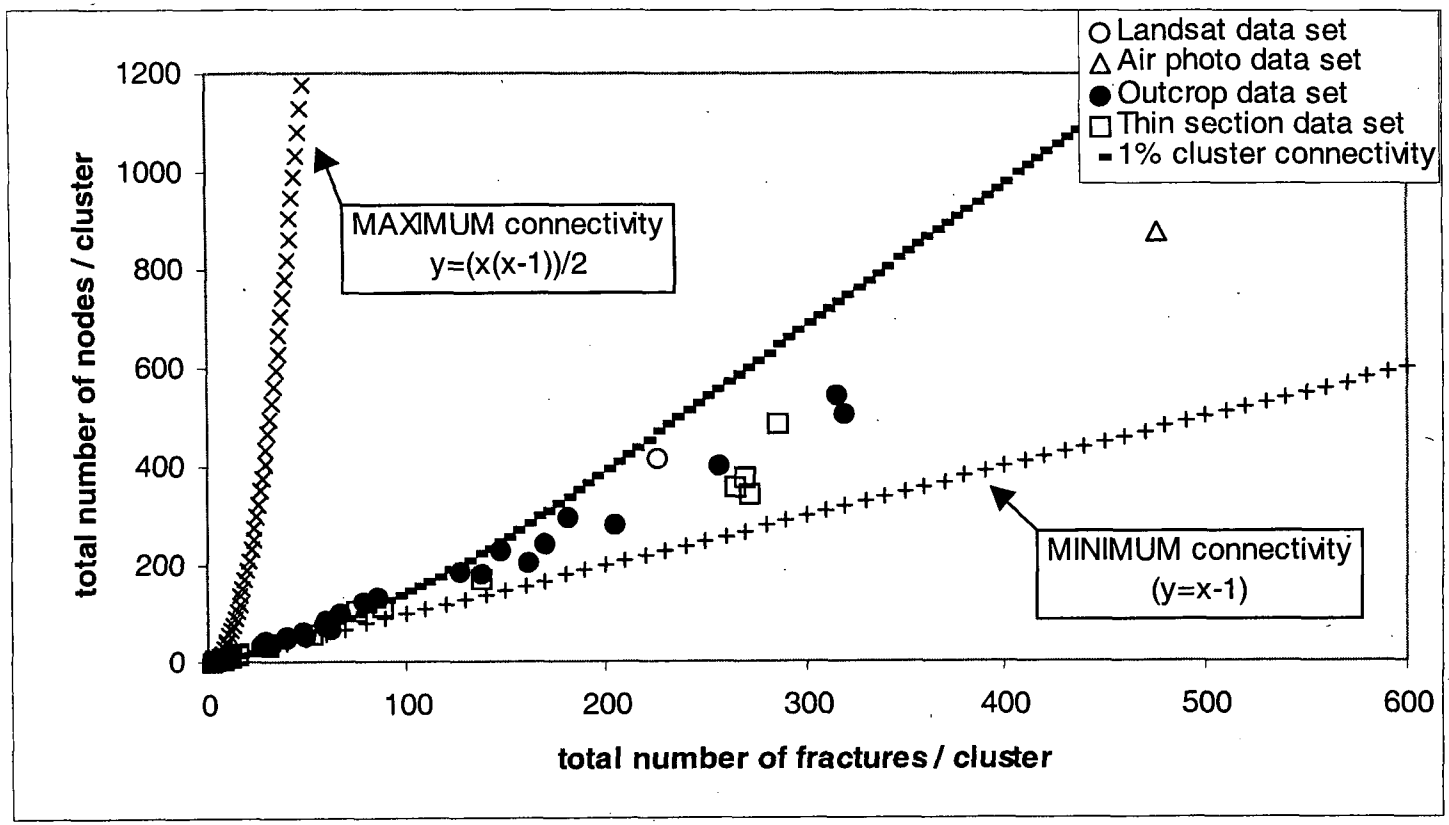

Figure 4.144 Total number of fractures per cluster 'v' total number of nodes per cluster for all data sets collected at thin section and outcrop scales, and from the air photograph and Landsat™ data sets, MTFC.

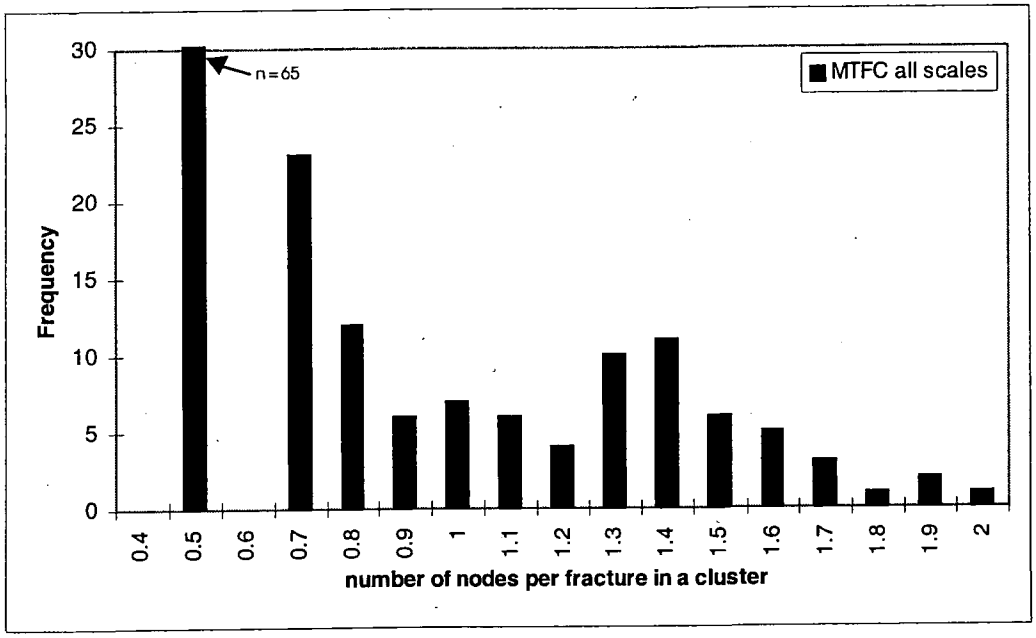

Figure 4.145 Histogram of the total number of nodes per fracture in a cluster for data sets measured adjacent to the VFP, HSFP and EFP from thin section, outcrop, air photograph and Landsat™ data sets

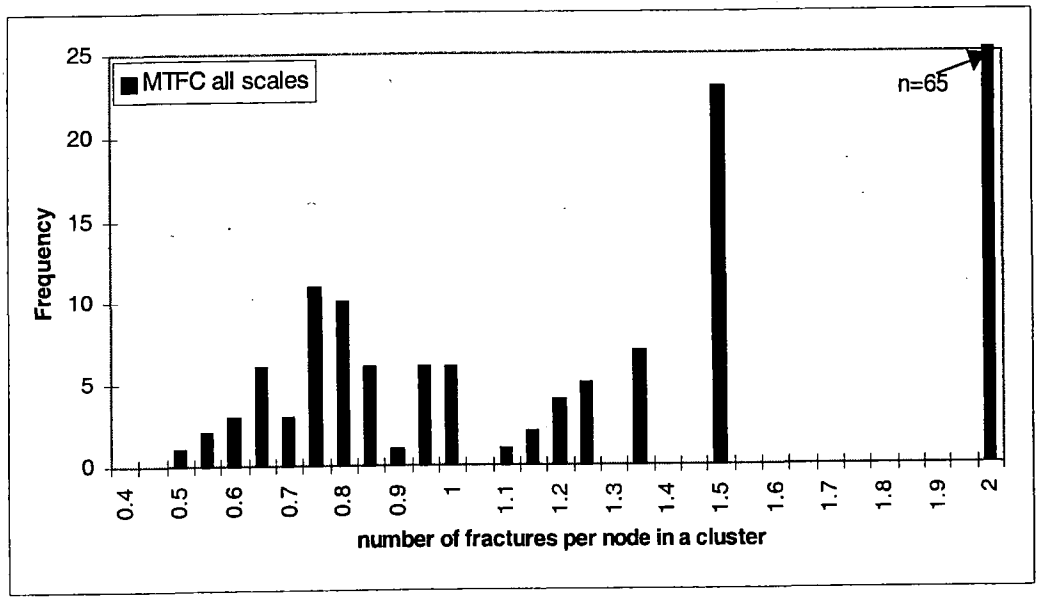

Figure 4.146 Histogram of the total number of fractures per node in a cluster for data sets measured adjacent to the VFP, HSFP and EFP from thin section, outcrop, air photograph and Landsat™ data sets

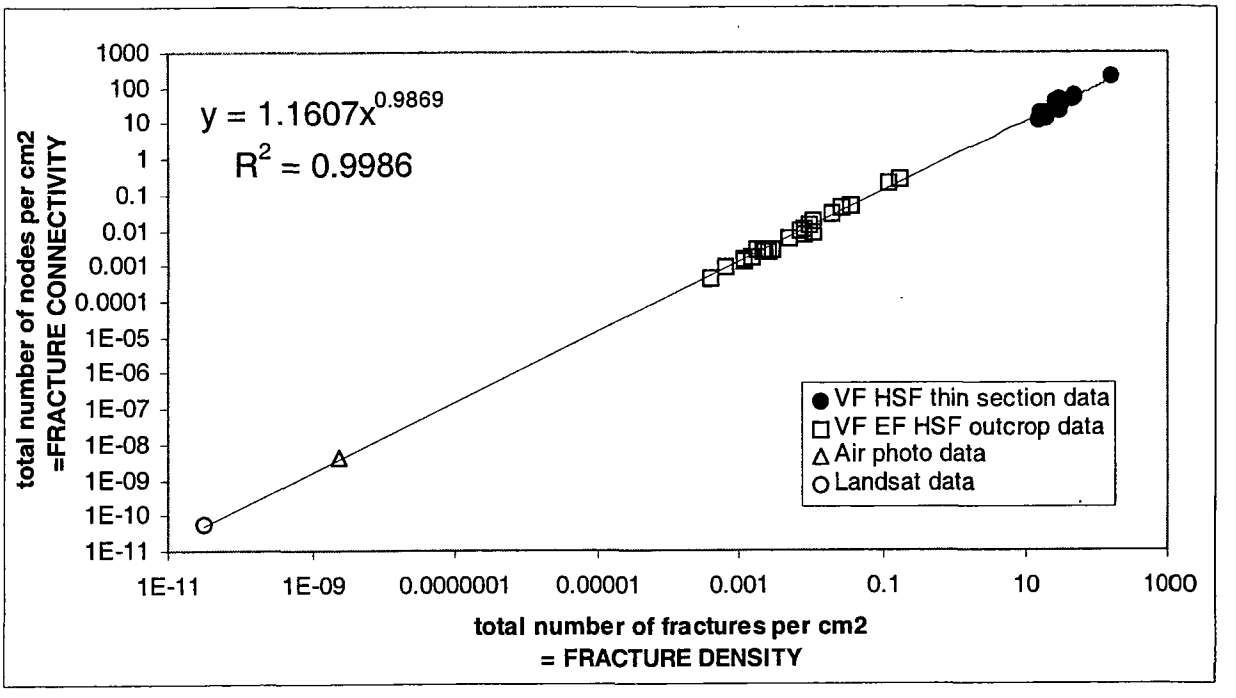

Figure 4.147 Fracture density 'v' fracture connectivity for data from all four scales (Landsat, air photograph, outcrop and thin section)

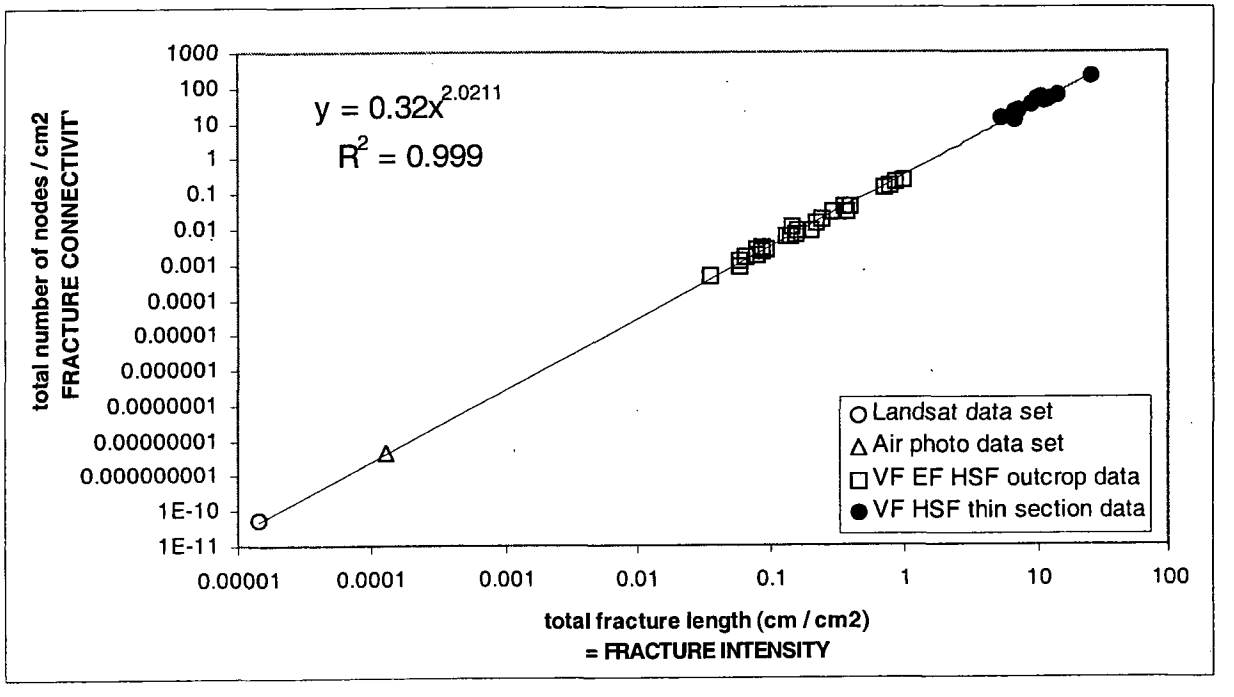

Figure 4.148 Fracture intensity 'v' fracture connectivity for data from all four scales (Landsat, air photograph, outcrop and thin section)

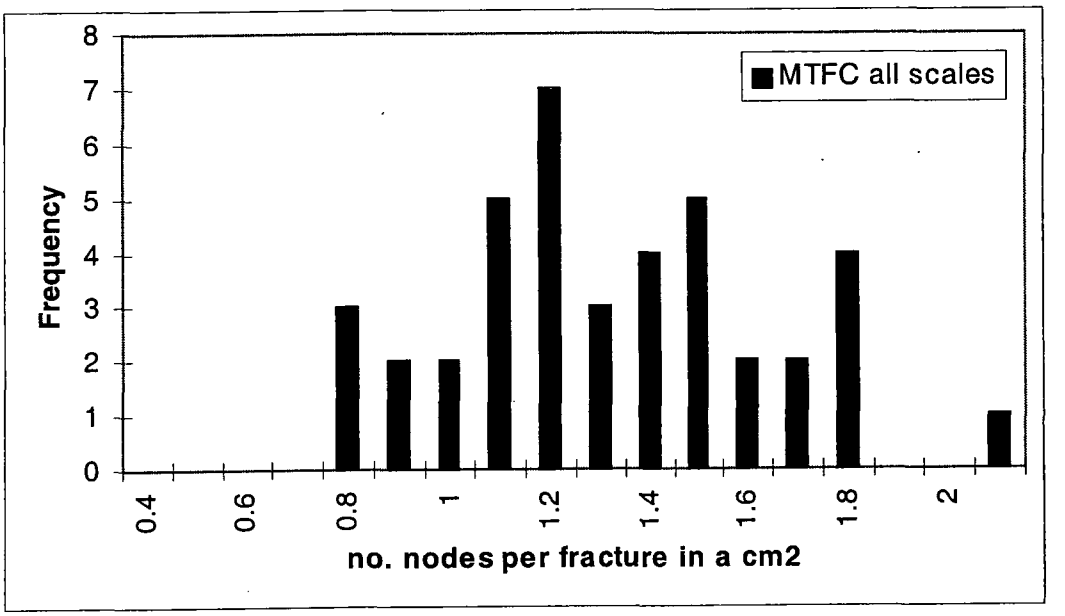

Figure 4.149 Histogram of the total number of nodes per fracture in a cm^2 for data sets measured adjacent to the VFP, HSFP and EFP from thin section, outcrop, air photograph and Landsat™ data sets

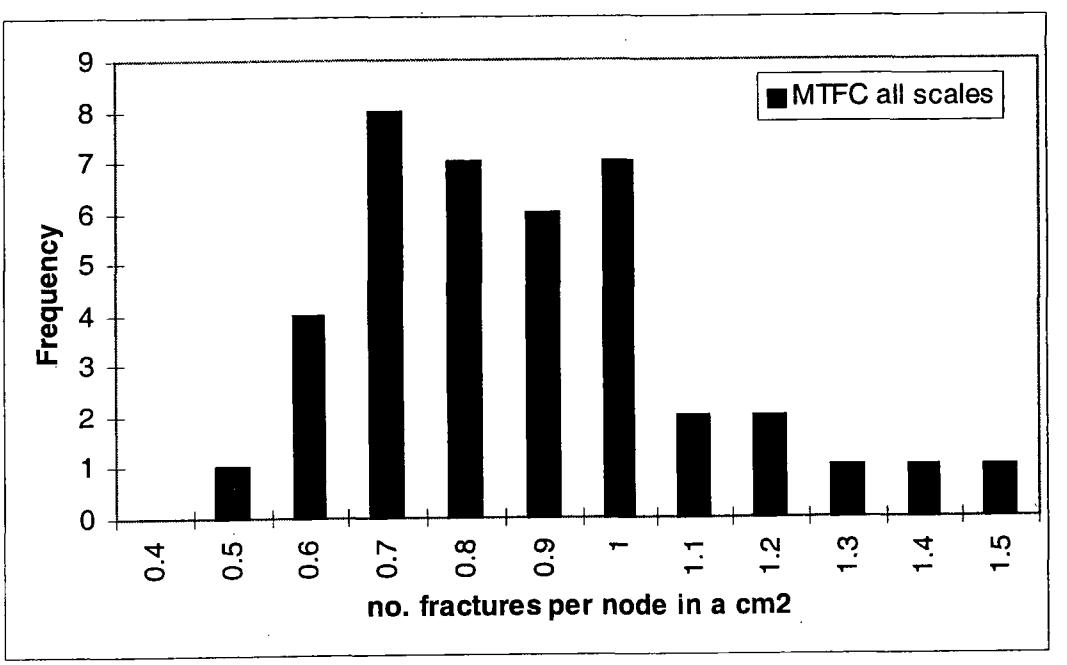

Figure 4.150 Histogram of the total number of fractures per node in a cm^2 for data sets measured adjacent to the VFP, HSFP and EFP from thin section, outcrop, air photograph and Landsat™ data sets

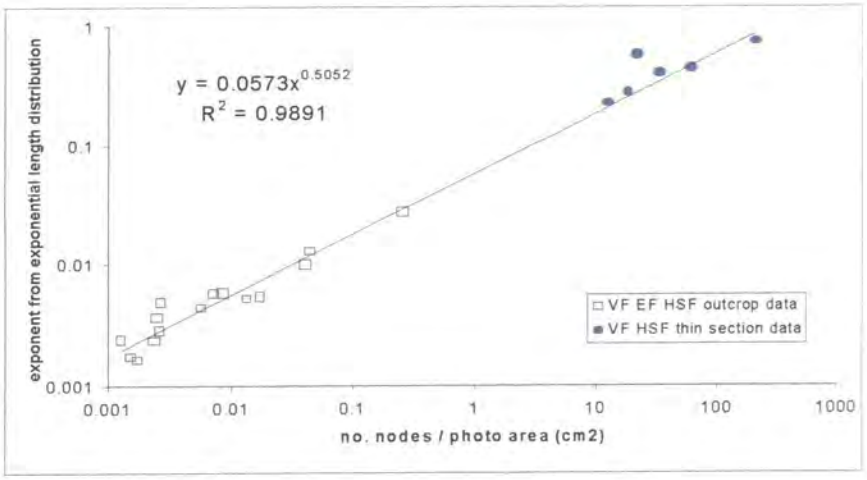

Figure 4.151 Exponent values from exponential fracture length distributions 'v' total number of nodes per cm² for data from thin section and outcrop scales, the air photograph and the Landsat™ image

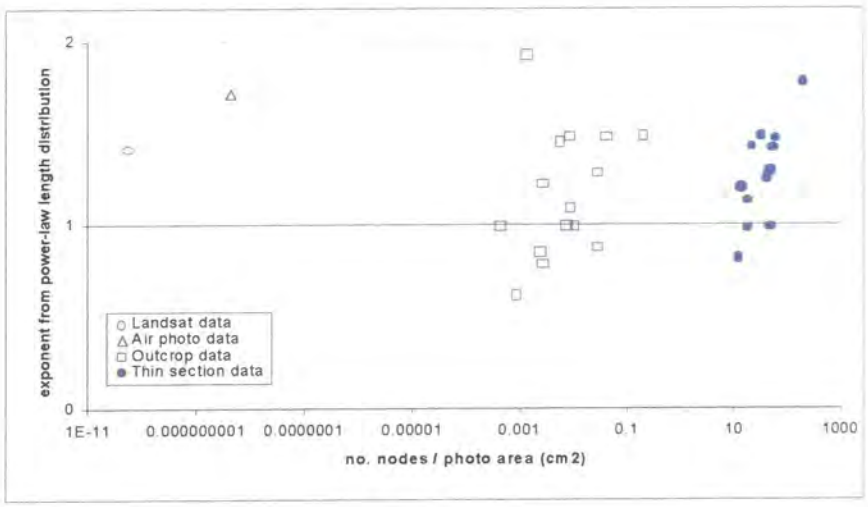

Figure 4.152 Exponent values from power-law fracture length distributions 'v' total number of nodes per cm² for data from thin section and outcrop scales, the air photograph and the Landsat™ image

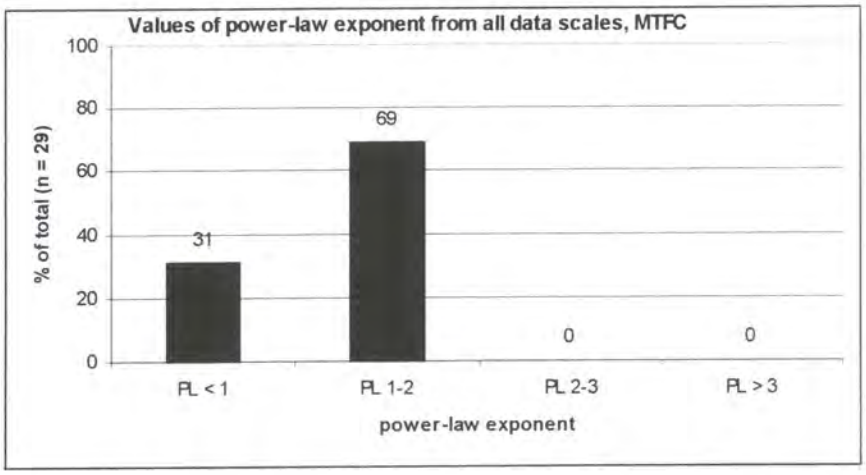

Figure 4.153 Histogram of power-law exponent values from length data collected at thin section and outcrop scales, and the air photograph and Landsat™ data sets

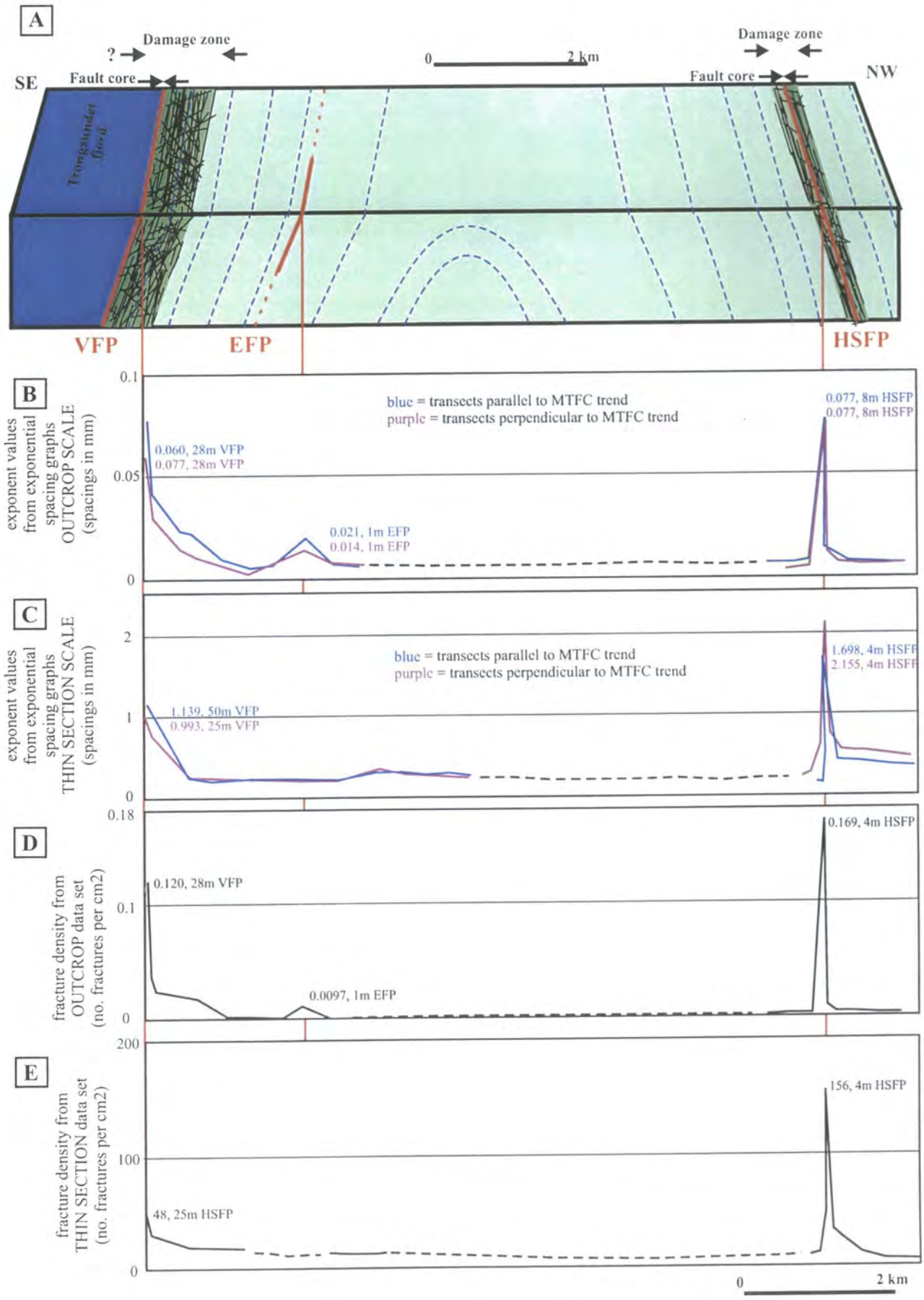

Figure 4.154 Variation in fracture spacing parameters adjacent to HSF, VF & EF within MTFC measured from 1-D transects across 2-D data sets.

A = representative cross-section across the MTFC

B - C = exponential exponent plots from outcrop and thin section data sets

D - E = fracture density plots from outcrop and thin section data sets

dashed line = interpreted, no data points

numbers adjacent to peaks = absolute peak value and distance that data was collected from fault plane (VF, EF or HSF)

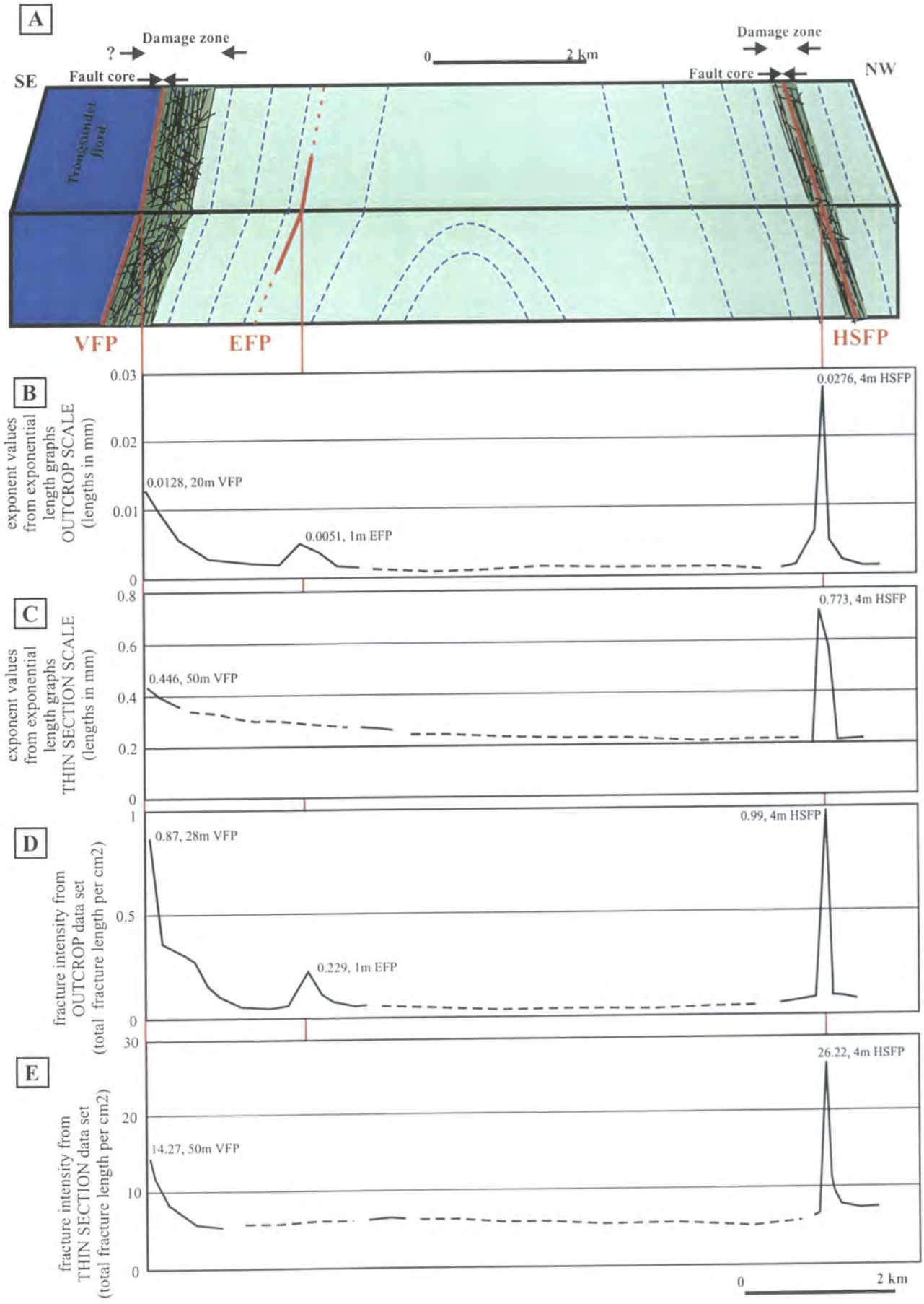

Figure 4.155 Variation in fracture length parameters adjacent to HSF, VF & EF within MTFC from 2-D data sets.

A = representative cross-section across the MTFC

B - C = exponential exponent plots from outcrop and thin section data sets

D - E = fracture intensity plots from outcrop and thin section data sets

dashed line = interpreted, no data points

numbers adjacent to peaks = absolute peak value and distance that data was collected from fault plane (VF, EF or HSF)

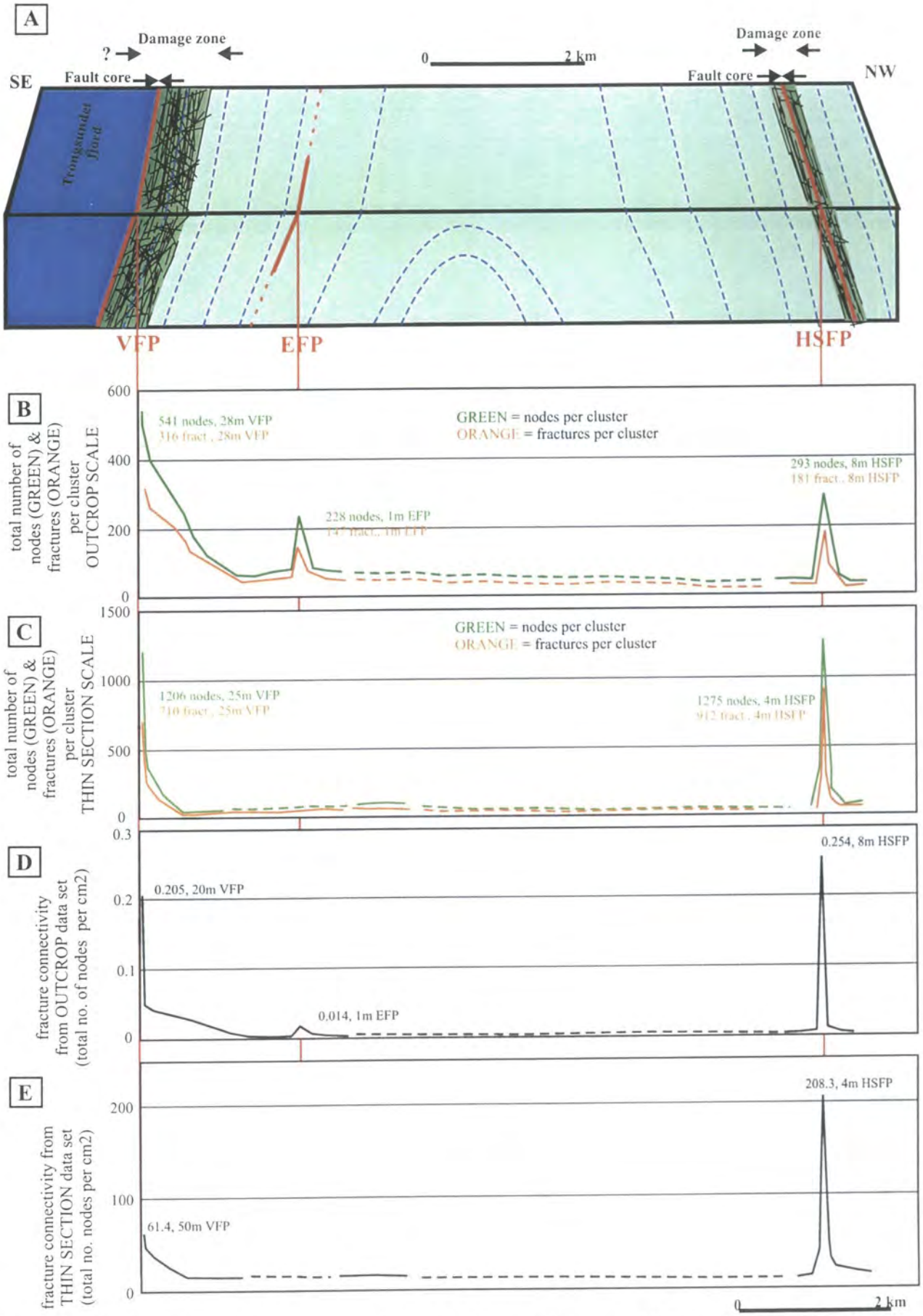

Figure 4.156 Variation in fracture connectivity parameters adjacent to HSF, VF & EF within MTFC from 2-D data sets.

A = representative cross-section across the MTFC

B-C = total number of fractures & nodes per cluster from outcrop & thin section data set

D-E = fracture connectivity plots (total number of nodes per cm2) from outcrop and thin section data sets

dashed line = interpreted, no data points

numbers adjacent to peaks = absolute peak value and distance that data was collected from fault plane (VF, EF or HSF)

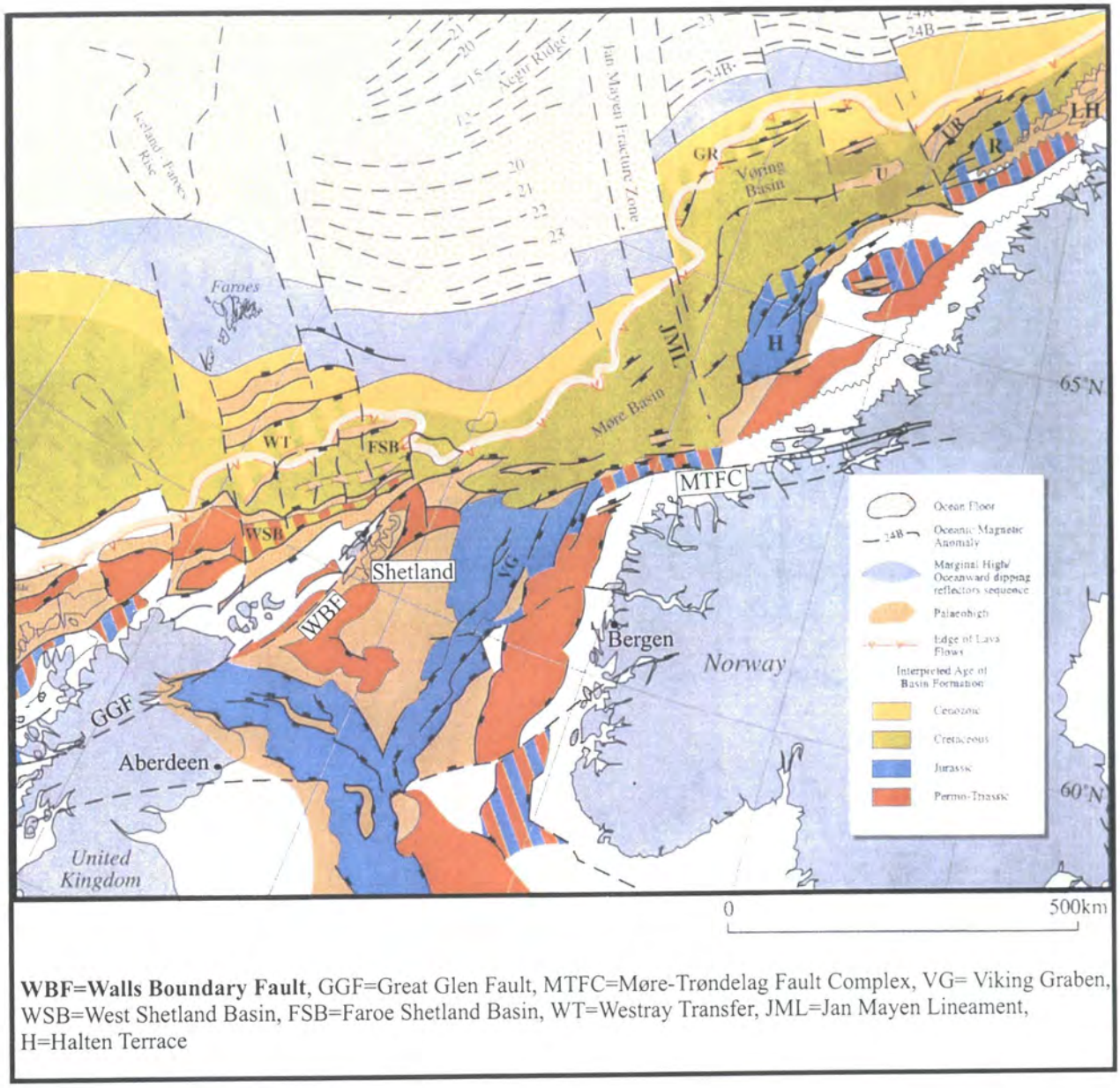

WBF=Walls Boundary Fault, GGF=Great Glen Fault, MTFC=Møre-Trøndelag Fault Complex, VG= Viking Graben, WSB=West Shetland Basin, FSB=Faroe Shetland Basin, WT=Westray Transfer, JML=Jan Mayen Lineament, H=Halten Terrace

Figure 5.1 Map to show the location of the Shetland Isles and the major offshore basins of the Northeast Atlantic margin
(adapted from Dore et al., 1997, and Watts 2001).

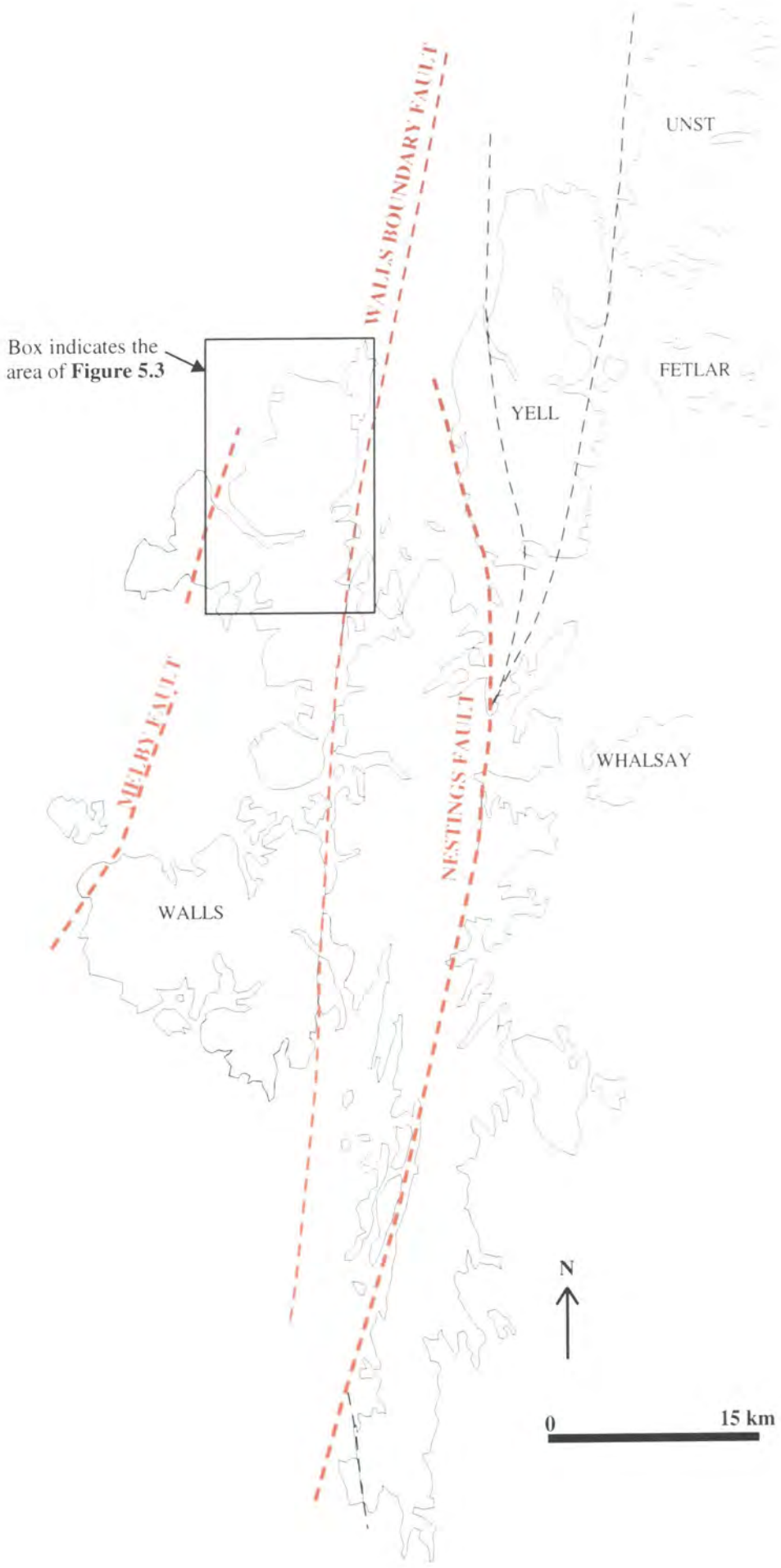

Figure 5.2 Map to show the location of the three major faults on Shetland. (After Flinn, 1977)

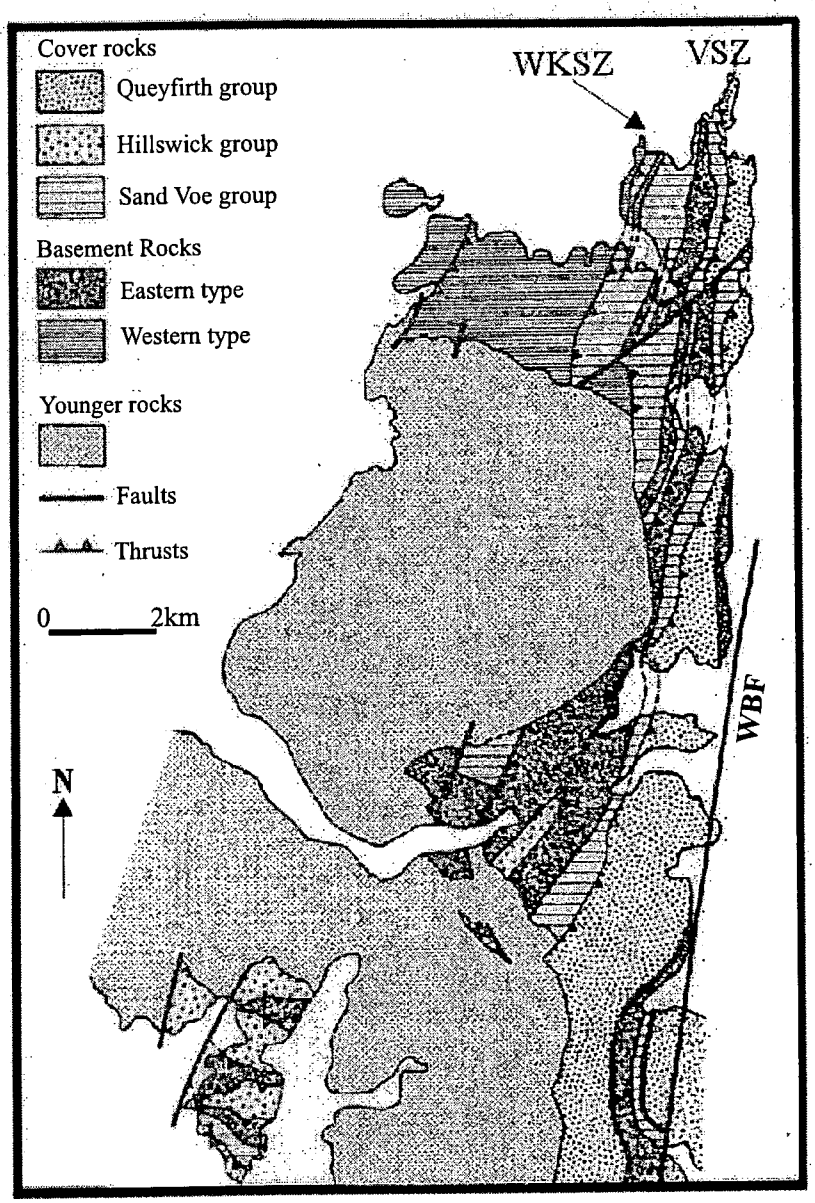

Figure 5.3 Geological map of the North Roe area, west of the Walls Boundary Fault (WBF)
VSZ = Virdbeck shear zone, WKSZ = Wester Keolka shear zone (adapted from Flinn 1985).

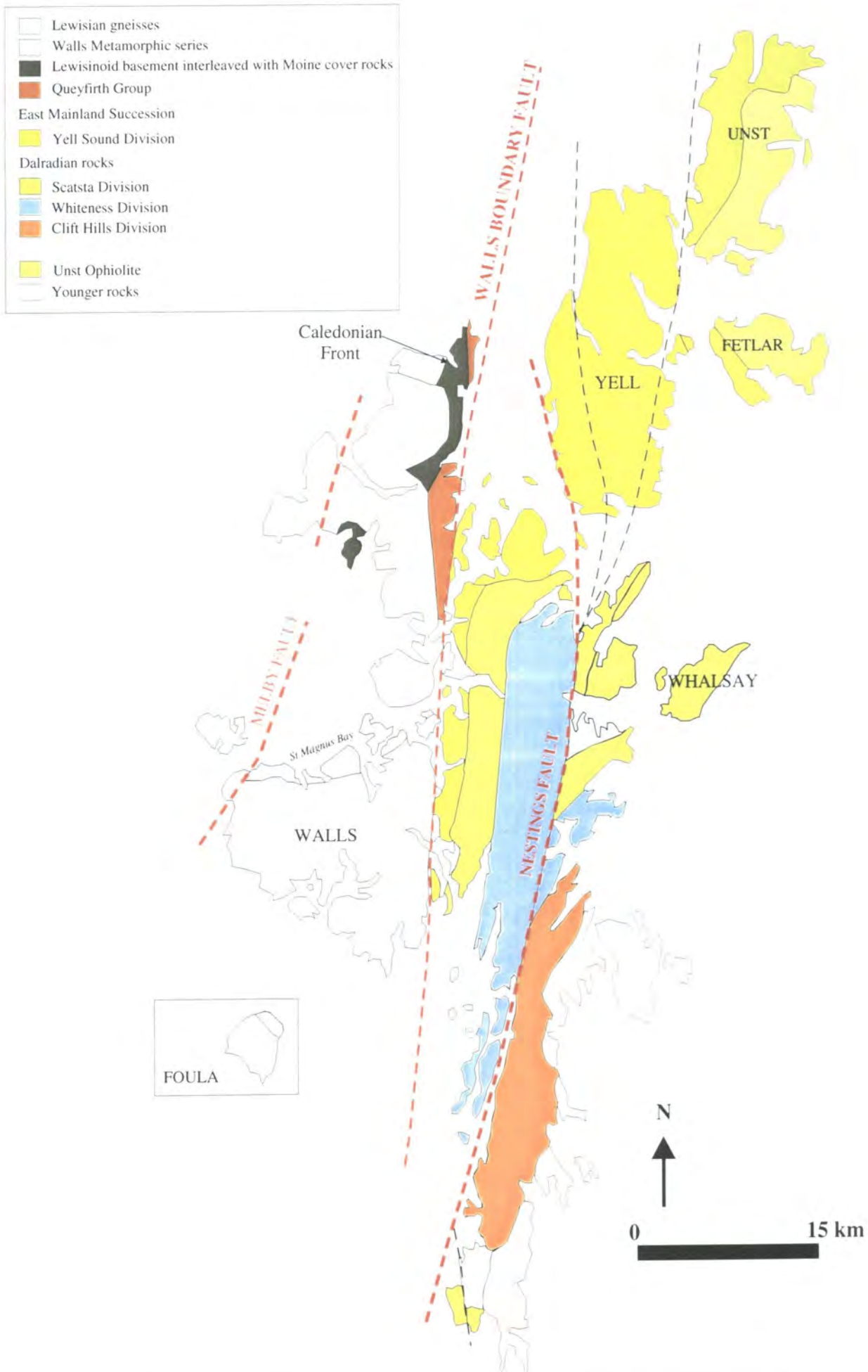

Figure 5.4 Map showing the location of Caledonian and older basement rocks of the Shetland Islands (after Watts 2001).

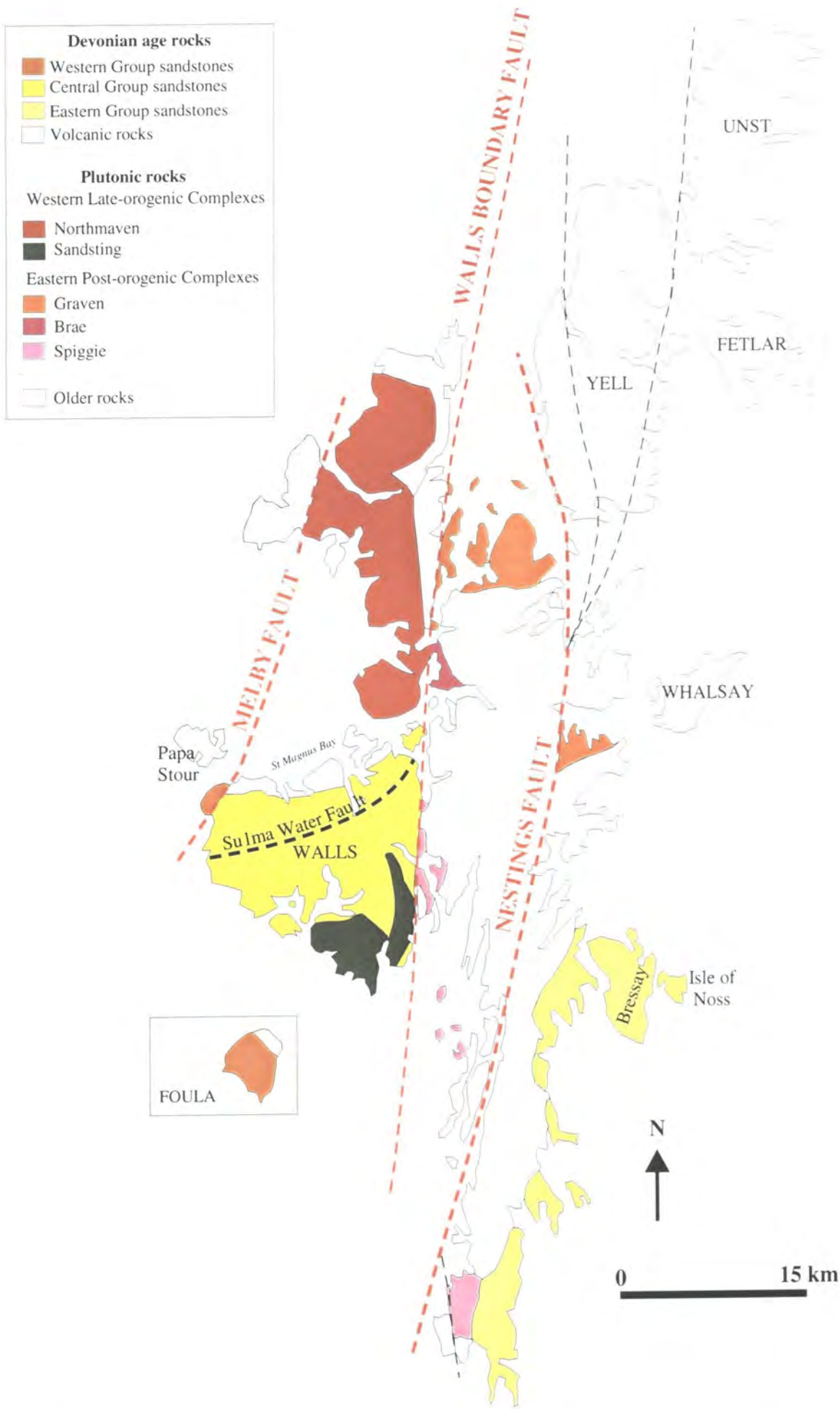

Figure 5.5 Geological map to show the location of Devonian sedimentary rocks and plutonic complexes on Shetland (after Watts 2001)

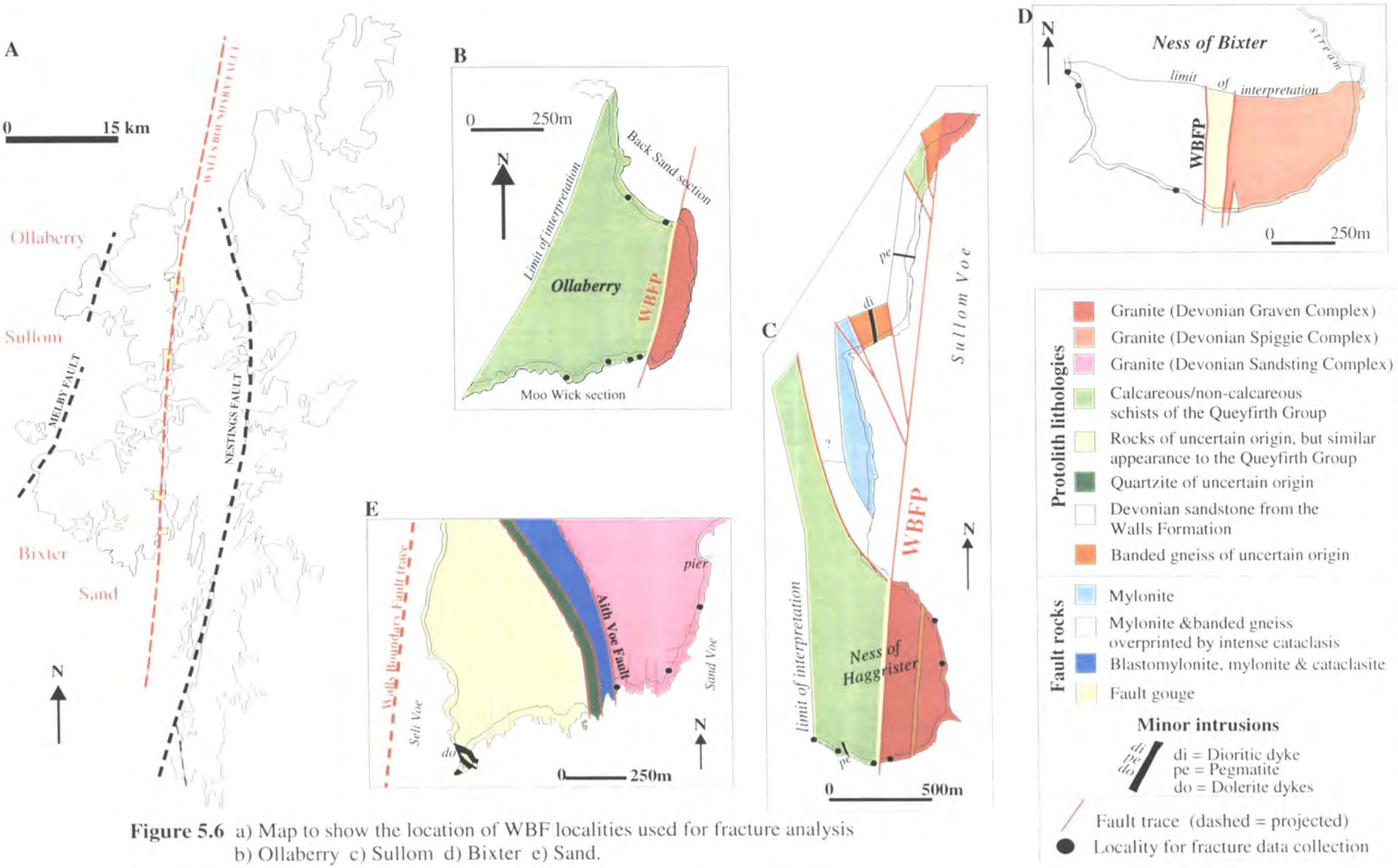

Figure 5.6 a) Map to show the location of WBF localities used for fracture analysis b) Ollaberry c) Sullom d) Bixter e) Sand.

Figure 5.7 Photograph illustrating the Back Sand section, on the northern side of the Ollaberry peninsula (there is a person on the beach for scale). The headland in the background is comprised of pink-coloured granite. The steep cliffs in the foreground are comprised of the Queyfirth group

Figure 5.8 Photographs of the Walls Boundary Fault Plane, exposed on the Back Sand section at Ollaberry.
A - looking North along the WBFP, **B** - looking SSE onto the WBFP

Figure 5.9 The core of the Walls Boundary Fault exposed at Sullom, on the southern side of the Ness of Haggrister, containing the WBFP
(photograph taken looking N)

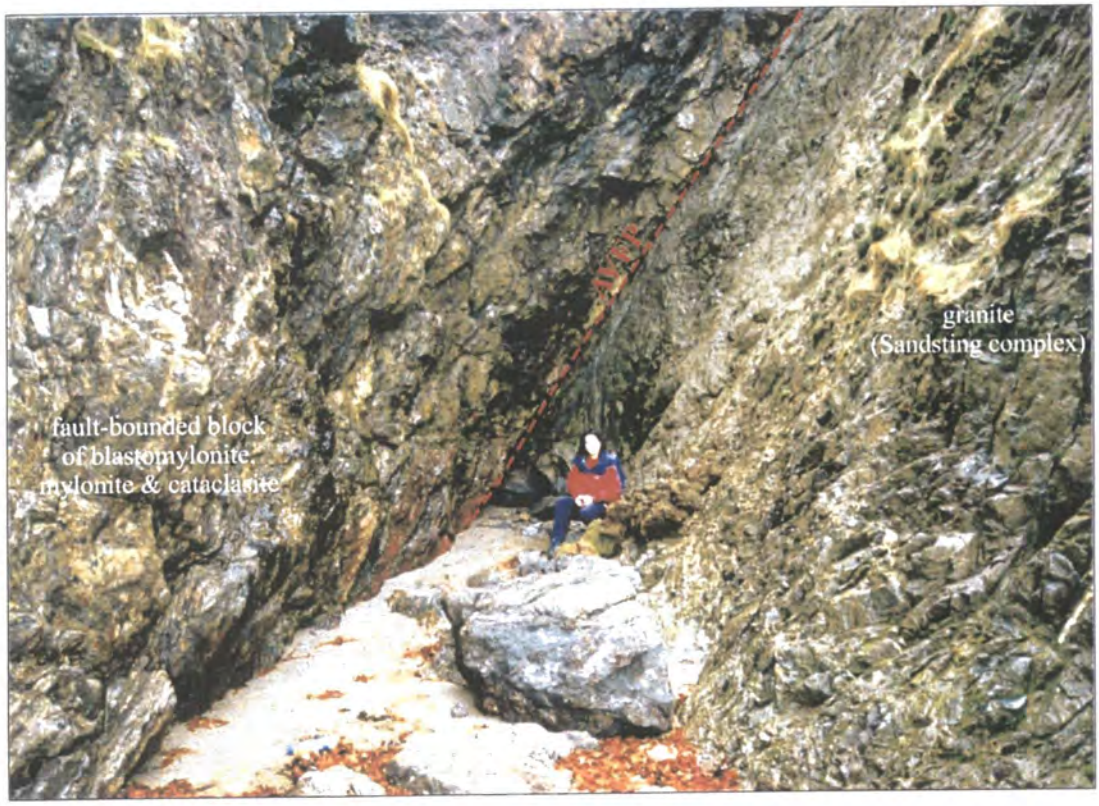

Figure 5.10 Photograph illustrating the Aith Voe Fault Plane, exposed at Sand locality.
(photograph taken looking N)

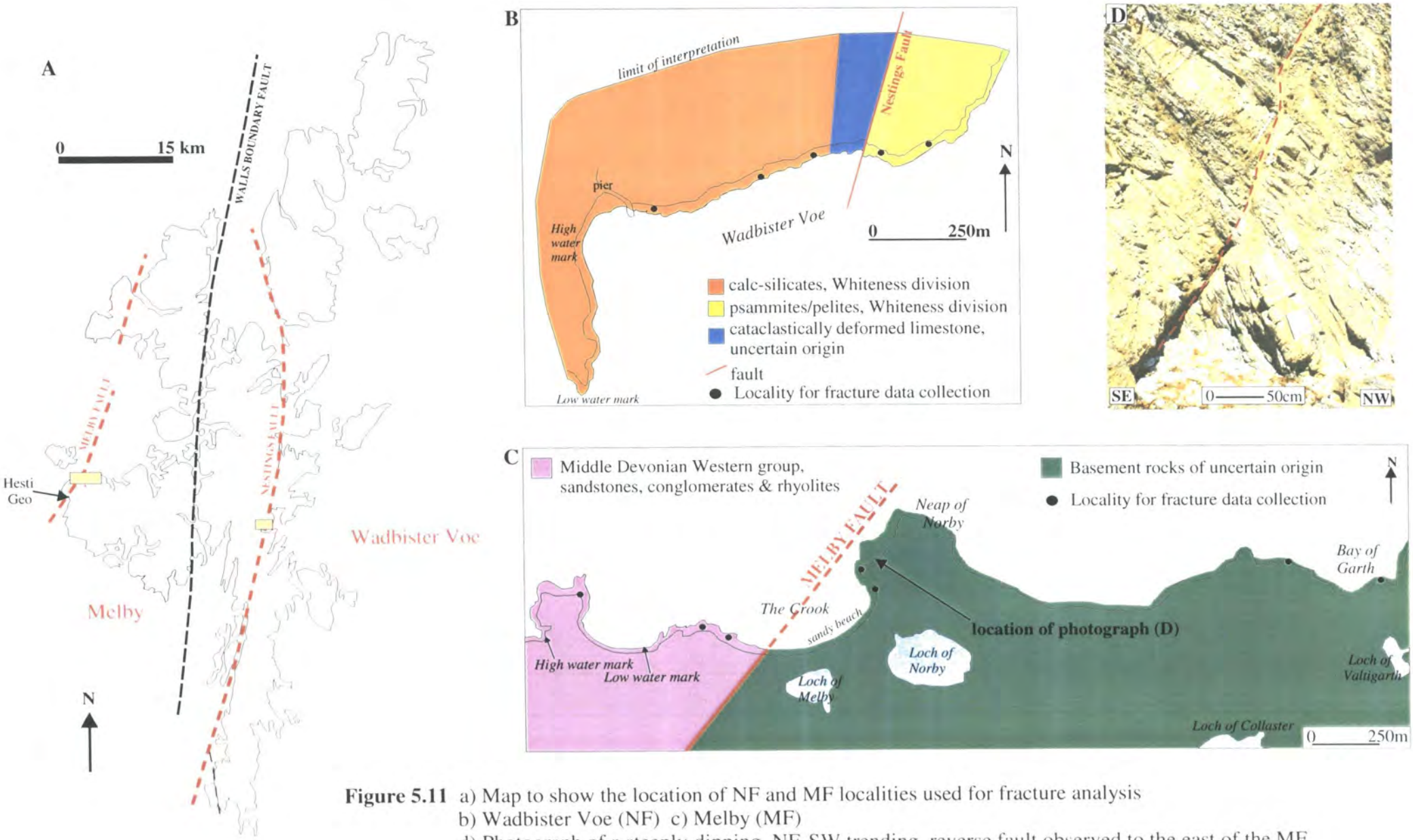

Figure 5.11 a) Map to show the location of NF and MF localities used for fracture analysis
b) Wadbister Voe (NF) c) Melby (MF)
d) Photograph of a steeply-dipping, NE-SW trending, reverse fault observed to the east of the MF within basement rocks (sub-vertical surface).

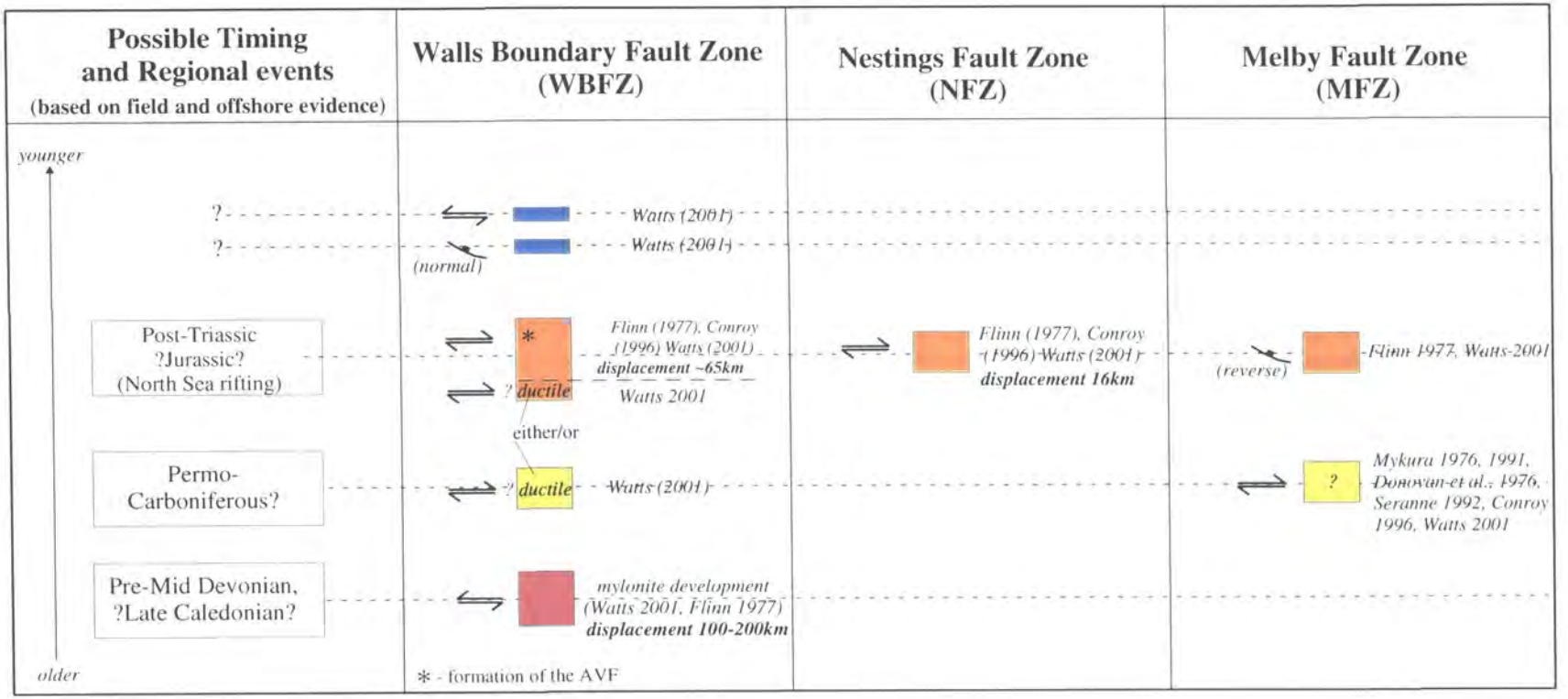

Figure 5.12 Diagram to show the relative kinematic histories for the Walls Boundary, Nestings and Melby Faults, with suggested timings based on field and offshore evidence.

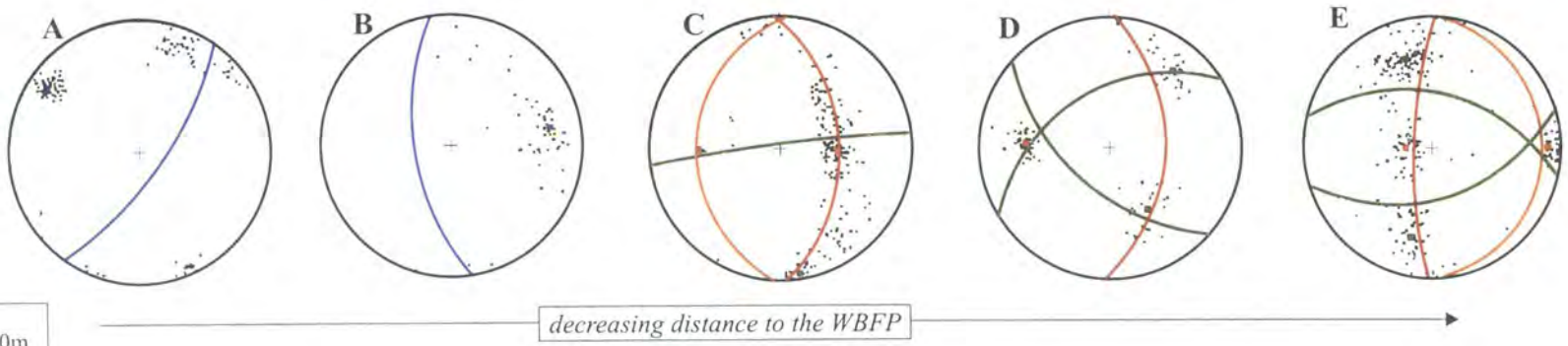

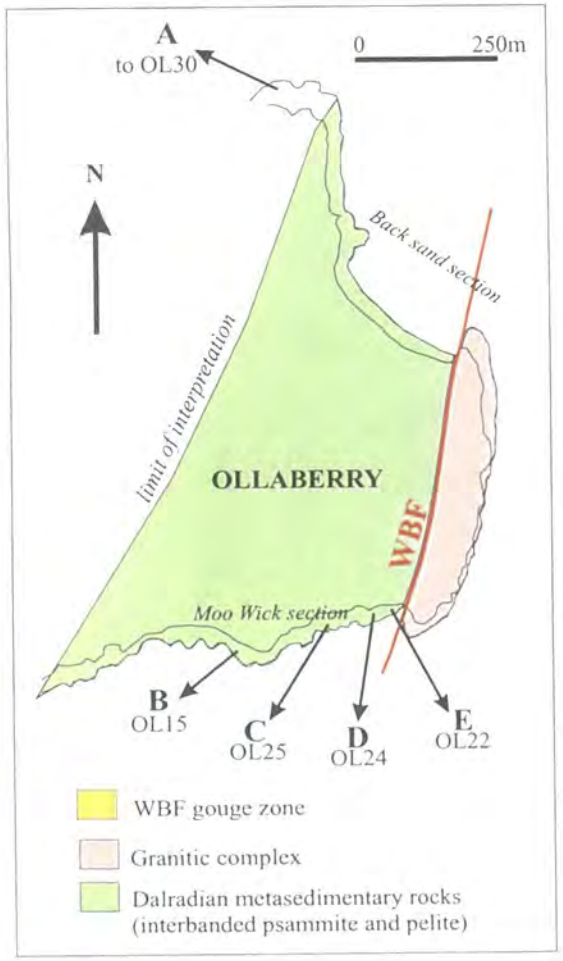

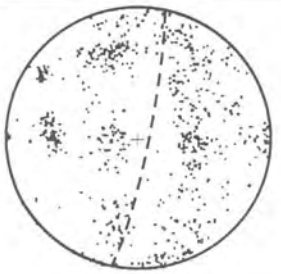

Stereonet showing all fractures measured within psammite at Ollaberry with the orientation of the WBFP at this locality (black dashed girdle 012/ 84 E) n = 798

		Stereonets				
		A	B	C	D	E
	Place	Ollaberry	Ollaberry	Ollaberry	Ollaberry	Ollaberry
	Locality	OL30	OL15	OL25	OL24	OL22
	Distance to WBFP	1300m	200m	130m	50m	20m
	no. data points	128	44	236	155	235
	lithology	psammite	psammite	psammite	psammite	psammite
	foliation orientation	032/ 76 E	179/ 70 W	177/ 50 E	000/ 53 E	004/ 80 W
mean girdles to fracture orientations	N-S steep (parallel to foliation) (RED)	-	172/ 67 W	178/ 52 E	002/ 55 E	002/ 78 W,
	N-S shallow (ORANGE)	-	-	003/ 36 W	-	000/ 16 E
	~NE-SW to NW-SE (GREEN)	-	-	083/ 88 N	058/ 54 N 132/ 64 S	073/ 58 S 103/ 56 N
	OTHER (BLUE)	035/ 75 E	-	-	-	-

Figure 6.1 Fracture orientation data measured adjacent to the WBFP within psammite **A - E** = stereographic projections of fracture orientations (details of which are given in the table), from localities illustrated on the map

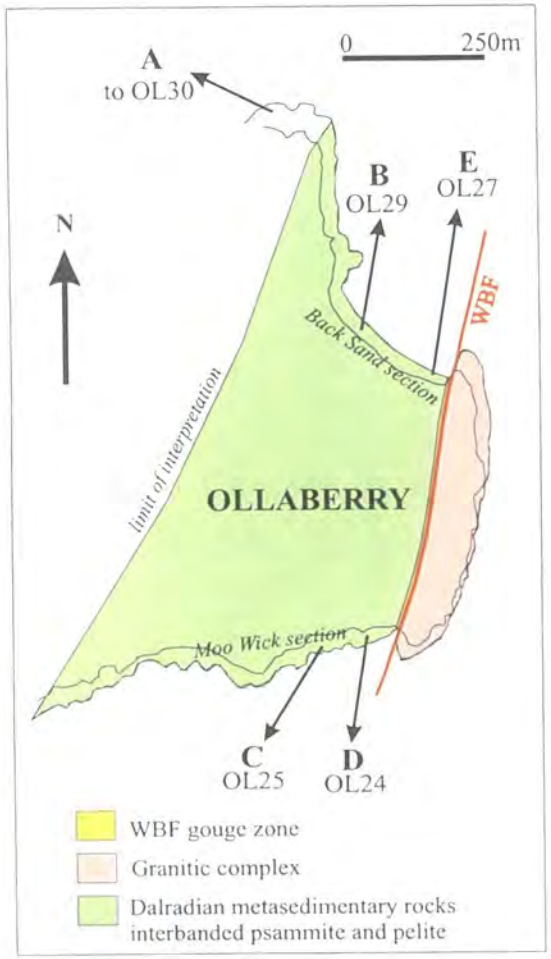

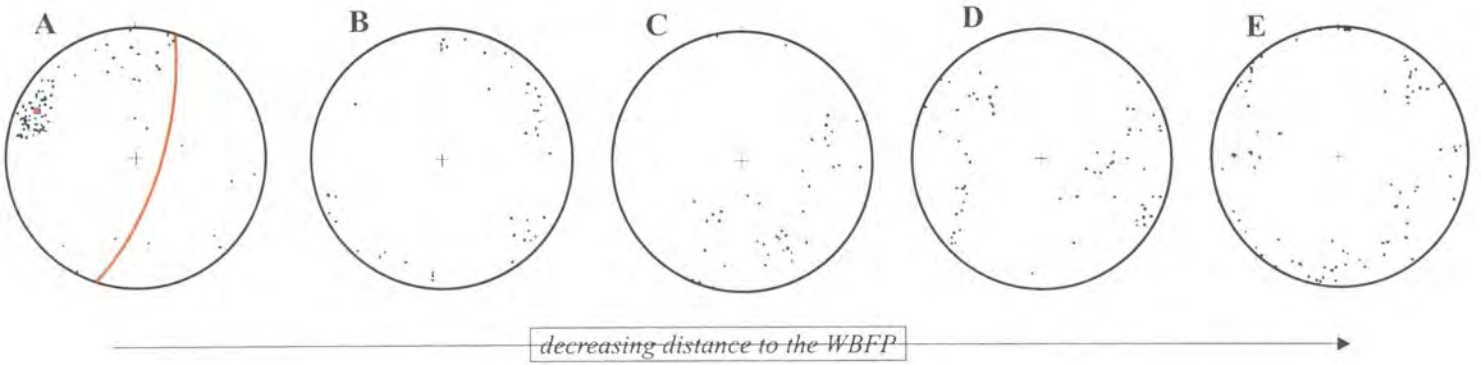

Stereonet showing all fractures measured within pelite at Ollaberry with the orientation of the WBFP at this locality (black dashed girdle 012/ 84 E) n = 335

	Stereonets				
	A	B	C	D	E
Place	Ollaberry	Ollaberry	Ollaberry	Ollaberry	Ollaberry
Locality	OL30	OL29	OL25	OL24	OL27
Distance to WBFP	1300m	170m	130m	50m	30m
no. data points	90	43	42	96	64
lithology	pelite	pelite	pelite	pelite	pelite
foliation orientation	018/ 66 E	003/ 84 W	178/ 54 E	179/ 54 E	012/ 50 E
fracture orientation clusters identified	016/ 74 S	none	none	none	none

Figure 6.2 Fracture orientation data measured adjacent to the WBFP within pelite
A - E = stereographic projections of fracture orientations (details of which are given in the table), from localities illustrated on the map

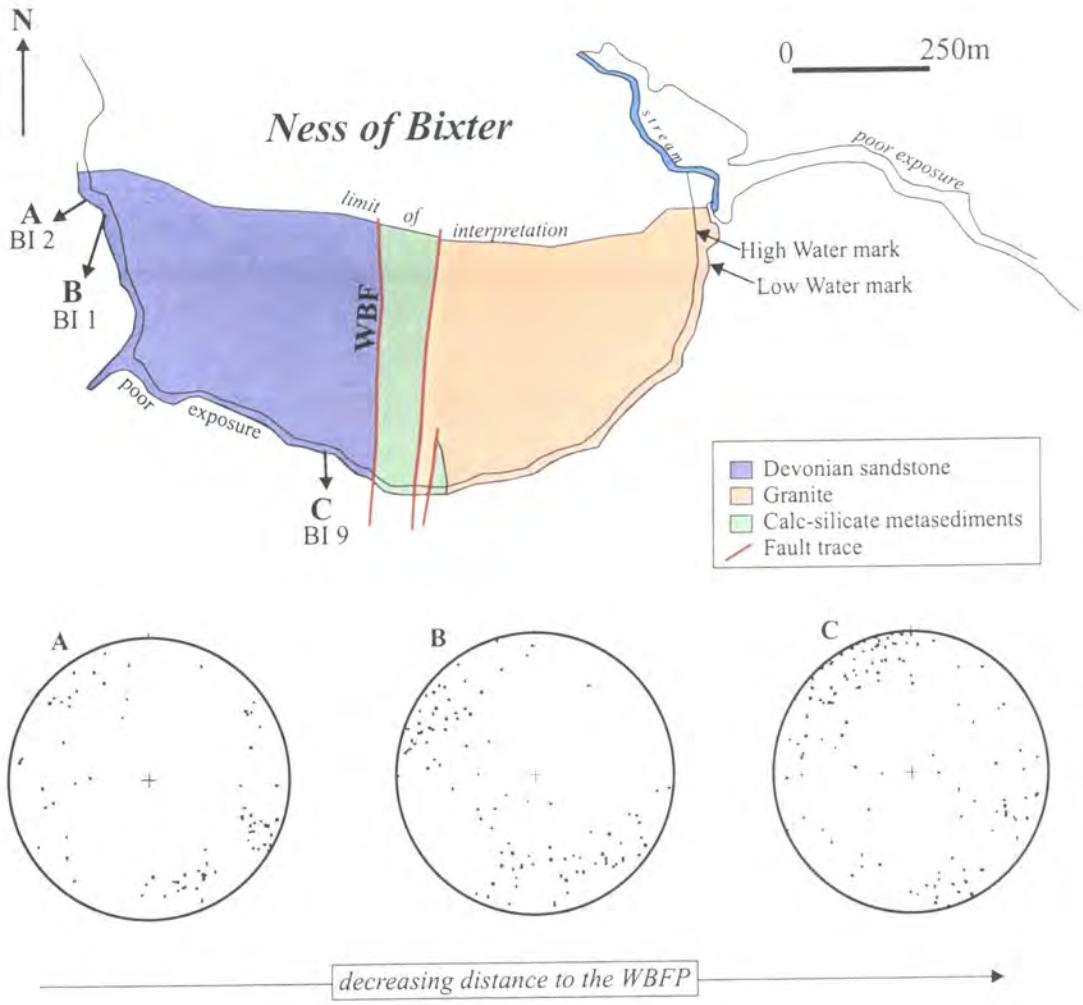

	Stereonet		
	A	**B**	**C**
Place	Bixter	Bixter	Bixter
Locality	BI 2	BI 1	BI 9
Distance to WBFP	535m	400m	100m
no. data points	77	99	126
lithology	sandstone	sandstone	sandstone
fracture orientation clusters identified	none	none	none

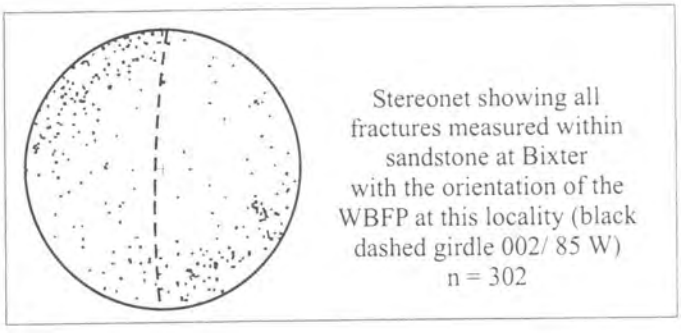

Figure 6.3 Fracture orientation data measured adjacent to the WBFP within sandstone **A - C** = stereographic projections of fracture orientations (details of which are given in the table), from localities illustrated on the map

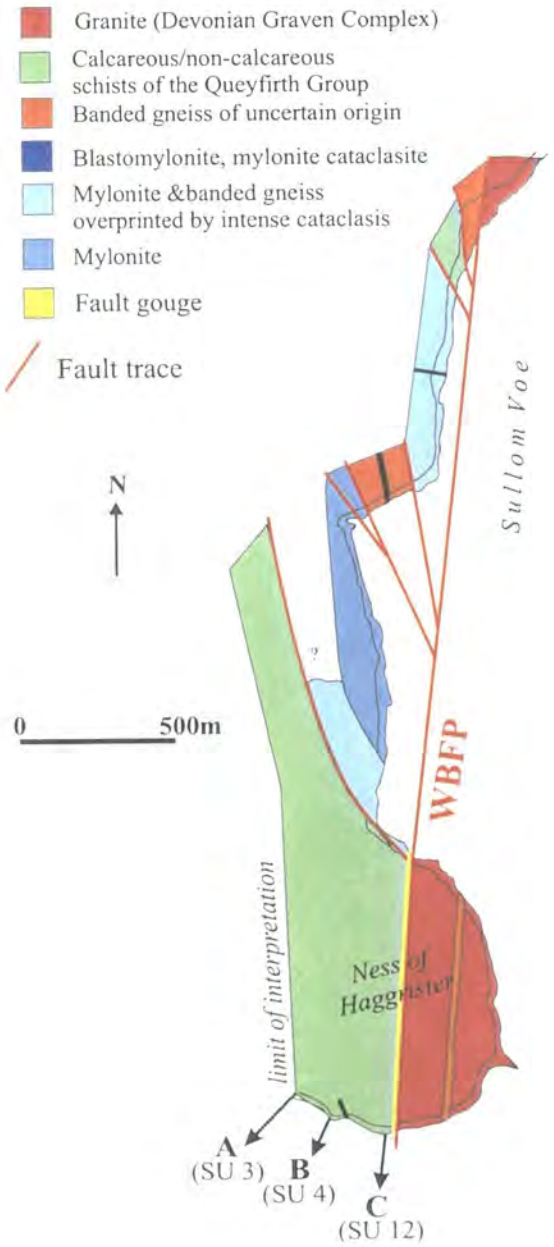

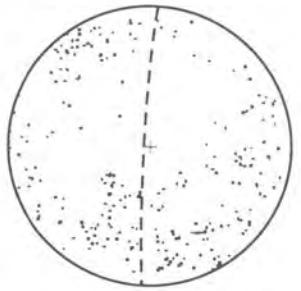

Stereonet showing all fractures measured within calc-silicate metasediments at Sullom, with the orientation of the WBFP at this locality (black dashed girdle 004/ 87 W) n = 263

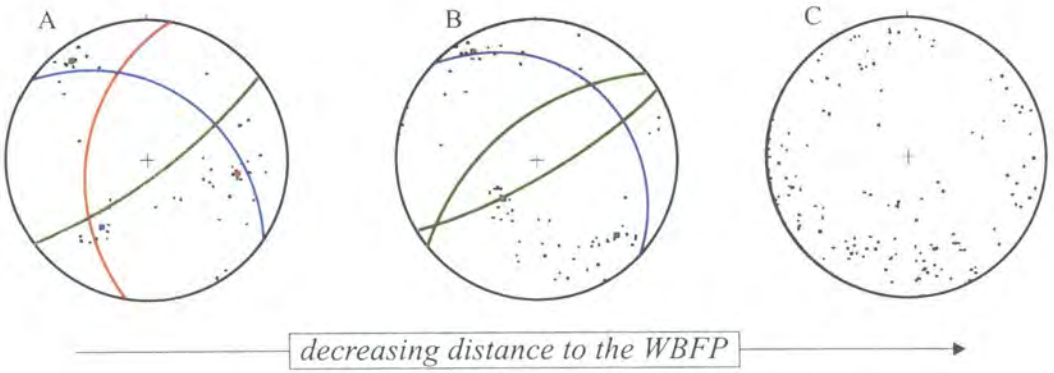

		Stereonet		
		A	B	C
	Place	Sullom	Sullom	Sullom
	Locality	SU3	SU4	SU12
	Distance to WBFP	245m	150m	15m
	no. data points	54	67	142
	lithology	calcareous meta-sediments		
	foliation orientation	130/ 50 N	131/ 47 N	174/ 84 E
fracture orientation clusters identified	foliation parallel (blue)	125/ 48 N	134/ 35 N	-
	WBFP parallel (red)	010/ 54 W	-	-
	other (green)	054/ 80 S	060/ 80 S 052/ 66 N	-

Figure 6.4 Fracture orientation data measured adjacent to the WBFP within calcareous metasediments
A - C = stereographic projections of fracture orientations (details of which are given in the table), from localities illustrated on the map

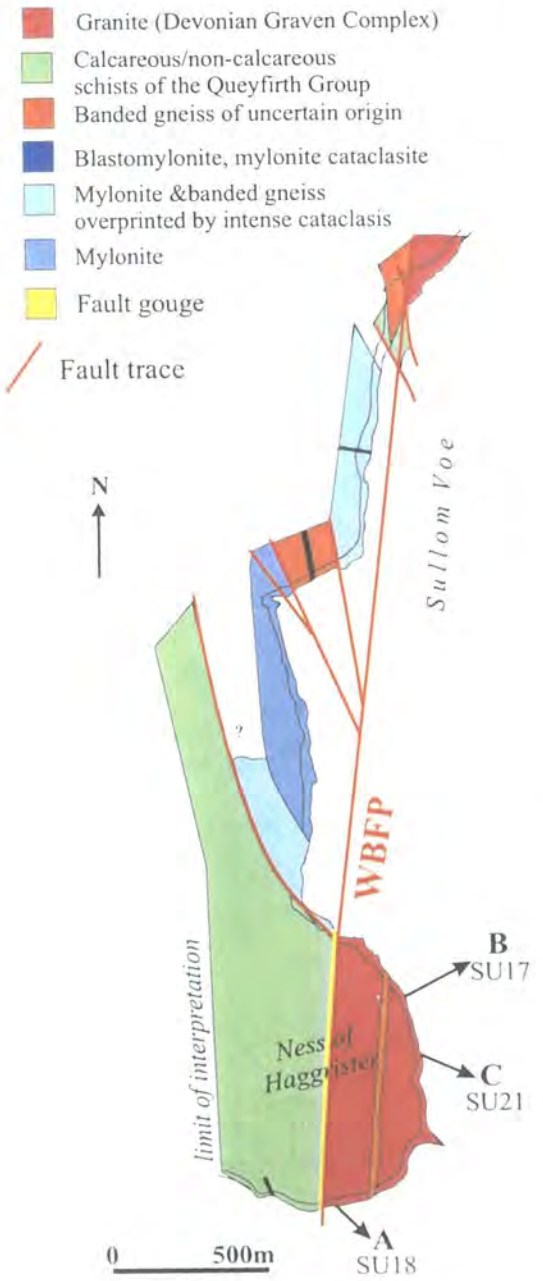

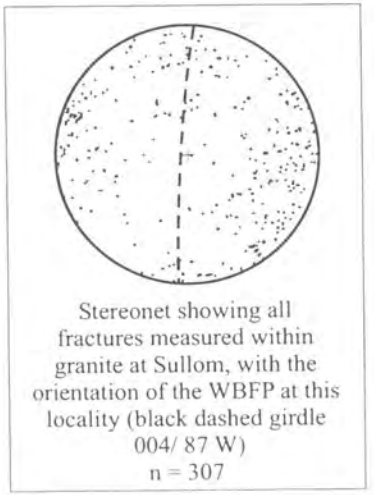

Stereonet showing all fractures measured within granite at Sullom, with the orientation of the WBFP at this locality (black dashed girdle 004/ 87 W)
n = 307

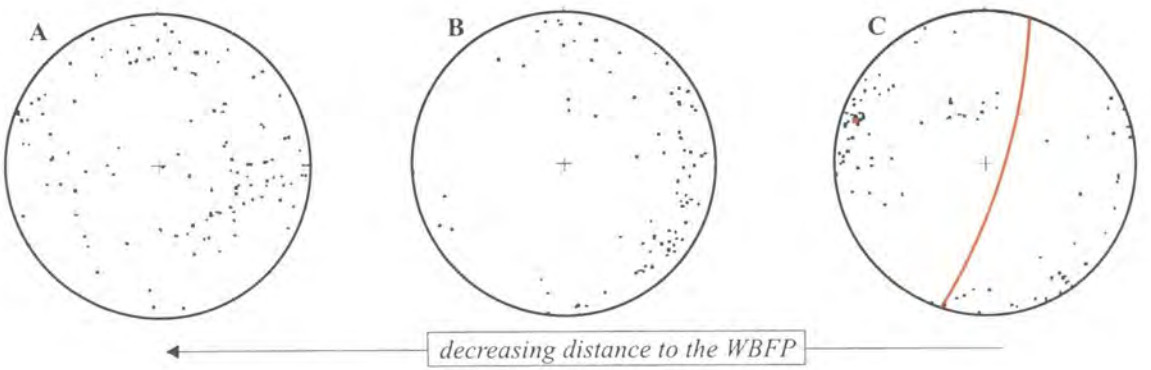

	Stereonets		
	A	B	C
Place	Sullom	Sullom	Sullom
Locality	SU18	SU17	SU21
Distance to WBFP	15m	225m	280m
no. data points	126	82	99
lithology	granite	granite	granite
fracture orientation clusters identified	none	none	018/ 80 E

Figure 6.5 Fracture orientation data measured adjacent to the WBFP within granite
A - C = stereographic projections of fracture orientations (details of which are given in the table), from localities illustrated on the map

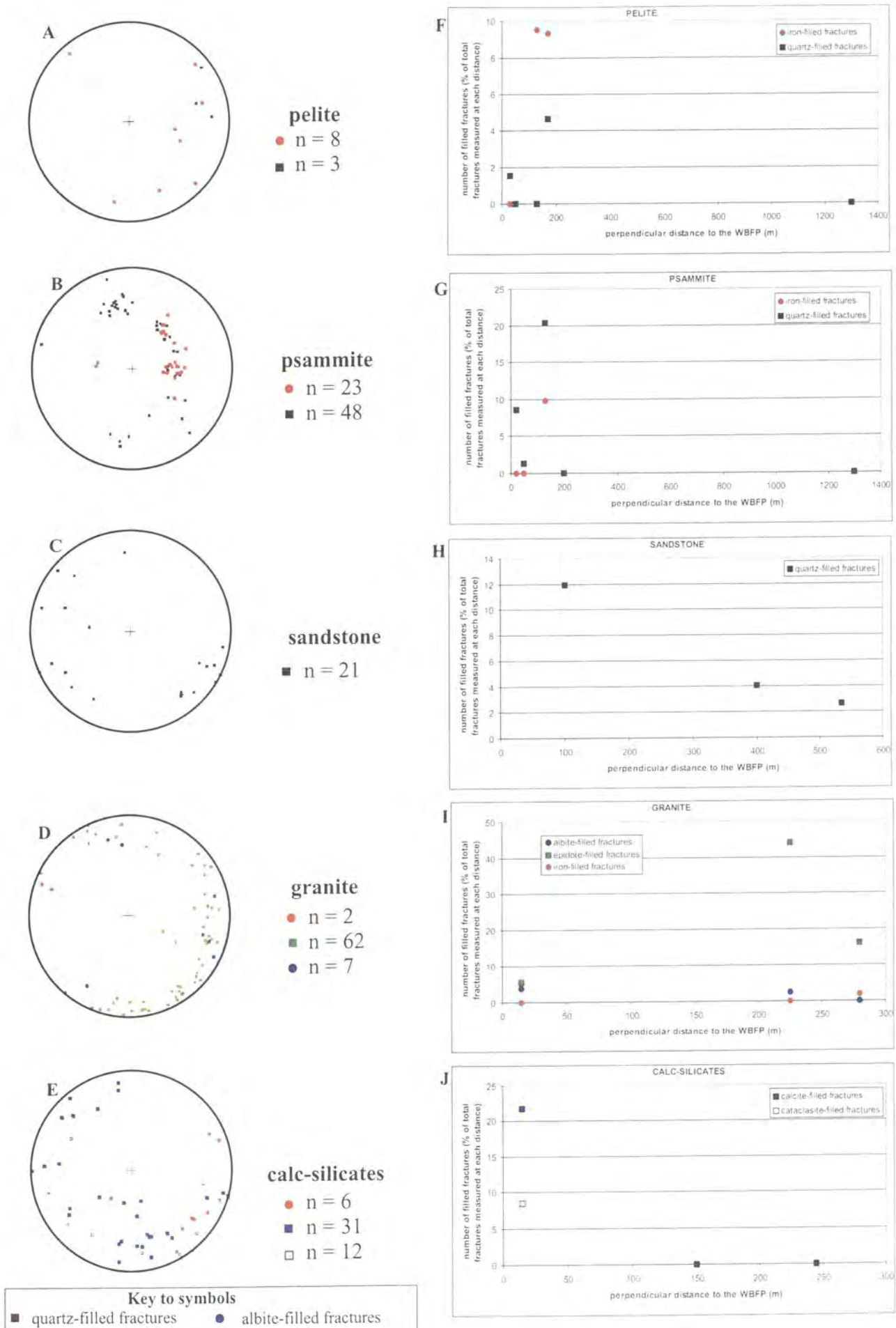

Figure 6.6 Filled-fractures recorded within lithologies adjacent to the WBFP
A - E = stereonets for each lithology, different infills identified
F - J = infill 'v' distance plots for each lithology

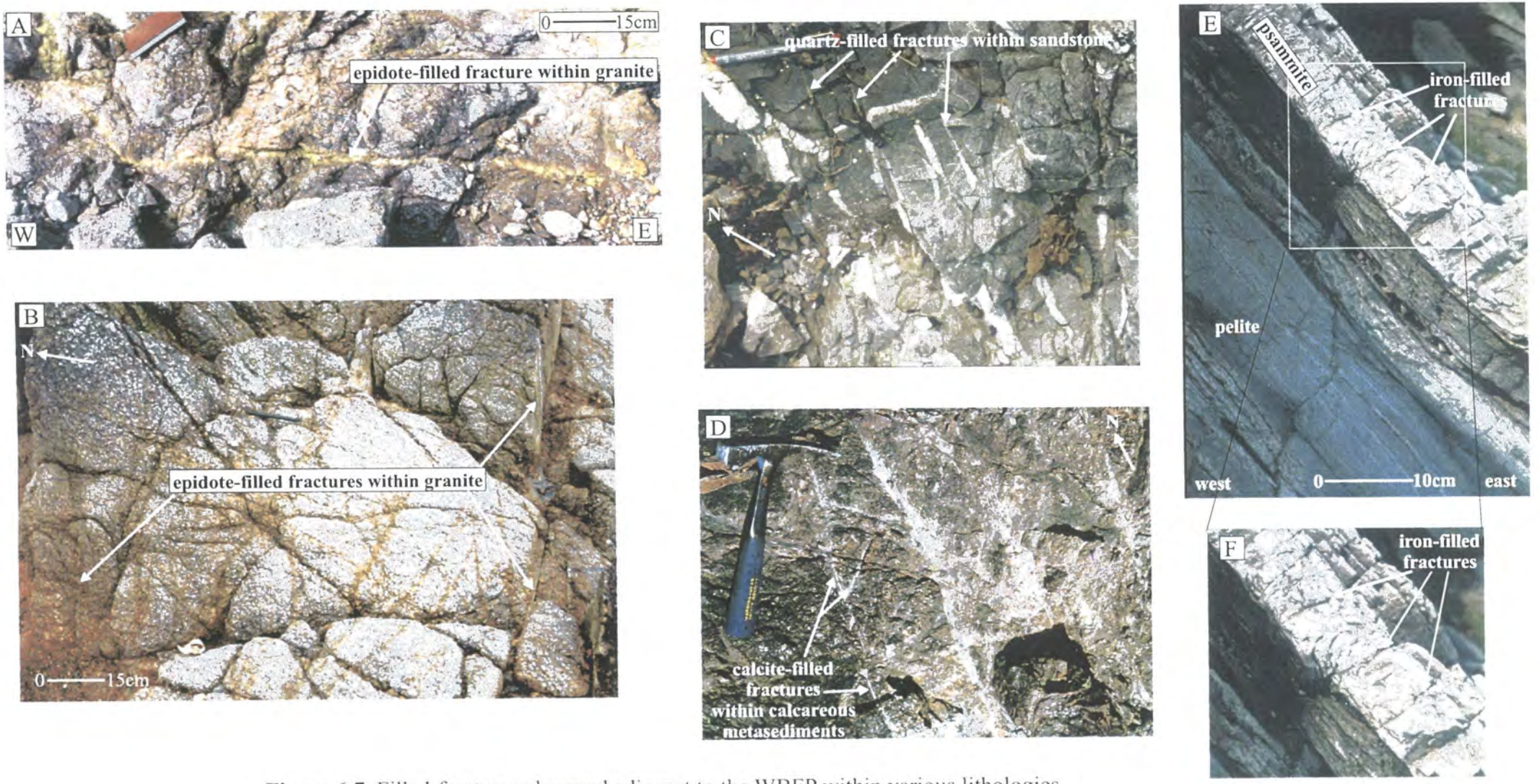

Figure 6.7 Filled-fractures observed adjacent to the WBFP within various lithologies
A & B - epidote-filled fractures within granite from Sullom localities
C - quartz-filled fractures within sandstone from Bixter locality
D - calcite-filled fractures within calcareous metasediments from Sullom locality
E & F - iron-filled fractures within psammite from Ollaberry locality
(A - D = plan view, E - F = sub-vertical surface)

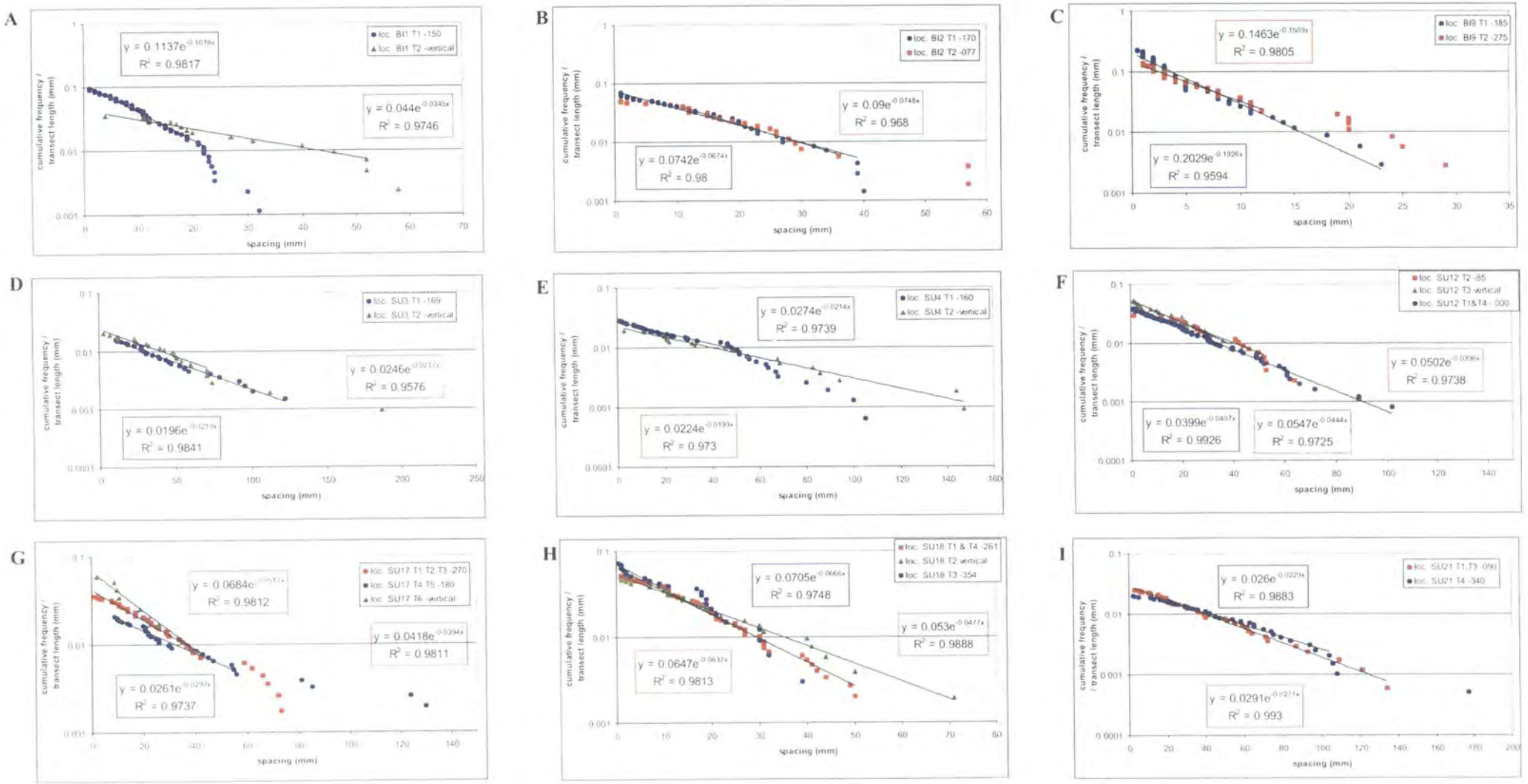

Figure 6.8 Cumulative frequency 'v' spacing plots for localities adjacent to the WBFP (continued on next 2 pages)

A - C = fractures measured within sandstone
D - F = fractures measured within calcareous metasediments
G - I = fractures measured within granite
J - O = fractures measured within psammite
P - U = fractures measured within pelite

blue data sets represent transects orientated parallel to the WBFP
red data sets represent transects orientated perpendicular to the WBFP
green data sets represent vertical transects

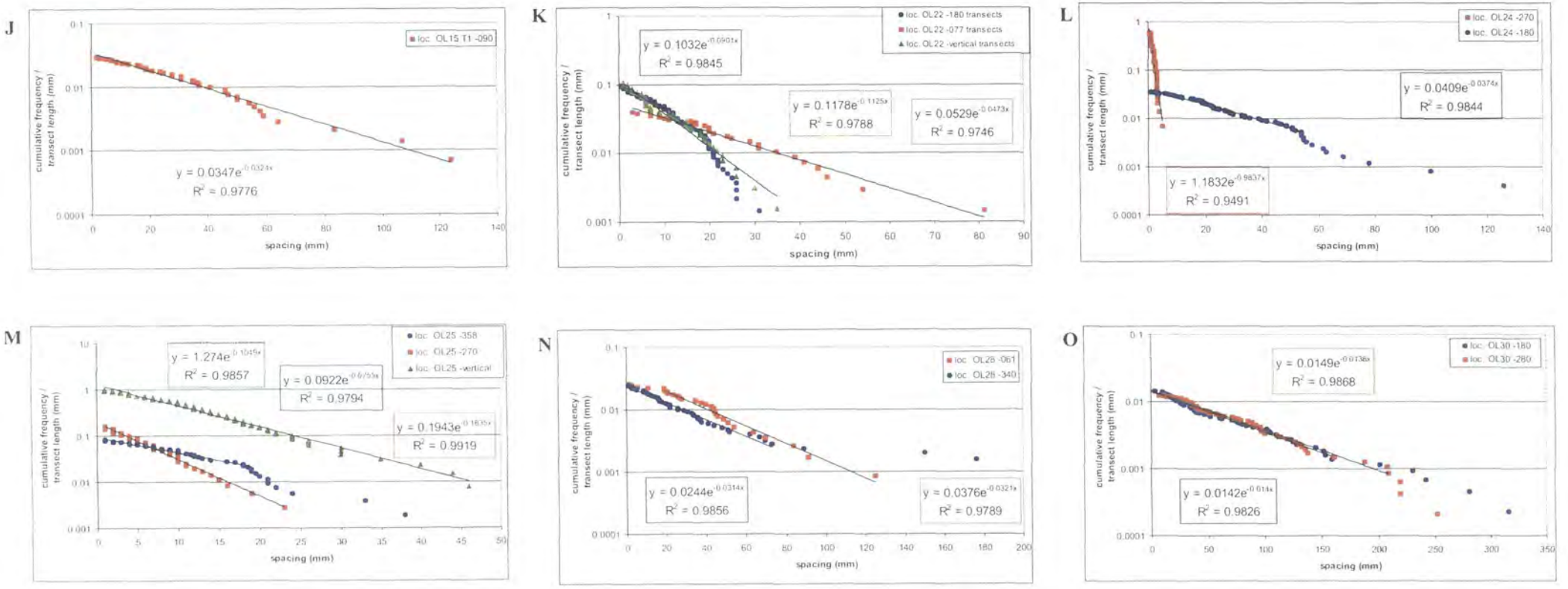

Figure 6.8 Cumulative frequency 'v' spacing plots for localities adjacent to the WBFP (continued from previous page and continued on next page)

A - C = fractures measured within sandstone
D - F = fractures measured within calcareous metasediments
G - I = fractures measured within granite
J - O = fractures measured within psammite
P - U = fractures measured within pelite

blue data sets represent transects orientated parallel to the WBFP
red data sets represent transects orientated perpendicular to the WBFP
green data sets represent vertical transects

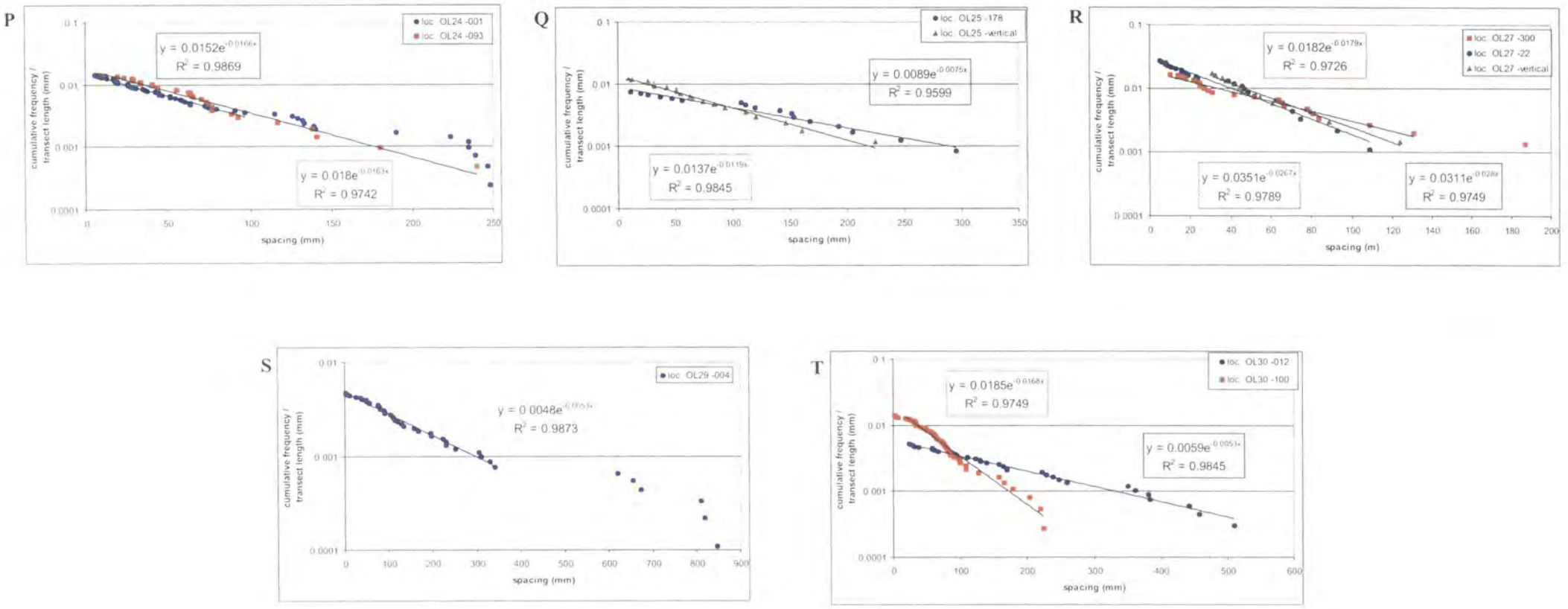

Figure 6.8 Cumulative frequency 'v' spacing plots for localities adjacent to the WBFP (continued from previous 2 pages)

A - C = fractures measured within sandstone
D - F = fractures measured within calcareous metasediments
G - I = fractures measured within granite
J - O = fractures measured within psammite
P - U = fractures measured within pelite

blue data sets represent transects orientated parallel to the WBFP
red data sets represent transects orientated perpendicular to the WBFP
green data sets represent vertical transects

a)

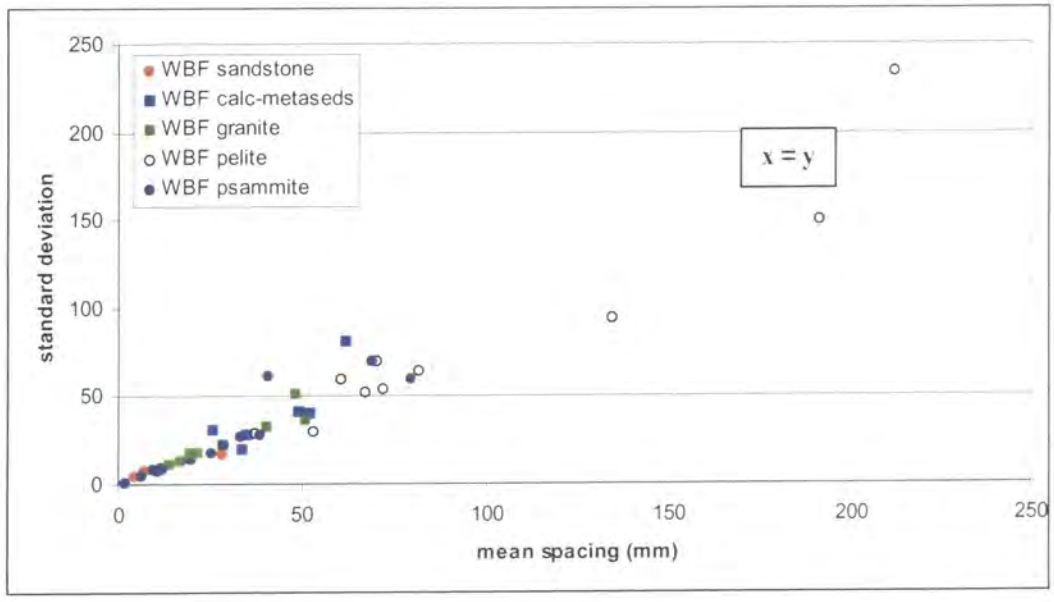

b)

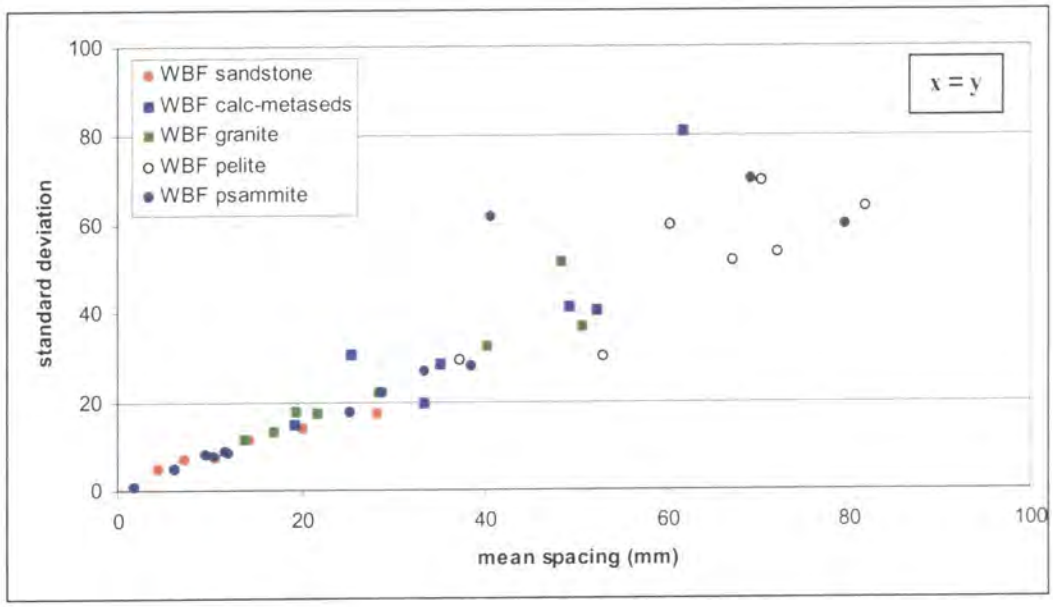

Figure 6.9 Mean spacing 'v' standard deviation plots (distinguished for different lithologies) for data collected adjacent to the WBFP.
A – all data sets, **B** – data sets with mean spacing values of 100mm or less.

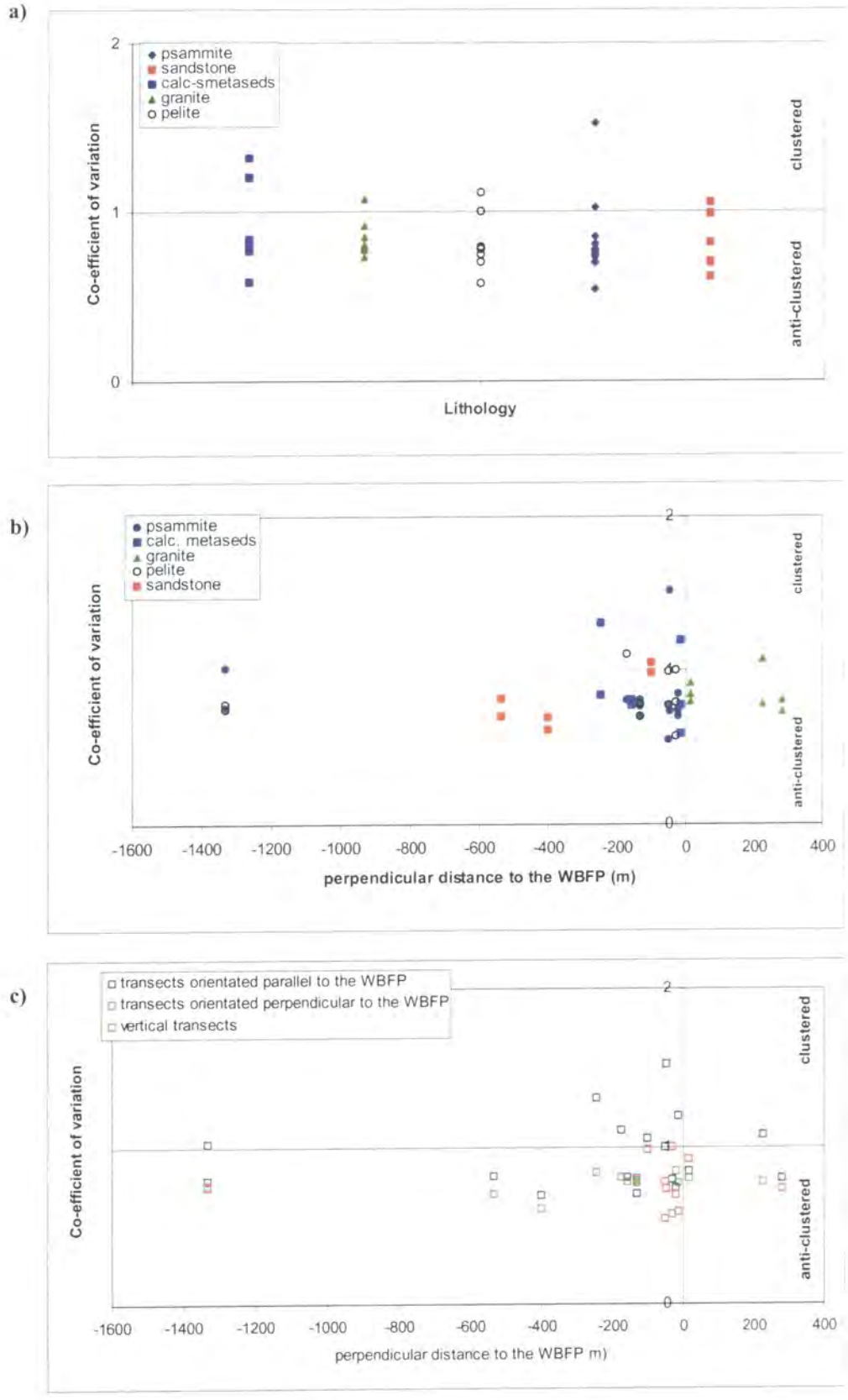

Figure 6.10 Co-efficient of variation (Cv) plots for data collected adjacent to the WBFP.
a) Cv values plotted for individual lithologies
b) Cv values plotted against perpendicular distance to the WBFP, distinguished for individual lithologies
c) Cv values plotted against perpendicular distance to the WBFP, distinguished for transect orientation

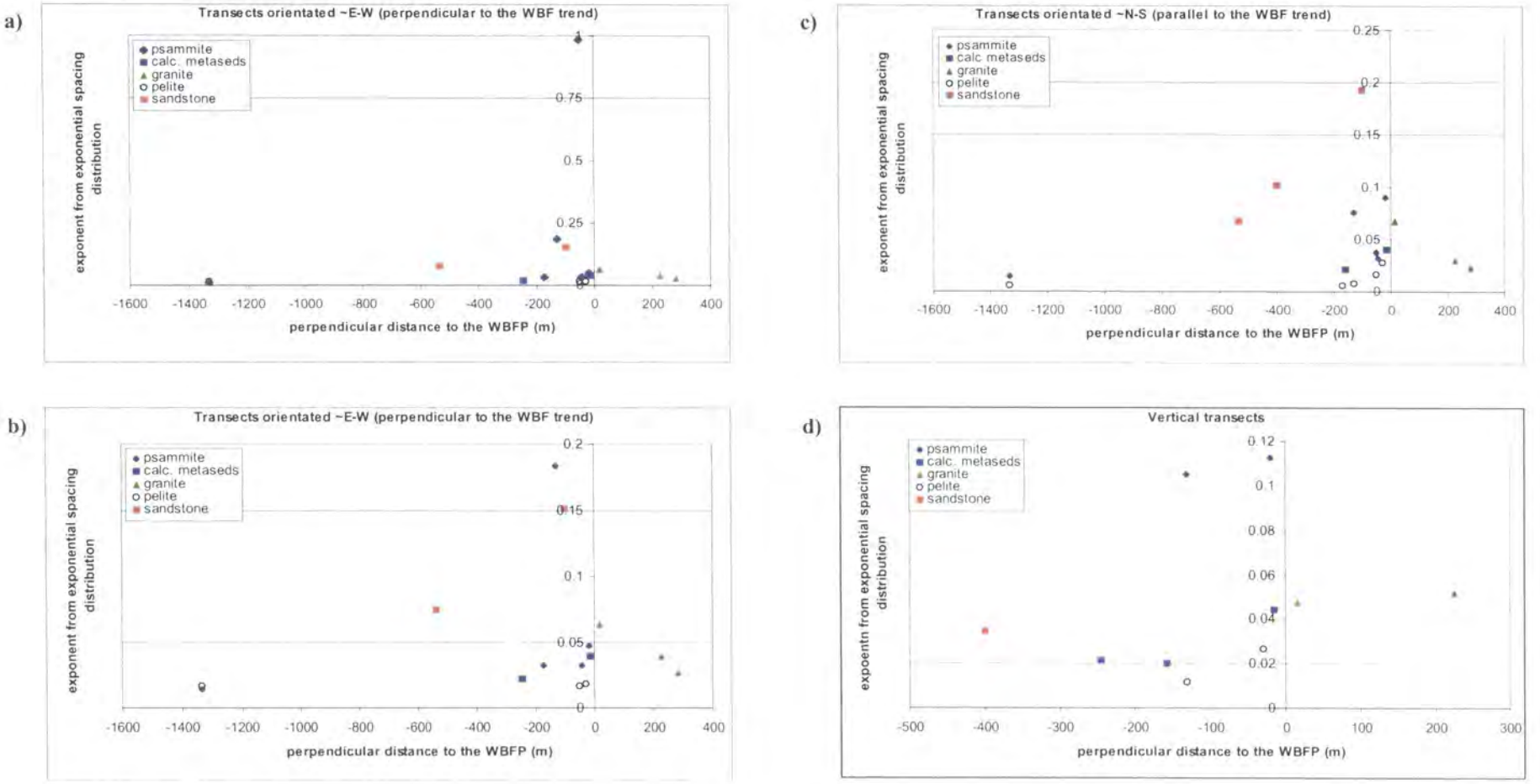

Figure 6.11 Exponent values from exponential data sets plotted against the perpendicular distance to the WBFP for different lithologies, and separated into different transect orientations.

a) – all exponent values from transects orientated perpendicular to the WBFP

b) – exponent values <0.2 from transects orientated perpendicular to the WBFP

c) – all exponent values from transects orientated parallel to the WBFP

d) – all exponent values from vertical transects

a)

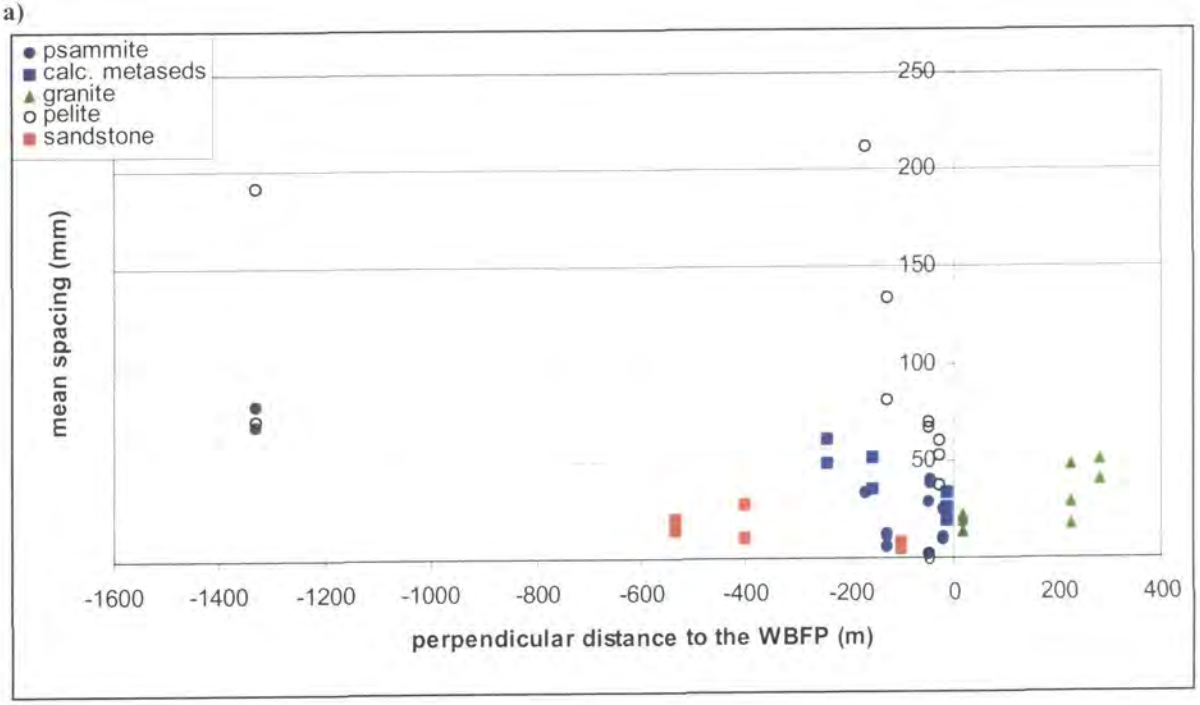

b)

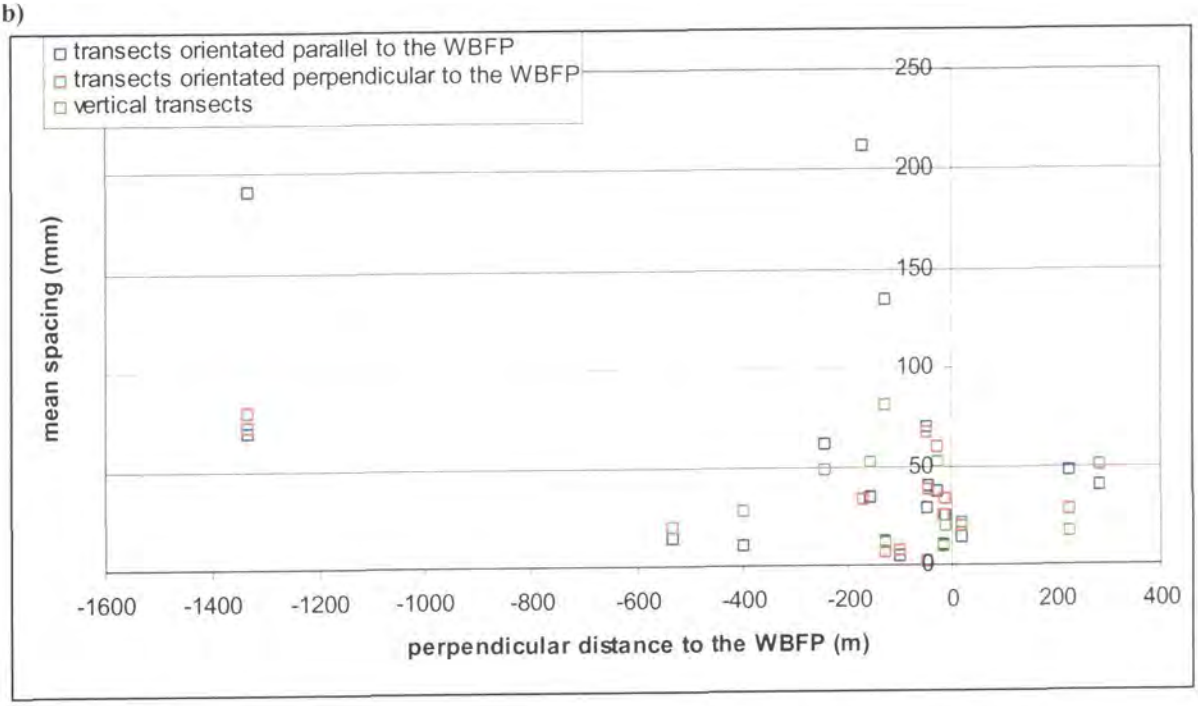

Figure 6.12 Mean fracture spacing (mm) 'v' perpendicular distance to the WBFP, data plotted by **a)** lithology and **b)** transect orientation

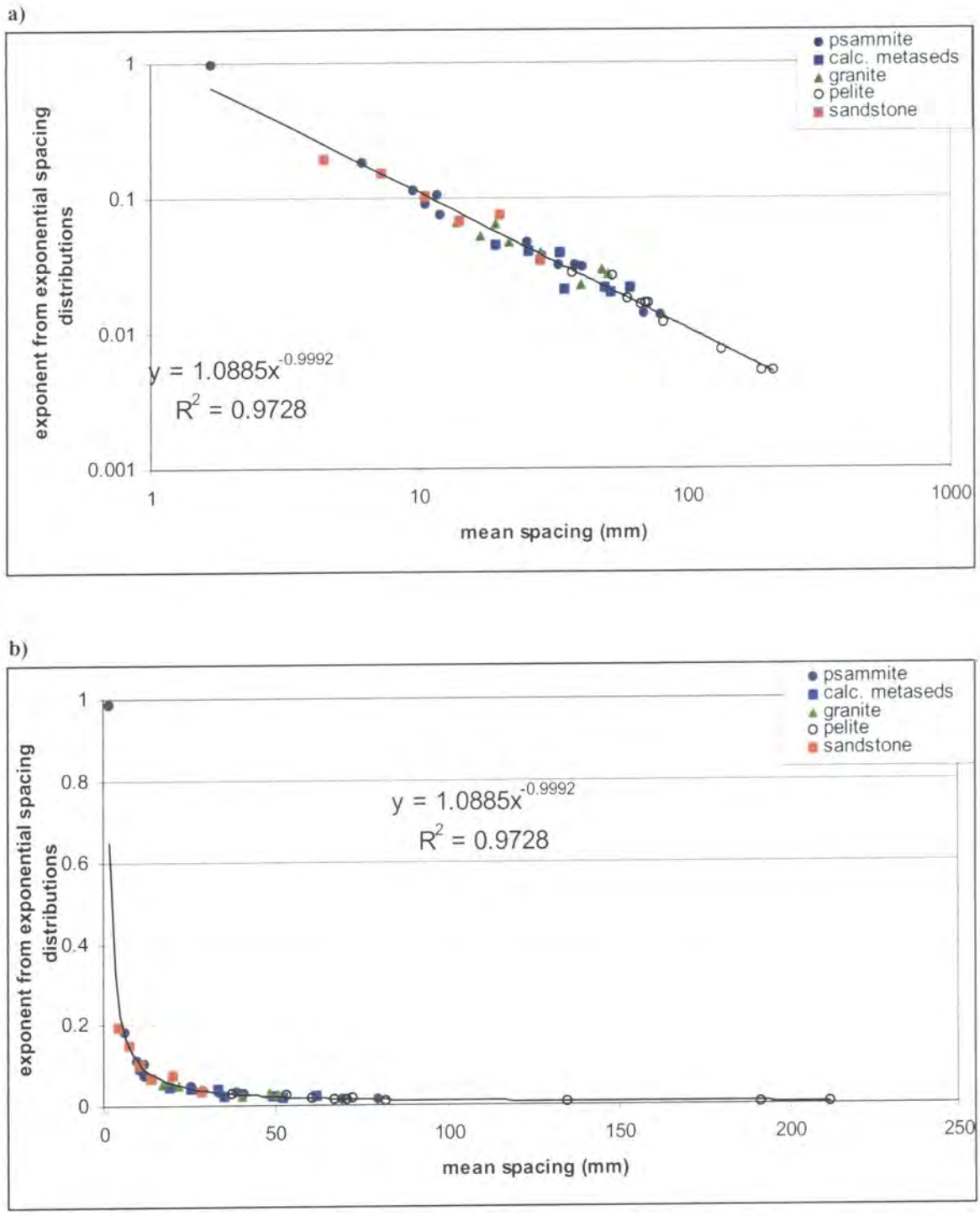

Figure 6.13 Mean spacing values plotted against exponent values from exponential spacing distributions, distinguished for lithology.
a) – data plotted on logarithmic axes, **b)** – data plotted on linear axes.

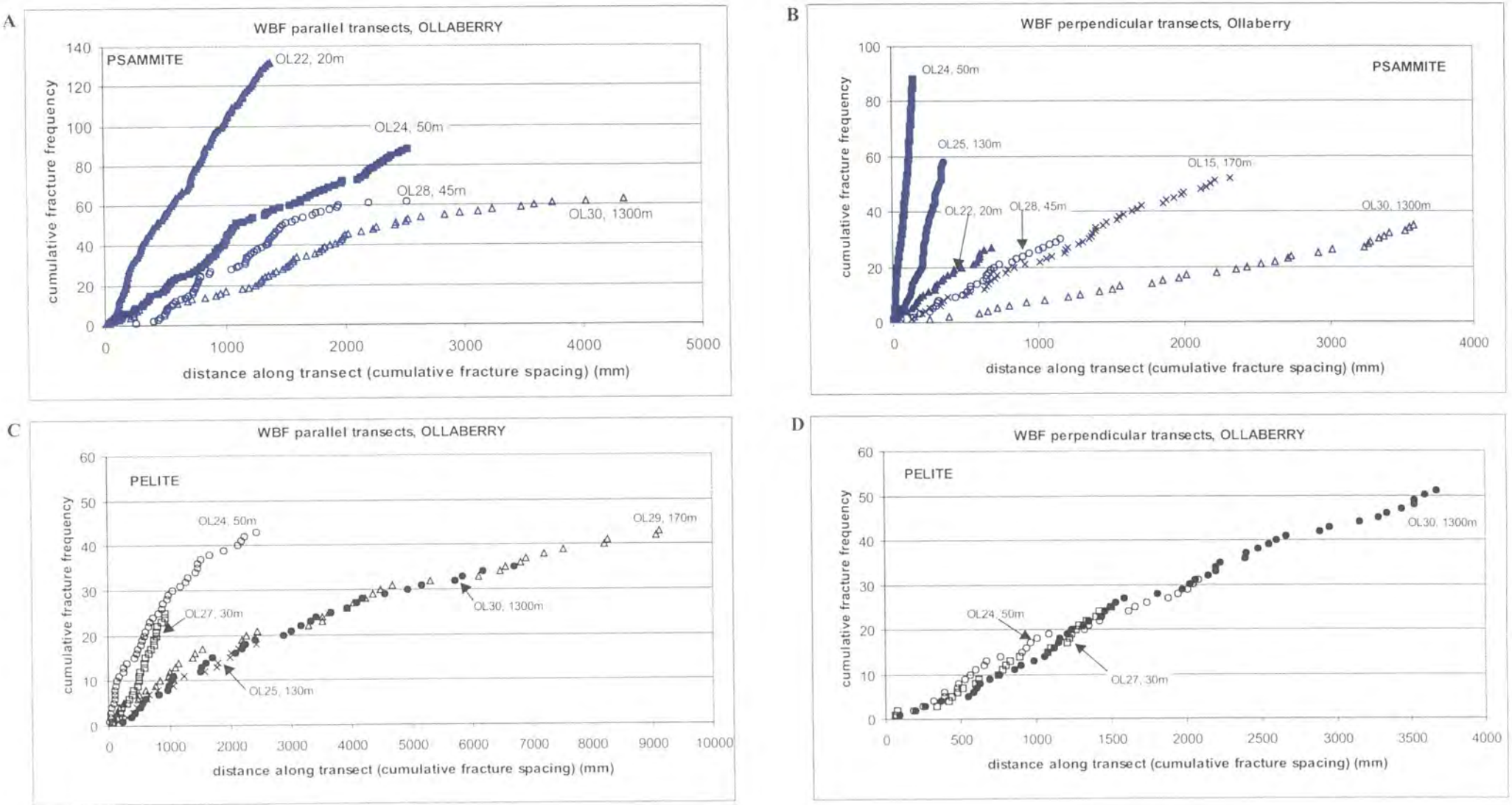

Figure 6.14 Cumulative fracture frequency 'v' distance along 1-dimensional line transects measured both parallel and perpendicular to the WBFP. Data sets are separated by lithology and transect orientation. Each transect is labelled with the locality name and distance to the WBFP.
A& B = psammite, **C&D** = pelite, **E&F** = sandstone, **F&H** = calcareous metasediments and granite.
A, C, E & G = transects orientated parallel to the WBFP, **B, D, F & H** = transects orientated perpendicular to the WBFP

(continued on next page)

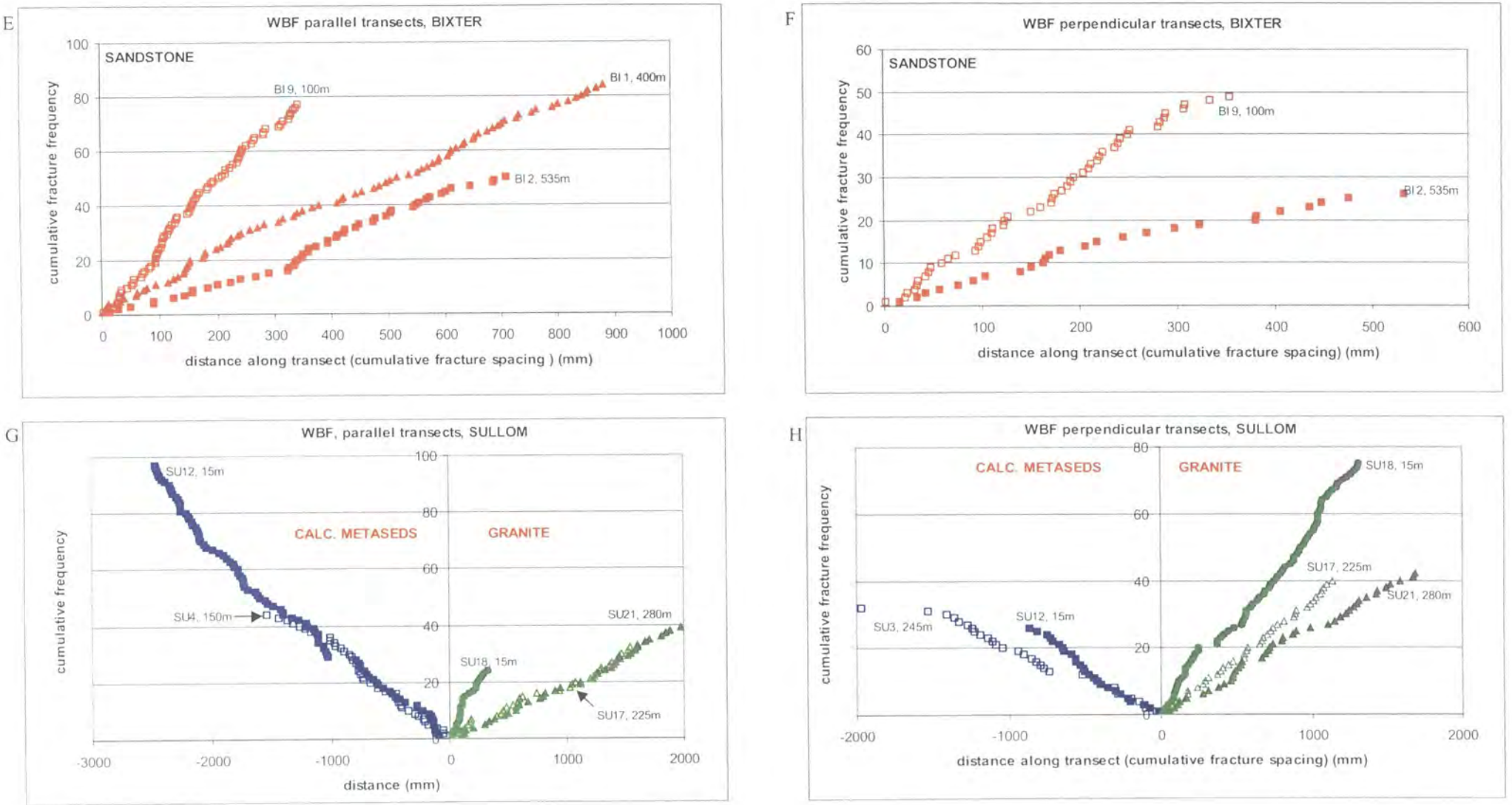

Figure 6.14 Cumulative fracture frequency 'v' distance along 1-dimensional line transects measured both parallel and perpendicular to the WBFP. Data sets are separated by lithology and transect orientation. Each transect is labelled with the locality name and distance to the WBFP.
A& B = psammite, **C&D** = pelite, **E&F** = sandstone, **F&H** = calcareous metasediments and granite.
A, C, E & G = transects orientated parallel to the WBFP, **B, D, F & H** = transects orientated perpendicular to the WBFP

(continued from previous page)

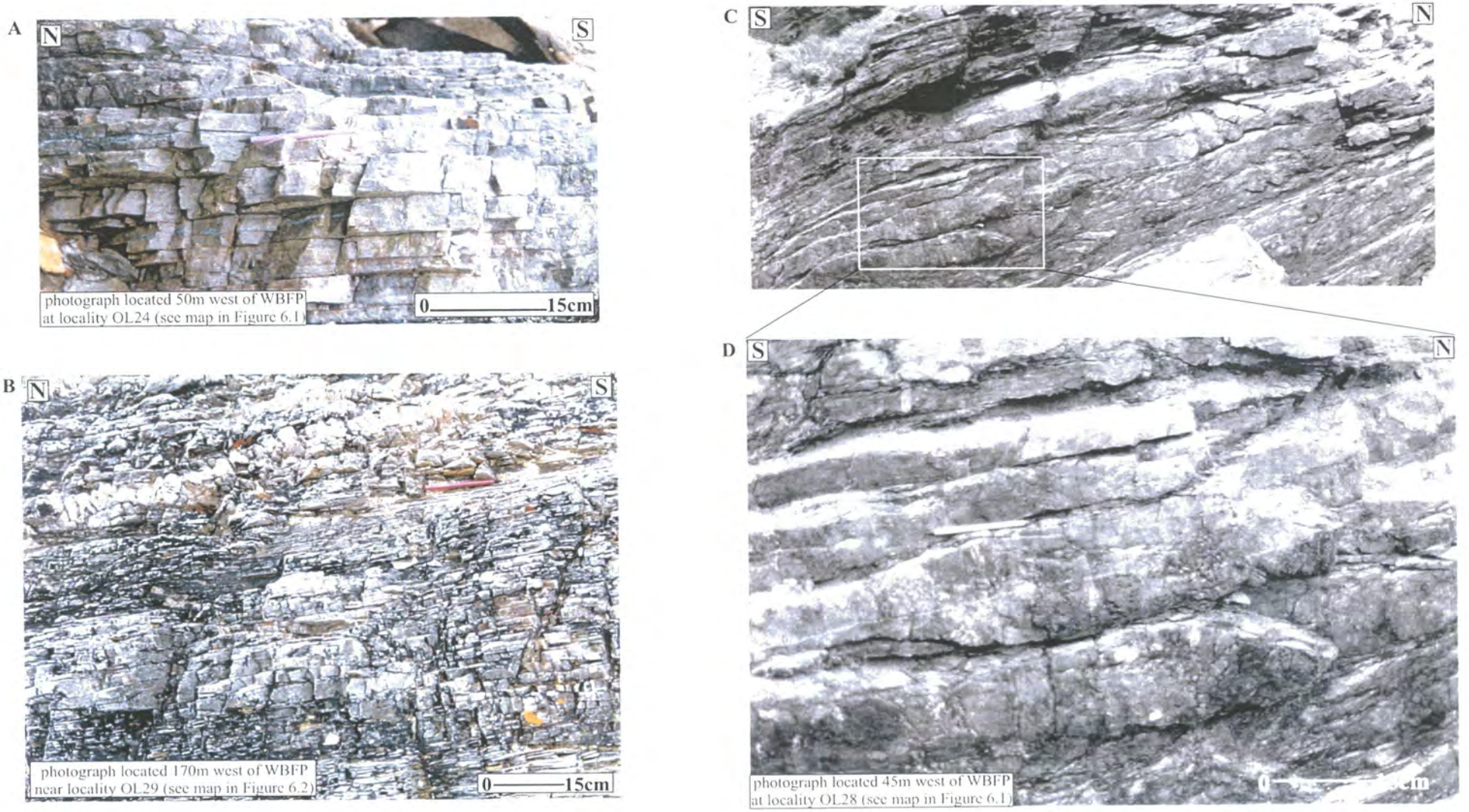

Figure 6.15 Fault-parallel fractures observed adjacent to the WBFP at Ollaberry within psammite
A & B illustrate closely spaced fault-parallel fractures located 50m and 170m west of the WBFP respectively
C & D illustrate wider spaced and more irregular fault-parallel fractures located 45m west of the WBFP

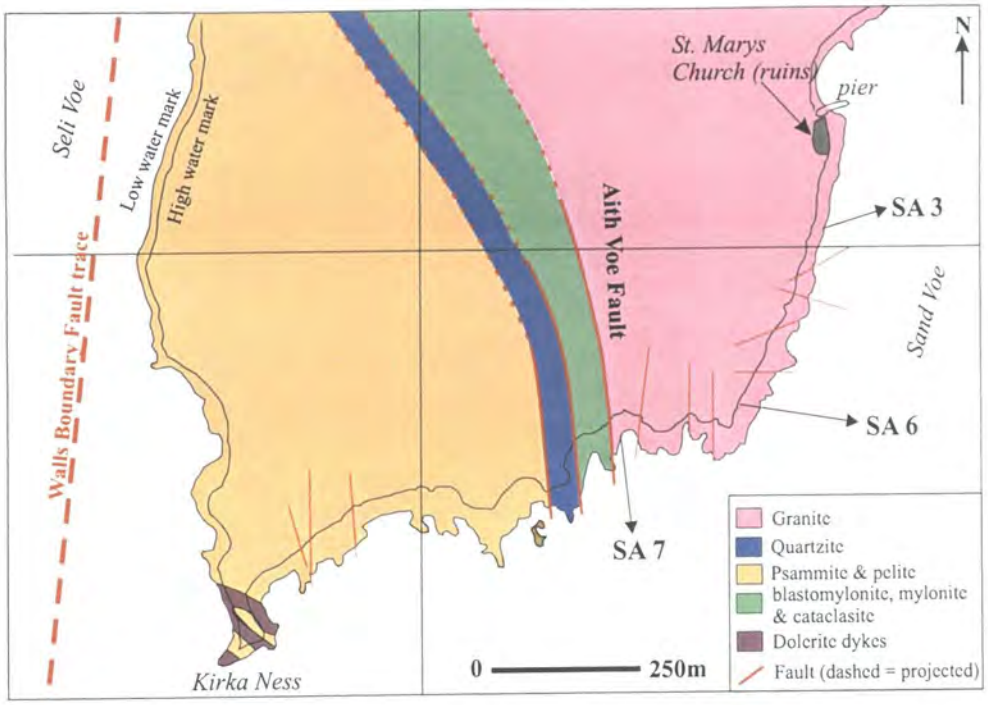

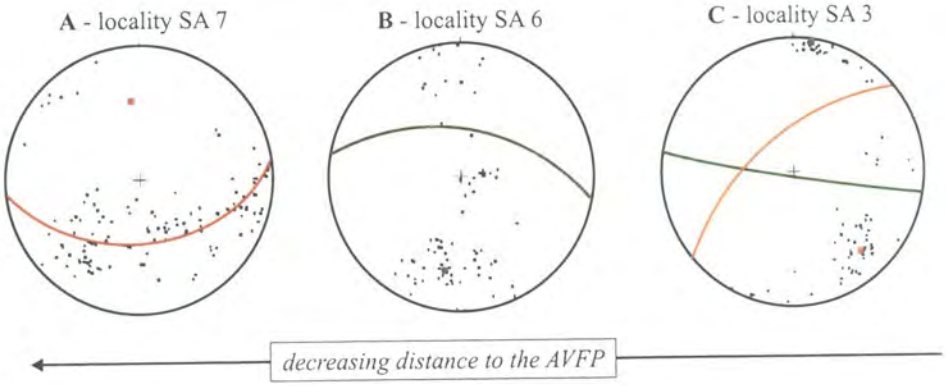

	Stereonets		
	A	B	C
Place	Sand	Sand	Sand
Locality	SA 7	SA 6	SA 3
Distance to WBFP	15m	240m	400m
no. data points	129	73	75
lithology	granite	granite	granite
fracture orientation clusters identified	poles to fracture planes lie on a girdle orientated 084/ 50 S	100/ 60 N	050/ 67 N 099/ 88 S

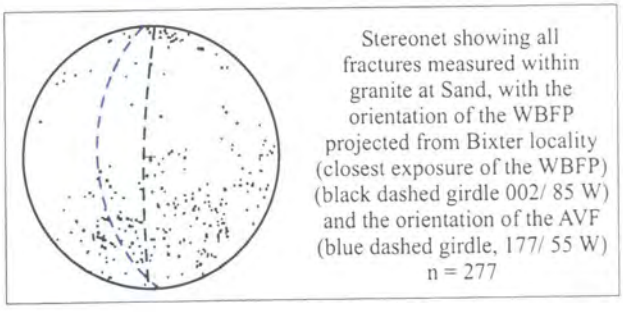

Stereonet showing all fractures measured within granite at Sand, with the orientation of the WBFP projected from Bixter locality (closest exposure of the WBFP) (black dashed girdle 002/ 85 W) and the orientation of the AVF (blue dashed girdle, 177/ 55 W) n = 277

Figure 6.16 Fracture orientation data collected from localities adjacent to the Aith Voe Fault Plane

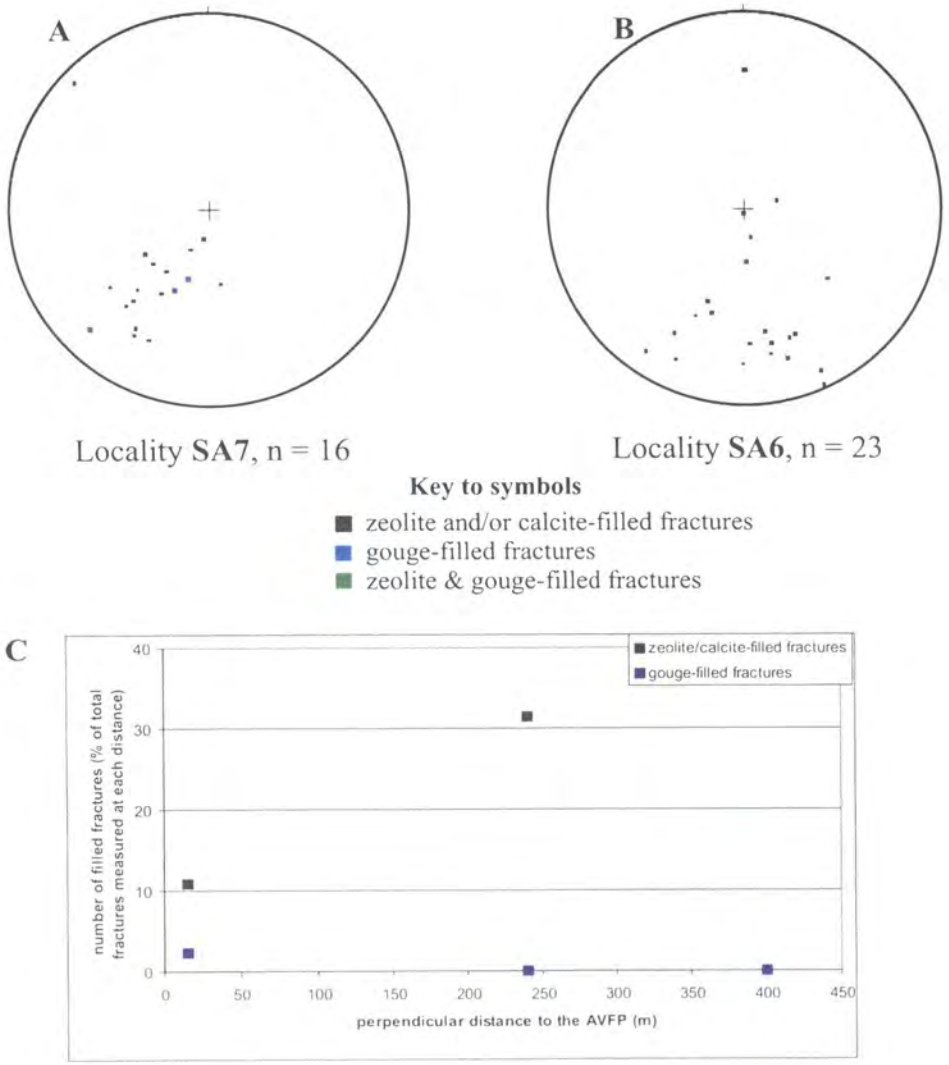

Figure 6.17 Filled-fractures observed adjacent to the AVF
A - stereonet from locality SA7
B - stereonet from locality SA6
C - Percentage of filled fractures at different distances to the AVFP

Figure 6.18 Zeolite-filled fractures observed adjacent to the AVFP at locality SA 7.

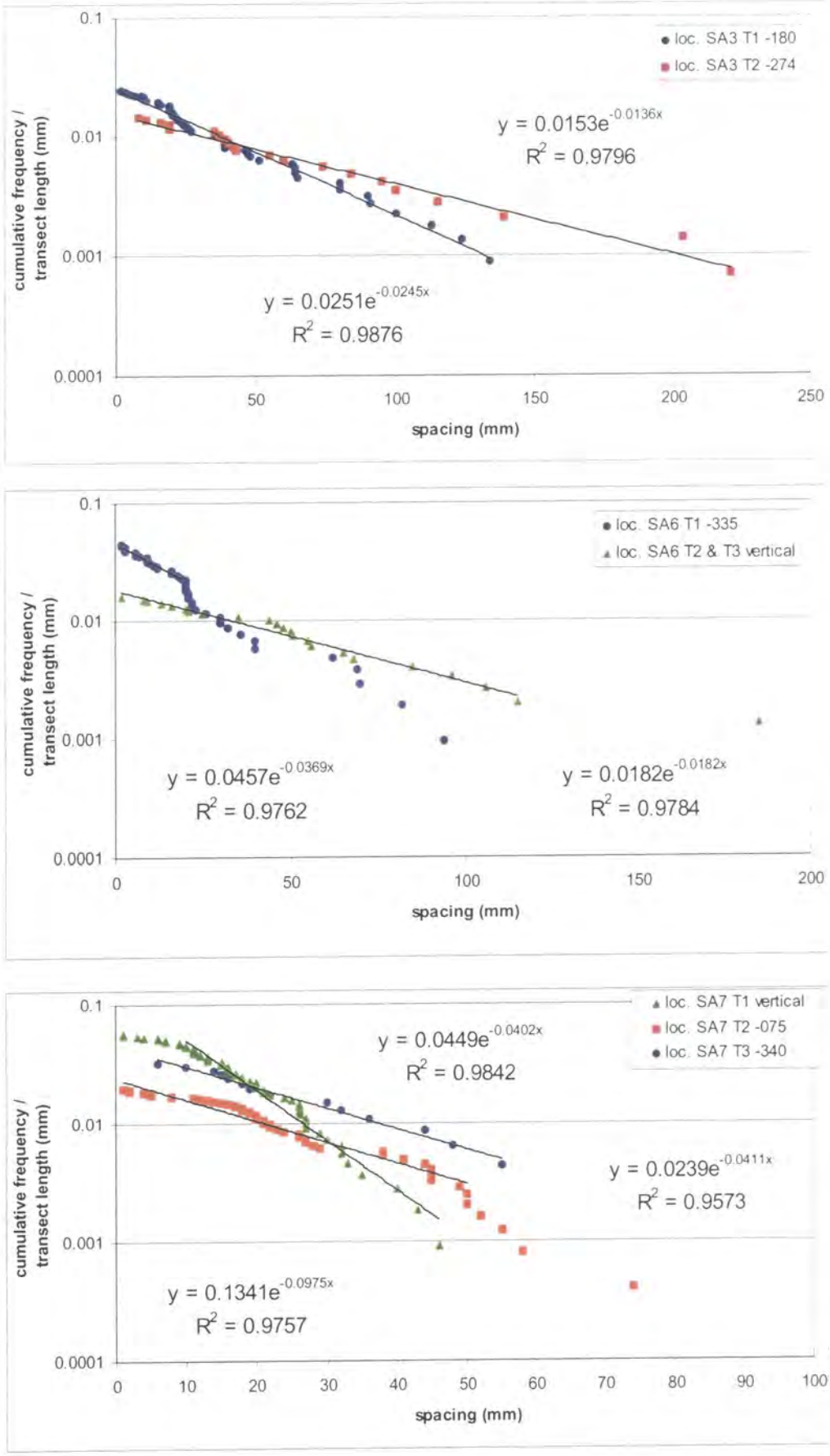

Figure 6.19 Cumulative frequency 'v' spacing plots for localities adjacent to the AVFP (blue data sets = transects parallel to the AVFP, red data sets = transects perpendicular to the AVFP, green data sets = vertical transects).

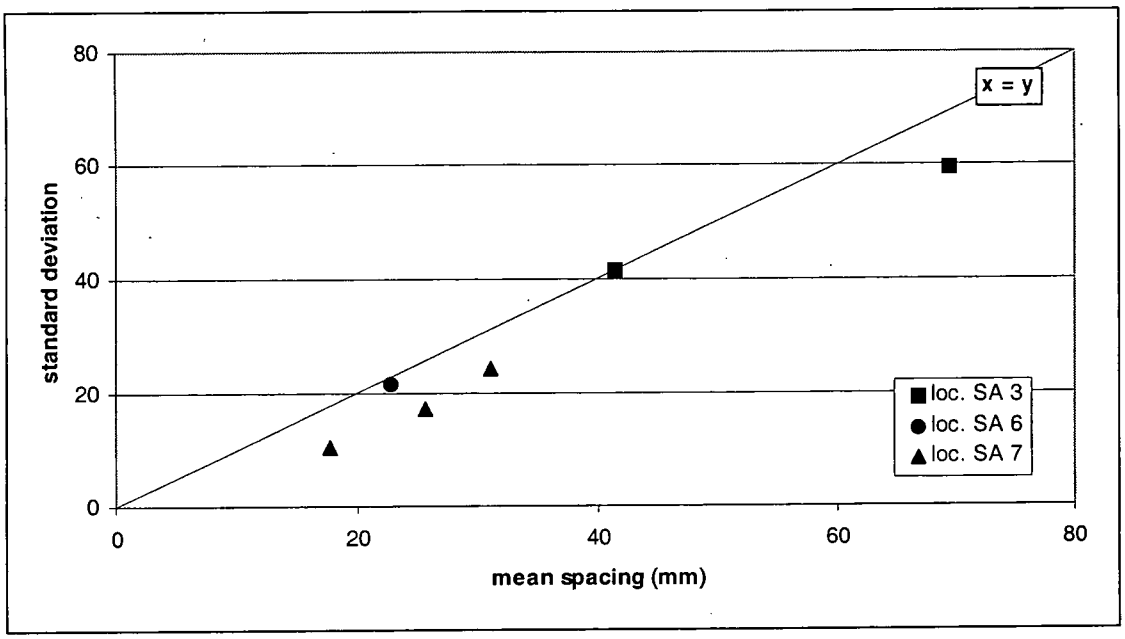

Figure 6.20 Mean spacing values 'v' standard deviation from data sets collected adjacent to the AVFP.

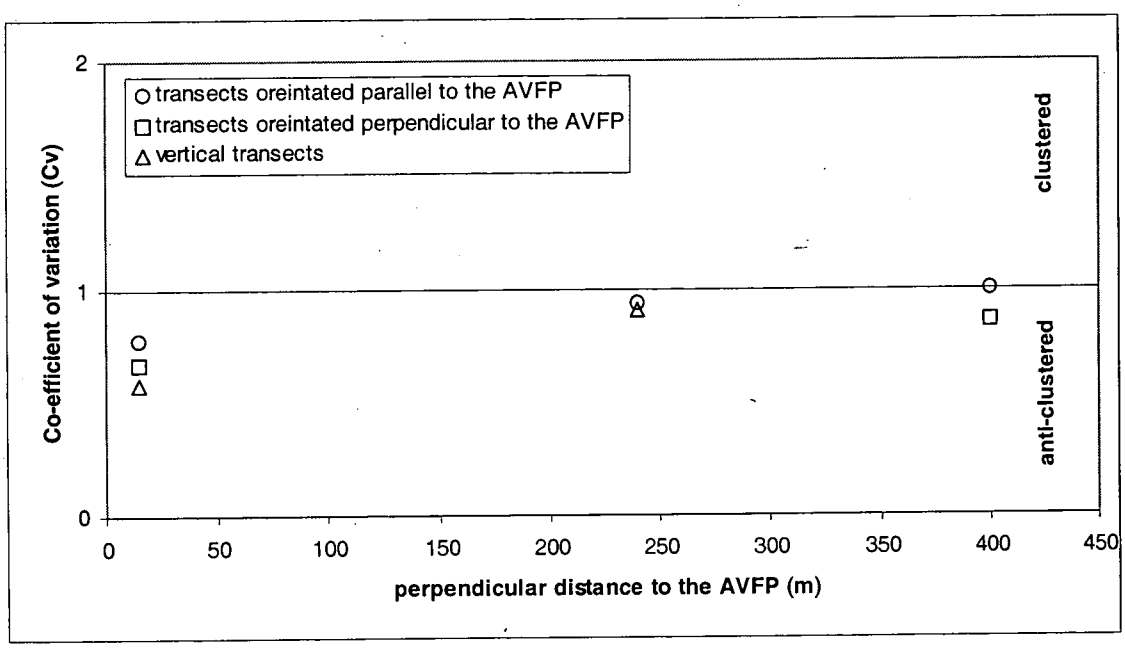

Figure 6.21 Co-efficient of variation values (Cv) 'v' perpendicular distance to the AVFP for data sets collected adjacent to the AVFP.

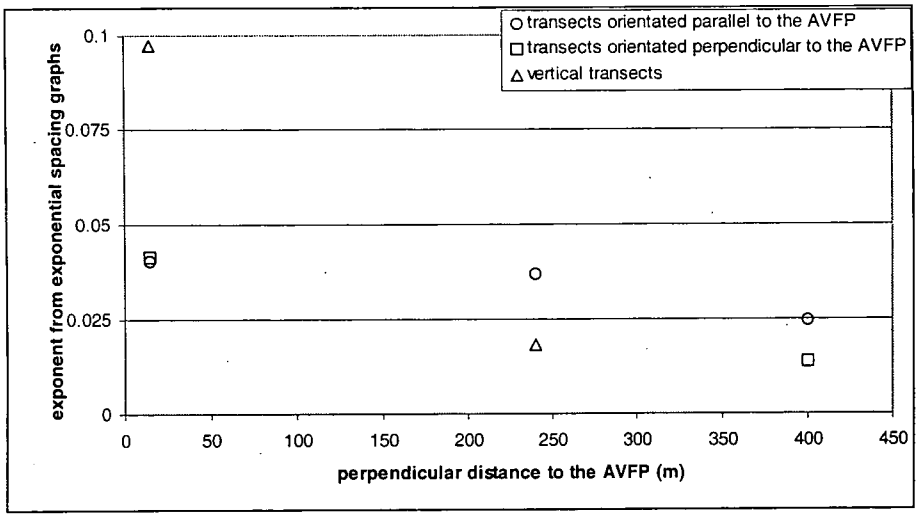

Figure 6.22 Exponential exponent values from spacing graphs 'v' perpendicular distance to the AVFP, for data sets collected adjacent to the AVFP.

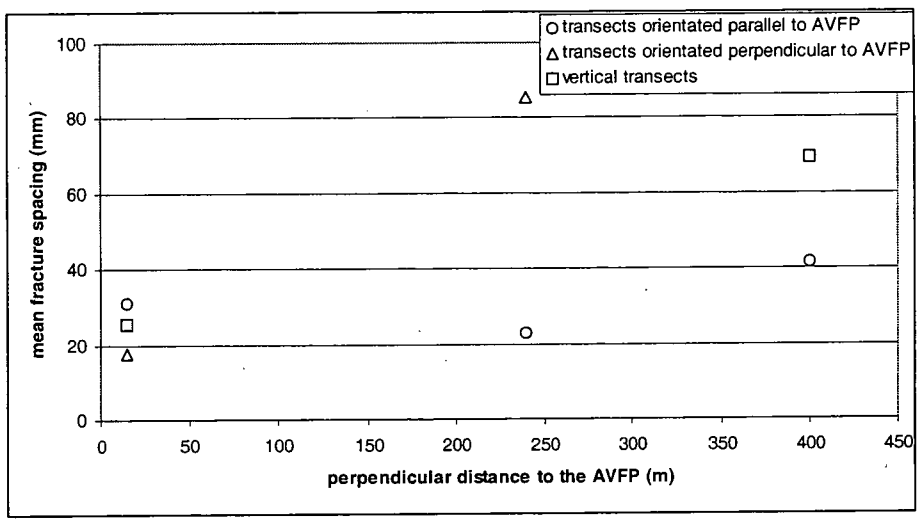

Figure 6.23 Mean spacing values 'v' perpendicular distance to the AVFP.

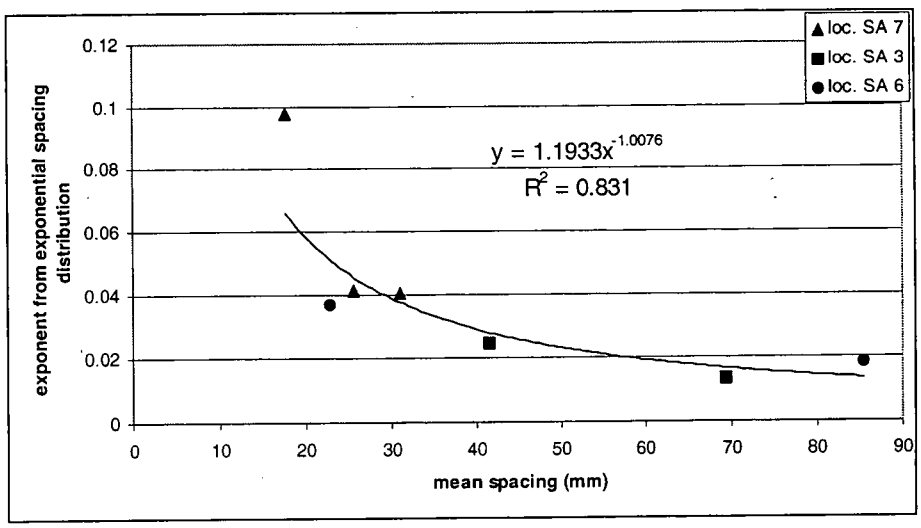

Figure 6.24 Mean spacing 'v' exponential exponent values from data sets collected adjacent to the AVFP.

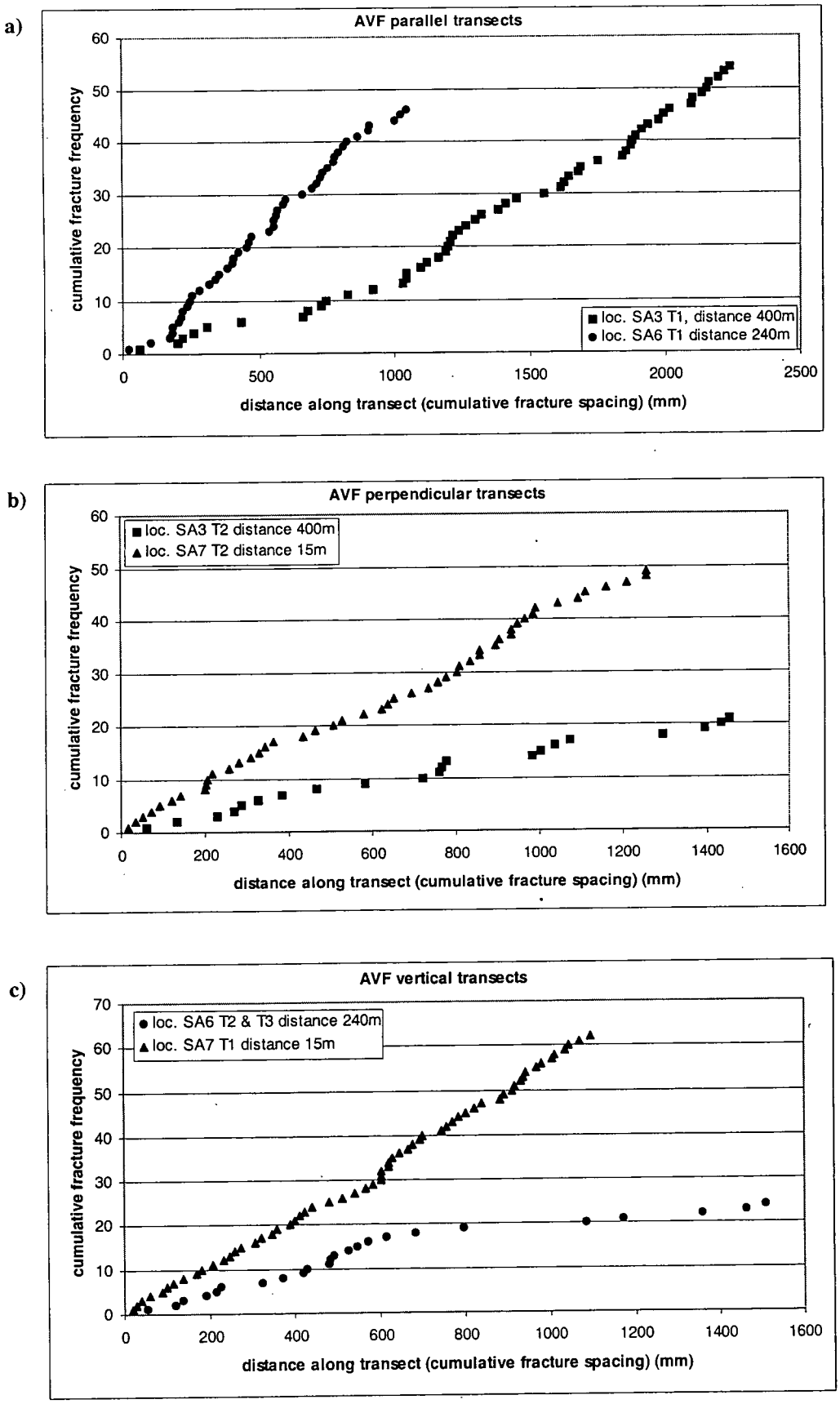

Figure 6.25 Cumulative frequency 'v' distance along 1-dimensional line transects carried out adjacent to the AVFP within granite.
a) transects orientated parallel to the AVFP, **b**) transects orientated perpendicular to the AVFP, **c**) vertical transects

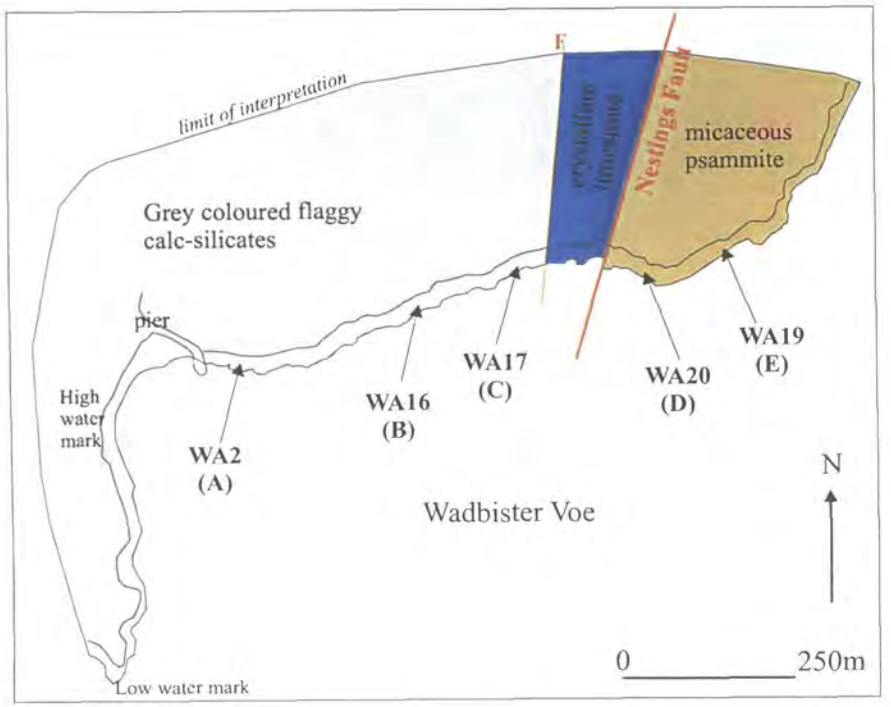

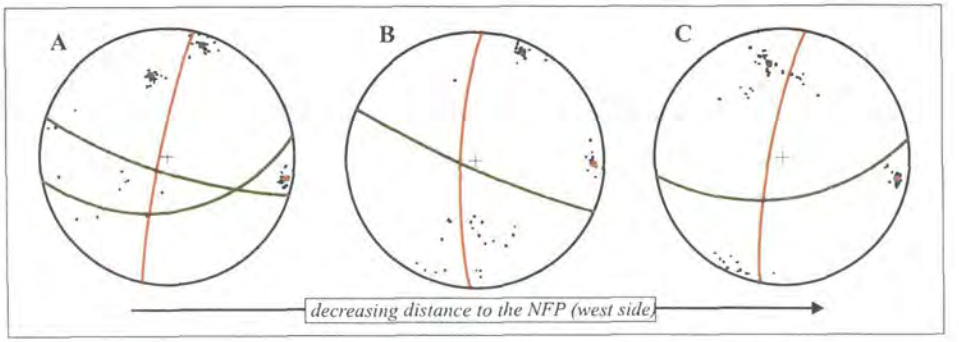

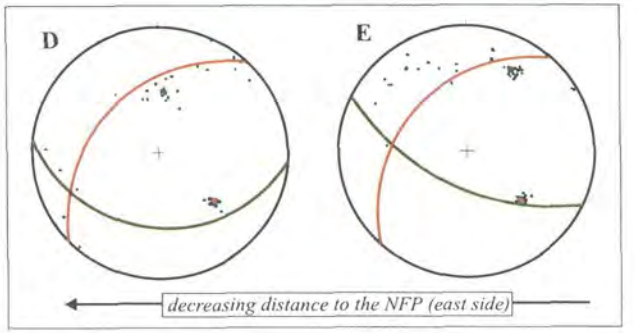

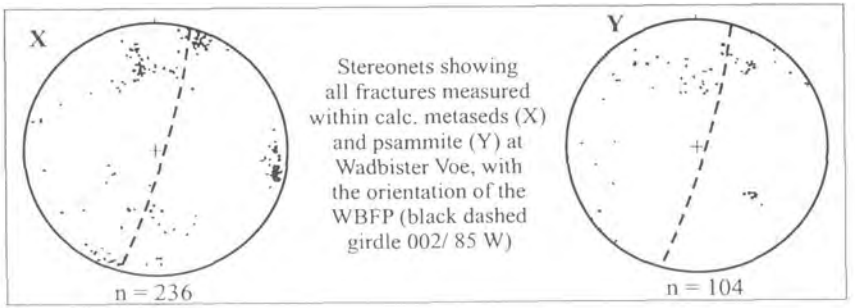

		Stereonets				
		A	B	C	D	E
Place		Wadbister Voe	Wadbister Voe	Wadbister Voe	Wadbister Voe	Wadbister Voe
Locality		WA2	WA16	WA17	WA20	WA19
Distance to NFP		520m	235m	70m	150m	50m
Number of data points		71	94	71	46	59
lithology		calcareous metasediments	calcareous metasediments	calcareous metasediments	psammite	psammite
foliation orientation		012/ 78 W	002/ 79 W	010/ 87 W	046/ 59 NW	041/ 49 NW
fracture orientation clusters identified	foliation parallel (RED)	012/ 85 W	003/ 80 W	011/ 81 W	045/ 48 NW	043/ 47 NW
	~ E-W (GREEN)	080/ 54 S 108/ 79 S	114/ 84 S	082/ 63 S	096/ 40 S	116/ 66 S

Figure 6.26 Fracture orientation data collected adjacent to the Nestings Fault Plane

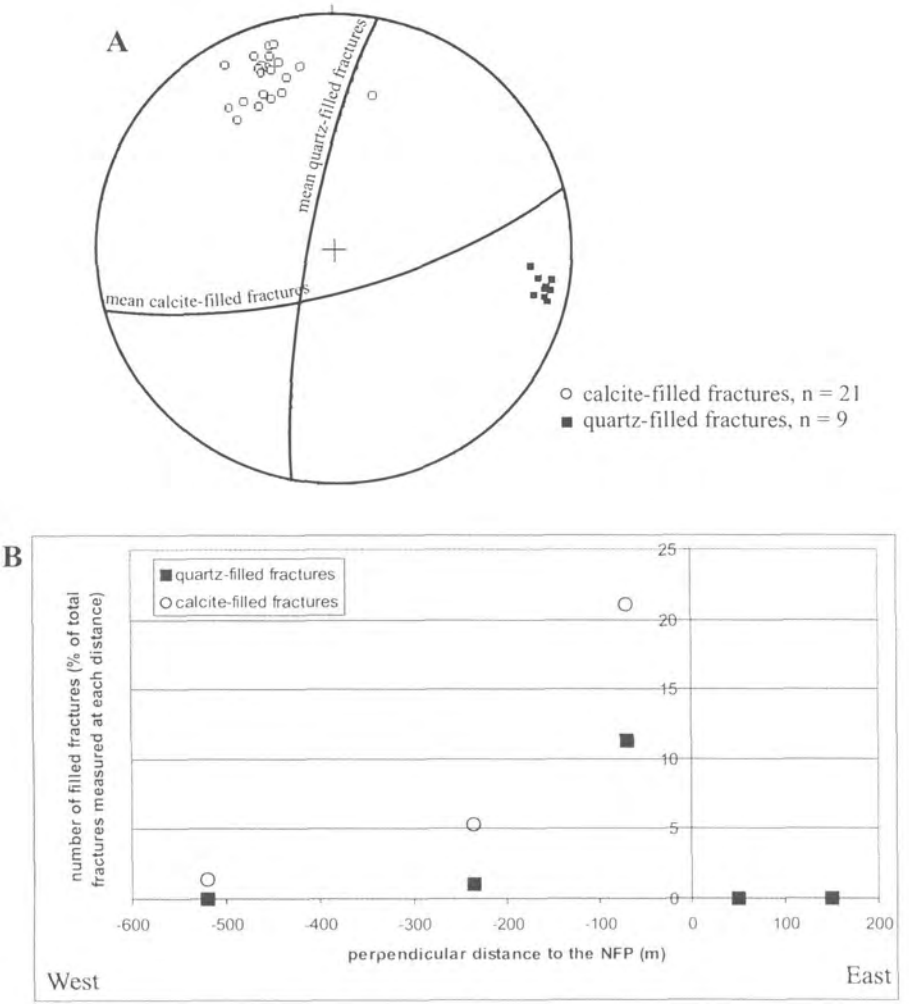

Figure 6.27 Filled fractures within calcareous metasediments to the west of the Nestings Fault Plane, on the northern shore of Wadbister Voe.
A - stereonet showing N-S fractures filled with quartz and ENE-WSW fractures filled with calcite
B - percentage of filled fractures 'v' distance plot
C - photograph illustrating N-S quartz-filled fractures
D - photograph illustrating ENE-WSW calcite-filled fracture

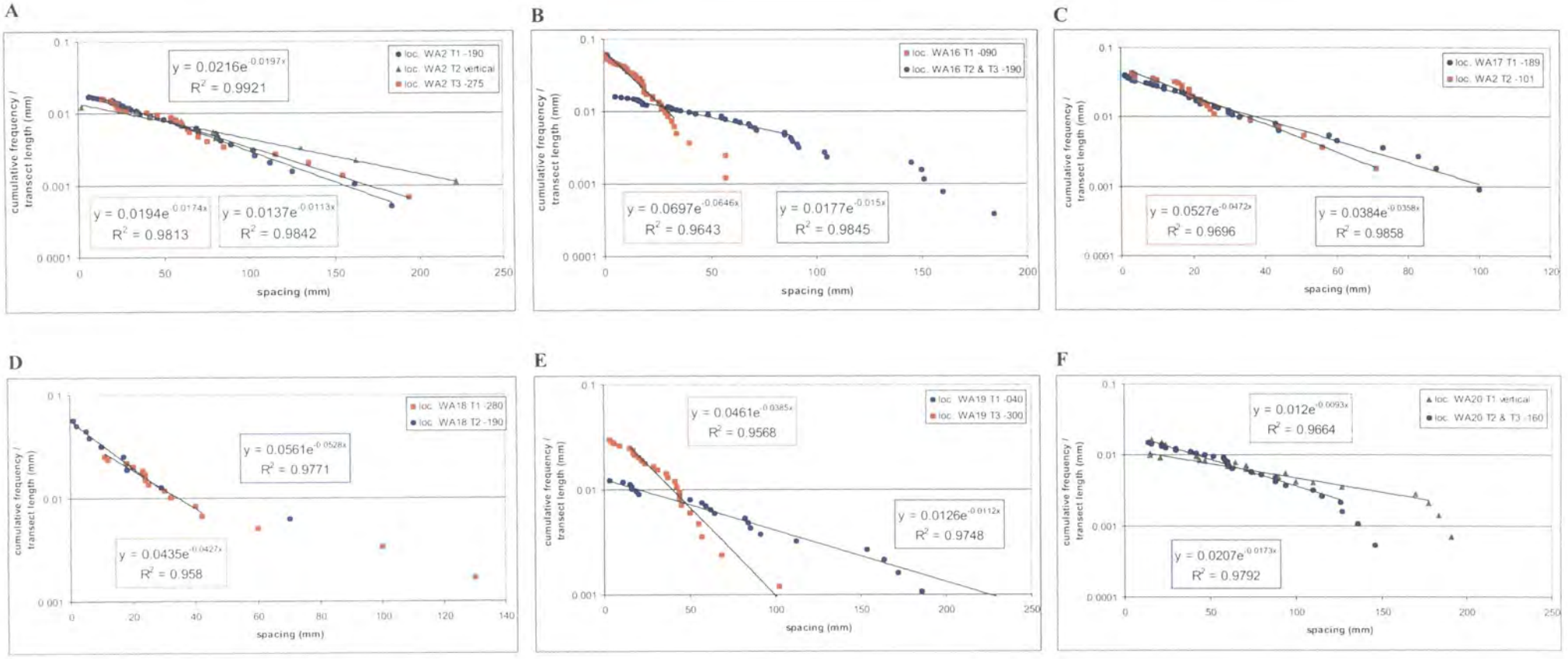

Figure 6.28 Cumulative frequency 'v' fracture spacing plots for data sets collected adjacent to the NFP
A - C = data sets collected to the west of the NFP within calcareous metasediments
D - F = data sets collected to the east of the NFP within psammite

blue data sets represent transects orientated parallel to the NFP
red data sets represent transects orientated perpendicular to the NFP
green data sets represent vertical transects

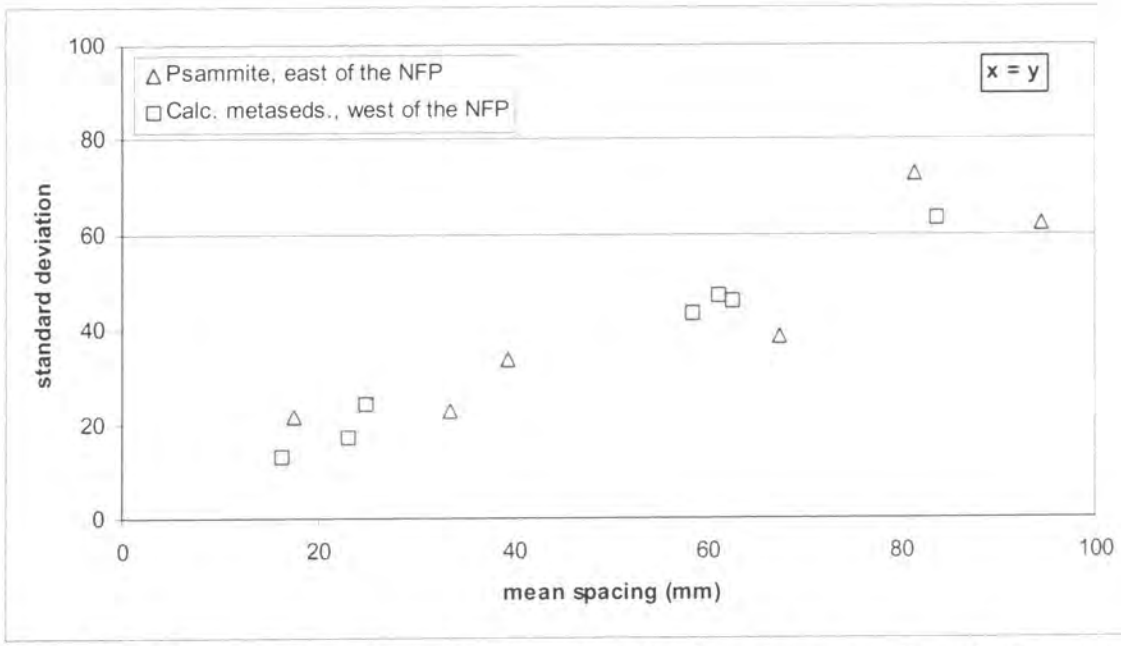

Figure 6.29 Mean spacing 'v' standard deviation plot from data sets collected adjacent to the NFP.

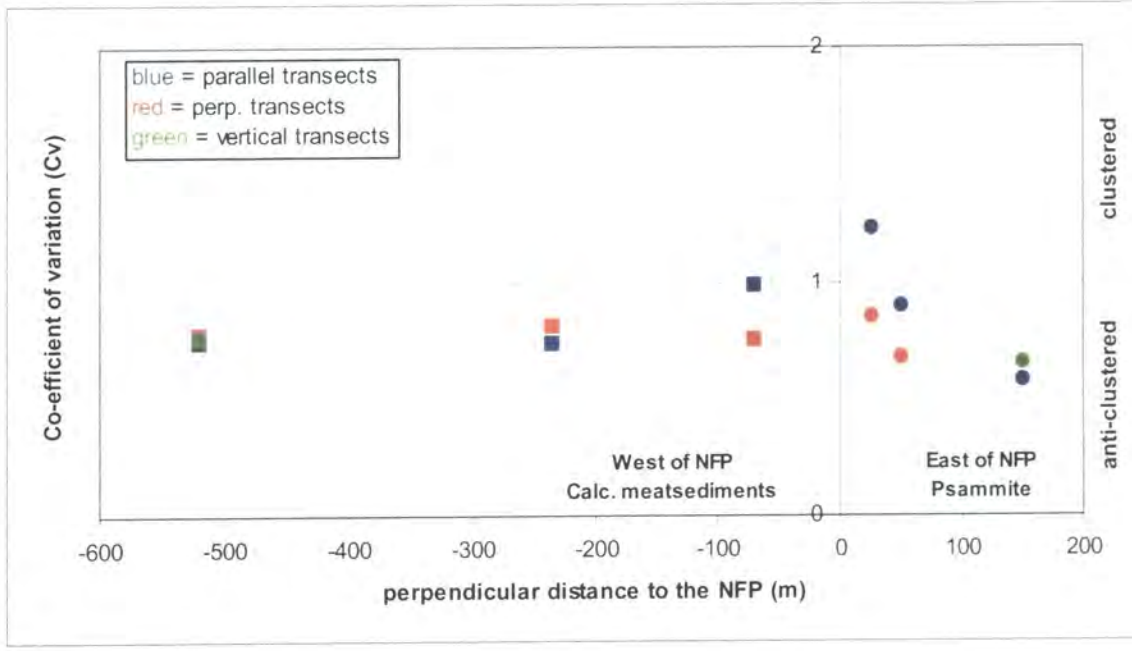

Figure 6.30 Co-efficient of variation values (Cv) 'v' perpendicular distance to the NFP for data sets collected adjacent to the NFP.

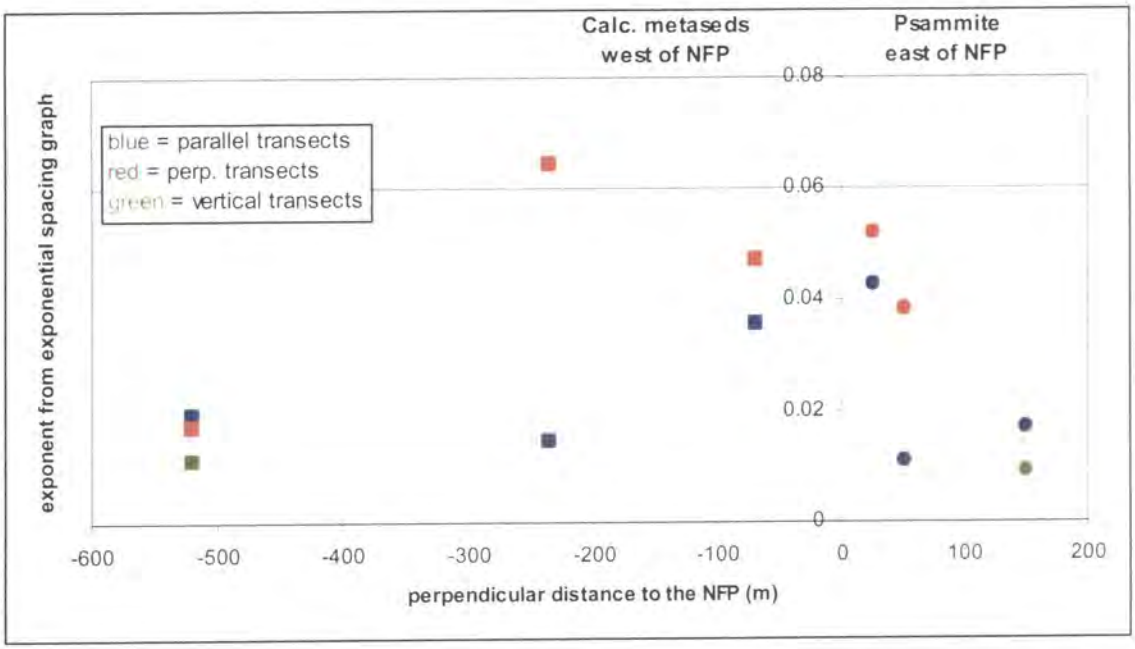

Figure 6.31 Exponential exponent values from spacing graphs 'v' perpendicular distance to the NFP, for data sets collected adjacent to the NFP.

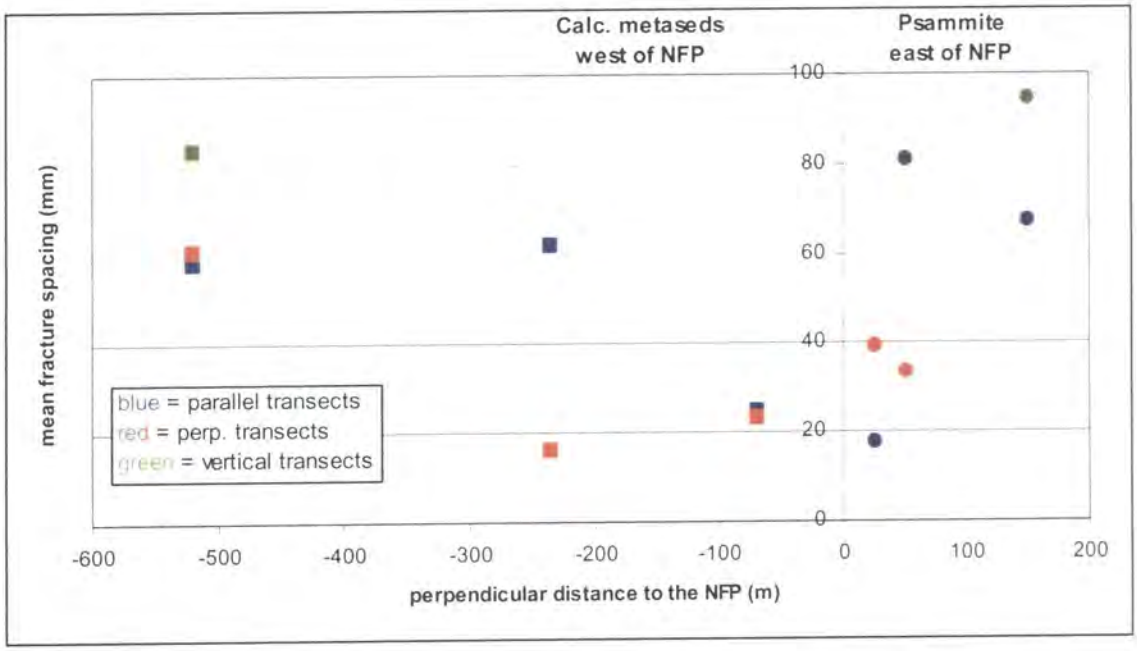

Figure 6.32 Mean spacing values 'v' perpendicular distance to the NFP, for data sets collected adjacent to the NFP.

a)

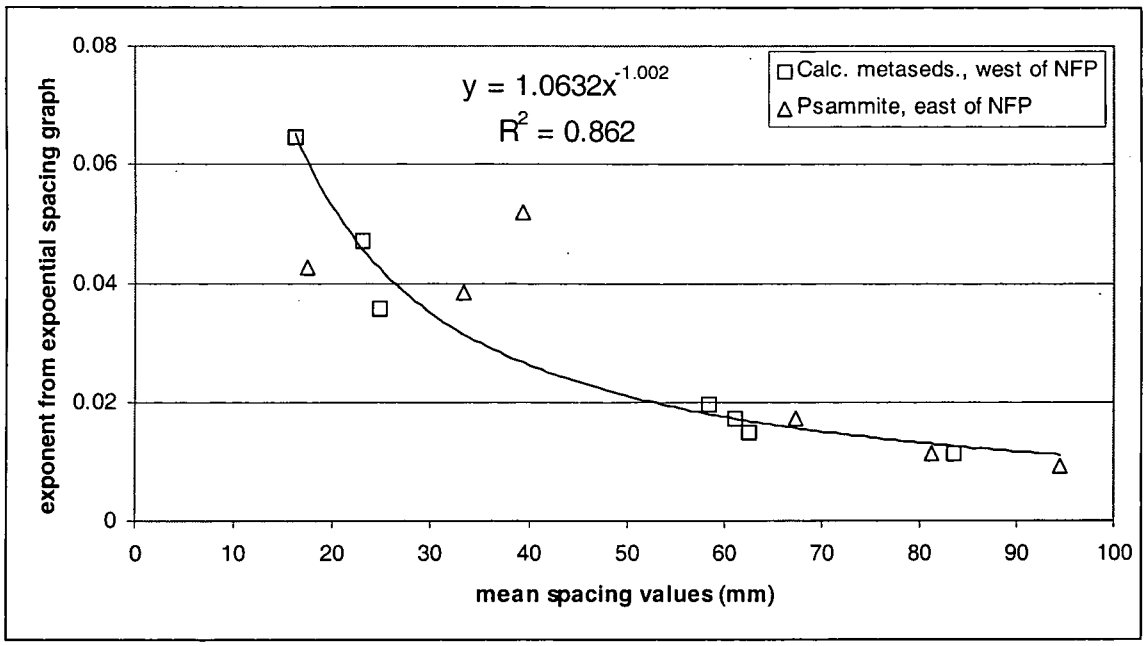

b)

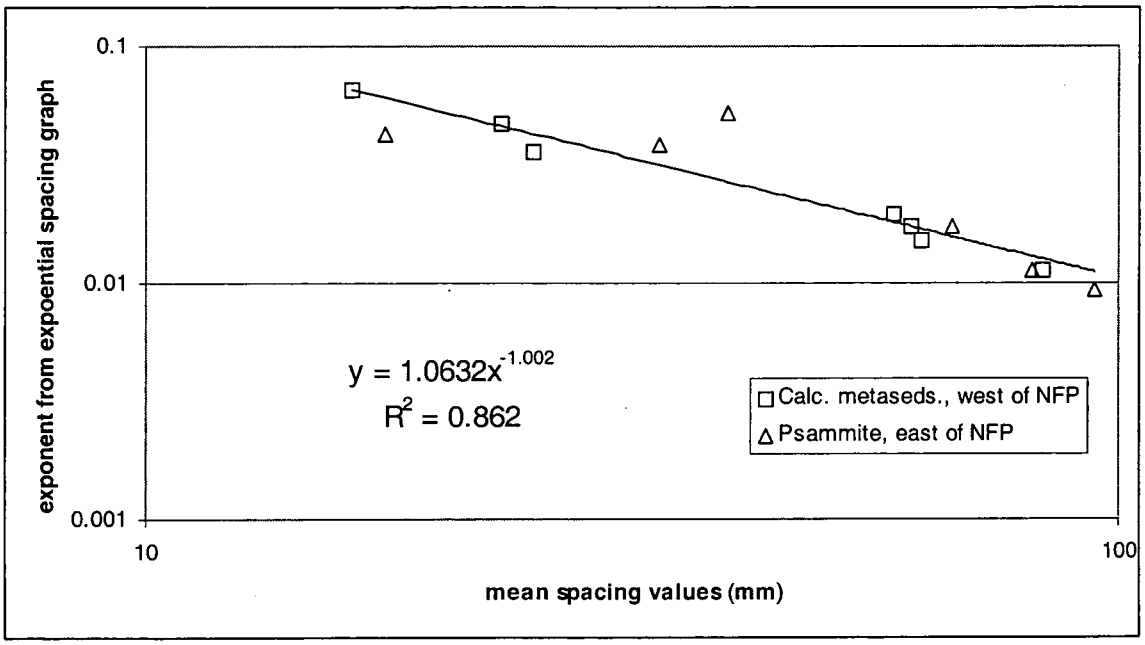

Figure 6.33 Mean spacing values plotted against exponent values from exponential spacing distributions, distinguished for lithology, for data sets collected adjacent to the NFP.
a) – data plotted on linear axes, **b)** – data plotted on logarithmic axes.

a)

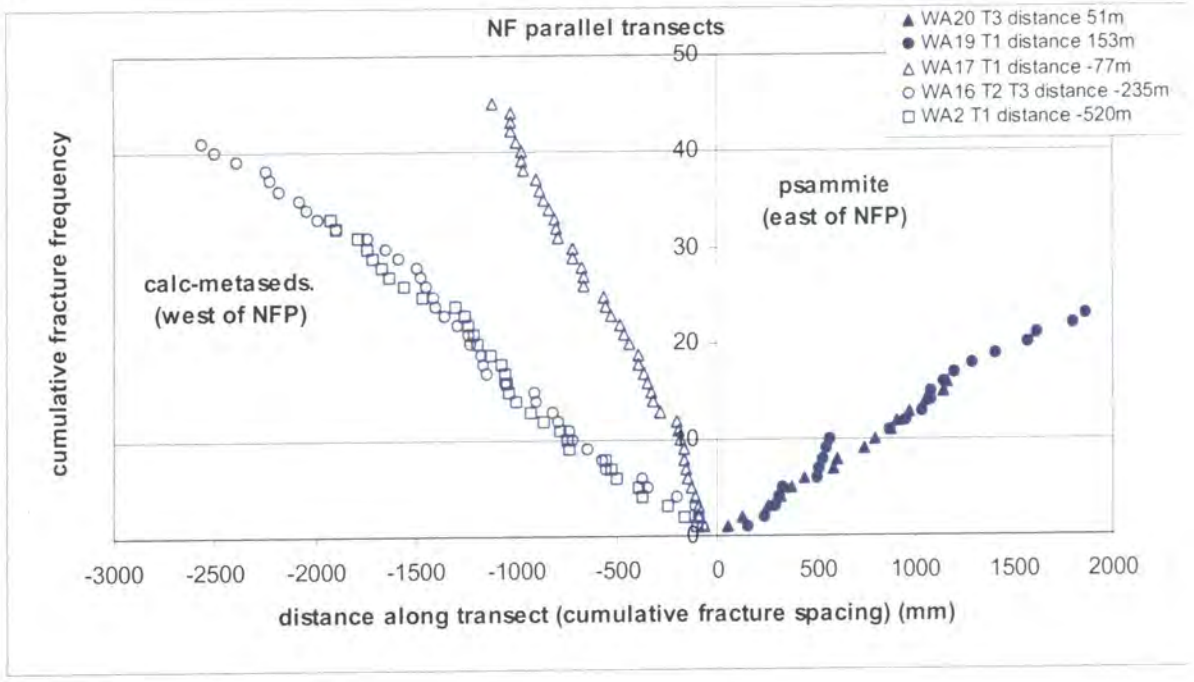

b)

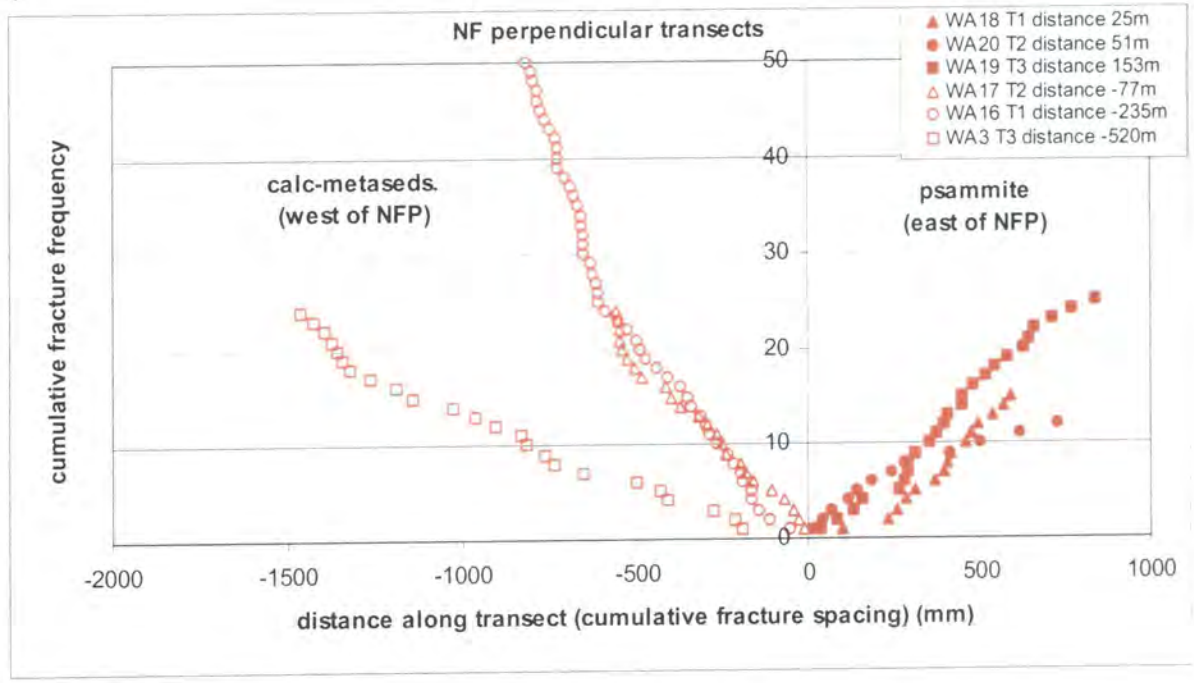

Figure 6.34 Cumulative frequency 'v' distance along 1-dimensional line transects carried out adjacent to the NFP within psammite and calcareous metasediments.
a) transects orientated parallel to the NFP,
b) transects orientated perpendicular to the NFP

		Stereonets					
		A	B	C	D	E	F
Place		Melby	Melby	Melby	Melby	Melby	Melby
Locality		ME 8	ME 2	ME 3	ME 5	ME 4	ME 10 & ME 11
Distance to MFP		660m	225m	150m	70m	140m	>1500m
Number of data points		57	86	107	96	78	128
lithology		Volcani-clastics	Volcani-clastics	Volcani-clastics	Basement	Basement	Basement
foliation orientation		165/ 70 W	050/ 70 NW	049/ 69 NW	043/ 48 SE	005/ 42 E	openly folded
fracture orientation clusters identified	MFP parallel	-	044/ 75 W	044/ 74 W	041/ 47 E	-	-
	other	165/ 78 W	-	161/ 57 W	-	-	-

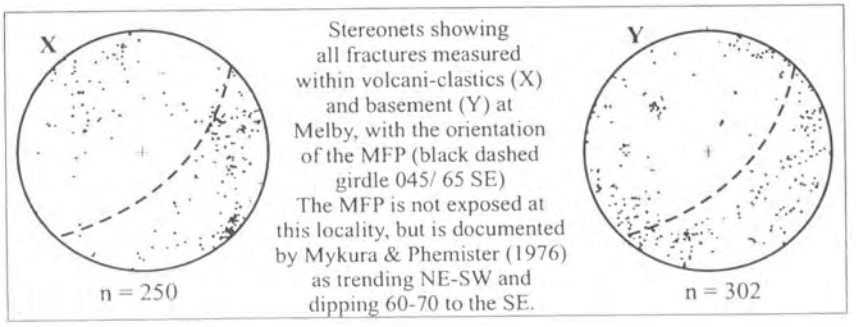

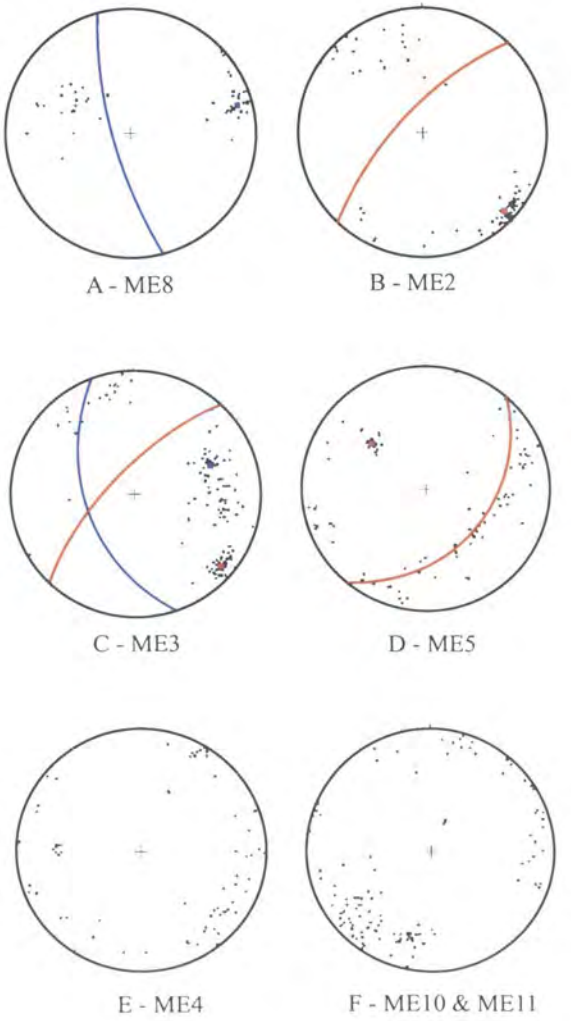

Figure 6.35 Fracture orientation data collected adjacent to the MFP

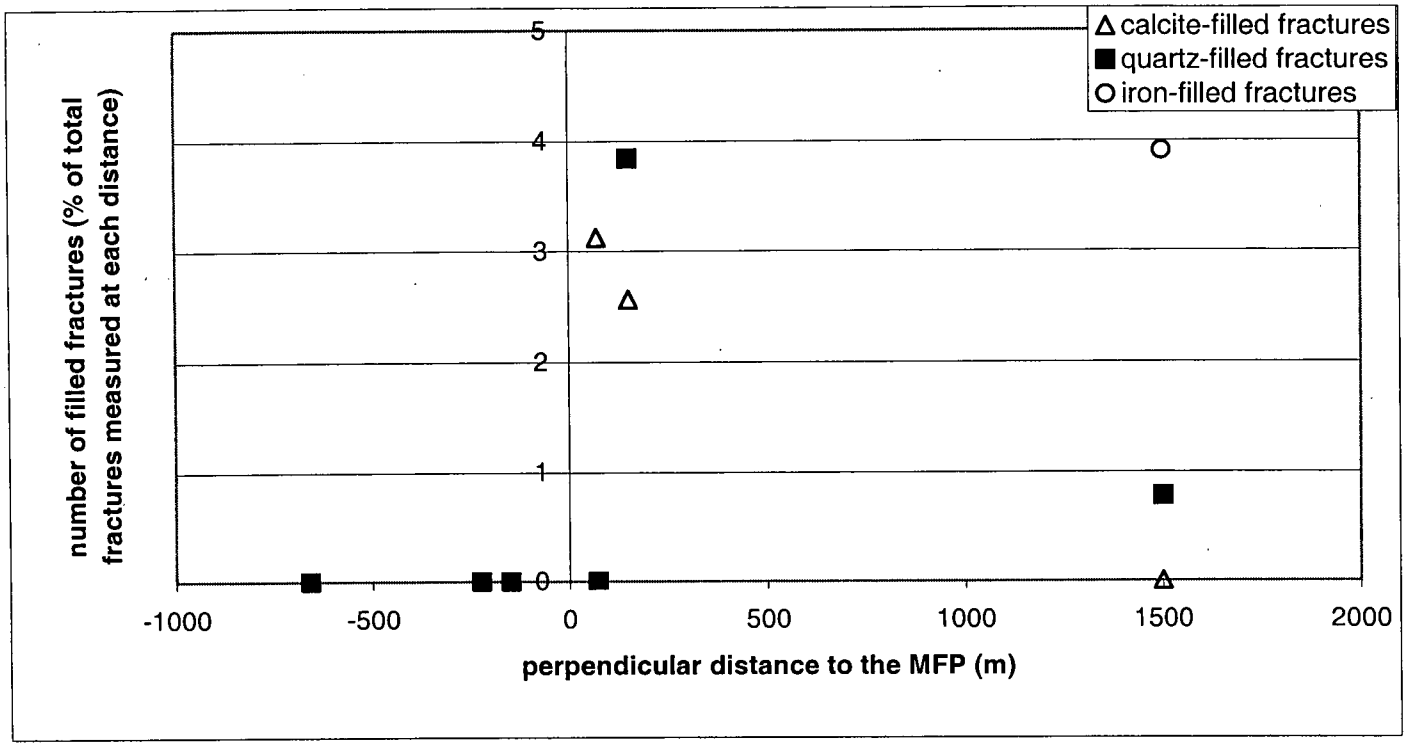

Figure 6.36 Percentage of filled fractures at different distances to the MFP. No filled fractures were observed to the west of the fault.

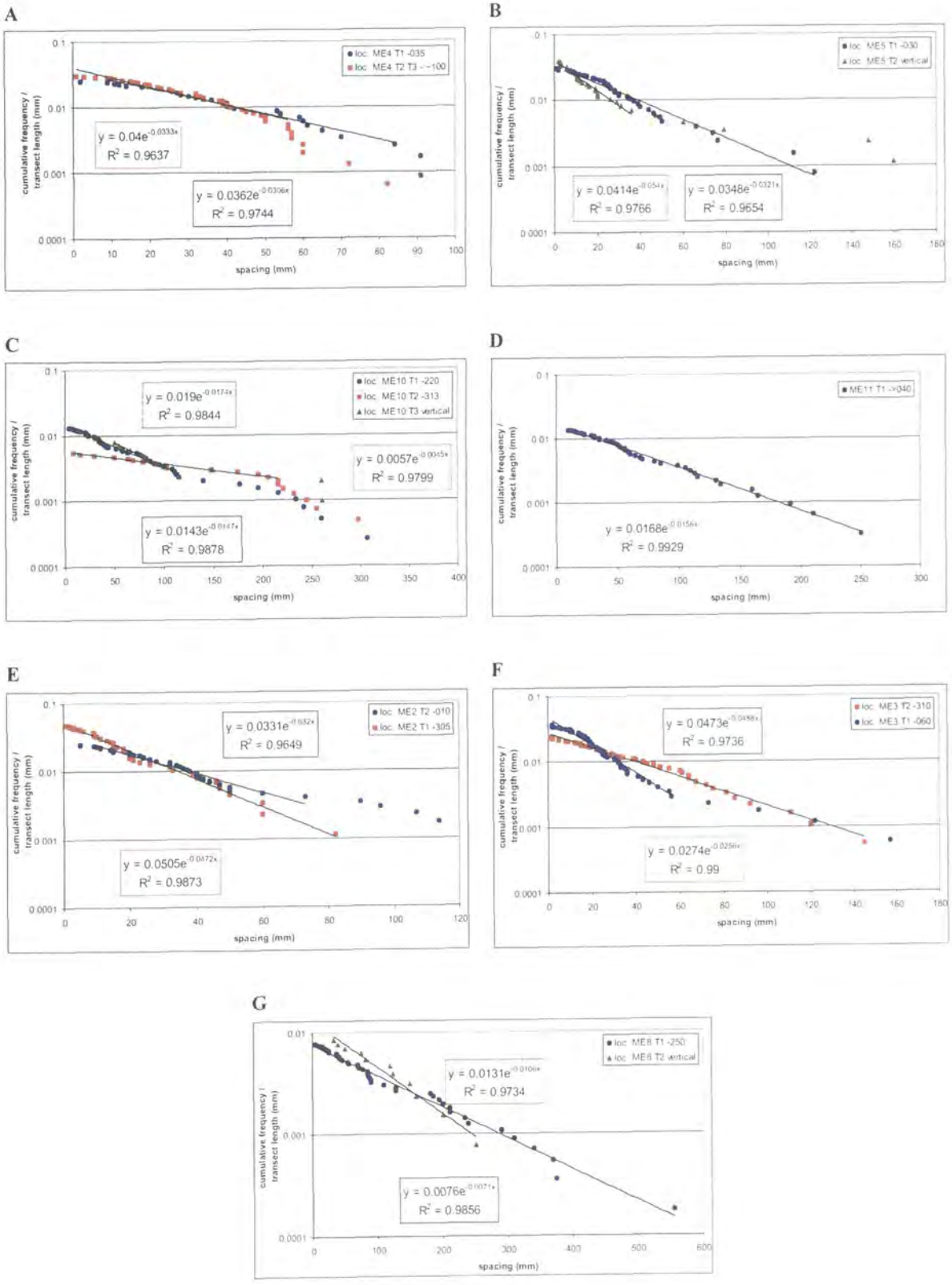

Figure 6.37 Cumulative frequency 'v' spacing plots for localities adjacent to the MFP
A - D = data sets collected from basement rocks
E - G = data sets collected from volcani-clastic rocks
(blue data sets = transects parallel to the MFP, red data sets = transects perpendicular to the MFP, green data sets = vertical transects).

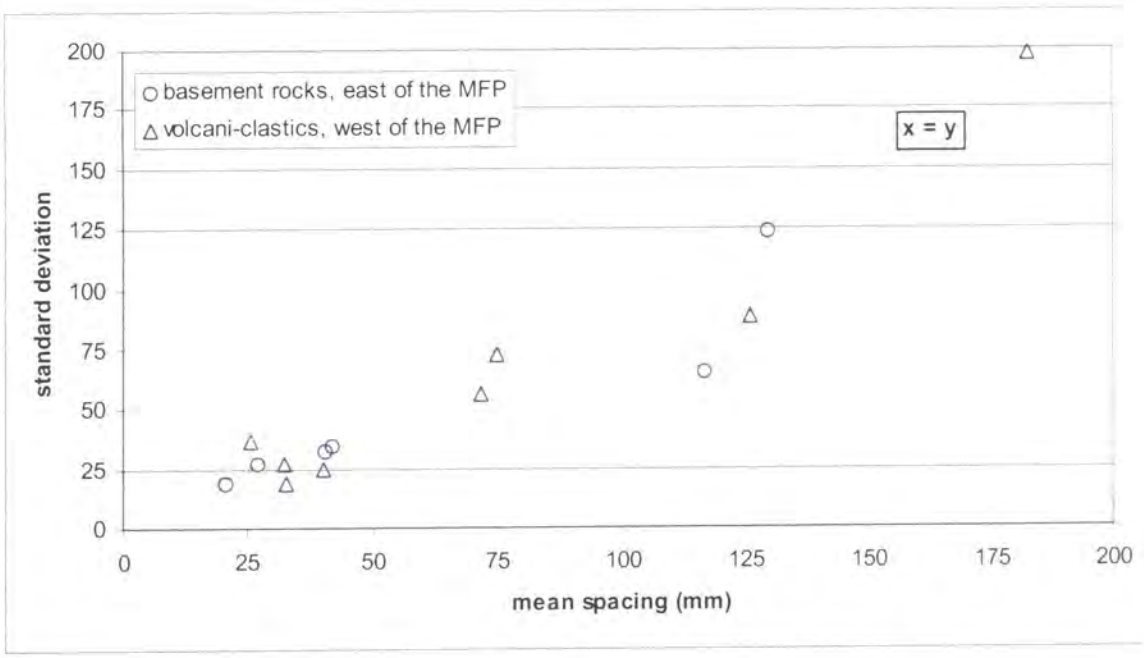

Figure 6.38 Mean spacing values 'v' standard deviation from data sets collected adjacent to the MFP.

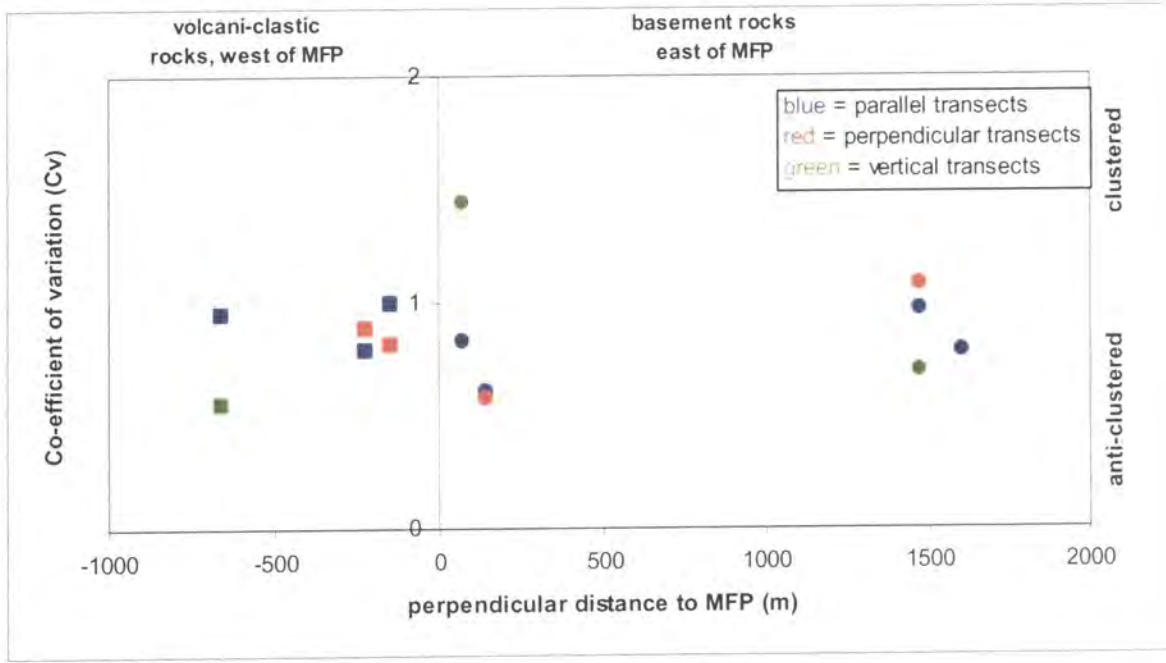

Figure 6.39 Co-efficient of variation values (Cv) 'v' perpendicular distance to the MFP for data sets collected adjacent to the MFP.

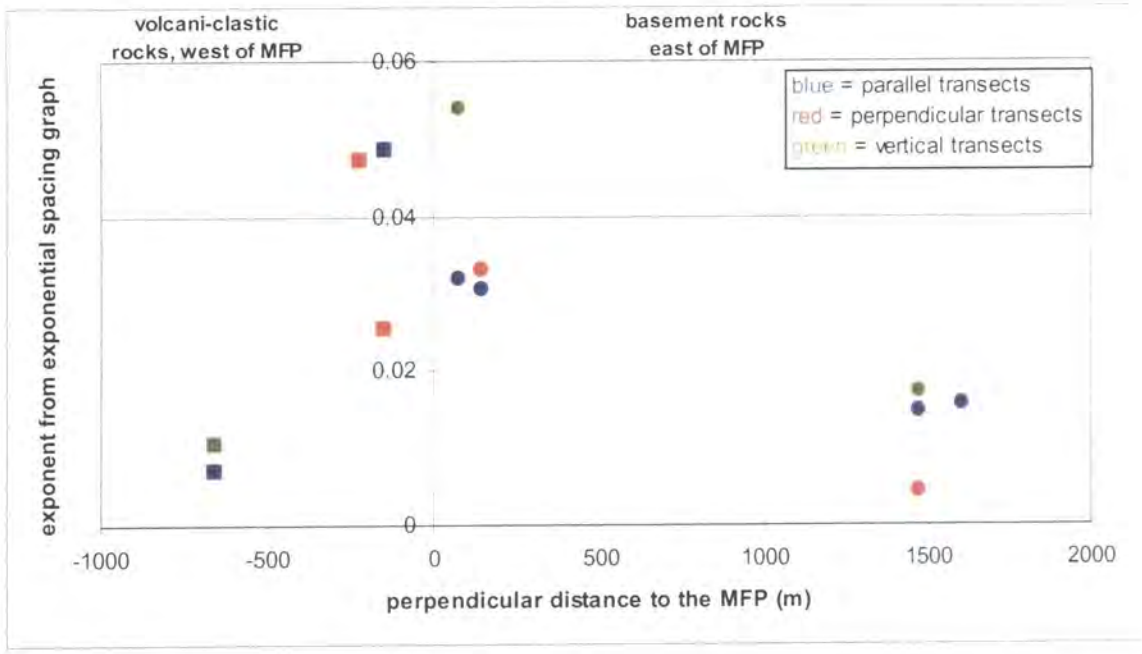

Figure 6.40 Exponential exponent values from spacing graphs 'v' perpendicular distance to the MFP, for data sets collected adjacent to the MFP.

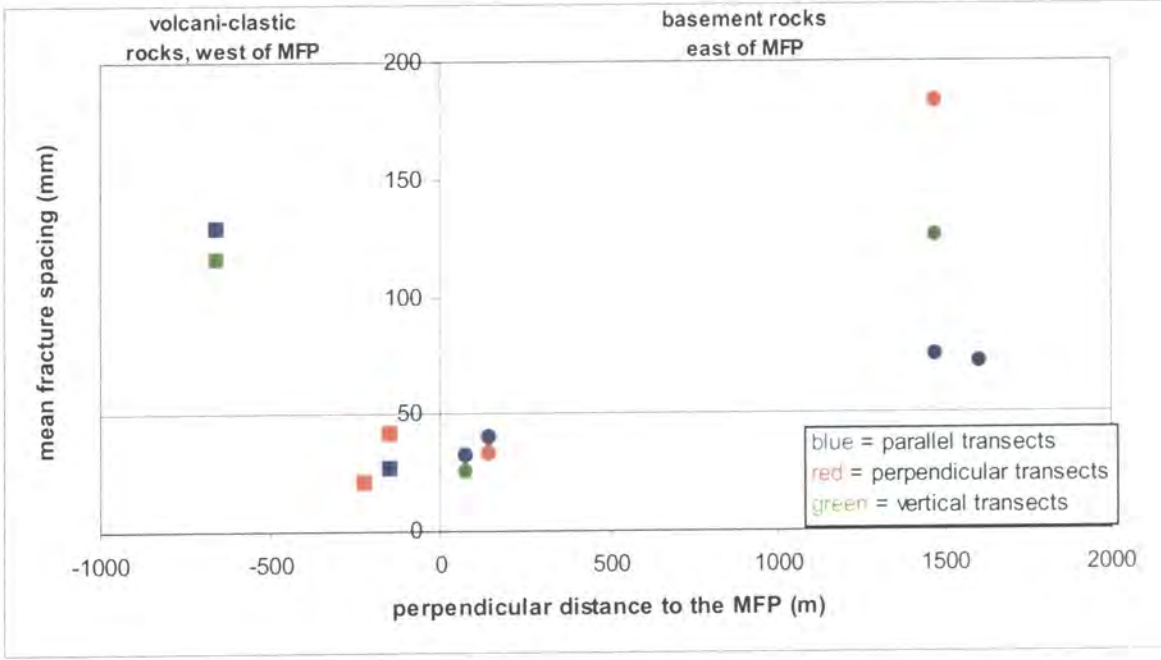

Figure 6.41 Mean spacing values 'v' perpendicular distance to the MFP, for data sets collected adjacent to the MFP.

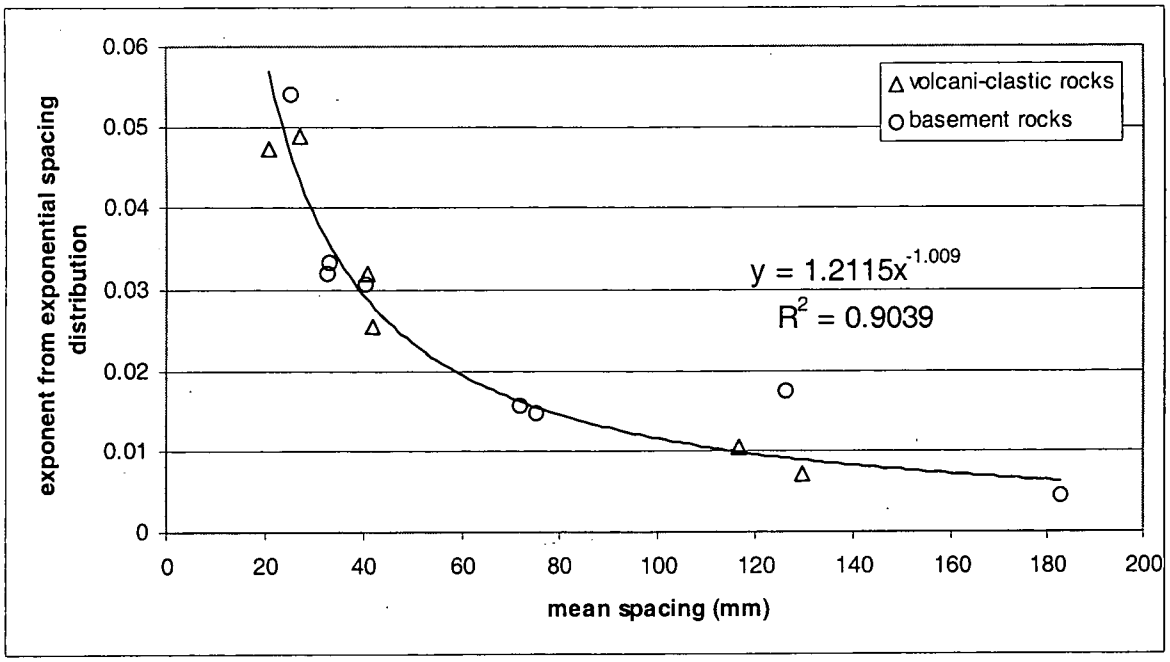

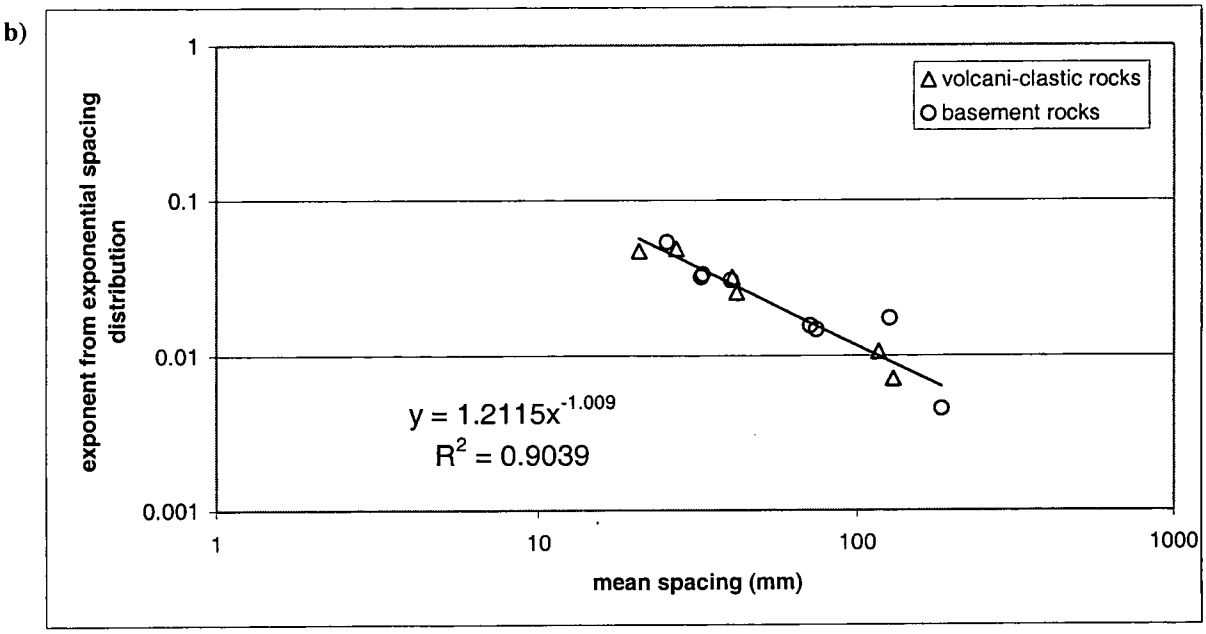

Figure 6.42 Mean spacing values plotted against exponent values from exponential spacing distributions, distinguished for lithology, for data sets collected adjacent to the MFP.
a) – data plotted on linear axes, **b)** – data plotted on logarithmic axes.

a)

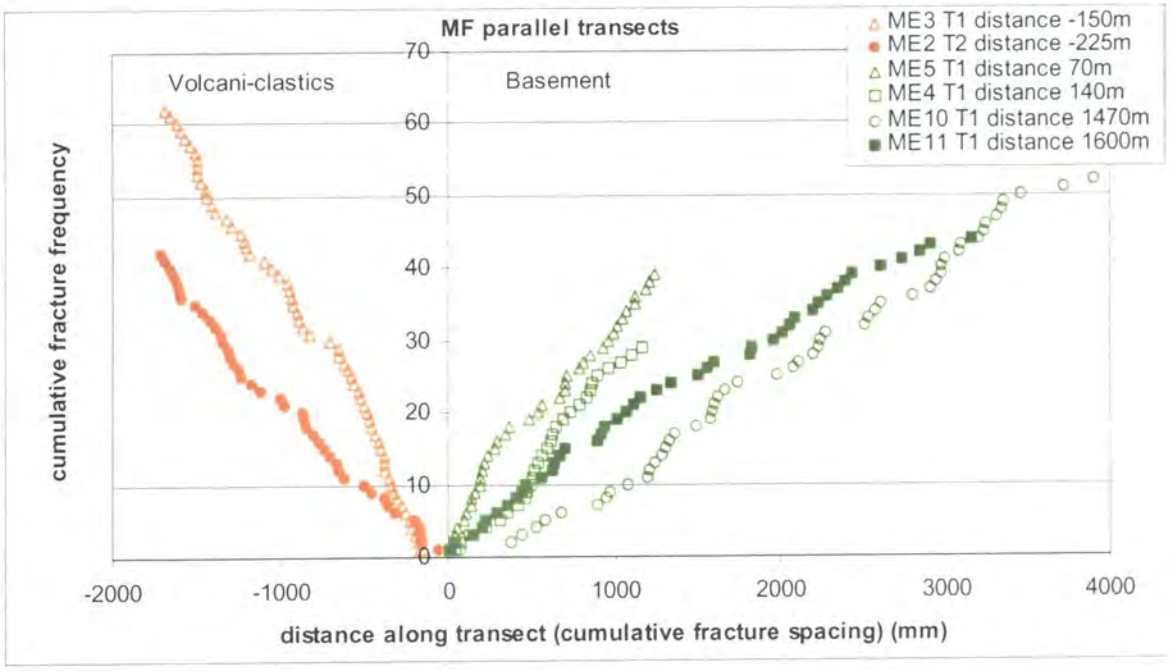

b)

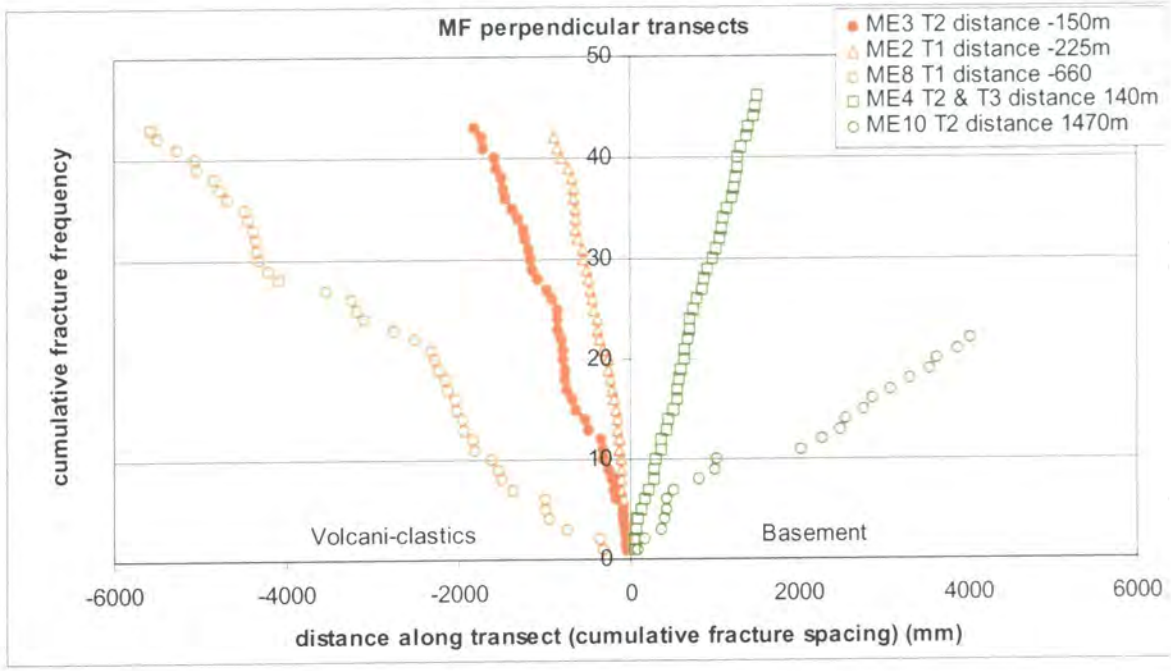

Figure 6.43 Cumulative frequency 'v' distance along 1-dimensional line transects carried out adjacent to the MFP within basement (to the east) and volcani-clastics (to the west).

a) transects orientated parallel to the MFP,

b) transects orientated perpendicular to the MFP,

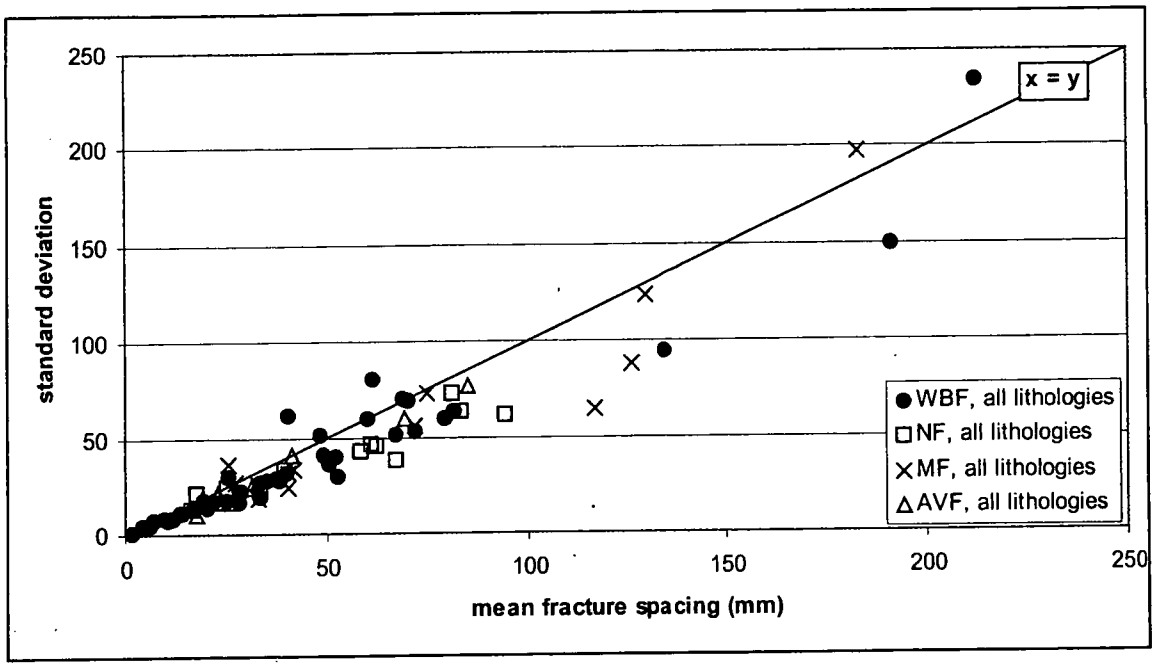

Figure 6.44 Mean 'v' standard deviation plot for spacing data collected along 1-D line transects adjacent to the WBF, AVF, NF and MF, within all lithologies

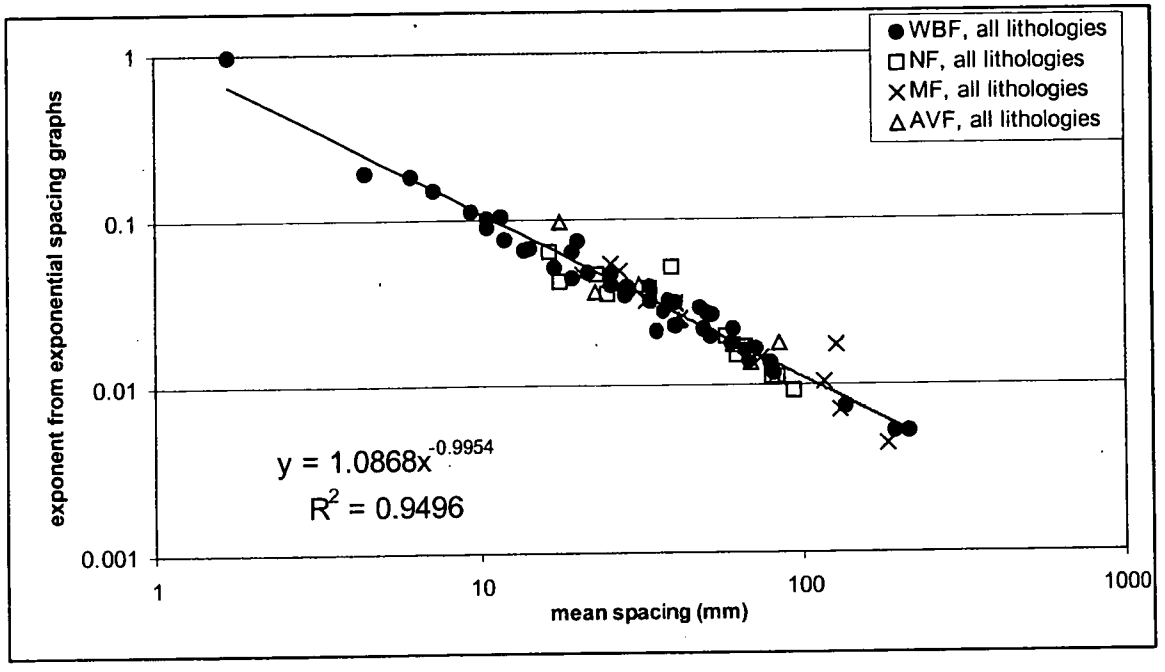

Figure 6.46 Mean spacing 'v' exponent from exponential spacing graphs, for data collected adjacent to all faults, and within all lithologies

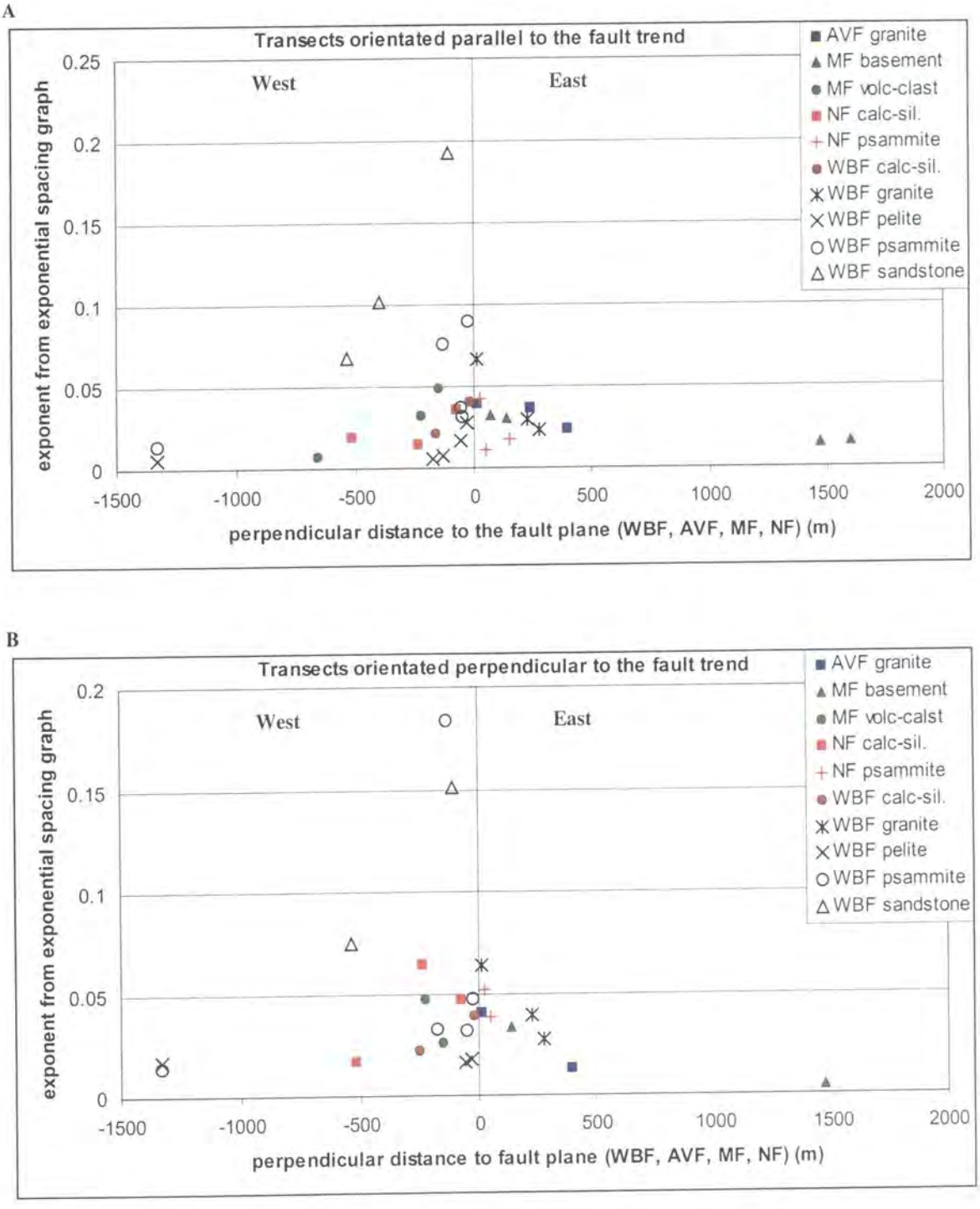

Figure 6.45 Exponential exponent values from (**A**) parallel, and (**B**) perpendicular transects carried out within all lithologies adjacent to the WBF (black symbols), AVF (blue symbols), NF (red symbols), and MF (green symbols).

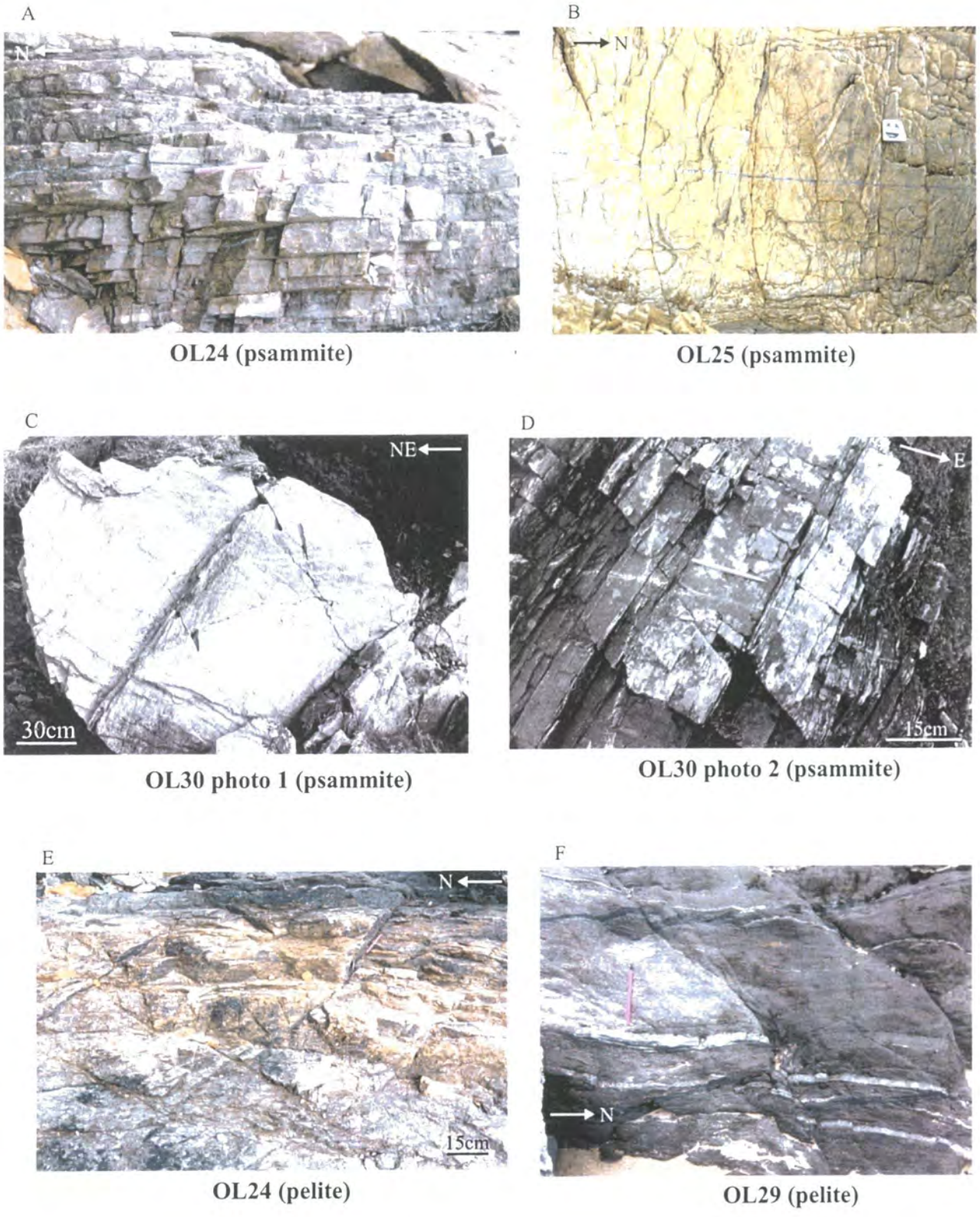

Figure 7.1 Outcrop data sets used to analyse fracture attributes in 2-D adjacent to faults in WBFS
A - D = psammite, Ollaberry (WBF)
E & F = pelite, Ollaberry (WBF)
G & H = granite, Sullom (WBF)
I & J = sandstone, Bixter (WBF)
K & L = calc. sil. Wadbister Voe (NF)
M & N - psammite Wadbister Voe (NF)
O - Q = granite, Sand (AVF)
R & S = volcani-clastics, Melby (MF)
T - W = basement, Melby (MF)
(see Table 7.1 for details) (continued on next 3 pages)

SU21 (granite)

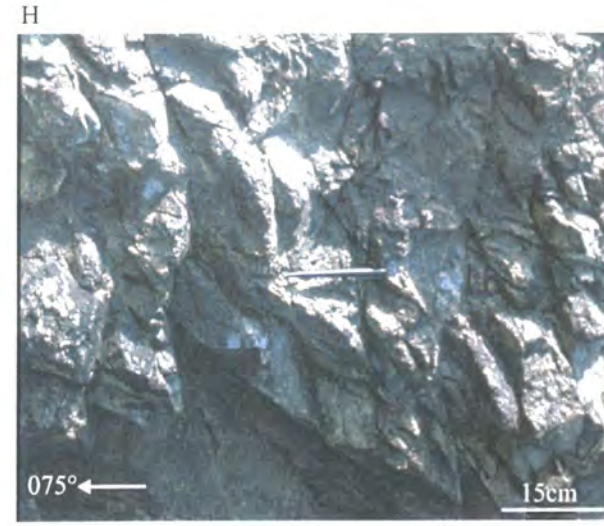

SU21 (granite)

BI 1 (sandstone)

BI 6 (sandstone)

Figure 7.1 Outcrop data sets used to analyse fracture attributes in 2-D adjacent to faults in WBFS
A - D = psammite, Ollaberry (WBF)
E & F = pelite, Ollaberry (WBF)
G & H = granite, Sullom (WBF)
I & J = sandstone, Bixter (WBF)
K & L = calc. sil. Wadbister Voe (NF)
M & N - psammite Wadbister Voe (NF)
O - Q = granite, Sand (AVF)
R & S = volcani-clastics, Melby (MF)
T - W = basement, Melby (MF)
(see Table 7.1 for details) (continued from previous page, & on next 2 pages)

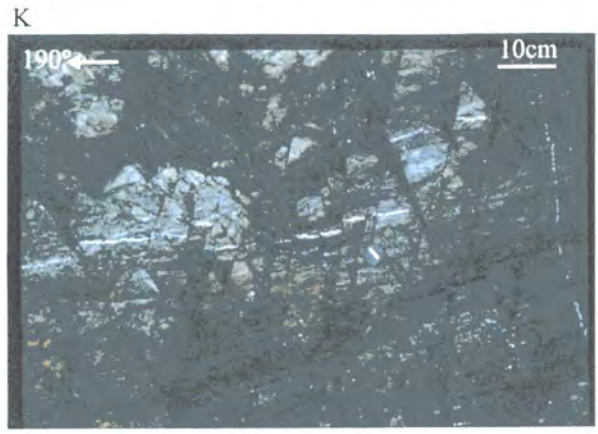

WA16 (calc. sil.)

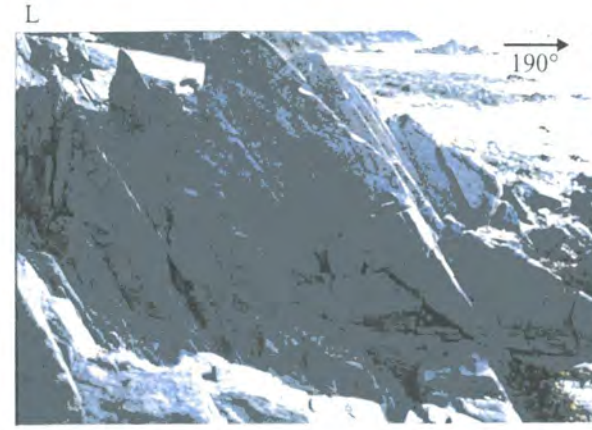

WA17 (calc. sil.)

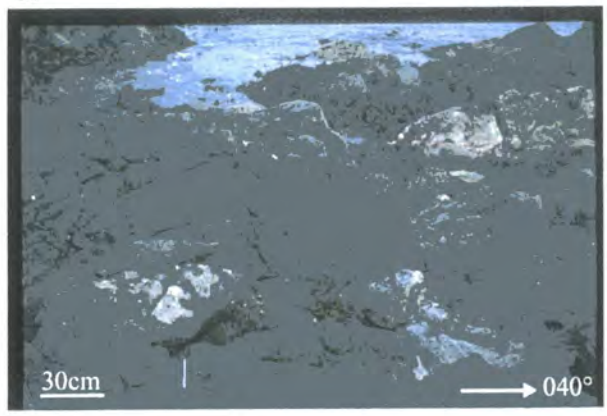

WA19 (psammite)

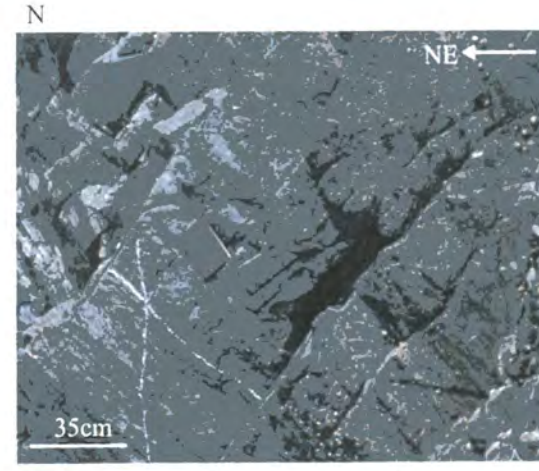

WA20 (psammite)

SA3 (granite)

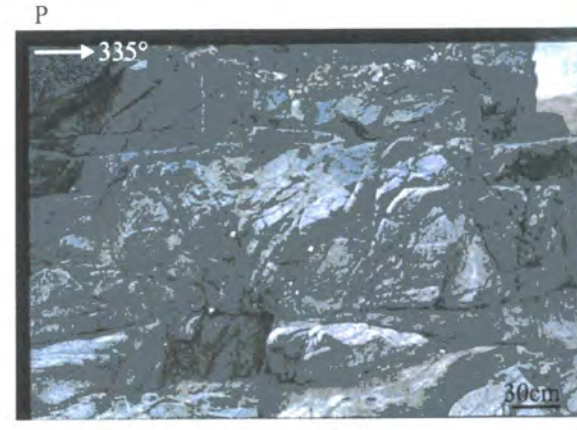

SA6 (granite)

SA7 (granite)

Figure 7.1 Outcrop data sets used to analyse fracture attributes in 2-D adjacent to faults in WBFS
A - D = psammite, Ollaberry (WBF)
E & F = pelite, Ollaberry (WBF)
G & H = granite, Sullom (WBF)
I & J = sandstone, Bixter (WBF)
K & L = calc. sil. Wadbister Voe (NF)
M & N - psammite Wadbister Voe (NF)
O - Q = granite, Sand (AVF)
R & S = volcani-clastics, Melby (MF)
T - W = basement, Melby (MF)
(see Table 7.1 for details)
(continued from previous 2 pages, & on next page)

ME 2

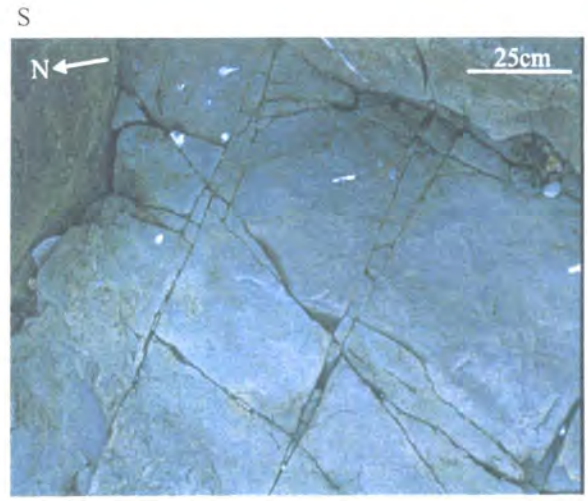

ME 8

ME 4

ME 5

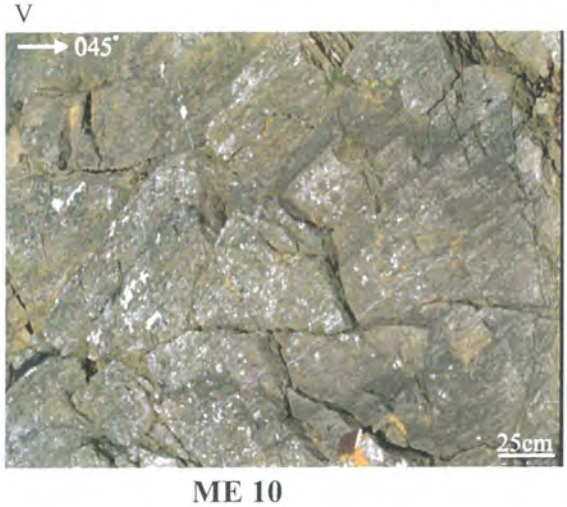

ME 10

ME 11

Figure 7.1 Outcrop data sets used to analyse fracture attributes in 2-D adjacent to faults in WBFS
A - D = psammite, Ollaberry (WBF)
E & F = pelite, Ollaberry (WBF)
G & H = granite, Sullom (WBF)
I & J = sandstone, Bixter (WBF)
K & L = calc. sil. Wadbister Voe (NF)
M & N = psammite Wadbister Voe (NF)
O - Q = granite, Sand (AVF)
R & S = volcani-clastics, Melby (MF)
T - W = basement, Melby (MF)
(see Table 7.1 for details) (continued from previous 3 pages)

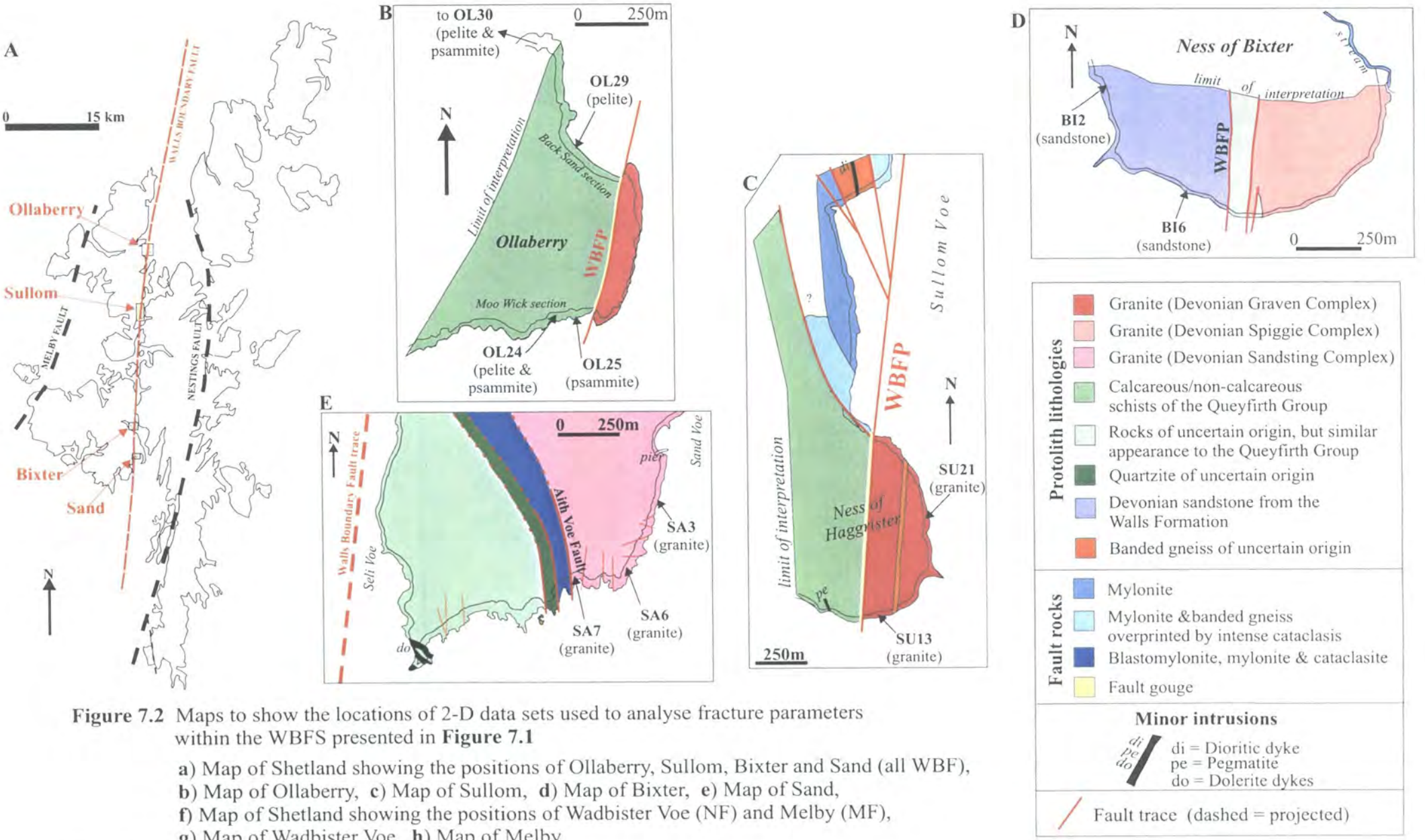

Figure 7.2 Maps to show the locations of 2-D data sets used to analyse fracture parameters within the WBFS presented in **Figure 7.1**

a) Map of Shetland showing the positions of Ollaberry, Sullom, Bixter and Sand (all WBF), **b**) Map of Ollaberry, **c**) Map of Sullom, **d**) Map of Bixter, **e**) Map of Sand, **f**) Map of Shetland showing the positions of Wadbister Voe (NF) and Melby (MF), **g**) Map of Wadbister Voe, **h**) Map of Melby

(continued on next page)

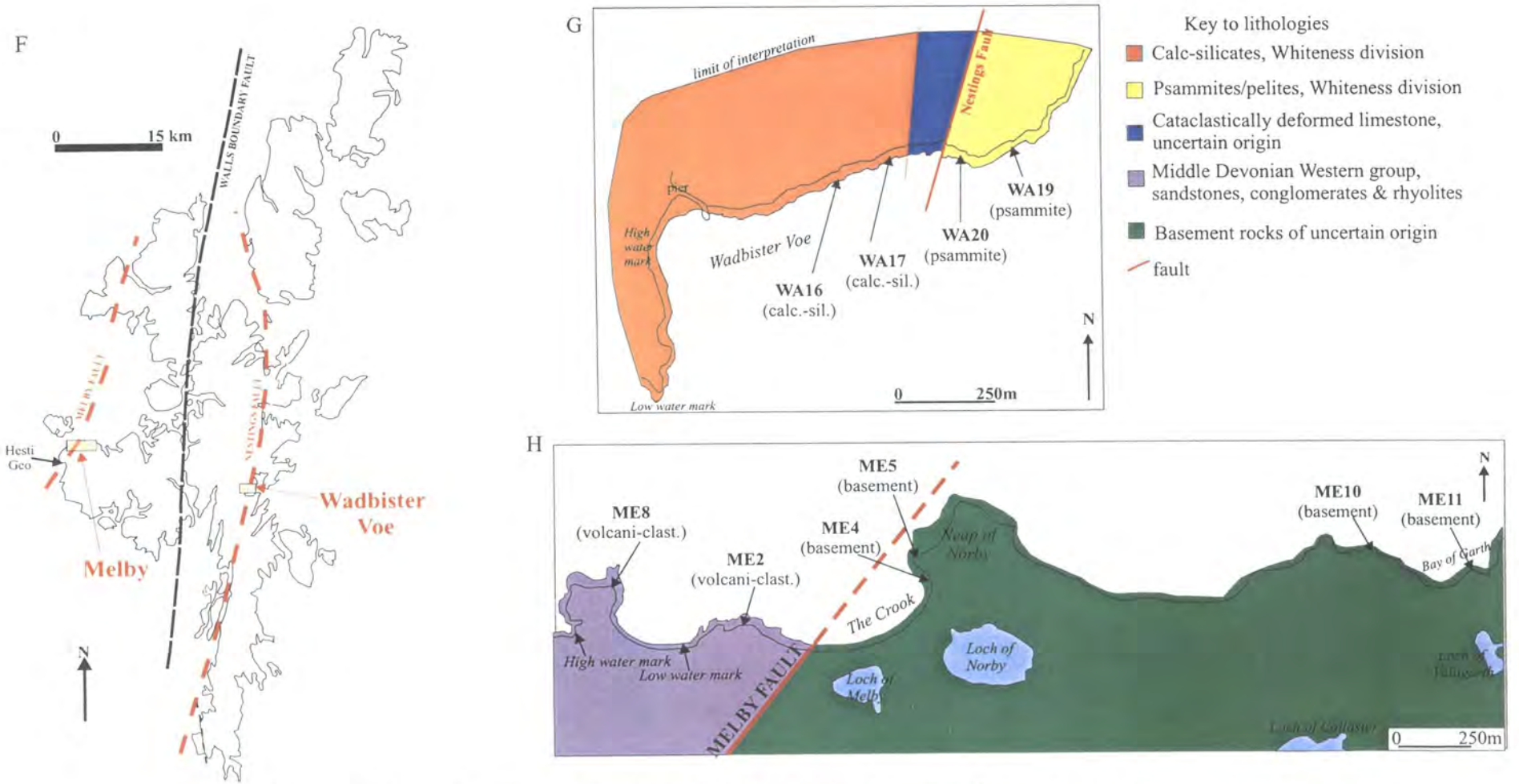

Figure 7.2 Maps to show the locations of 2-D data sets used to analyse fracture parameters within the WBFS presented in **Figure 7.1**

a) Map of Shetland showing the positions of Ollaberry, Sullom, Bixter and Sand (all WBF), **b**) Map of Ollaberry, **c**) Map of Sullom, **d**) Map of Bixter, **e**) Map of Sand, **f**) Map of Shetland showing the positions of Wadbister Voe (NF) and Melby (MF), **g**) Map of Wadbister Voe, **h**) Map of Melby

(continued from previous page)

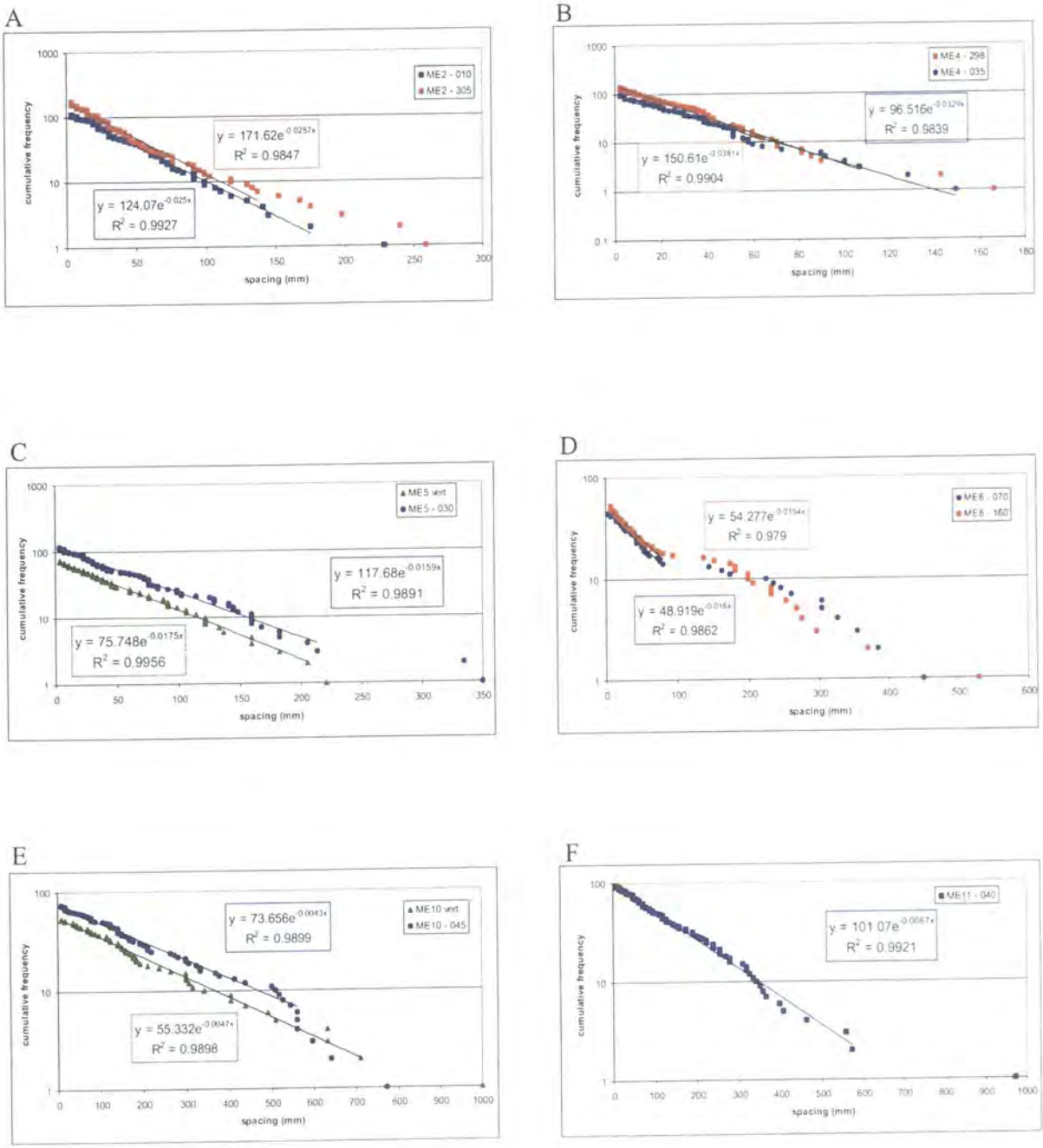

Figure 7.3 Spacing 'v' cumulative frequency plots for data collected adjacent to faults within the WBFS (continued on next 2 pages)
A-F = data collected adjacent to the MF
G-J = data collected adjacent to the NF
K-M = data collected adjacent to the AVF
N-W = data collected adjacent to the WBF

Blue data sets represent transects carried out ~parallel to the fault trend
Red data sets represent transects carried out ~perpendicular to the fault trend
Green data sets represent vertical transects

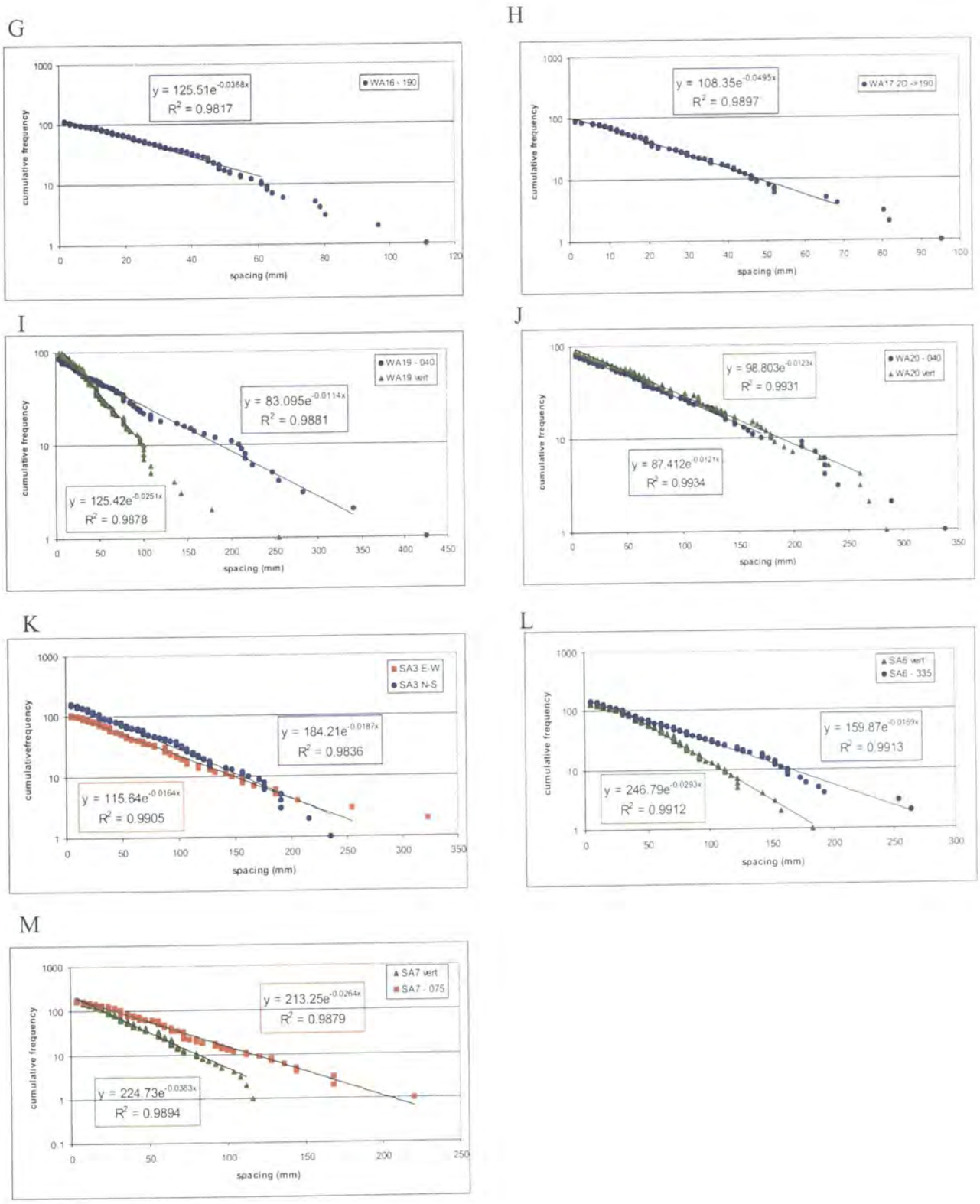

Figure 7.3 Spacing 'v' cumulative frequency plots for data collected adjacent to faults within the WBFS (continued from previous page, and continued on next page)
A-F = data collected adjacent to the MF
G-J = data collected adjacent to the NF
K-M = data collected adjacent to the AVF
N-W = data collected adjacent to the WBF

Blue data sets represent transects carried out ~parallel to the fault trend
Red data sets represent transects carried out ~perpendicular to the fault trend
Green data sets represent vertical transects

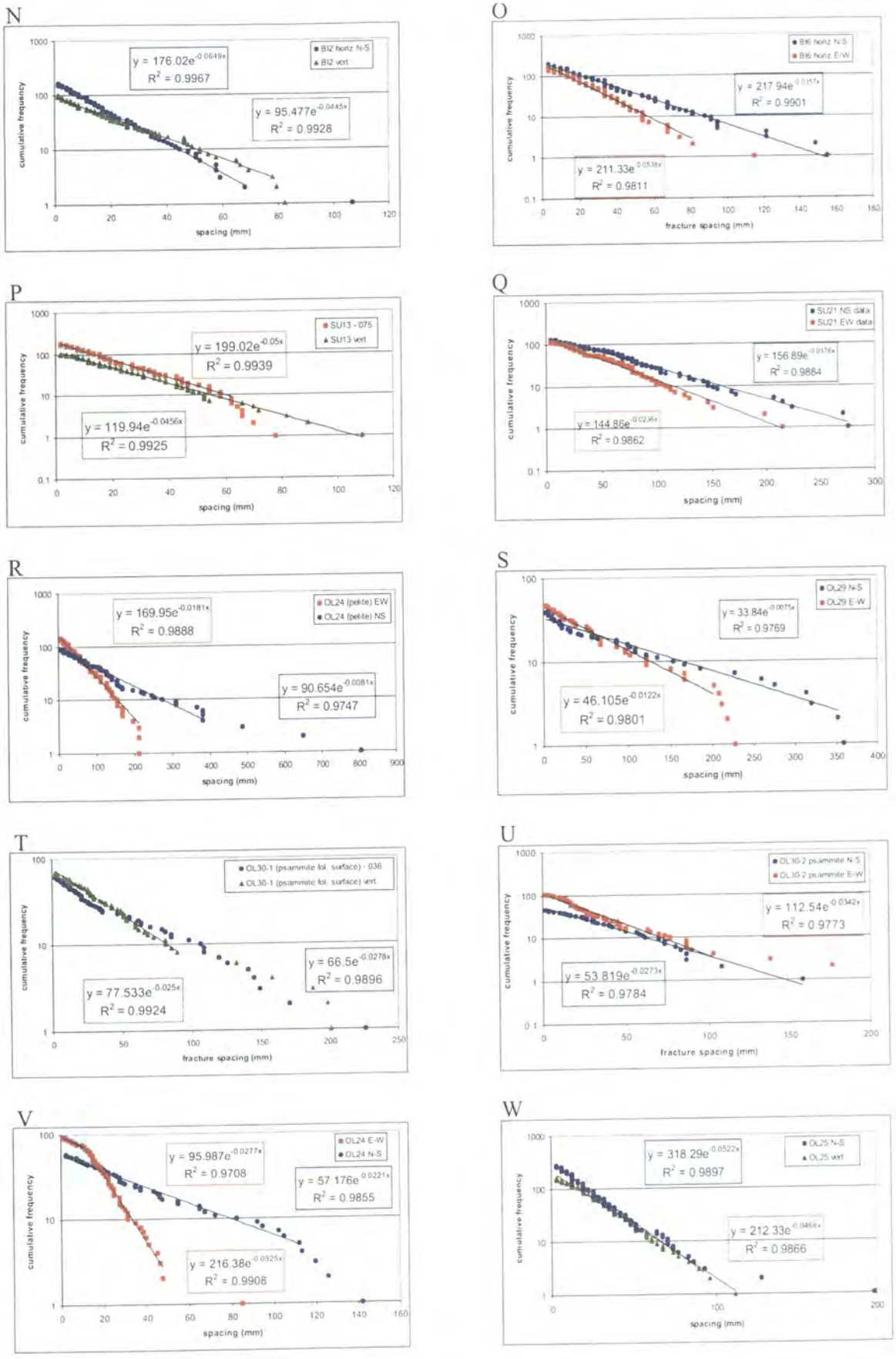

Figure 7.3 Spacing 'v' cumulative frequency plots for data collected adjacent to faults within the WBFS (continued from previous 2 pages)
A-F = data collected adjacent to the MF
G-J = data collected adjacent to the NF
K-M = data collected adjacent to the AVF
N-W = data collected adjacent to the WBF

Blue data sets represent transects carried out ~parallel to the fault trend
Red data sets represent transects carried out ~perpendicular to the fault trend
Green data sets represent vertical transects

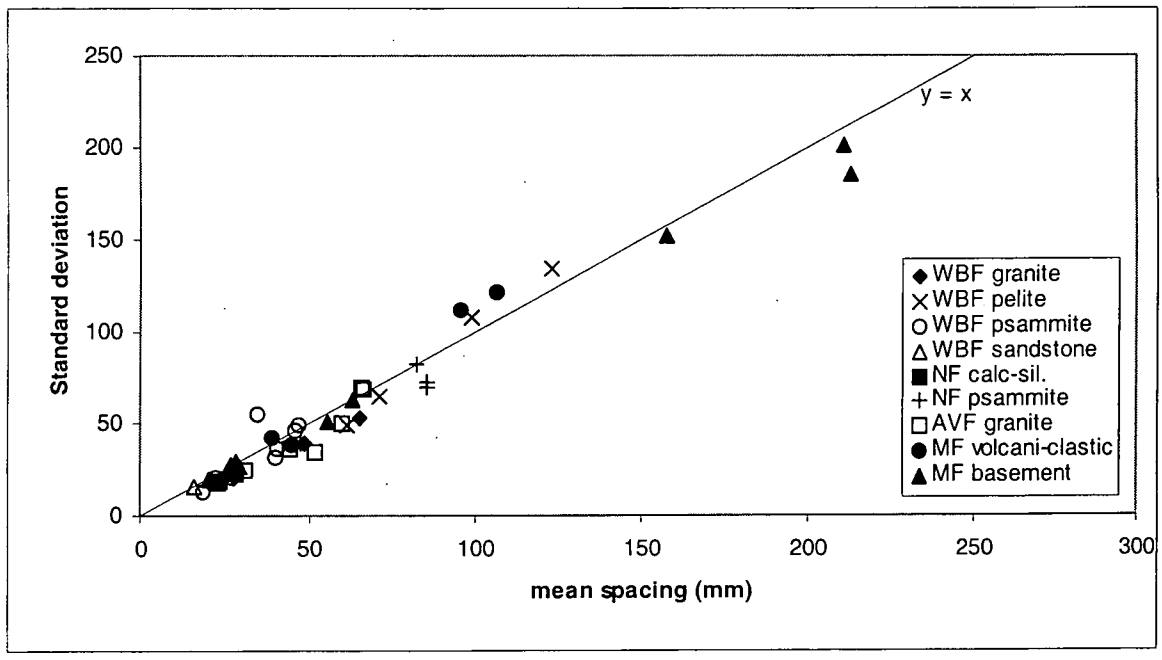

Figure 7.4 Mean spacing 'v' standard deviation plot for fracture data collected adjacent to faults within the WBFS.

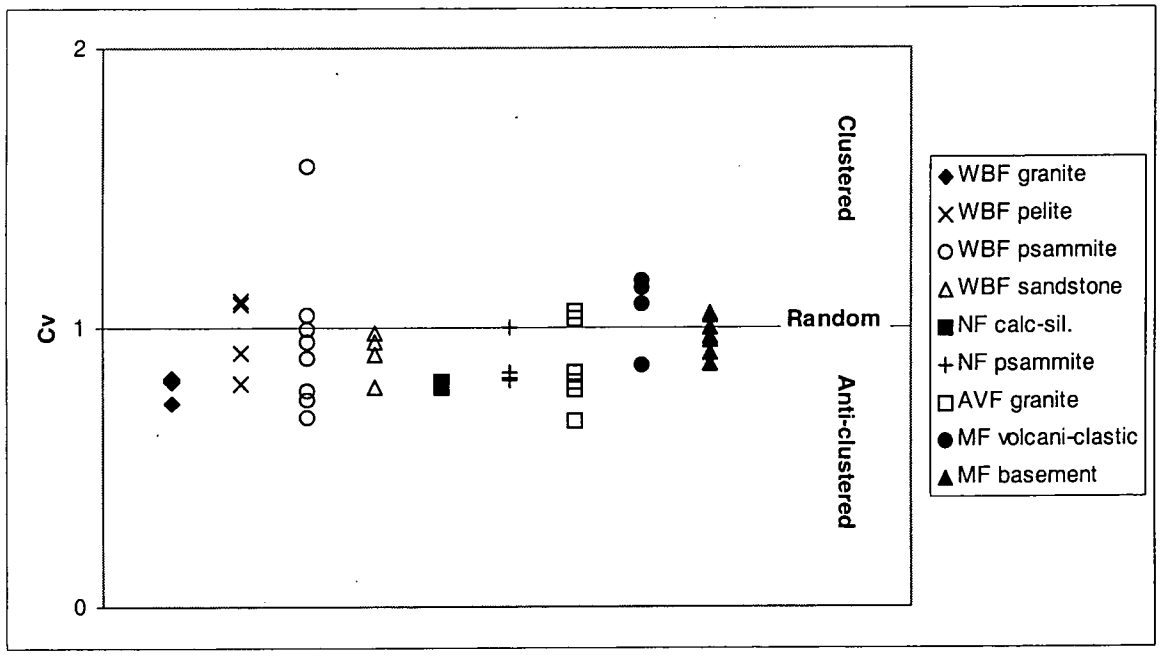

Figure 7.5 Co-efficient of variation values for fracture data collected adjacent to faults within the WBFS.

a)

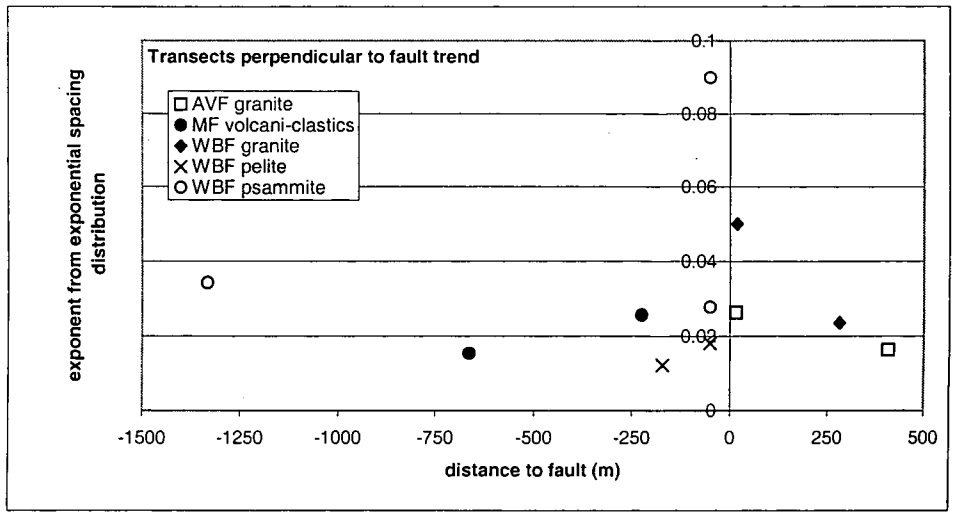

b)

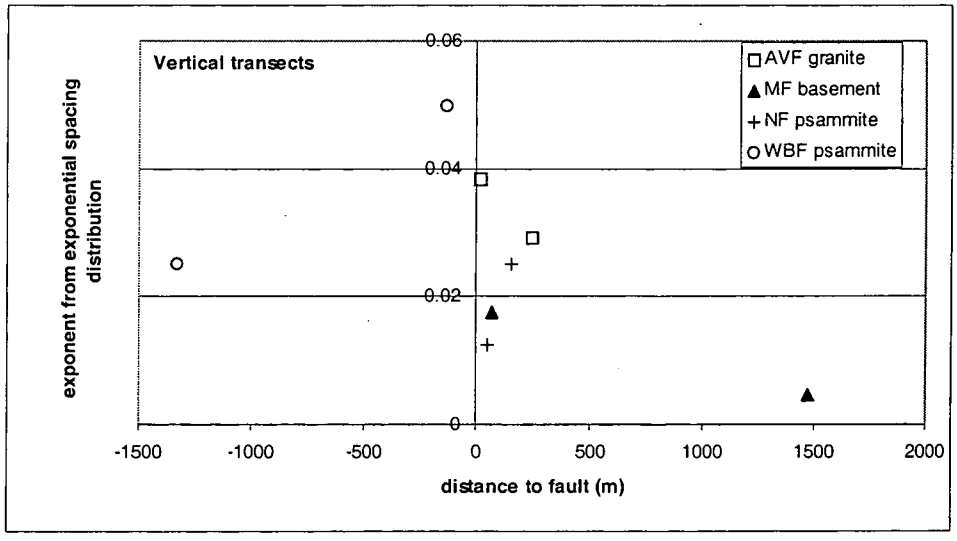

c)

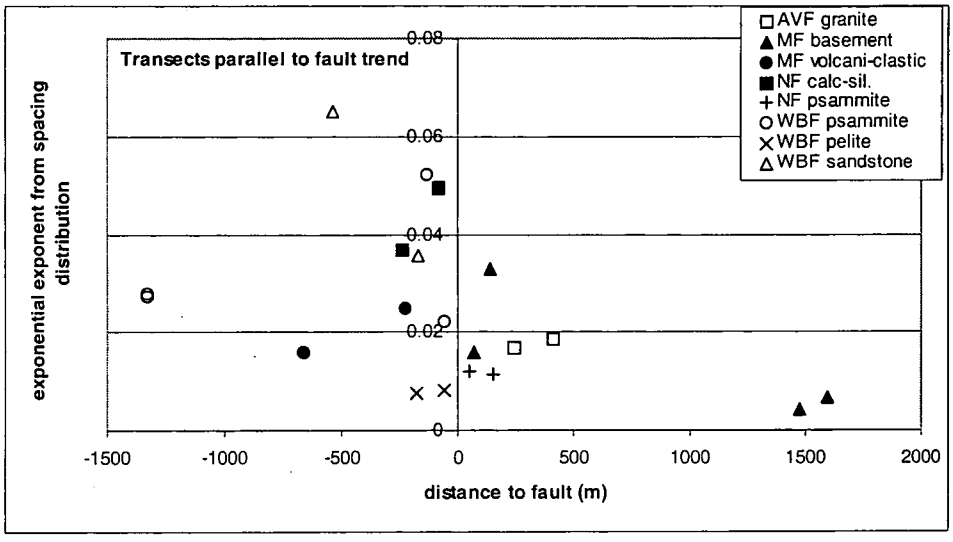

Figure 7.6 Exponent values from exponential spacing distributions plotted against the perpendicular distance to faults within the WBFS.

a) Transects orientated perpendicular to the fault trend

b) Vertical transects

c) Transects orientated parallel to the fault trend (N-S or NE-SW).

a)

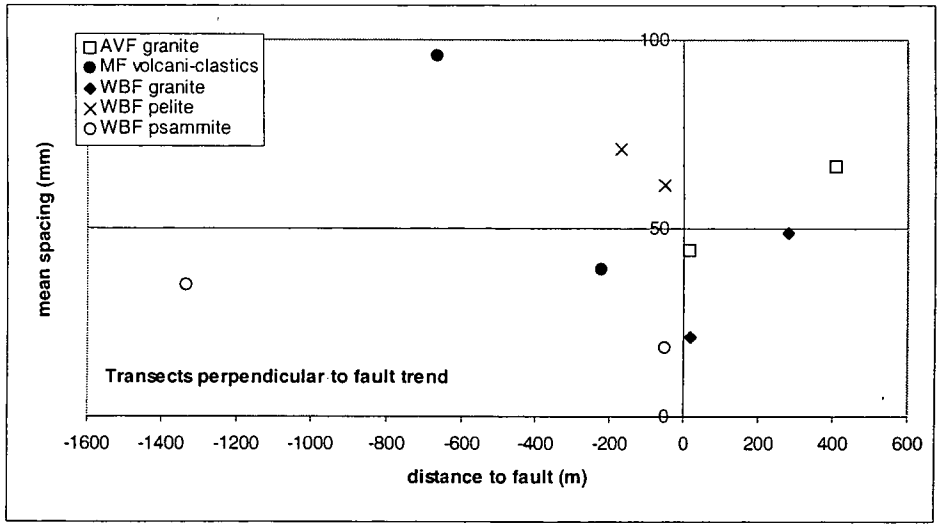

b)

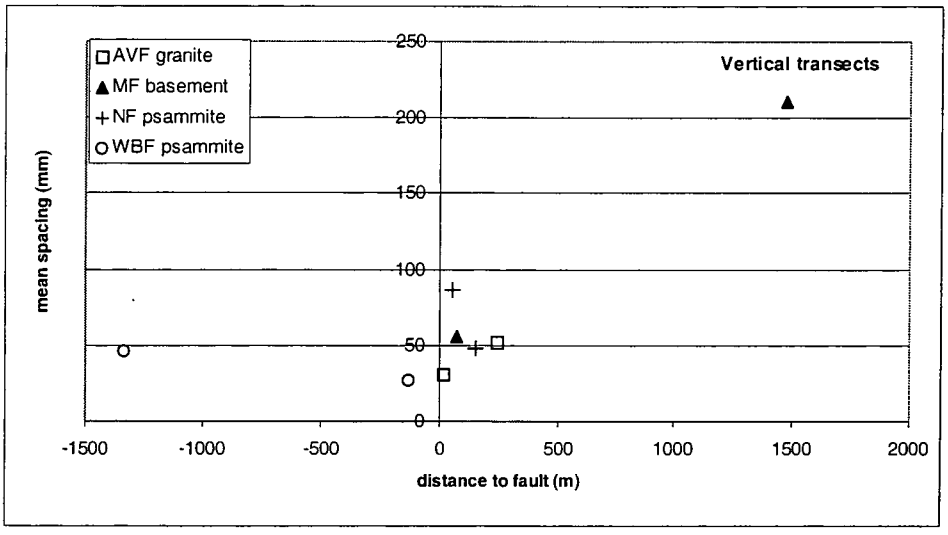

c)

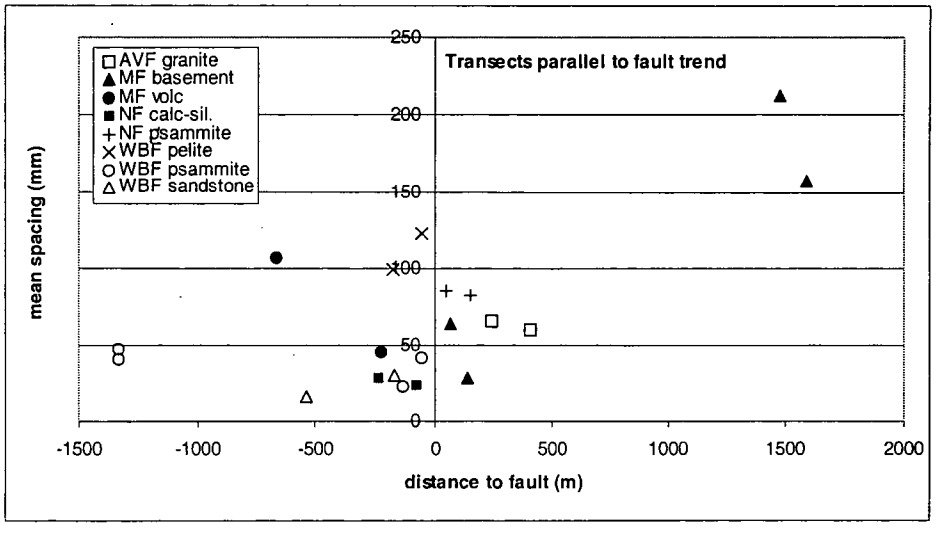

Figure 7.7 Mean spacing values plotted against the perpendicular distance to faults within the WBFS.

a) Transects orientated perpendicular to the fault trend

b) Vertical transects

c) Transects orientated parallel to the fault trend (N-S or NE-SW).

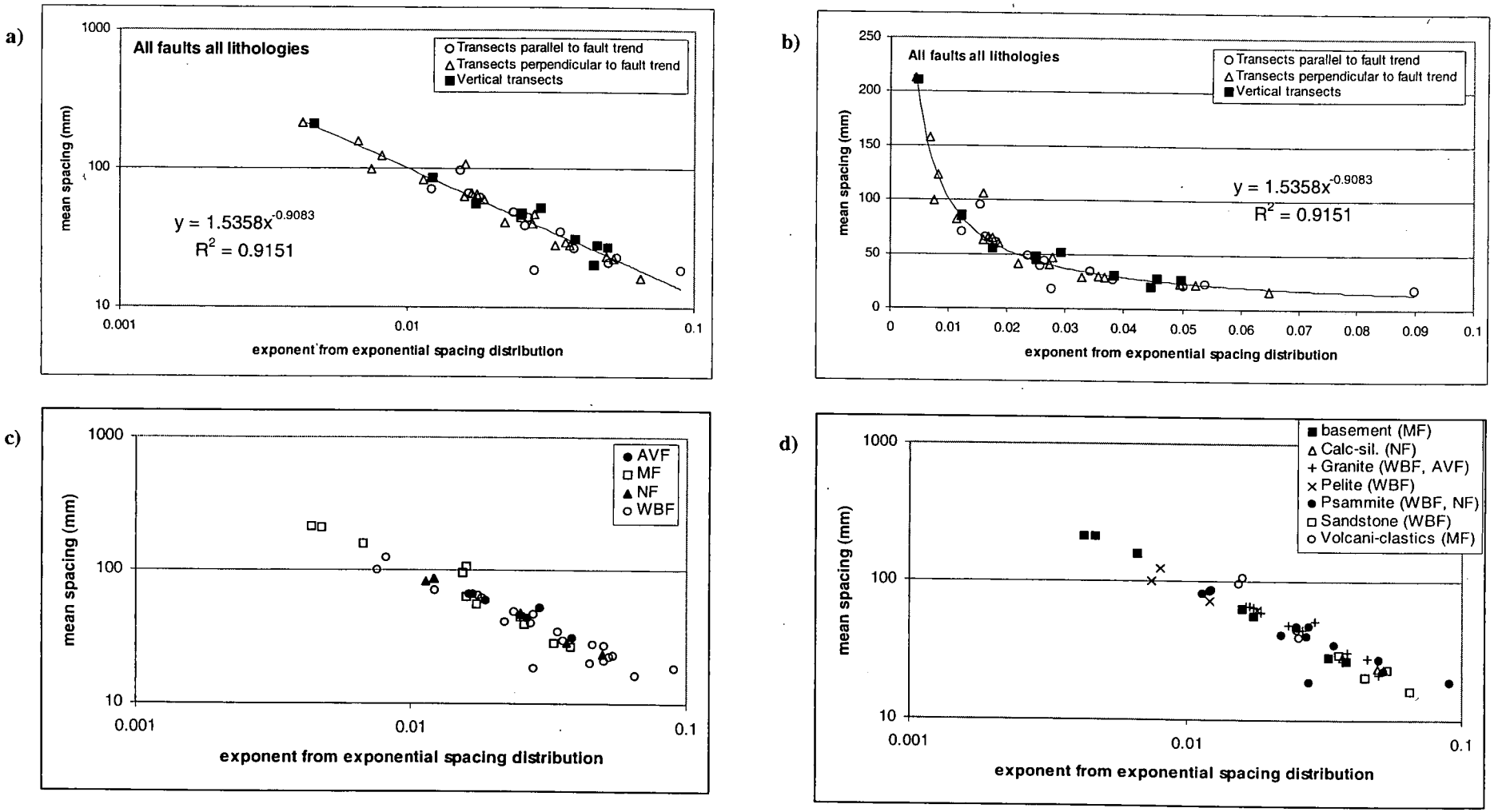

Figure 7.8 Exponent values from exponential spacing distributions 'v' mean spacing for data collected adjacent to the WBFS.
a) data plotted for each transect orientation on logarithmic axes
b) data plotted for each transect orientation on linear axes
c) data plotted for each fault data set on logarithmic axes
d) data plotted for each lithological data set on logarithmic axes

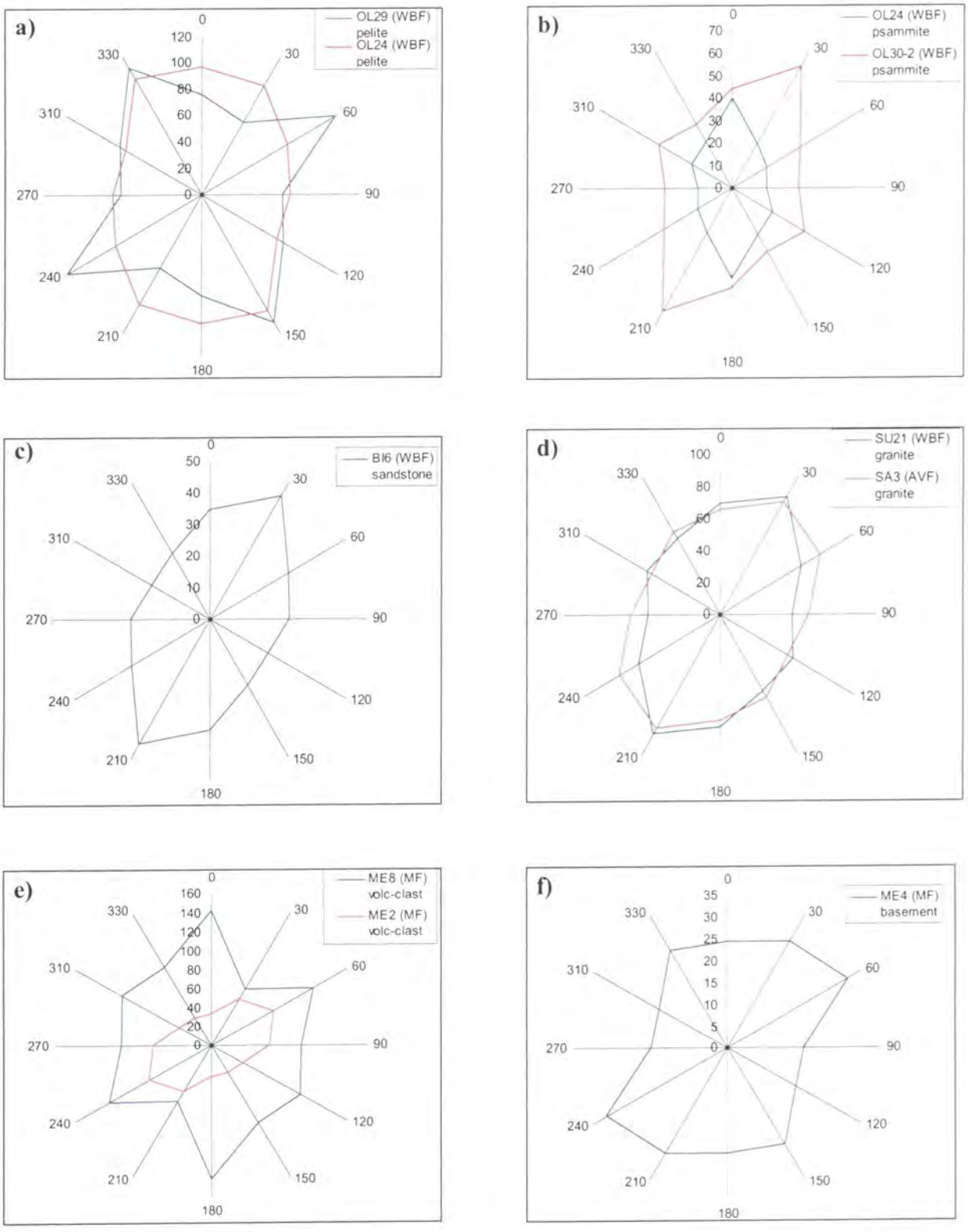

Figure 7.9 Mean spacing ellipses created for data sets collected on horizontal surfaces adjacent to faults within the WBFS. (Mean spacings are measured in mm.) The legend on each plot provides the locality name, lithology and fault adjacent to which the data was collected

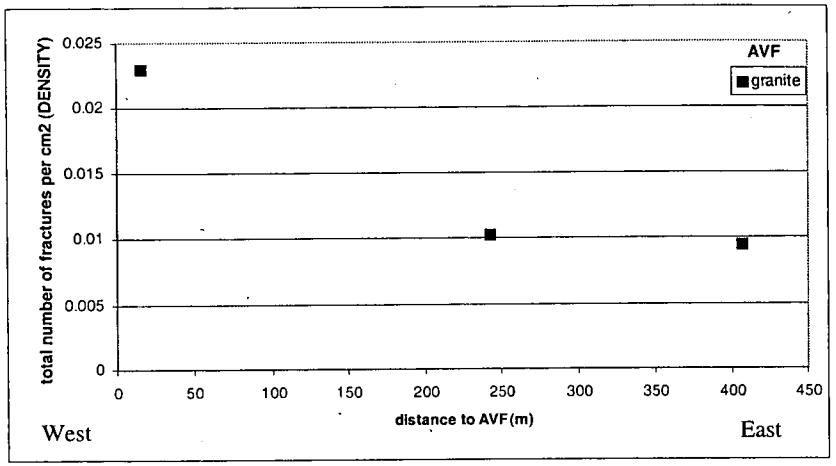

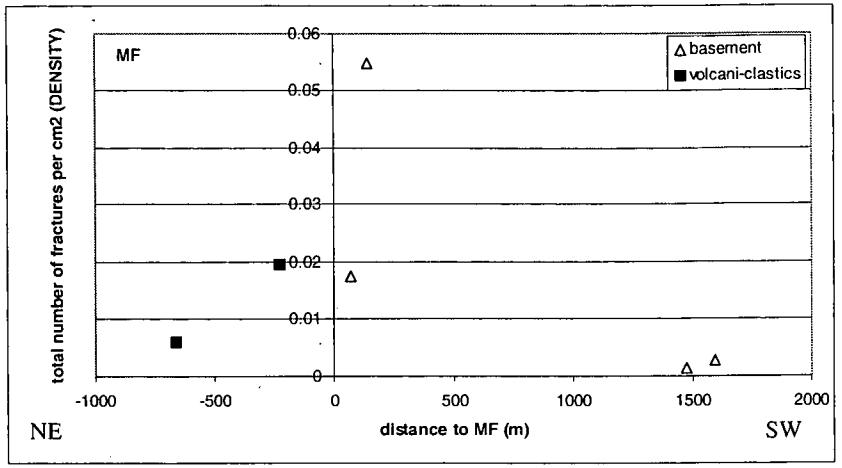

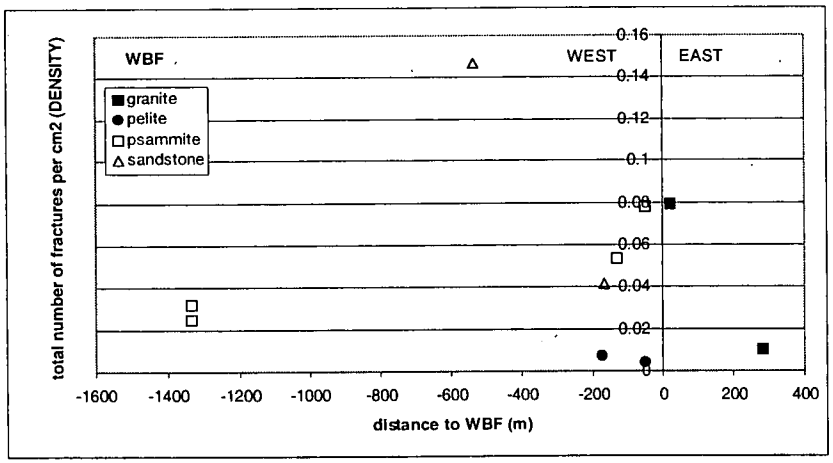

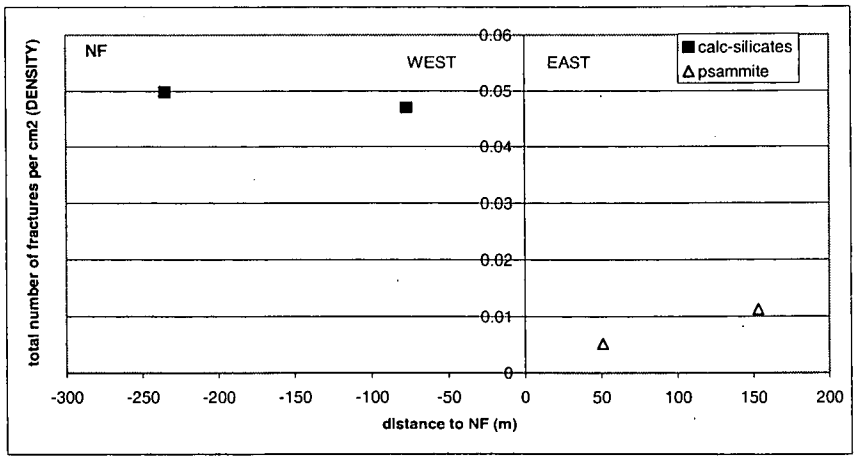

Figure 7.10 Fracture density (total number of fractures per cm²) 'v' perpendicular distance to faults within the WBFS.

a) AVF
b) MF
c) WBF
d) NF

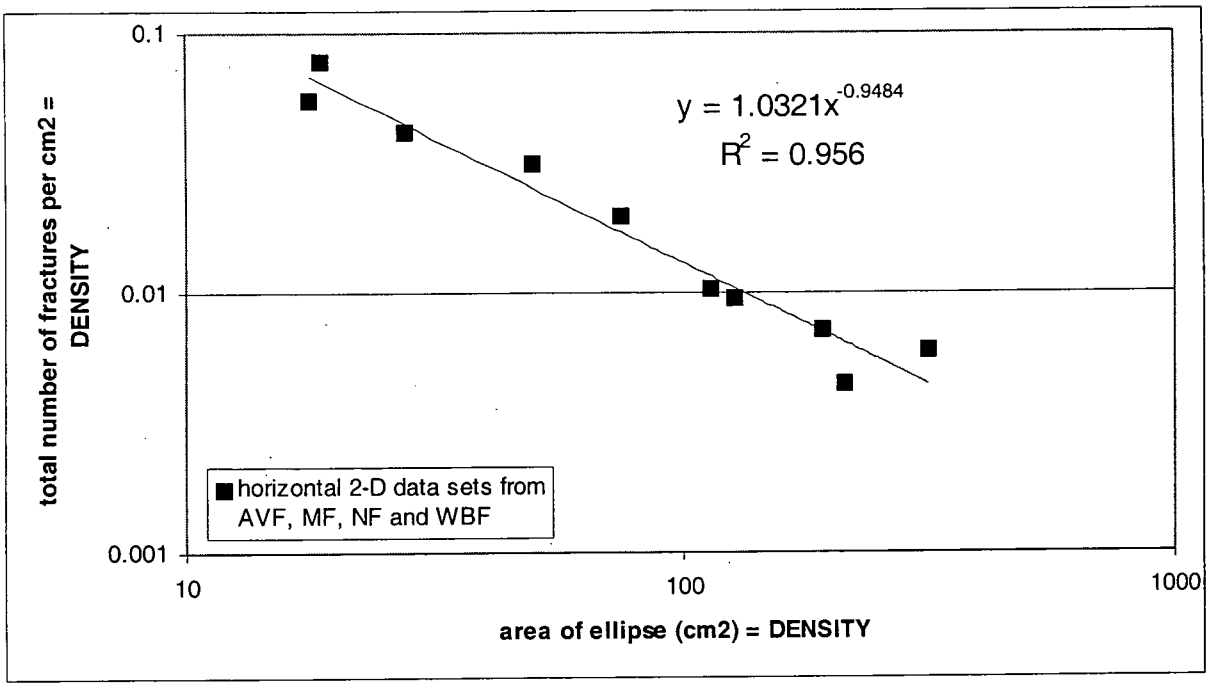

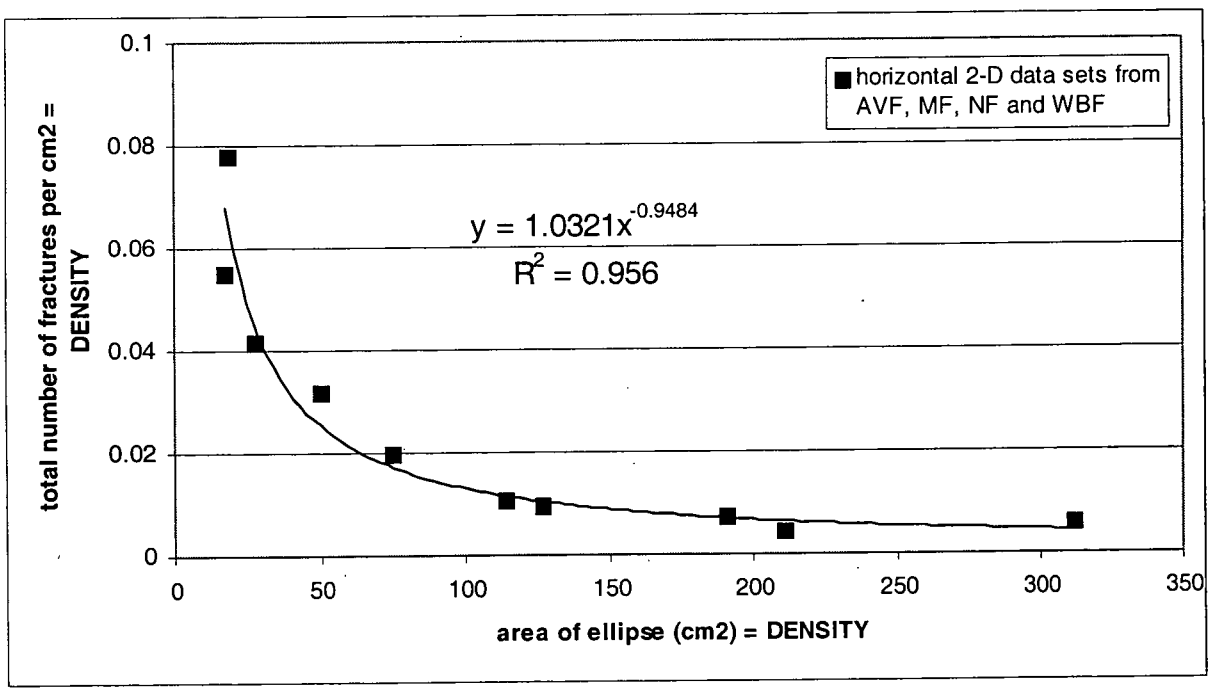

Figure 7.11 Fracture density measured in two ways (number of fractures per cm^2) and area of mean spacing ellipse) plotted against each other on a) logarithmic axes, and b) on linear axes

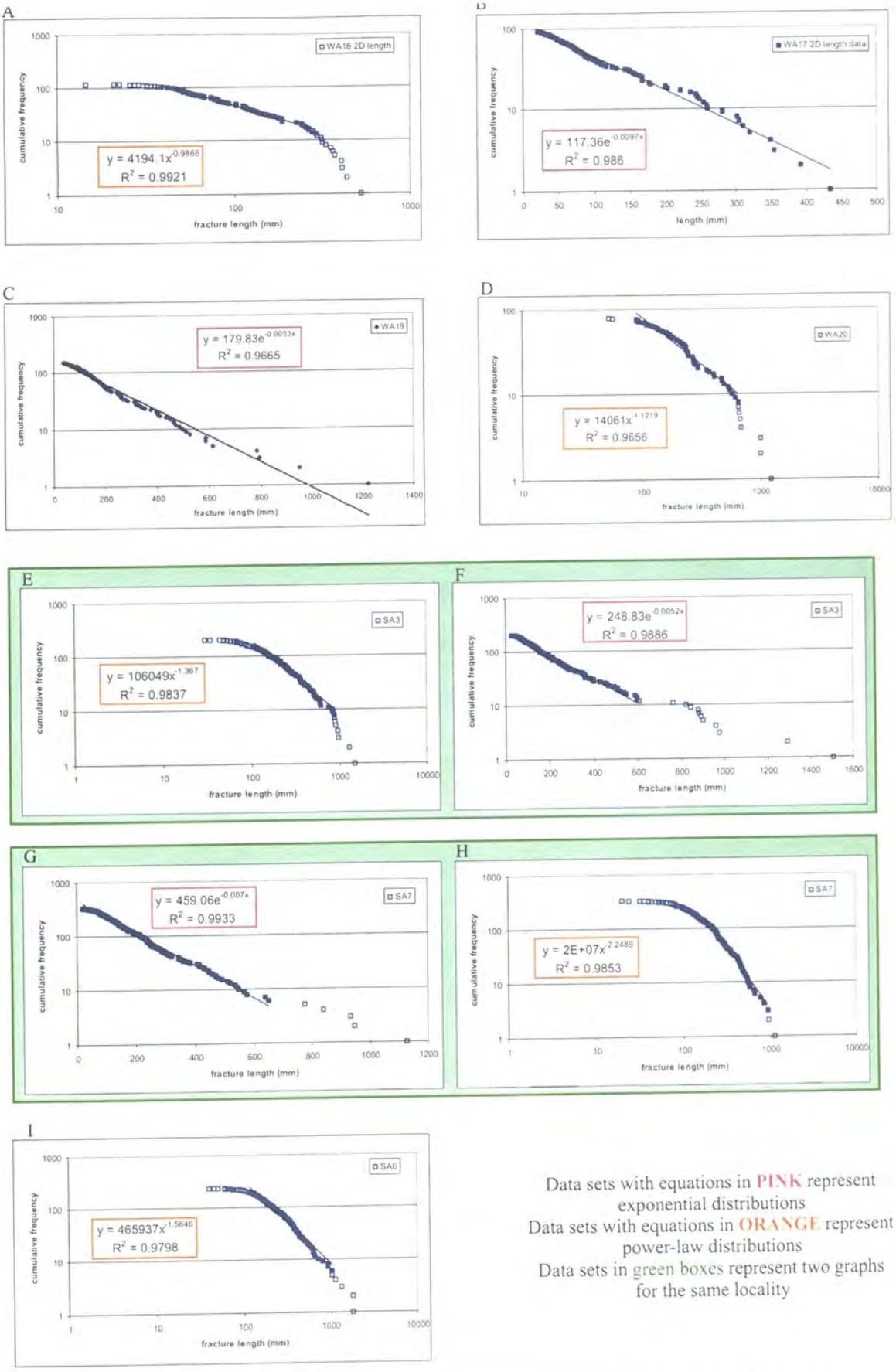

Data sets with equations in PINK represent exponential distributions
Data sets with equations in ORANGE represent power-law distributions
Data sets in green boxes represent two graphs for the same locality

Figure 7.12 Fracture length 'v' cumulative frequency plots for data collected adjacent to faults within the WBFS (continued on next 3 pages)
A - D = data collected adjacent to the NF
E - I = data collected adjacent to the AVF
J - P = data collected adjacent to the MF
Q - AE = data collected adjacent to the WBF

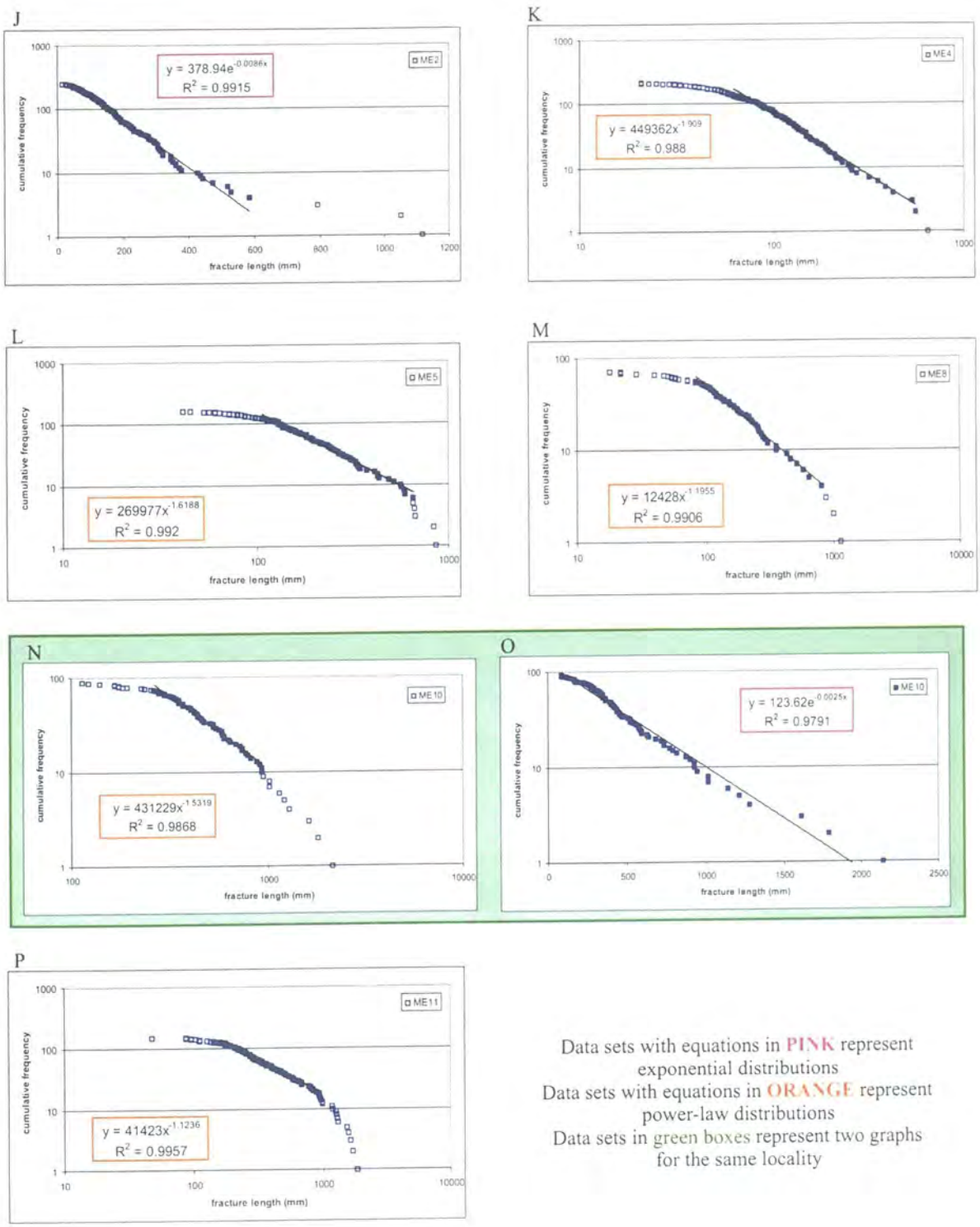

Data sets with equations in PINK represent exponential distributions
Data sets with equations in ORANGE represent power-law distributions
Data sets in green boxes represent two graphs for the same locality

Figure 7.12 Fracture length 'v' cumulative frequency plots for data collected adjacent to faults within the WBFS (continued from previous page, and continued on next 2 pages)
A - D = data collected adjacent to the NF
E - I = data collected adjacent to the AVF
J - P = data collected adjacent to the MF
Q - AE = data collected adjacent to the WBF

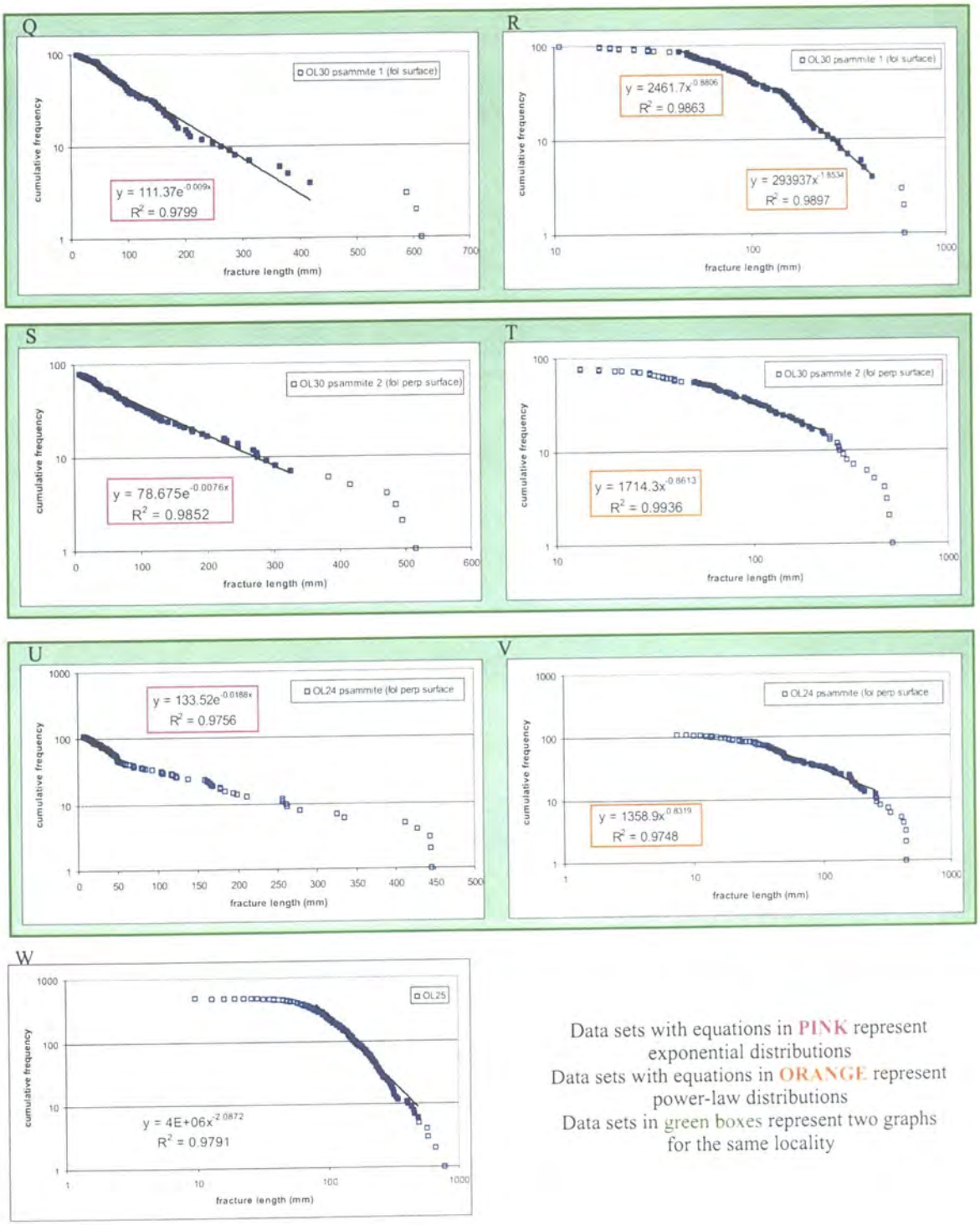

Data sets with equations in PINK represent exponential distributions
Data sets with equations in ORANGE represent power-law distributions
Data sets in green boxes represent two graphs for the same locality

Figure 7.12 Fracture length 'v' cumulative frequency plots for data collected adjacent to faults within the WBFS (continued from previous 2 pages, continued on next page)
A - D = data collected adjacent to the NF
E - I = data collected adjacent to the AVF
J - P = data collected adjacent to the MF
Q - AE = data collected adjacent to the WBF

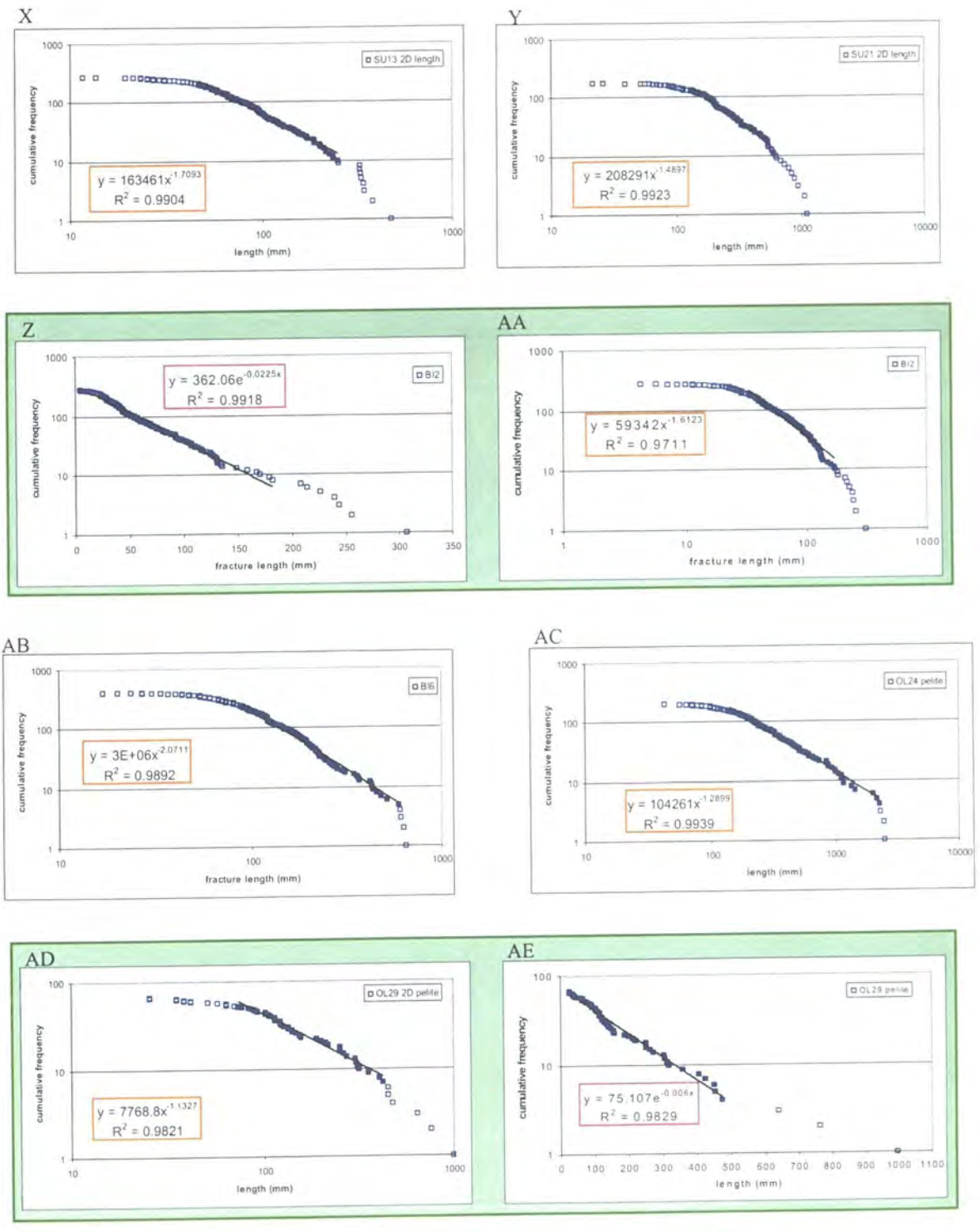

Figure 7.12 Fracture length 'v' cumulative frequency plots for data collected adjacent to faults within the WBFS (continued from previous 3 pages)
A - D = data collected adjacent to the NF
E - I = data collected adjacent to the AVF
J - P = data collected adjacent to the MF
Q - AE = data collected adjacent to the WBF

Data sets with equations in PINK represent exponential distributions
Data sets with equations in ORANGE represent power-law distributions
Data sets in green boxes represent two graphs for the same locality

a)

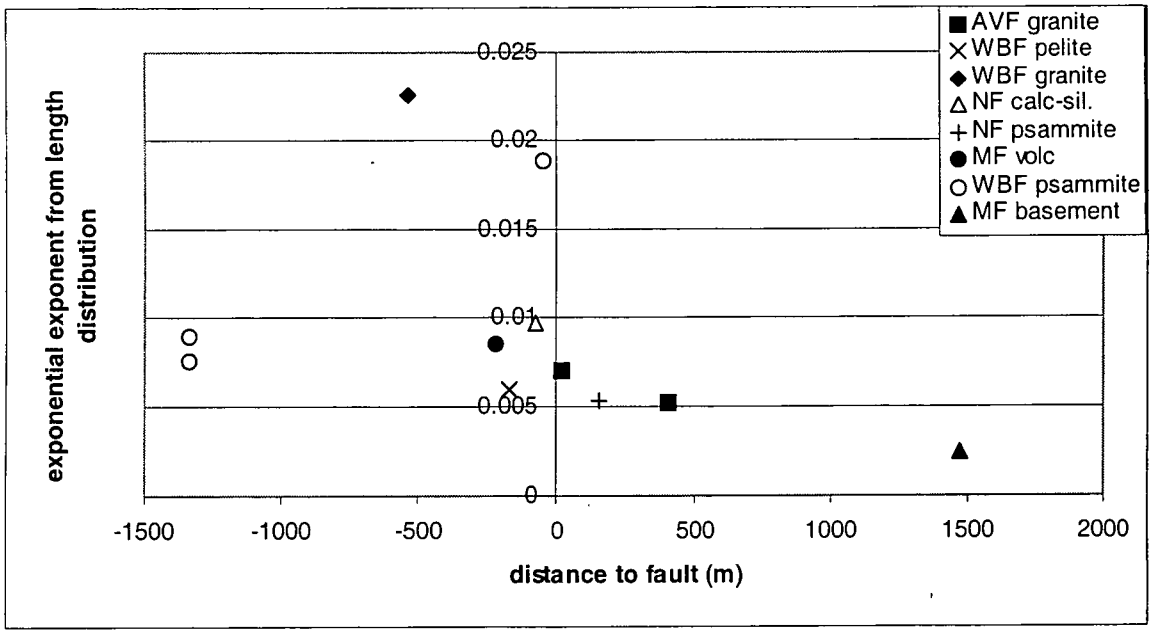

b)

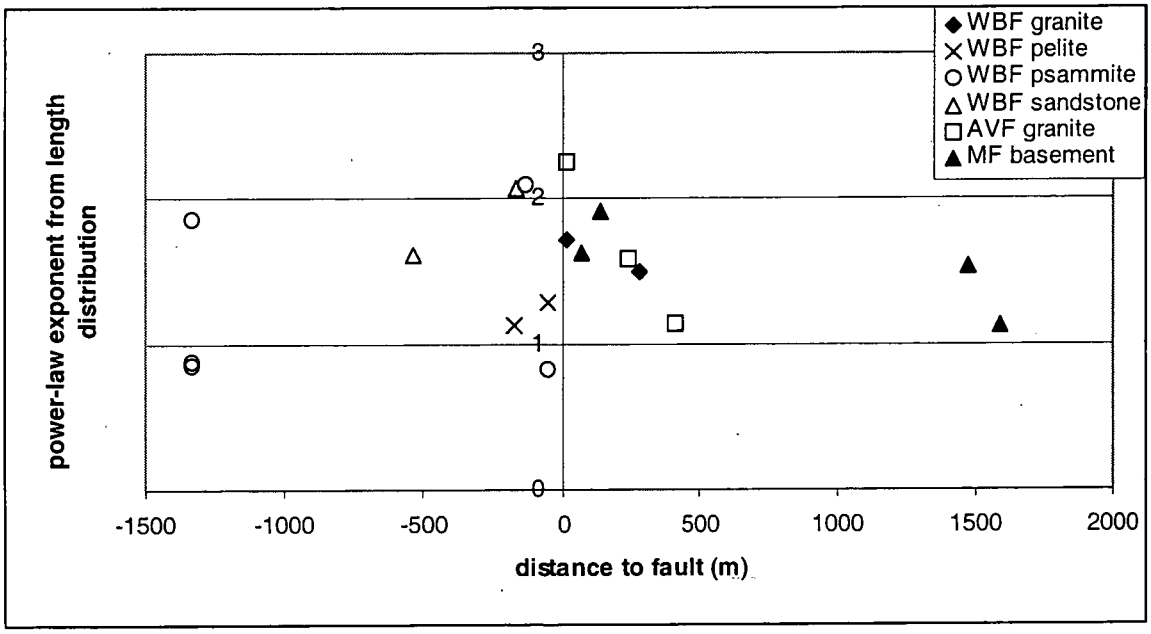

Figure 7.13 Exponent from best-fitting fracture length distributions 'v' perpendicular distance to faults within the WBFS.
A – exponential exponents
B – power-law exponents

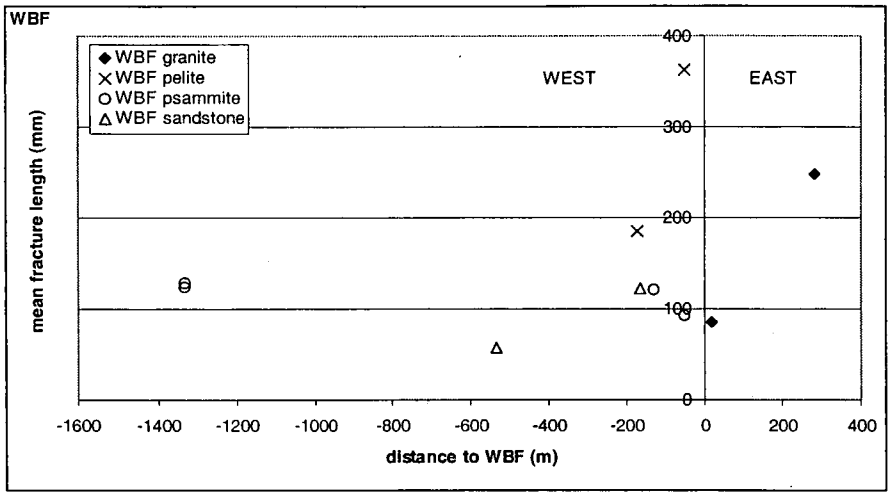

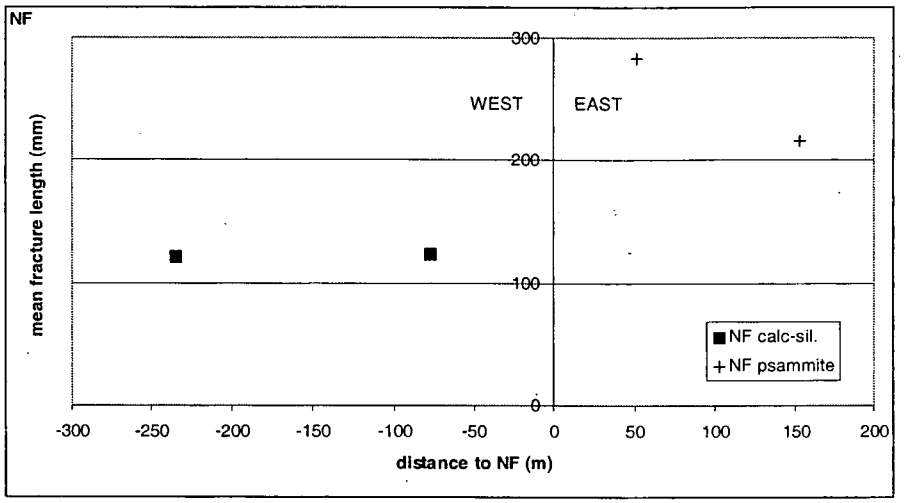

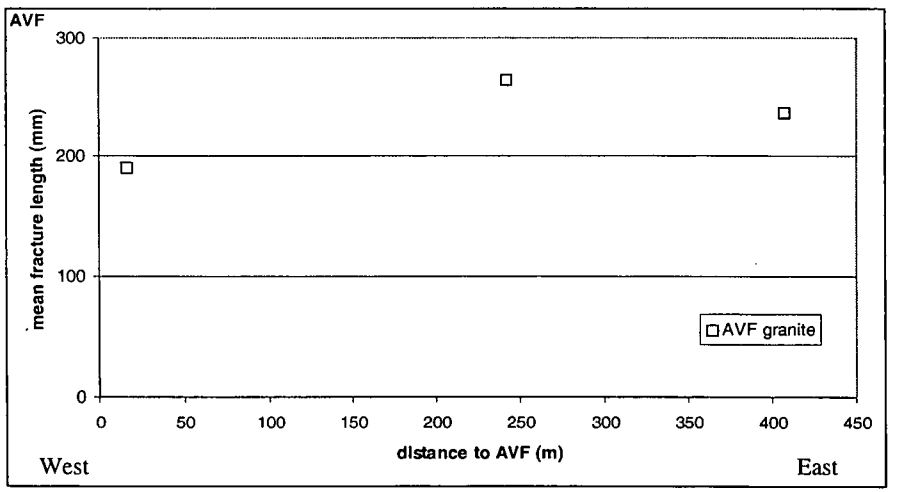

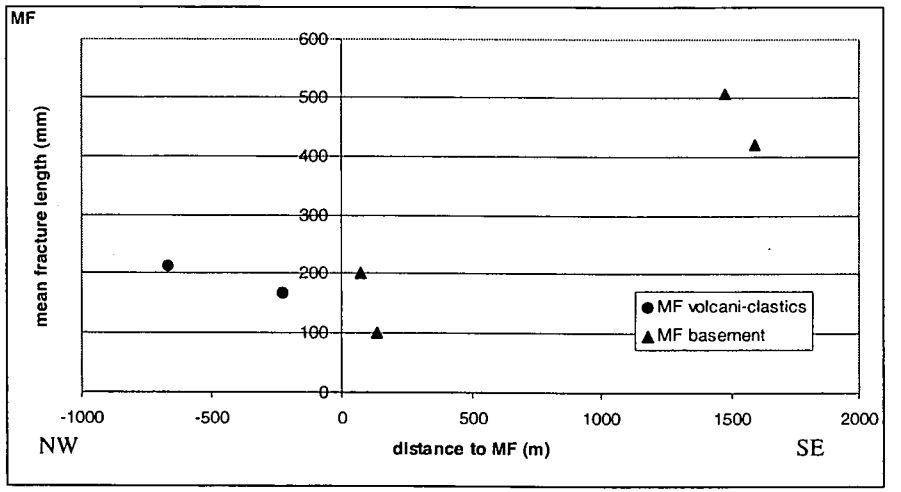

Figure 7.14 Mean fracture length plotted against the perpendicular distance to faults within the WFBS.

a) WBF
b) NF
c) AVF
d) MF

a)

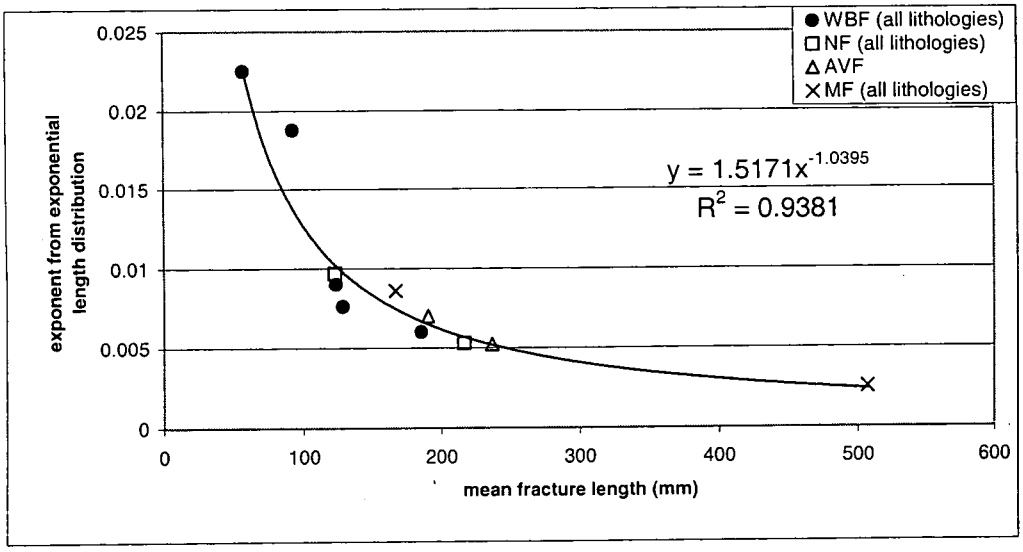

b)

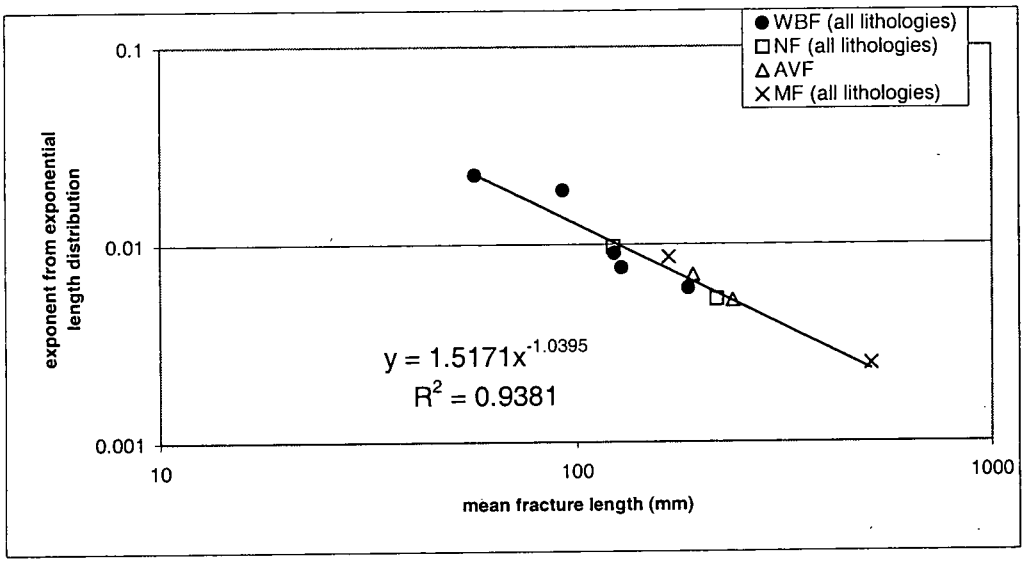

c)

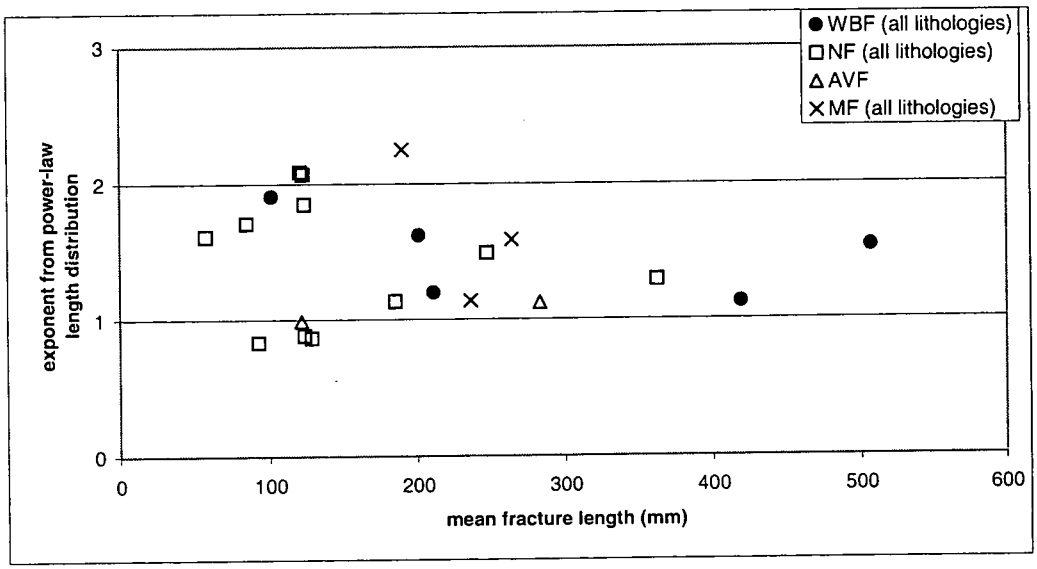

Figure 7.15 Exponent values from fracture length distributions 'v' mean fracture length for data collected adjacent to faults within the WBFS.
a) exponential exponents 'v' mean length plotted on linear axes
b) exponential exponents 'v' mean length plotted on linear axes
c) power-law exponents 'v' mean length plotted on linear axes

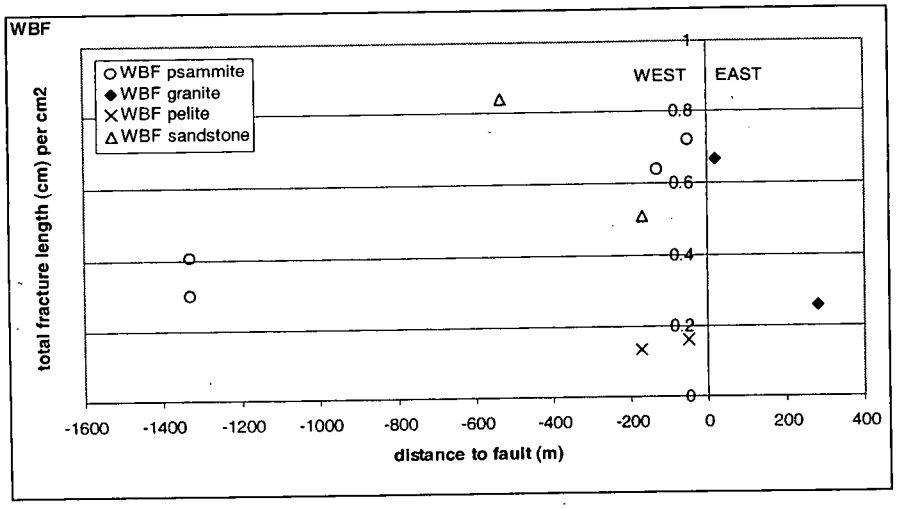

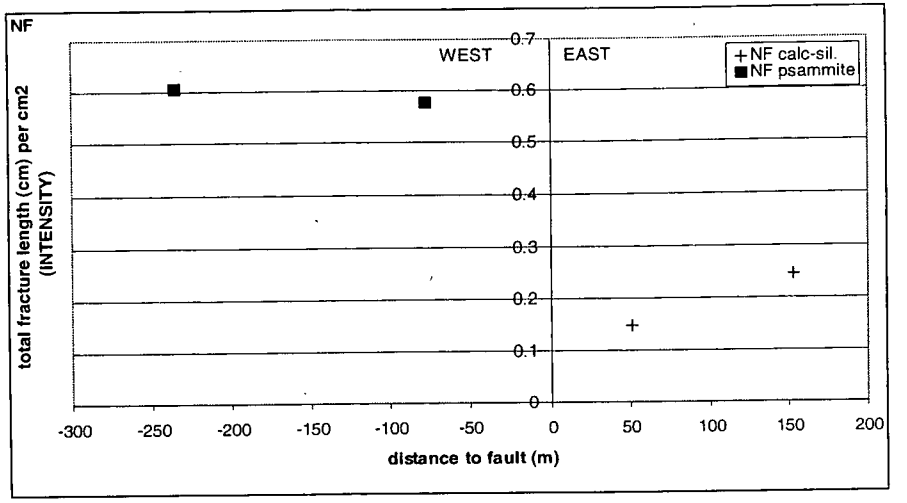

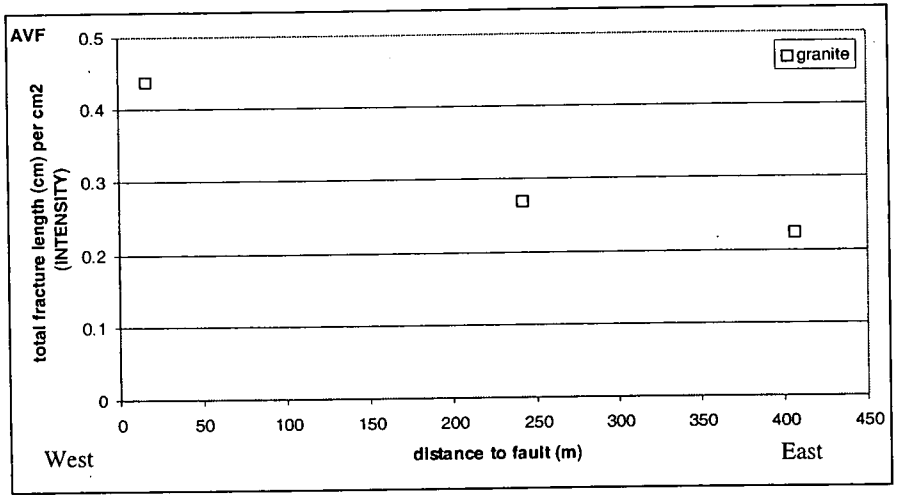

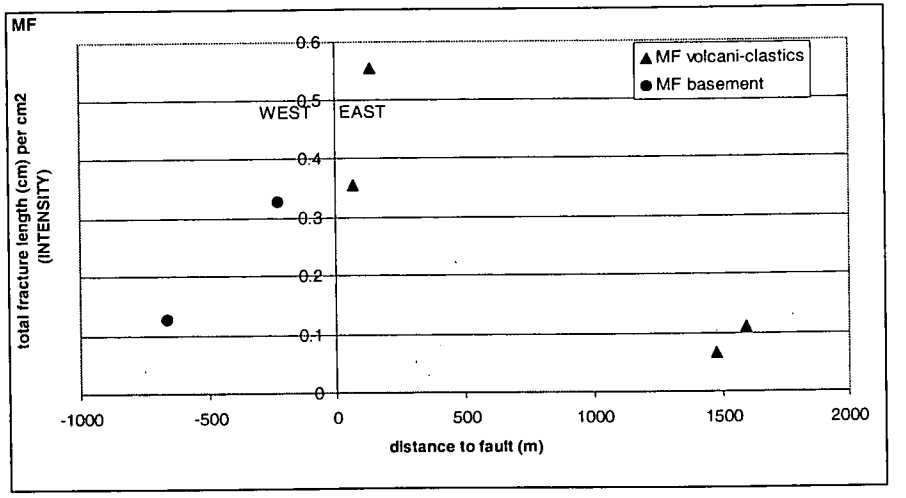

Figure 7.16 Fracture intensity (total fracture length (cm) per cm²) 'v' perpendicular distance to faults within the WBFS.

a) WBF
b) NF
c) AVF
d) MF

a)

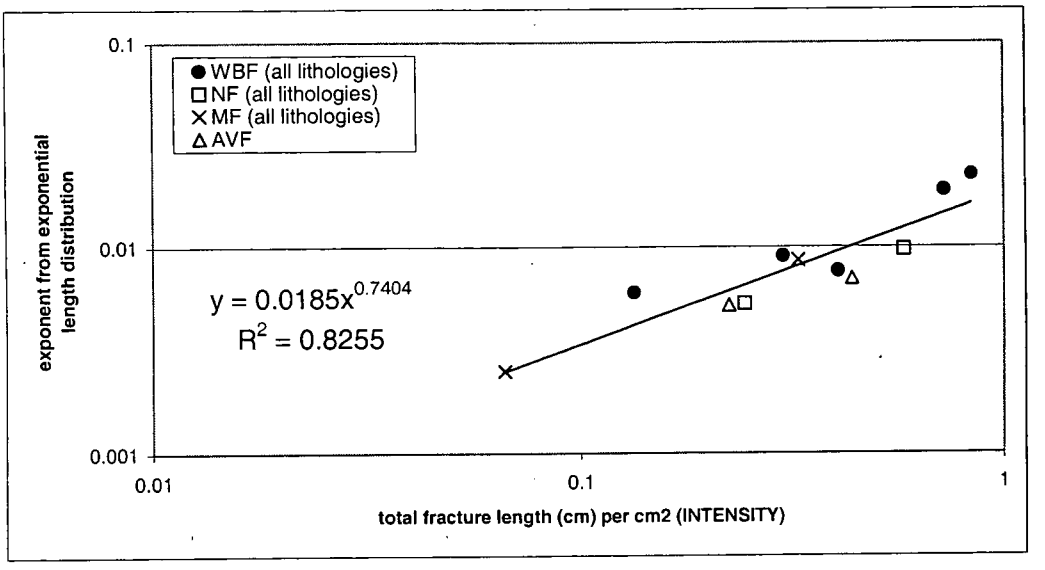

b)

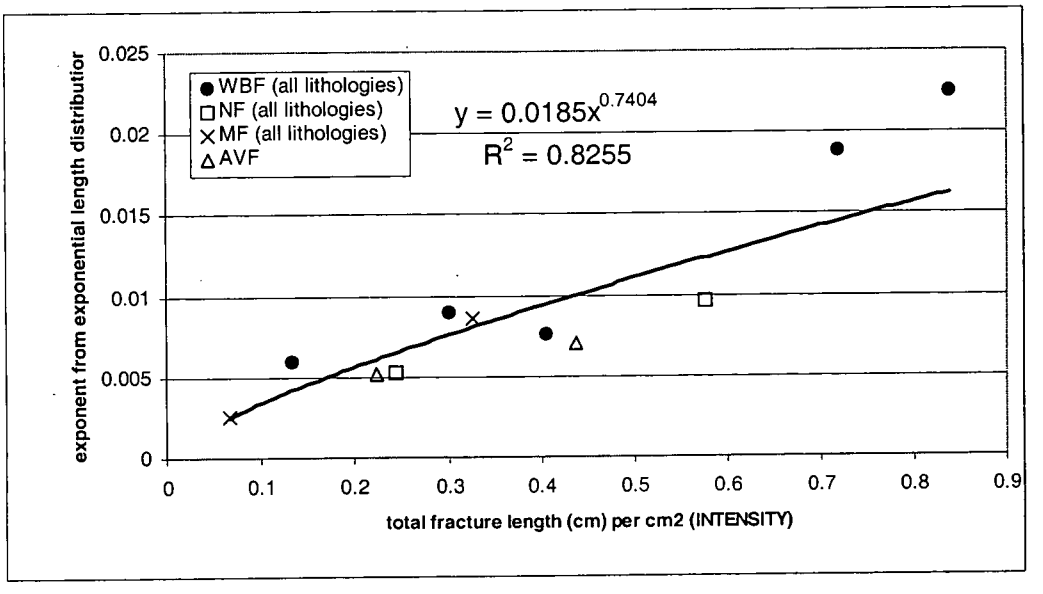

c)

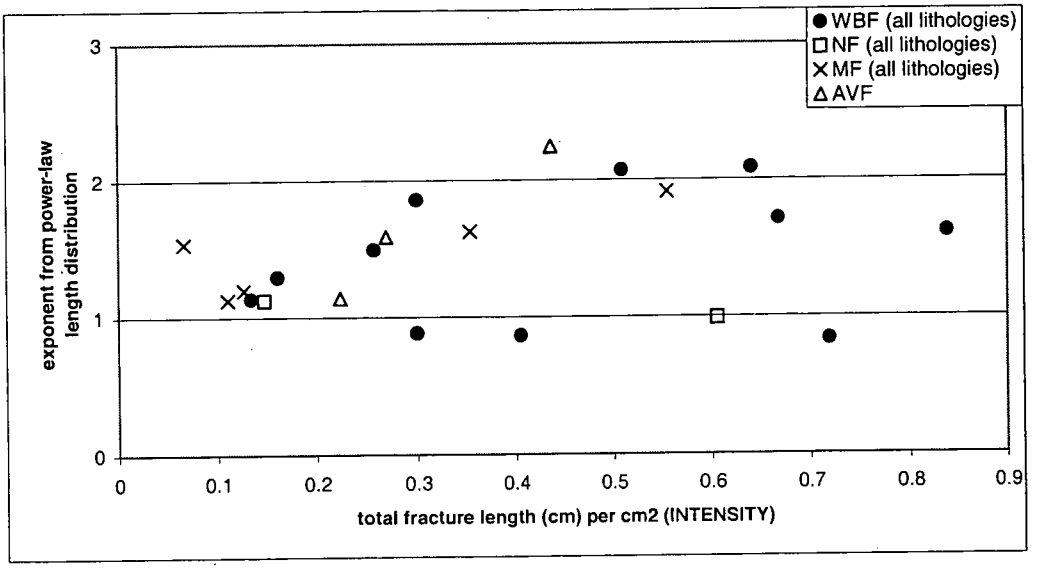

Figure 7.17 Exponent from best-fitting fracture length distributions 'v' fracture intensity (total fracture length (cm) per cm²)
a) exponentially distributed fracture length data sets plotted on logarithmic axes
b) exponentially distributed fracture length data sets plotted on linear axes
c) power-law length data sets

a)

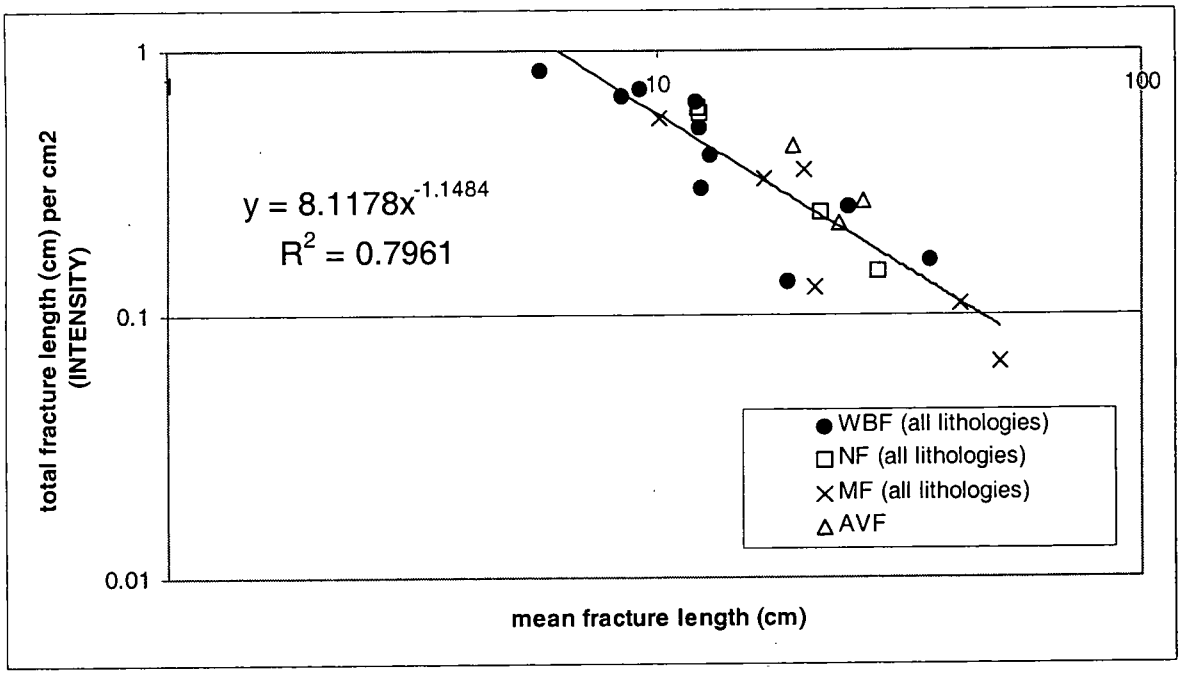

b)

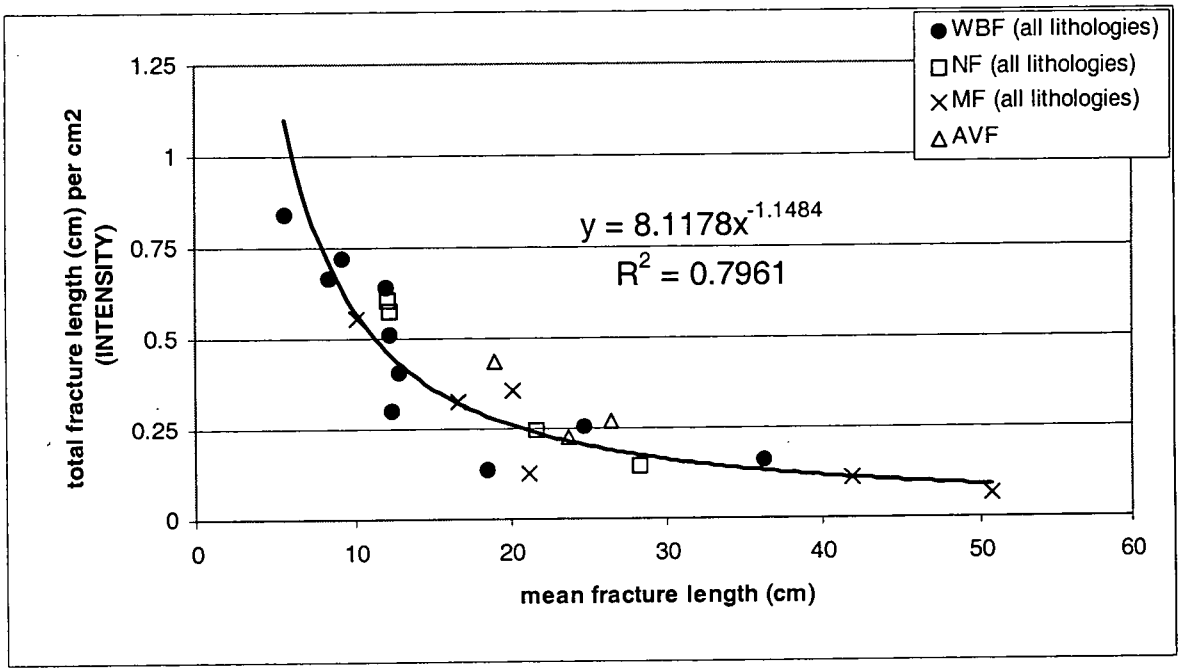

Figure 7.18 Fracture intensity (total fracture length (cm) per cm²) 'v' mean fracture length plotted on (a) logarithmic and (b) linear axes

a)

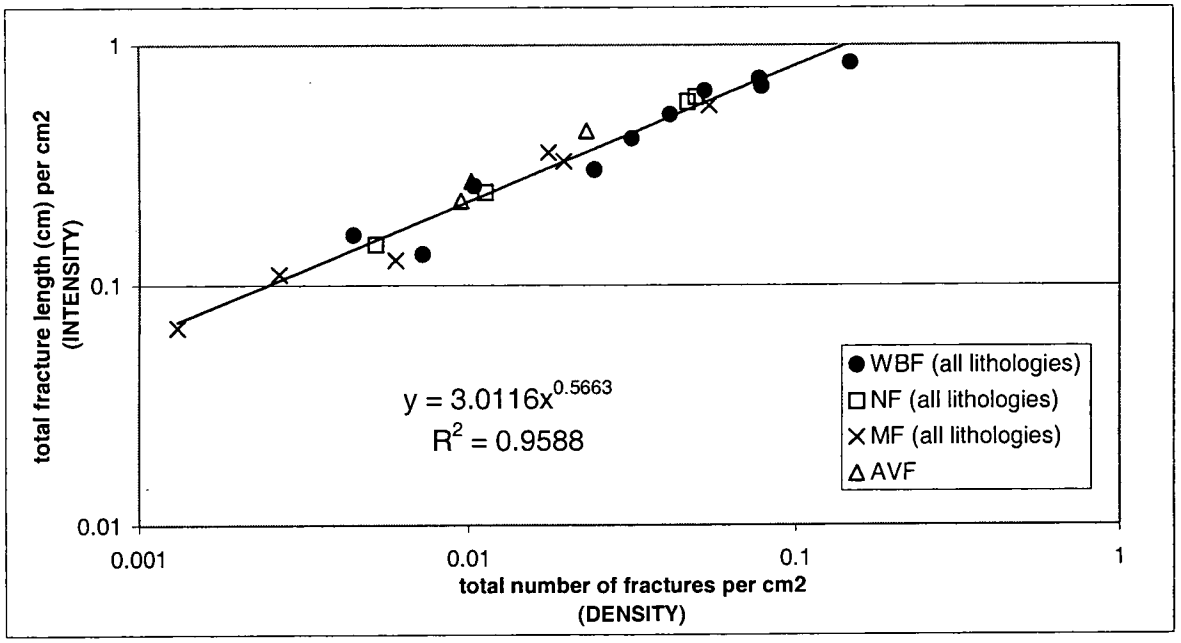

b)

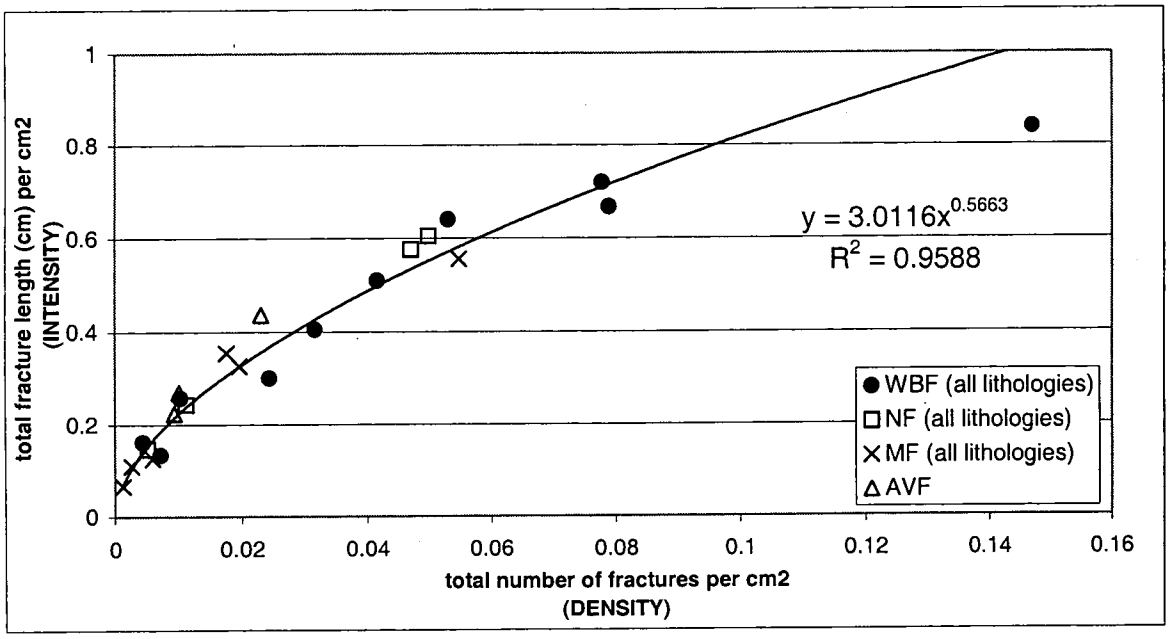

Figure 7.19 Fracture density (total number of fractures per cm²) 'v' fracture intensity (total fracture length (cm) per cm ²)
a) data plotted on logarithmic axes
b) data plotted on linear axes

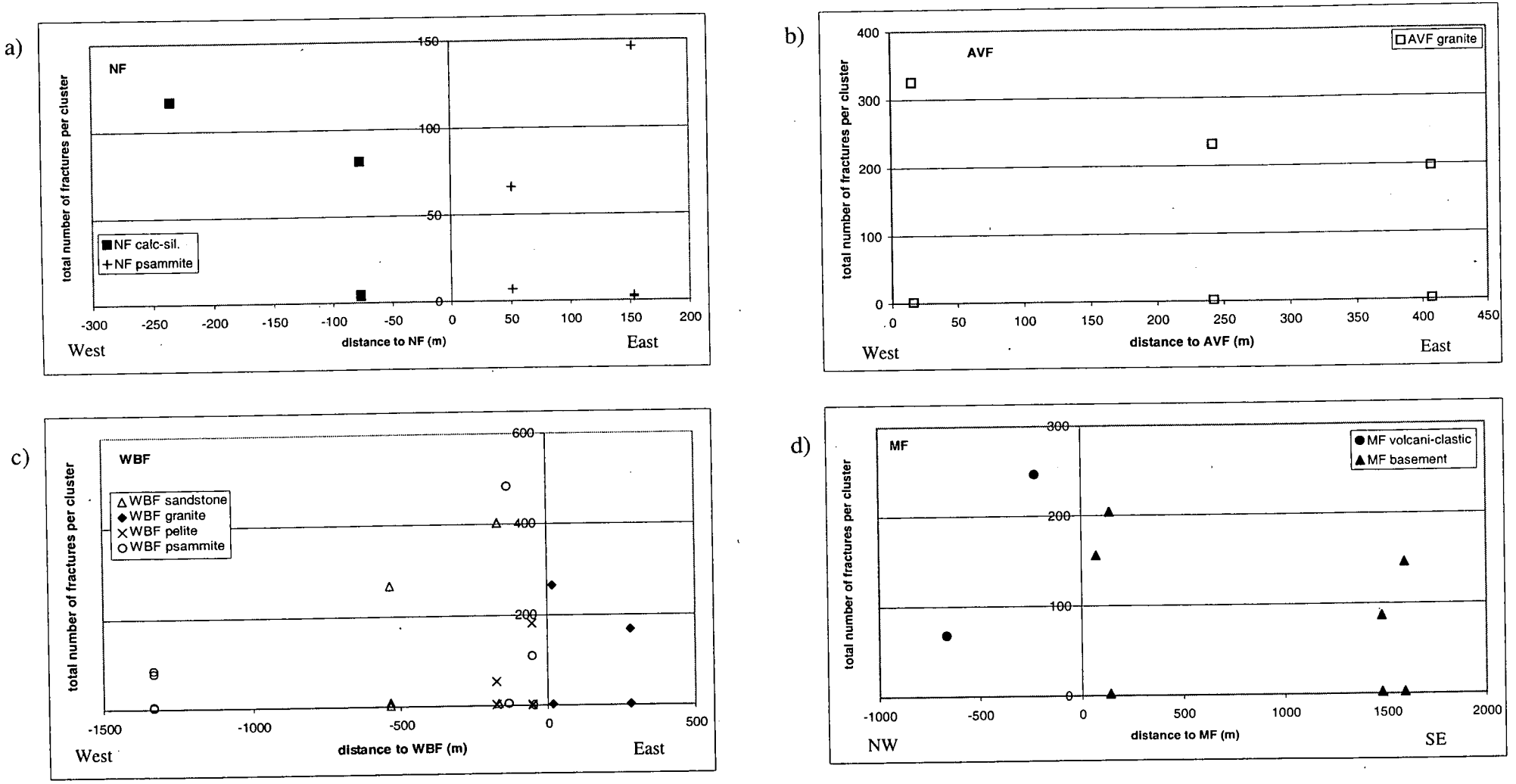

Figure 7.20 Total number of fractures per cluster 'v' perpendicular distance to faults within the WBFS.
a) - NF
b)- AVF
c) - WBF
d) - MF

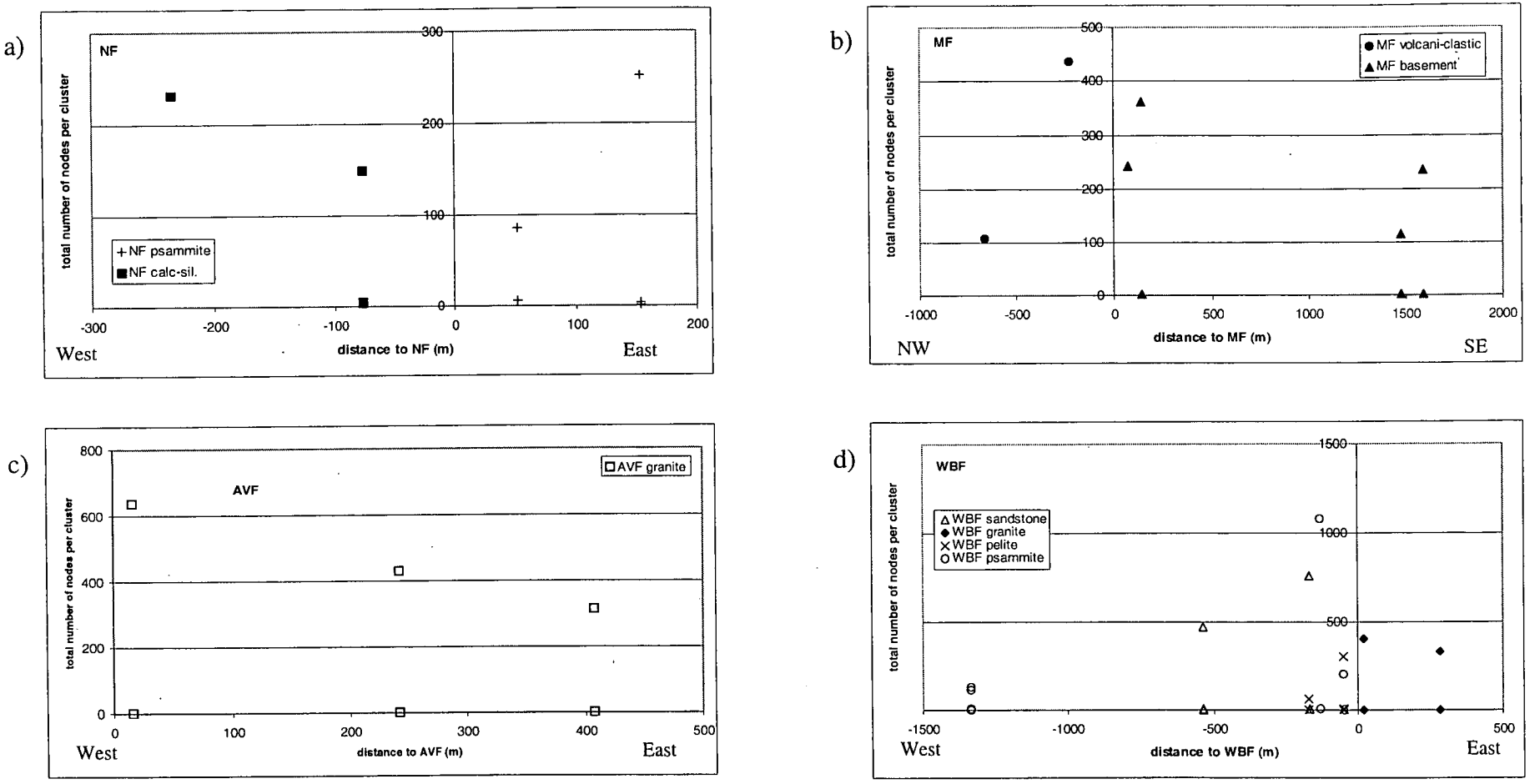

Figure 7.21 Total number of nodes per cluster 'v' perpendicular distance to faults within the WBFS
a) NF
b) MF
c) AVF
d) WBF

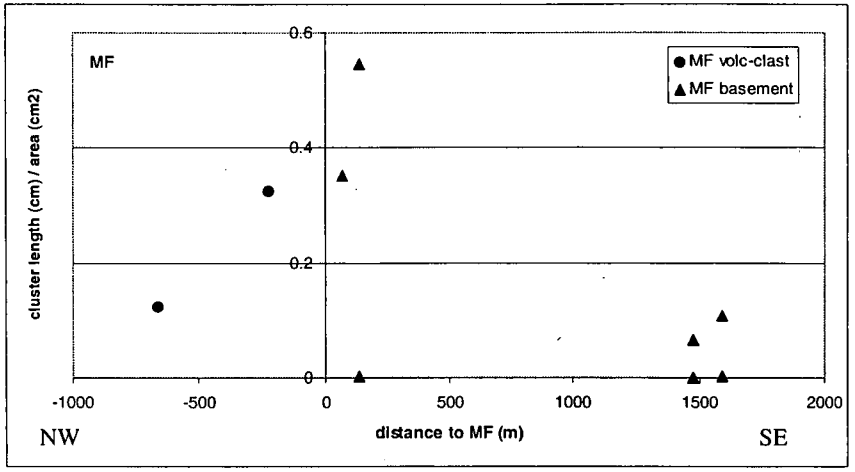

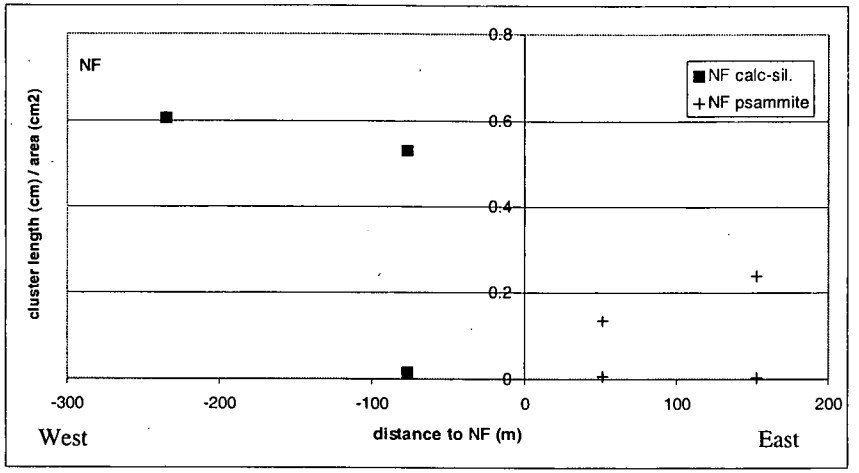

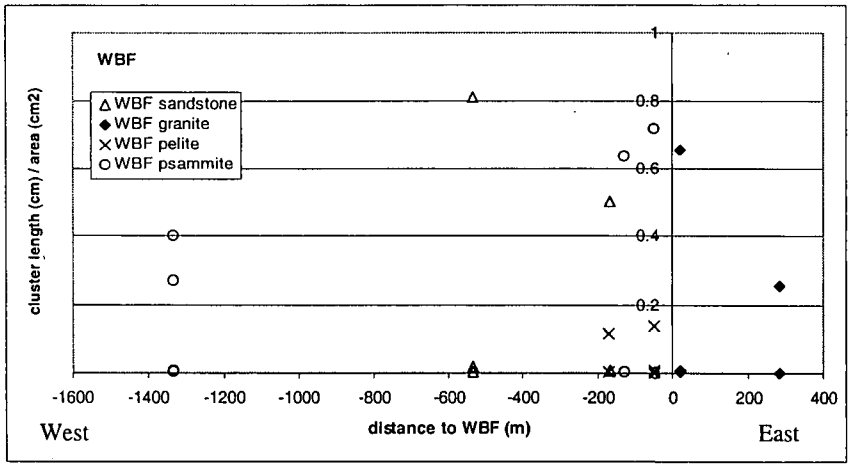

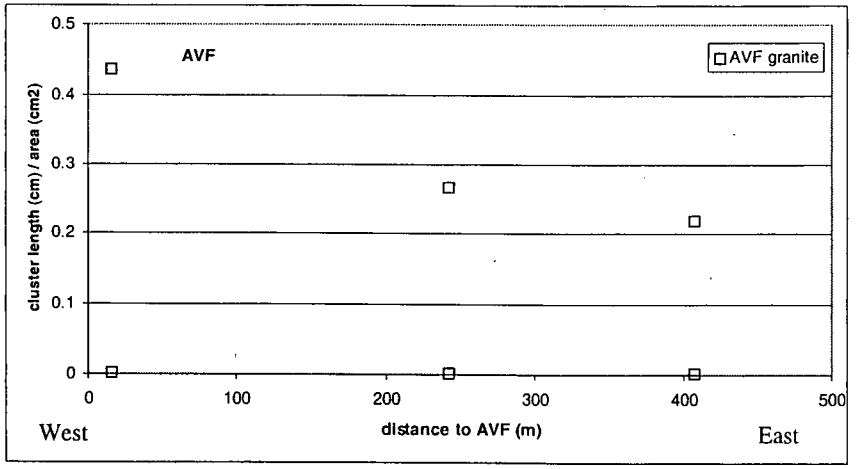

Figure 7.22 Total cluster length (cm) per cm² 'v' perpendicular distance to faults within the WBFS
a) MF
b) NF
c) WBF
d) AVF

A

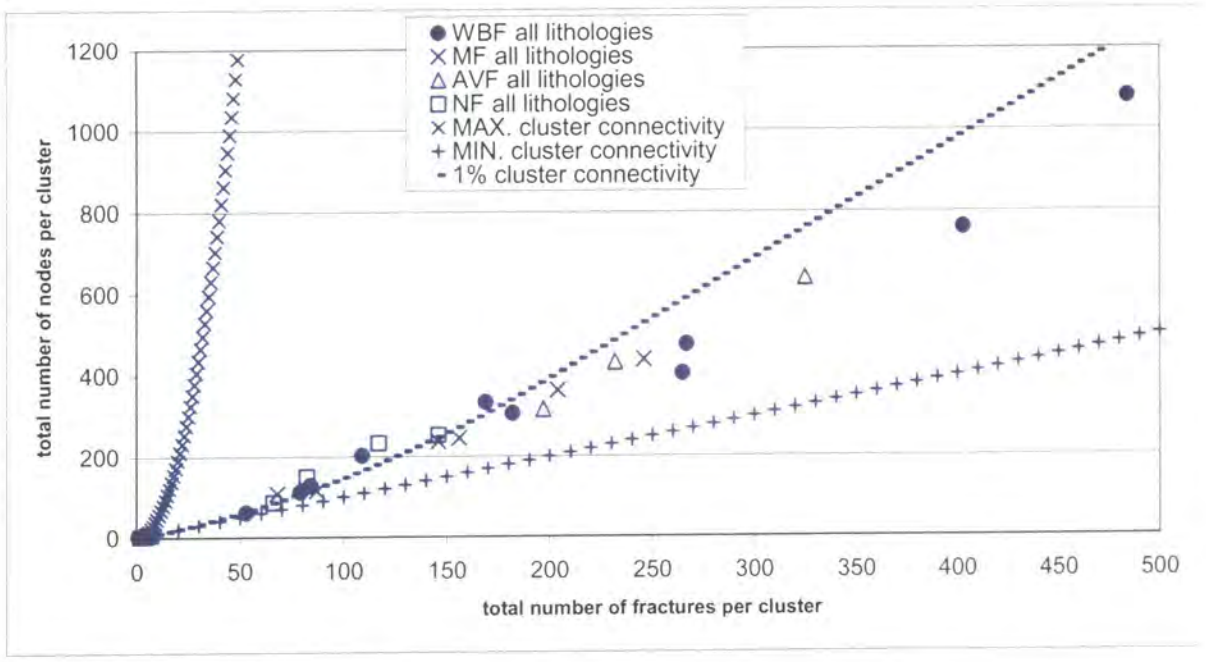

B

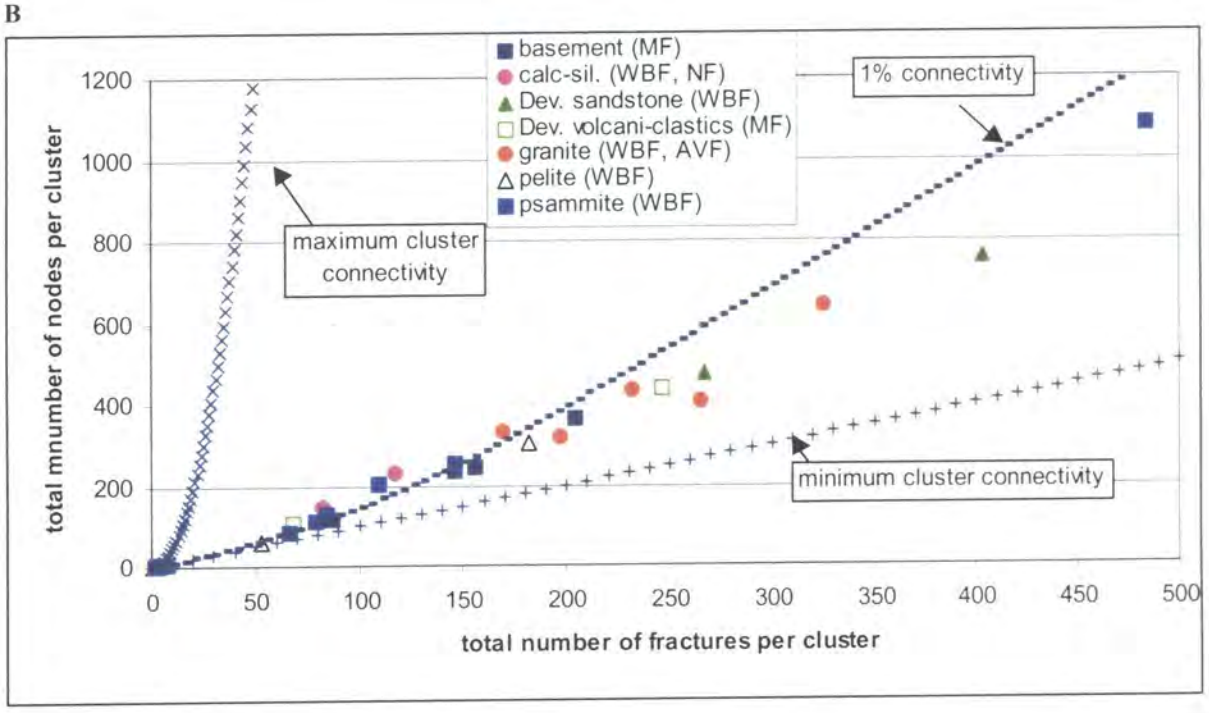

Figure 7.23 Total number of fractures per cluster 'v' total number of nodes per cluster for data sets collected adjacent to faults within the WBFS
A – data separated for each fault
B – data separated for each lithology

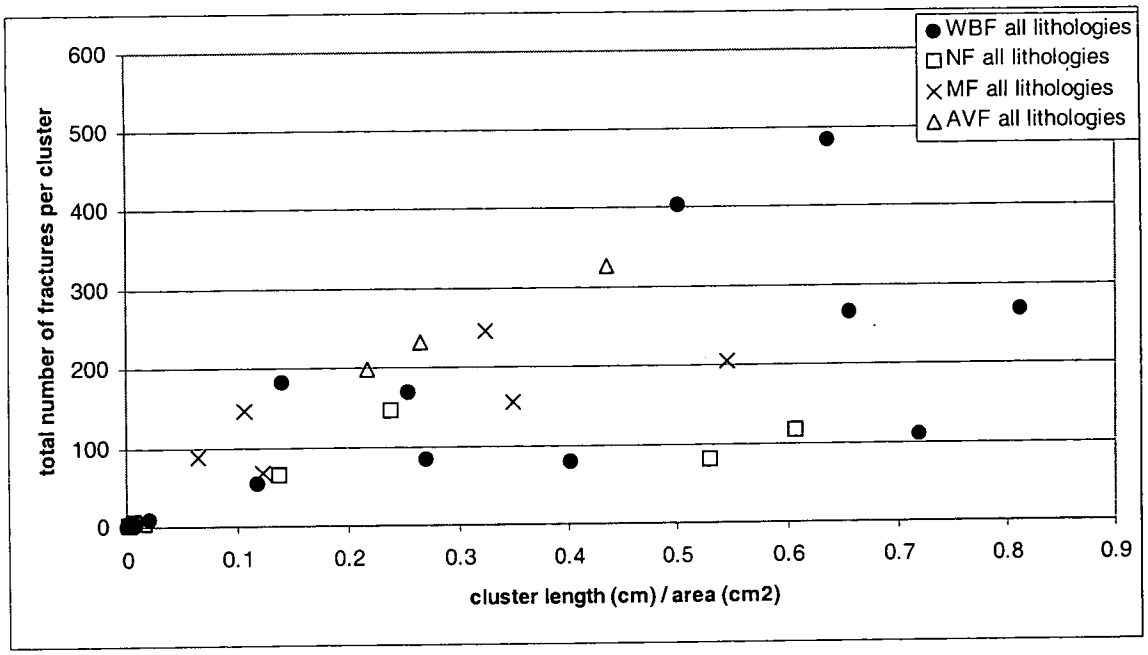

Figure 7.24 Total fracture cluster length (cm) per cm² 'v' total number of fractures per cluster for data sets collected adjacent to faults within the WBFS

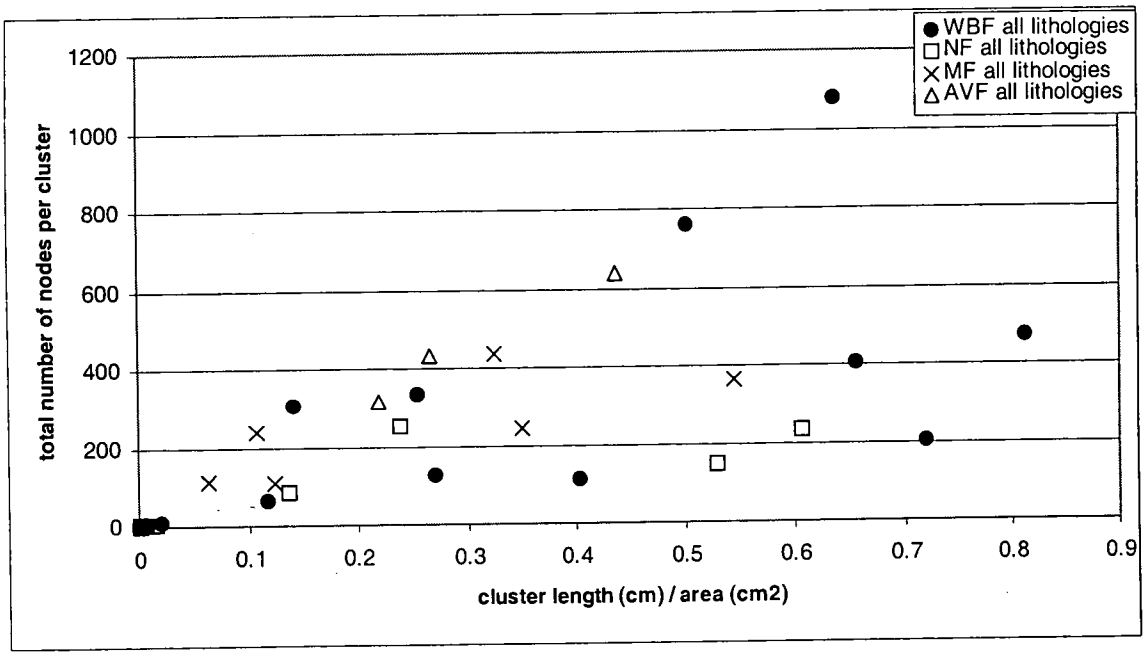

Figure 7.25 Total fracture cluster length (cm) per cm² 'v' total number of nodes per cluster for data sets collected adjacent to faults within the WBFS

a)

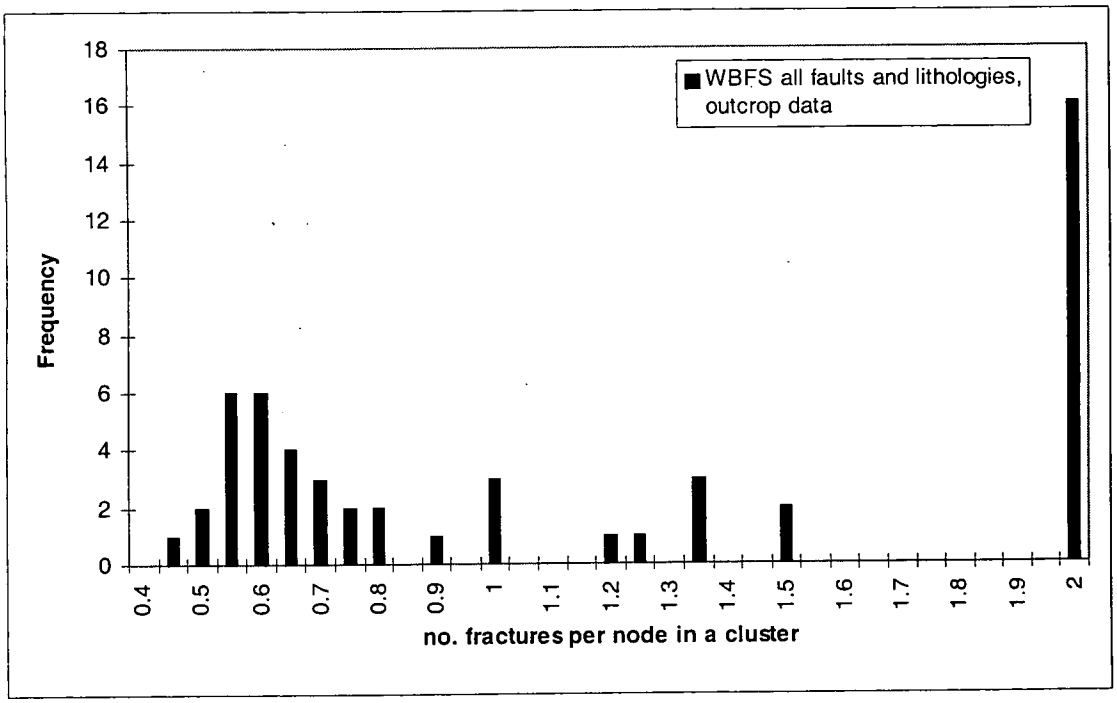

b)

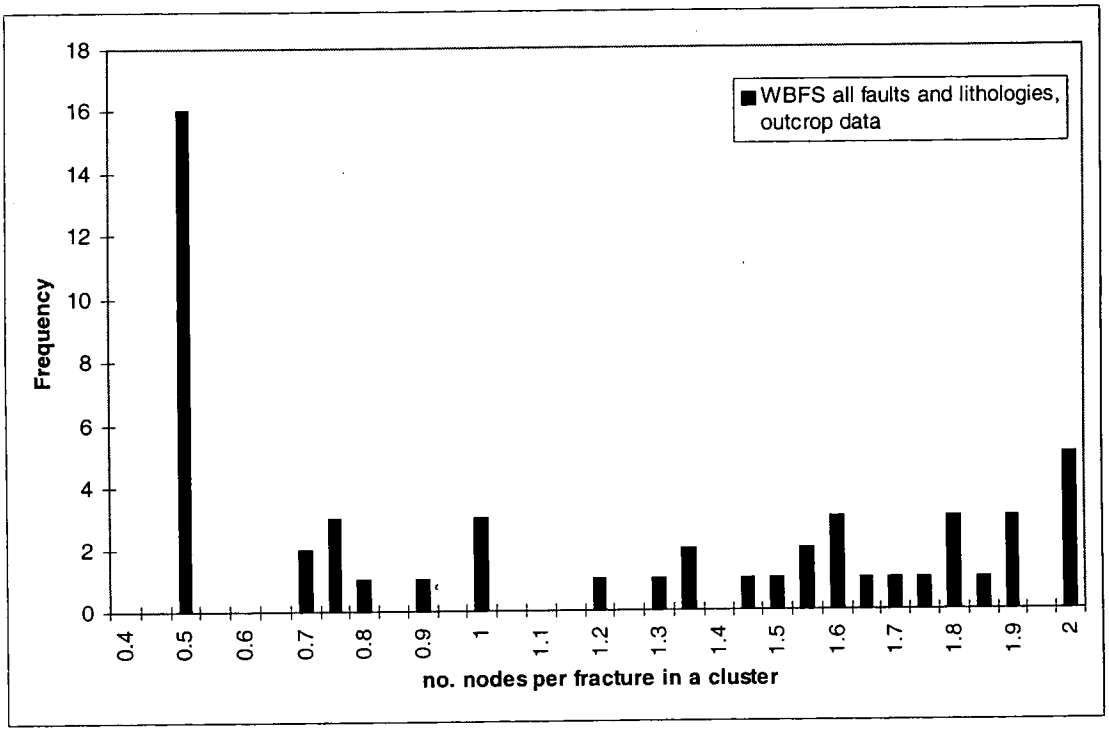

Figure 7.26 Histograms of **a**) total number of fractures per node in a cluster and **b**) total number of nodes per fracture in a cluster for data collected adjacent to faults within the WBFS.

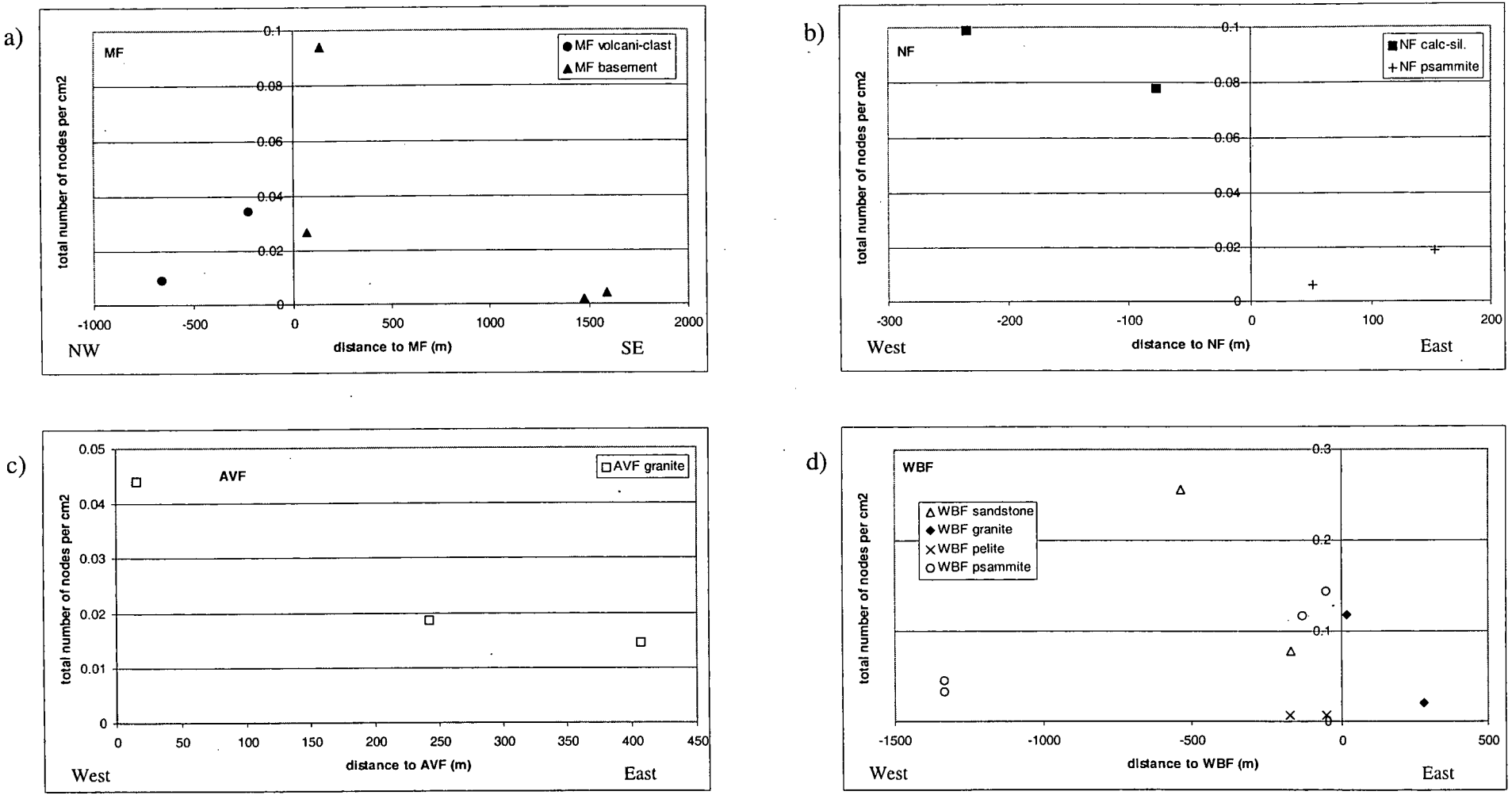

Figure 7.27 Total number of nodes per cm² 'v' perpendicular distance to faults within the WBFS

a) MF
b) NF
c) AVF
d) WBF

a)

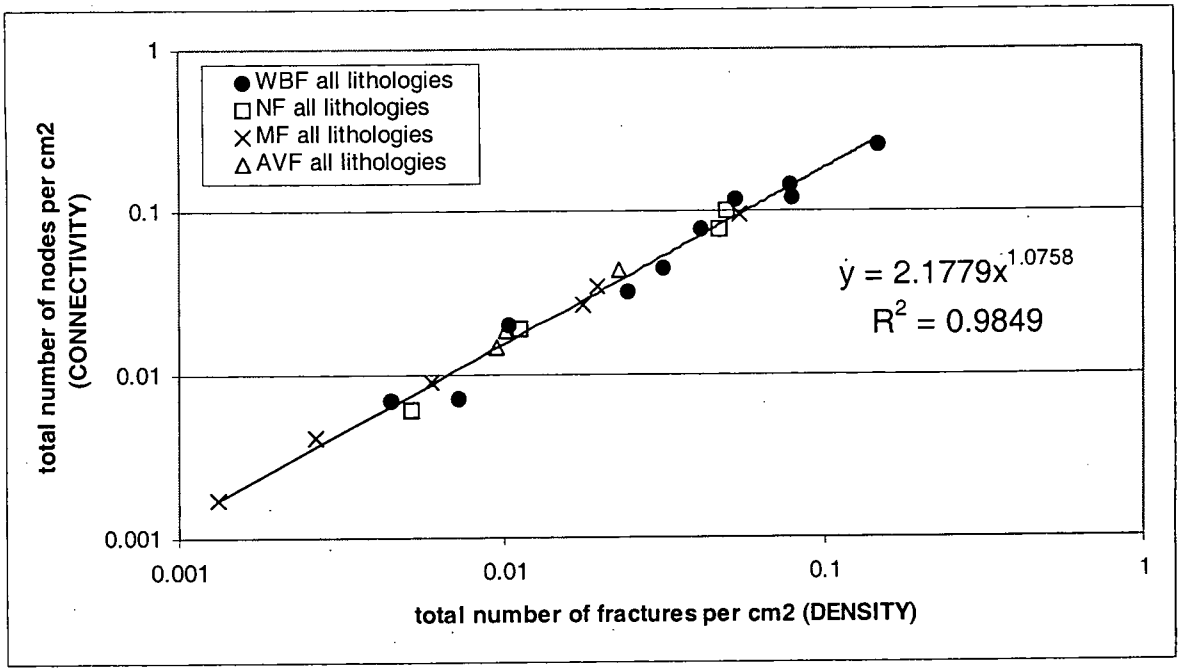

b)

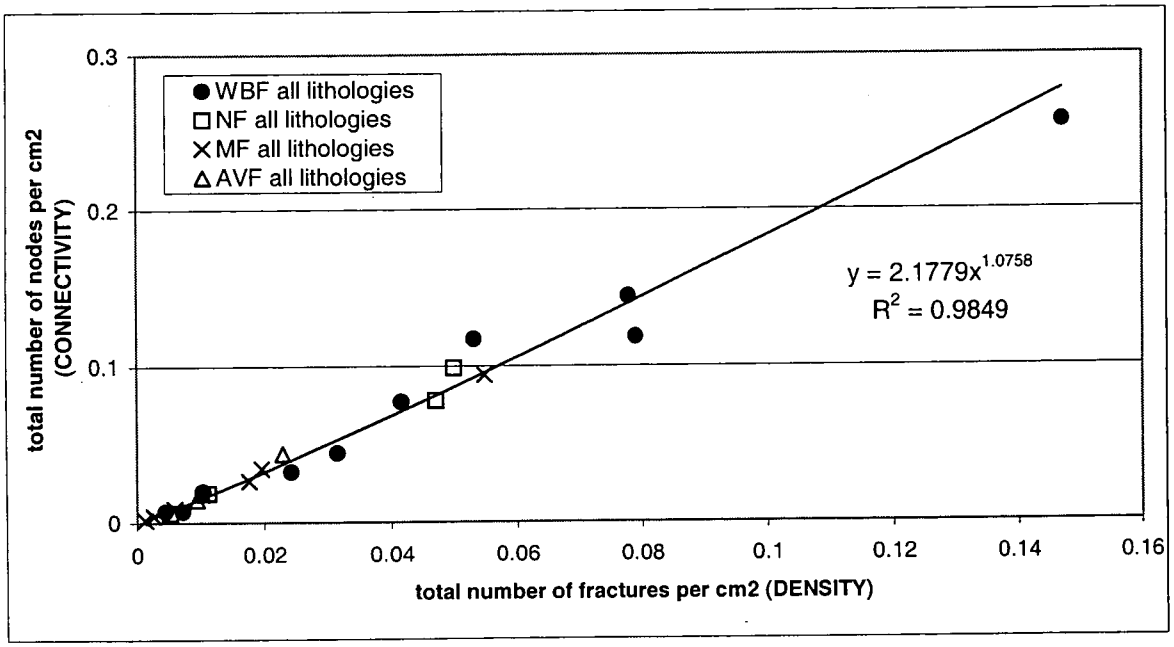

Figure 7.28 Fracture density (total number of fractures per cm²) 'v' fracture connectivity (total number of nodes per cm²) plotted on **a**) logarithmic axes, and **b**) linear axes

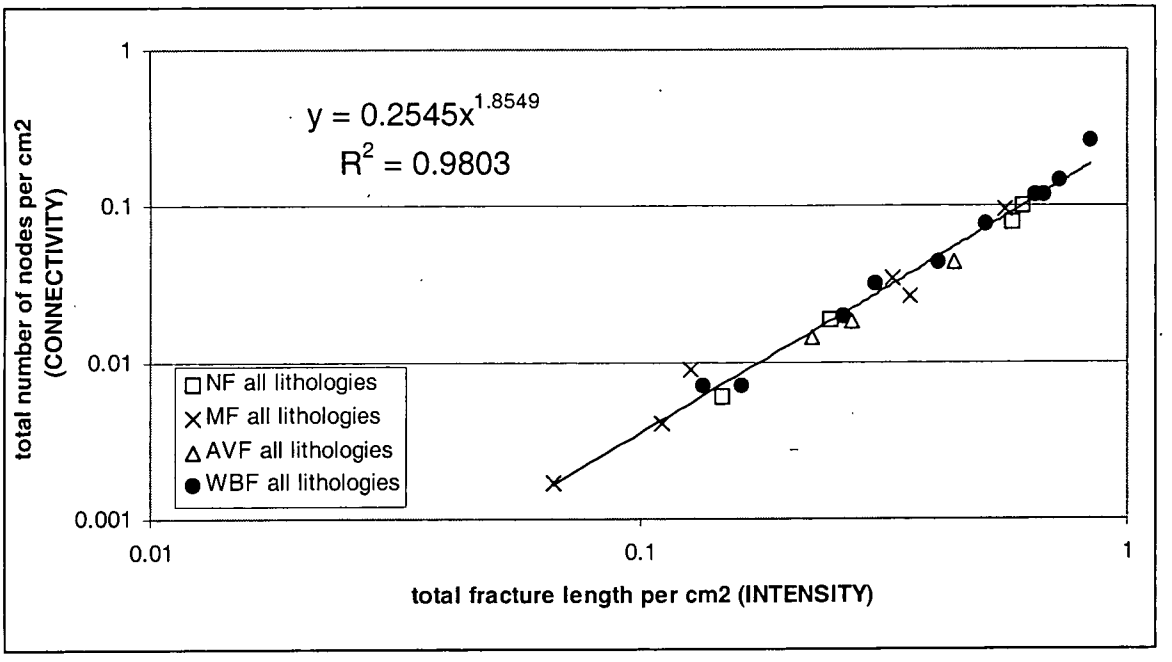

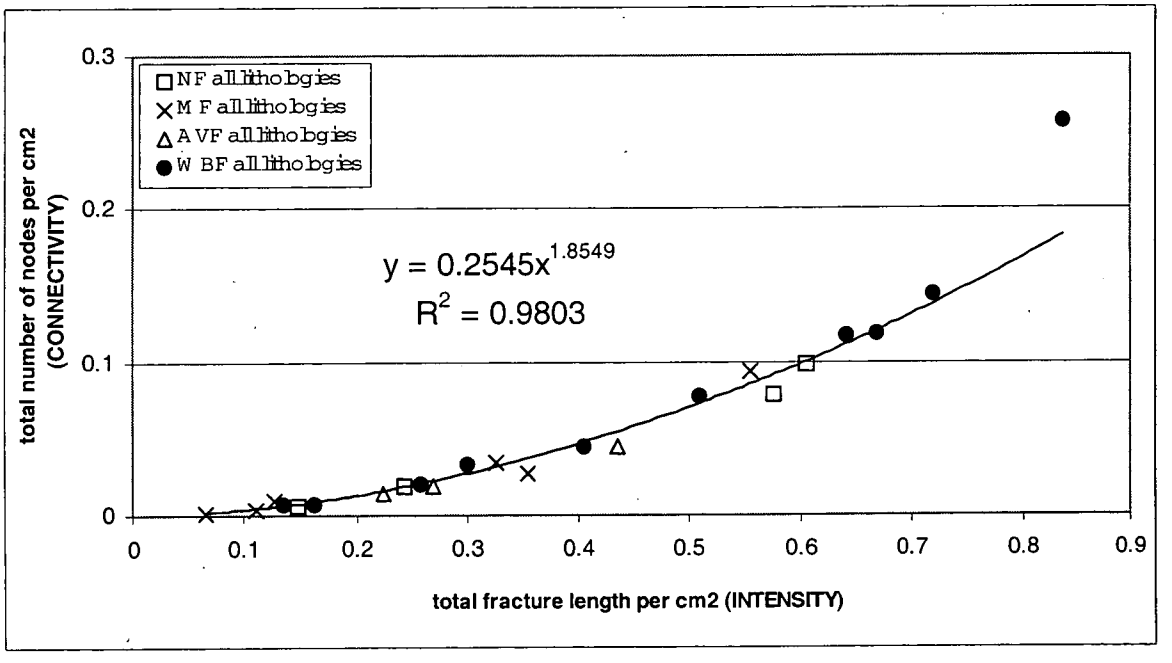

Figure 7.29 Fracture intensity (total fracture length per cm²) 'v' fracture connectivity (total number of nodes per cm²) plotted on **a**) logarithmic axes and **b**) linear axes

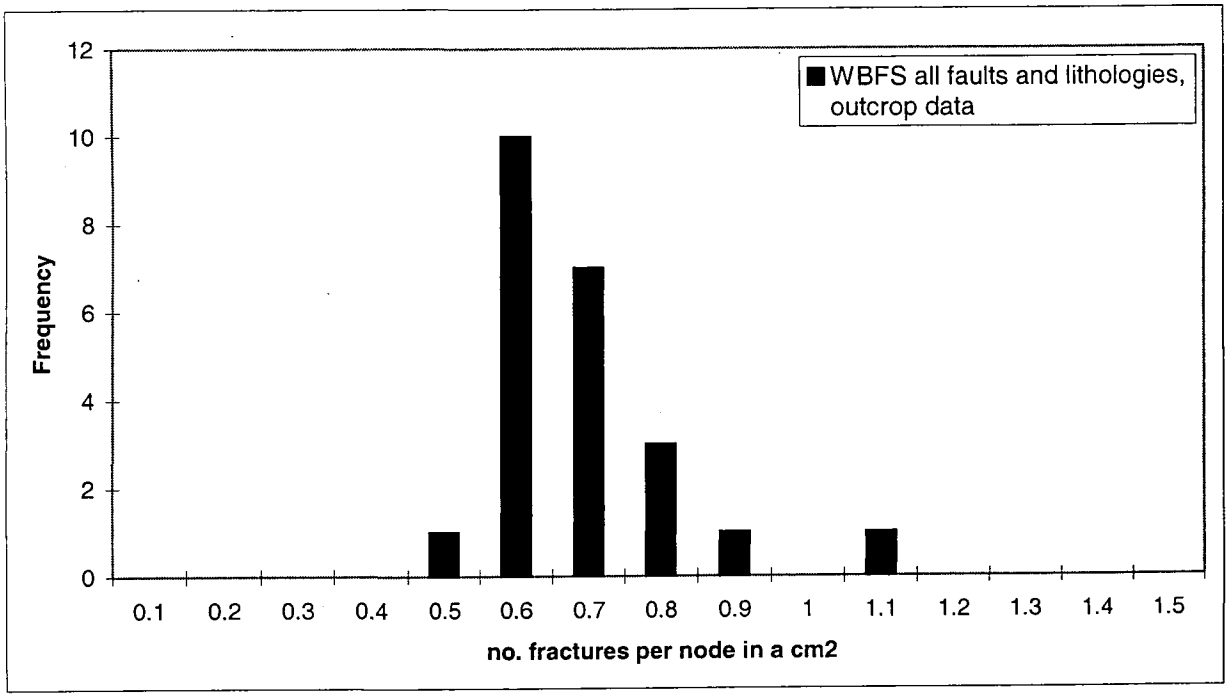

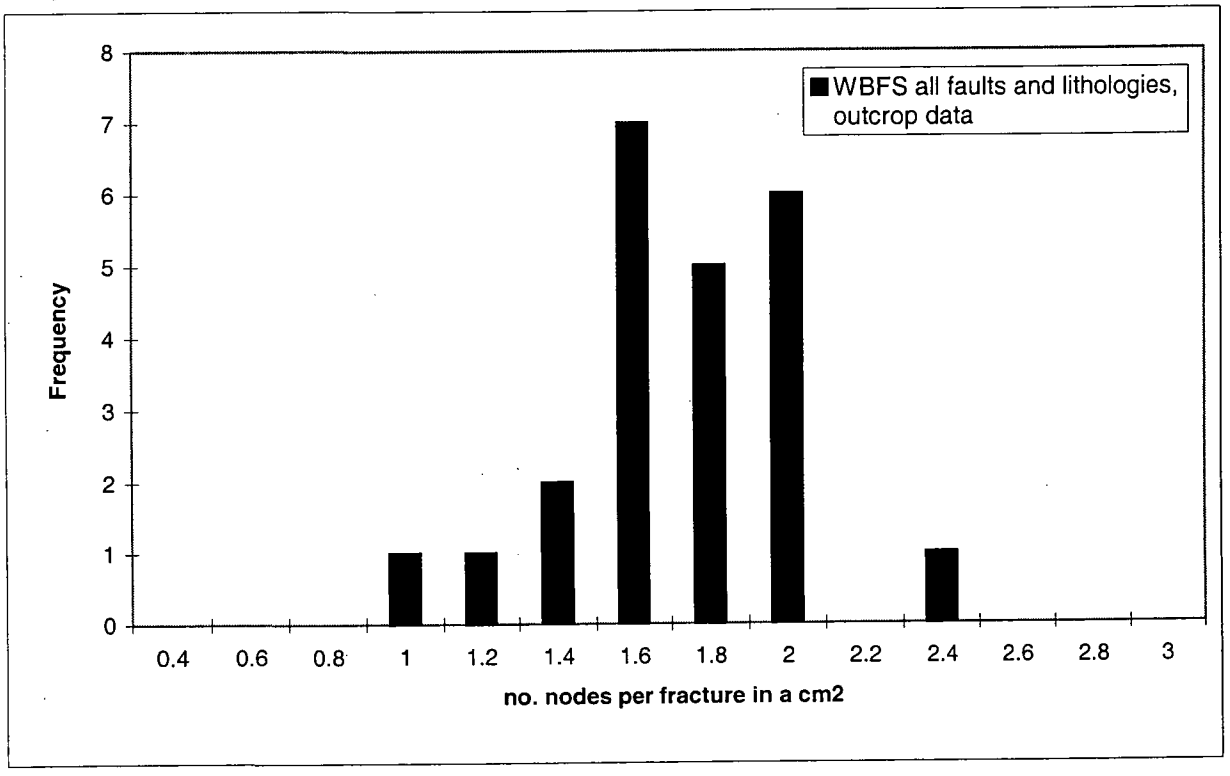

Figure 7.30 Histograms of **a**) total number of fractures per node in a cm^2, and **b**) total number of nodes per fracture in a cm^2 for data collected adjacent to faults within the WBFS.

a)

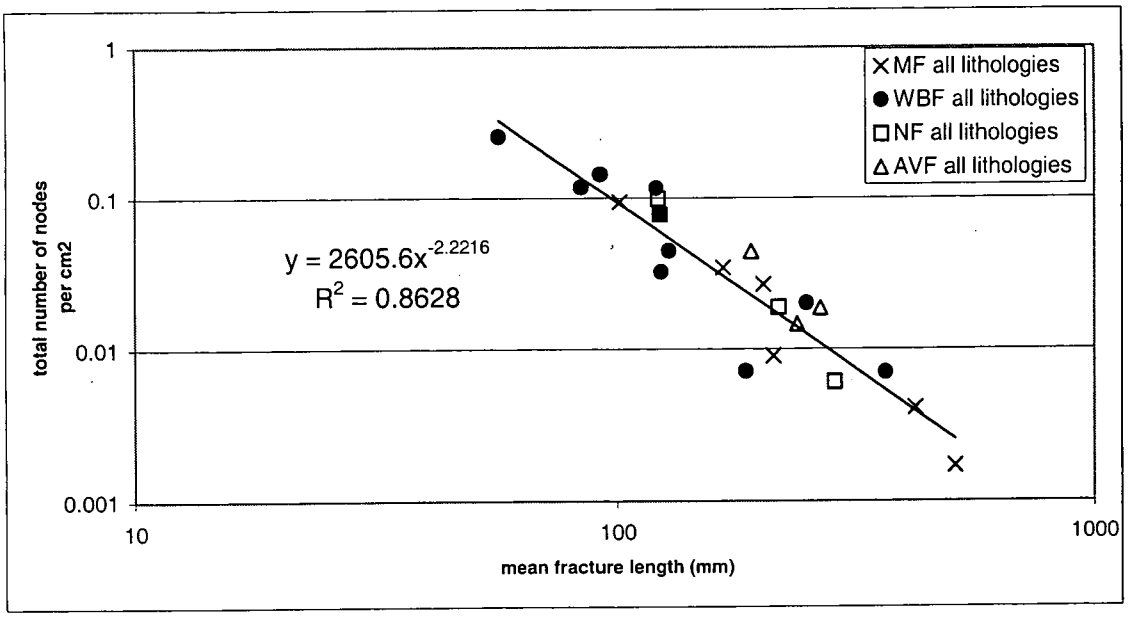

b)

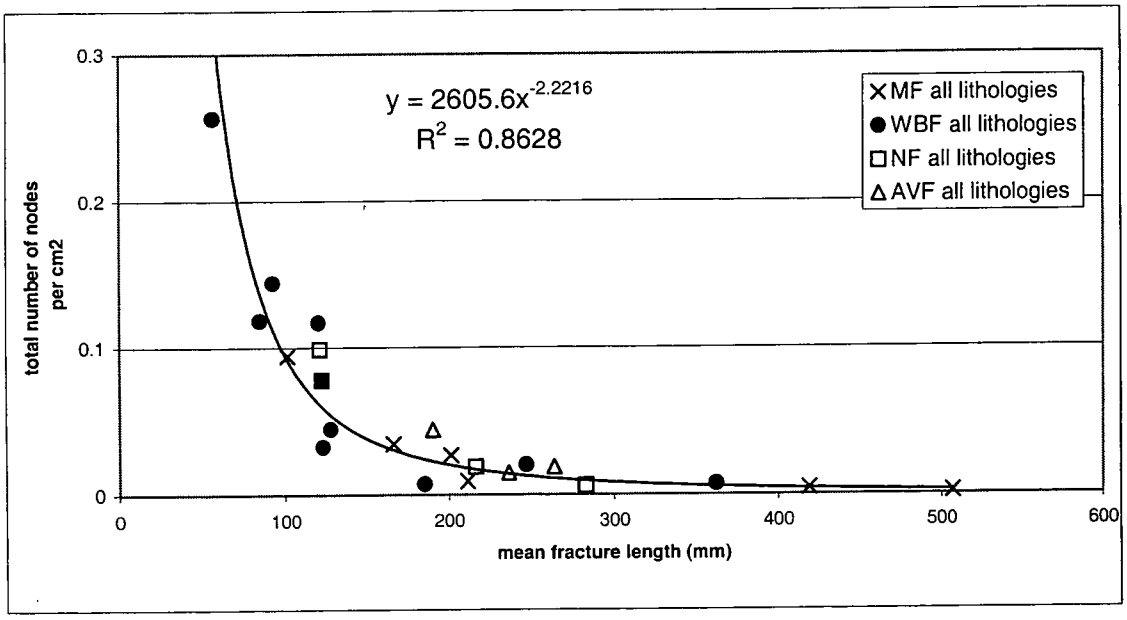

Figure 7.31 Mean fracture length 'v' total number of nodes per cm² (connectivity) plotted on **a**) logarithmic axes and **b**) on linear axes for data collected adjacent to faults within the WBFS.

a)

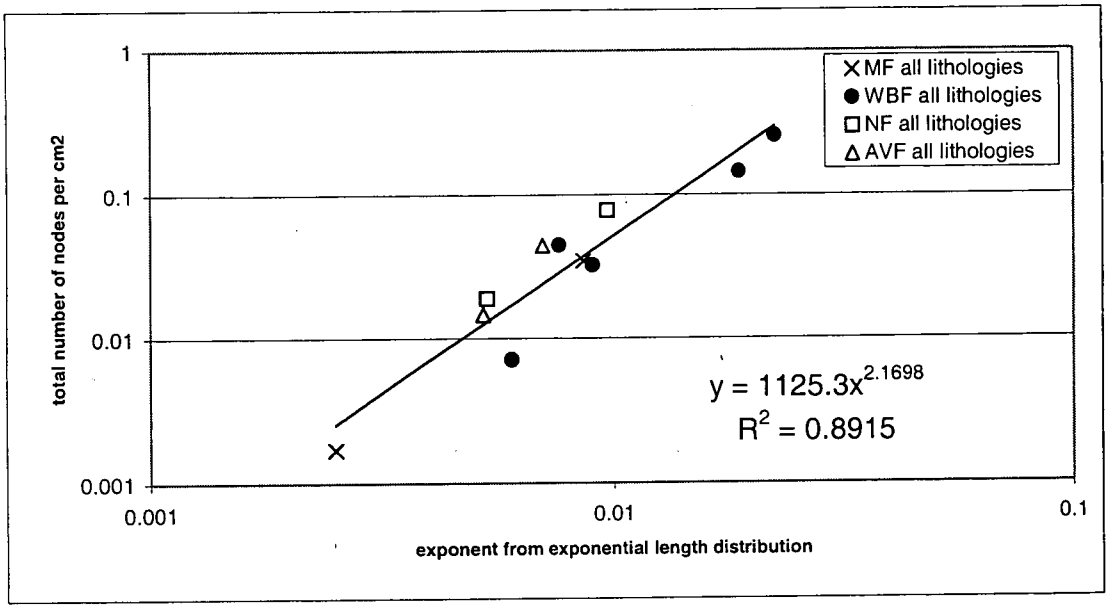

b)

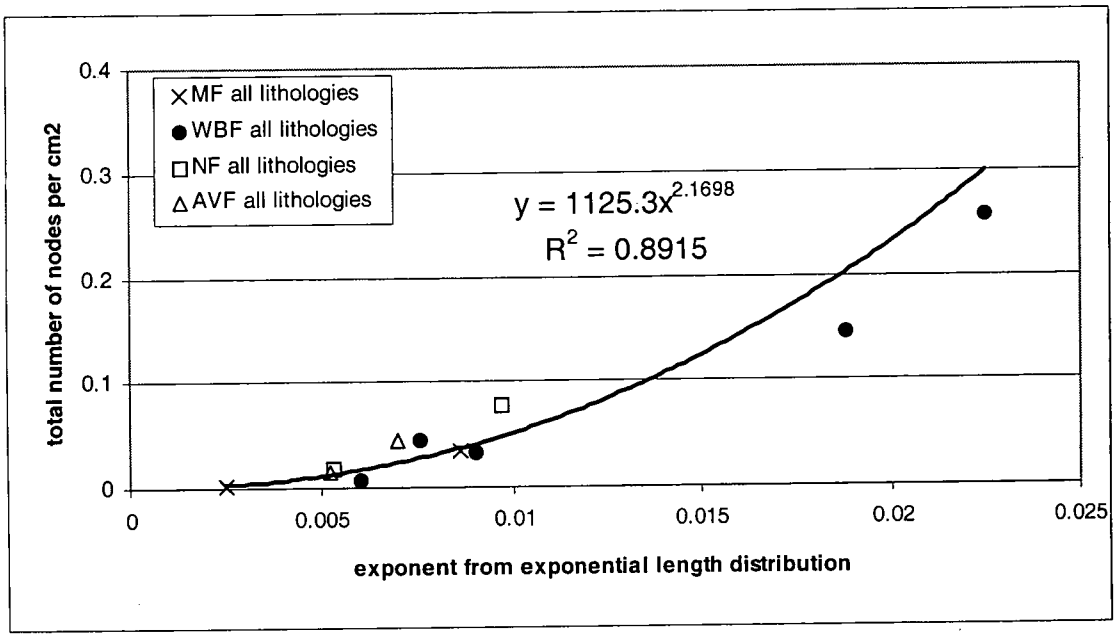

Figure 7.32 Exponent from exponential length distributions 'v' total number of nodes per cm² plotted on **a**) logarithmic axes and **b**) on linear axes for data collected adjacent to faults within the WBFS.

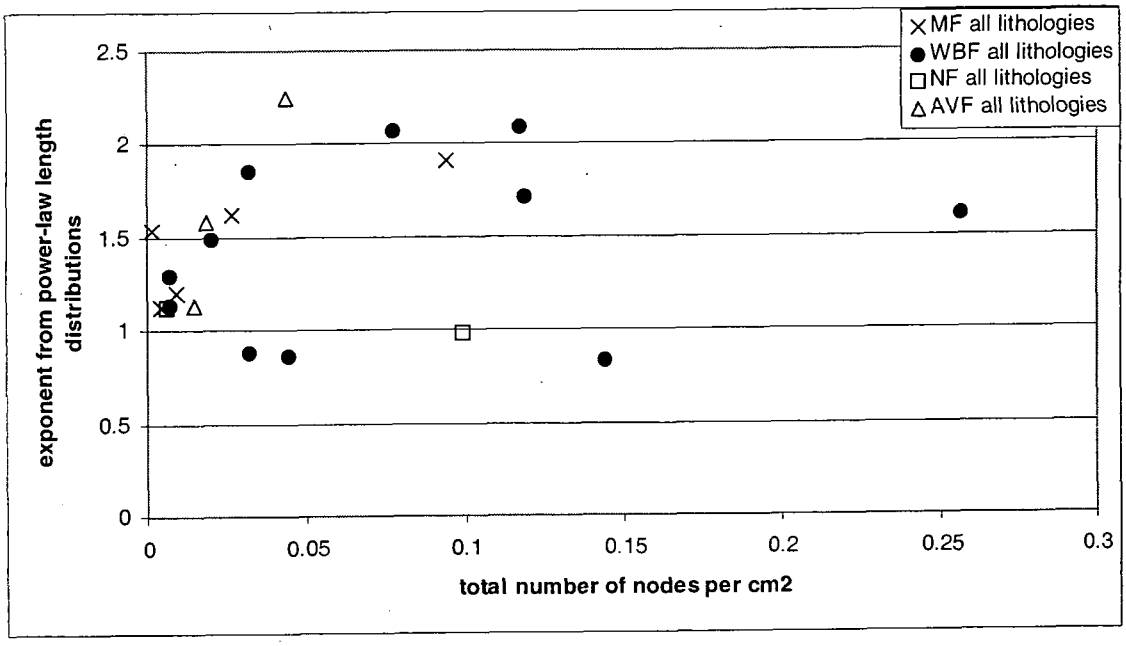

Figure 7.33 Exponent from power-law length distribution 'v' total number of nodes per cm^2 for data collected adjacent to faults within the WBFS, plotted on linear axes.

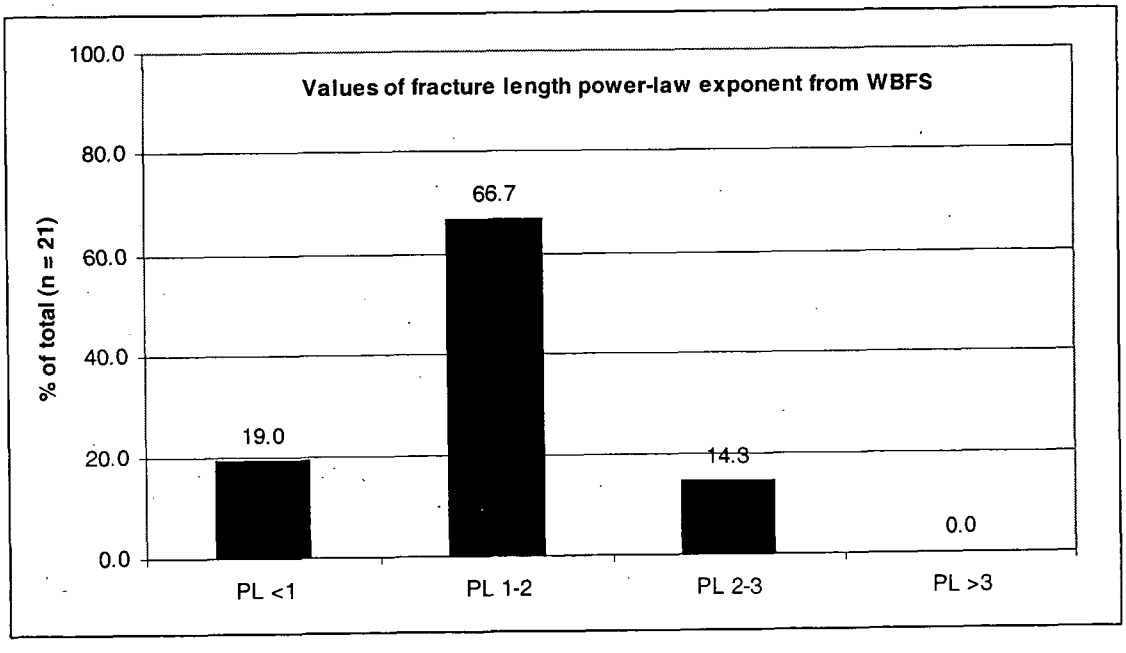

Figure 7.34 Histogram of power-law exponent values from fracture length data collected adjacent to faults within the WBFS.

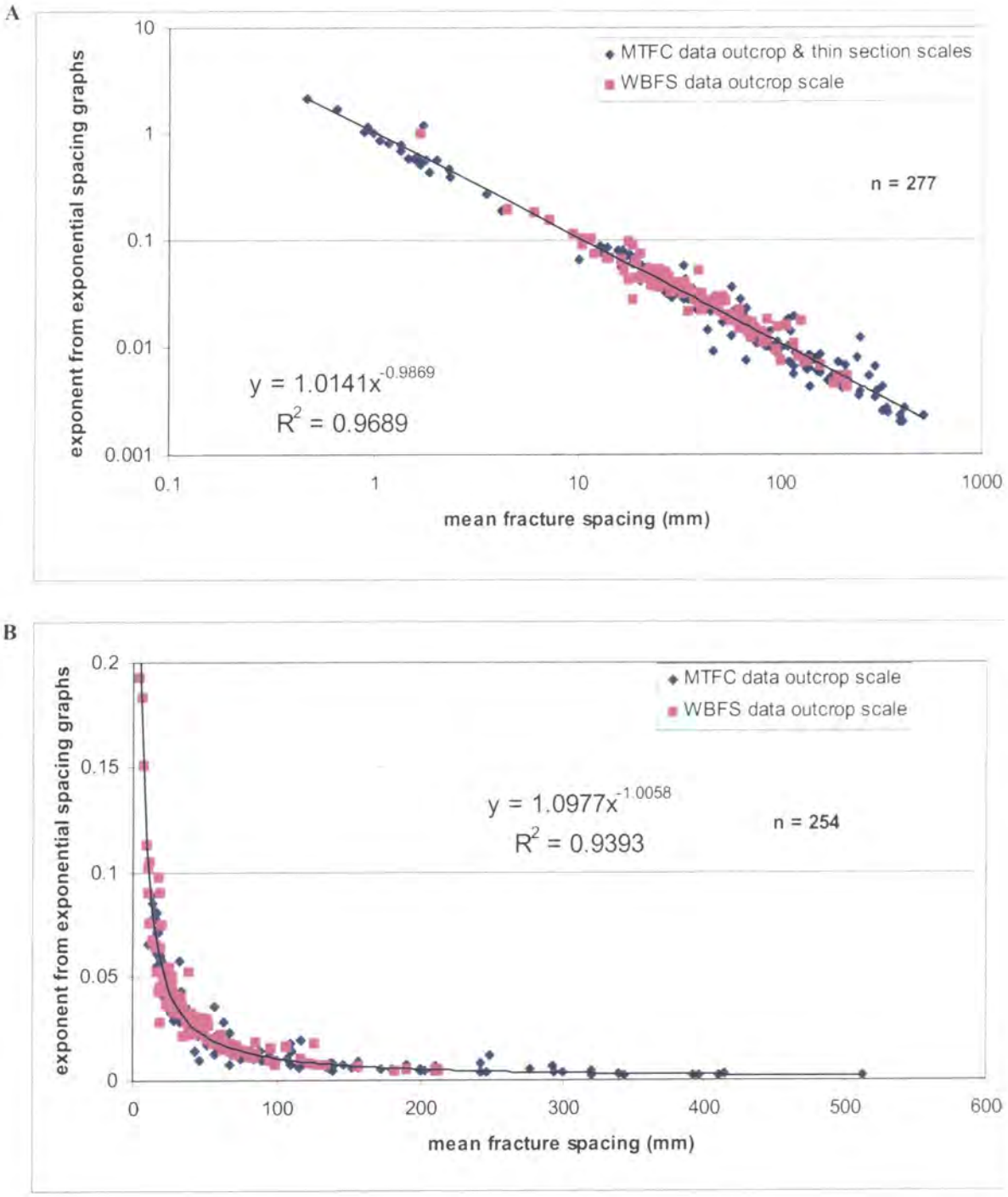

Figure 8.1 Graphs showing the good relationship between mean & exponent values from exponentially distributed spacing data sets from the MTFC & the WBFS.
A – outcrop data (measured from 1D transects in the field and from 2D data sets) and thin section data from the MTFC, plus outcrop data (measured from 1D transects in the field and from 2D data sets) from the WBFS. Data is plotted on log-log axes due to the range of values present
B – Outcrop data only from the MTFC and the WBFS (measured from 1D transects in the field and from 2D data sets). Data is plotted on linear axes.

(Some scatter is observed, and is probably related to the calculation of mean values being from the whole data set, whereas the exponent values may not necessarily encompass the whole spacing data set)

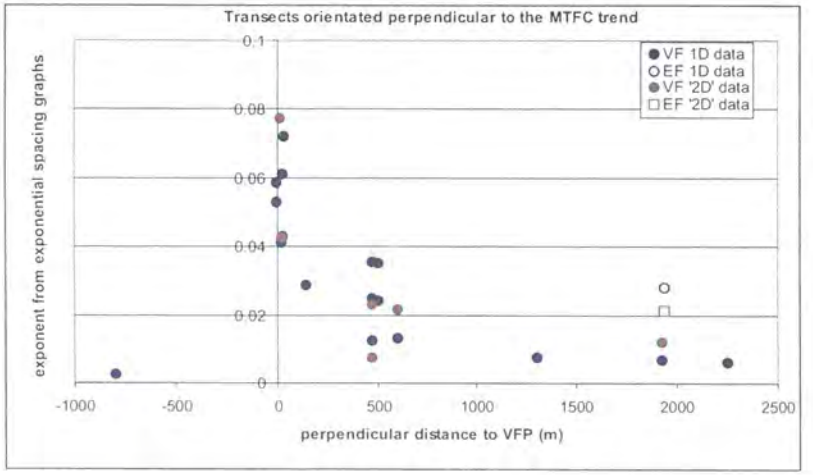

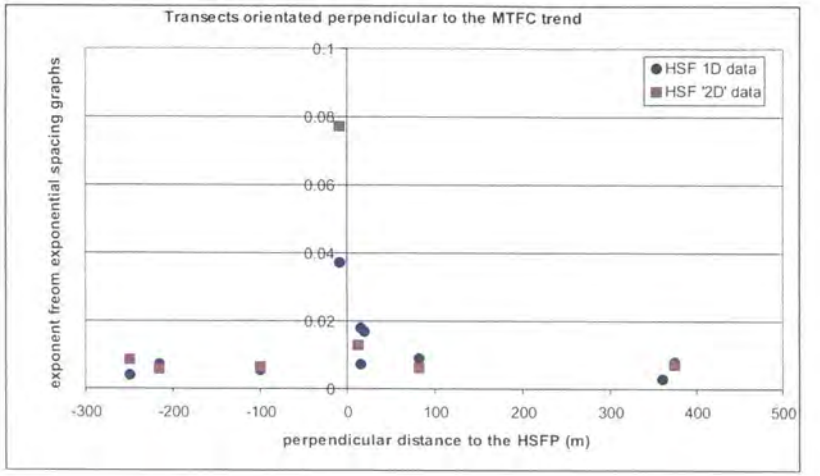

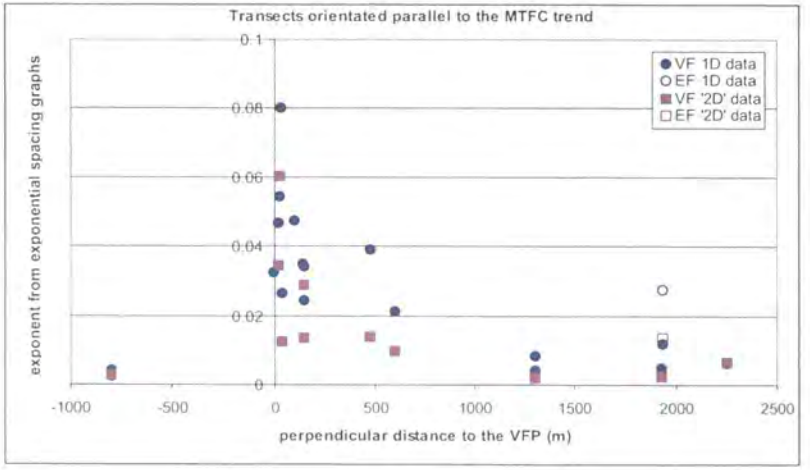

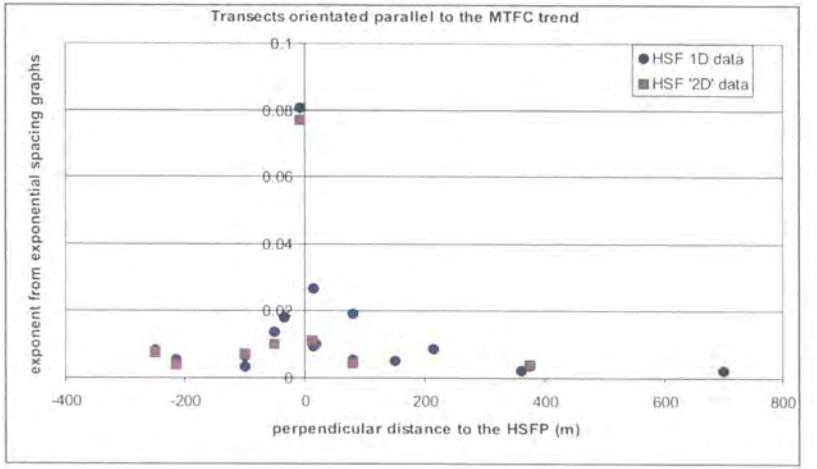

Figure 8.2 Exponent values from exponentially distributed spacing graphs, calculated from 1) 1-D line transects in the field (1D data in legends) and 2) multi-line transects across 2-D photograph data sets ('2D' data in legends)
A & B = data collected adjacent to the VFP and EFP, along transects orientated perpendicular and parallel to the MTFC trend respectively
C & D = data collected adjacent to the HSFP, along transects orientated perpendicular and parallel to the MTFC trend respectively

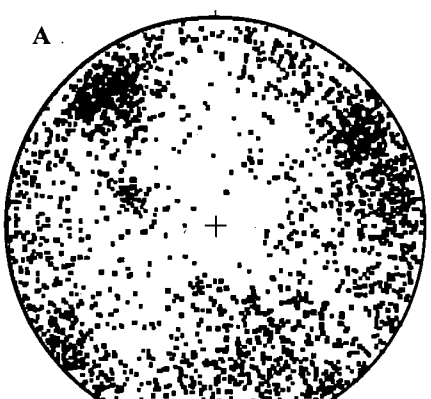

VF, EF & RF all 1D transect data
n = 2979, clusters = 050/ 75 S, 149/ 75 W

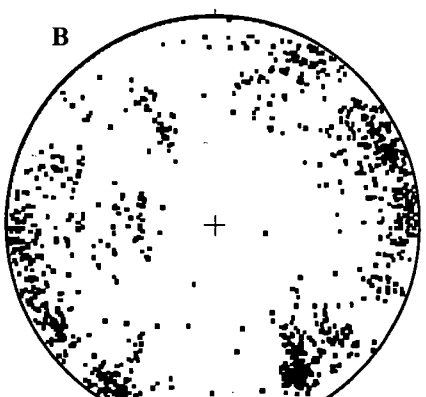

HSF all 1D transect data
n = 1463,
clusters = 060/ 72 N, 122/ 81 N, 158/ 81 W

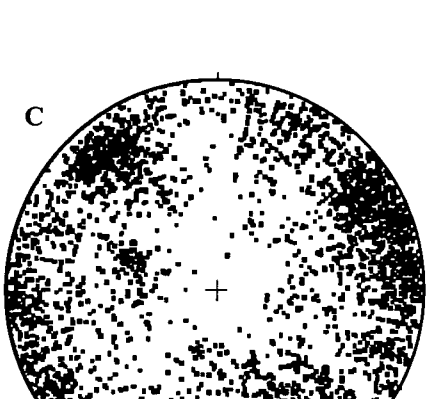

VF, EF, RF & HSF all 1D transect data
n = 4442,
clusters = 050/ 74 S, 060/ 71 N, 150/ 76 W, 173/ 82 W

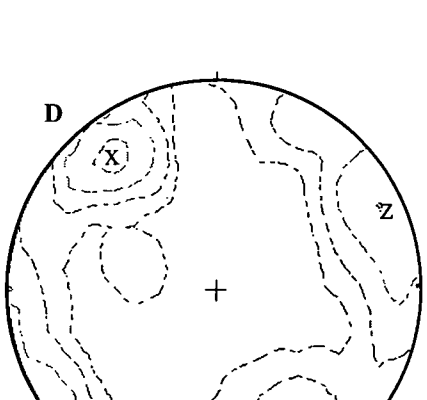

equal-area contour plot of
VF, EF, RF & HSF all 1D transect data
n = 4442,
clusters - x = 051/ 70 S, y = 060/ 73 N,
plus a large cluster centred around 155/ 78 W (z),
probably contains 2 clusters, trending N-S and NW-SE

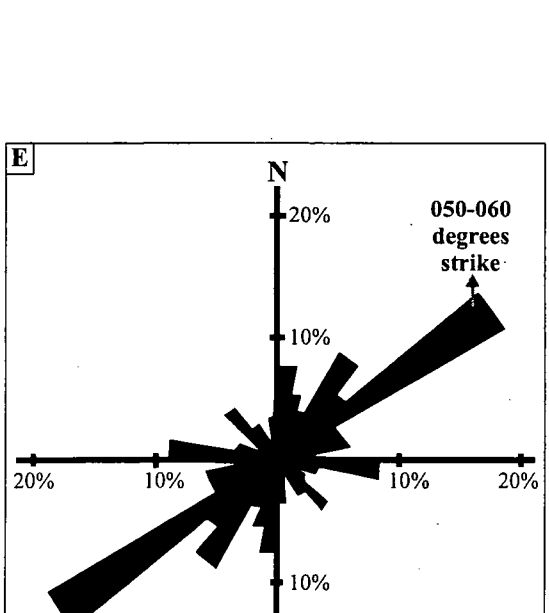

Rose diagram of lineament trends from
Air Photograph over the VFS within the MTFC

Figure 8.3 Fracture orientations within the MTFC (all data plotted as poles to fracture planes)
A - fracture data collected within the VFS
B - fracture data collected adjacent to HSF
C - all fracture data collected from the MTFC
D - all data from the MTFC, contoured
E - rose diagram of lineament strike measurements from the air photograph data set

A

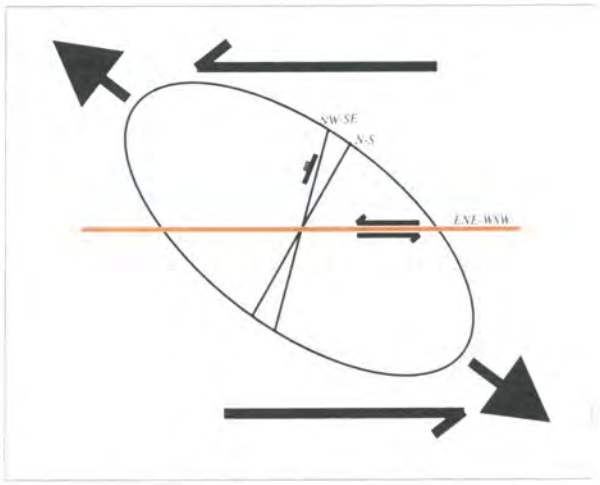

B

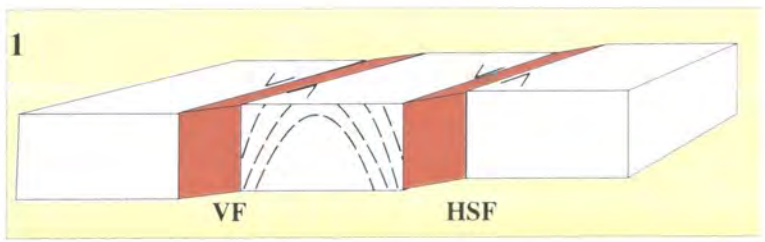

HSF and VF initiated as two parallel ductile shear zones on the opposite limbs of a regional antiform, mylonites have been dated at 409 ±12 Ma (Watts 2001)

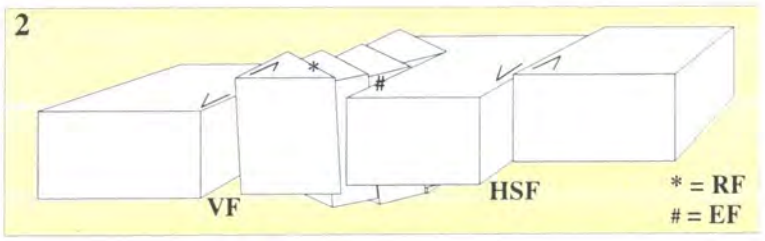

Brittle reactivation occurred as sinstral transtensional movements along VF & HSF with the initiation of RF minor movements along EF, and the creation the present day fracture network. Epiote-rich cataclasites & coeval pseudotachylites produced during this event are dated at 291 ±14 Ma (Watts 2001)

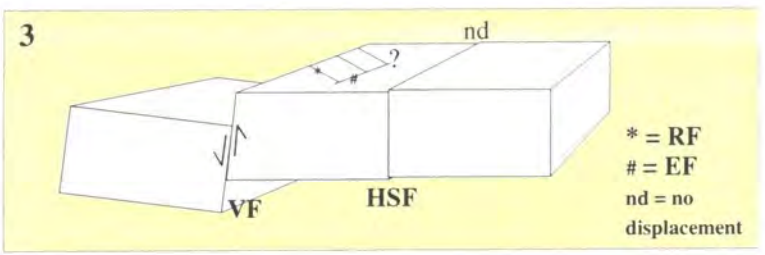

Minor dip-slip normal reactivation occurred along the VF with little/no displacement along HSF. Movements along RF and EF are unknown.

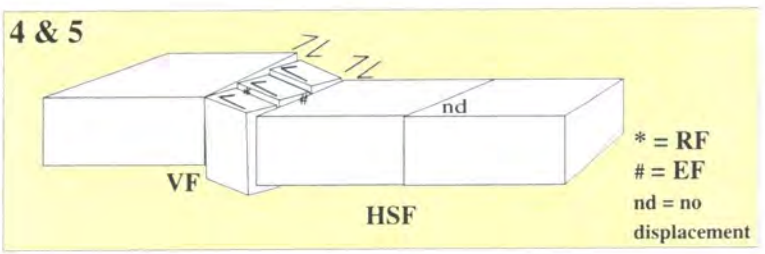

Two dextral strike-slip events are recognised by Watts (2001). A major phase in Mesozoic times associated with zeolite & calcite, with movements recognised along VF, RF and EF. The second, more minor, phase is associated with incohesive fault gouge observed along VF only

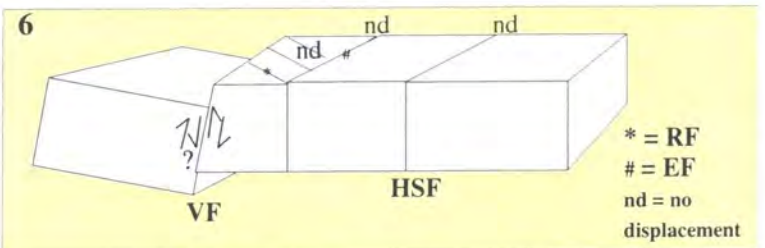

A second incohesive fault gouge is observed along VF, associated with dip-slip movements

Figure 8.4 The main fracture network associated with the MTFC

A - summary of 4 main clusters observed within the MTFC, 2 parallel to the overall fault trend (ENE-WSW), one ~N-S and one ~NW-SE, all consistent with initiation during sinistral transtensional movements.

B - (after Watts 2001) Series of schematic block diagrams to show the initiation and development of faults within the MTFC. Note that the sinistral transtension event (#2) is inferred to have initiated the present day fracture network.

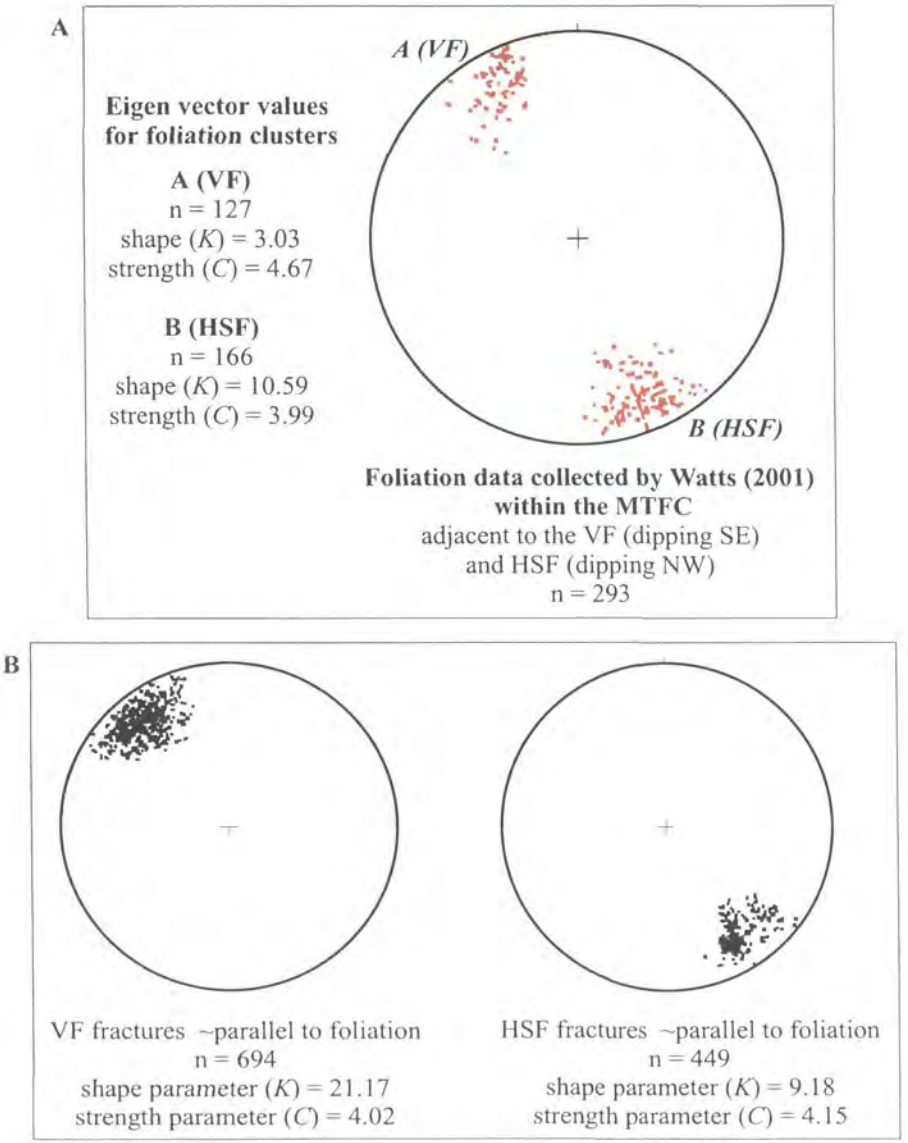

Figure 8.5 Stereonets and eigen vector values for (**A**) foliation and (**B**) fracture data collected within the MTFC. (Foliation data collected by Watts (2001)).

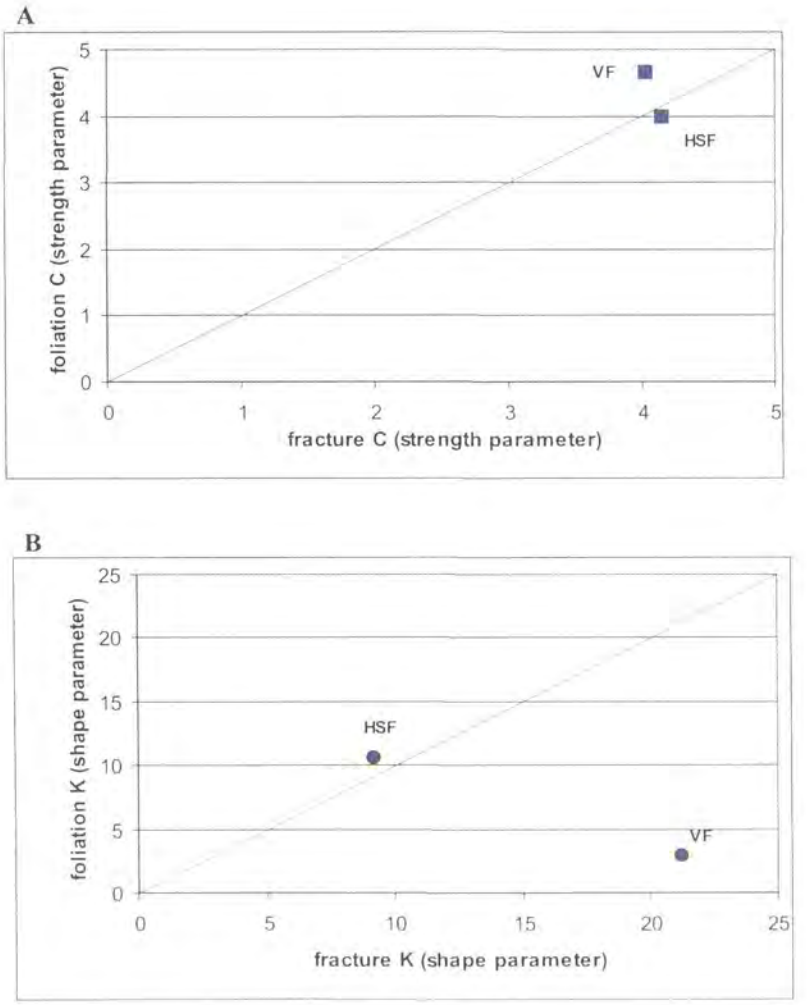

Figure 8.6 Eigen vector plots for foliation and fracture data collected within the MTFC.
(**A**) = strength parameter *C*
(**B**) = shape parameter *K*

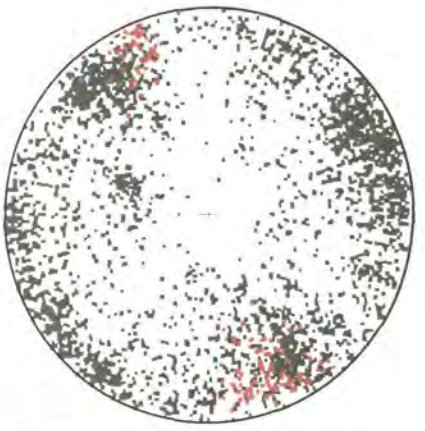

All fracture data collected at outcrop
scale within MTFC (**black squares, poles to planes**)
with foliation data collected adjacent to the VF and HSF
by Watts (2001) (red squares, poles to planes)

Figure 8.7 Stereonet of all fracture orientations (black) collected from the MTFC. Superimposed in red are foliation readings measured by Watts (2001). Note that the foliation and fracture clusters are not geometrically coincident.

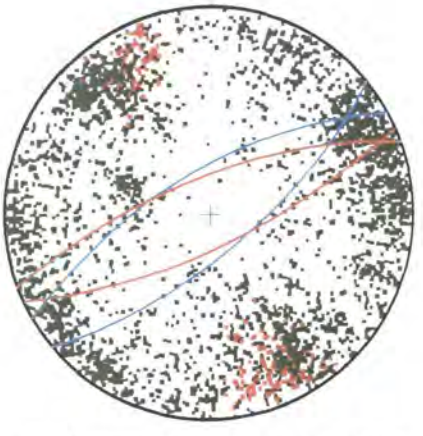

All fracture data collected at outcrop
scale within MTFC (**black squares, poles to planes**)
with foliation data collected adjacent to the VF and HSF
by Watts (2001) (red squares, poles to planes)
Red girdles represent mean foliation planes
Blue girdles represent brittle fault orientations (VF and HSF)

Figure 8.8 Stereonet of fracture and foliation readings from within the MTFC with mean girdles for foliation (on each fold limb, red) and for the orientations of the two major brittle faults (VF & HSF, blue). Note that the fracture clusters are parallel to the brittle fractures and not the ductile foliation.

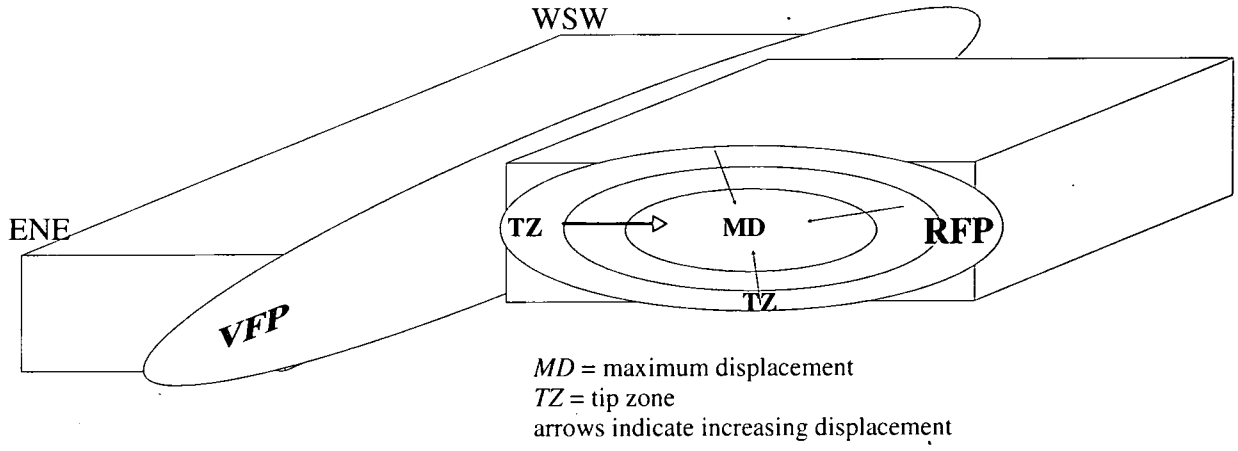

Figure 8.9 Schematic diagram (not to scale) to illustrate the possible explanation for increasing fracture density to the north, along strike of the Rautingdalen Fault (RF), away from the intersection zone between the RF and the Verran Fault (VF). Red arrow indicates increasing displacement towards the centre of the RFP, and away from the intersection of the VFP, and it's suggested that here, fracture density may increase due to increasing displacement along RFP

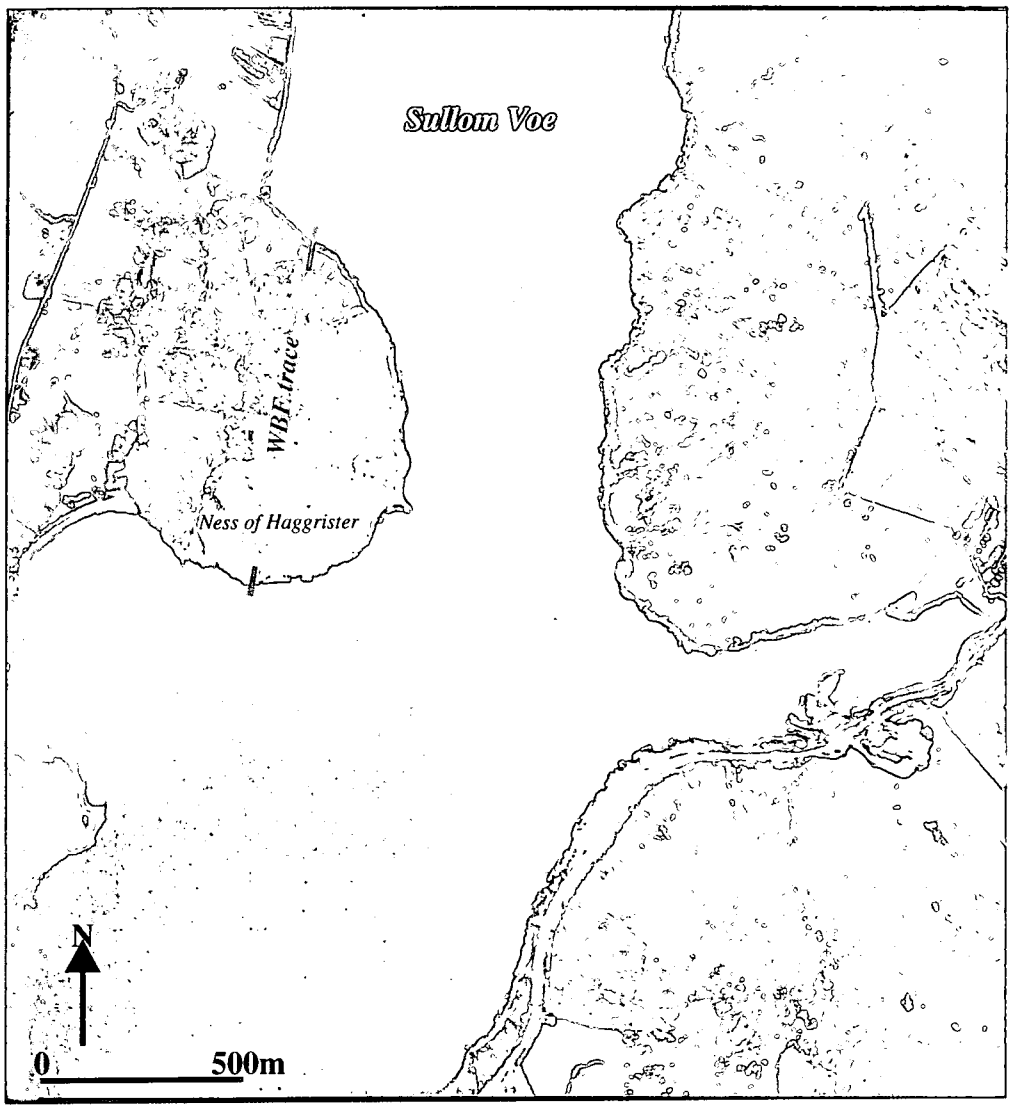

Figure 8.10 Air Photograph taken over the Sullom/Ness of Haggrister localities of the WBF. The WBF trace (based on field evidence) is indicated by the black lines, and cannot easily be traced inland due to the extensive peat cover.

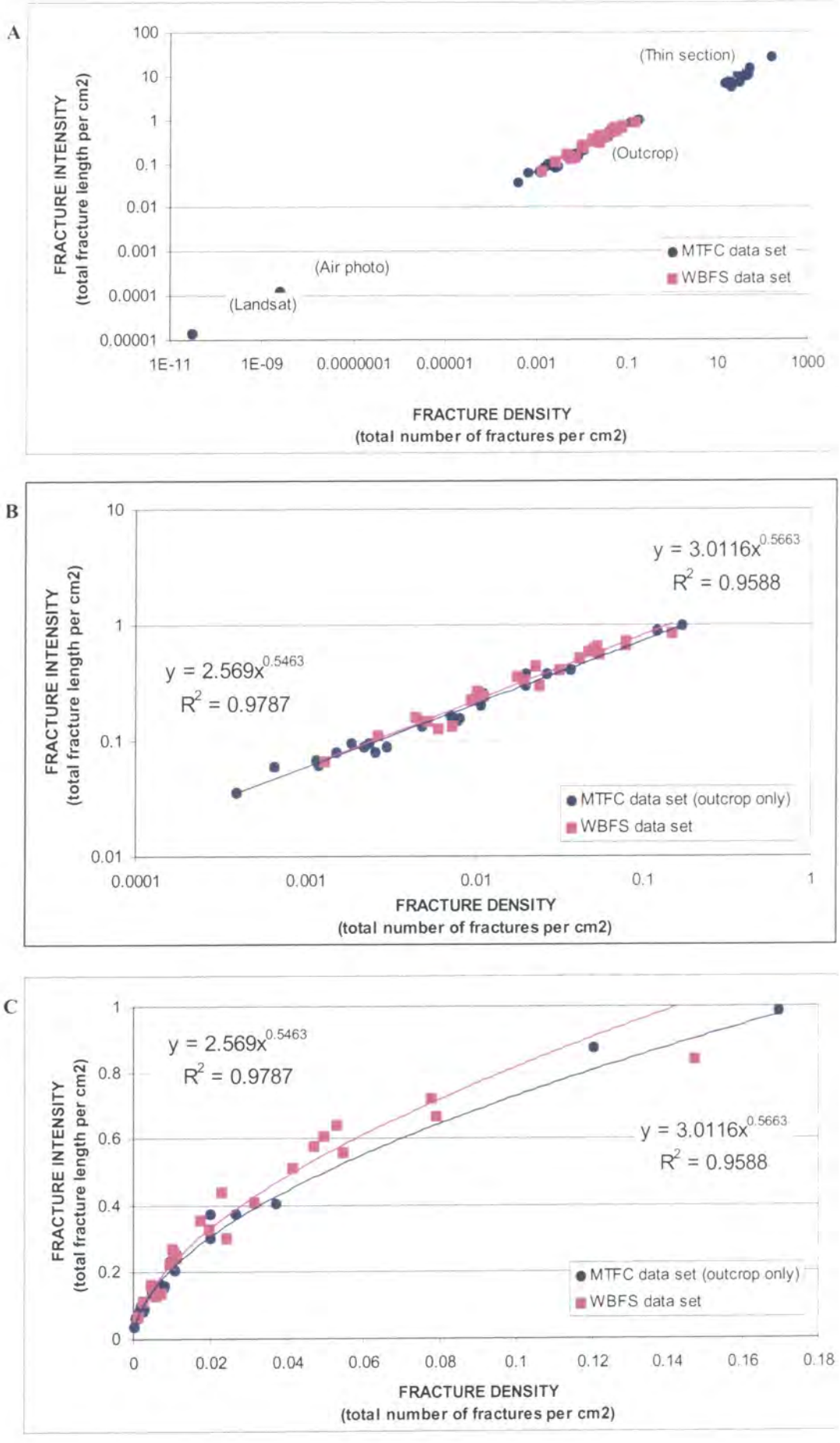

Figure 8.11 Fracture density 'v' fracture intensity data from the MTFC and the WBFS. **A** – data collected at all scales for both fault systems, on logarithmic axes **B** & **C** – data collected at outcrop scale only for both fault systems, on logarithmic and linear axes respectively

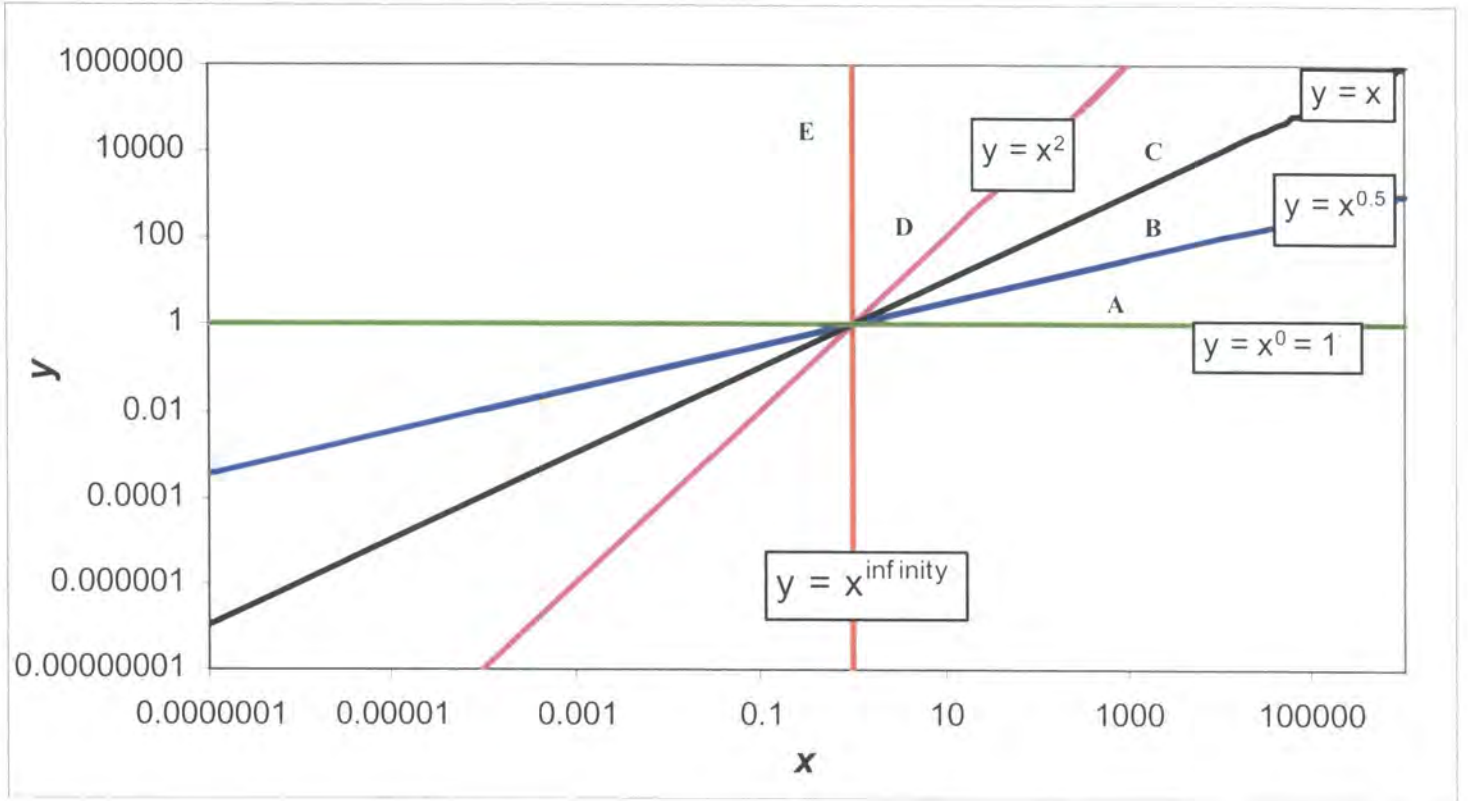

Figure 8.12 Graph to show the different relationships between fracture parameters (i.e. x & y) based on the exponent values. Each line represents a different exponent value.

A – exponent = 0, *x* parameter has no influence on the *y* parameter

B – exponent = 0.5, relatively little variation in *y* parameter as *x* parameter values change (c.f. density & intensity, MTFC & WBFS)

C – exponent = 1, parameters *x* and *y* are directly proportional (c.f. density & connectivity, MTFC & WBFS)

D – exponent = 2, x parameter values change significantly with respect to changes in y parameter values (c.f. intensity & connectivity, MTFC & WBFS)

E – exponent = infinite, *y* parameter has no influence on the *x* parameter

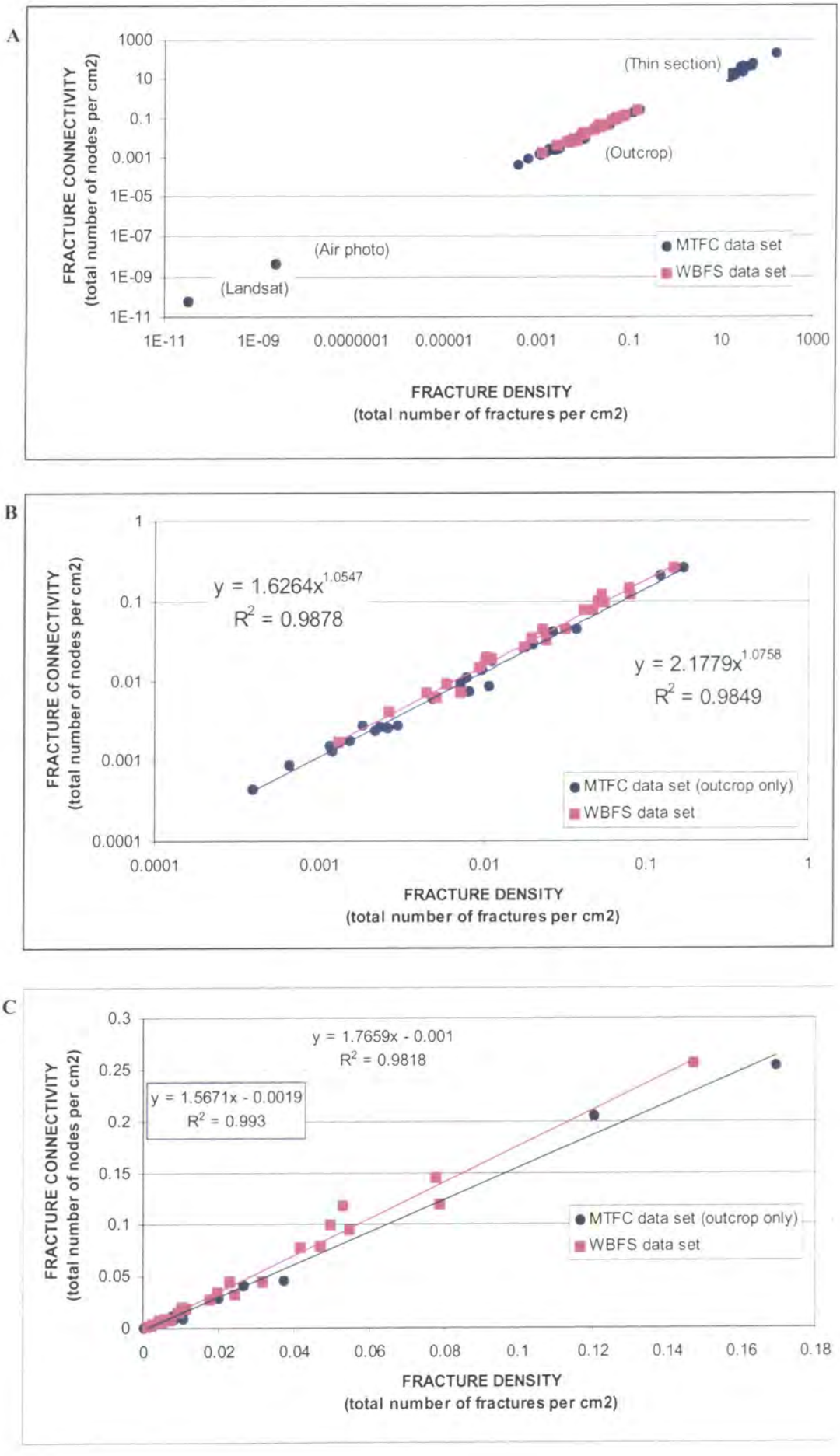

Figure 8.13 Fracture density 'v' fracture connectivity data from the MTFC & the WBFS. **A** – data collected at all scales for both fault systems, on logarithmic axes **B** & **C** – data collected at outcrop scale only for both fault systems, on logarithmic and linear axes respectively

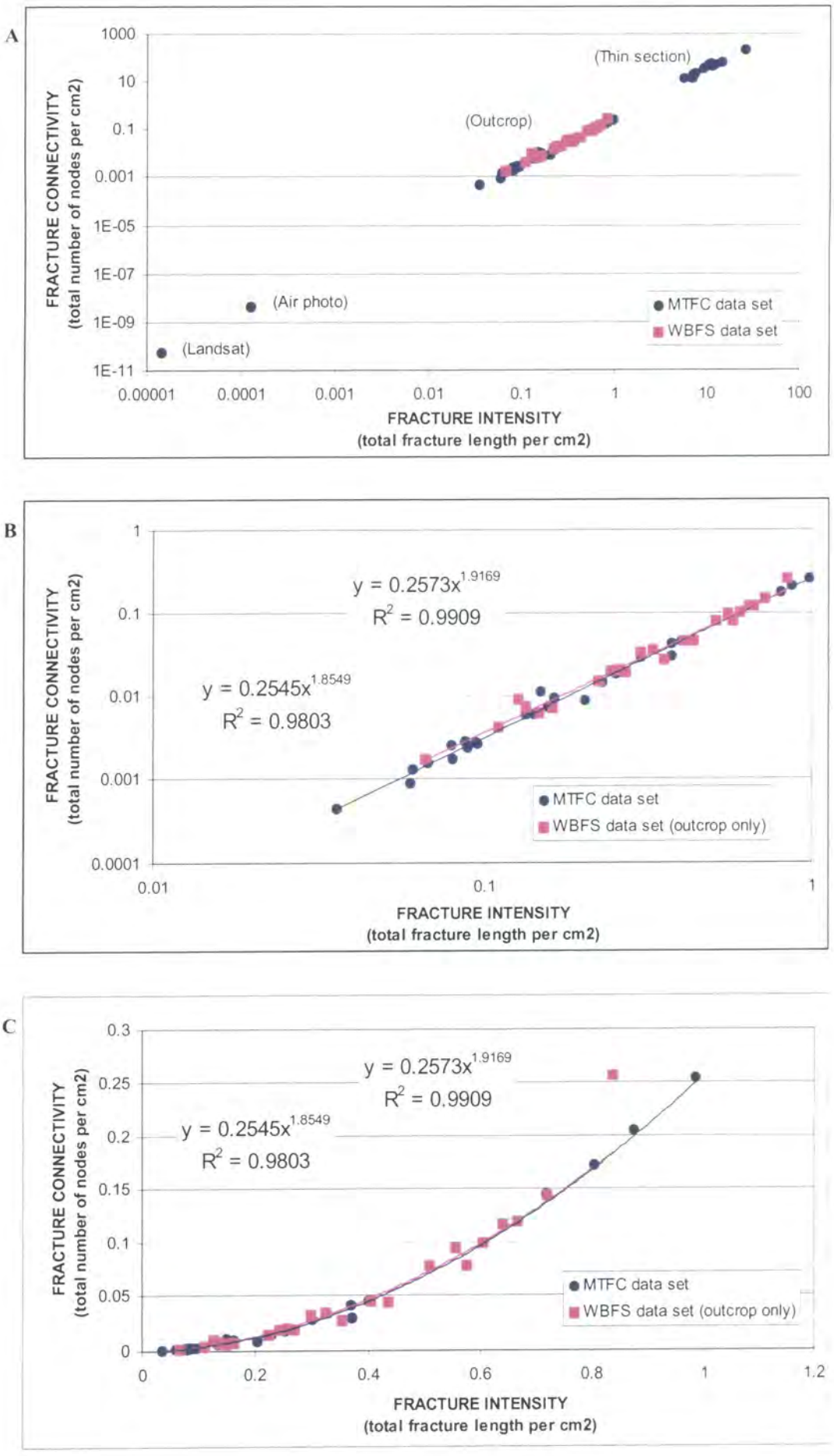

Figure 8.14 Fracture intensity 'v' fracture connectivity data from the MTFC & the WBFS.
A – data collected at all scales for both fault systems, on logarithmic axes
B & **C** – data collected at outcrop scale only for both fault systems, on logarithmic and linear axes respectively

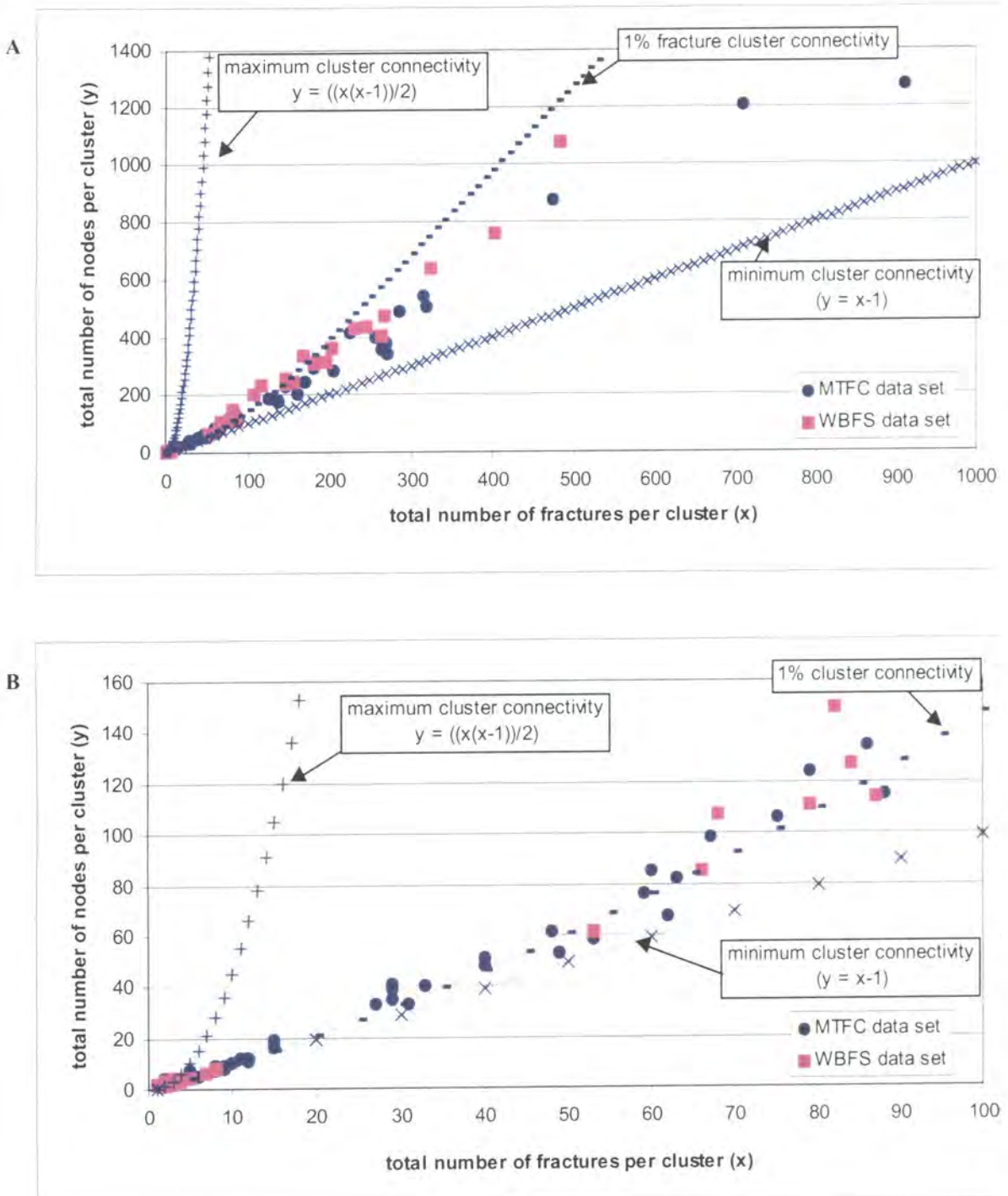

Figure 8.15 Fracture cluster connectivity (number of nodes and fractures per cluster) for the MTFC and WBFS data sets.
A – All values from both fault data sets
B – Clusters containing less than or equal to 100 fractures, from the MTFC and WBFS data sets

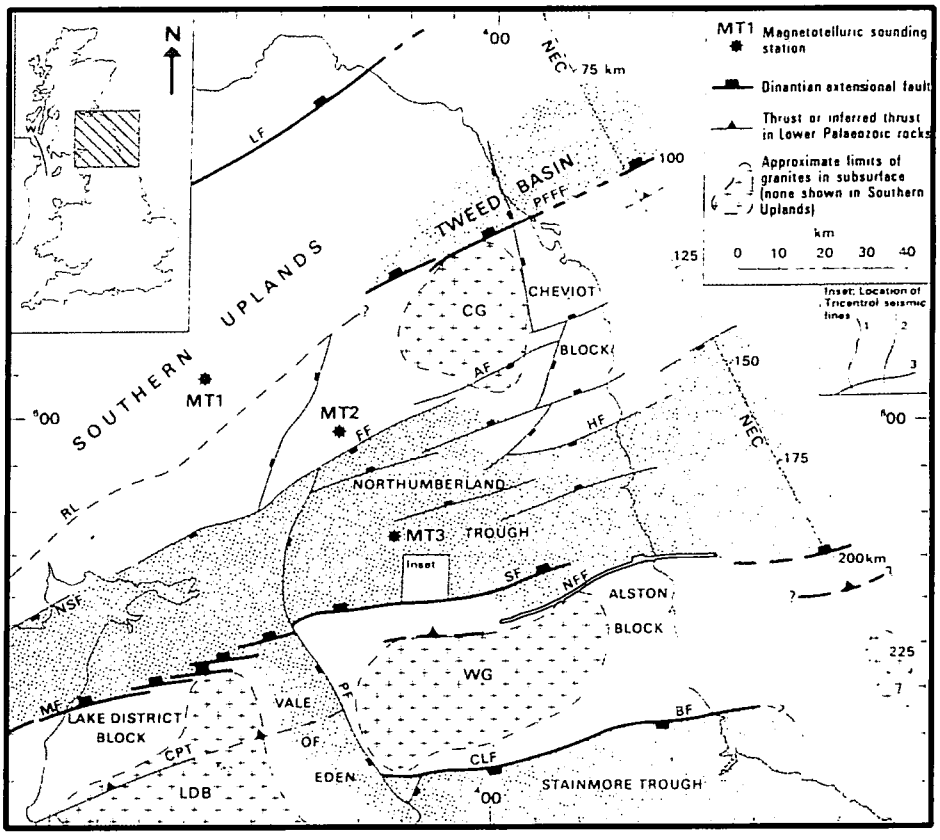

Figure 8.18 Map showing the major structural features of North East England
AF = Alwinton fault, BF = Butterknowle fault, CLF = Closehouse-Lunedale fault, CPT = Causey Pike thrust, FF = Featherwood fault, HF = Hauxley fault, LF = Lammermuir fault, MF = Maryport fault, **NFF = Ninety Fathom fault (*in red*)** NSF = North Solway fault, PF = Penine faults, PFFF = Pressen-Flodden-Ford faults RL = Riccarton line, SF = Stublick faults, CG = Cheviot granite, LDB - Lake District batholith, WG = Weardale granite
(after Chadwick and Holliday 1991)

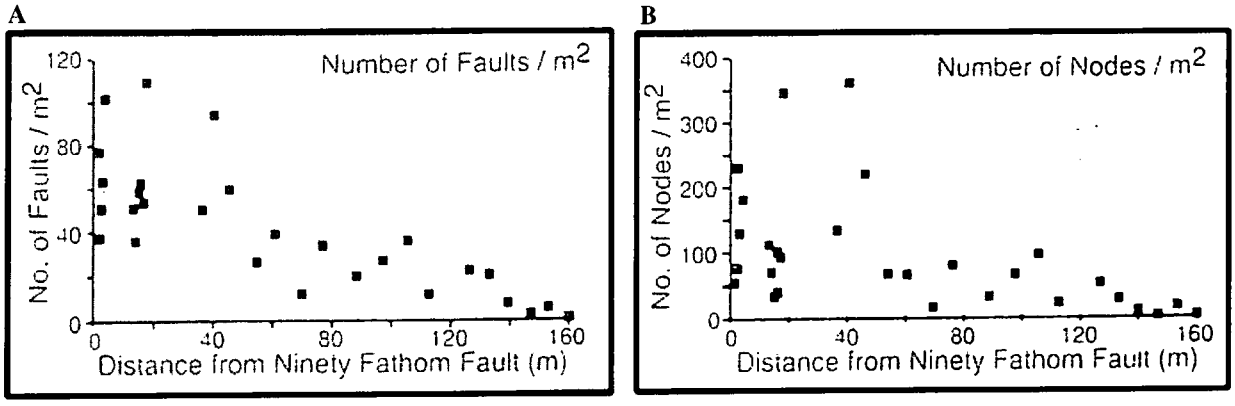

Figure 8.19 Graphs of fault density (**A**) and connectivity (**B**) adjacent to the Ninety Fathom Fault (after Knipe 1998)

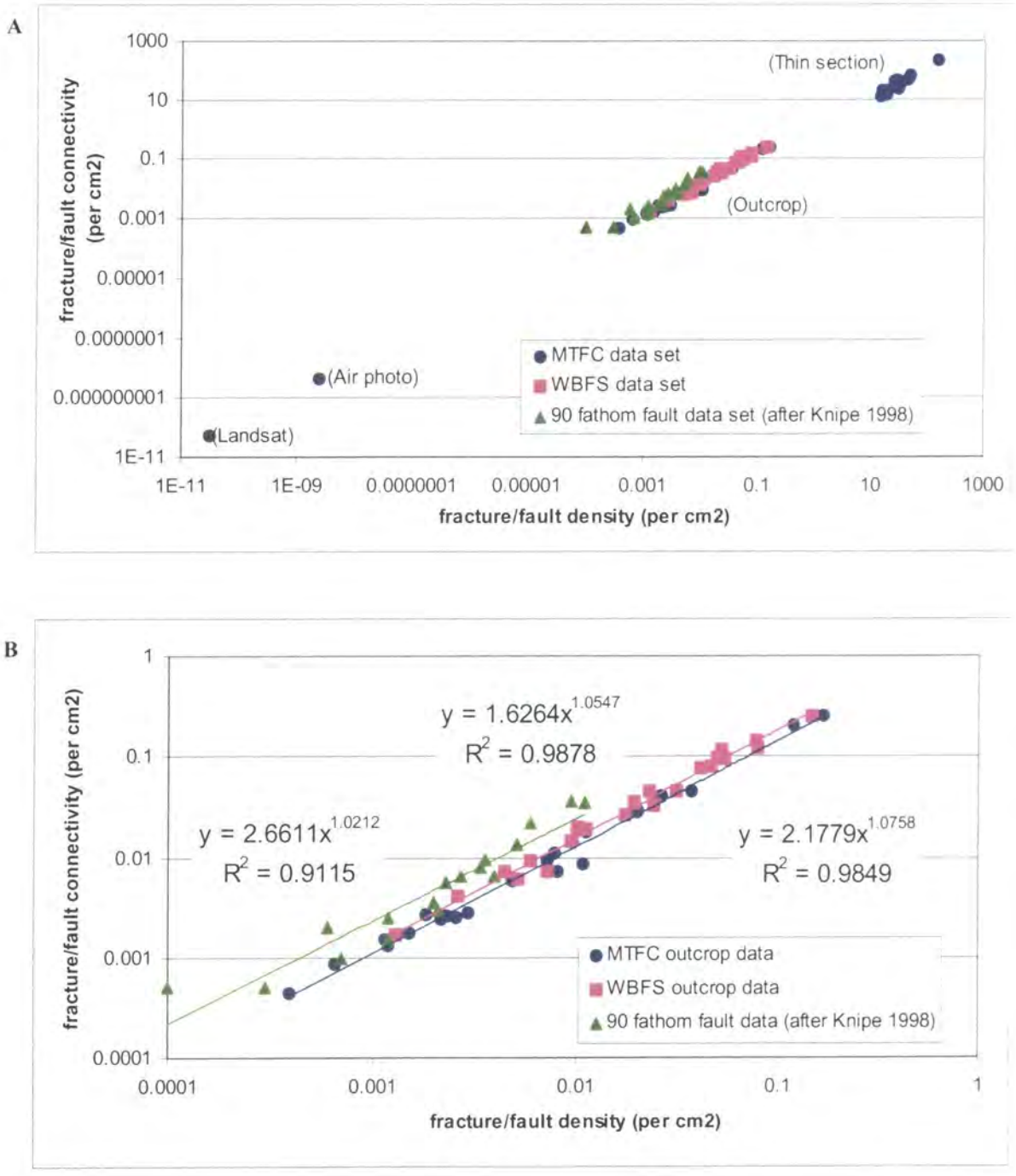

Figure 8.20 Fracture/fault density 'v' fracture/fault connectivity data from the MTFC, WBFS and the Ninety Fathom fault.

A – data collected at all scales from all fault systems, on logarithmic axes

B – data collected at outcrop scale only from all faults, on logarithmic axes

C – data collected at outcrop scale only from all faults, on linear axes

D - data collected at outcrop scale only (up to density of 0.06), on linear axes

(continued overleaf)

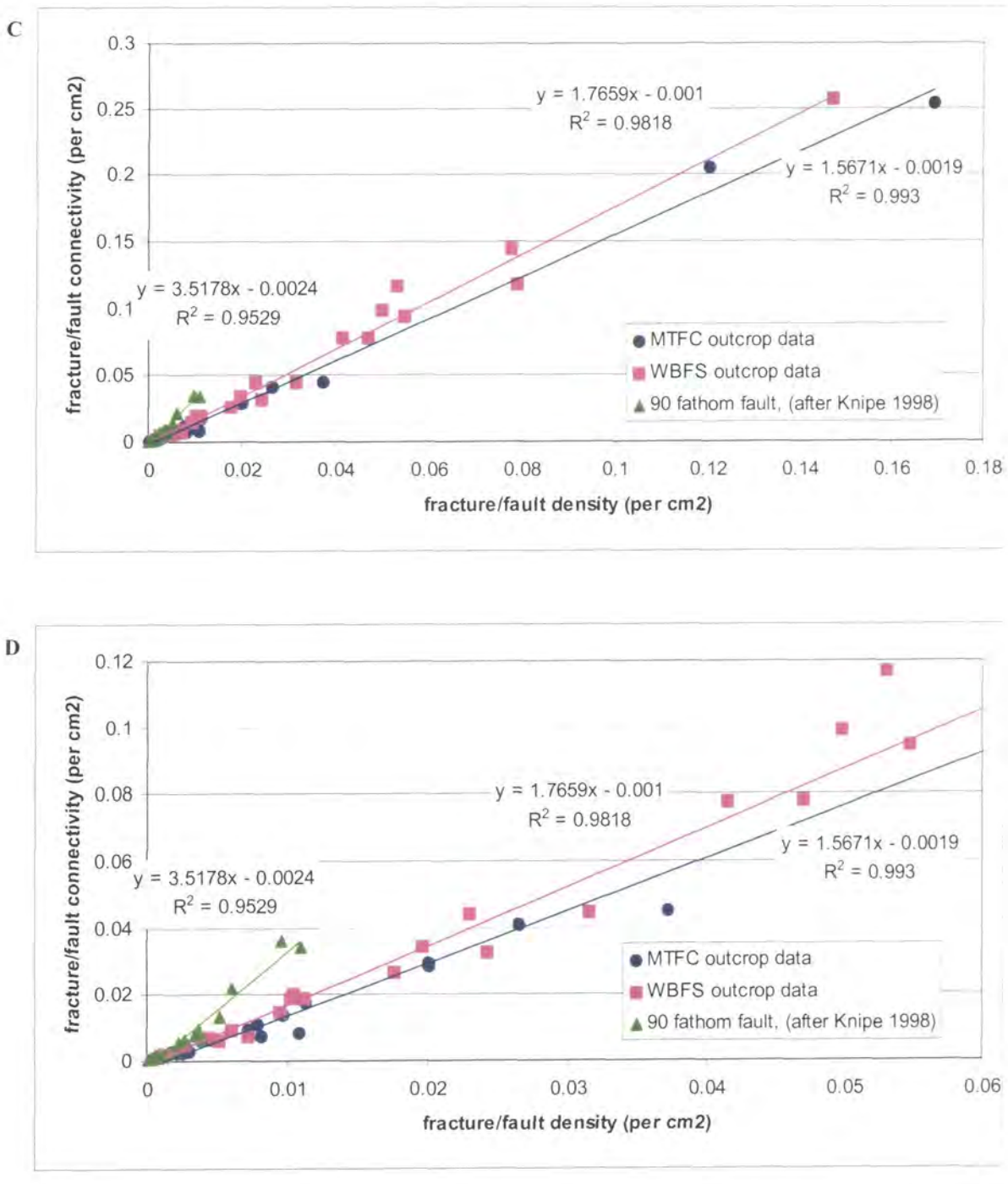

Figure 8.20 Fracture/fault density 'v' fracture/fault connectivity data from the MTFC, WBFS and the Ninety Fathom fault.
A – data collected at all scales from all fault systems, on logarithmic axes
B – data collected at outcrop scale only from all faults, on logarithmic axes
C – data collected at outcrop scale only from all faults, on linear axes
D - data collected at outcrop scale only (up to density of 0.06), on linear axes

(continued from previous page)

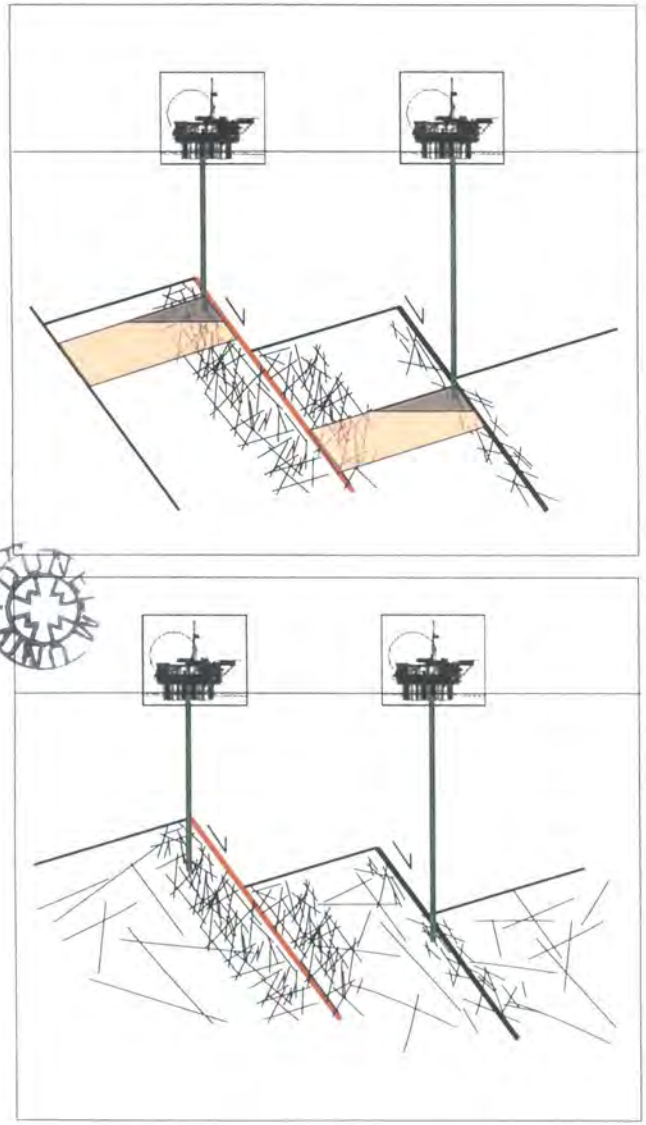

A - oil is accumulated in porous and permeable sandstone layers adjacent to 2 faults. One is highly reactivated (RED), the other is not (**BLACK**). The reactivated fault is associated with more fracturing & a wider damage zone, therefore more compartmentalisation of the reservoir occurs, inhibiting oil extraction

B - oil is accumulated within fractures, in an impermeable rock (e.g. basement, chalk). The impermeable rock is faulted, one fault is highly reactivated (RED), the other is not (**BLACK**). The reactivated fault is associated with more fracturing & a wider damage zone, therefore more oil can be stored adjacent to the reactivated fault, and fluid flow is enhanced, enabling easier oil extraction. Adjacent to the non-reactivated fault, fewer fractures occur, and connectivity is less.

Figure 8.21 Schematic diagrams illustrating the effects of reactivated faults being associated with wider, more connected damage zones, in porous and permeable rocks (**A**) and in impermeable rocks (**B**)

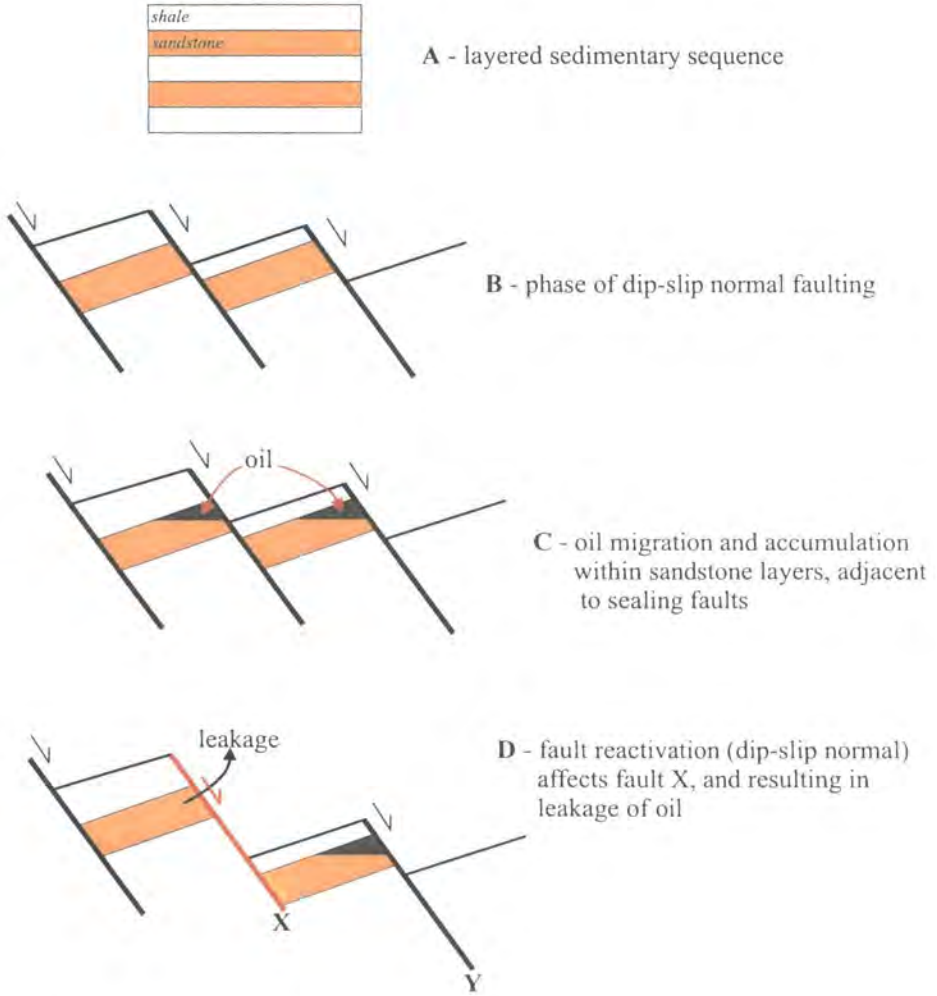

Figure 8.22 Schematic diagram to illustrate the effects of fault reactivation on oil migration and accumulation. Reactivation with the same successive kinematic movements is often very difficult to recognise. If fault reactivation occurs after oil migration, traps can be breached resulting in leakage of hydrocarbons, where they otherwise may be expected to be found.